Investigations of Hybrid Inorganic-Organic Network Solids

A Thesis Submitted for the Degree of

Doctor of Philosophy

By

A. Thirumurugan

Chemistry and Physics of Materials Unit

Jawaharlal Nehru Centre for Advanced Scientific Research

(A Deemed University)

Bangalore- 5600064, India

March 2008

“Fraction Demands - Totality Supplies”

-Guru Vethathiri Maharishi.

Dedicated to
All My
Beloved Teachers!

DECLARATION

I hereby declare that the matter embodied in this thesis entitled "**Investigations of Hybrid Inorganic-Organic Network Solids**" is based on the work carried out by me in the ***Chemistry and Physics of Materials Unit***, **Jawaharlal Nehru Centre for Advanced Scientific Research**, Jakkur, Bangalore, India, under the supervision of **Professor C. N. R. Rao, FRS**.

In keeping with the general practice of reporting scientific observations, due acknowledgement has been made wherever the work described is based on the findings of other investigations. Any omission that might have occurred by oversight or error in judgement is regretted.

March 2008,

Bangalore (A. Thirumurugan)

CERTIFICATE

Certified that the work described in the thesis entitled "**Investigations of Hybrid Inorganic-Organic Network Solids**" is the result of investigations carried out by **Mr. A. Thirumurugan** in the ***Chemistry and Physics of Materials Unit***, **Jawaharlal Nehru Centre for Advanced Scientific Research**, Jakkur, Bangalore, under my supervision.

March, 2008

Bangalore

(Prof. C. N. R. Rao)

Acknowledgements

I am deeply grateful to my thesis advisor, ***Prof. C. N. R. Rao, FRS,*** *for his invaluable guidance, love and affection during my study and research at JNCASR. His perpetual energy, passion for science and enthusiasm in research had motivated all who have come into his contact, including me. In addition, he is always accessible and willing to help me in all the possible ways. As a result, research life became smooth and rewarding for me. I am truly blessed to learn how to explore research problems in a scientific manner with in-depth exploration and global understanding. I am sure the values imparted by him will always guide me in all my future endeavors so that society which I live in will certainly benefit.*

I am extremely happy to thank ***Prof. S. Natarajan*** *of IISc from whom I have received important guidance during my first steps in research. I have learnt from him how to do research systematically starting from analyzing the PXRDs to drawing the crystal structures in a nice presentable way. I will always cherish the moments I have spent with him and the advices he gave to me on various aspects of life.*

I am thankful to all the faculty members of CPMU and especially Profs. G. U. Kulkarni, N. Chandrabhas, S. Balasubramanian, K. S. Narayan and Shobhana Narasimhan for the various discussions and courses. I also thank Drs. A. Sundaresan, M. Eswaramoorthy and T. Maji for their help in various aspects of my research. I am very happy to thank Profs. T.N. Guru Row, P.Balaram and Anuradha of IISc for their extremely useful and enjoyable courses.

I thank all my lab mates and seniors especially Drs. Sandip, Sukhendu, Anupama and Reji for their help and support in crystallography lab. I also thank Drs. Meenakshi, Beheraji, Prabha along with Ganesh, Partha, Claudy, Jyoti, Raju, Ramakrishna, Sujith, Avinash, Suchethan, Sowmiya, Dr. Padmanabhan and Dr. K. Bhat who made our lab a convivial place to work and enjoy. I am grateful to Dr.A. Govindaraj for his many helps and useful tips in day-today lab activities. I thank Prof. Bhat for giving me an opportunity to teach the students of Project oriented chemical education program. I am extremely happy to thank Dr. Ayan

Dutta, Sairam and Prof. S. K. Pati of Theoretical sciences unit in JNCASR for the help in many calculations and fruitful discussion.

I am indebted to my many friends in JNCASR, Chandu, V.P.Bhat, Ayan, Ved, Kabra, Vijay, Gopal, Kalyani, Vegadesh, Subbu, Leela, Rakesh, Saikrishna, Gurunath, Prakash, Sudip, Sameer, Vivek, Pavan, Kalyan, Madhu, KKR Datta, Dinesh, Pranab, Neenu, Gomathi, Radha, Kavitha and Manoj for providing me a stimulating and fun environment in JNCASR.

I express my gratitude to all the technical staff of JNCASR, Anil Kumar, Srinivas, Srinath for their help in the powder and single crystal X-ray diffractometers, Vasu for the TGA and IR, UV-Vis spectrometers, Basavaraj, Selvi and Usha Madam for their help with the SEM and TEM. I also thank Mr. Arogyanathan and Moorthy from the workshop. I sincerely thank all the office staff in CSIR-COE, JNCASR, Mrs. Shasi, Mrs. Sudha, Gowda, Xavier and Victor for offering help with all the official work.

It is a pleasure to thank Mrs. Indumati Rao and Sanjay Rao for being nice to me and for the very nice dinners at their residence.

I thank the Council of Scientific and Industrial Research (CSIR), Government of India for the award of Junior and Senior research fellowships.

I am deeply indebted to all my teachers from my school and college and it is difficult to overstate my gratitude towards them for teaching me to live with an inquisitive and open mind in all the aspects towards knowledge. This thesis would not have been possible without them. I dedicate this thesis to all my respected teachers.

I cannot end without thanking my parents, my brother and my family, on whose constant encouragement, sacrifice, unflagging love and support I have relied throughout my life. I earnestly hope I will make my family extremely satisfied by serving the society through science and make their sacrifice meaningful.

Preface

Hybrid inorganic–organic network compounds constitute an important class of materials that have been studied extensively over the last few years due to their potential applications in catalysis, gas separation and storage. Other properties which draw attention to these materials include magnetic, optical and electronic properties. An effective and widely used strategy for the design of hybrid framework solids is based on the selection of metal and ligand geometries to produce desired network topologies. The mode of linkage and the dimensionality of the inorganic sub network, along with the size, geometry, chemical functionality and various coordinating modes of the linkers, provide excellent means of controlling and modulating the properties in these solids. In an attempt to understand these aspects and design hybrid frameworks with novel structural features and properties, hybrid dicarboxylates have been explored in this thesis in terms of dimensionality and extended inorganic connectivity. In pursuit of the above understanding, benzene-, cyclohexane- and aliphatic-dicarboxylic acids have been employed to synthesize hybrid inorganic-organic frameworks of di- and trivalent metal ions with or without chelating amines. To understand the process of formation of a three-dimensional zinc terephthalate, a systematic time and temperature dependent transformation study has been carried out. Investigations were also carried out to synthesize novel hybrid solids and nano materials by employing ionic liquids as solvents.

After providing an brief overview on hybrid inorganic-organic frameworks (Chapter 1), the thesis presents the results of the investigations of the hybrid benzenedicarboxylates (BDCs) of the three isomeric (1,2-, 1,3- and 1,4-) benzenedicarboxylic acids with divalent cations of Zn, Cd, Pb and trivalent cations of lanthanides (in Chapter 2). Several coordination polymers and the hybrids with extended inorganic connectivity of BDCs in different dimensionality have been prepared under hydrothermal conditions. Few of them have been doped Eu and Tb and they exhibit the lanthanide-centered red and green emission sensitized by the ligands at room temperature. The studies on zinc terephthalates show that a progressive transformation of a one-dimensional structure to a three-dimensional structure and the possible presence of a dimensional hierarchy.

Chapter 3 presents the results of the investigations of the hybrid cyclohexane and cyclohexenedicarboxylates (CHDCs and CHeDCs) of the three isomeric (1,2-, 1,3- and 1,4-) flexible cyclohexanedicarboxylic acids in different conformation with cations of Mn, Cd, Pb and La and 1,2-cyclohex(4)enedicarboxylic acid with Cd(II) cation. Several coordination polymers and the hybrids with extended inorganic connectivity in different dimensionality have been prepared under hydrothermal conditions.

Chapter 4 presents the results of the investigations of the hybrid aliphatic-dicarboxylates. These novel hybrid networks with extended inorganic connectivity, have been synthesized hydrothermally by employing single (homoleptic) and mixture (heteroleptic) of aliphatic dicarboxylicacids with the potentially lone pair active, flexible coordinating Pb(II) cation with larger ionic radii.

Chapter 5 presents the results of the investigations on a hybrid dihydroxybenzoate. A novel three-dimensional coordination network of lead 2,6-dihydroxybenzoate with (3,6) 3D net topology, has been synthesized and characterized.

Chapter 6 presents the results of the investigations on the exploration of ionic liquids as solvents to synthesize novel hybrid frameworks and nano materials. Ionic liquids are salts with low melting points ($<100^{o}C$), consisting of a bulky organic cation and an organic or inorganic anion. Two imidazolium bromoplumbates which exhibit unusual supramolecular organization with channel structures have been obtained by heating imidazolium bromide-based ionic liquids with lead (II) salts under ionothermal conditions. Nanocrystals, nanorods, nanowires and nanobelts of various elemental chalcogens and metal oxides have been synthesized by using imidazolium [BMIM]-based ionic liquids as solvents at 100 – 200 °C.

CONTENTS

Chapter 3. Hybrid Networks of Metal Cyclohexanedicarboxylates

Chapter 4. Hybrid Networks of Lead Aliphaticdicarboxylates with Extended Inorganic connectivity

Chapter 1

Hybrid Inorganic-Organic Network solids - A Brief Overview*

1.1. Introduction

Hybrid inorganic–organic network compounds constitute an important class of materials that have been studied extensively over the last few years due to their potential applications in catalysis, gas separation and storage. Other properties which draw attention to these materials include magnetic, optical and electronic properties.[1] It is necessary to understand where hybrid materials belong relative to conventional coordination compounds. Starting with the pioneering work of Werner on coordination compounds, for which he was awarded the Nobel Prize in Chemistry in 1913, the field of coordination polymers has turned out to be rich and varied. Coordination compounds with infinite structures, the so-called coordination polymers, have been intensively studied, in particular compounds with backbones constructed from metal ions as nodes and ligands as linkers. The term, "coordination polymers" appeared in the early 1960s, and the area was first reviewed[2] in 1964.

A vast range of coordination polymers and supramolecular architectures with one, two and three dimensional structures have been discovered. Examples of 1-D coordination polymers are relatively common in the early literature, even though they were not recognized at the time as part of a vast and remarkable family of materials. Examples include porphyrin coordination polymers with

* A topical review on the subject has been published in *J. Phys: Condens. Matter* (2008).

interesting magnetic properties, first discovered by Basolo and co-workers in the 1970s and characterized by X-ray diffraction at a later date.[3,4] Early examples of nanoporous 3-D coordination polymers can be found in the work of Gravereau, Garnier and Hardy in the late 1970s, in which zeolitic materials with ion-exchange properties were made by linking hexacyanoferrate units with tetrahedrally coordinated Zn^{2+} cations.[5] The components of coordination polymers are connected through coordination bonds, which are weaker in energy than the strong Si/Al-O bonds that sustain the structures of zeolites. Thus, coordination polymers have rather poorer thermal stability, though they are sufficiently robust for many applications, especially in systems with extended inorganic connectivity, e.g. metal-oxygen-metal bonds.

The development of hybrid inorganic-organic network materials may be traced back to a strategy that was originally used to increase the interlayer spacing in layered compounds, the most notable being the layered zirconium phosphonates.[6,7] However, there was relatively little interest in hybrid materials until the 1990s, when several groups, particularly those of Robson, Hoffman and Yaghi, recognized that rigid, polyfunctional organic molecules could be used to bridge metal cations or clusters into extended arrays. Robson published a landmark paper[8] in 1990, laying the groundwork for an important part of the field of crystal engineering – the science of predicting basic networks with potentially useful characteristics and then using appropriate molecular building blocks to synthesize them.[9-11] For the synthesis of porous materials, networks are often envisioned where rigid organic molecules and metal atoms or clusters replace bonds and atoms in classical inorganic structures.[12] Since then, several groups have focused

on synthesizing and characterizing novel hybrid metal oxides based on carboxylates.[13-18]

Hybrid inorganic–organic network materials are defined as compounds that contain both inorganic and organic moieties as integral parts of a network with infinite bonding connectivity in at least one dimension.[18] This definition excludes systems that are molecular or oligomeric. Most of the known hybrid networks may be divided into two categories. The coordination polymers, or metal organic frameworks (MOFs) as they are also known (especially when they are porous), can be defined as extended arrays composed of isolated metal atoms or clusters that are linked by multifunctional organic ligands, L; these are based upon M–L–M connectivity. Second, there are systems that contain extended arrays of inorganic connectivity, referred to as extended inorganic hybrids. At present, the vast majority of known materials in this area are based upon oxygen bridges. These hybrid metal oxides, which contain infinite metal–oxygen–metal (M–O–M) arrays as a part of their structures, represent a sub-group of a larger class in which there is extended M–X–M bonding via other atoms such as Cl, N or S.

1.2. Classification

In Table 1, we show the range of possibilities in terms of M–ligand–M, ($\boldsymbol{O^m}$, where $\boldsymbol{m}$ represents the dimensionality of the ligand bridging) or extended inorganic dimensionalities ($\boldsymbol{I^n}$, where $\boldsymbol{n}$ represents the dimensionality of the inorganic connectivity). The overall dimensionality of the structure is then represented with the notation $\boldsymbol{I^nO^m}$. The sum of the exponents gives the overall dimensionality of the structure ($m + n \leq 3$, $n = 0$ to 3 and $m = 3 - n$). The entire family of molecular coordination compounds are contained within a single box ($\boldsymbol{I^0O^0}$) in Table 1.1 {i.e. both M–L–M (m) and inorganic connectivity (n) = 0}. The

remaining three boxes in the first column represent the coordination polymers with overall dimensionality 1 to 3. The three boxes in the second column represent hybrid compounds with one-dimensional inorganic connectivity ($\boldsymbol{I^1}$) and with an overall dimensionality between 1 and 3. The two boxes in the third column represent hybrid compounds with two-dimensional inorganic connectivity ($\boldsymbol{I^2}$) and

Table 1.1 ***Classification of Inorganic-organic hybrid network solids***

Metal–organic–metal connectivity, O^n (n = 0–3) \ Dimensionality of inorganic connectivity, I^n (n = 0–3)	0	1	2	3
0	Molecular complexes I^0O^0	Hybrid inorg. chains I^1O^0	Hybrid inorg. layers I^2O^0	3-D Inorg. hybrids I^3O^0
1	Chain coordination polymers I^0O^1	Mixed inorg.–organic layers I^1O^1	Mixed inorg.–organic 3-D framework I^2O^1	—
2	Layered coordination polymers I^0O^2	Mixed inorg.–organic 3-D framework I^1O^2	—	—
3	3-D Coordination polymers I^0O^3	—	—	—

with the overall dimensionality of 2 or 3. The first box in the fourth column represents a rare class of hybrid compound ($\boldsymbol{I^3O^0}$) with a three-dimensional inorganic connectivity ($\boldsymbol{I^3}$) and with the overall dimensionality of 3. There are examples of all of these classes of hybrid materials[19-28] (Table 1.2 and Fig. 1.1). Hybrid compounds with zero-inorganic connectivity are coordination polymers, which can be represented as $_{\boldsymbol{x}}\boldsymbol{I^0O^m}$ where $\boldsymbol{x}$ represents the nuclearity of the metal

site. For compounds with isolated metal sites, $x = 1$ and for cluster metal sites, $x > 1$.

Table 1.2 ***Examples of the different classes of inorganic-organic hybrid compounds***

I^nO^m	Compound	Figure	Ref
I^0O^1	Zinc oxalate	1(a)	[19]
I^0O^1	Zinc oxalate	1(b)	[19]
I^0O^2	Zinc oxalate	1(c)	[20]
I^0O^3	Zinc terephthalate	1(d)	[21]
I^1O^0	Strontium dihydroxybenzoate	1(e)	[22]
I^1O^1	Nickel succinate	1(f)	[23]
I^1O^2	Nickel gallate	1(g)	[24]
I^2O^0	Cobalt succinate	1(h)	[25]
I^2O^1	Cobalt phosphonate	1(i)	[26]
I^3O^0	Nickel succinate	1(j)	[27]
I^3O^0	Cadmium malonate	1(k)	[28]

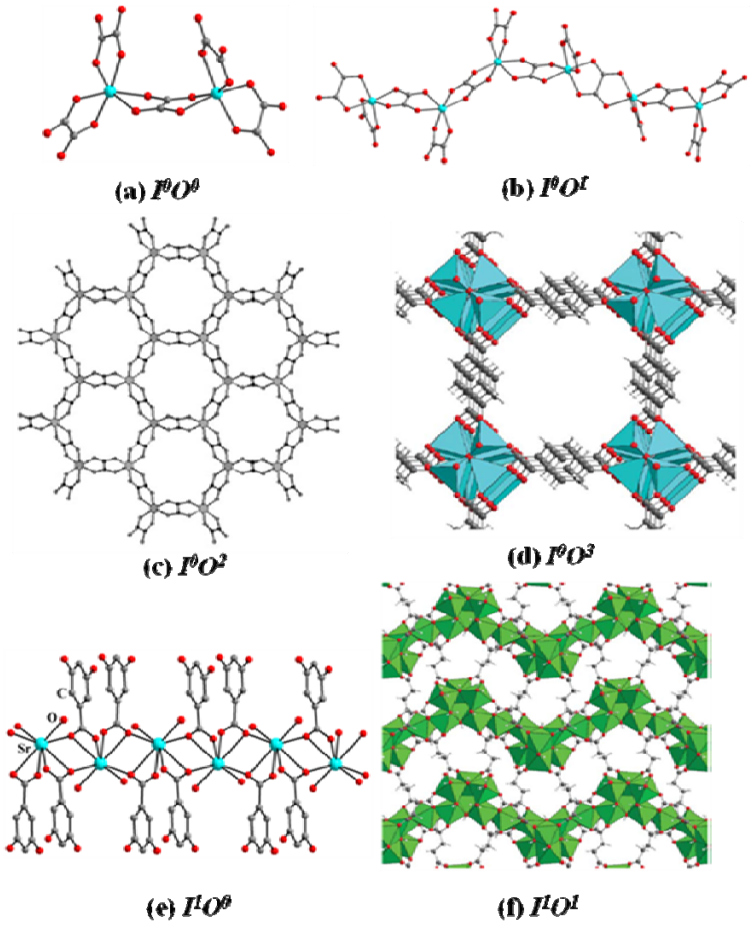

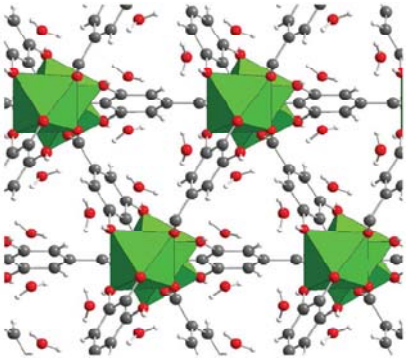

(g) I^1O^2

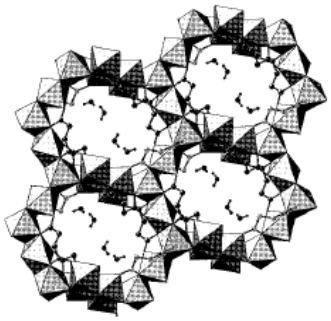

(h) I^2O^0

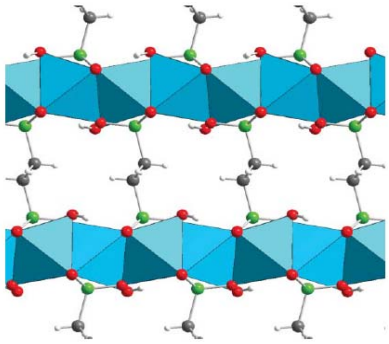

(i) I^2O^1

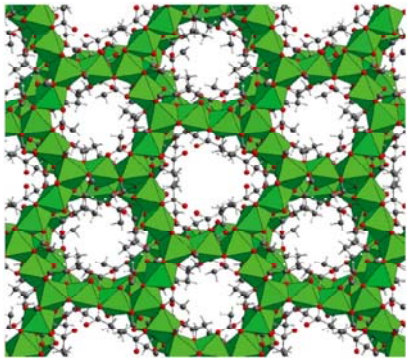

(j) I^3O^0

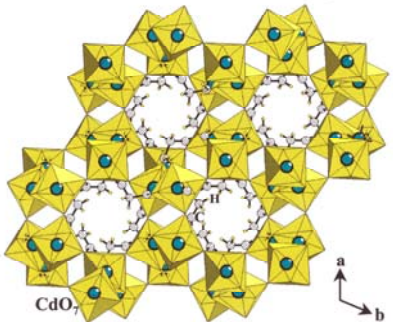

(k) I^3O^0

Fig.1.1a) – k) Examples of all the classes of hybrid materials

1.3. Synthetic methods

The synthesis of crystalline hybrid network materials while preventing the precipitation of amorphous solid remains a challenge, and novel methodologies are being investigated to access them. Synthetic strategies[29] for the preparation of crystalline hybrid materials may be categorized as follows: (i) coordination-directed assembly of metal complexes by multifunctional organic ligands, or the bottom-up method. The structural integrity of the building units is maintained

throughout the reactions which allow their use as modules in the assembly of extended structures. (ii) pH-controlled condensation of metal hydroxide or hydrate units to form extended M-O-M linkages. (iii) combination of the above two, i.e. partial condensation of oxide components intercepted by coordination and linking by multidentate ligands. The extent of oxide bridging and structure condensation increases with reaction temperature.

The above strategies are realized in terms of two important techniques of crystallization, namely i) diffusion based crystallization and ii) hydro/solvo/iono-thermal methods. Good quality single crystals can be generally obtained by layered diffusion, which is preferred for coordination polymers of desired stoichiometry. Hybrid compounds with extended inorganic connectivity are generally prepared by hydro/solvo thermal methods to overcome the differing solubilities of the organic as well as inorganic components and to enhance the degree of condensation.[30] Ionothermal methods have been employed recently for the synthesis of the hybrid compounds, wherein ionic liquids are used as solvents.[31,32]

The use of hydrothermal methods and relatively high reaction temperatures (up to, say, 250^{o}C) generally produces compounds with increased M-O-M connectivity. For example, five different cobalt succinate structures could be synthesized using identical starting mixtures by varying only the temperature.[33] The extent of oxide bridging and structure condensation increases with reaction temperature. In a more comprehensive study of the cobalt succinate system by high throughput experimentation, the trends as a function of pH and time were also examined.[34] It was found that extended inorganic hybrid structures are also favored at high pH, where the formation of M-O-M linkages arise due to the elimination of water or hydroxide groups by condensation reactions. The evolution of reaction

products as a function of time, however, showed relatively few changes, supporting the idea that thermodynamic factors are often very important in hybrid synthesis.

Hybrid compounds have also been synthesized by microwave-assisted solvothermal synthesis.[35-38] An advantage in this method is that local superheating of the solvent (or the organic ligand, L) can lead to hot spots that nucleate crystal growth all over the system. More seeds lead to faster growth and higher yields. Once the seeds start to grow, the available reactants get quickly depleted. The size of the crystals can therefore be varied by adjusting the reactant concentration. The ability of the microwave technique to control the nucleation process leads to a narrow size distribution, because all of the crystals are nucleated at once. It also allows new types of networks to be discovered readily since the growth process is not depending on nucleation on the walls or dust particles. Since the hot spots in microwave-assisted reactions with certain organic solvents are known to produce excessive pressure and heat, extra care must be taken. Since ionic liquids with high polarizability and ionic conductivity exhibit excellent microwave absorption behavior, they are used as solvents for microwave-assisted ionothermal synthesis of hybrid compounds.[32]

Another recent method is the high-throughput hydrothermal method, which involves in the systematic studies of the role that various synthesis parameters and this help for a quick investigations.[33] Recently high-throughput methods can be successfully applied to developing a robust synthesis protocol for zeolitic imidazolate frameworks (ZIFs)[39]. 25 different ZIF crystals were synthesized from "only" 9600 microreactions of either zinc(II)/cobalt(II) and imidazolate/imidazolate-type linkers. Some of them have high porosity (with

surface areas up to 1970 square meters per gram), and they exhibit unusual selectivity for CO_2 capture from CO_2/CO mixtures and extraordinary capacity for storing CO_2: 1 liter of ZIF-69 can hold ~83 liters of CO_2 at 273 kelvin under ambient pressure.

1.4. Crystal engineering and rational synthesis

Crystal engineering, the design of solids, is the synthesis of functional solid-state structures from neutral or ionic building blocks, using intermolecular interactions in the design strategy. Hydrogen bonds, coordination bonds, and other less directed interactions define sub-structural patterns, referred to in the literature as supramolecular synthons and secondary building units. Crystal engineering has considerable overlap with supramolecular chemistry, X-ray crystallography, materials science, and solid-state chemistry and yet it is a distinct discipline in itself. A definition of crystal engineering, is given as "the understanding of intermolecular interactions in the context of crystal packing and in the utilisation of such understanding in the design of new solids with desired physical and chemical properties".[40] The subject today includes three distinct activities: i) the study of intermolecular interactions ii) the study of packing modes, in the context of these interactions and with the aim of defining a design strategy; and iii) the study of crystal properties and their fine-tuning with deliberate variations in the packing.[41]

An effective and widely used strategy for the design of hybrid network solids, based on the selection of metal and ligand geometries to produce given network topologies, has been around for some 15 years now.[8] This strategy can be highly rewarding, allowing, for example, the targeting of certain network topologies (e.g. diamond) which are likely to produce acentric structures,[42] the design of magnetically interesting nets such as the Kagome´ lattice,[43] or the

synthesis of highly porous materials.[44] Despite this, however, the crystal engineering of coordination polymers can still be a highly unpredictable pursuit.[45] The first challenge is to coax the building blocks (Fig. 1.2. shows some of the building blocks of metals and ligands; Fig. 1.3. shows net topology of square SBUs and 2 connecting ligands) to behave as predicted. This may sound trivial, but it many cases it is not. Flexible ligands can be particularly difficult to predict their final geometry, but even rigid ligands can refuse to coordinate, or can show multiple bonding modes. Metal coordination geometries can also unpredictable, particularly for those malleable metal ions which possess two or more common coordination geometries. Even if the ligand and metal ion coordination geometries are correctly predicted, further complications can arise. There are, for example, numerous networks possible with only 3-connecting nodes.[47,48] These can range from one-dimensional (e.g. ladders) to two-dimensional [(6,3) sheets] to three-dimensional [e.g. (8,3), (10,3), (10,3), (12,3), and so forth]. Thus, controlling the local coordination geometries controls only this; the overall network topology is still out of our complete control. Even for tetrahedrally connected networks, where diamond is the overwhelmingly dominant topology, the question remains: why? There are other perfectly feasible nets possible for tetrahedral nodes, such as Lonsdaleite and quartz. Why is diamond so special? The answer may lie in the high underlying symmetry of the net[49] as it is the most highly symmetric and simplest of the nets containing tetrahedral nodes. Indeed it has been argued, quite reasonably, that the diamond net is the 'default' topology for tetrahedral nodes.[49] Even low-symmetry structures with asymmetric or flexible ligands or nodes form this net regularly. Nonetheless, even for tetrahedral nodes, other network topologies are possible and have been formed. A further complication can arise for

networks with significant cavities and channels: how are these filled? For two-dimensional (and one-dimensional) networks, there are three main ways in which the packing efficiency can be maximised: interdigitation, interpenetration and intercalation,[50] and which method (or combination of methods) occurs can be affected by subtleties. Interpenetration also provides its own complications. The first question is: will it occur, and if so, how many nets? The mode of interpenetration is another possible variable.

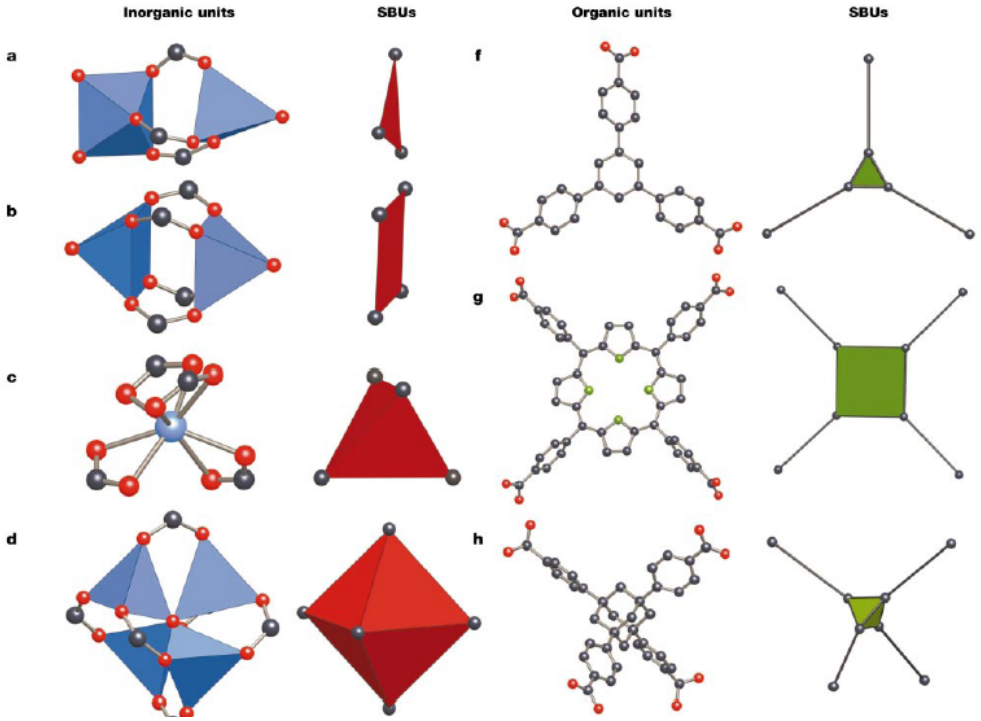

Fig. 1.2 Building blocks of metals and ligands. Reproduced from Ref. 44.

All these factors contribute to the formation of polymorphs, which encapsulate the challenges of structure prediction or design for the crystal engineer. Pseudopolymorphism, where structures differ in the numbers or types of included solvent molecules.[51,52] It also illustrates the problems of kinetic versus thermodynamic products. Related to the problem of polymorphism is structure templation of network topology by counterions, solvents or guest molecules. Modest variation of one of these variables can result in very different structures.

Cation templation is a good example. Anionic metal oxalate networks form (6,3) sheets when crystallised with tetraalkyl or tetraaryl amines or phosphines, but form chiral (10,3)-a three-dimensional networks when $[M(2,2'\text{-bipyridine})_3]^{2+}$ cations are used.[53,54] The solvent also plays a vital role in structure design. The first question to be answered is: will the solvent coordinate, be intercalated, or be ignored in the crystallisation process? If the solvent is not ignored, then it can have a crucial structure-directing effect.

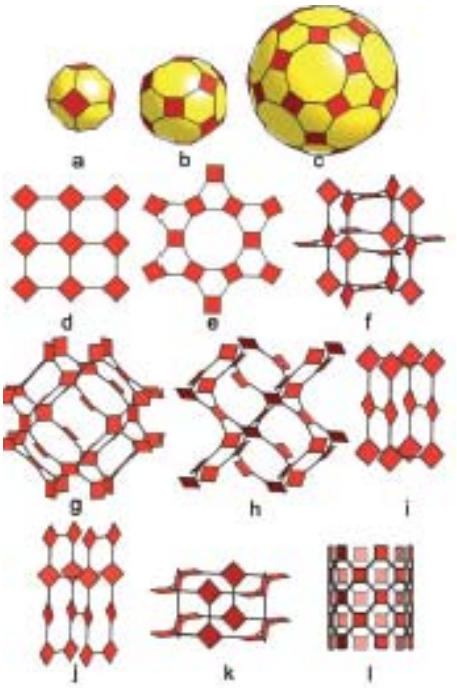

Fig. 1.3 Various Net topologies from square SBUs and 2-connecting ligands. Reproduced from Ref. 46.

Despite these important challenges for the future, there is no doubt the modular, net-based approach is an essential part of crystal engineering, for both the design and analysis of crystal structures. It has produced some fascinating results. Thus, Yaghi et al used reticular synthesis to obtain series of isoreticular structures with different topology.[55] Figure 1.2 shows some of the possible organic and inorganic secondary building units (SBUs) available for reticular synthesis and

figure 1.3 shows the possible structures for linking square SBUs by linear linkers into polyhedra and networks. Reticular chemistry is concerned with linking judiciously designed rigid molecular secondary building blocks into predetermined periodic structures using strong bonds.[44] The principle of **reticular** chemistry is synthesized from both **ret**ero synthesis approach of organic chemistry and supramole**cular** chemistry.

Férey et al used another concept, known as the 'scale chemistry'[55] for the design and synthesis where playing on the size of the SBU, it was illustrated that, whatever the size of the SBU, the topology of the resulting structure remains invariant and, in terms of porosity, 'the larger the brick, the larger the pores'. Therefore, the principle of scale chemistry is very simple: larger the brick, larger the pore. The brick, primitively of chemical nature, becomes a *topological* building unit. The only important point is that it keeps its connectivity. With these simple principles, it becomes easy to imagine 'hyperstructures' with very large pores.[55] Two examples based on the same topology will illustrate this point. Thus a semiconducting indium sulfides in which the SBU is an assembly of ten InS_4 tetrahedra, the truncated octahedron delineated by the centers of these supertetrahedra is a sodalite-type cage of order three (with a 25.6 Å free diameter), compared to the parent sodalite structure[56] and a supercristobalite structure,[57] with SBU containing this time twenty tetrahedral were described. Similarly, zeotype cubic structures of trinuclear chromium cluster-based benzene di- and tri-carboxylates which possess very large surface areas and unit cell volumes going up to 700000 $Å^3$ were described based on the super tetrahedron SBU.[58]

However, despite the increasing number of examples of true structure design, we should not be blind to the limitations and challenges of this approach.

We can, at best, direct rather than predict structures i.e. we can create the conditions under which our desired structure is possible, but we cannot be certain of its formation. This is nonetheless a considerable achievement, and its significance should not be underestimated. However, this area is still very much an experimental pursuit, with surprises and subtleties at every turn. This is not necessarily a bad thing while one aim to predict and understand, the most enjoyable and rewarding structures are often those unexpected ones.

1.5. Characterization

1.5.1. Single-Crystal X-ray diffraction

Single crystal structure determination provides complete and unambiguous information about the internal structure of a material. For example, it tells about the types of atoms and their space arrangement, internal symmetry of crystals, coordinates of atoms, population of atoms (occupancies), anisotropic thermal parameters, connectivity and the stereochemistry of the molecule, bond length and bond angle information etc. It also allows one to correlate between the property observed for the material with its structure. For X-ray data collection the crystal should (i) have a uniform internal structure (i.e. it must not be twinned or composed of microscopic subcrystals. The existence of two different orientation of a lattice in one crystal is called twinning. The crystal should not be grossly fractured, bent or otherwise physically distorted. However, it need not have uniform or neatly formed external surfaces), (ii) it must be of proper size and shape (the preferred crystal size is 0.1-0.3 mm, but should not exceed 0.5 x 0.5 mm).

1.5.2. Powder X-ray diffraction

The first step in characterizing the solid isolated from synthesis mixture is powder X-ray diffraction (PXRD). Powder X-ray diffraction is a non-destructive

powerful technique widely used for qualitative and quantitative analysis of crystalline compounds. As the name suggests, the sample is usually a powder, containing fine grains of single crystalline material, which are randomly-oriented. Each crystalline solid has its unique characteristic PXRD pattern, which is used as a 'fingerprint' for its identification. The peak positions and the systematic absences are used for crystallographic structural analysis and unit cell determinations. The intensity information is used to assess the type and nature of atoms. If there are more than one phase present in a sample then the relative intensity of the peaks is used to quantitatively estimate the amount of different phases present. The intensity distribution of diffraction pattern can be used to determine the texture of the sample, i.e. if the individual grains of the sample show any preferred orientation. This preferred orientation can also be of hindrance for quantitative identification of different phases in a mixture. The width of the diffracted peak is used to determine crystallite size and micro-strain in the sample. Various informations can be obtained from the different features of the PXRD pattern. Few examples include; a) Peak position parameter helps in unit cell parameter refinement, pattern indexing, space group determination (from absent reflections) and qualitative phase identification b) Intensity can be used to extract information on phase abundance, crystal structure analysis (whole pattern), Rietveld refinement (whole pattern), search/match, quantitative phase identification and preferred orientation and texture analysis. C) Width/breadth and shape of each peak in the pattern can be used for the analysis of microstructure (crystallite size, size distribution, lattice distortion, dislocations, microstrain etc).

In the case of microporous and hybrid network materials, powder diffraction data is most commonly used to identify a newly synthesized material, to

check the purity of the product. For mixture of phases it is also used to identify the relative proportion of the different phases present. PXRD method is also used to monitor the phase changes that take place as a function of changes in reaction conditions or to monitor the effects of post-synthesis treatment. The PXRD of the solid is generally taken for 2θ values between 5 to 40°. It is within this range that the most intense peaks characteristic of a particular compound occurs. Microporous materials are identified by the presence of peaks at low 2θ values, i.e. high "d" values. The measured patterns are compared with an existing one, either with the pattern in the collection of simulated XRD powder patterns for known microporous materials or the powder diffraction file of the Inorganic Chemistry Diffraction Database (ICDD). If the PXRD pattern does not match with any of the existing ones and is found to contain peaks at low values of 2θ, then it is identified as a new microporous material.

In recent years the powder method has also been used for the determination of crystal structures by *ab initio* methods.[59,60] Powerful methods are available for pattern indexing, extraction of integrated intensities, structure solution and refinement of the structure model with the Rietveld method.[61,62] Efficient Rietveld programs like FULLPROF from Rodriguea-Carvajal, GSAS from Von Dreele and RIETAN from Izumi are available which can be used for the crystal structure refinement.

1.5.3. Computer simulation

Early work on *ab initio* structure determination[60,61] from powder diffraction was done independent of simulations, but simulations have now become an integral part of structure determination, gradually incorporating global

optimisation techniques that are traditionally used in the field of structure prediction.[56] However, the design of materials with increasingly large pores carries, especially for hybrid network solids, the risk of interpenetration of the skeletons within structures. In addition, although the structural characterization of such solids with large cells is usually possible when single crystals are available, the probability of getting the solutions is known to drastically decrease or even to become zero when the cell dimensions increase too much[63]. These problems have restricted the number of discovered porous solids with extra-large pores, of which cloverite, with a cell volume of ~125,000 $Å^3$ and pore diameters close to 30 Å is the largest.[64]

A recently developed a strategy to overcome these limitations based on the combination of targeted chemistry and computer simulations. Hybrid porous solids result from the three-dimensional covalent connection of inorganic clusters and organic moieties that act as linkers, and the first step in this approach is to control the nature of the inorganic cluster and the chemical conditions required for its formation and stability in solution.[65] In the second step involve the use computational strategies, typically the global optimization AASBU (automated assembly of secondary building units) method [66-68] as recently adapted to hybrids,[69] or other closely related methods.[70] The AASBU method explores how an inorganic cluster and an organic linker, or even predefined hybrid building blocks, may connect in three-dimensional space to form periodic lattices. A virtual library of candidate networks is produced, along with their crystallographic features (space group, cell parameters and atomic coordinates) and their simulated x-ray diffraction (XRD) patterns. The comparison of the simulated pattern of each candidate structure with the experimental one identifies the targeted experimental

structure, giving direct access to the structural solution without any recourse to single crystals. The final structure is refined with the Rietveld method from powder data, the guest species being localized from Fourier difference maps. While tackling the underlying issue of polymorphism of hybrid materials, this computational approach provides a direct-space tool for solving structures that may be highly complex.

On the one hand, structure determination may benefit from remarkable advances in the ways of exploiting the diffraction data using the recently developed charge flipping techniques[71,72] and microdiffraction technique[73] with the combination of other techniques such as electron microscopy[71,74] or radial distribution measurements[75]. On the other hand, structure predictions will benefit from the advances in quantum chemistry calculations in the exploration of polymorphism[76] and the understanding of structure–energy relationships. Such progress already extends the limits of the solids that were considered as tractable by both the structure prediction and structure determination areas.

1.5.4. Other techniques

Besides single-crystal and powder X-ray diffraction, other techniques like thermogravimetric analysis, elemental analysis, infrared (IR) spectroscopy, UV-VIS spectroscopy, absorption studies, magnetic susceptibility measurement, NMR technique etc are routinely used to characterize microporous materials. These methods provide useful information about structure and property of the material.

The network materials are routinely characterized by thermogravimetric analysis (TGA). Typically, the material is heated under a flow of air or oxygen or nitrogen and the mass loss occurring due to the stepwise decomposition of the various species present in the material is measured as a function of temperature.

The temperature range at which mass loss occurs and the amount of mass loss gives a quantitative estimation of the specific species present in the material, which can be used to verify the composition of the material, besides determining the thermal stability of the material. The product of calcination is characterized by powder X-ray diffraction technique.

IR spectroscopy provides informations about the functional groups present in the compound. Vibrations in the Far-IR region provide information about metal-ligand bonding. NMR spectroscopy is used extensively to obtain information on structural features of microporous materials. It has been used to determine the coordination environment of the network atoms. *In situ* NMR technique is used to study the reaction kinetics and mechanism of formation of microporous materials, the evolution of different phases etc.

Adsorption studies have been routinely used to determine the pore volume. Several probe molecules have been routinely employed for this purpose (e.g. O_2, N_2, CO_2, n-butane, alcohol, n-hexane, CH_4, H_2 etc). Generally adsorption of probe molecules within microporous materials results in type I adsorption isotherm. Adsorption studies also reveal information about the nature of the pore (hydrophobicity, hydrophillicity).

Magnetic susceptibility measurements provide useful information about the oxidation state of the metals and also about the distances and connectivity between the metal atoms in the network.

1.6. Magnetic properties

Magnetic properties of hybrid inorganic-organic compounds in which extended inorganic networks or local paramagnetic centers (mostly of transition

metal and lanthanide ions) are linked by diamagnetic linkers that can efficiently mediate magnetic exchange, has evoked considerable interest. The mode of linkage and the dimensionality of the inorganic sub network, along with the size, geometry, chemical functionality and various coordinating modes of the linkers, provide excellent means of controlling and modulating the magnetic properties in these solids. Synthesis, structural and magnetic features of hybrid Co and Ni carboxylates have been reviewed recently.[77]

Table 1.3 *Magnetic properties of representative inorganic-organic hybrid compounds*

a) Ferromagnetic (FM)

S.No	Formula	I^nO^m	Description of properties	Figure	Ref.
1	Glutarate $[Ni_{20}(H_2O)_8(C_5H_6O_4)_{20}\cdot 40H_2O]$	I^3O^0	$T_c \approx 4K$	1.4	[78]
2	1,4-cyclohexane dicarboxylate $[Co_5(OH)_8(CHDC)\cdot 4H_2O]$	I^2O^1	$T_c \approx 60K$	1.5	[79]
3	Succinate $[Ln_2(C_4H_4O_4)_3(H_2O)_2]\cdot 0.5H_2O$ Ln = Gd, Dy.	I^1O^2	Super exchange interaction	-	[80]
4	cyclohexane-1,3,5-tricarboxylate $[Ni_3(H_2O)_4(CTC)_2\cdot 5H_2O]$	I^1O^2	Dominant AFM interaction till 190K, FM-LRO at lower temp	-	[81]

b) Ferrimagnetic (FiM)

S.No	Formula	I^nO^m	Description of properties	Figure	Ref.
1	Succinate $[Co_5(OH)_2(C_4H_4O_4)_4]$	I^2O^1	$T_N \approx 10K$	1.6	[82]
2	Succinate $[Co_4(OH)_2(H_2O)_2(C_4H_4O_4)_3\cdot 2H_2O]$	I^2O^0	$T_N \approx 10K$	1(h)	[25]
3	Fumarate $[Ni_3(OH)_2(H_2O)_4(C_4H_2O_4)_2\cdot 2H_2O]$	I^1O^2	$T_N \approx 20K$	1.7	[83]
4	3,4-pyridinecarboxylate $[Mn_3(OH)_2(3,4\text{-pyda})2(H_2O)_2]$	I^1O^2	$T_N \approx 7K$	-	[84]

c) Metamagnetic (MM)

S.No	Formula	I^nO^m	Description of properties	Figure	Ref.
1	Terephthalate $[Co_2(OH)_2(1,4\text{-BDC})]$	I^2O^1	Intralayer FM And interlayer AFM ($T_N \approx 48K$)	1.8	[85]
2	Azide $[Cu_2(N_3)_4(L)]$, (L = 1,2-bis(tetrazol-1-yl)ethane, 1,4-bis-(tetrazol-1-yl)butane	I^2O^1	Short range FM and interlayer AFM	-	[86]
3	1,4-naphthalenedicarboxylate $[Co(C_{12}H_6O_4)]$	I^1O^2	$T_C \approx 5.5K$, Intrachain FM and interchain AFM	1.9	[87]

d) Canted antiferromagnetic (CAFM)

S.No	Formula	I^nO^m	Description of properties	Figure	Ref.
1	Terephthalate $[Co_2(OH)_2(1,4\text{-BDC})]$	I^2O^1	T < 45K	1.8	[85]
2	Terephthalate $V^{IV}{}_2O_2F_2\{O_2C\text{-}C_6H_4\text{-}CO_2\}$	I^2O^1	T < 20K	-	[88]
3	2,5-pyridinedicarboxylate $[Co_3(NC_5H_3(CO2)_2)(OH)_2(H_2O)_2]$	I^1O^2	T < 30K	1.10	[89]

e) Antiferromagnetic (AFM)

S.No	Formula	I^nO^m	Description of properties	Figure	Ref.
1	Succinate $[Co_6(OH)_2(C_4H_4O_4)5\cdot H_2O]$	I^2O^1	$T_N \approx 26K$	-	[90]
2	Ethylenediphosphonate $M^{II}{}_2(H_2O)_2(O_3P(CH_2)_2PO_3)$, M= Co and Ni	I^2O^1	$T_N \approx 7K$, M=Co $T_N \approx 13K$, M=Ni	1(i)	[26]
3	Terephthalate $V(OH)\{1,4\text{-BDC}\}.x(1,4\text{-}H_2BDC)$	I^1O^2	$T_N \approx 95K$	-	[91]
4	Terephthalate $Fe_2O\{O_2C\text{-}CH_3\}_2\{1,4\text{-BDC}\}.2CH_3OH$	I^1O^2	$T_N \approx 5K$	-	[92]

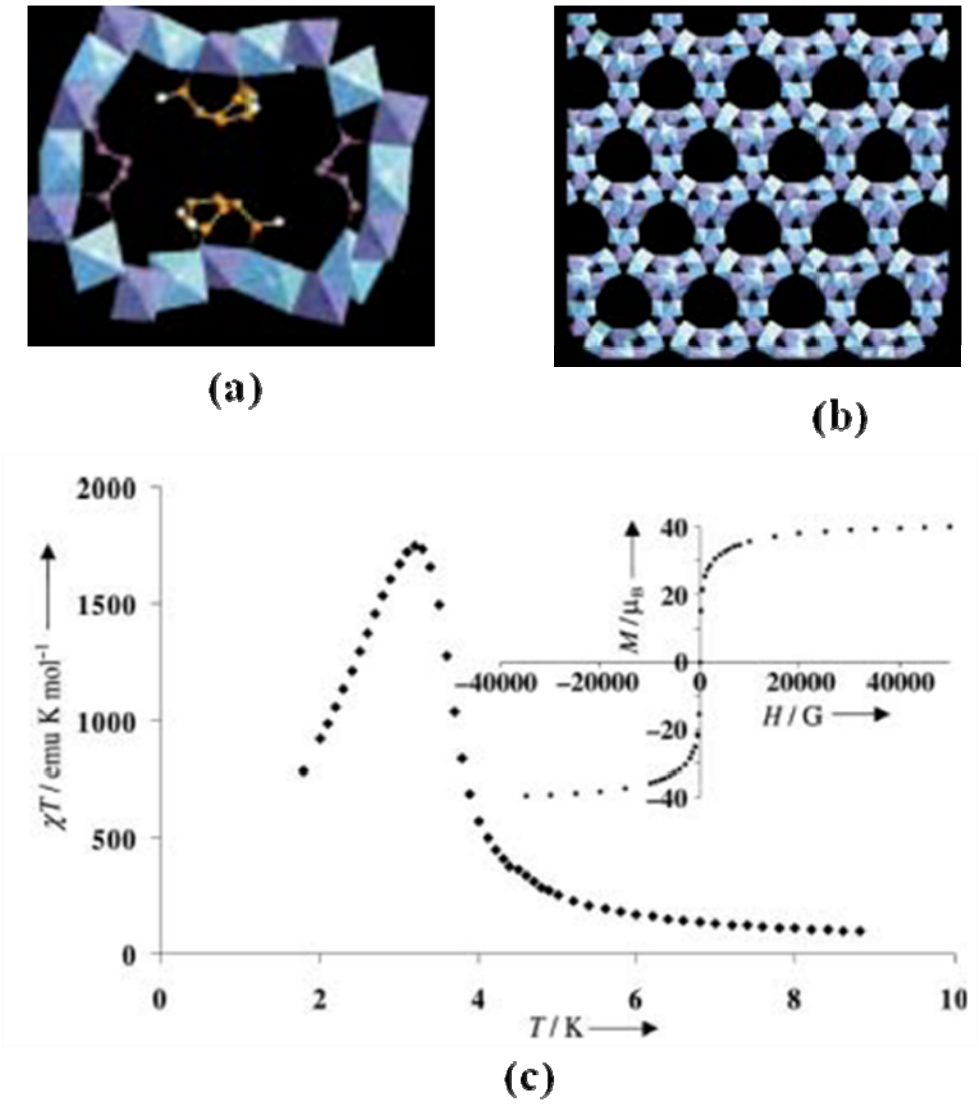

Fig. 1.4 (a) Polyhedral view of a corrugated 20-membered ring with two independent glutarate ions, (b) a view of the nickel oxide tunnels down [111] in 3D glutarate $[Ni_{20}(H_2O)_8(C_5H_6O_4)_{20}\cdot 40H_2O]$ and (c) thermal dependence of the χT product. The inset shows the magnetization versus the applied magnetic field at 2 K. Reproduced from Ref. 78.

A variety of magnetic properties have been found with hybrid materials. Of particular interest being those with ferromagnetic (FM) properties (Table 1.3). For example, a chiral three-dimensional nickel glutarate, $[Ni_{20}(H_2O)_8(C_5H_6O_4)_{20}\cdot 40H_2O]$ shows a pure cooperative ferromagnetic behavior (

$T_c \approx 4K$), without any spin frustration.[77,78] The $\boldsymbol{I^3O^0}$ type three-dimensional connectivity in this compound arises as the helices of edge-sharing octahedra connected to four parallel neighboring ones through a nickel octahedron. The oxide network is walled by two independent glutarate anions (Fig. 1.4). The low T_c value is due to the weakness of the ferromagnetic interaction for a Ni-O-Ni bridge angle significantly larger than 90^o.

A cobalt 1,4-cyclohexane dicarboxylate, $[Co_5(OH)_8(CHDC)\cdot 4H_2O]$, has a T_c of 60 K, a temperature that is among the highest observed in this class of compounds.[77,79] Its structure is based on metal–hydroxide octahedral–tetrahedral layers pillared by dicarboxylate ions ($\boldsymbol{I^2O^1}$ type). These layers are closely related to the brucite type but with one out of every four octahedra removed and replaced by two tetrahedra above and below the layer (Fig. 1. 5). Each tetrahedron shares three corners with octahedra and the cobalt coordination is completed by unidentate carboxylate groups of the CHDC pillars. A 3D network is thus formed that contains channels filled with water. The dehydration–rehydration process is reversible, thereby conferring to this hybrid some porous properties. Removal of the water molecules leads to a shift of the layers combined with a tilt and a rotation of the organic moieties and a shortening of the interlayer space of about 1 Å.

From *cis*,*cis*-cyclohexane-1,3,5-tricarboxylic acid (H_3CTC), three-dimensional hybrid compounds with both cobalt and nickel, $[M_3(H_2O)_4(trans\text{-}CTC)_2\cdot 5H_2O]$, have been synthesized.[77,81] The structure comprises a lozenge-shaped tunnel topology with inorganic chains connected by the organic moiety. The four oxide chains in this compound are all connected through two central tricarboxylates into a three dimensional structure. The chains are constructed by dimers of edge-sharing octahedra, connected through a third octahedron which

shares its *trans* vertices with two neighbouring dimers through a μ_2-OH_2. These compounds behave as short-range coupled low-dimensional chains with a tendency to ferrimagnetic alignment of the moments for the cobalt compound and ferromagnetic for the nickel compound.

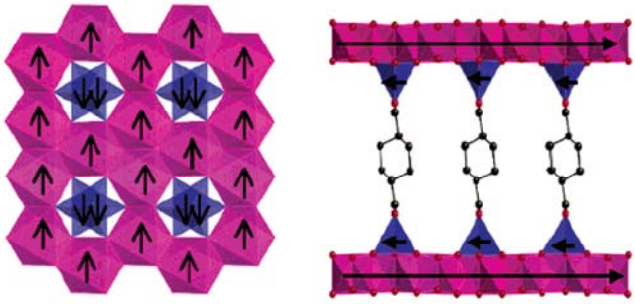

(a)

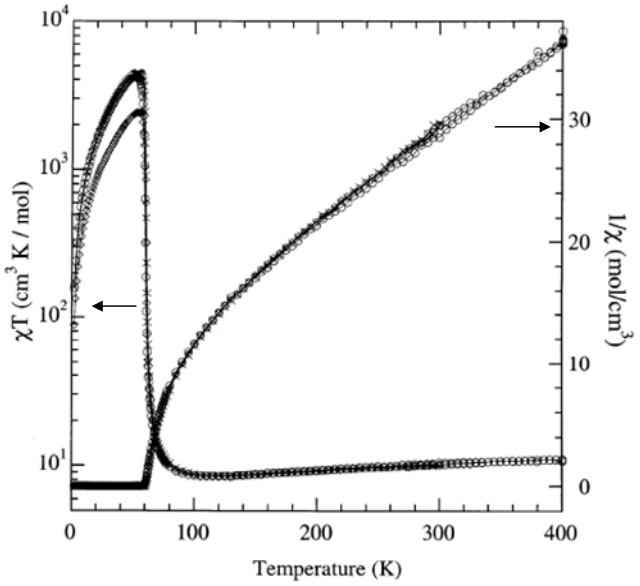

(b)

Fig. 1.5 (a) Diagrammatic representation of the proposed magnetic ordering at the tetrahedral and octahedral cobalt(II) sites in1,4-cyclohexane dicarboxylate, [Co5$(OH)_8$(1,4-CHDC)·$4H_2O$] and (b) temperature dependence of the inverse magnetic susceptibility and of the product of susceptibility and temperature: virgin (O), dehydrated (X) and rehydrated (♦). Reproduced from Ref. 78.

The cobalt succinate, [$Co_5(OH)_2(C_4H_4O_4)_4$], exhibiting ferrimagnetic interactions, is a two-dimensional metal oxide network pillared by the succinate moiety into a three-dimensional network[77,82] (***I²O¹***). It is constructed from zig-zag

layers of edge-sharing cobalt octahedra that generate pentamers of octahedra and 12-membered ring cavities (Fig. 1. 6). The succinate moieties act as bridges between the sheets. This compound exhibits ferrimagnetic behavior below 10K, which results from (i) antiferromagnetic couplings within the pentamers, (ii) ferromagnetic coupling between the pentamers to avoid the compensation of the moments, which implies a ferromagnetic interaction in agreement with the largest superexchange angles of the structure, and (iii) ferromagnetic coupling between the layers. According to Goodenough, d^7–d^7 superexchange 180° interactions are always antiferromagnetic, the 90° ones can be either antiferromagnetic (e_g–p–t_{2g}) or ferromagnetic (e_g–p_σ–p_σ–e_g). Another ferrimagnetic cobalt succinate, $[Co_4(OH)_2(H_2O)_2(C_4H_4O_4)_3 \cdot 2H_2O]$, of the type $\boldsymbol{I^2O^0}$, contains a two-dimensional Co-O-Co network with 14-membered ring windows and can be described as parallel "helicoidal" chains of octahedra connected by tetrameric units of co-planar octahedra through edge sharing. Succinate anions link the cobalt atoms within each layer.[25] The occluded and coordinated water can be removed from this compound in a reversible process. This compound is ferrimagnetic below 10 K due to antiferromagnetic coupling within the helicoidal chain and ferromagnetic coupling in the tetramer. It is well-known that in 90° superexchange interactions, small variations of the angle around the superexchange "blank angle" can invert the sign of the coupling constant (90-100°, depending on the nature of the 3d transition metal cation). Large superexchange angles lead to antiferromagnetic interactions while weaker ones induce ferromagnetic coupling. In this case, the blank angle is in the 98-99° range.

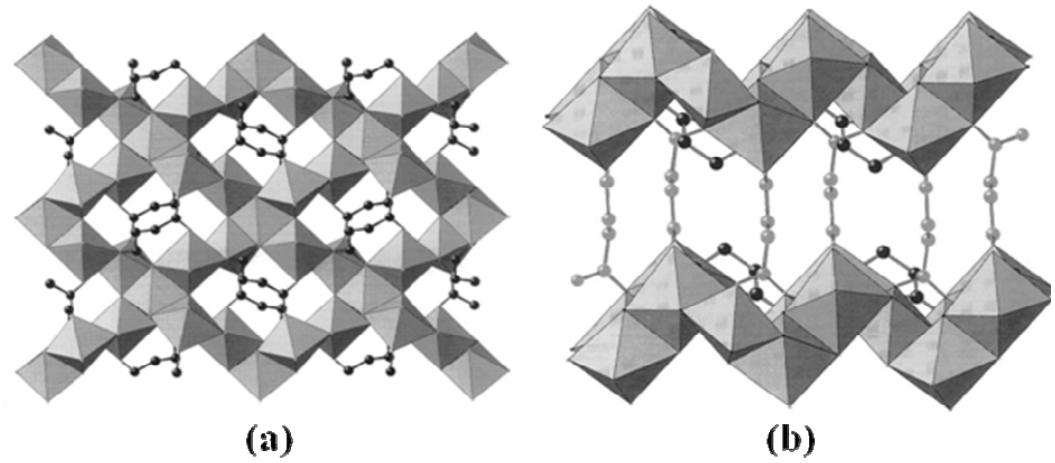

Fig. 1.6 (a) View of the 2-D inorganic layer in a 3-D cobalt succinate $[Co_5(OH)_2(C_4H_4O_4)_4]$ and (b) a view of the 3-D structure where 2-D layers are connected by succinate anions. Reproduced from Ref. 82.

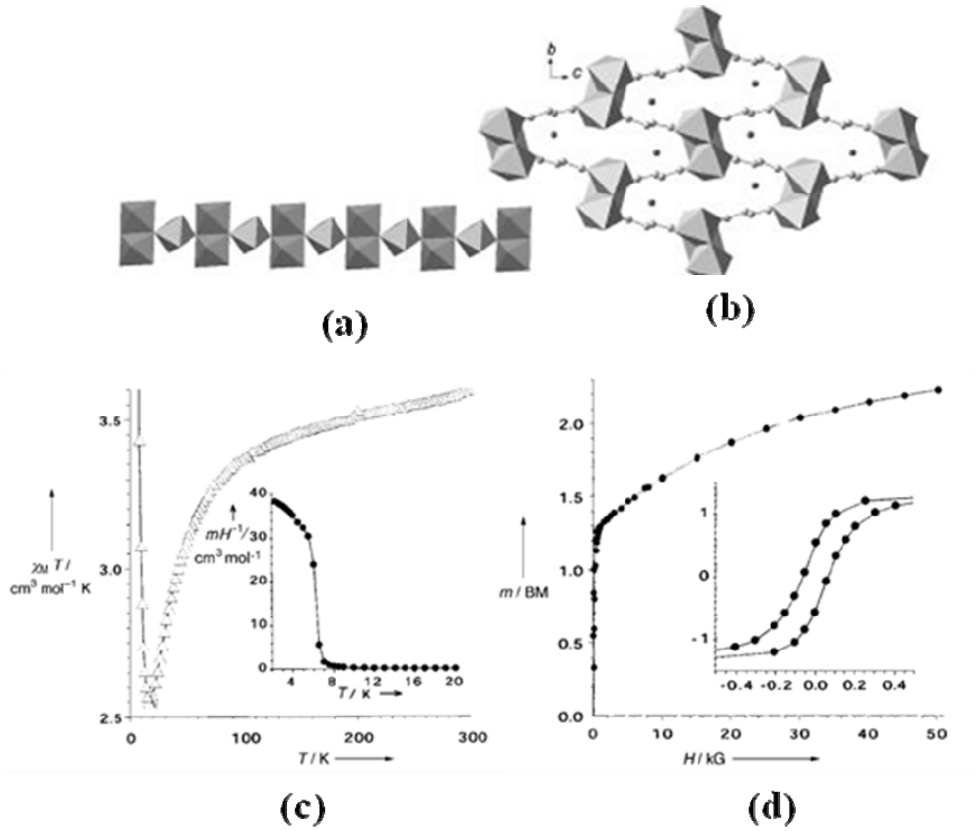

Fig. 1.7 (a) The 1-D Nickel oxide chain in 3-D fumarate, $[Ni_3(OH)_2(H_2O)_4(C_4H_2O_4)_2 \cdot 2H_2O]$, b) view of the 3-D structure where 1-D chains are connected by fumarate anions, (c) Plot of $\chi_M T$ versus T. Inset shows field-cooled magnetization curve (under an applied magnetic field H=100 G) showing ferromagnetic order at 6 K and (d) Magnetization curve at 2K. Reproduced from Ref. 77 and 83.

The nickel fumarate, $[Ni_3(OH)_2(H_2O)_4(C_4H_2O_4)_2 \cdot 2H_2O]$, consists of a metal oxide chain built from trimers consisting of two edge-sharing octahedra linked by a μ_3-OH to a vertex of a third one. The chains are connected by fumarate ions to form a 3D framework of the type $\boldsymbol{I^1O^2}$ (Fig. 1.7).[77,83] This compound behaves as a ferrimagnet, T<20 K, with a spontaneous magnetization below 6 K. A possible spin-orbit coupling along with a small spin frustration due to additional exchange pathways through fumarate ions explain the three-dimensional co-operative magnetization.

A three-dimensional cobalt terephthalate, $[Co_2(OH)_2(1,4\text{-BDC})]$, of the $\boldsymbol{I^2O^1}$ type is built up from inorganic layers where two types of parallel tilted chains of edge-sharing octahedra are linked by OH bridges.[77,85] The layers are then connected together through terephthalate linkers into a 3D architecture (Fig. 1. 8). Magnetic studies show that the intralayer exchange interaction between Co(II) ions is ferromagnetic, but the whole system orders antiferromagnetically at 48 K with a metamagnetic (MM) transition above a threshold field of 0.2 T. The existence of conjugated π electrons in the terephthalate bridges explains the antiferromagnetic interactions between the layers. Below 45 K, the compound exhibits canted antiferromagnetism associated with a non-collinear orientation of the moments between the layers. The magnetization loop shows a large coercive field of 5.9 T at 4.2 K, which must be related to extremely large single-ion anisotropy on the Co sites. The copper analogue of the above cobalt terephthalate, however, exhibits ferromagnetic coupling through the terephthalate bridge between the ferromagnetic sheets with in-plane interaction J = +5.5 K, probably due to Jahn-Teller effects.

A simple cobalt 1,4-naphthalenedicarboxylate, $[Co(C_{12}H_6O_4)]$, of the $\boldsymbol{I^1O^2}$ type consists of chains of metal octahedral connected by the organic moiety

into a 3D framework. The chain is zig-zag and constructed from edge-sharing cobalt octahedra (Fig. 1.9).[77,87] The compound exhibit metamagnetic behavior (T_C = 5.5 K) with strong ferromagnetic intra-chain interactions and antiferromagnetic inter-chain interactions.

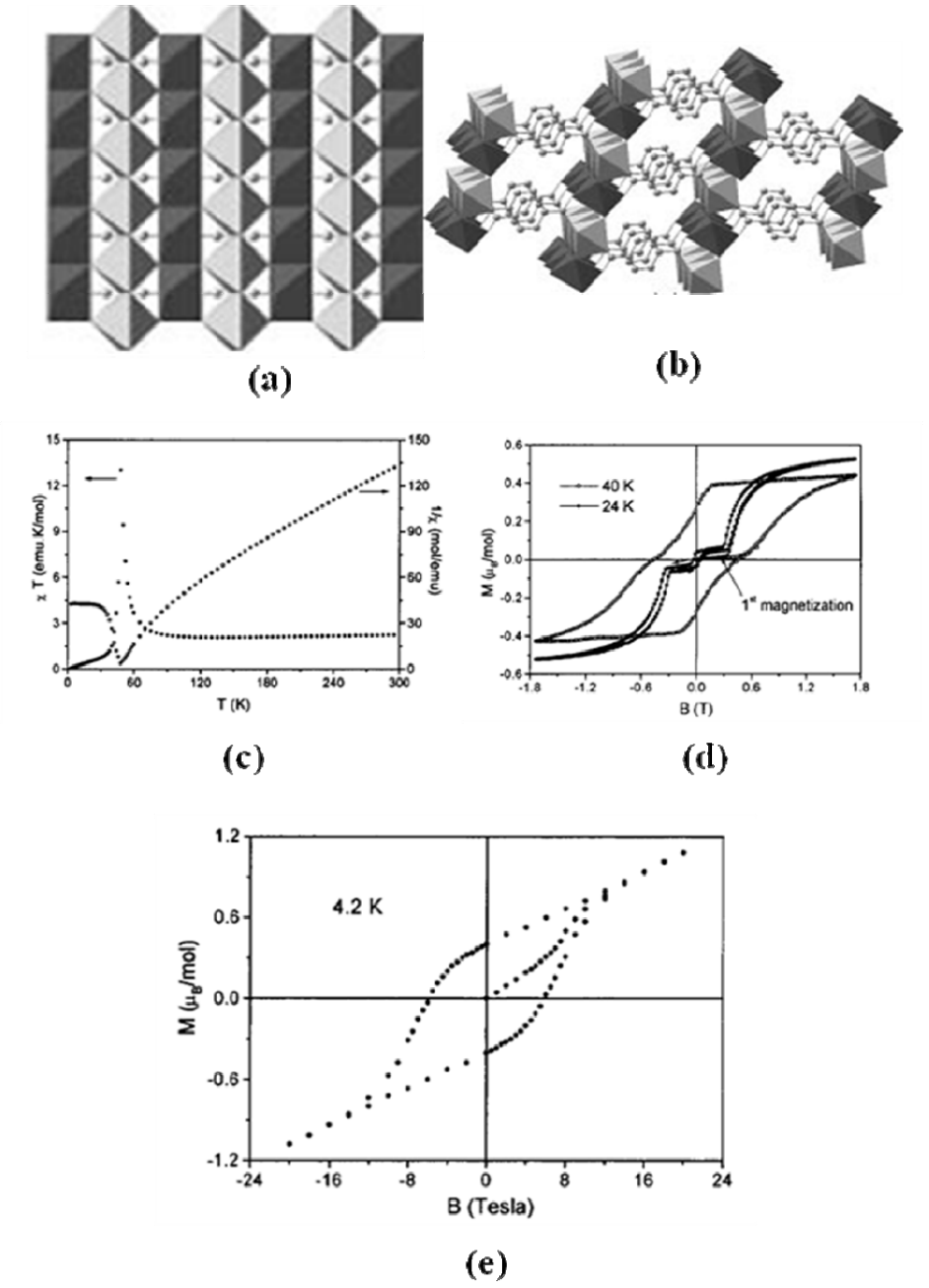

Fig. 1.8(a) View of the 2-D inorganic layer in a 3-D cobalt 1,4-benzenedicarboxylate [$Co_2(OH)_2$(1,4-BDC)], (b) view of the 3-D structure where 2-D layers are connected by 1,4-BDC anions, (c) temperature dependence of the static χ^{-1} and χT at 50 Oe, (d) Field-dependent magnetization at 40, 24 K and (e) High field magnetization up to 20 T for at 4.2 K. Reproduced from Ref. 77 and 85.

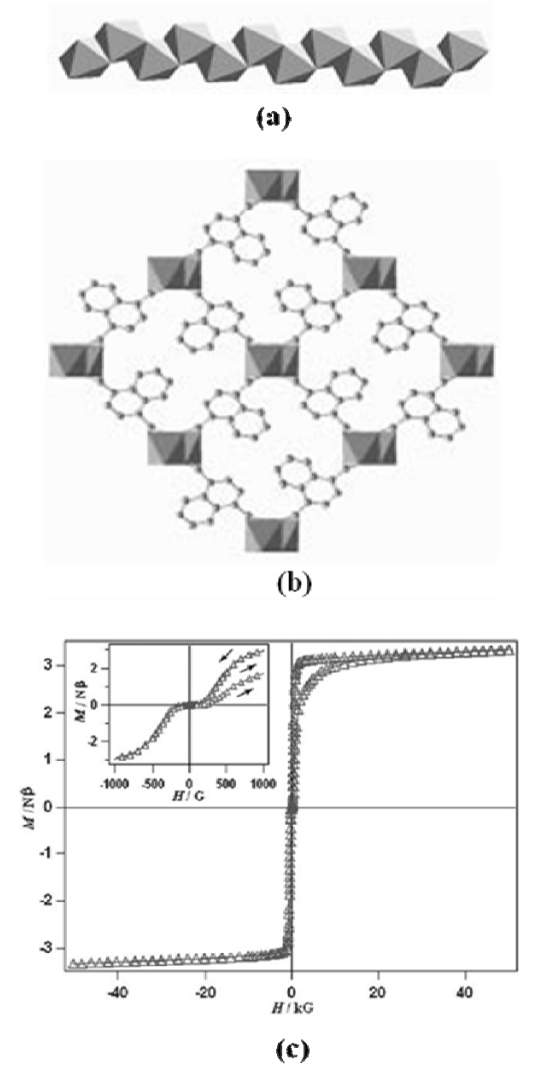

Fig. 1.9 (a) The 1-D cobalt oxide chain in 3-D 1,4-naphthalenedicarboxylate, [M(1,4-NDC)], M=Co, Mn, b) view of the 3-D structure where 1-D chains are connected by 1,4-NDC anions and (c) Magnetic hysteresis loop at 2 K (inset: details in a low field showing a sigmoidal curve corresponding metamagnetic behaviour). Reproduced from Ref. 77 and 87.

An interesting cobalt 2,5-pyridinecarboxylate, $[Co_3(NC_5H_3\{CO2\}_2)(OH)_2(H_2O)_2]$, with a three dimensional structure of the $\boldsymbol{I^1O^2}$ type consists of chains of CoO_x (X= 5 and 6) polyhedra with three different geometry.[89] These chains of hydroxide-bridged scalene triangles (not equilateral) that share edges and vertices, and are further connected by the ligand into a three-dimensional structure (Fig. 1.10).

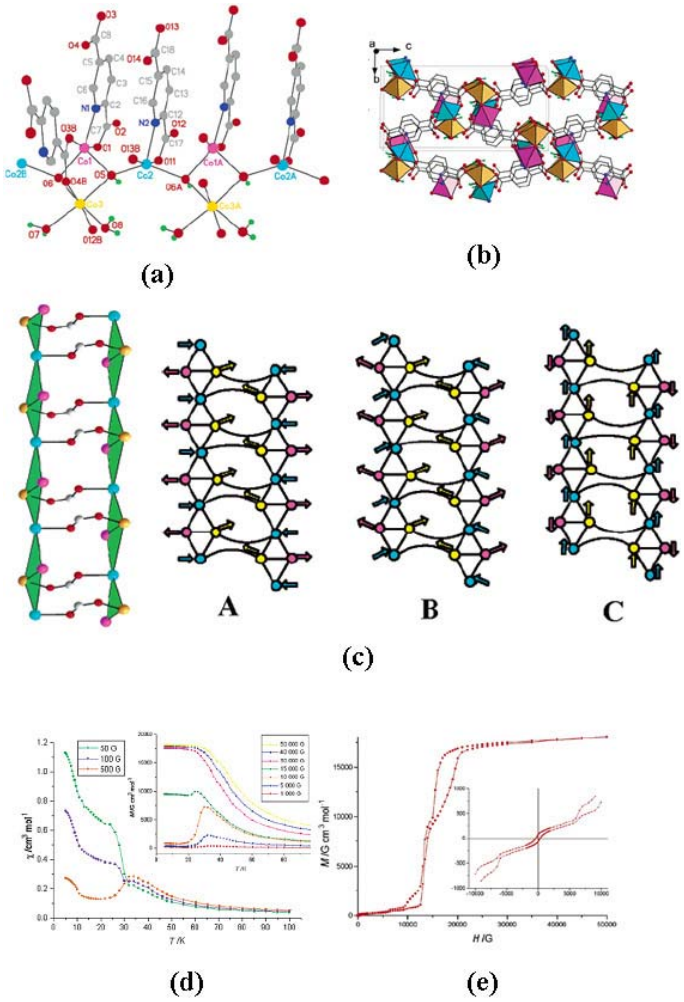

Fig. 1.10 (a) Crystal structure of cobalt 2,5-pyridinedicarboxylate, $[Co_3(NC_5H_3\{CO_2\}_2)(OH)_2(H_2O)_2]$ showing complete coordination environments of the three Co^{2+} ions, (b) view of the 3D structure, (c) parallel chains of edge- and vertex-sharing triangles with *syn-anti*-carboxylate bridges. Green triangles have μ3-hydroxide-O at their center (omitted) and suggested arrangement for the spins on the cobalt ions for (A) $H < 10\,000$ G, (B) $10\,000 < H < 15\,000$ G, and (C) $H > 15\,000$ G, (d) plot of χ versus T in small external applied fields, with magnetization data in larger applied external fields (inset) and (e) hysteresis loop for the partially aligned state recorded at 5.0 K, zero field region inset. Reproduced from Ref. 89.

In small fields below 30 K the susceptibility increases as the measuring field decreases, which is consistent with canted antiferromagnetism producing a small but significant coercive field of 200 G. Three different areas of bistability (A-less than 500G, B-5000 to 12000G and C-above 18000G) have been observed due to the field-induced reorientation of spins. The magnetization saturates at slightly more than 18000 G cm^3 mol^{-1} compared with 62077 G cm^3 mol^{-1}

calculated for ferromagnetic alignment, which suggests a spin structure in which 1/3 of the Co(II) ions are uncompensated (e.g., as shown in Fig.1.10C). Magnetic bistability may be observed in materials with ferromagnetic, ferrimagnetic, canted antiferromagnetic, or metamagnetic spin arrangements, but it is rare to observe more than one area of bistability in a single material. This behavior is ascribed to the competing superexchange and dipolar exchange pathways, the different *g* values associated with different coordination geometries, and the structural anisotropy of the material.

A large number of hybrid compounds with $\boldsymbol{I^1O^x}$ frameworks exhibit AFM interactions (Table 1.3e)[26,90-92], especially compounds of the type $\boldsymbol{I^1O^1}$ and $\boldsymbol{I^1O^2}$. Also compounds with $\boldsymbol{I^0}$ (zero inorganic connectivity- first column in Table 1.1) generally show AFM interactions. Compounds with FM interactions are of greater interest, but good examples of hybrid compounds with strong FM interactions are yet to be discovered. Such compounds, especially if they are nanoporous, would be valuable since they might be able to separate nitrogen and oxygen making use of paramagnetism of molecular oxygen. Hybrid frameworks with homo or hetero-metalic clusters linked by various types of organic connectors would be of interest as model compounds to understand low-dimensional magnetism and frustrated magnetic systems.

Several transition metal compounds possessing the Kagome structure wherein hexagonal bronze type inorganic layers are templated by organic amines have been synthesized and characterized in the last few years.[93,94] An example of the amine templated metal sulfate is shown in (Fig. 1.11). One would expect all Kagome compounds to exhibit magnetic frustration, characteristic of a triangular lattice[95]. Kagome compounds containing Mn^{2+}, Co^{2+}, Fe^{2+}, Fe^{3+} and Ni^{2+} exhibit

different magnetic properties as shown in Table 1.4. We readily see that Kagome compounds comprising transition metal ions with non-integral spins such as Mn^{2+}, Co^{2+} and Fe^{3+} exhibit magnetic frustration or low-temperature antiferromagnetism. Magnetic frustration is minimized in compounds containing transition metal ions with integral spins such as Ni^{2+} and Fe^{2+}. Furthermore they also show evidence for ferromagnetic interactions. Theoretical investigations suggest that the spin magnitude of the transition metal ion plays a crucial role in determining the magnetic frustration and related properties of the Kagome compounds.[96]

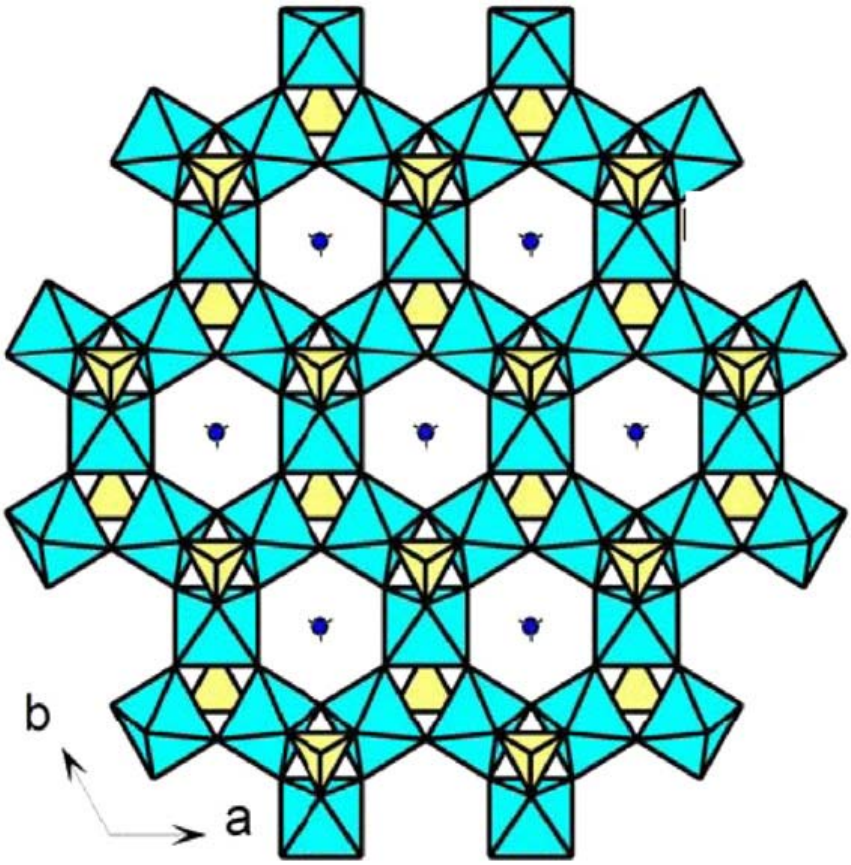

Fig. 1.11 View of the Kagome layer in amine templated $\{[C_6N_2H_8][NH_4]_2[Ni_3F_6(SO_4)_2]\}$. . Reproduced from Ref. 93.

Table 1.4 ***Magnetic properties of organically templated Kagome compounds***

TM ion	Spin (S)	Magnetic properties
Mn^{2+}	5/2	AFM interaction
Fe^{3+}	5/2	Magnetic frustration and AFM interaction
Co^{2+}	3/2	Magnetic frustration and AFM ordering
Fe^{2+}	2	Ferromagnetic interaction
Ni^{2+}	1	Canted AFM interaction

Clearly, the magnetic properties of hybrid materials offer much scope for further investigations. Some of the challenges would be to synthesize high T_c ferromagnets, ferromagnets with channels and those showing magnetoresistance.

1.7. Optical properties

Table 1.5 ***Optical properties of representative inorganic-organic hybrid Compounds***
Photoluminescence (PL)

S.No	Formula	I^nO^m	Origin of PL	Figure	Ref.
1	Phthalate $[Cd(1,2\text{-}BDC)(H_2O)]$	I^2O^0	π–π* intraligand fluorescence	-	[97]
2	Oxalate $[Cd_2(C_2O_4)(OH)_2]$	I^2O^1	π* → n intraligand transition and LMCT	1.12	[98]
3	Glutarate $[Gd_{1-x}Er_x\ (glu)].4H_2O$	I^1O^2	ligand-sensitized metal-centered emission (FRET)	-	[100]
4	Terephthalate $Ln_3(BDC_{3.5})(OH)_2(H_2O)_2]\cdot H_2O$, Ln = Y:Er-Yb	I^0O^3	FRET and upconversion	-	[103]

Optical properties of hybrid network materials are of interest partly because of their greater stability compared with molecular materials, since adequate thermal, chemical and optical stability is a pre-requisite for commercial

applications. Porous, chiral and magnetic hybrids exhibiting photo- and electro-luminescence (Table 5) and non-linear optical activity have evoked interest.

1.7.1. Photoluminescence

Many hybrid networks that exhibit photoluminescence (PL) do so as a result of intra-ligand transitions or charge transfer [metal to ligand (MLCT) or ligand to metal (LMCT)] excitations. Another important source is metal-centered PL, especially with hybrids containing rare-earth ions. Ligand-centered emissions may be significantly enhanced due to the rigidity of the network, which reduces energy losses due to radiationless decay (σ–σ^* or π–π^*) compared to free molecules. The lifetime of the emission can be tuned by introducing heavy metals like lead with increased spin-orbit coupling, thereby reducing the radiative lifetime of triplets resulting in room temperature phosphorescence. A range of examples are given in Table 1.5.

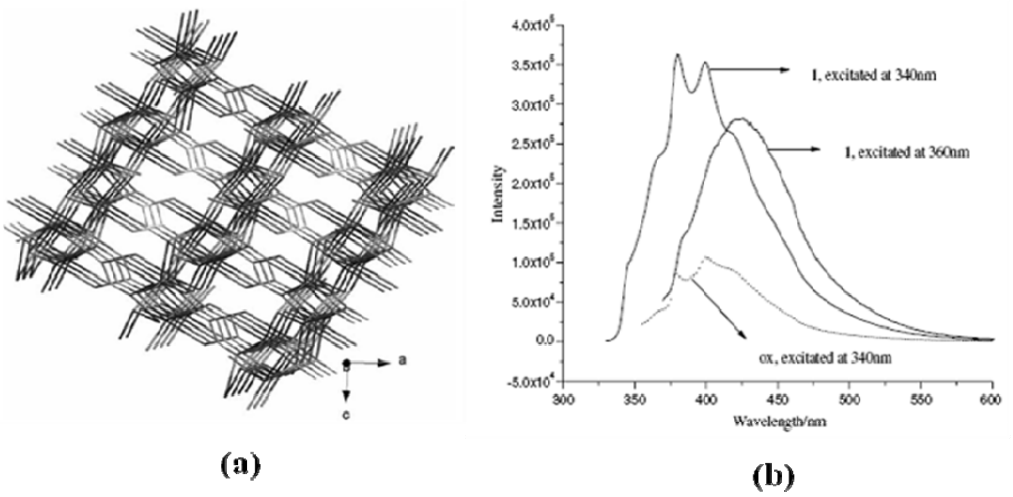

Fig. 1.12 (a) View of the 3-D structure of a cadmium oxalate, $[Cd_2(C_2O_4)(OH)_2]$ and (b) fluorescence emission spectra at room temperature for oxalic acid and the compound. Reproduced from Ref.98.

The two-dimensional cadmium phthalate, [Cd(1,2-BDC)(H_2O)], of the type I^2O^0, exhibits strong fluorescent emission in the solid state at room temperature. The structure consists of a honeycomb inorganic Cd-O-Cd layer with edge and

corner shared (CdO_7) pentagonal bipyramids. The short π–π* luminescence [λ_{max} = 407 nm, τ = 0.021 ms] was assigned to intra-ligand fluorescent emission.[97] A three dimensional cadmium oxalate, $[Cd_2(C_2O_4)(OH)_2]$, of the type $\boldsymbol{I^2O^1}$, with infinite cadmium hydroxide corrugated layers connected through oxalate units, exhibits strong fluorescent emission bands in the solid state at room temperature at 380 and 400 nm (λ_{ex} = 340 nm). These are attributed to a π* → n intra-ligand transition (Fig. 1.12).[98] It also exhibits another strong emission at 432 nm (λex = 360 nm), which was assigned to ligand-to-metal charge transfer (LMCT).

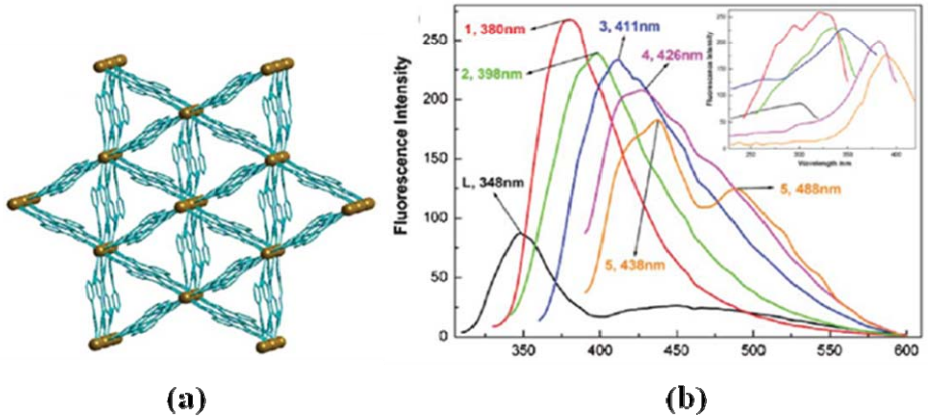

Fig. 1.13 (a) View of the 3-D structure $[Cd_3L_6](BF_4)_2$-$(SiF_6)(OH)_2 \cdot 13.5H_2O$, L = 2,6-di-(4-triazolyl)pyridine), without the guest water molecules and anions and (b) luminescence emission spectra at room temperature for ligand (black) and the compound at various degrees of hydration and dehydration (inset shows excitation spectra).

A three-dimensional porous, $[Cd_3L_6](BF_4)_2$-$(SiF_6)(OH)_2 \cdot 13.5H_2O$, where L = 2,6-di-(4-triazolyl)pyridine), exhibits tunable emission between UV and visible wavelengths (Fig. 1.13).[99] The compound and a series of its dehydrated derivatives display intense luminescence with emission maxima ranging from the UV (380 nm- intraligand fluorescence) to the visible region (438 nm- LMCT). With rehydration, the fluorescent emissions shift back from visible light (438 nm) to the UV region (382 nm). This phenomenon was attributed to weak interactions of the solvent molecules, which not only stabilize the supramolecular structures but also

absorb the UV light, preventing the transfer of energy effectively from the ligand to the metal centre.

Luminescence from rare earth (RE) based hybrid compounds occurs mainly due to two important processes: a) emission from the rare earth ion due to direct photo excitation in the rare earth ion b) emission from the rare earth ion due to the fluorescence resonance energy transfer (FRET) from the ligand to the metal centre (antenna effect). The efficiency of the emission depends on the rare earth and the degree of the FRET, i.e. energy level comparison between ligand and rare earth. Early work on a very open rare-earth glutarate, $[Gd_{1-x}Er_x\ (glu)].4H_2O$, with an $\boldsymbol{I^1O^2}$ architecture similar to that shown in Fig. 1.9 illustrated the potential of this area.[100] The as-synthesized material has water molecules in the channels between the chains, but they can be removed reversibly. It has been shown that the photoluminescent lifetime of the Eu^{3+}-dopant depends upon the degree of dehydration because the coordinating water molecules act as relaxation agents. Such materials clearly have the potential to be used as sensors. In another example, the 3-D pyridine-2,5-dicarboxylate, $[Ln_3(OH)_4(2,5\text{-}pydc)(2,5\text{-}Hpydc)_3(H_2O)_4]$ (Ln = Dy, Eu) exhibits characteristic emission corresponding to the RE ion. The structure consists of helical dodecahedral chains connected as in a (3,4) net with $\boldsymbol{I^3}$ Ln-O-Ln connectivity.[101]

A neodymium 1,4-naphthalenedicarboxylate, $[Nd_2(NDC)_3(DMF)_4]\cdot H_2O$, (DMF = N,N-dimethylformamide), where dinuclear of tricapped trigonal prism are connected into a layered structure by the dicarboxylate ligands, exhibits both PL and up-conversion properties.[102] Under excitation of 488 nm, the compound displays a strong emission band at 1059 nm ($^4F_{3/2} \rightarrow {}^4I_{11/2}$), an emission band at 893 nm ($^4F_{3/2} \rightarrow {}^4I_{9/2}$) with a much lower intensity, and a weak band at 1333 nm

($^4F_{3/2} \rightarrow {}^4I_{13/2}$). A weak UV up-conversion emission at about 391.6 nm and a much stronger blue emission at about 449.5 nm show up upon pulse laser excitation at 580 nm. The intense absorption at 580 nm corresponds to the $^4I_{9/2} \rightarrow {}^4G_{5/2}$ transition, which is a hypersensitive band, satisfying the selection rules of $\Delta J = \pm 2$, $\Delta L = \pm 2$ and $\Delta S = 0$.

1.7.2. Electroluminescence

Semiconducting luminescent materials would have a filled valence band and an empty conduction band. When an appropriate alternating current (ac) is applied between the two electrodes of a device containing such a material, electron-hole pairs are generated with the possibility of recombination to give emitted light (electroluminescence, EL). The requirements for good EL performance are the ability to transport electrons and holes, and high luminescence efficiency. Hybrid materials, such as semiconducting nanoparticles within a organic polymer matrix or coordination complexes such as $[Ru(bpy)_3]^{2+}$ have been used in EL devices. Strong EL at a low driving voltage was first reported by Tang and Van Slyke in 1987. Thus, the coordination compound, tris(8-hydroxyquinoline)aluminum (Alq_3) has played an important role in light-emitting diodes and has been studied extensively.[104] Tunable emission colors have been obtained by doping other electroluminescent materials into Alq_3, by introducing different substituents into the quinolinolate ligands, or by embedding Alq_3 into mesoporous materials[105].

The use of hybrid inorganic-organic networks in EL is relatively new and is receiving attention as materials capable of yielding efficient electroluminescent devices. The well known three dimensional Zn_4O(dicarboxylate) ($\boldsymbol{I^0O^3}$ type), also called MOFs, comprise Zn_4O_{13} units linked by various dicarboxylate ligands. In

view of the structural similarities between the zinc clusters in the nodes and semiconductor zinc oxide quantum dots (doped and undoped semiconducting zinc compounds), the MOFs might be expected to exhibit interesting optoelectronic properties. An EL device was made by spreading a uniform film of as-synthesized MOF-5 (zinc 1,4-benzenedicarboxylate) as a wet paste with DMF onto a transparent conductive ITO electrode. From this device, EL emission at about 565 nm was obtained, which is very close to the value of 540 nm found for the corresponding photoluminescence emission maximum. The λ_{EL}(max) obtained for MOF-5 is also very close to the value of 555 nm, which is the wavelength of maximum sensibility of the human eye. By applying an alternating current of 60 V and 180 Hz, a light intensity of 0.4 cd m^{-2} was obtained, which approximately corresponds to an electricity-to-light efficiency conversion of about two lumens $watt^{-1}$. MOF-5 also can be an active component in photovoltaic cells. Similarly, the porosity of MOF networks and the possibility of designing them with suitable organic components offer opportunities to have materials with high EL efficiency.[106]

1.7.3. Non-linear optical properties

The availability of novel methods to generate the required asymmetry (both structural as well as electronic asymmetry) in hybrid inorganic-organic compounds, along with their thermal stability and optical transparency, render them to be candidates as non-linear optical (NLO) materials. Structural asymmetry can be easily generated in hybrid networks by using acentric or chiral centers (asymmetric linkers, nodes, polar H-bonds, head-to-tail alignment of dipolar guests confined in channels etc.) to create structures with polar or chiral space groups. The use of polarizable ligands and metals with efficient donor-acceptor charge

transfer (LMCT or MLCT), or "hard" and "soft" ligands trans to one another at the metal center, can ensure electronic asymmetry. Some hybrid materials with NLO properties have been reported (Table 1.6).

Table 1.6 ***NLO properties of representative inorganic-organic hybrid Compounds***

S.No	Formula	I^nO^m	Type of NLO	Figure	Ref.
1	$[ZnCl_2(HQA)]\cdot 2.5H_2O$, (HQA = 6-methoxyl-(8S,9R)-cinchonan-9-ol-3-carboxylic acid)	I^0O^1	SHG	1.14	[109]
2	Oxalate-glutarate $Nd_4(H_2O)_2(OOC(CH_2)_3COO)_4(C_2O_4)_2]$	I^1O^2	SHG	-	[110]
3	$[Zn(CN_4\text{-}C_6H_4\text{-}C_{12}H_7N\text{-}C_5H_4N)_2]\cdot 1.5H_2O$	I^0O^3	SHG	1.15	[112]
4	β-ferrocenylacrylates, $[Pb(OOCCH=CHFc)_2(phen)]$ and $[Cd(OOCCH=CHFc)_2(H_2O)_2]\cdot(H_2O)_4$	I^0O^3	THG and self-focusing behavior	-	[113]
5	(2,6-dicarboxy-4-hydroxypyridine), $[Zn(C_7H_3O_5N)]\cdot H_2O$	I^0O^2	THG and self-focusing behavior	-	[114]

Ward and Lin[107,108] are perhaps the first to develop strategies to engineer non-centrosymmetric networks for use as nonlinear optical materials. Here we focus on some recent examples. A powdered sample of one-dimensional $[ZnCl_2(HQA)]\cdot 2.5H_2O$, (HQA = 6-methoxyl-(8S,9R)-cinchonan-9-ol-3-carboxylic acid) shows a strong SHG response of ca. 20 times larger than that for KDP (KH_2PO_4). Each ligand acts as a bidentate spacer through the nitrogen and carboxylic acid group that links two Zn centers and leads to the formation of a 1-D coordination polymer. The compound crystallizes in a chiral space group (*P*1), which belongs to polar point group (*C*1). Such a strong SHG response was attributed to the presence of intramolecular charge separation due to a zwitterionic moiety generating a large dipole moment ($\mu = qd$, where q is charge and d is

distance) (Fig. 1.14). A good donor-acceptor chromophore in the ligand was also an essential factor for the observed nonlinear optical behavior.[109]

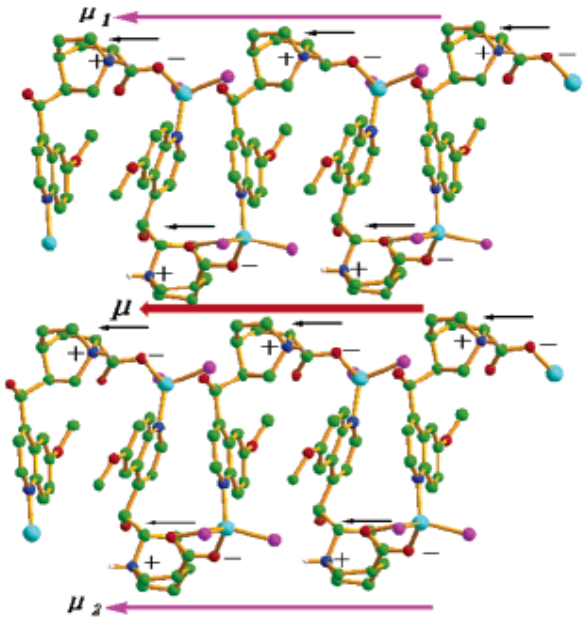

Fig. 1.14 Perspective view of two chains along the *a* axis with the dipolar moment direction in 1-D $[ZnCl_2(HQA)]\cdot 2.5H_2O$, (HQA = 6-methoxyl-(8S,9R)-cinchonan-9-ol-3-carboxylic acid). The red arrow is the total dipolar moment (***μ***), while the purple arrows are the chain dipolar moments ***μ***1 and ***μ***2. From ref. 109.

A three-dimensional mixed oxalate-glutarate of neodymium, $Nd_4(H_2O)_2(OOC(CH_2)_3COO)_4(C_2O_4)_2]$, comprising a helical column formed by grafting the oxalate unit onto helical NdO_9 chains, cross-linked by the glutarate anions[110], exhibits a frequency-doubled green beam at 532 nm on excitation with a Nd-YAG laser emitting at 1.06 μm. A powdered sample with the homochiral space group $P2_1$ shows about 11 times the SHG activity of KDP. A three-dimensional zinc compound of β-dehydroamino acid, $[Zn\{(E)\text{-}3\text{-}C_5H_4N\text{-}C(NH_2)=CH\text{-}COO\}]ClO_4$, obtained from the low-symmetry, racemic 3-pyridyl-3-aminopropionic acid[111] crystallizes in a chiral space group ($P2_12_12_1$) and shows a strong SHG response. The presence of the amino group, which is considered to be

a good donor, may be expected to enhance the electronic asymmetry (pull-push effect) and advantageous for nonlinear optical behavior.

Two three-dimensional diamond-like networks, $(CN_4\text{-}C_6H_5)_2Zn$ and $(NH_2\text{-}C_5H_3N\text{-}CN_4)_2Zn$ and one two-dimensional square grid network, $[(CN_4\text{-}C_6H_4\text{-}C_{12}H_7N\text{-}C_5H_4N)_2\text{-}Zn]\cdot 1.5H_2O$ were crystallized in the non-centrosymmetric space groups *I*-42*d* and *Fdd*2, respectively. The ligands involve a non-center A-D (acceptor-donor) system, a one-center A-D system, and a two-center A-D system, respectively, in those three compounds (Fig. 1.15)[112]. All three compounds display strong second harmonic generation (SHG) responses. Among the three complexes, the third one shows the largest SHG effect, which is about 50 and 500 times those of urea and KDP (KH_2PO_4), respectively. The two-center A-D system (multicenter push-pull electronic effect) may be responsible for it having the largest SHG effect.

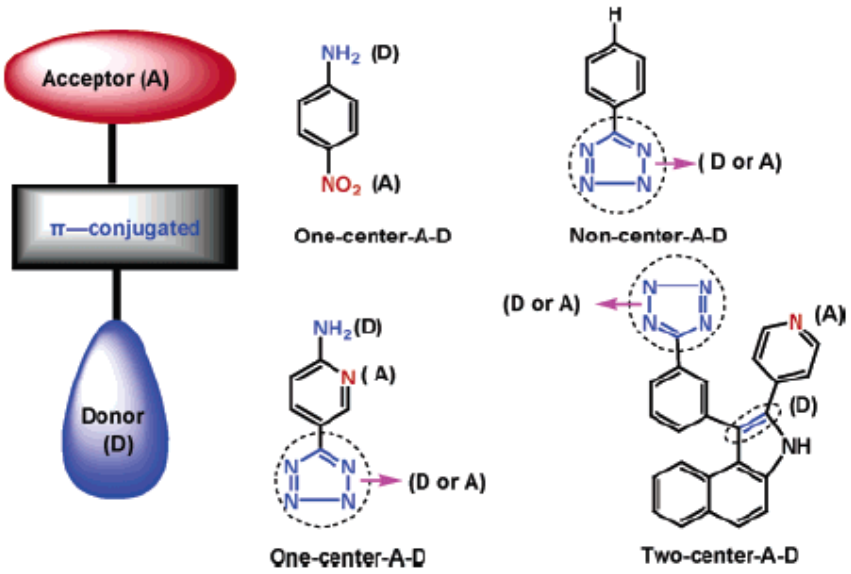

Fig. 1.15 Different types of donor-acceptor systems in various ligands. Ref. 112.

The one dimensional *β*-ferrocenylacrylates, $[Pb(OOCCH{=}CHFc)_2(phen)]$ and $[Cd(OOCCH{=}CHFc)_2(H_2O)_2]\cdot(H_2O)_4$ show third-order NLO properties. Both

the chain structures possess infinite one-dimensional M-O-M linkages. The compounds have the same positive sign for the refractive nonlinearity, which gives rise to self-focusing behavior.[113] Their hyperpolarizability (γ) values are calculated to be 5.19×10^{-30} and 1.57×10^{-29} esu for the lead and cadmium compounds, respectively. The γ value of the Cd compound is slightly larger than the Pb compound, which indicates that the metal ions play an important role in the NLO properties of these materials.

A two-dimensional zinc compound of chelidamic acid (2,6-dicarboxy-4-hydroxypyridine), $[Zn(C_7H_3O_5N)]\cdot H_2O$, shows large static third-order polarizability and the convergence value of γ_{xxxx} reaches 6.86 $\times10^{-33}$ esu in the case of zero input photon energy; is about three orders of magnitude greater than those of typical organic materials ($\times10^{-36}$ esu). The third-order, non-linear refractive index value (n2) was calculated to be 4.15×10^{-11} esu. The structure consists of anticlockwise windmill-like connectivity of metal and ligand with spiroconjugation and an infinitely delocalized π-bond systems over the molecular layer.[114]

Besides hybrid phosphors, designing materials with other interesting optical properties, specially non-linear properties would be of value. Just like one uses mixture of inorganic phosphors or polymer-inorganic composites, it should be possible to design hybrids with optical emission properties for potential applications.

1.8 Electronic properties

Tuning the electronic band structure and thereby controlling the electron-transport properties in hybrid network compounds has attracted attention because

of the availability of various methods for tuning the structure and porosity by a proper selection of donor and acceptor moieties.

The cadmium formate-4,4'-biphenyldicarboxylate, $[Cd_{11}(HCOO)_6(bpdc)_9]\cdot 9DMF\cdot 6H_2O$), has a rare *bcu* topology (***I*^{0}*O*^{3}** type) in which undecanuclear cadmium clusters are connected by the bpdc units into a three-dimensional structure with large pores. It shows good sorption, optical and semiconducting properties.[115] Photovoltaic (PV) transients can be used to characterize semiconductor materials, and a PV signal will arise whenever light-induced excess charge carriers are separated in space. PV transients at different intensities of the exciting laser pulse (355 nm) were measured (Fig. 1.16) and clearly exhibit a time lag caused by the slow and independent diffusion of excess electrons and holes. The times of the PV maxima are similar ($t \approx 0.013$ s) with the different exciting laser pulses (0.05, 0.10, 0.20, and 0.30 mJ). These maxima are related to the separation of charge at the hybrid-indium tin oxide (ITO) interface, and the gradient of excess electron and hole concentrations is caused by the nonhomogeneous absorption of light with photons with *hv* larger than the optical bandgap (E_g). The PV transient signals are positive, which indicates that the photo excited electrons move faster than holes towards the interface. The maxima of the transients are linearly enhanced when the intensity of the pulse is increased from 0.05 to 0.30 mJ. This observation implies that this compound possesses the characteristics of a diffusion PV transient, but not of a Dember PV transient, which is similar to the case for nanosized metal oxide semiconductors. As mentioned earlier, MOF-5, a terephthalate with quantum dot like Zn_4O_{13} units, also exhibits semiconducting properties, including photocatalysis with reverse shape-selectivity, solar photovoltaic and electroluminescence properties.[106]

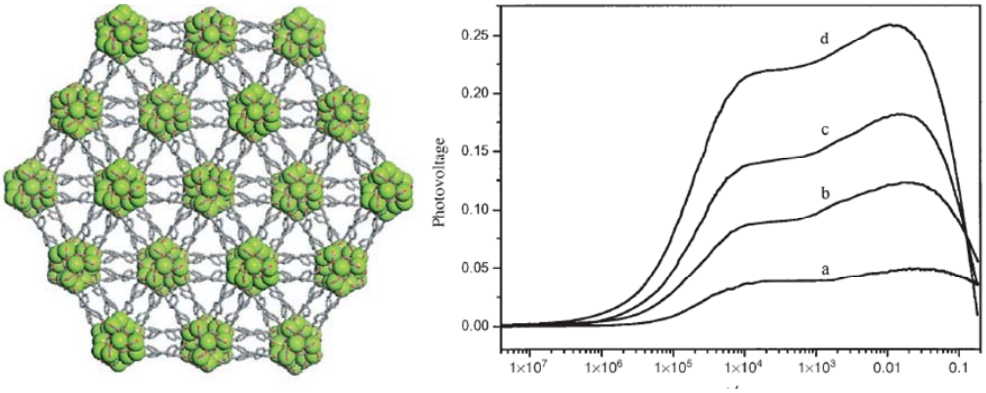

(a) **(b)**

Fig. 1.16 (a) View of a rare *bcu* topology in 3-D cadmium formate-4,4'-biphenyldicarboxylate, $[Cd_{11}(HCOO)_6(bpdc)_9]\cdot 9DMF\cdot 6H_2O)$ along the [001] direction and (b) PV transients upon illumination by a 355-nm pulse laser at intensities of a- 0.05, b- 0.10, c- 0.20, and d- 0.30 mJ. From ref. 115.

A three-dimensional compound, $Cu(DCNQI)_2$, (DCNQI=N,N'-dicyano quinodiimine) formed by the linkages between Cu ion donors and organic DCNQI acceptors exhibit an interesting metal–insulator (M–I) transition under high pressure.[116] This behavior is due to the interaction between the localized 3d-electron bands of the Cu ions and the p-electron conductive bands of DCNQI. Another one-dimensional ribbon, copper-5,6,11,12-tetraazanaphthacene, [Cu^I(TANC)], with alternative metal and ligand shows a high conductivity of 50 Scm^{-1} along the *a* axis at 300 K, but the conductivity sinks rapidly[117] with decreasing temperature, reaching to 10^{-6} Scm^{-1} at 10 K. This behavior indicates semiconducting behavior at ambient pressure. Calculations based on the tight-binding approximation yield a 1D energy band and an open Fermi surface. The temperature dependence of the resistivity can be well fitted by the variable-range-hopping (VRH) formula. Application of pressure up to 6.5 GPa increases the purity of the one-dimensionality and the strength of the random potential.

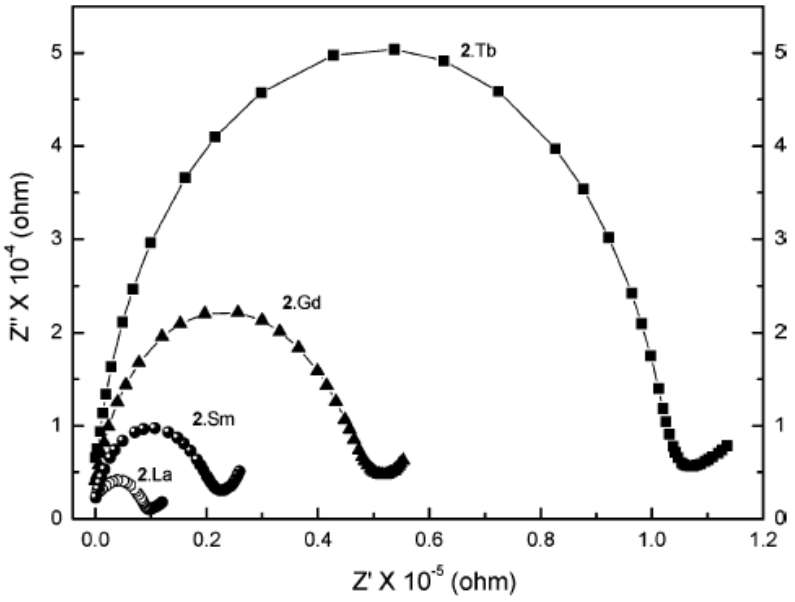

Fig. 1.17 Impendence spectroscopy measurements of the electrical resistance of $[Ln_6Cu_{24}(OH)_{30}(Ala)_{12}(Ac)_6(ClO_4)(H_2O)_{12}]\cdot(ClO_4)10\cdot(OH)_7\cdot(H_2O)_{34}$, at room temperature. From Ref. 118.

Impedance spectroscopic measurements on a series of novel 3d-4f heterometallic Ln_6Cu_{24} clusters $[Ln_6Cu_{24}(OH)_{30}(Ala)_{12}(Ac)_6(ClO_4)(H_2O)_{12}]\cdot(ClO_4)10\cdot(OH)_7\cdot(H_2O)_{34}$, (Ln = Tb, Gd, Sm, and La) with L-alanine as the ligand reveal that they are ionic conductors (Fig. 1.17).[118] The metal skeleton of the cluster may be described as a Ln_6Cu_{12} octahedron (constructed with six Ln^{III} ions located at the vertices and 12 inner Cu^{II} ions located at the midpoints of the edges) connected by 12 additional Cu^{II} ions (every two are connected to one Ln^{III} vertex). Conductivity measurements showed typical behavior of an ionic conductor, with a semicircle at high frequencies (from 150 Hz to 300 kHz) and a linear spike at low frequencies (from 20 to 150 Hz). The sample resistance from this plot is 103 K, giving a conductivity of 7.72×10^{-6} Scm^{-1}. The La, Sm, and Gd compounds show similar behavior. The sample resistances and conductivities of these complexes are 8.6, 20.2, and 45.8 KΩ and 9.25, 3.94 and 1.74×10^{-5} S cm^{-1}, respectively.

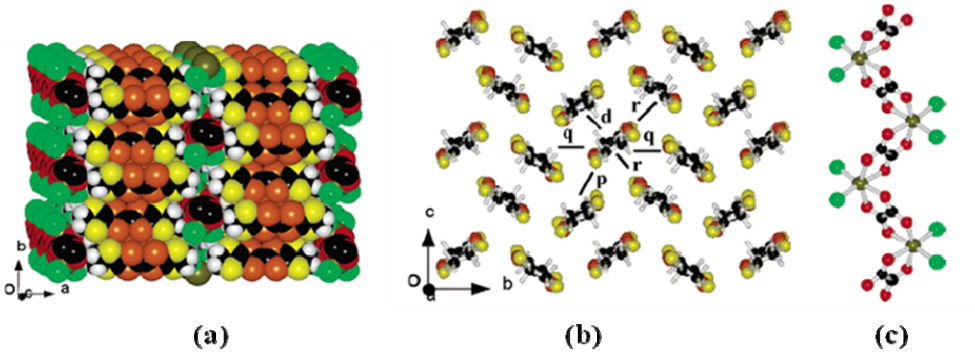

Fig. 1.18 (a) Structure of *k*-$BETS_2[Fe(C_2O_4)Cl_2]$: a space-filling view of the packing of BETS layers and $[Fe(C_2O4)Cl_2]_n$ chains in the crystal, viewed along the *c* axis. Color scheme: C, black; H, white; O, red; S, yellow; Cl, green; Fe, brown-green; Se, orange, (b) BETS layer showing the *k*-type packing of the donors with the definition of the overlap integrals and (c) $[Fe(C_2O4)Cl_2]_n$ chain, viewed along the *a* axis. From Ref. 119.

A novel hybrid compound, κ-$BETS_2[Fe^{III}(C_2O_4)Cl_2]$, (BETS = bis(ethylenedithio) tetraselenafulvalene, with both conducting building blocks (π electron) and magnetic molecular building blocks (d electron) in the structure, has reported been recently.[119] The structure consist of parallel donor layers, two per unit cell, displaying a κ type packing of $BETS^{0.5+}$ within the *bc* plane, and anionic magnetic chains, $[Fe(C_2O4)Cl_2]^-_n$, running along the *c* axis (Fig. 1.18). It displays metallic behavior down to 4.2 K, with a large optical anisotropy. The band structure consists of a 1-D band and a hole pocket, characteristic of κ phases. The magnetic properties were modeled by the sum of a 1D antiferromagnetic chain contribution from the d spins of Fe^{3+}, a temperature-independent paramagnetic contribution, and a Curie impurity term. At 4.5 K, there is a signature of long-range magnetic ordering to a canted-antiferromagnetic state in the zero-field-cooled-field-cooled magnetizations, and at 2 K, a small hysteresis loop is observed.

A rather different example of electronic behaviour should be mentioned. Kepert and co-workers[120] have discovered an interesting case of spin-crossover in a nanoporous hybrid metal-organic network compound,

$[Fe_2(azpy)_4(NCS)_4 \cdot (guest)]$, (azpy is *trans*-4,4'-azopyridine). The crossover is triggered by the uptake or release of molecules into the cavities, providing another example of a sensor system based upon a nanoporous hybrid network.

Amongst the hybrid materials with novel electronic properties, those which seem feasible are materials which may become superconducting (even at low temperature) and those which exhibit metal-insulator transitions.

1.9. Dielectrics

It is not surprising that some of the hybrid networks exhibit interesting dielectric properties, such as ferroelectricity and other types of ferroic behavior. For example, a one-dimensional chiral $[ZnCl_2(HQA)] \cdot 2.5H_2O$, (HQA = 6-methoxyl-(8S,9R)-cinchonan-9-ol-3-carboxylic acid) shows a dipolar chain relaxation process and a high dielectric constant (ε_0 = 37.3), with a strong SHG response that is ca. 20 times larger than that for KDP (KH_2PO_4). The properties are attributed to the presence of intramolecular charge separation due to the zwitterionic moiety and a good donor-acceptor chromophore.[109]

A three-dimensional $[Cd(papa)(Hpapa)]ClO_4 \cdot H_2O$, Hpapa = 3-(3-pyridyl)-3-aminopropionic acid, crystallizes in a noncentric (*Cc*) polar (C_S) space group. The 3-D structure posses a novel topology which arises from the connectivity of cadmium ions through papa unit.[111] This compound exhibits good ferroelectric properties with a dielectric hysteresis loop with a remnant polarization (P_r) of 0.18-0.28 μCcm^{-2} and coercive field (E_c) of 12 $kVcm^{-1}$. The saturation spontaneous polarization (P_s) is about 1.2-1.8 μCcm^{-2}, while that of ferroelectric KDP and triglycine sulfate are 5.0 and 3.0 μCcm^{-2}, respectively.

Another three-dimensional cadmium compound, Cd(TBP)Cl, HTBP = *N*-(4-(1*H*-tetrazol-5-yl)benzyl)praline, crystallized in a noncentric (*Cc*) polar (C_S) space group. This compound exhibit ferroelectric behavior associated with dielectric loss and thus a relaxation process.[121] The electric hysteresis loop shows typical ferroelectric features with a remnant polarization (P_r) of ca. 0.38 μCcm^{-2} and coercive field (E_c) of ca. 2.10 kVcm^{-1}. Saturation of the spontaneous polarization (*P*s) occurs at ca. 0.50 μCcm^{-2}, which is significantly higher than that for a typical ferroelectric compound (e.g., $NaKC_4H_4O_6 \cdot 4H_2O$, Rochelle salt; usually *P*s = 0.25 μCcm^{-2}). A relaxation process was also observed, suggesting that the dielectric loss changes with temperature at different frequencies with the peak maxima. The relaxation process (peak) is probably associated with dipolar Cd-Cl bond vibrations or the displacement of the proton on the tetrazoyl group in the ligand. It also shows an SHG response of ca. 10 times that of KDP. Two multiferroic, homochiral two-dimensional compounds, [Cu((R)-hmp)(dca)] and [Cu((S)-hmp)(dca)], consists of Cu_2O_2 units connected by dicyanamide (dca) and α -methyl-2-pyridinemethanol (hmp) linkers. Both phases show ferroelectric behavior along with a strong antiferromagnetic interaction. They also exhibit an SHG response that is approximately 0.6 times that of urea.[122]

Finally, a three-dimensional porous manganese formate, $[Mn_3(HCOO)_6] \cdot (C_2H_5OH)$, with one-dimensional channels along the *b*-axis, exhibits a ferroelectric transition at 165 K and a ferrimagnetic transition at 8.5 K. The compound is a nice example of a hybrid in which the porous host lattice exhibits magnetic order and the behavior of guest molecules can induce ferroelectric behaviour. It is also a rare example of a multiferroic system in which ferroelectricity and ferromagnetism coexist (Fig. 1.19).[123]

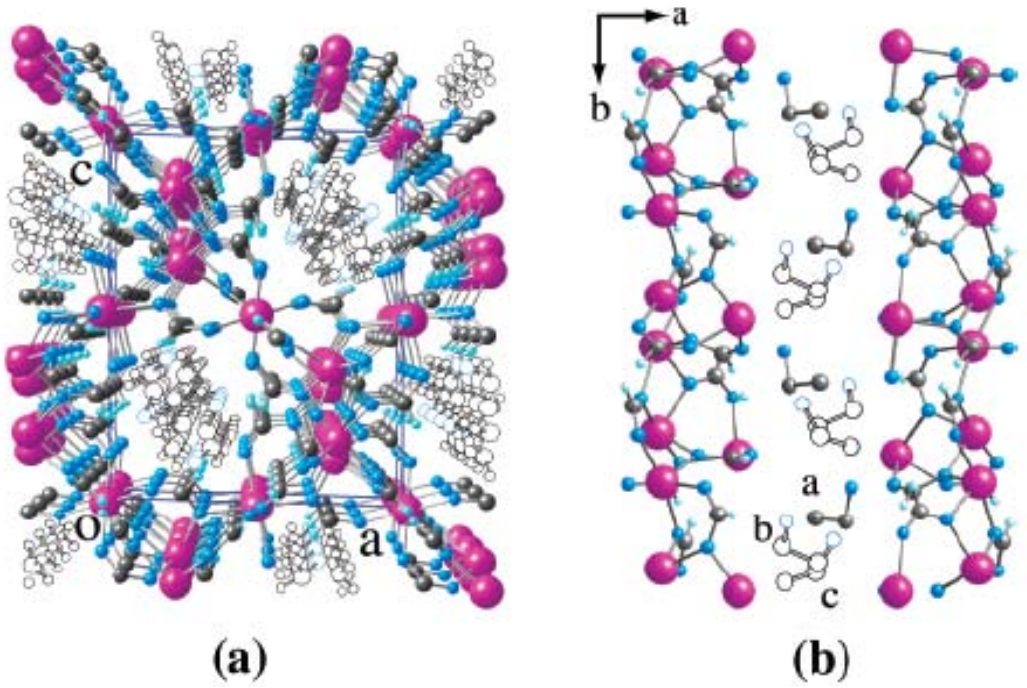

Fig. 1.19(a) View of the 3-D structure of $[Mn_3(HCOO)_6](C_2H_5OH)$ viewed along the *b*-axis: Mn, pink; C, gray; O, blue; H, pale sky blue. The C and O atoms of guest C_2H_5OH molecules are shown by open circles and (b) the arrangement of guest ethanol molecules along the channel at 90 K. From. Ref 123.

Besides hybrid materials exhibiting ferroelectricity and related ferroic properties, it would be fascinating to have hybrids which are multiferroic and magnetoelectric. This would require designing materials which are magnetic and are at the same time ferroelectric, preferably with coupling between the electrical and magnetic order parameters.

1.10. Nanoporous hybrids

Properties of nanoporous hybrid network solids have been investigated extensively due to their potential applications in catalysis, gas storage, guest exchange, sorption, separation, sensing and other areas.[18,124] Porous network solids are conveniently classified into three generations.[125,126] The 1st generation compounds have porous networks that are often sustained only with guest molecules and the structure may collapse irreversibly on removal of guest

molecules. The 2nd generation porous networks have stable and robust networks, which show permanent porosity without any guest molecules in the pores. The 3rd generation hybrid compounds possess flexible and dynamic networks, which respond to external stimuli such as light, electric fields and guest molecules, and are able to change their structure reversibly. The 1st generation compounds constitute inorganic porous materials constructed by covalent bonds, and include zeolite analogues such as organically templated silicates, phosphates, sulphates etc. The 2nd and 3rd generation compounds are mainly from hybrid inorganic-organic network solids. In Table 1.7, we list typical examples of porous hybrid materials. In what follows we briefly indicate some of the unusual properties of a few of the porous hybrid network compounds discovered in recent years.

Most hybrid porous networks are coordination polymers of the type $\boldsymbol{I^0O^3}$. They were realized through crystal engineering by utilizing various geometrical shapes of metal cores (secondary building units-SBUs) as nodes and multifunctional organic ligand as the linkers. Some of the materials in this class have remarkably large pores and low densities. For example, a series of MOFs (metal organic frameworks) with high porosity and low densities have been constructed by bridging Zn_4O SBUs via rigid aromatic di- or tricarboxylates[127]. A notable member of the series is MOF-177, Zn_4O(1,3,5-benzenetribenzoate)$_2$, which will store 7.5% hydrogen by weight at 77 K and a pressure of 70 bar[128]. A three-dimensional coordination polymer of the type $\boldsymbol{I^0O^3}$, the chromium terephthalate, $Cr_3F(H_2O)_2O[(O_2C)\text{-}C_6H_4\text{-}(CO_2)]_3.nH_2O$ (n = 25) (MIL-101), based on a trinuclear chromium SBU, has an extremely large unit cell (702,000 Å^3), very large pore sizes (29 to 34 Å), and one of the highest internal surface area reported to date

(5900 m^2 g^{-1}) (Fig. 1.20).[58] Some of the porous metal terephthalate (M = Cr and Fe) are being studied for use in drug delivery applications.[129]

Table 1.7 ***Porous properties of representative inorganic-organic hybrid compounds***

S.No	Formula	I^nO^m	Porous property	Figure	Ref.
1	Zn_4O(1,3,5-benzenetribenzoate)$_2$	I^0O^3	7.5% H_2 storage by weight (77 K, 70 bar)	-	[128]
2	Terephthalate, $Cr_3F(H_2O)_2O$[(1,4-BDC]$_3$.nH_2O (n = 25)	I^0O^3	cell dimensions (702,000 $Å^3$), pore sizes (29 to 34 Å), surface area (5900 m^2 g^{-1})	1.20	[58]
3	[Tb(BTB)(H_2O)]·2($C_6H_{12}O$), (BTB = 1,3,5- benzene trisbenzoate)	I^1O^2	Pore dim. =10 Å, surface area >1000 m^2 g^{-1}.	-	[130]
4	1,4-phenylendiacetate, [Er_2(PDA)$_3$(H_2O)]·2H_2O	I^1O^2	stable up to 450 °C, pore dim. = 3.4 Å, selectivity for CO_2 sorption	-	[131]
5	1,3,5-benzenetricarboxylate, Dy(BTC)(H_2O)· DMF	I^0O^1	Stable up to 350 ^oC, surface area = 655 m^2 g^{-1}, H_2 and CO_2 storage capability	-	[132]
6	Terephthalate, [M(OH)(1,4-BDC)], M = Cr, Fe, Sc	I^1O^2	Stable up to 500 ^oC, surface area = 1500 m^2 g^{-1}, breathing effect	1.21	[133]
7	Ni_2(4,4'-bipyridine)$_3$ (NO_3)$_4$·2ROH	I^0O^1	Dynamic porosity, hysteresis in H_2 sorption, pore dim.= 8.3 Å	-	[134]
8	[Ni(bpe)$_2${N(CN)$_2$}] ·{N(CN)2}·5H_2O	I^0O^3	Dynamic porosity, Anion exchange, selective gas sorption.	-	[135]

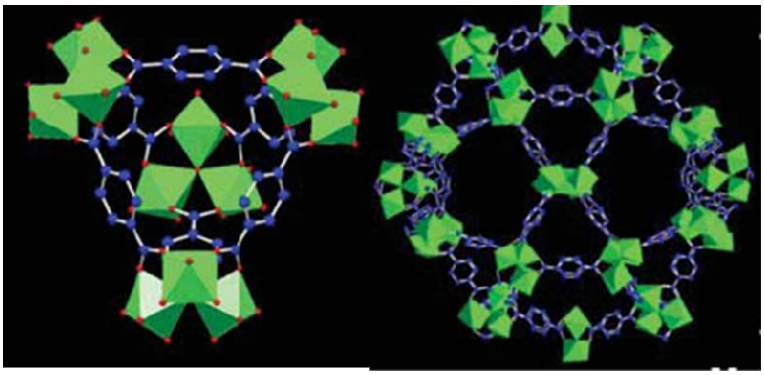

Fig. 1.20 (a) The super tetrahedron (ST) unit in a 3-D chromium terephthalate, $Cr_3F(H_2O)_2O[(O_2C)\text{-}C_6H_4\text{-}(CO_2)]_3.nH_2O$ (n = 25), where trinuclear chromium SBUs are connected by 1,4-BDC anions and (b) a view of the porous structure built up from the ST units. From Ref. 58.

A three-dimensional lanthanide carboxylate $[Tb(BTB)(H_2O)]\cdot 2(C_6H_{12}O)$, (BTB = 1,3,5- benzene trisbenzoate), with a $\boldsymbol{I^1O^2}$ type structure, based upon chains of edge-sharing TbO_9 polyhedra connected by the extended tritopic BTB^{3-} ligand, has 1-D hexagonal pores containing free cyclohexanol molecules. When the solvent is removed, this compound with free cylinders of ca. 10 Å diameter, exhibits a high surface area (>1000 $m^2\ g^{-1}$).[130]

Not all the interesting properties are to be found in systems with large pores. A highly robust three-dimensional erbium 1,4-phenylendiacetate, $[Er_2(PDA)_3(H_2O)]\cdot 2H_2O$ reversibly undergoes dehydration of both coordinated and lattice water molecules to form $[Er_2(PDA)_3]$ of the type $\boldsymbol{I^1O^2}$. Thermogravimetric analysis show that $[Er_2(PDA)_3]$ remains stable[131] up to 450 °C. With an effective pore window size of 3.4 Å, it adsorbs CO_2 into its pores and shows nonporous behavior toward Ar or N_2. There is a general correlation between the pore size and the kinetic diameters of the adsorbates (CO_2 = 3.3 Å, Ar =3.40 Å, and N_2 = 3.64 Å). The selectivity of CO_2 over Ar arises from the combined differentiations on size and on host-guest interactions. A three-dimensional 1,3,5-

benzenetricarboxylate, Dy(BTC)(H_2O)· DMF, with an $\boldsymbol{I^0O^1}$ type structure and excellent thermal stability (350 °C), shows a high surface area of 655 m^2 g^{-1} as well as hydrogen and carbon dioxide storage capability due to the availability of Lewis-acid metal sites.[132]

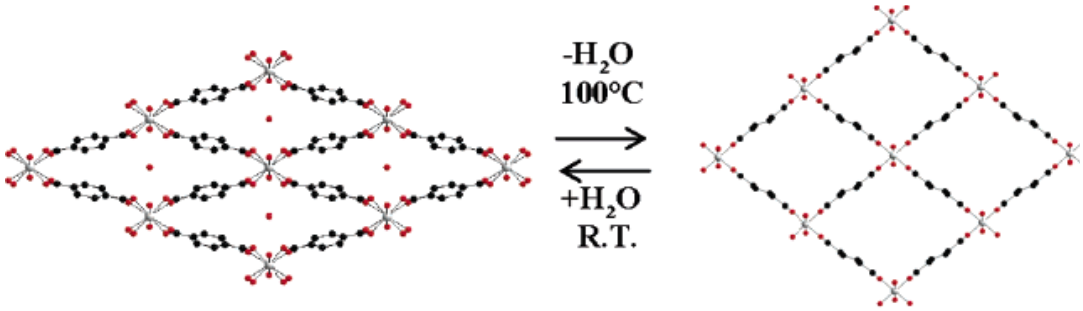

Fig. 1.21 Breathing effect in 3-D 1,4-benzenedicarboxylate [M(OH)(OOC–C_6H_4–COO)], M = Cr, Fe, Sc. From Ref. 133

Turning to 3rd generations systems, the three-dimensional metal terephthalate, [M(OH)(OOC–C_6H_4–COO)], M = Cr^{III}, Fe^{III}, Sc^{III}, of the type $\boldsymbol{I^1O^2}$ exhibits dynamic porosity based on host-guest interactions. This novel dynamic property or the "breathing effect" occurs when the structure is sufficiently flexible that it can adapt its structure to accommodate sorbates of different sizes and loadings. The structure contains one-dimensional chains of corner-sharing MO_6 octahedra that are cross-linked by the benzene-1,4-dicarboxylate groups to form a three-dimensional network (Fig. 1.21). The surface area of the dehydrated form of the Cr(III) member of the MIL-53 family is 1500 m^2 g^{-1} and it is stable[133] up to 500°C. The dehydrated structure contracts when water is adsorbed due to hydrogen bonding between the water molecules and the oxygen atoms of the benzene-1,4-dicarboxylate groups.

Two one–dimensional coordination polymers, Ni_2(4,4'-bipyridine)$_3$(NO_3)$_4$·$2CH_3OH$ and Ni_2(4,4'-bipyridine)$_3$(NO_3)$_4$·$2C_2H_5OH$, also

exhibit dynamic porosity. Both contain linear chains of metal centers bridged by bipy, which in turn are connected by further bipy coordination into pairs. These pairs are aligned parallel to each other in the methanol compound and perpendicular in ethanol system, giving maximum pore cavity dimensions of 8.3 Å with flexible linkers in which the pore openings appear to be too small to allow H_2 to pass. However, they show hysteresis in the adsorption and desorption kinetics above the supercritical temperature of H_2, reflecting the dynamical opening of the windows between pores. This behavior allows H_2 to be adsorbed at high pressures but stored at lower pressures.[134]

Another three-dimensional compound which exhibits dyanamic porosity is a bimodal microporous two-fold interpenetrating network of $[Ni(bpe)_2\{N(CN)_2\}]\cdot\{N(CN)2\}\cdot 5H_2O$ (bpe = 1,2-bis(4-pyridyl)ethane; $N(CN)_2$ = dicyanamide). It has two types of channels, one for anionic dicyanamide and the other for neutral water molecules.[135] The dehydrated framework provides a dual function of specific anion exchange of free dicyanamide for the smaller N_3^- anions and selective gas sorption. The N_3^- exchanged framework leads to a dislocation of the mutual positions of the two interpenetrating frameworks, resulting in an increase in the effective pore size in one of the channels and a higher adsorbate capacity than in the initial compound, thereby illustrating the controlled sorption properties of flexible porous frameworks.

Of the various porous hybrid materials that would be of interest, specially important would be materials with high hydrogen uptake. Such materials should have metal sites with little or marginal interaction with hydrogen and possess small or moderate sized pores, surface area not being of great importance. It would be

exciting to separate oxygen and nitrogen by passing air through a hybrid material with small magnetic channels.

1.11. Outlook

The foregoing discussion underlines the wide variety of properties that have already been discovered in hybrid inorganic-organic network materials, but nevertheless, there remains an enormous amount of scope for further work in this area. The number of chemical and structural variations that can be envisaged for hybrid network compounds is literally infinite, making the scope of this emerging field arguably larger than that of organic and inorganic materials combined. There has been a strong emphasis to date on the study of porous coordination polymers, or MOFs, but, as argued in a recent article,[136] there is a great deal of untapped potential in the area of dense materials, many of which have excellent stability. It is also worth remembering that the vast majority of the interesting phenomena studied by physicists are found in dense rather than porous phases.

There are many properties that are yet to be discovered in hybrid systems, such as thermoelectricity, superconductivity, lasing and metal-insulator transitions. In addition, certain potential combinations of properties may be unique to hybrids. For example, it would be exciting if we could make a hybrid high T_c superconductor with channels into which molecules could be adsorbed. Other unique opportunities may arise from the ease with which homochiral extended solids can be made in this area, opening up the possibility of probing the impact of chirality on other physical properties. Another emerging application of porous hybrids is in catalysis and photochemistry, where host-guest interactions in hybrid networks have been exploited to use them as carriers for naked nanoparticles and metal-organic chemical vapor deposition precursors.[137-139] Depositing hybrid

compounds on to solid surfaces as thin films for potential applications in surface chemistry and physics is also emerging in recent years.[140]

There also remains a pressing need for theory and simulation in the hybrid area. One of the challenges lies in predicting the architectures of possible hybrid networks and using such predictions to guide synthesis.[141] Other opportunities lie in adapting first principles and force-field methods for the study of hybrids in order to better understand the energetics of such systems.[142,143] Why, for example, is it so difficult to introduce mixed valency into transition metal hybrids in the quest to discover interesting magnetic and electronic properties? These are some of the many areas where condensed matter physicists will find exciting challenges in this rapidly emerging field.

1.12. References

1) S. Kitagawa, R. Kitaura and S-i. Noro, *Angew. Chem. Int. Ed.*, **2004**, 43, 2334.

2) J. C. Bailar and Jr., *Prep. Inorg. React*. 1**964**, 1, 1.

3) D. A. Summerville, T. W. Cape, E. D. Johnson and F. Basolo, *Inorg.Chem*., **1978**, 17, 3297.

4) J. S. Miller, C. Vazquez, N. L. Jones, R. S. McLean and A. J. Epstein, *J. Mater. Chem*., **1995**, 5, 707.

5) P. Gravereau, E. Garnier and A. Hardy, *Acta Crystallogr. Sect. B: Struct. Crystallogr. Cryst.Chem.*, **1979**, 35**,** 2843.

6) G. Alberti, U. Constantino, S. Allulli and N. Tomassini, *Inorg. Nucl. Chem*., **1978**, 40, 1113.

7) M. D. Poojary, H-L. Hu, F. Campbell III and A. Clearfield, *Acta Crystallogr.,Sect. B: Struct. Sci.*, **1993**, 49, 996.

8) B. F. Hoskins and R. Robson, *J. Am. Chem. Soc*., **1990**, 112, 1546.

9) R. Robson, *J. Chem. Soc*., *Dalton Trans.*, **2000**, 3735.

10) B. Moulton and M. J. Zaworotko, *Chem. Rev*., **2001**, 101, 1629.

11) B. Moulton and M. J. Zaworotko, *Curr. Opin. Solid State Mater. Sci*., **2002**, 6, 117.

12) M. O'Keeffe, M. Eddaoudi, H. Li, T. Reineke and O. M. Yaghi, *J. Solid State Chem.*, **2000**, 152, 3.

13) A. Clearfield, *Curr. Opin. Solid State Mater. Sci.*, **2002**, 6, 495.

14) A. K. Cheetham and P. M. Forster, *Topics in Catalysis*, **2003**, 24, 79.

15) J. L. C. Rowsell and O. M. Yaghi, *Microporous Mesoporous Mater*., **2004**, 73, 3.

16) M. J. Rosseinsky, *Microporous Mesoporous Mater.*, 2004, 73, 15.

17) C. N. R. Rao, S. Natarajan and R. Vaidhyanathan, *Angew. Chem. Int. Ed*., **2004**, 43, 1466.

18) A. K. Cheetham, C. N. R. Rao and R. K. Feller, *Chem. Commun*., **2006**, 4780

19) M. Dan and C. N. R. Rao, *Angew. Chem. Int. Ed.*, **2006**, 45, 281.

20) E. Coronado, J. R. G-Mascarós and C. M-Gastaldo, *J. Mater. Chem.*, **2006**, 16, 2685.

21) H. Li, M. Eddaoudi, M. O' Keeffe and O. M. Yaghi, *Nature*, **1999**, 402, 276.

22) M. Dan, A. K. Cheetham and C. N. R. Rao, *Inorg. Chem*., **2006**, 45, 8227.

23) N. Guillou, C. Livage, W. van Beek, M. Nogues and G. Férey, *Angew. Chem., Int. Ed*., **2003**, 42, 644.

24) R. K. Feller and A. K. Cheetham, *Solid State Sci*., **2006**, 8, 1121.

25) C. Livage, C. Egger and G. Férey, *Chem. Mater.*, **1999**, 11, 1546.

26) C. A. Merrill and A. K. Cheetham, *Inorg. Chem.*, **2007**, 46, 278.

27) P. M. Forster and A. K. Cheetham, *Angew. Chem. Int. Ed.*, **2002**, 41, 457.

28) R. Vaidhyanathan, S Natarajan and C. N. R. Rao, *Dalton Trans.*, **2003**, 1459.

29) D. Bradshaw, J. B. Claridge, E. J. Cussen, T. J. Prior and M. J. Rosseinsky, *Acc. Chem. Res*., **2005,** 38, 273.

30) K. Byrappa, M. Yoshimura, *Handbook of Hydrothermal Technology:Technology for Crystal Growth and Materials Processing*, William Andrew Inc, Salem, MA, **2001.**

31) E. R. Parnham and R. E. Morris, *Acc. Chem. Res*., **2007**, 40, 1005.

32) Z. Lin, S. Wragg and R. E. Morris *Chem. Commun*., **2006**, 2021.

33) P. M. Forster, A. R. Burbank, C. Livage, G. Férey and A. K. Cheetham, *Chem. Commun*., **2004**, 368.

34) P. M. Forster, N. Stock and A. K. Cheetham, *Angew. Chem., Int. Ed*., **2005**, 44, 7608.

35) Z. Ni and R. I. Masel, *J. Am. Chem. Soc*., **2006**, 128, 12394.

36) S. H. Jhung, J-H. Lee, P. M. Forster, G. Férey, A. K. Cheetham and J-S Chang, *Chem. Eur. J.*, **2006**, 12**,** 7899.

37) S. H. Jhung, T. Jin, Y. K. Hwang and J-S. Chang, *Chem. Eur. J.*, **2007**, 13, 4410.

38) S. H Jhung, J-H Lee, J. W. Yoon, C. Serre, G. Férey and J-S Chang, *Adv. Mater.*, **2007**, 19, 121.

39) R. Banerjee, A. Phan, B. Wang, C. Knobler, H. Furukawa, M. O'Keeffe, O. M. Yaghi, Science, **2008**, 319, 939.

40) G. R. Desiraju, *Crystal Engineering - The Design of Organic Solids*, Elsevier, Amsterdam, **1989.**

41) G. R. Desiraju, *Angew. Chem., Int. Ed*., **2007**, 46, 8342.

42) O.R. Evans and W. Lin, *Chem. Mater*., **2001**, 13, 2705.

43) B. Moulton, J. Lu, R. Hajndl, S. Hariharan and M. J. Zaworotko, *Angew. Chem. Int. Ed*., **2002**, 41, 2821.

44) O.M. Yaghi, M. O'Keeffe, N.W. Ockwig, H.K. Chae, M. Eddaoudi and J. Kim, *Nature*, **2003**, 423, 705.

45) S.R. Batten and K.S. Murray, *Aust. J. Chem*., **2001**, 54, 605.

46) M. Eddaoudi, J. Kim, D. Vodak, A. Sudik, J. Wachter, M. O'Keeffe and O.M. Yaghi, PNAS, **2002**, 99, 4900.

47) A.F. Wells, *Further Studies of Three-dimensional Nets*, ACA Monograph No. 8, American Crystallographic Association, **1979.**

48) M. O'Keeffe and B.G. Hyde, *Crystal Structures. I. Patterns and Symmetry*, Mineralogical Society of America Monograph, Mineralogical Society of America, Washington, DC, **1996.**

49) N.W. Ockwig, O. D-Friedrichs, M. O'Keeffe and O.M. Yaghi, *Acc. Chem. Res*., **2005**, 38, 176.

50) S.R. Batten, B.F. Hoskins and R. Robson, *Chem. Eur. J*., **2000**, 6, 156.

51) A. Nangia and G.R. Desiraju, *Chem. Commun*., **1999**, 605.

52) V.S.S. Kumar, S.S. Kuduva and G.R. Desiraju, *J. Chem. Soc., Perkin Trans*., **1999**, 2, 1069.

53) P. Day, *J. Chem. Soc., Dalton Trans*., **1997**, 701.

54) S. Decurtins, H. Schmalle and R. Pellaux, *N. J. Chem*., **1998**, 22, 117.

55) G. Férey, *J. Solid State Chem*., **2000**, 152, 37.

56) H. Li, A. Laine, M. O'Keeffe and O.M. Yaghi, *Science*, **1999**, 123, 1145.

57) H. Li, J. Kim, T.L. Groy, M. O'Keeffe and O.M. Yaghi, *J. Am. Chem. Soc*., **2001**, 123, 4867.

58) G. Férey, C. M-Draznieks, C. Serre, F. Millange, J. Dutour, S. Surblé and I. Margiolake, *Science*, **2005**, 309**,** 2040.

59) W. I. F. David, K. Shankland, L. B. McCusker and C. Baerlocher, *Structure Determination from Powder Diffraction Data*, Oxford Science Publications.

60) A. L. Bail, Trends in Structure Determination by Powder Diffractometry. http://sdpd.univ-lemans.fr/postscript/ecm18.pdf

61) H. M. Rietveld, *Acta Crystallogr.*, 1967, **22**, 151.

62) H. M. Rietveld, *J. Appl. Crystallogr.*, 1969, **2**, 65.

63) S. R. Batten, R. Robson, *Angew. Chem. Int. Ed.*, **1998**, 37, 1460.

64) M. Estermann, L. B. McCusker, C. Baerlocher, A.Merrouche, H. Kessler, *Nature*, **1991**, 352, 320.

65) C. Serre, F. Millange, S. Surblé and G. Férey, *Angew. Chem. Int. Ed*., **2004**, 43, 6286.

66) C. M-Draznieks, S. Girard and G. Férey, *J. Am. Chem. Soc*., **2002**, 124, 15326.

67) C. M-Draznieks, S. Girard, G. Férey, J. C. Schön, Z. Cancarevic and M. Jansen, *Chem. Eur. J*., **2002**, 8, 4102.

68) C. M-Draznieks, J. M. Newsam, A. M. Gorman, C. M. Freeman and G. Férey, *Angew. Chem. Int. Ed*., **2000**, 39, 2271.

69) C. M-Draznieks, J. Dutour, G. Férey, *Angew. Chem. Int. Ed.*, **2004**, 43, 6290.

70) C. M-Draznieks, J. Dutour and G. Férey, *Z. Anorg. Allg. Chem*., **2004**, 630, 2599.

71) C. Baerlocher, F. Gramm, L. Massüger, L. B. Mc Cusker, Z. He, S. Hovmöller and X. Zou, *Science*, **2007**, 315, 1113.

72) J. Wu, K. Leinenweber, J. C. H. Spence and M. O'Keeffe, *Nature*, **2006**, 5, 647.

73) C. Volkringer, D. Popov, T. Loiseau, N. Guillou, G. Férey, M. Haouas, F. Taulelle, C. M-Draznieks, M. Burghammer and C. Riekel, *Nature Mat*., **2007**, 6, 760.

74) F. Gramm, C. Baerlocher, L. B. McCusker, S. J. Warrender, P. A. Wright, B. Han, S. B. Hong, Z. Liu, T. Ohsuna and O. Terasaki, *Nature*, **2006**, 444, 79.

75) P. Juhas, D. M. Cherba, P. M. Duxbury, W. F. Punch and S. J. L. Billinge, *Nature*, **2006**, 440, 655.

76) R. Martonak, D. Donadio, A. R. Oganov and M. Parrinello, *Nature*, **2006**, 5, 623.

77) N. Guillou, C. Livage and G. Férey, *Eur. J. Inorg. Chem.*, **2006**, 4963.

78) N. Guillou, C. Livage, M. Drillon and G. Férey, *Angew. Chem. Int. Ed*., **2003**, 42, 5314.

79) M. Kurmoo, H. Kumagai, S. M, Hughes and C. J. Kepert, *Inorg. Chem.*, **2003**, 42, 6709.

80) S. C. Manna, E. Zangrando, A. Bencini, C. Benelli and N. R. Chaudhuri, *Inorg. Chem*., **2006**, 45, 9114.

81) S. O. H. Gutschke, D. J. Price, A. K. Powell and P. T. Wood, *Angew. Chem. Int. Ed*., **2001**, 40, 1920.

82) C. Livage, C. Egger, M. Noguès and G. Férey, *J. Mater. Chem.*, **1998**, 8, 2743.

83) N. Guillou, S. Pastre, C. Livage and G. Férey, *Chem. Commun.*, **2002**, 2358 and S. Konar, P. S. Mukherjee, E. Zangrando, F. Lloret and N. R. Chaudhuri, *Angew. Chem. Int. Ed* ., **2002**, 41, 1561.

84) M-L. Tong, J. Wang and S. Hu, *J.Solid State Chem.*, **200**5, 178, 1518.

85) Z-L. Huang, M. Drillon, N. Masciocchi, A. Sironi, J-T. Zhao, P. Rabu and P. Panissod, *Chem. Mater.*, **2000**, 12, 2805.

86) P-P. Liu, A-L. Cheng, N. Liu, W-W. Sun and E-Q. Gao, *Chem. Mater*., **2007**, 19, 2724.

87) T. K. Maji, W. Kaneko, M. Ohba and S. Kitagawa, *Chem. Commun.*, **2005**, 4613.

88) K. Barthelet, K. Adil, F. Millange, C. Serre, D. Riou and G. Férey, *J. Mater. Chem*., **2003**, 13, 2208.

89) S. M. Humphrey and P. T. Wood, *J. Am. Chem. Soc.*, **2004**, 126, 13236.

90) L-S. Long, X-M. Chen, M-L. Tong, Z-G. Sun, Y-P. Ren, R-B. Huang and L-S. Zheng, *J. Chem. Soc., Dalton Trans.*, **2001**, 2888 .

91) K. Barthelet, J. Marrot, D. Riou and G. Férey, *Angew. Chem. Int. Ed*., **2002,** 41, 281.

92) C. Serre, F. Millange, S. Surblé, J-M. Grenéche and G. Férey, *Chem. Mater*., **2004**, 16, 2706.

93) J. N. Behera and C. N. R. Rao, *J. Am. Chem. Soc*., **2006**, **128,** 9334.

94) J. N. Behera and C. N. R. Rao, *Dalton Trans*., **2007**, 669.

95) A. P. Ramirez, *Annu. Rev. Mater. Sci*., **1994**, 24, 453.

96) S. K. Pati and C. N. R. Rao, *J. Chem. Phys*., **2005**, 123, 234703.

97) S. Wang, Y. Hou, E. Wang, Y. Li, L. Xu, J. Peng, S. Liua and C. Hua, *New J. Chem*., **2003**, 27, 1144.

98) J. Lu, Y. Li, K. Zhao, J-Q. Xu, J-H. Yu, G-H. Li, X. Zhang, H-Y. Bie and T-G. Wang, *Inorg. Chem. Commun*., **2004**, 7, 1154.

99) Y-Q, Huang, B, Ding, H-B, Song, B, Zhao, P, Ren, P, Cheng, H-G, Wang, D-Z, Liao and S-P Yan, *Chem. Commun.*, **2006**, 4906.

100) F. Serpaggi, T. Luxbacher, A. K. Cheetham and G. Férey, *J. Solid State Chem*., **1999**, 145, 580.

101) Y-G. Huang, B-L. Wu, D-Q. Yuan, Y-Q. Xu, F-L. Jiang and M-C. Hong, *Inorg. Chem.*, **2007**, 46, 1171.

102) J. Yang, Q. Yue, G-D. Li, J-J. Cao, G-H. Li and J-S. Chen, *Inorg. Chem.*, **2006**, 45, 2857.

103) D. Weng, X. Zheng and L. Jin, *Eur. J. Inorg. Chem.*, **2006**, 4184

104) S. Wang, *Coord. Chem. Rev.*, **2001**, 215, 79.

105) G. S. Huang, X. L. Wu, Y. Xie, F. Kong, Z. Y. Zhang, G. G. Siu and P. K. Chu, *App. Phys. Lett.*, **2005**, 87, 151910.

106) F. X. L. i Xamena, A. Corma and H. Garcia, *J. Phys. Chem. C,* **2007**, 111, 80.

107) K. T. Holman, A. M. Pivovar, J. A. Swift and M. D. Ward, *Acc. Chem. Res*., **2001**, 34, 107.

108) O. R. Evans and W. B. Lin, *Acc. Chem. Res*., **2002**, 35, 511.

109) Y-Z. Tang, X-F. Huang, Y-M. Song, P. W. H. Chan and R-G. Xiong, *Inorg. Chem.*, **2006**, 45, 4868.

110) R. Vaidhyanathan, S. Natarajan and C. N. R. Rao, *J. Solid State Chem*., **2004**, 177, 1444.

111) Z-R. Qu, H. Zhao, Y-P. Wang, X-S. Wang, Q. Ye, Y-H. Li, R-G. Xiong, B. F. Abrahams, Z-G. Liu, Z-L. Xue and X-Z. You, *Chem. Eur. J*., **2004**, 10, 53.

112) Q. Ye, Y-H. Li, Y-M. Song, X-F. Huang, R-G. Xiong and Z. Xue, *Inorg. Chem.*, **2005**, 44, 3618.

113) L. K. Li, Y. L. Song, H. W. Hou, Y. T. Fan and Y. Zhu, *Eur. J. Inorg. Chem.*, **2005**, 16, 3238.

114) G-W. Zhou, Y-Z. Lan, F-K. Zheng, X. Zhang, M-H. Lin, G-C. Guo and J-S. Huang, *Chem. Phys. Lett*., **2006**, 426, 341.

115) Q-R. Fang, G-S. Zhu, Z. Jin, M. Xue, X. Wei, D-J. Wang and S-L. Qiu, *Angew. Chem. Int. Ed.*, **2006**, 45, 6126.

116) R. Kato, *Bull. Chem. Soc. Jpn.*, **2000**, 73, 515.

117) M. Tadokoro, S. Yasuzuka, M. Nakamura, T. Shinoda, T. Tatenuma, M. Mitsumi, Y. Ozawa, K. Toriumi, H. Yoshino, D. Shiomi, K. Sato, T. Takui, T. Mori and K. Murata, *Angew. Chem. Int. Ed.*, **2006**, 45, 5144.

118) J-J. Zhang, T-L. Sheng, S-Q. Xia, G. Leibeling, F. Meyer, S-M. Hu, R-B. Fu, S-C. Xiang and X-T. Wu, *Inorg. Chem.*, **2004**, 43, 5472.

119) B. Zhang, Z. Wang, Y. Zhang, K. Takahashi, Y. Okano, H. Cui, H. Kobayashi, K. Inoue, M. Kurmoo, F. L. Pratt and D. Zhu, *Inorg. Chem.*, **2006**, 45, 3275.

120) G.J. Halder, C. J. Kepert, B. Moubaraki, K. S. Murray and J. D. Cashion, *Science*, **2002**, 298, 1762.

121) Q. Ye, Y-M. Song, G-X. Wang, K. Chen, D-W. Fu, P. W. H. Chan, J-S. Zhu, S. D. Huang and R-G. Xiong, *J. Am. Chem. Soc.*, **2006**, 128, 6554.

122) Z-G. Gu, X-H. Zhou, Y-B. Jin, R-G. Xiong, J-L. Zuo and X-Z. You, *Inorg. Chem.*, **2007**, 46, 5462.

123) H. Cui, Z. Wang, K. Takahashi, Y. Okano, H. Kobayashi and A. Kobayashi, *J. Am. Chem. Soc*., **2006**, 128, 15074.

124) D. Maspoch, D. R-Molina and J. Veciana, *Chem. Soc. Rev*., **2007**, 36, 770.

125) S. Kitagawa and M. Kondo, *Bull. Chem. Soc. Jpn*., **1998**, 71, 1739.

126) S. Kitagawa and K. Uemura, *Chem. Soc. Rev*., **2005**, 34, 109.

127) A. G. W-Foy, A. J. Matzger and O. M. Yaghi, *J. Am. Chem. Soc.*, **2006**, 128, 3494.

128) H. Furukawa, M. A. Miller and O. M. Yaghi, *J. Mater. Chem.*, **2007**, 17, 3197.

129) P. Horcajada, C. Serre, M. V-Regi, M. Sebban, F. Taulelle and G. Férey, *Angew. Chem. Int. Ed.*, **2006**, 45, 5974.

130) T. Devic, C. Serre, N. Audebrand, J. Marrot and G. Férey, *J. Am. Chem. Soc.*, **2005**, 127, 12788.

131) L. Pan, K. M. Adams, H. E. Hernandez, X. Wang, C. Zheng, Y. Hattori and K. Kaneko, *J. Am. Chem. Soc.*, **2003**, 125, 3062.

132) X. Guo, G. Zhu, Z. Li, F. Sun, Z. Yang and S. Qiu, *Chem. Commun*., **2006**, 3172.

133) T. Loiseau, C. Serre, C. Huguenard, G. Fink, F. Taulelle, M. Henry, T. Bataille, G. Férey, *Chem.Eur. J*., **2004**, 10, 1373.

134) X. Zhao, B. Xiao, A. J. Fletcher, K. M. Thomas, D. Bradshaw and M. J. Rosseinsky, *Science*, **2004**, 306, 1012.

135) T. K. Maji, R. Matsuda and S. Kitagawa, *Nature Mat*., **2007**, 6, 142.

137) A. K. Cheetham and C. N. R. Rao, *Science*, **2007**, 318, 58.

137) S. Hermes, M-K. Schröter, R. Schmid, L. Khodeir, M. Muhler, A. Tissler, R.W. Fischer, and R.A. Fischer, *Angew. Chem. Int. Ed.*, **2005**, 44, 6237.

138) S. Hermes, F. Schröder, R. Chelmowski, C. Wöll and R. A. Fischer, *J. Am. Chem. Soc.*, **2005**, 127, 13744.

139) O. Shekhah, H. Wang, T. Strunskus, P. Cyganik, D. Zacher, R. Fischer and C. Wöll, *Langmuir*, **2007**, 23, 7440.

140) J. A. Theobald, N. S. Oxtoby, M. A. Phillips, N. R. Champness and P. H. Beton, *Nature*, **2003**, 424, 1029.

141) C. M-Draznieks, *J. Mater. Chem.*, **2007**, 17, 4348.

142) C. Lee, C. M-Draznieks, B. Slater, G. Wu, W. T. A. Harrison, C. N. R. Rao and A. K. Cheetham, *Chem. Comm*., **2006**, 2687.

143) H. G. Harvey, B. Slater and M. P. Attfield, *Chem. Eur. J.*, **2004**, 10, 3270.

Chapter 2

Hybrid Networks of Metal Benzenedicarboxylates

Summary*

In an attempt to understand the structural features of hybrid dicarboxylate frameworks in terms of dimensionality and extended inorganic connectivity, we have employed the three isomeric (1,2-, 1,3- and 1,4-) benzenedicarboxylic acids to synthesize hybrid inorganic-organic frameworks of Zn, Cd, Pb and lanthanides with or without chelating amines.

Six one-dimensional (I^0O^1) coordination polymers [with zero inorganic connectivity (I^0O^1)] of metal 1,2-benzenedicarboxylates with 1,10-phenanthroline or 2,2'-bipyridine as the chelating amines have been obtained. [$Zn(H_2O)$(1,2-BDC)(1,10-phen)].H_2O, **I**, and [$Cd(H_2O)$(1,2-BDC)(2,2'-bipy)], **II**, have helical chain structures. [$Cd(H_2O)$(1,2-BDC)(1,10-phen)], **III**, has a one-dimensional ribbon like structure, which contains four-membered rings and the $^2\mathbf{D_2}$ dimers. [Description of dimer SBUs and terminology are given in the appendix {see Appendix. 2.7(a)}]. [Y_2(1,2-BDC)$_3$(1,10-phen)$_2$]·H_2O, **IV**, is also a one-dimensional structure but with two types of dimers ($^2\mathbf{D_0}$ & $^4\mathbf{D_2}$), which are related to the paddlewheel SBU. [Y_2(1,2-BDC)$_3$(1,10-phen)], **V**, has a one-dimensional structure with two types of paddlewheel dimer SBUs ($^4\mathbf{D_0}$ & $^4\mathbf{D_2}$).

*Papers based on these studies have been published in *Proc. Indian Acad. Sci.* (*Chem. Sci.*) (2003), *Dalton. Trans*. (2004), *Eur.J. Inorg. Chem.* (2004), *Solid State Sci.* (2004), *Inorg. Chem. Commun.* (2004), *J. Mater. Chem.* (2005), *Inorg. Chimica Acta* (2005), *J. Mater. Chem.* (2005) and *Crystal Growth & Design* (2005).

$[Dy_2(1,2\text{-BDC})_3(1,10\text{-phen})]$, **VI**, has a one-dimensional structure with two types of eight-membered ring dimer SBUs ($^2\mathbf{D_0}$ & $^2\mathbf{D_2}$). Four 1,3-benzenedicarboxylates of lanthanides with 1,10-phenanthroline or 2,2'-bipyridine as the chelating amines have been obtained. Two of them, $[Y_2(1,3\text{-BDC})_3(2,2'\text{-bipy})_2]$, **VII**, and $[Nd_2(1,3\text{-BDC})_3(1,10\text{-phen})_2]$, **X**, have two-dimensional ($\boldsymbol{I^0O^2}$) augmented square lattice structure and the other two, $[Y_2(1,3\text{-BDC})_3(2,2'\text{-bipy})_2]\cdot H_2O$, **VIII**, and $[Y_2(1,3\text{-BDC})_3(1,10\text{-phen})_2]$, **IX**, have three-dimensional ($\boldsymbol{I^0O^3}$) augmented $CdSO_4$ structure. These structures contain dimers of paddle wheel ($^4\mathbf{D_0}$) or paddle wheel related SBUs.

$[Cd(1,4\text{-BDC})(1,10\text{-phen})].H_2O$, **XI**, has a two-dimensional layer structure ($\boldsymbol{I^0O^2}$). The two chelating 1,10-phen molecules in each dimeric unit project into opposite sides of the layer, thereby preventing the formation of a three-dimensional interpenetrating network of the 1,4-BDC.

Two heteroleptic benzenedicarboxylates of yttrium coordination polymers, $[Y_2(1,2\text{-BDC})_2(1,3\text{-BDC})(1,10\text{-phen})_2]$, **XII**, and $[Y_2(1,2\text{-BDC})_2(1,4\text{-BDC})(1,10\text{-phen})_2]$, **XIII**, have similar two-dimensional structures of the type ($\boldsymbol{I^0O^2}$), where ladders formed by the ($^2\mathbf{D_0}$) dimers and the 1,2-BDC anions are connected by the 1,4-BDC anions in to the layer structure. $[La_2(H_2O)_2(1,2\text{-BDC})_2(1,4\text{-BDC})(1,10\text{-phen})_2(H_2O)_2]\cdot H_2O$, **XIV**, has a three-dimensional structure with zero inorganic connectivity ($\boldsymbol{I^0O^3}$), where ladders formed by the ($^2\mathbf{D_2}$) dimers and the 1,2-BDC anions are cross-linked by the 1,4-BDC anions in to the three-dimensional structure.

Two heteroleptic benzenedicarboxylates without any chelating amines, **XV** and **XVI**, have been obtained with a three-dimensional structure ($\boldsymbol{I^0O^3}$), both with the same formula, $[M_2(1,2BDC)_2(1,4BDC)(H_2O)_4]$, (For **XV**, M = La, Pr and for

XVI, Gd, Dy, and Y). Both these structures contain layers formed by the dimers and the 1,2-BDC anions, which are cross-linked by the 1,4-BDC anions in to the three-dimensional structure but they differ in their dimers ($^{3}\mathbf{D_2}$ for **XV** and $^{2}\mathbf{D_0}$ for **XVI**). A two dimensional Gd phthalate, $[Gd_2(1,2\text{-}BDC)_4(H_2O)_2].(H_2Pip)$, **XVII**, templated by protonated piperazine contains $^{2}\mathbf{D_0}$ dimer SBUs connected by the 1,2-BDC anions. $(OPb_4)(1,3\text{-}BDC)_3(H_2O)$, **XVIII**, has a three-dimensional structure with zero inorganic connectivity ($\boldsymbol{I^0O^3}$). It has (2,8) 3D-periodic net topology, where hexanuclear SBUs are connected by the 1,3-BDC anions.

Seven hybrid frameworks of metal benzenedicarboxylates with extended inorganic connectivity were obtained with or without chelating amines. Of these, $[M_3(1,2\text{-}BDC)_4(1,10\text{-}phen)_3(H_2O)]\cdot 0.5H_2O$, **XIX**, and $[M_3(1,2\text{-}BDC)_4(1,10\text{-}phen)_2(NO_3)]\cdot H_2O$, **XX,** (where M = La and Pr) have a one-dimensional structure with one-dimensional inorganic connectivity ($\boldsymbol{I^1O^0}$). Compound **XIX** has two types of dimer SBUs ($^{3}\mathbf{D_2}$ **&** $^{2}\mathbf{D_1}$), and **XX** has three types of dimer SBUs ($^{2}\mathbf{d_2}$**,** $^{2}\mathbf{D_2}$ **&** $^{3}\mathbf{D_2}$). Eu and Tb doped compounds of **XIX** exhibit the ligand sensitized lanthanide-centered red and green emissions respectively at room temperature.

Two polymorphs of the same formula, $M_2(1,2\text{-}BDC)_3(H_2O)$, (Y=**XXI**, and Dy= **XXII**), with a two-dimensional structure and one-dimensional inorganic connectivity ($\boldsymbol{I^1O^1}$) have been obtained. Though the inorganic connectivity and the M…M interaction within the layer are different, the interlayer $\pi\ldots\pi$ interactions appears to be similar for these two structures. $[Pr_2(1,2\text{-}BDC)_2(PipDPDA)]$, **XXIII**, (where PipDPDA = N,N'-Piperazine diphthalidodiamide dianion, generated *in-situ* under hydrothermal conditions) has a two-dimensional structure ($\boldsymbol{I^1O^1}$) with one-dimensional inorganic connectivity ($\boldsymbol{I^1O^1}$), where infinite Pr-O-Pr chains, made up of ($^{4}\mathbf{D_2}$) dimers and connected by the PipDPDA anions into the layer structure. The

isophthalate, [Cd(1,3-BDC)(H_2O)], **XXIV**, has a two-dimensional structure ($\boldsymbol{I^1O^1}$), where infinite Cd-O-Cd chains, made up of ($\boldsymbol{^2D_2}$) dimers are connected by the 1,3-BDC anions in to the layer structure. The terephthalate, Pb(1,4-BDC), **XXV**, has a three-dimensional structure with two-dimensional inorganic connectivity ($\boldsymbol{I^2O^1}$), where the infinite two-dimensional Pb-O-Pb layers of the $\boldsymbol{I^2O^0}$ type, with a (3,6) 2D-net topology are connected by the 1,4-BDC anions in to the three-dimensional structure.

To understand the process of formation of three-dimensional zinc terephthalates, we have carried out a systematic time and temperature dependent transformation study. The study shows the transformation of a one-dimensional structure to a three-dimensional structure, and the possible presence of a dimensional hierarchy.

2.1. Introduction

Design and synthesis of new materials with novel structures constitutes an important area of research. According to the generally accepted definition, the process of "design" incorporates the creation of a topology / shape / form, which fulfils a given function as well as possible, and is also considered aesthetically pleasing. An additional fundamental aspect of "design" is that in general it is imbued with an artistic component. Currently, the field of coordination polymers is burgeoning worldwide. For this class of compounds, a nearly inflationary use of the term "design" has developed.[1] As in organic chemistry, one employs a system of independent structure increments that are connected by means of polycondensation or donor–acceptor interactions. The required building units must be stable under the reaction conditions and on the time scale of the reaction, and they must exhibit the necessary correctly matching sites for the interconnection.

With a clever choice of increments, a very reliable prediction of the structures is possible, even without a large computational effort. However, since the desired compounds are collective solids, the traditional concepts of molecular chemistry for directing the synthesis process do not apply. Steering the reaction towards the target compound must, in contrast, be controlled by means of the solubility product, and nucleation and growth processes.[2]

Inorganic–organic hybrid compounds prepared using multi-functional benzene carboxylic acids belong to this class and attracted much attention.[3–19] Benzenedicarboxylic acids are ideal ligands to design novel coordination polymers and open framework structures.[7-19] In the last few years, several metal-organic frameworks (MOFs) have been reported in the literature, with interesting properties such as porosity, sorption, catalysis, non-linear optics, luminescence, and magnetism.[20-23] A particular focus is on open-pored, three-dimensional framework structures, since they are thought to have high potential for important applications such as gas storage and heterogeneous catalysis. Thus, Yaghi and coworkers have reported interesting cubic zinc benzenedicarboxylates with porous structures having some hydrogen sorption properties.[24-26] Though the literature abounds on the report of novel benzene carboxylates, those formed from specific building units or with a inorganic core are rare. An interesting aspect of benzenedicarboxylic acids is their ability to form novel structures in the presence or absence of chelating aromatic amines by utilizing supramolecular interactions along with solvent molecules, which may be coordinated or present as solvent of crystallization. The structures formed by benzenedicarboxylic acids vary from one-dimensional chains to three-dimensional architectures. There are, however very few examples of systems wherein structures with all the three dimensionalities

occur with the same metal or the ligands.[27,28] Though porosity is an important property, it is important to have inorganic connectivity in the structure for stability and many important physical properties. Our particular interest is in the overall dimensionality as well as the inorganic connectivity of the metal benzenedicarboxylates (BDCs). We have carried out a systematic investigation of the compounds formed by zinc, cadmium, lead and lanthanides with the three isomeric benzenedicarboxylic acids in order to examine the structural and dimensional variations caused by the different dispositions of the two carboxylic acid groups, the values of dispersion angles being 60^o, 120^o, 180^o respectively in the 1,2-, 1,3- and 1,4- isomers. We have carried out the synthesis of these BDCs in the presence and absence of 2,2'-bipyridine (2,2'-bipy) or 1,10-phenanthroline (1,10-phen) and tried to examine the role of the amine and the water molecules on the dimensionality of the BDCs. The study has enabled us to arrive some generalizations on the factors determining the dimensionality of the BDCs. More importantly, we have examined the mode of evolution of the three-dimensional structures of the BDCs and have been able to show how a one-dimensional chain may be a precursor of the three-dimensional structure.

2.2. Scope of the present investigations

In order to design novel hybrid frameworks with potential applications, it is necessary to understand the geometrical preferences of the linkers (ligands) and the coordination preferences of the metal cations. The main aim of the present study was to understand structural aspects of hybrid dicarboxylate frameworks in terms of dimensionality modulation and extended inorganic connectivity. For the purpose of a systematic study, we have employed the three isomeric (1,2-, 1,3- and 1,4-) benzenedicarboxylic acids to synthesize coordination polymers and hybrid

frameworks with extended inorganic connectivity of Zn, Cd, Pb and lanthanides with or without chelating amines. Understanding of their structural chemistry will assist in the rational design of novel materials.

2.2.1. Coordination Polymers of Metal Benzenedicarboxylates

Hybrid inorganic-organic metal benzenedicarboxylates with zero inorganic connectivity (***I^{0}O^y***, ***y = 1*** to ***3***) have been synthesized. These coordination polymers are the three isomeric benzenedicarboxylates (1,2-, 1,3- and 1,4-) of Zn, Cd, Pb and lanthanides with or without chelating amines.

(a) Metal dicarboxylates with chelating amines

Six one-dimensional (***I^{0}O^1***) coordination polymers [with zero inorganic connectivity (***I^{0}O^1***)] of metal 1,2-benzenedicarboxylates with 1,10-phenanthroline or 2,2'-bipyridine as the chelating amines have been obtained. [Zn(H_2O)(1,2-BDC)(1,10-phen)].H_2O, **I**, and [Cd(H_2O)(1,2-BDC)(2,2'-bipy)], **II**, have helical chain structures. [Cd(H_2O)(1,2-BDC)(1,10-phen)], **III**, has a one-dimensional ribbon like structure, which contains four-membered rings and the **$^2D_2$** dimers. [Description of dimer SBUs and terminology are given in the appendix {see Appendix. 2.7(a)}]. [Y_2(1,2-BDC)$_3$(1,10-phen)$_2$]·H_2O, **IV**, is also a one-dimensional structure but with two types of dimers (**$^2D_0$ & $^4D_2$**) related to the paddlewheel SBU. [Y_2(1,2-BDC)$_3$(1,10-phen)], **V**, has a one-dimensional structure with two types of paddlewheel dimer SBUs (**$^4D_0$ & $^4D_2$**). [Dy_2(1,2-BDC)$_3$(1,10-phen)], **VI**, has a one-dimensional structure with two types of eight-membered ring dimer SBUs (**$^2D_0$ & $^2D_2$**).

Four 1,3-benzenedicarboxylates of lanthanides with 1,10-phenanthroline or 2,2'-bipyridine as the chelating amines have been obtained. Two of them, [Y_2(1,3-BDC)$_3$(2,2'-bipy)$_2$], **VII**, and [Nd_2(1,3-BDC)$_3$(1,10-phen)$_2$], **X**, have two-

dimensional (***I*^{0}*O*^{2}**) augmented square lattice structure while the other two, [Y_2(1,3-BDC)$_3$(2,2'-bipy)$_2$]·H_2O, **VIII**, and [Y_2(1,3-BDC)$_3$(1,10-phen)$_2$], **IX**, have three-dimensional (***I*^{0}*O*^{3}**) augmented $CdSO_4$ structure. These structures contain dimers of paddle wheel or paddle wheel related SBUs.

[Cd(1,4-BDC)(1,10-phen)].H_2O, **XI**, has a two-dimensional layer structure (***I*^{0}*O*^{2}**). The two chelating 1,10-phen molecules in each dimeric unit project into opposite sides of the layer, thereby preventing the formation of a three-dimensional interpenetrating network of the 1,4-BDC.

Two heteroleptic benzenedicarboxylates of yttrium coordination polymers, [Y_2(1,2-BDC)$_2$(1,3-BDC)(1,10-phen)$_2$], **XII**, and [Y_2(1,2-BDC)$_2$(1,4-BDC)(1,10-phen)$_2$], **XIII**, have similar two-dimensional structures of the type (***I*^{0}*O*^{2}**), where ladders formed by the (**^{2}D$_0$**) dimers and the 1,2-BDC anions are connected by the 1,4-BDC anions in to the layer structure. [$La_2(H_2O)_2$(1,2-BDC)$_2$(1,4-BDC)(1,10-phen)$_2(H_2O)_2$]·H_2O, **XIV**, has a three-dimensional structure with zero inorganic connectivity (***I*^{0}*O*^{3}**), where ladders formed by the (**^{2}D$_2$**) dimers and the 1,2-BDC anions are cross-linked by the 1,4-BDC anions in to the three-dimensional structure.

(b) Metal dicarboxylates without chelating amines

Two heteroleptic benzenedicarboxylates without any chelating amines, **XV** and **XVI**, have been obtained with three-dimensional structure (***I*^{0}*O*^{3}**) with the same formula, [M_2(1,2BDC)$_2$(1,4BDC)$(H_2O)_4$], (For **XV**, M = La, Pr and for **XVI**, Gd, Dy, and Y). Both these structures contain layers formed by the dimers and the 1,2-BDC anions, which are cross-linked by the 1,4-BDC anions in to the three-dimensional structure but they differ in their dimers (**^{3}D$_2$** for **XV** and **^{2}D$_0$** for **XVI**). The two dimensional Gd phthalate, [Gd_2(1,2-BDC)$_4(H_2O)_2$].(H_2Pip), **XVII**,

templated by protonated piperazine contains $^{2}\mathbf{D_0}$ dimer SBUs connected by the 1,2-BDC anions. $(OPb_4)(1,3\text{-}BDC)_3(H_2O)$, **XVIII**, has a three-dimensional structure with zero inorganic connectivity ($\boldsymbol{I^0O^3}$). It has (2,8) 3D-periodic net topology, where hexanuclear SBUs are connected by the 1,3-BDC anions.

2.2.2. Hybrid Networks of Metal Benzenedicarboxylates with Extended Inorganic Connectivity

(a) Metal 1,2-benzenedicarboxylates with chelating amines

Two hybrid frameworks of metal benzenedicarboxylates with extended inorganic connectivity were obtained with chelating amines. $[M_3(1,2\text{-}BDC)_4(1,10\text{-}phen)_3(H_2O)]\cdot 0.5H_2O$, **XIX**, and $[M_3(1,2\text{-}BDC)_4(1,10\text{-}phen)_2(NO_3)]\cdot H_2O$, **XX,** (where M = La and Pr) have a one-dimensional structure with one-dimensional inorganic connectivity ($\boldsymbol{I^1O^0}$). Compound **XIX** has two types of dimer SBUs ($^{3}\mathbf{D_2}$ & $^{2}\mathbf{D_1}$), and **XX** has three types of dimer SBUs ($^{2}\mathbf{d_2}$, $^{2}\mathbf{D_2}$ & $^{3}\mathbf{D_2}$). Eu and Tb doped compounds of **XIX** exhibit the lanthanide-centered red and green emissions respectively at room temperature, sensitized by the ligands.

(b) Metal benzenedicarboxylates without chelating amines

Five hybrid frameworks of metal benzenedicarboxylates with extended inorganic connectivity were obtained without chelating amines. Two polymorphs of the same formula, $M_2(1,2\text{-}BDC)_3(H_2O)$, (Y=**XXI**, and Dy= **XXII**), have been obtained with two-dimensional structure with one-dimensional inorganic connectivity ($\boldsymbol{I^1O^1}$). Though the inorganic connectivity and the M…M interaction within the layer are different, the interlayer $\pi\ldots\pi$ interactions appear to be similar for these two structures. $[Pr_2(1,2\text{-}BDC)_2(PipDPDA)]$, **XXIII**, (where PipDPDA = N,N'-Piperazine diphthalidodiamide dianion and generated *in-situ* under

hydrothermal conditions) has a two-dimensional structure ($\boldsymbol{I^1O^1}$) with one-dimensional inorganic connectivity ($\boldsymbol{I^1O^1}$), where infinite Pr-O-Pr chains, made up of ($^4\mathbf{D_2}$) dimers and connected by the PipDPDA anions into the layer structure. The isophthalate, [Cd(1,3-BDC)(H_2O)], **XXIV**, has a two-dimensional structure ($\boldsymbol{I^1O^1}$), where infinite Cd-O-Cd chains, made up of ($^2\mathbf{D_2}$) dimers are connected by the 1,3-BDC anions in to the layer structure. The terephthalate, Pb(1,4-BDC), **XXV**, has a three-dimensional structure with two-dimensional inorganic connectivity ($\boldsymbol{I^2O^1}$), where the infinite two-dimensional Pb-O-Pb layers of the $\boldsymbol{I^2O^0}$ type, with a (3,6) 2D-net topology are connected by the 1,4-BDC anions into the three-dimensional structure.

2.2.3. Process of Formation of a Three-dimensional Zinc Terephthalate

To understand the process of formation of a three-dimensional zinc terephthalate, we have carried out a systematic time and temperature dependent transformation study on zinc terephthalates. These studies show that the transformation of a one-dimensional structure to a three-dimensional structure and the possible presence of a dimensional hierarchy.

2.3. Experimental

2.3.1. Synthesis

The metal dicarboxylates were synthesized under hydrothermal conditions by heating homogenized reaction mixtures in a 23 or 7ml PTFE-lined bomb in the temperature range 150 - 200 °C for 72 h under autogeneous pressure. The pH of the starting reaction mixture was generally in the range 5-7. The pH after the reaction did not show appreciable change. The products of the hydrothermal

reactions were vacuum-filtered and dried under ambient conditions. The starting compositions and synthetic conditions for the different compounds synthesized by us are given in Tables 2.1-2.4. All the compounds were obtained as single phase, except few. Crystals of **VII** and **VIII** were obtained admixed with small quantities of polycrystalline powder of each other. Crystals of **XVIII** were obtained admixed with small quantities of polycrystalline powder of an unknown compound. The crystals were separated under a polarizing microscope and used for all the characterization. In syntheses, where 1,2-dicyanobenzene (1,2-DCB) was used, it has been hydrolyzed under the hydrothermal synthesis conditions to give rise to phthalic acid. Similar cases of *in-situ* hydrolysis were reported earlier also.[29-31]

2.3.2. Characterization

Infrared (IR) spectra of KBr pellets of the compounds were recorded in the mid IR region (Bruker IFS-66v). Compounds show characteristic bands for the functional groups.[32-34] The bands around 1550 and 1400 cm^{-1} are assigned to carboxylate $\nu_{as\ C=O}$ and $\nu_{s\ C=O}$ stretching and the absence of a band at 1700 cm^{-1} confirms the binding of carboxylate group to the lead cation. The bands around 3550 ($\nu_{as\ O-H}$), 3470 ($\nu_{s\ O-H}$), indicates the presence of water molecules. IR spectra of **IV** (a) and **IX** (b) are given in Fig 2.3.1 as representative examples.

Thermogravimetric analysis (TGA) was carried out (Metler-Toledo) in oxygen atmosphere (flow rate = 50 ml/min) in the temperature range 25 to 800 °C (heating rate = 5 °C/min). Analyses show single or multistep weight losses in these compounds. The total weight loss matches very well with the loss of CO_2, with or without H_2O and the formation of M_xO_y in all the cases. TGA plots of **IV** (a) and **IX** (b) are given in Fig 2.3.2 as representative examples.

The UV-VIS spectra was recorded on a Perkin-Elmer spectrometer (lamda-900) equipped with a double beam set-up employing a halogen lamp (150 watt) as the source and a photo-multiplier tube as the detector. The spectrum was recorded in the solid state using the diffuse reflectance mode. For the photoluminescence studies, a Perkin-Elmer spectrometer (LS-55) with a single beam set-up was employed using a xenon lamp (50 watt) as the source and a photo-multiplier tube as the detector. The experiment was carried out in the solid state at room temperature in the fluorescence mode with a scan speed of 200 nm/min.

A suitable single crystal of each compound was carefully selected under a polarizing microscope and glued to a thin glass fiber. Crystal structure determination by X-ray diffraction was performed on a Bruker-Nonius diffractometer with Kappa geometry attached with an APEX - II-CCD detector and a graphite monochromator for the X-ray source (Mo Kα radiation, $\lambda = 0.71073$Å) operating at 50 kV and 30 mA. An empirical absorption correction based on symmetry equivalent reflections was applied using the SADABS program.[35] The structure was solved and refined using SHELXTL-PLUS suite of program.[36] For the final refinement the hydrogen atoms on the cyclohexane rings were placed geometrically and held in the riding mode. The hydrogen atoms on the water molecules were located in the difference Fourier map and the O-H distance was constrained to 0.85 Å. Final refinement included atomic positions for all the atoms, anisotropic thermal parameters for all the non-hydrogen atoms and isotropic thermal parameters for the hydrogen atoms. All the hydrogen atoms were included in the final refinement, except few. The hydrogen atoms of a water molecule in these few compounds could not be located in the difference Fourier map. Details of the structure solution and final refinements for the compounds **I** to **XXV** are given

in Tables 2.5-2.11. Atomic coordinates for the compounds **I** to **XXV** are given in the appendix (see 2.7. Appendix, Tables A2.1-A.2.25).

Powder XRD patterns of the products were recorded using Cu Kα radiation (Rich-Seifert, 3000TT). The patterns agreed with those calculated for single crystal structure determination. Simulated and experimental powder XRD patterns of **IV** (a) and **IX** (b) are given in Fig 2.3.3 as representative examples.

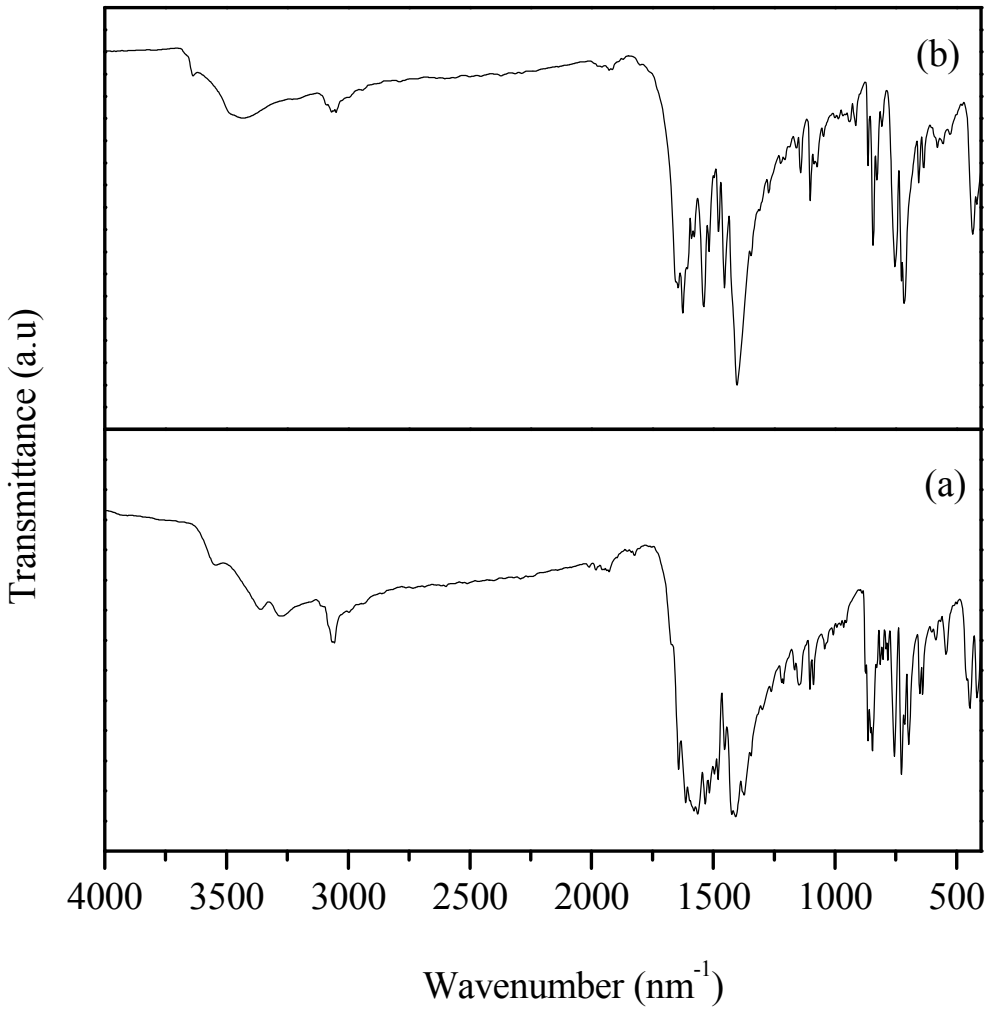

Fig. 2.3.1. IR spectra of **IV** (a) and **IX** (b).

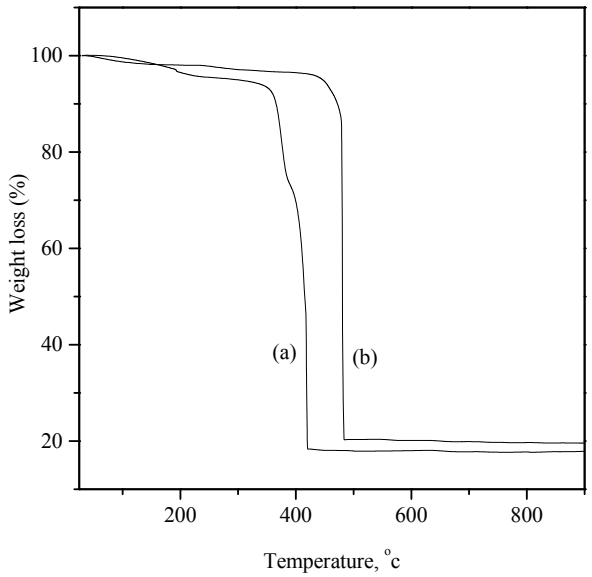

Fig. 2.3.2. TGA plots of **IV** (a) and **IX** (b).

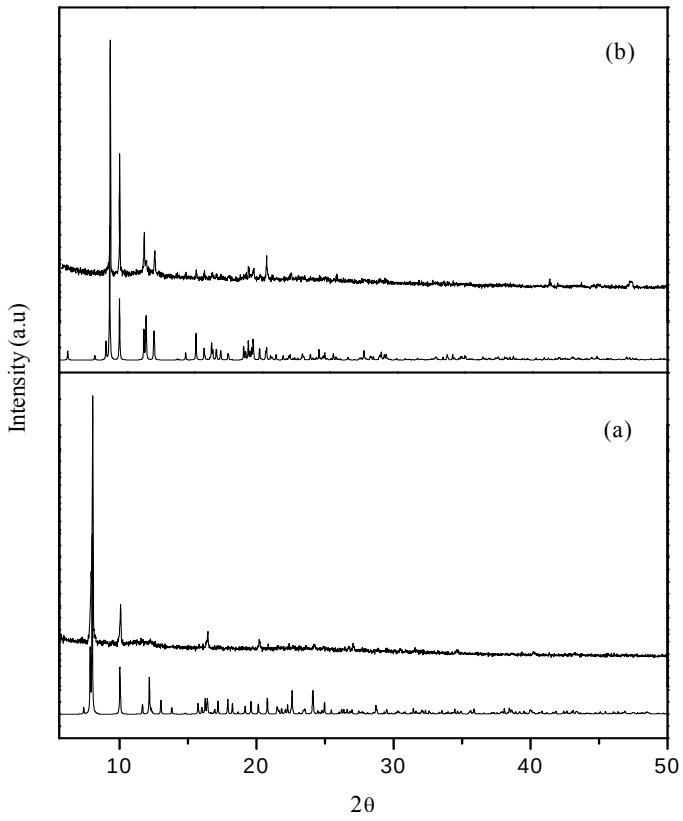

Fig. 2.3.3. Simulated and experimental powder XRD patterns of **IV** (a) and **IX** (b).

Table 2.1

Compound No.	Formula	Composition					Temperature, ºC
		Metal salt	Acid	Additive 1	Additive 2	Water	
I	$[Zn(H_2O)(1,2\text{-BDC})(1,10\text{-phen})].H_2O$	$Zn(OAc)_2 \cdot 2H_2O$ (1mmol)	$1,2\text{-}H_2BDC$ (1mmol)	1,10-phen (1mmol)	NaOH (2 mmol)	H_2O (278mmol)	180
IIA	$[Cd(H_2O)(1,2\text{-BDC})(2,2'\text{-bipy})]$	$Cd(OAc)_2 \cdot 2H_2O$ (1mmol)	$1,2\text{-}H_2BDC$ (1mmol)	2,2'-bipy (1mmol)	Piperidine (1mmol)	H_2O (278mmol)	180
IIB					Piperidine (2mmol)		
III	$[Cd(H_2O)(1,2\text{-BDC})(1,10\text{-phen})]$	$Cd(OAc)_2 \cdot 2H_2O$ (1mmol)	$1,2\text{-}H_2BDC$ (1mmol)	1,10-phen (1mmol)	NaOH (2 mmol)	H_2O (278mmol)	180
IV	$[Y_2(1,2\text{-BDC})_3(1,10\text{-phen})_2] \cdot H_2O$	$Y(NO_3)_3$ (1mmol)	$1,2\text{-}H_2BDC$ (2mmol)	1,10-phen (3mmol)	NaOH (3 mmol)	H_2O (278mmol)	180
V	$[M_2(1,2\text{-BDC})_3(1,10\text{-phen})]$, (M = Y, Gd and Dy)	$Y(NO_3)_3$ (1mmol)	$1,2\text{-}H_2BDC$ (2mmol)	1,2-DCB (1mmol)	1,10-phen (1 mmol) & Piperazine (1mmol)	H_2O (278mmol)	180
VI	$[Dy_2(1,2\text{-BDC})_3(1,10\text{-phen})]$	$Dy(NO_3)_3$ (1mmol)	$1,2\text{-}H_2BDC$ (2mmol)	1,10-phen (1mmol)	DABCO (2mmol)	H_2O (278mmol)	180

Table 2.2

Compound No.	Formula	Composition					Temperature, ºC
		Metal salt	Acid	Additive 1	Additive 2	Water	
VII	$[M_2(1,3\text{-BDC})_3(2,2'\text{-bipy})_2]$, (M = Y, Gd and Dy)	$M(NO_3)_3$ (1mmol)	1,3-H_2BDC (2mmol)	2,2'-bipy (3mmol)	Piperidine (3mmol)	H_2O (278mmol)	180
VIII	$[M_2(1,3\text{-BDC})_3(2,2'\text{-bipy})_2]\cdot H_2O$ (M = Y, Gd and Dy)	$M(NO_3)_3$ (1mmol)	1,3-H_2BDC (2mmol)	2,2'-bipy (3mmol)	Piperazine (3 mmol)	H_2O (278mmol)	180
IX	$[Y_2(1,3\text{-BDC})_3(1,10\text{-phen})_2]$	$Y(NO_3)_3$ (1mmol)	1,3-H_2BDC (2mmol)	1,10-phen (3mmol)	NaOH (3 mmol)	H_2O (278mmol)	180
X	$[Nd_2(1,3\text{-BDC})_3(1,10\text{-phen})_2]$	$Nd(NO_3)_3$ (1mmol)	1,3-H_2BDC (2mmol)	1,10-phen (2mmol)	TMA-OH (5 mmol)	H_2O (278mmol)	180
XI	[Cd(1,4-BDC) (1,10-phen)].H_2O	$Cd(OAc)_2\cdot 2H_2O$ (1mmol)	1,2-H_2BDC (1mmol)	1,10-phen (1mmol)	-	H_2O (278mmol)	180

TMA-OH = Tetramethylammonium hydroxide

Table 2.3

Compound No.	Formula	Composition					Temperature, ºC
		Metal	Acid	Additive 1	Additives 2…	Water	
XII	$[Y_2(1,2\text{-BDC})_2(1,3\text{-BDC})(1,10\text{-phen})_2]$	$Y(NO_3)_3$ (1mmol)	1,3-H_2BDC (1mmol)	1,2-DCB (1mmol)	1,10-phen (1 mmol) & NaOH (2 mmol)	H_2O (278mmol)	180
XIII	$[Y_2(1,2\text{-BDC})_2(1,4\text{-BDC})(1,10\text{-phen})_2]$	$Y(NO_3)_3$ (1mmol)	1,4-H_2BDC (1mmol)	1,2-DCB (1mmol)	1,10-phen (1 mmol) & NaOH (2 mmol)	H_2O (278mmol)	180
XIV	$[Pr_2(1,2\text{-BDC})_2(1,4\text{-BDC})(1,10\text{-phen})_2(H_2O)_2]\cdot H_2O$	$Pr(NO_3)_3$ (0.3mmol)	1,4-H_2BDC (0.3mmol)	1,2-DCB (0.3mmol)	1,10-phen (0.3 mmol) & NaOH (0.6 mmol)	H_2O (111mmol)	180
XV	$[M_2(1,2\text{BDC})_2(1,4\text{BDC})(H_2O)_4]$, (M = La and Pr)	$M(NO_3)_3$ (1mmol)	1,4-H_2BDC (1mmol)	1,2-DCB (1mmol)	NaOH (2 mmol)	H_2O (278mmol)	180
XVI	$[M_2(1,2\text{BDC})_2(1,4\text{BDC})(H_2O)_4]$, (M = Gd, Dy, and Y)	$M(NO_3)_3$ (1mmol)	1,4-H_2BDC (1mmol)	1,2-DCB (1mmol)	NaOH (2 mmol)	H_2O (278mmol)	180
XVII	$[Gd_2(1,2\text{-BDC})_4(H_2O)_2].(H_2Pip)$	$Gd(NO_3)_3$ (1mmol)	1,2-H_2BDC (2mmol)	1,10-phen (1mmol)	Piperazine (2 mmol)	H_2O (278mmol)	180
XVIII	$(OPb_4)(1,3\text{-BDC})_3(H_2O)$	$Pb(NO_3)_3$ (1mmol)	1,3-H_2BDC (0.5mmol)	-	Piperazine (0.5 mmol)	H_2O (278mmol)	150

1,2-DCB = 1,2-dicyanobenzene

Table 2.4

Compound No.	Formula	Composition					Temperature, ºC
		Metal salt	Acid	Additive 1	Additive 2	Water	
XIX	$[M_3(1,2\text{-BDC})_4(1,10\text{-phen})_3(H_2O)]\cdot 0.5H_2O$, (M = La and Pr)	$M(NO_3)_3$ (1mmol)	1,2-H_2BDC (2mmol)	1,10-phen (2mmol)	TMA-OH (5 mmol)	H_2O (278mmol)	180
XX	$[M_3(1,2\text{-BDC})_4(1,10\text{-phen})_2(NO_3)]\cdot H_2O$, (M = La and Pr)	$M(NO_3)_3$ (1mmol)	1,2-H_2BDC (1mmol)	1,2-DCB (1mmol)	1,10-phen (1 mmol) & Piperazine (1mmol)	H_2O (278mmol)	180
XXI	$Y_2(1,2\text{-BDC})_3(H_2O)$	$Y(NO_3)_3$ (1mmol)	1,2-H_2BDC (2mmol)	-	NaOH (6 mmol)	H_2O (278mmol)	180
XXII	$Dy_2(1,2\text{-BDC})_3(H_2O)$	$Dy(NO_3)_3$ (1mmol)	1,2-H_2BDC (2mmol)	1,10-phen (2mmol)	NaOH (1 mmol)	H_2O (278mmol)	200
XXIII	$[M_2(1,2\text{-BDC})_2(PipDPA)]$, (M = La and Pr)	$M(NO_3)_3$ (0.3mmol)	1,2-H_2BDC (0.6mmol)	2,2'-bipy (0.6mmol)	Piperazine (0.6 mmol)	H_2O (111mmol)	180
XXIV	$[Cd(1,3\text{-BDC})(H_2O)]$	$Cd(OAc)_2\cdot 2H_2O$ (1mmol)	1,3-H_2BDC (1mmol)	-	1,2-DAP (1mmol)	H_2O (278mmol)	180
XXV	[Pb(1,4-BDC)]	$Pb(NO_3)_3$ (1mmol)	1,4-H_2BDC (0.5mmol)	-	Piperazine (0.5 mmol)	H_2O (278mmol)	150

1,2-DCB = 1,2-dicyanobenzene; TMA-OH = Tetramethylammonium hydroxide;
1,2-DAP =1,2-diaminopropane

Table 2.5. Crystal data and structure refinement parameters for **I-III**.

Structure parameter	**I**	**IIA**	**IIB**	**III**
Empirical formula	$C_{20}H_{16}ZnN_2O_6$	$C_{18}H_{14}CdN_2O_5$	$C_{18}H_{14}CdN_2O_5$	$C_{40}H_{26}Cd_2N_4O_9$
Formula weight	445.75	450.71	450.71	929.47
Crystal system	Monoclinic	Monoclinic	Orthorhombic	Monoclinic
Space group	$P2_1/n$, (no. 14)	$P2_1/n$, (no. 14)	$Pna2_1$, (no. 33)	C2/c, (no. 15)
a /Å	9.6430 (0)	9.8105(2)	10.4092(2)	22.1574(4)
b /Å	8.9796(1)	9.9054(2)	19.7245(5)	10.1982(2)
c /Å	21.4183(3)	17.7854(2)	8.4632(2)	30.7709(2)
β /°	90.7590(10)	101.7710(10)	90	102.3600(10)
V /Å^3	1854.45(3)	1691.99(5)	1737.63(7)	6792.00(19)
Z	4	4	4	8
D (calc) /gcm^{-3}	1.596	1.769	1.723	1.822
μ /mm^{-1}	1.366	1.323	1.289	1.320
Total data collected	7392	6704	6895	13674
Unique data	2648	2435	2406	4864
Observed data [$I > 2\sigma(I)$]	2364	2008	2318	4077
R_{merg}	0.0191	0.0321	0.0242	0.0295
R indexes [$I > 2\sigma(I)$]	$R_1 = 0.0261$[a]; $wR_2 = 0.0701$[b]	$R_1 = 0.0257$[a]; $wR_2 = 0.0651$[b]	$R_1 = 0.0160$[a]; $wR_2 = 0.0369$[b]	$R_1 = 0.0268$[a]; $wR_2 = 0.0614$[b]
R indexes [all data]	$R_1 = 0.0306$[a]; $wR_2 = 0.0723$[b]	$R_1 = 0.0356$[a]; $wR_2 = 0.0690$[b]	$R_1 = 0.0169$[a]; $wR_2 = 0.0372$[b]	$R_1 = 0.0372$[a]; $wR_2 = 0.0659$[b]

[a] $R_1 = \Sigma ||F_0|-|F_c|| / \Sigma |F_0|$; [b] $wR_2 = \{\Sigma[w(F_0^2 - F_c^2)^2] / \Sigma[w(F_0^2)^2]\}^{1/2}$. $w = 1/[\sigma^2(F_0)^2 + (aP)^2 + bP]$, $P = [\max.(F_0^2,0) + 2(F_c)^2]/3$, where $a = 0.0383$ and $b = 1.2413$ for **I**, $a = 0.0368$ and $b = 0.1976$ for **IIA**, $a = 0.0171$ and $b = 0.0$ for **IIB** and $a = 0.0247$ and $b = 10.2529$ for **III**.

.

Table 2.6. Crystal data and structure refinement parameters for **IV** - **VI**

Structure parameter	**IV**	**V**	**VI**
Empirical formula	$C_{48}H_{30}Y_2N_4O_{13}$	$C_{36}H_{20}Y_2N_2O_{12}$	$C_{36}H_{20}Dy_2O_{12}N_2$
Formula weight	1048.58	3280.62	997.54
Crystal system	Triclinic	Triclinic	Triclinic
Space group	P-1 (no. 2)	P-1, (no. 2)	P-1, (no. 2)
a./Å	12.0953(2)	11.5750(3)	10.9683(2)
b /Å	12.8460(2)	11.9321(4)	16.9557(2)
c /Å	15.7650(3)	13.5561(3)	20.3927(3)
α /°	109.62(1)	104.2860(10)	69.5170(10)
β /°	112.231(1)	107.1040(10)	86.4580(10)
γ /°	90.290(1)	107.3490(10)	71.5070(10)
V /Å^3	2111.17(6)	1589.14(8)	3364.13(9)
Z	2	2	2
D (calc) /gcm^{-3}	1.650	1.777	1.970
μ /mm^{-1}	2.811	3.707	4.477
Total data collected	8694	6684	14041
Unique data	5862	4477	9431
Observed data [I > 2σ (I)]	4695	3680	6986
R_{merg}	0.0416	0.0318	0.0578
R indexes [I > 2σ (I)]	$R_1 = 0.0333^a$; $wR_2 = 0.0769^b$	$R_1 = 0.0395^a$; $wR_2 = 0.0935^b$	$R_1 = 0.0502^a$; $wR_2 = 0.1192^b$
R indexes [all data]	$R_1 = 0.0412^a$; $wR_2 = 0.0824^b$	$R_1 = 0.0526^a$; $wR_2 = 0.1009^b$	$R_1 = 0.0662^a$; $wR_2 = 0.1333^b$

[a] $R_1 = \Sigma ||F_0|-|F_c|| / \Sigma |F_0|$; [b] $wR_2 = \{\Sigma[w(F_0^2 - F_c^2)^2] / \Sigma[w(F_0^2)^2]\}^{1/2}$. $w = 1/[\sigma^2(F_0)^2 + (aP)^2 + bP]$, $P = [\max.(F_0^2,0) + 2(F_c)^2]/3$, where $a = 0.00394$ and $b = 0.0$ for **IV**, for $a = 0.0444$ and $b = 0.0$ **V**, and $a = 0.0539$ and $b = 0.0$ for **VI**.

Table 2.7. Crystal data and structure refinement parameters for **VII** - **X**

Structure parameter	**VII**	**VIII**	**IX**	**X**
Empirical formula	$C_{44}H_{28}Y_2N_4O_{12}$	$C_{44}H_{30}Y_2N_4O_{13}$	$C_{48}H_{28}N_4Y_2O_{12}$	$C_{48}H_{28}O_{12}N_4\,Nd_2$
Formula weight	982.54	1000.55	1030.56	1141.22
Crystal system	Triclinic	Monoclinic	Triclinic	Triclinic
Space group	P-1, (no. 2)	C2/c, (no. 15)	P-1, (no. 2)	P-1, (no. 2)
a /Å	11.4060(2)	17.4993(3)	12.352(3)	10.7548(3)
b /Å	11.9991(1)	13.1290	13.105(4)	14.5063(4)
c /Å	16.5355(4)	18.7591(3)	16.560(4)	14.6246(4)
α /°	92.0110(10)	90	81.722(2)	92.8600(10)
β /°	106.7560(10)	111.8950(10)	71.43(2)	104.5960(10)
γ /°	105.9300	90	61.93(2)	97.75
V /Å^3	2067.68(7)	3999.00(10)	2242.1(10)	2179.44(10)
Z	2	4	2	2
D (calc) /gcm^{-3}	1.578	1.662	1.527	1.739
μ /mm^{-1}	2.862	2.963	2.644	2.426
Total data collected	8555	8037	8496	9239
Unique data	5790	2863	5712	6174
Observed data [I > 2σ(I)]	4392	2476	4325	4819
R_{merg}	0.0355	0.0285	0.0432	0.0311
R indexes [I > 2σ(I)]	R_1 = 0.0399[a]; wR_2 = 0.0868[b]	R_1 = 0.0273[a]; wR_2 = 0.0617[b]	R_1 = 0.0460[a]; wR_2 = 0.0948[b]	R_1 = 0.0289[a]; wR_2 = 0.0665[b]
R indexes [all data]	R_1 = 0.0625[a]; wR_2 = 0.0972[b]	R_1 = 0.0353[a]; wR_2 = 0.0653[b]	R_1 = 0.0532[a]; wR_2 = 0.1018[b]	R_1 = 0.0433[a]; wR_2 = 0.0719[b]

[a] $R_1 = \Sigma\,||F_0|-|F_c|| / \Sigma\,|F_0|$; [b] $wR_2 = \{\Sigma[w(F_0^2 - F_c^2)^2] / \Sigma[w(F_0^2)^2]\}^{1/2}$. $w = 1/[\sigma^2(F_0)^2 + (aP)^2 + bP]$, $P = [\max.(F_0^2,0) + 2(F_c)^2]/3$, where a = 0.0354 and b = 0.0 for **VII**, for 0.0287 and b = 4.5321 for **VIII**, a = 0.0372 and b = 0.0 for **IX** and a = 0.0134 and b = 0.0 for **X**.

Table 2.8. Crystal data and structure refinement parameters for **XI** - **XIV**

Structure parameter	**XI**	**XII**	**XIII**	**XIV**
Empirical formula	$C_{40}H_{26}CdN_4O_9$	$C_{48}H_{14}Y_2N_2O_6$	$C_{48}H_{14}Y_2N_2O_6$	$C_{24}H_{17}PrN_2O_8$
Formula weight	931.47	1030.56	1030.56	602.31
Crystal system	Monoclinic	Monoclinic	Monoclinic	Monoclinic
Space group	$P2_1/n$, (no. 14)	$P2_1/n$, (no. 14)	$P2_1/n$, (no. 14)	C2/c, (no. 15)
a /Å	10.4883(2)	7.5167(16)	7.1718(3)	12.6745(3)
b /Å	13.1483(1)	15.328(4)	16.0831(7)	22.8681(6)
c /Å	13.1207(2)	17.540(5)	17.5050(7)	15.4254(4)
β /°	106.6530(10)	90.759(14)	91.479(1)	92.5930(10)
V /Å^3	1733.50(5)	2020.8(9)	2018.44(15)	4466.3(2)
Z	2	4	4	8
D (calc) /gcm^{-3}	1.784	1.661	1.696	1.791
μ /mm^{-1}	1.293	2.928	2.937	2.236
Total data collected	7056	8404	8208	9281
Unique data	2485	2914	2883	3212
Observed data [I > 2σ(I)]	2058	2091	2342	2633
R_{merg}	0.0317	0.0842	0.0392	0.0413
R indexes [I > 2σ(I)]	R_1 = 0.0277[a];	*R*1 = 0.0529a;	*R*1 = 0.0304[a];	R_1 = 0.0258[a];
	wR_2 = 0.0622[b]	*wR*2 = 0.1359[b]	*wR*2 = 0.0593[b]	wR_2 = 0.0572[b]
R indexes [all data]	R_1 = 0.0392[a];	*R*1 = 0.0824[a];	*R*1 = 0.0466[a];	R_1 = 0.0368[a];
	wR_2 = 0.0668[b]	*wR*2 = 0.1479[b]	*wR*2 = 0.0647[b]	wR_2 = 0.0609[b]

[a] $R_1 = \Sigma ||F_0|-|F_c|| / \Sigma |F_0|$; [b] $wR_2 = \{\Sigma[w(F_0^2 - F_c^2)^2] / \Sigma[w(F_0^2)^2]\}^{1/2}$. $w = 1/[\sigma^2(F_0)^2 + (aP)^2 + bP]$, $P = [\max.(F_0^2,0) + 2(F_c)^2]/3$, where a = 0.0253 and b = 1.6834 for **XI**, for a = 0.0848 , b = 0.0 for **XII**, a = 0.0111 and b = 1.7975 for **XIII** and a = 0.0190 and b = 3.4092 for **XIV**.

Table 2.9. Crystal data and structure refinement parameters for **XV** - **XVIII**

Structure parameter	**XV**	**XVI**	**XVII**	**XVIII**
Empirical formula	$C_{24}H_{20}La_2O_{16}$	$C_{12}H_{10}YO_8$	$C_{36}H_{32}Gd_2N_2O_{18}$	$C_{24}H_{14}Pb_4O_{14}$
Formula weight	842.16	371.11	1095.14	1355.15
Crystal system	Triclinic	Triclinic	Monoclinic	Monoclinic
Space group	P-1 (no. 2)	P-1, (no. 2)	$P2_1/n$, (no. 14)	$P2_1/c$, (no. 14)
a /Å	6.2428(2)	6.1272(1)	13.1671(3)	15.2585(4)
b /Å	8.9794(2)	8.8099(3)	13.7336(3)	13.5990(4)
c /Å	25.3905(7)	12.8788(4)	11.3100(1)	14.0418(4)
α /°	88.954(1)	95.060(2)	90	90
β /°	86.896(1)	99.143(1)	115.411(1)	112.584(1)
γ /°	70.920(1)	110.302(2)	90	90
V /Å^3	1343.14(6)	635.97(3)	1847.34(6)	2690.25(13)
Z	2	1	4	4
D (calc) /gcm^{-3}	2.063	1.938	1.969	3.346
μ /mm^{-1}	3.217	4.624	3.644	25.030
Total data collected	5569	2652	7500	49320
Unique data	3748	1773	4023	4918
Observed data [$I > 2\sigma(I)$]	2868	1658	2658	4129
R_{merg}	0.041	0.0165	0.0351	0.0299
R indexes [$I > 2\sigma(I)$]	$R_1 = 0.0351$[a]; $wR_2 = 0.0823$[b]	$R_1 = 0.0401$[a]; $wR_2 = 0.1073$[b]	$R_1 = 0.0238$[a]; $wR_2 = 0.0566$[b]	$R_1 = 0.0211$[a]; $wR_2 = 0.0388$[b]
R indexes [all data]	$R_1 = 0.0519$[a]; $wR_2 = 0.0928$[b]	$R_1 = 0.0436$[a]; $wR_2 = 0.1092$[b]	$R_1 = 0.0238$[a]; $wR_2 = 0.0566$[b]	$R_1 = 0.0321$[a]; $wR_2 = 0.0414$[b]

[a] $R_1 = \Sigma ||F_0|-|F_c|| / \Sigma |F_0|$; [b] $wR_2 = \{\Sigma[w(F_0^2 - F_c^2)^2] / \Sigma[w(F_0^2)^2]\}^{1/2}$. $w = 1/[\sigma^2(F_0)^2 + (aP)^2 + bP]$, $P = [\max.(F_0^2,0) + 2(F_c)^2]/3$, where $a = 0.0089$ and $b = 0.0$ for **XV**, for $a = 0.0737$ and $b = 1.0849$ for **XVI**, $a = 0.0261$ and $b = 0.0$ for **XVII** and $a = 0.0142$, $b = 5.8290$ for **XVIII**.

Table 2.10. Crystal data and structure refinement parameters for **XIX-XXI**.

Structure parameter	**XIX**	**XX**	**XXI**
Empirical formula	$C_{136}H_{84}N_{12}O_{35}La_6$	$C_{112}H_{66}N_{10}O_{39}La_3$	$C_{48}H_{28}O_{26}Y_4$
Formula weight	3280.62	3007.21	1376×31
Crystal system	Triclinic	Triclinic	Triclinic
Space group	$P2_1/n$, (no. 2)	P-1 (no. 2)	P-1 (no. 2)
a./Å	15.9715(1)	12.8146(2)	12.6669 (2)
b /Å	17.7227(2)	13.1192(2)	13.8538 (2)
c /Å	22.4201(3)	17.5359(2)	16.0289 (3)
α /°	90.00	89.1100	75.201 (1)
β /°	103.2090(10)	79.8090(10)	69.012 (1)
γ /°	90.00	65.9370(10)	65.529 (1)
V /Å^3	6178.29(11)	2644.16(7)	2371.28 (7)
Z	4	1	2
D (calc) /gcm^{-3}	1.763	1.889	1.922
μ /mm^{-1}	2.117	2.465	4.943
Total data collected	24949	11111	9745
Unique data	8789	7456	6566
Observed data [I > 2σ (I)]	6314	6019	5252
R_{merg}	0.0601	0.0340	0.0292
R indexes [I > 2σ (I)]	R_1 = 0.0353[a]; wR_2 = 0.0579[b]	R_1 = 0.0330[a]; wR_2 = 0.0701[b]	R_1 = 0.0339[a]; wR_2 = 0.0724b
R indexes [all data]	R_1 = 0.0676[a]; wR_2 = 0.0661[b]	R_1 = 0.0453[a]; wR_2 = 0.0741[b]	$R1$ = 0.0506a; $wR2$ = 0.0805[b]

[a] $R_1 = \Sigma ||F_0|-|F_c|| / \Sigma |F_0|$; [b] $wR_2 = \{\Sigma[w(F_0^2 - F_c^2)^2] / \Sigma[w(F_0^2)^2]\}^{1/2}$. $w = 1/[\sigma^2(F_0)^2 + (aP)^2 + bP]$, $P = [\max.(F_0^2,0) + 2(F_c)^2]/3$, where $a = 0.0184$, $b = 0.0$ for **XIX**, $a = 0.0131$ and $b = 0$ for **XX** and $a = 0.0232$ and $b = 0.8469$ for **XXI**.

Table 2.11. Crystal data and structure refinement parameters for **XXII-XXV**.

Structure parameter	**XXII**	**XXIII**	**XXIV**	**XXV**
Empirical formula	$C_{24}H_{14}Dy_2O_{13}$	$C_{18}H_{12}PrNO_7$	$C_8H_6CdO_5$	$C_8H_4PbO_4$
Formula weight	835.35	495.20	294.53	371.31
Crystal system	Monoclinic	Triclinic	orthorhombic	orthorhombic
Space group	P21/c, (no. 14)	P-1, (no. 2)	Pbcm, (no. 57)	Pbca, (no. 61)
a /Å	7.9529(2)	7.3545(7)	6.5021(1)	7.7475(1)
b /Å	26.4843(6)	9.9774(9)	6.9509(2)	10.2448(2)
c /Å	11.6177(3)	12.0780(11)	18.3199(1)	18.3638(3)
α /°	90	74.103(2)	90.0	90
β /°	106.8630(10)	88.675(2)	90.0	90
γ /°	90	78.7230	90	90
V /Å^3	2341.78(10)	835.48(13)	829.15(11)	1457.56(4)
Z	4	2	4	8
D (calc) /gcm^{-3}	2.369	1.968	2.335	3.384
μ /mm^{-1}	6.407	2.959	2.627	23.121
Total data collected	9772	3527	3106	5320
Unique data	3550	2352	621	1370
Observed data [$I > 2\sigma(I)$]	2985	2146	541	1241
R_{merg}	0.0466	0.0325	0.0374	0.0260
R indexes [$I > 2\sigma(I)$]	$R_1 = 0.0271$[a]; $wR_2 = 0.0643$[b]	$R_1 = 0.0308$[a]; $wR_2 = 0.0750$[b]	$R_1 = 0.0221$[a]; $wR_2 = 0.0610$[b]	$R_1 = 0.0346$[a]; $wR_2 = 0.0908$[b]
R indexes [all data]	$R_1 = 0.0337$[a]; $wR_2 = 0.0661$[b]	$R_1 = 0.0346$[a]; $wR_2 = 0.0760$[b]	$R_1 = 0.0253$[a]; $wR_2 = 0.0626$[b]	$R_1 = 0.0378$[a]; $wR_2 = 0.0920$[b]

[a] $R_1 = \Sigma ||F_0|-|F_c|| / \Sigma |F_0|$; [b] $wR_2 = \{\Sigma[w(F_0^2 - F_c^2)^2] / \Sigma[w(F_0^2)^2]\}^{1/2}$. $w = 1/[\sigma^2(F_0)^2 + (aP)^2 + bP]$, $P = [\max.(F_0^2,0) + 2(F_c)^2]/3$, where $a = 0.0312$, $b = 0.0$ for **XXII**, $a = 0.0348$ and $b = 0$ for **XXIII** $a = 0.0353$ and $b = 0.2568$ for **XXIV** and $a = 0.0254$ and $b = 23.5591$for **XXV**.

2.4. Results and discussion

2.4.1. Coordination polymers of metal benzenedicarboxylates

Hybrid inorganic-organic metal benzenedicarboxylates with zero inorganic connectivity ($\boldsymbol{I^0O^y}$, $\boldsymbol{y = 1}$ to $\boldsymbol{3}$) have been synthesized and characterized. These coordination polymers are the three isomeric benzenedicarboxylates (1,2-, 1,3- and 1,4-) of Zn, Cd, Pb and lanthanides with or without chelating amines.

2.4.1.1 Metal dicarboxylates with chelating amines

(a) 1,2-Benzenedicarboxylates

Six one-dimensional ($\boldsymbol{I^0O^1}$) coordination polymers of metal 1,2-benzenedicarboxylates with 1,10-phenanthroline or 2,2'-bipyridine as the chelating amines have been obtained. Two of them have helical chain structures. The structures of the remaining four compounds can be understood based on the dimer SBUs [see the appendix 2.7(a) for dimer SBU description].

[$Zn(H_2O)$(1,2-BDC)(1,10-phen)].H_2O, **I**, has a helical one-dimensional chain structure ($\boldsymbol{I^0O^1}$). It has an asymmetric unit with 94.5 non-hydrogen atoms (Fig. 2.4.1a). There are one Zn^{2+} cation, a phthalate (1,2-BDC) dianion, a chelating 1,10-phenanthroline molecules, a terminal water molecule and a lattice water molecule in the asymmetric unit. The distorted ZnN_2O_4 octahedra (with one coordinated water and a terminal chelating 1,10-phen) are connected by the two different tridentate carboxylic acid molecules with (1110) connectivity[37]. This connectivity results in a helical chain with a pitch of 8.980 Å, where the neighboring Zn…Zn distance is 5.986 Å. The helical structure (Fig. 2.4.1b) is stabilized in the crystal by weak interchain C-H…π interaction between the 1,10-phen and 1,2-BDC (3.010 Å, 137.9°), the interchain π…π interactions between the

1,10-phen molecules (3.687 to 3.789 Å) and the C-H…O hydrogen bonds between the coordinated water and 1,10-phen (2.424 Å, 170.3°) or 1,2-BDC (2.574 Å, 136.5°). The Zn-O bond distance in **I** ranges from 2.177 to 2.538 Å and the Zn-N bond distances are 2.143 and 2.155 Å.

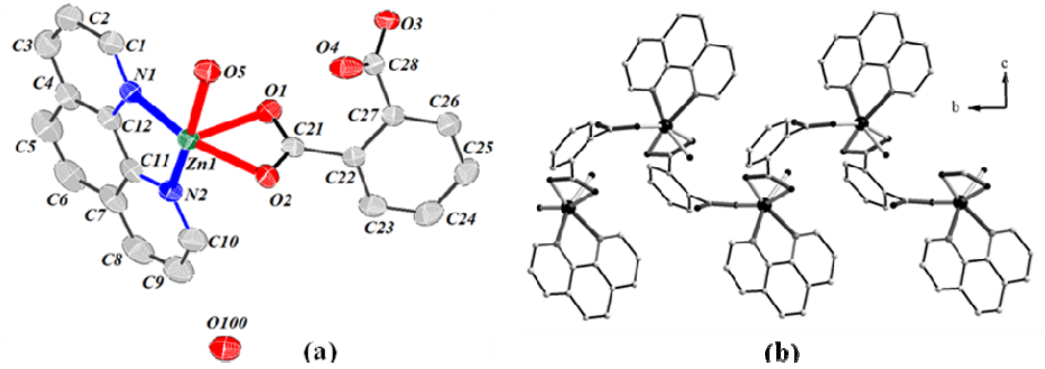

Fig. 2.4.1. (a) ORTEP plot of **I** (Thermal ellipsoids are shown at 50% probability) and (b) 1D helical chain structure of **I**.

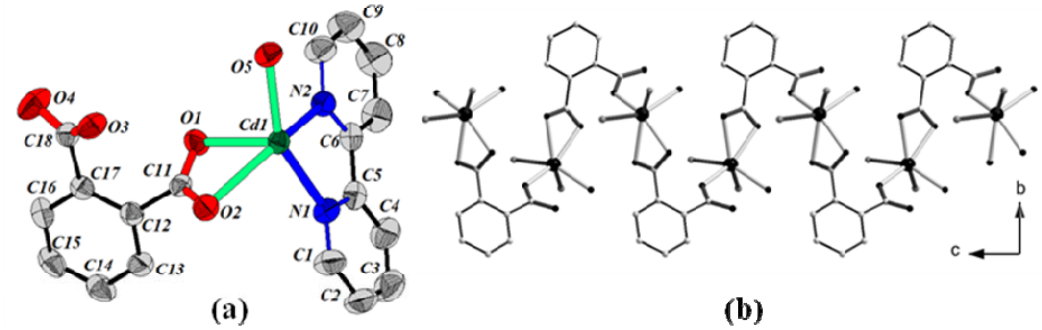

Fig. 2.4.2. (a) ORTEP plot of **II** (Thermal ellipsoids are shown at 50% probability) and (b) 1D helical chain structure of **II** (2,2'-bipy molecules are not shown).

We have been able to isolate a 1,2-BDC of Cd with 2,2'-bipyridine [$Cd(H_2O)$(1,2-BDC)(2,2'-bipy)], **II** in two polymorphic forms, monoclinic (**IIA**) and orthorhombic (**IIB**). Both the polymorphs consist of one-dimensional helical chains formed by distorted CdN_2O_4 octahedra linked by the dicarboxylic acid ($\boldsymbol{I^0O^1}$) (Fig. 2.4.2b). The polymorphs exist as racemic mixtures of right- and left-handed infinite helical one-dimensional chains. The Cd-O bond distance ranges from 2.226 to 2.445 Å in **IIA** and from 2.213 to 2.429 Å in **IIB.** The CdN_2O_4

octahedron coordinates to a terminal 2,2'-bipy and to a water molecule. The remaining three oxygen atoms come from two different carboxylic acid molecules, one with the monodentate and the other with the bidentate carboxylate group. Thus each tridentate carboxylic acid molecule with (1110) connectivity[37], links two cadmium atoms, giving rise to a half turn unit of the helical one-dimensional chain. The neighboring Cd…Cd distances are 5.974 Å and 5.597 Å respectively in **IIA** and **IIB** and the pitches of the helical chains are 9.905 Å and 8.463 Å. These differences arise because of the difference in the dihedral angles between the carboxylate groups in the two polymorphs. The helical structure of **II** is stabilized in the crystal by interchain C-H…π and C-H…O interactions. The interchain C-H…π interactions between the 2,2-bipy and the carboxylic acid rings are 2.983 Å, 139.1° and 2.998 Å, 146.7° respectively in **IIA** and **IIB**, while the interchain C-H…O interactions are 2.211 Å, 161.8° and 2.446 Å, 166.4°. These interactions seem to be stronger in the monoclinic form than in the orthorhombic form. Fig. 2.4.3a and b show packing arrangements in **IIA** and **IIB** respectively.

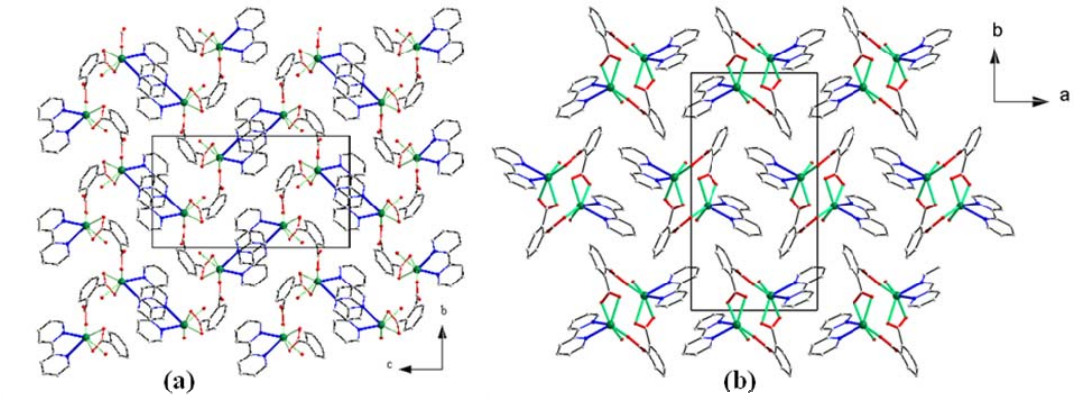

Fig. 2.4.3. (a) Packing arrangement in **IIA** viewed along the *a* axis and (b) packing arrangement in **IIB** viewed along the *c* axis.

Cadmium also forms a 1,2-BDC with 1,10-phen, with a one-dimensional chain structure, the composition being, [Cd(H_2O)(1,2-BDC)(1,10-phen)], **III.** The

asymmetric unit (Fig. 2.4.4a) contains Cd in two crystallographically independent distorted octahedral environments. In the CdN_2O_4 octahedra, the Cd-O bond distance ranges from 2.177 to 2.538 Å and the Cd-N bond distance from 2.343 to 2.391 Å. Sharing of the edges of two similar octahedra gives rise to a dinuclear unit, and two such dinuclear units get connected by four carboxylic acid molecules with two different type of coordination [(1110) and (2110) connectivity], giving rise to a four-membered ring.

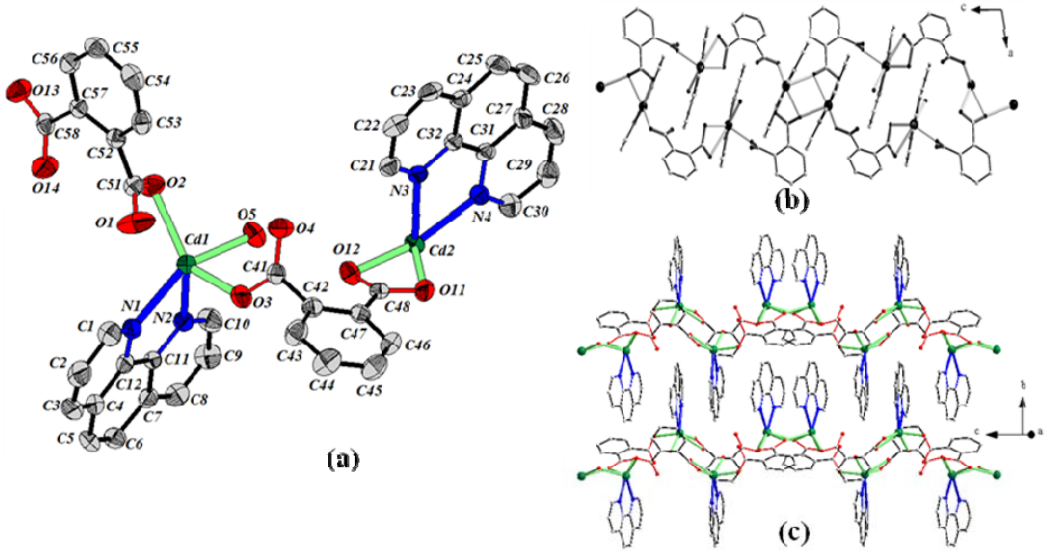

Fig. 2.4.4. (a) ORTEP plot of **III** (Thermal ellipsoids are shown at 50% probability) and (b) 1D ribbon like chain structure of **III** and (c) packing arrangement in **III** viewed along the *a* axis

These rings are connected to each other by the $^{2}\mathbf{D_2}$ dimer SBUs. [Description of dimer SBUs and terminology are given in the appendix {see Appendix. 2.7(a)}] Such a connectivity of these Cd rings yields a ribbon like structure ($\boldsymbol{I^0O^1}$) (Fig. 2.4.4b), stabilized by inter and intra chain π-π stacking interactions (3.476 to 3.651 Å) in the crystal (Fig. 2.4.4c).

The asymmetric unit of $[Y_2(1,2\text{-BDC})_3(1,10\text{-phen})_2]\cdot H_2O$, **IV** consists of 67 non-hydrogen atoms, of which there are two crystallographically distinct Y^{3+} atoms. Six carboxylate oxygen atoms and two nitrogen atoms from the 1,10-

phenanthroline coordinate each Y atom, giving rise to a distorted dodecahedral geometry. The average Y–O distance of 2.334 Å and Y–N distance of 2.522 Å result from this bonding. The Y atoms are connected to the 1,2-BDC through oxygen atoms and to 1,10-phenanthroline through the nitrogen atoms. There are three distinct 1,2-BDC anions with different connectivities [(1211), (1110) and (1111)] to the Y^{3+} ions. The structure of **IV** consists of a linkage between Y^{3+}, 1,10-phenanthroline and 1,2-BDC anions giving rise to one-dimensional chains. The connectivity between YN_2O_6 distorted dodecahedra and the carboxylic acids

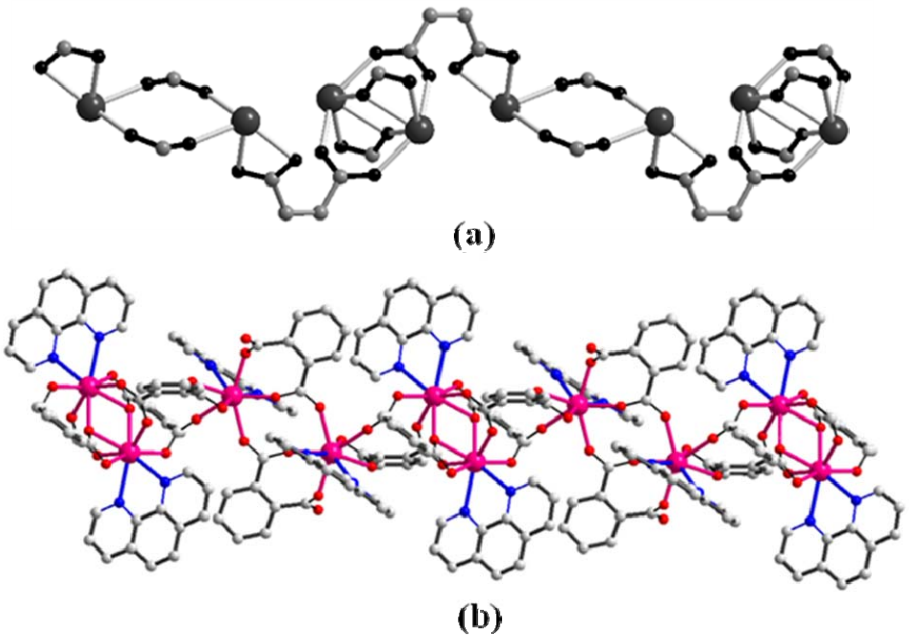

Fig. 2.4.5. (a) Connectivity of dimer SBUs and (b) 1D chain structure in **IV**.

give rise to two different building units. Thus, Y(1) is connected by two carboxylate anions forming a eight-membered ring, $^{2}\mathbf{D_0}$ dimer SBU [Description of dimer SBUs and terminology are given in the appendix {see Appendix. 2.7(a)}], while Y(2) is connected through two three-coordinated (μ_3) oxygen atom, forming a dimer which is further connected by carboxylate units forming a paddle-wheel like $^{4}\mathbf{D_2}$ dimer SBU. The 1,10-phenanthroline molecules, bound to the Y atoms, are situated above and below the plane of the building units. The two SBUs

alternate along the direction of the chain and are connected by the carboxylate moieties (Fig. 2.4.5a, part of the benzene rings are not shown). These connectivities lead to the formation of an infinite one dimensional-structure (***I*^{0}*O*^{1}**) (Fig. 2.4.5b). Due to the close proximity between the 1,10-phenanthroline and the benzene rings considerable π…π interactions have been observed, which may also contribute for the structural stability. The water molecules occupy spaces between the chains.

$[M_2(1,2\text{-BDC})_3(1,10\text{-phen})]$, **V**, (where M = Y, Gd and Dy) has a one-dimensional structure with zero inorganic connectivity (***I*^{0}*O*^{1}**). It has an asymmetric unit with 52 non-hydrogen atoms. There are two M^{3+} cations in two crystallographically distinct positions, three phthalate (1,2-BDC) dianions and a chelating 1,10-phenanthroline molecule in the asymmetric unit. The three BDC anions [acid-1, acid-2 and acid-3] exhibit three different coordination modes with the torsional angle of 20.46(2), 60.47(3) and 43.65 (1)º respectively. They have (1121), (1111) and (1111) connectivities respectively. Acid-1 binds to three M^{3+} cations [one M(1) and two M(2)], acid-2 binds to four M^{3+} cations [two M(1) and two M(2)] and acid-3 binds to three M^{3+} cations [two M(1) and one M(2)]. M(1) is seven-coordinated (MN_2O_5) with five oxygen atoms from five different 1,2-BDC anions and two nitrogen atoms from a chelating 1,10-phenanthroline molecule. All the five oxygen atoms of $M(1)N_2O_5$ are having $\boldsymbol{\mu}_2$ connectivity (one is from the acid-1 and two each from acid-2 and acid-3). These oxygen atoms link two $M(1)N_2O_5$ via four carboxylate moieties into a paddle wheel $^4\mathbf{D_0}$ dimer SBU. The M-O bond lengths are in the 2.266(3) - 2.322(3) Å range for M = Y, 2.307(4) - 2.388(4) Å range for M = Gd and 2.282(4) - 2.301(4) Å range for M = Dy. The M-N bond lengths are 2.504(4) and 2.564(4) Å for M = Y, 2.543(5) and 2.616(5) Å

for M = Gd and 2.522(4) and 2.575(4) Å for M = Dy. M(2) is eight-coordinated (MO_8) with eight oxygen atoms from five different 1,2-BDC anions. Among the six oxygens of MO_8, two oxygen atoms having μ_2 connectivity (connecting a M atom and a C atom) and other two with μ_3 connectivity. These connectivities link two $M(2)O_8$ via two oxygen atoms (μ_3) and two carboxylate moieties, forming another SBU, $^4\mathbf{D_2}$, structurally related to the paddle wheel SBU. The M-O bond lengths are in the 2.298(3) – 2.456(3) Å range for M = Y, 2.337(4) - 2.500(4) Å range for M = Gd and 2.310(3) - 2.474(3) Å range for M = Dy.

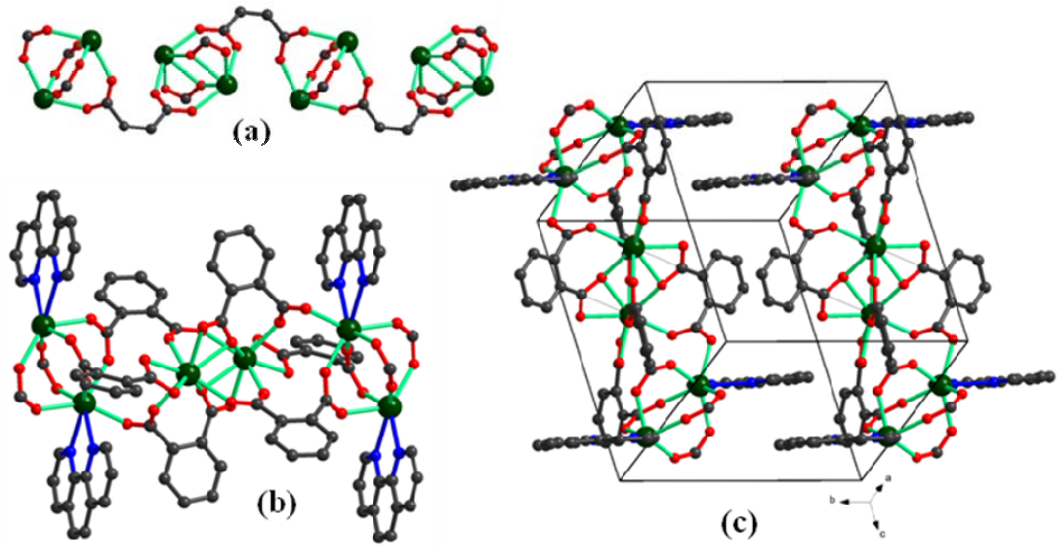

Fig. 2.4.6. (a) Connectivity of dimer SBUs (b) 1D chain structure and (c) packing arrangement in **V**.

The connectivities in these two polyhedra lead to the formation of two different SBUs [M(1) dimer (paddle wheel) - $^4\mathbf{D_0}$ and M(2) dimer - $^4\mathbf{D_2}$]. These two SBUs are connected alternatively (Fig. 2.4.6a) by the six 1,2-BDC anions (two each of acid-1, acid-2 and acid-3) in to an infinite one dimensional-structure ($\boldsymbol{I^0O^1}$) (Fig. 2.4.6b). The chelating 1,10-phenanthroline molecules are projecting out from both side of the $^4\mathbf{D_0}$ SBU and decorating the chain structure. The one-dimensional

chain structure is stabilized by π…π and C-H…π interactions among and between the BDC anions and 1,10-phenanthroline molecules (Fig. 2.4.6c).

$[Dy_2(1,2\text{-BDC})_3(1,10\text{-phen})]$, **VI**, has a one-dimensional structure with zero inorganic connectivity ($\boldsymbol{I^0O^1}$) (Fig. 2.4.7). It has an asymmetric unit with 104 non-hydrogen atoms. There are four Dy^{3+} cations in four crystallographically distinct positions, six phthalate (1,2-BDC) dianions and two chelating 1,10-phenanthroline molecules in the asymmetric unit. The six BDC anions [acid-1 to acid-6] exhibit three different coordination modes with the torsional angle of 45.06(2), 40.46(3), 49.33(4), 45.05(3), 41.43(3) and 43.55(4)º respectively. Acids-1, -2 and -3 have (1121) connectivities, acids-4 and -6 have (1111) connectivities and acid-5 has (1221) connectivities. Every 1,2-BDC anion binds to three Dy^{3+} cations. Acid-1 binds to two Dy(1) and one Dy(2). Acid-2 and -3 binds to one each of Dy(1), Dy(2) and Dy(3). Acid-4 binds to one each of Dy(2), Dy(3) and Dy(4). Acid-5 and -6 binds to one Dy(3) and two Dy(4).

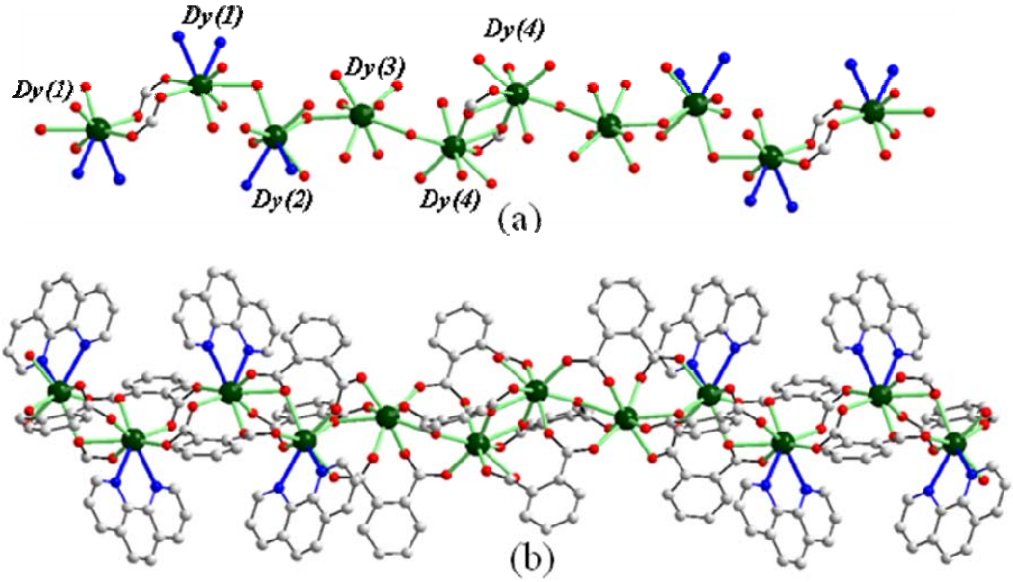

Fig. 2.4.7. (a) Connectivity of dimer SBUs and (b) 1D chain structure in **VI**.

Dy(1) is eight-coordinated (DyN_2O_6) with six oxygen atoms from four different 1,2-BDC anions and two nitrogen atoms from a chelating 1,10-

phenanthroline molecule. Among the six oxygen atoms of $Dy(1)N_2O_6$, four are having $\boldsymbol{\mu}_2$ connectivity and the remaining two are having $\boldsymbol{\mu}_3$ connectivity. Thus $\boldsymbol{\mu}_3$ oxygen atoms link Dy(1) to Dy(2) via an edge. The Dy-O bond lengths are in the 2.286(7) - 2.636(7) Å range. The Dy-N bond lengths are 2.537(9) and 2.578(9) Å. Dy(2) is nine-coordinated (DyN_2O_7) with seven oxygen atoms from four different 1,2-BDC anions and two nitrogen atoms from a chelating 1,10-phenanthroline molecule. Among the seven oxygen atoms of $Dy(2)N_2O_7$, four are having $\boldsymbol{\mu}_2$ connectivity and the remaining three are having $\boldsymbol{\mu}_3$ connectivity. These $\boldsymbol{\mu}_3$ oxygen atoms link Dy(2) to Dy(1) via an edge and to Dy(3) through a corner. The Dy-O bond lengths are in the 2.305(7) - 2.854(7) Å range. The Dy-N bond lengths are 2.522(9) and 2.563(8) Å. Dy(3) is eight-coordinated (DyO_8) with the oxygen atoms from five different 1,2-BDC anions. Among the eight oxygen atoms, six are having $\boldsymbol{\mu}_2$ connectivity and the remaining two are having $\boldsymbol{\mu}_3$ connectivity. These $\boldsymbol{\mu}_3$ oxygen atoms link Dy(3) to Dy(2) and to Dy(4) via two different corners. The Dy-O bond lengths are in the 2.248(8) - 2.686(8) Å range. Dy(4) is also eight-coordinated (DyO_8) with the oxygen atoms from five different 1,2-BDC anions. Among the eight oxygen atoms, five are having $\boldsymbol{\mu}_2$ connectivity and the remaining three are having $\boldsymbol{\mu}_3$ connectivity. These $\boldsymbol{\mu}_3$ oxygen atoms link Dy(4) to an another Dy(4) via edge and to Dy(3) through corner. The Dy-O bond lengths are in the 2.230(8) - 2.459(7) Å range.

The connectivities in these four polyhedra lead to the formation of a linear tetramer of [Dy(1)-Dy(2)-Dy(3)-Dy(4)] sequence. These tetramers are connected at the Dy(4) end (where two Dy(4) polyhedra share an edge, $^2\mathbf{D_2}$ dimer) into a linear octamer (1234-4321) (Fig. 2.4.7a). These sequential octamers are further get

connected at Dy(1) $^2\mathbf{D_0}$ dimer by the 1,2-BDC anions in to an infinite one-dimensional structure ($\boldsymbol{I^1O^0}$) (Fig. 2.4.7b). Chelating 1,10-phenanthroline molecules are projecting out from the chain structure alternatively for every four polyhedra (12-21) in the sequence resulting in a eight continuous M-O-M moieties in the sequence broken periodically by the carboxylate (M-COO-M) moieties. The one-dimensional chain structure is further stabilized by π…π and C-H…π interactions among the BDC anions and 1,10-phenanthroline molecules and also between BDC anions and 1,10-phenanthroline molecules.

(b) 1,3-Benzenedicarboxylates

Four 1,3-benzenedicarboxylates of lanthanides with 1,10-phenanthroline or 2,2'-bipyridine as the chelating amines have been obtained. Two of them have two-dimensional ($\boldsymbol{I^0O^2}$) augmented square lattice structure and the other two have three-dimensional ($\boldsymbol{I^0O^3}$) augmented $CdSO_4$ structure. The structures contain dimers of paddle wheel or paddle wheel related SBUs.

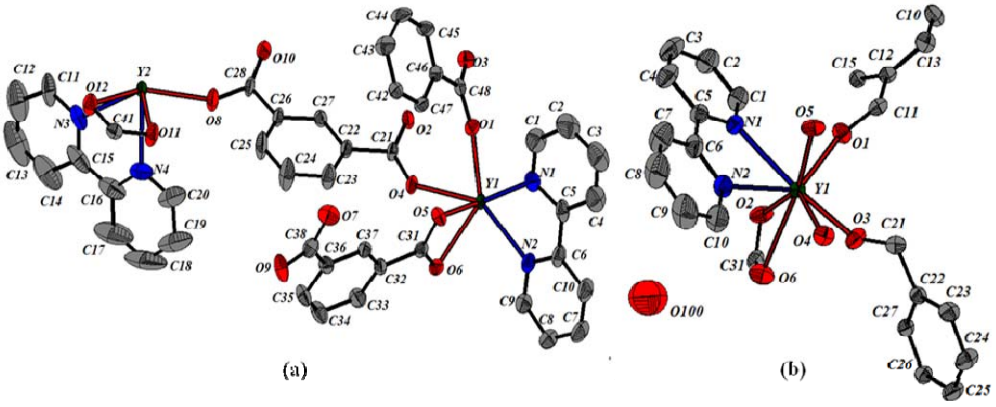

Fig. 2.4.8. ORTEP plot of (a) **VII** and (b) **VIII** (Thermal ellipsoids are shown at 50% probability).

$[M_2(1,3\text{-BDC})_3(2,2'\text{-bipy})_2]$, **VII**, (where M=Y, Gd and Dy), has a two-dimensional augumented square lattice ($\boldsymbol{I^0O^2}$) structure, consists of a network of MO_6N_2 distorted dodecahedral units, chelating 2,2-bipy ligands and 1,3-BDC anions with (1111) connectivity. The dodecahedral units are linked through the

carboxylate anions giving rise to a two-dimensional layered structure with the 2,2'-bipy ligands hanging into the interlamellar spaces from the metal center. The asymmetric unit of **VII** is shown in Fig. 2.4.8a. The M-O bond distances are in the range 2.248(3)-2.478(3) Å (av. 2.348 Å for Y, 2.392 Å for Gd, and 2.359 Å for Dy), and the M-N bond distances have an average distance of 2.572 Å for Y, 2.607 Å for Gd, and 2.574 Å for Dy. The two-dimensional structure can be described based on simple SBUs. Thus, two MO_6N_2 units are connected by the carboxylate anions forming a paddle wheel $^4\mathbf{D_0}$ dimer SBU. The SBU is formed by two M atoms, two 2,2'-bipy ligands and six carboxylate linkers. The two chelating 2,2'-bipy ligands projects out from the SBU. All the six carboxylates linkers have the same type of connectivity with the metal centers. To understand the structure, it is preferable to differentiate the isophthalates as acid-1 and acid-2, respectively. It may be noted that, of the six vertices of the paddle wheel-like SBU, only four vertices are available for bonding with neighboring SBUs as two vertices are bonded to terminal 2,2'-bipy ligands. Thus, each paddle wheel unit is connected to four other paddle wheel units involving six 1,3-BDC anion linkers (two acid-1 and four acid-2). This gives rise to two SBUs being connected by two 1,3-BDC units (acid-2), and the remaining two by one 1,3-BDC unit each (acid-1). This kind of bonding gives rise to a two-dimensional augumented square lattice ($\boldsymbol{I^0O^2}$) structure with apertures (Fig. 2.4.9a). As can be noted, the connectivity resembles the (4,4) net topology commonly observed in many hybrid compounds (Fig. 2.4.10a). The 2,2'-bipy ligands, connected to the M^{3+} ions, project into the interlamellar region, giving rise to considerable intralayer $\pi\cdots\pi$ interactions between the 2,2'-bipy ligands and interlayer $\pi\cdots\pi$ and $CH\cdots\pi$ interactions.

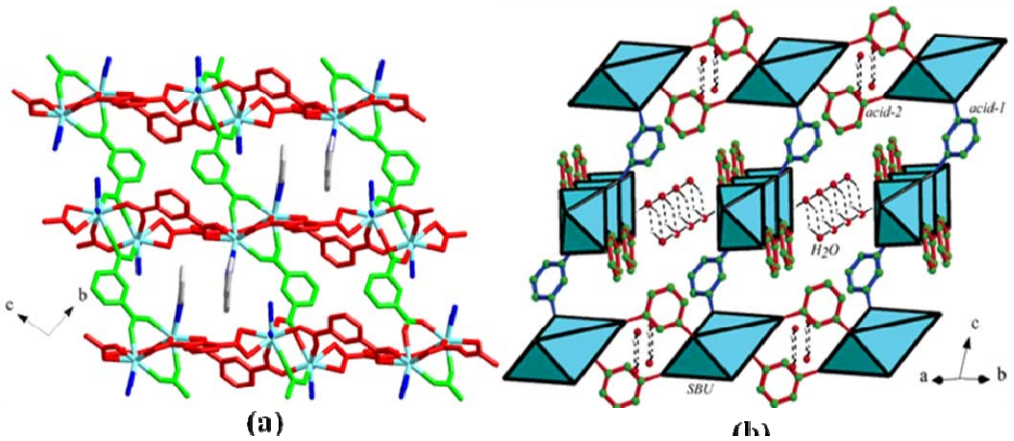

Fig. 2.4.9. (a) 2D structure of **VII** and (b) 3D structure of **VIII** (2,2'-bipy molecules are not shown for clarity).

$[M_2(1,3\text{-BDC})_3(2,2'\text{-bipy})_2]\cdot H_2O$, **VIII**, (where M=Y, Gd and Dy), has a *three-dimensional structure, consists of a network of* MO_6N_2 *distorted* dodecahedral units, 2,2-bipy ligands and 1,3-BDC anions with (1111) connectivity. The asymmetric unit of **VIII** is shown in Fig. 2.4.8b. The M-O bond distances are in the range 2.281(2)-2.543(3) Å (ave 2.352 Å for Y, 2.387 Å for Gd, and 2.366 Å for Dy), and the M-N bond distances have an average distance of 2.558 Å for Y, 2.592 Å for Gd, and 2.566 Å for Dy. The structure of **VIII** also possesses identical paddle wheel like $^4D_0$ dimer SBUs as in **VII**. In **VIII**, the connectivity between the SBUs through the 1,3-BDC units gives rise to layers related to the (4,4) two-dimensional nets. The observed 3-D structure of **VIII**, then, is due to the presence of a second identical 2-D layer in a direction perpendicular to the first layer (Fig. 2.4.10b). The water molecules occupy the channel spaces within the structure (Fig. 2.4.9b). More importantly, strong hydrogen-bond interactions exist between the water molecules giving rise to a pseudo one-dimensional ladder-like arrangement. It is highly likely that the position of the water molecules and its hydrogen-bond interactions with the framework oxygen atoms would have resulted in the formation of a 3-D structure with interpenetrating 2-D layers. This cross-linking of

the (4,4) two-dimensional net gives rise to an unusual arrangement and a novel three-dimensional structure ***(I^0O^3)***. This unique structure can be described as a "Lincoln log" arrangement. Whitesides and co-workers described the mesoscale assembly of polyurethane rods in which adjacent rods lie at right angles to each other as Lincoln logs[38]. This orthogonal stacking of the (4,4) augmented square nets in **VIII** is identical to the $CdSO_4$ network[39-42] (Fig. 2.4.7b). Considerable intralayer $\pi\cdots\pi$ interactions between the 2,2'-bipy ligands and interlayer $\pi\cdots\pi$ and $CH\cdots\pi$ interactions also stabilize the structure.

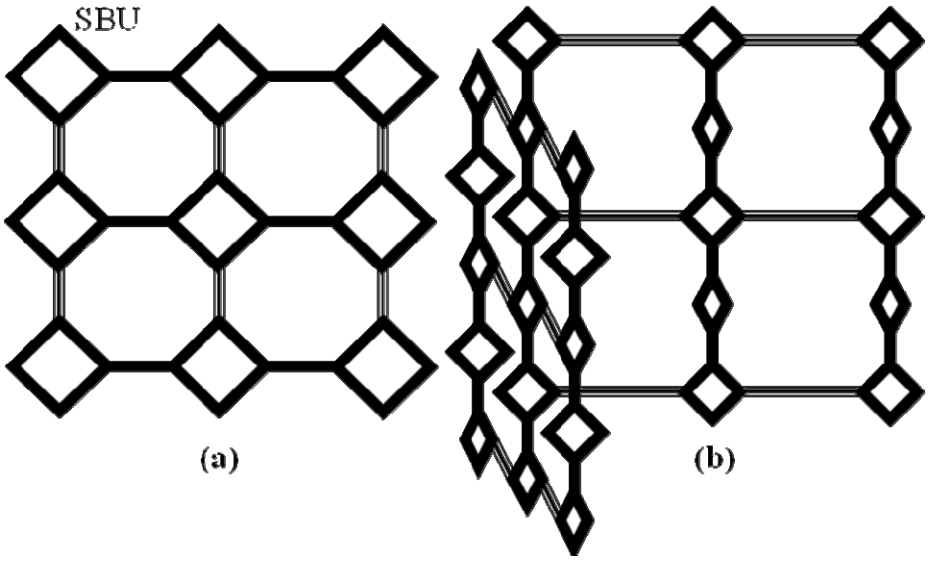

Fig. 2.4.10. Schematic showing the arrangement of the SBU in **VII** and **VIII**. (a) The augmented square lattice and (b) the $CdSO_4$ lattice.

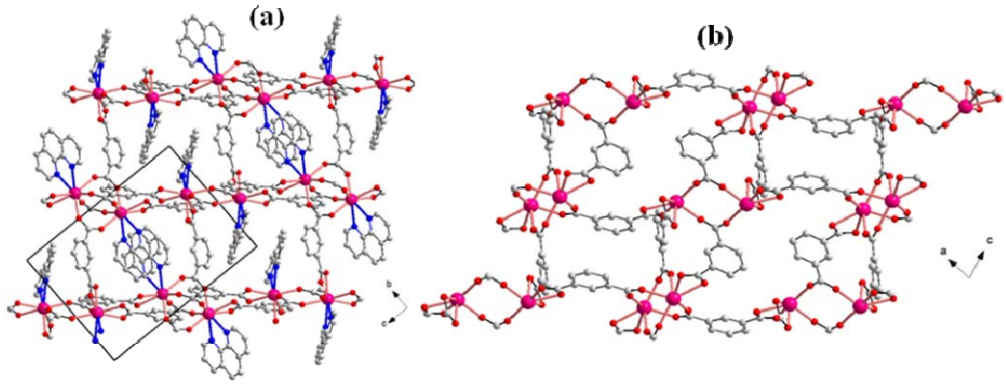

Fig. 2.4.11. Stucture of **IX** viewed (a) along the *a* axis and along (b) the *b* axis.

The three-dimensional $[Y_2(1,3\text{-BDC})_3(1,10\text{-phen})_2]$, **IX**, (Fig. 2.4.11), have an asymmetric unit with 66 non-hydrogen atoms, of which two Y atoms are crystallographically independent. Both the Y atoms have distorted dodecahedral coordination with respect to six carboxylate oxygen atoms and two nitrogen atoms from the 1,10-phenanthroline. The average Y–O distance of 2.336 Å and Y–N distance of 2.554 Å result from this bonding. The Y atoms are connected to the 1,3-BDC through oxygen atoms and to 1,10-phenanthroline through the nitrogen atoms. All the three 1,3-BDC anions have identical connectivity (1111) with the Y^{3+} ions, with one bis-bidendate and two monodentate connectivity. The structure of **IX** consists of a linkage between Y^{3+}, 1,10-phenanthroline and 1,3-BDC anions giving rise to an extended three-dimensional of structure ($\boldsymbol{I^0O^3}$). Though the structure is the augumented $CdSO_4$ as in **VIII**, it possesses two distinct SBUs. Thus, Y(1) forms a eight-membered ring, $^{2}\mathbf{D_0}$ dimer, and the Y(2) forms a paddle-wheel unit, $^{4}\mathbf{D_0}$ dimer. The absence of three-coordinated $\boldsymbol{\mu}_3$ oxygen atoms in **IX** gives rise to the typical paddlewheel arrangement, observed in many benzene dicarboxylate compounds. The connectivity between Y^{3+} and carboxylate anions gives rise to a three-dimensional structure with inter-penetrating channels. The view of the structure in the *bc* plane shows square channels formed by six Y^{3+} ions and six 1,3-dicarboxylate anions (Fig. 2.4.11a). These are further cross-linked by 1,3-BDC to give rise to the three-dimensional structure ($\boldsymbol{I^0O^3}$). In the *ac* plane, an alternating narrow and wide elliptical channels are observed formed by eight Y^{3+} ions and four 1,3-BDC anions (Fig. 2.4.11b). The 1,10-phenanthroline molecules project into these channels from the Y centers and completely occupy the channels. The structure of **IX** is stabilized by only intralayer $\pi\cdots\pi$ interactions between the

1,10-phen ligands unlike **VII** and **VIII**, where both intra as well as interlayer $\pi\cdots\pi$ interactions stabilize the structure.

$[Nd_2(1,3\text{-BDC})_3(1,10\text{-phen})_2]$, **X**, (Fig. 2.4.12), has a two-dimensional square lattice structure with zero inorganic connectivity ($\boldsymbol{I^0O^2}$) similar to **VII**. It has an asymmetric unit with 66 non-hydrogen atoms. There are two Nd^{3+} cations in two crystallographically distinct positions, three isophthalate (1,3-BDC) dianions and two chelating 1,10-phenanthroline molecules in the asymmetric unit. The three BDC anions [acid-1 to acid-3] exhibit two different coordination modes with the torsional angle of 7.77(4), 10.67(5) and 12.14(4)º respectively. Acids-1, -2 and -3 have (1111), (1111) and (2111) connectivities respectively. Acid-1 and -2 bind to three Nd^{3+} cations each. Acid-3 binds to four Nd^{3+} cations. Acid-1 binds to one Nd(1) and two Nd(2). Acid-2 binds to two Nd(1) and one Nd(2). Acid-3 binds to two each of Nd(1) and Nd(2).

Nd(1) is nine-coordinated (NdN_2O_7) with seven oxygen atoms from five different 1,3-BDC anions and two nitrogen atoms from a chelating 1,10-phenanthroline molecule. Among the seven oxygens of $Nd(1)N_2O_7$, five oxygen atoms having $\boldsymbol{\mu_2}$ connectivity (connecting a M atom and a C atom) and other two with $\boldsymbol{\mu_3}$ connectivity. These connectivities link two $Nd(1)N_2O_7$ polyhedra via two oxygen atoms ($\boldsymbol{\mu_3}$) and two carboxylate moieties into $\boldsymbol{^4D_2}$ dimer SBU (SBU-1 or A). The Nd-O bond lengths are in the 2.393(3) – 2.731(3) Å range. The Nd-N bond lengths are 2.653(4) and 2.678(4) Å. Nd(2) is eight-coordinated (NdN_2O_6) with six oxygen atoms from five different 1,3-BDC anions and two nitrogen atoms from a chelating 1,10-phenanthroline molecule. All the six oxygen atoms of $Nd(2)N_2O_6$ are having $\boldsymbol{\mu_2}$ connectivity (two each from acid-1, acid-2 and acid-3). These

oxygen atoms link two $Nd(2)N_2O_6$ via four carboxylate moieties into a paddle wheel $^4\mathbf{D_0}$ dimer SBU (SBU-2 or B). The Nd-O bond lengths are in the 2.370(4) - 2.514(4) Å range. The Nd-N bond lengths are 2.660(4) and 2.708(4) Å.

The connectivities in these two polyhedra lead to the formation of two different SBUs [Nd(1) dimer (A) - SBU-1, $^4\mathbf{D_0}$ and Nd(2) paddle wheel dimer (B) - SBU-2, $^4\mathbf{D_2}$]. These two SBUs are connected by the two 1,3-BDC anions (acid-1 and acid-2). Thus, the alternative connectivity of A and B via acid-1 and -2 (double connectivity) lead to the formation of an infinite one dimensional chain (A=B=A=B). Acid-3 further connects (single connectivity) these chains through A and B alternatively (A-B-A-B) in to an infinite two-dimensional structure ($\boldsymbol{I^0O^2}$) (Fig. 2.4.12). The chelating 1,10-phenanthroline molecules are projecting out from both sides of the layer and decorating the structure. The structure is stabilized by intralayer π…π and C-H…π interactions among the BDC anions and 1,10-phenanthroline molecules and also between BDC anions and 1,10-phenanthroline molecules.

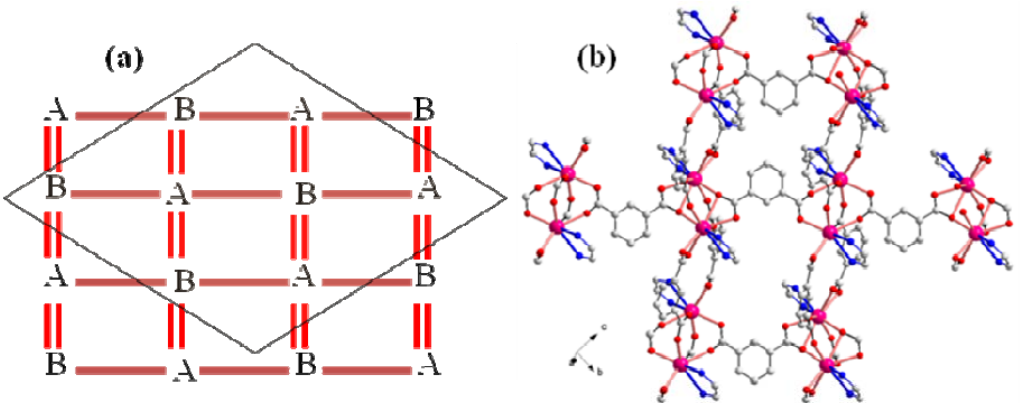

Fig. 2.4.12. (a) Schematic showing the arrangement of the SBU in **X** and (b) the 2D square lattice structure in **X** (1,10-phen molecules are not shown for clarity).

Though all these four isophthalates (**VII** – **X**) have structures related to the square lattice net, variation in the size of the cation and the chelating amines brought out the difference in π…π (intra- and interlayer) interactions in these

compounds with different types of dimer SBU in these isomers and represents an example for supramolecular isomerism.

(c) 1,4-Benzenedicarboxylate

[Cd(1,4-BDC)(1,10-phen)].H_2O, **XI**, has a two-dimensional layer structure ($\boldsymbol{I^0O^2}$), with Cd in a distorted pentagonal bipyramidal environment. The asymmetric unit is shown in Fig. 2.4.13a. The CdN_2O_5 polyhedron has Cd-O bond distances in the 2.341 - 2.590 Å range and the Cd-N bond distances are 2.340 and 2.408 Å. Each Cd atom is coordinated to the two nitrogen atoms of a terminal 1,10-phen molecule, two oxygens from a chelating carboxylate group (11) of a carboxylic acid molecule with (1111) connectivity and three oxygens from a tridentate carboxylate (21) of another carboxylic acid molecule with (2121) connectivity. Two such polyhedra form an edge-sharing dimer ($^2\mathbf{D_2}$ SBU) by sharing the μ_2 oxygen atom from a tridentate carboxylate (21). This carboxylic acid unit links the dimer units into an one-dimensional chain. Two chelating bidentate carboxylates of another carboxylic acid unit (1111) connect the one-dimensional chains into an extended two-dimensional square network (4,4-net) (Fig. 2.4.13b and c).

The two chelating 1,10-phen molecules in each dimeric unit project into opposite sides of the layer, thereby preventing the formation of a three-dimensional interpenetrating network of the 1,4-BDC. The structure is stabilized by interlayer CH-π interaction (2.604 Å, 141.3°) between the 1,10-phen and 1,4-BDC along with the C-H…O interaction (2.349 Å, 175.2°) between the 1,10-phen and free water molecule.

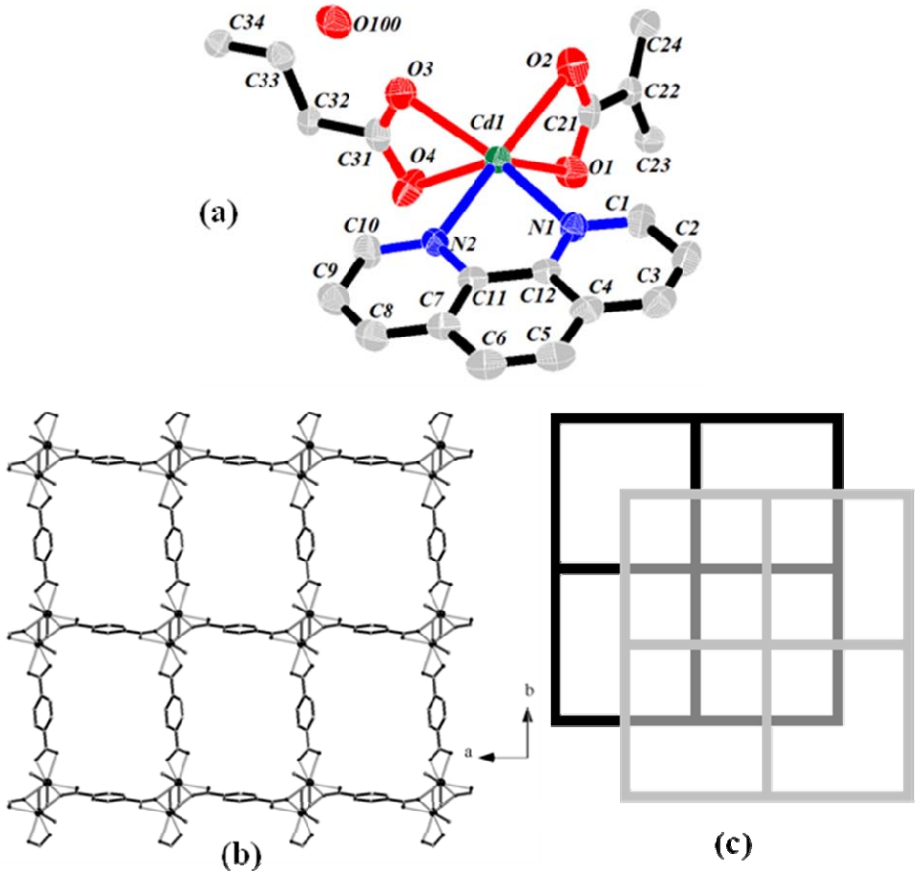

Fig. 2.4.13. (a) ORTEP plot of **XI** (Thermal ellipsoids are shown at 50% probability) (b) 2D layered structure of **XI** and (c) schematic showing the packing arrangement of the layers in **XI.**

(d) Heteroleptic Benzenedicarboxylates

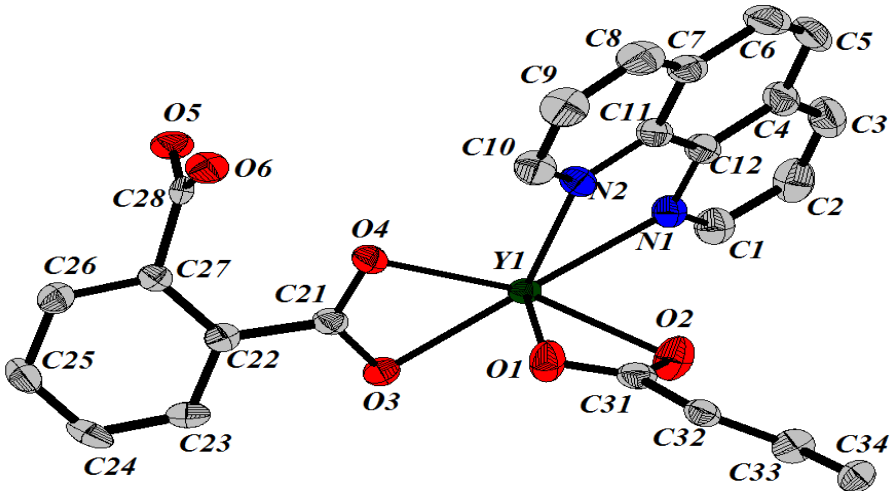

Fig. 2.4.14. ORTEP plot of **XII** (Thermal ellipsoids are shown at 50% probability).

Two yttrium coordination polymers, $[Y_2(1,2\text{-BDC})_2(1,3\text{-BDC})(1,10\text{-phen})_2]$, **XII**, and $[Y_2(1,2\text{-BDC})_2(1,4\text{-BDC})(1,10\text{-phen})_2]$, **XIII**, have similar two-dimensional structures of the type ($\boldsymbol{I^0O^2}$). The asymmetric unit of both **XII** and **XIII** consists of 33 nonhydrogen atoms, of which one Y atom is crystallographically independent (Fig. 2.4.14). Six carboxylate oxygen atoms and two nitrogen atoms from the 1,10-phenonthroline coordinate each Y atom, giving rise to distorted dodecahedron geometry. The average Y–O distances of 2.51 and 2.356 Å, and Y–N distances of 2.485 and 2.499 Å, respectively, for **XII** and **XIII**, result from this bonding. The O–Y–O and O–Y–N bond angles have average values of 97.15◦ and 106.52◦, respectively. The 1,2-BDC anions (1111) show a bis-bidendate connectivity with respect to one carboxylate unit and a monodendate connectivity with respect to the other in both the compounds. The 1,3-BDC acid (1111), in the case of **XII**, is disordered with one of the carbon atom occupying the crystallographic two-fold axis. Both the structures consist of connectivities between YO_6N_2 distorted dodecahedra and the 1,2-BDC anions, which give rise to $^2\mathbf{D_0}$ dimer SBUs. The 1,10-phenonthroline molecules, bound to the Y atoms, are situated on either side of the plane of the building units. The building units are connected together forming a one-dimensional chain, which are cross-linked by the 1,3-BDC anions in **XII** and 1,4-BDC anions in **XIII**, respectively, giving rise to the two-dimensional structure in the *ab* plane (Fig. 2.4.15a). In Fig. 2.4.15b, the arrangement of layers in both the compounds, in the *bc* plane, are shown. As can be noted, the 1,10-phenonthroline molecules hang from the layer in a direction perpendicular to the layers and occupy the interlamellar region. This arrangement of the 1,10-phenonthroline molecules gives rise to considerable $\pi \ldots \pi$ interactions, which, probably, lends additional structural stability to these materials.

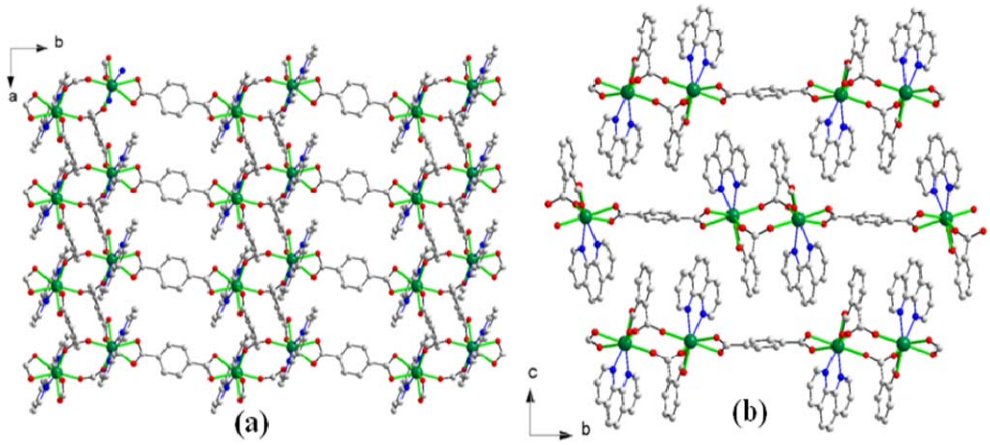

Fig. 2.4.15. (b) 2D layered structure of **XIII** and (c) the packing arrangement of the layers in **XIII.**

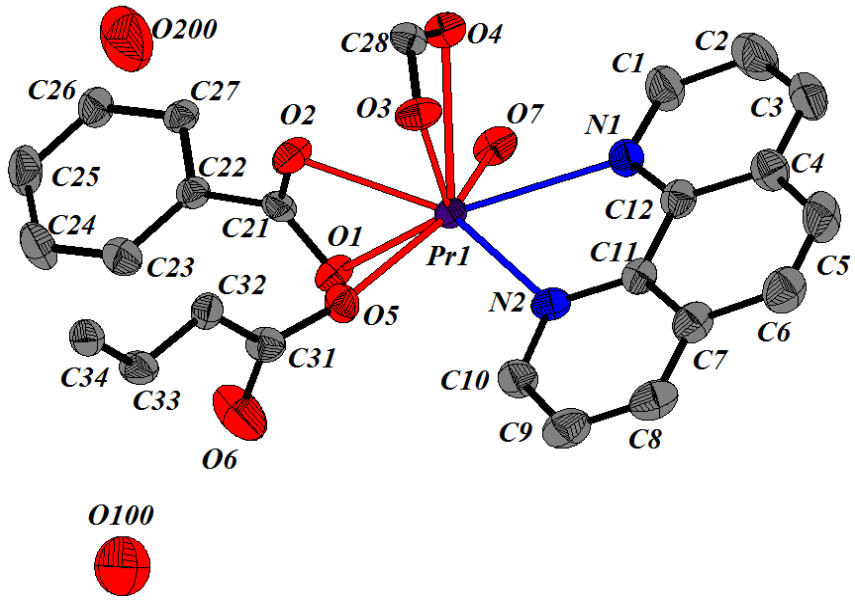

Fig. 2.4.16. ORTEP plot of **XIV** (Thermal ellipsoids are shown at 50% probability).

$[Pr_2(H_2O)_2(1,2\text{-BDC})_2(1,4\text{-BDC})(1,10\text{-phen})_2(H_2O)_2]\cdot H_2O$, **XIV**, has a three-dimensional structure with zero inorganic connectivity ($\boldsymbol{I^0O^3}$). It has an asymmetric unit with 35 non-hydrogen atoms (Fig. 2.4.16). There are one M^{3+} cation, one phthalate (1,2-BDC) dianion, one half of terephthalate (1,4-BDC) dianion, one chelating 1,10-phenanthroline molecule, one terminal water molecule and two lattice water molecules with 0.5 occupancy in the asymmetric unit. The BDC anions [1,2- and 1,4-BDC] exhibit two different coordination modes with the torsional angle of 72.75(6) and 0º respectively. 1,2-BDC with (2111) connectivity

binds to three M^{3+} cations. 1,4-BDC with (1010) connectivity binds to two M^{3+} cations. Pr^{3+} cation is nine-coordinated (PrN_2O_7) with six oxygen atoms from four different BDC anions (three 1,2- and one 1,4-BDC), one oxygen atom from a terminal water molecule and two nitrogen atoms from a chelating 1,10-phenanthroline molecule. Among the six carboxylate oxygens of MN_2O_7, four oxygen atoms (three from 1,2-BDCs and one from 1,4-BDC) having μ_2 connectivity and other two (both from 1,2-BDCs) with μ_3 connectivity.

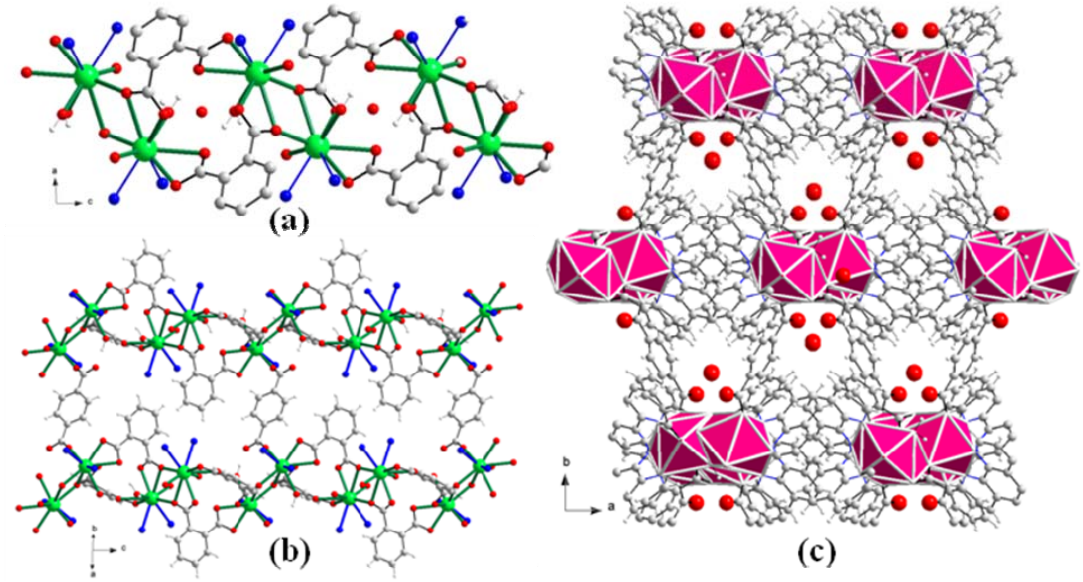

Fig. 2.4.17. (a) Showing the connectivity of dimers into ID chains (b) the connectivity of 1D chains into 2D layer and (c) view of the 3D structure along the *c* axis in **XIV**.

These connectivities link two PrN_2O_7 polyhedra via two oxygen atoms (μ_3) and two carboxylate moieties into a dimer ($^2\mathbf{D_2}$ SBU) of edge sharing polyhedra. Two 1,10-phenanthroline molecules are projecting out from these dimers. The dimers get connected by the 1,2-BDC anions into an infinite one-dimensional chain (Fig. 2.4.17a, rings in the 1,10-phen are not shown). These chains are further cross-linked by the 1,4-BDC anions into a three-dimensional structure ($\boldsymbol{I^0O^3}$) with open channels (Fig. 2.4.17b-c). The lattice water molecules reside in these

channels and hydrogen bonded to the terephthalate oxygen atoms. The structure is further stabilized by π…π and C-H…π interactions among and between the phenanthroline molecules and the BDC anions. The Pr-O bond lengths are in the 2.386(2) - 2.749(2) Å range. The Pr-N bond lengths are 2.700(3) and 2.717(3) Å.

2.4.1.2. Metal dicarboxylates without chelating amines

(a) Heteroleptic Benzenedicarboxylates

Two rare earth mixed benzenedicarboxylates (two different dicarboxylate ligands) have been obtained with three-dimensional structure (***I*^{0}*O*^{3}**) of the same formula, $[M_2(1,2BDC)_2(1,4BDC)(H_2O)_4]$, (M = La, Pr, Gd, Dy, and Y). They can be grouped into two distinct classes based on the coordination environment around the central metal ion and the connectivity with the carboxylate units. Thus, M = La and Pr, form type-1, and M = Gd, Dy, and Y, form type-2.

The asymmetric unit of type-1 compounds, $[M_2\{(1,2BDC)_2(1,4BDC)(H_2O)_4\}]$, **XV**, (M = La and Pr), contains 44 non-hydrogen atoms, of which two M atoms are crystallographically independent (Fig. 2.4.18a). The structure is built up by the connectivity involving M and the carboxylate units. The coordination environment around the nine coordinated M atoms is an idealized *D*3*h* triply capped trigonal prism. The structure of the type-1 compounds, has two types of 1,2-BDC and one chelating 1,4-BDC anions with [(1121) for 1,2-BDC and (1111) for 1,4-BDC] different connectivities. Each M atom is coordinated by seven carboxylate oxygens and two terminal oxygen atoms, from water molecules. Among the seven carboxylate oxygens (five from 1,2-BDC and two from 1,4-BDC) two have μ_3 connectivity, connect the M atoms through a three-coordinate bond, leading to formation of the **^{3}D$_2$** dimer SBU. The M-O distances are in the 2.397(6)-2.923(5) Å range.

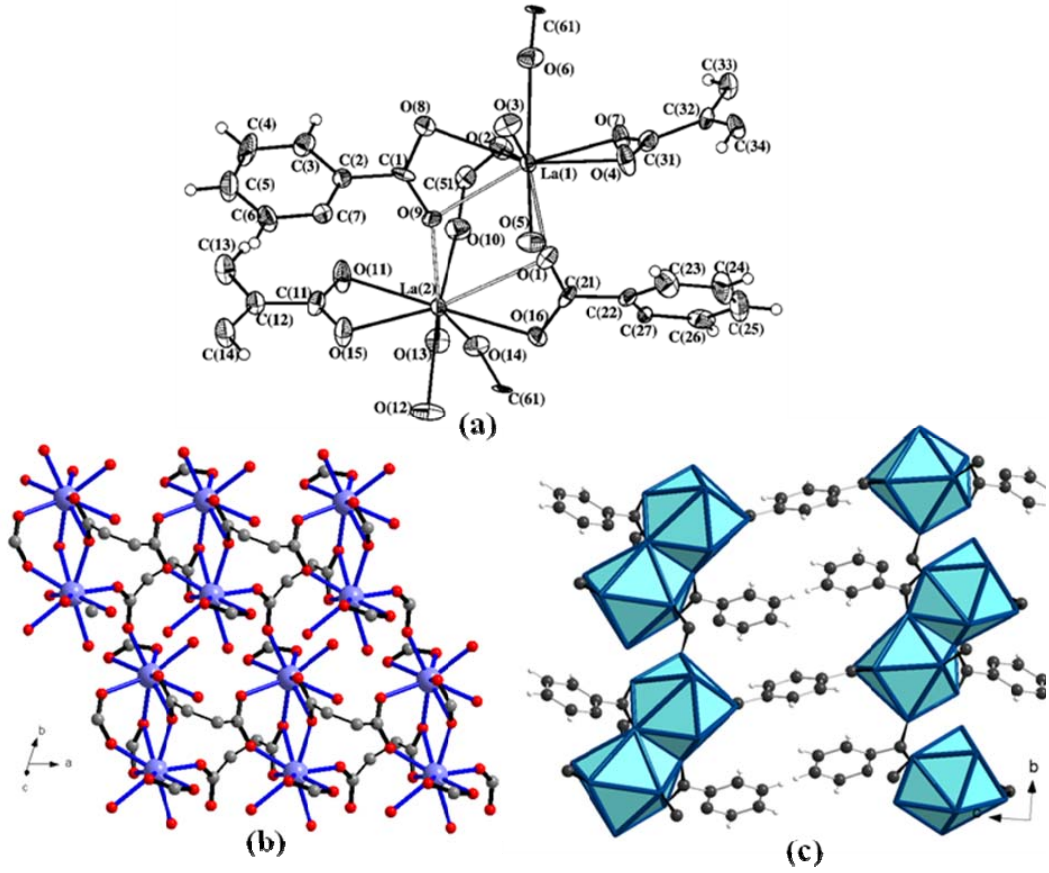

Fig. 2.4.18. (a) ORTEP plot of **XV** (Thermal ellipsoids are shown at 50% probability) (b) View of the connectivity of dimers into 2D layer and (c) view of the 3D structure along the *a* axis in **XV**.

The framework structure of the type-1 compounds can be understood in terms of simpler building units. The dimers are connected into a ladder like arrangement by the connectivity of a single –COO units. The 1,2-BDC connects these ladders giving rise to a corrugated sheet of M-carboxylate networks in the *ab* plane (Fig. 2.4.18b). The M-M atoms are separated by 4.3 Å within the dimer and 6.293 Å between the dimers in the same ladder. The corrugated sheets are cross-linked by the 1,4-BDC completing the three-dimensional structure as shown in (Fig. 2.4.18c). The connectivity between the M, 1,2-BDC and 1,4-BDC gives rise to rhombic one-dimensional channels. The two water molecules bound to the M ions project into the channels.

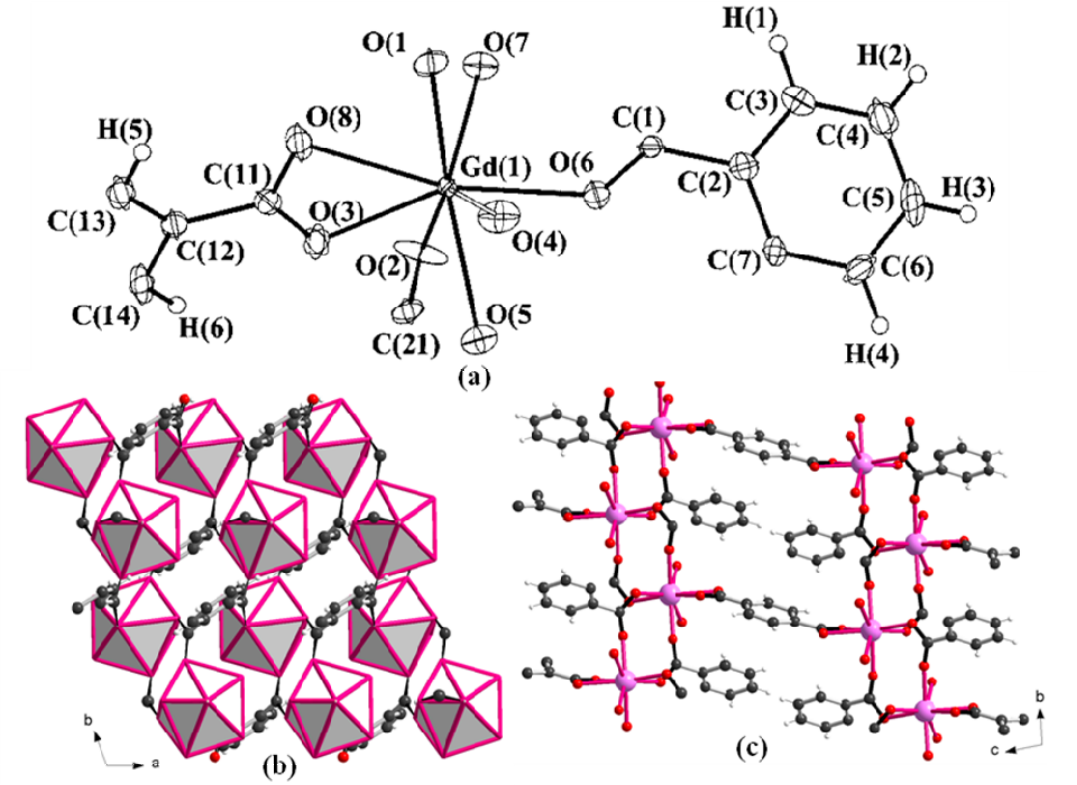

% probability) (b) View of the connectivity of dimers into 2D layer and (c) view of the 3D structure along the *a* axis in **XVI**.

The asymmetric unit of type-2 compounds, $[M_2(1,2BDC)_2(1,4BDC)(H_2O)_4]$, **XVI**, (M = Gd, Dy, and Y), have 21 non-hydrogen atoms, of which one M atom is independent (Fig. 2.4.19a). The M atoms are eight-coordinated with oxygen atoms that have M-O distances in the range 2.262(4)-2.509(4) Å (av. 2.381 for Gd, 2.411 for Dy, and 2.370 Å for Y). The coordination environment around the central M atom is a distorted dodecahedron. The M atom has two terminal M-O linkages with an average distance of 2.405 Å, which are water molecules. The structure of the type-2 compounds, has two 1,2-BDC and one chelating 1,4-BDC anions with (1111) connectivity. Each M atom is coordinated by six carboxylate oxygens and two terminal oxygen atoms, from water molecules. All the six carboxylate oxygens (four from 1,2-BDC and two

from 1,4-BDC) have μ_2 connectivities leading to formation of the $^2\mathbf{D_0}$ dimer SBU (8-membered ring).

The connectivity between the M atoms and the 1,2-BDC acid, similar to type-1 compounds, gives rise to a corrugated step-like ladder arrangement and a layer (*ab* plane) (Fig. 2.4.19b), but with the $^2\mathbf{D_0}$ dimer SBUs. Similar to the type-1 compounds, the distance between the M atoms varies between 4.910-6.116 Å. The connectivity between the 1,2-BDC, 1,4-BDC and the M atoms gives rise to rhombic one-dimensional channels (Fig. 2.4.19c) (view along the *a* axis). The two water molecules bound to the M atoms project into these channels. The arrangement of the benzene carboxylates in the *ab* plane clearly indicates that direct π···π interactions have been avoided.

(b) 1,2-Benzenedicarboxylate

The two-dimensional structure of piperazine templated, Gd phthalate, $[Gd_2(1,2\text{-BDC})_4(H_2O)_2].(H_2Pip)$, **XVII**, contains 29 non-hydrogen atoms in the asymmetric unit, of which 26 belong to the framework and 3 atoms belong to half of the piperazine molecule, the C–C bond in the piperazine has a center of symmetry (Fig. 2.4.20a). The Gd^{3+} ion is coordinated to eight oxygen atoms with the Gd–O bond distances are in the range 2.301(3)–2.559(3) Å. The local coordination environment around the Gd^{3+} ions can be described as distorted dodecahedra formed by seven carboxylate oxygen atoms and a water molecule. There are two crystallographically unique 1,2-BDC anions (acid-1 and acid-2) in the structure, which show differences in their connectivity [(1111) and (1101)]. The Gd^{3+} ion is connected to three acid-1 and two acid-2 anions and possesses one terminal water molecule. Of the two carboxylate units of acid-1, one has a bis-bidendate coordination while the other has monodendate connectivity with two

Gd^{3+} ions. The acid-2 has one carboxylate unit in bis-bidendate coordination and the other connects with only one Gd^{3+} ion and possesses a terminal C–O linkage. The structure consists of a network of Gd dimers of the type, $^{2}\mathbf{D_0}$ SBUs and 1,2-BDC anions.

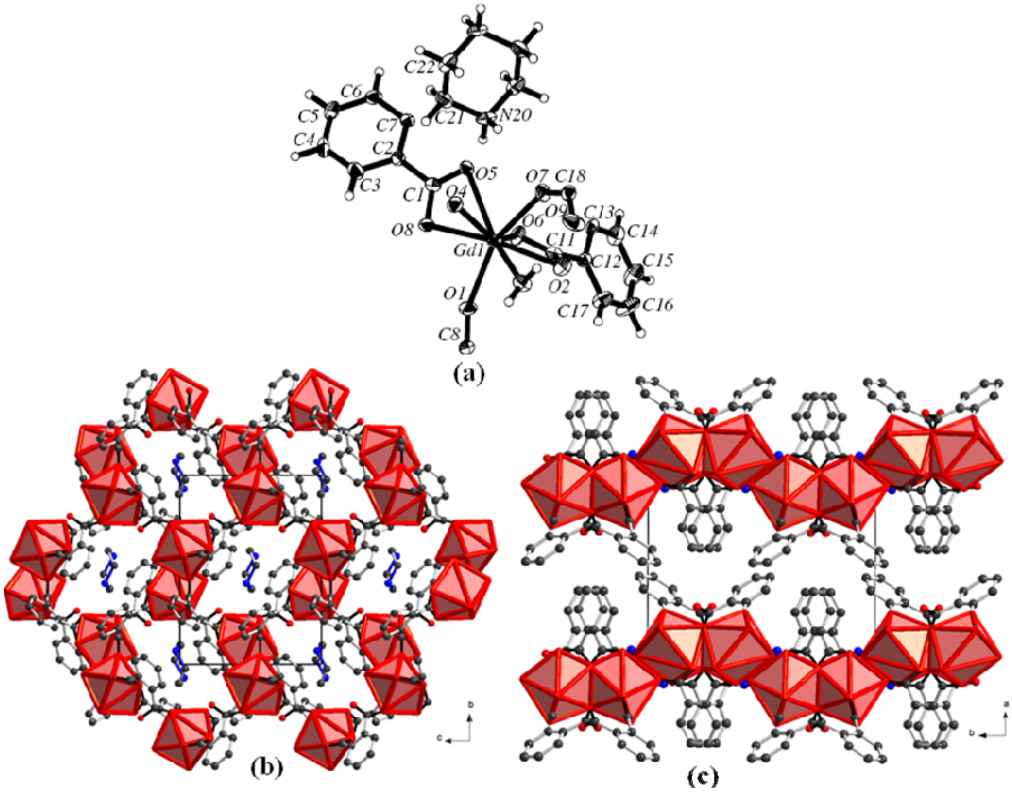

Fig. 2.4.20. (a) ORTEP plot of **XVII** (Thermal ellipsoids are shown at 50% probability) (b) view of the connectivity of dimers into 2D layer and (c) view of the packing arrangement in **XVII**.

The connectivity between Gd^{3+} ions and 1,2-BDC anions gives rise to two-dimensional macroanionic sheet structure ($\boldsymbol{I^0O^2}$) with large apertures (Fig. 2.4.20b). The charge compensating protonated piperazine molecules are located in the middle of the apertures within the sheet. This situation is to be contrasted with other compounds possessing two-dimensional open-framework structures. The charge compensating amine molecules, in general, are located in between the anionic sheets in most of the layered structures and the presence of the amine molecule, in **XVII**, within the sheet is noteworthy. The view of the arrangement of

the layers is shown in (Fig. 2.4.20c). As can be noted, the benzene rings project into the inter-layer spaces. It is likely that the presence of the bulky benzene rings and the associated p electron cloud may be responsible for the piperazine molecule to occupy the apertures within the layers rather than the inter-lamellar spaces.

(c) 1,3-Benzenedicarboxylate

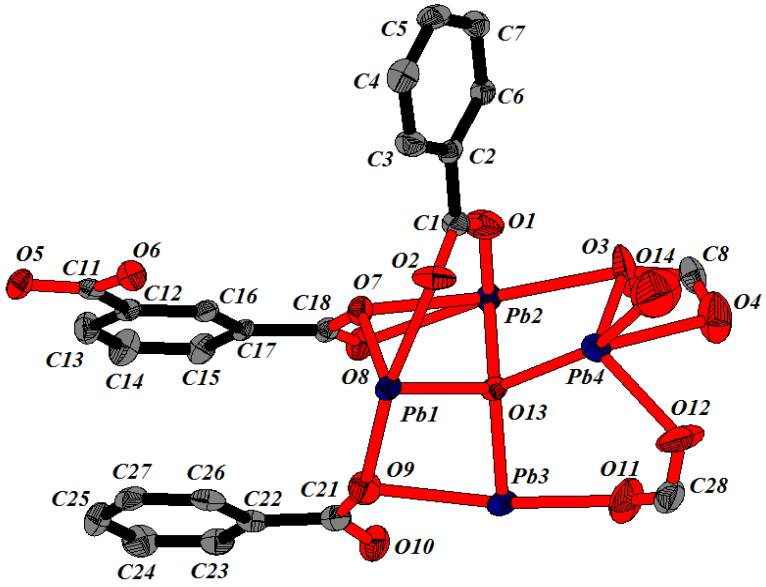

Fig. 2.4.21. ORTEP plot of **XVIII** (Thermal ellipsoids are shown at 50% probability).

$(OPb_4)(1,3\text{-}BDC)_3(H_2O)$, **XVIII**, has a three-dimensional structure with zero inorganic connectivity ($\boldsymbol{I^0O^3}$). It has an asymmetric unit with 42 non-hydrogen atoms. There are four Pb^{2+} cations in four crystallographically distinct positions, three isophthalate (1,3-BDC) dianions, a terminal water molecule and an independent oxo dianion in the asymmetric unit (Fig. 2.4.21). The three BDC anions [acid-1, acid-2 and acid-3] exhibit three different coordination modes with the torsional angle of 32.59(1), 3.83(1) and 14.81(1)º respectively. They have (1112), (1222) and (1122) connectivities respectively. Acid-1 binds to four Pb^{2+} cations [one Pb(1), two Pb(2) and one Pb(4)], acid-2 binds to five Pb^{2+} cations [two Pb(1) and one each of Pb(2), Pb(3) and Pb(4)] and acid-3 binds to six Pb^{2+}

cations [three Pb(3), and one each of Pb(1), Pb(2) and Pb(4)]. The independent oxo dianion binds to all the four Pb^{2+} cations [Pb(1) - Pb(4)] to form a OPb_4 tetrahedron.

Pb(1) is hemidirected and coordinated by six oxygen atoms (PbO_6). Among the six oxygens of $Pb(1)O_6$, one with μ_2 connectivity is from the acid-1, four with μ_3 connectivity (connecting two Pb atoms and a C atom) are from three different 1,3-BDC anions and the remaining one with μ_4 connectivity (connecting four Pb atoms) is the oxo dianion. These oxygen atoms link Pb(1) with Pb(2) and Pb(4) by sharing an edge with each and with Pb(3) by sharing a face. The Pb-O bond lengths are in the 2.284(4) – 2.871(5) Å range. Pb(2) is also hemidirected and coordinated by six oxygen atoms (PbO_6). Among the six oxygens of $Pb(2)O_6$, one oxo anion has μ_4 connectivity. The remaining oxygens are from four different 1,3-BDC anions with two oxygens having μ_2 connectivity (connecting a Pb atom and a C atom) and other three with μ_3 connectivity. These oxygens link Pb(2) with Pb(1), Pb(3) and Pb(4) by sharing an edge with each. The Pb-O bond lengths are in the 2.271(4) – 2.857(4) Å range. Pb(3) is also hemidirected but coordinated by five oxygen atoms (PbO_5). Among the six oxygens of $Pb(2)O_6$, one oxo anion is having μ_4 connectivity. The remaining four oxygens are from four different 1,3-BDC anions and three are with μ_3 connectivity and the remaining one is with μ_2 connectivity. These oxygens linking Pb(3) with Pb(1) by sharing a face, with one Pb(2) by sharing an edge and with one Pb(4) by sharing a corner. The Pb-O bond lengths are in the 2.53(4) – 2.660(6) Å range. Pb(4) is also hemidirected and coordinated by six oxygen atoms (PbO_6). Among the six oxygens of $Pb(2)O_6$, one

oxo anion has μ_4 connectivity. Among the remaining oxygens one is from terminal water molecule and four others are from three different 1,3-BDC anions with two oxygens having μ_2 connectivity and other two with μ_3 connectivity. These oxygens link Pb(4) with Pb(1) and Pb(2) by sharing an edge with each and with Pb(3) by sharing a corner. The Pb-O bond lengths are in the 2.372(6) – 2.805(4) Å range.

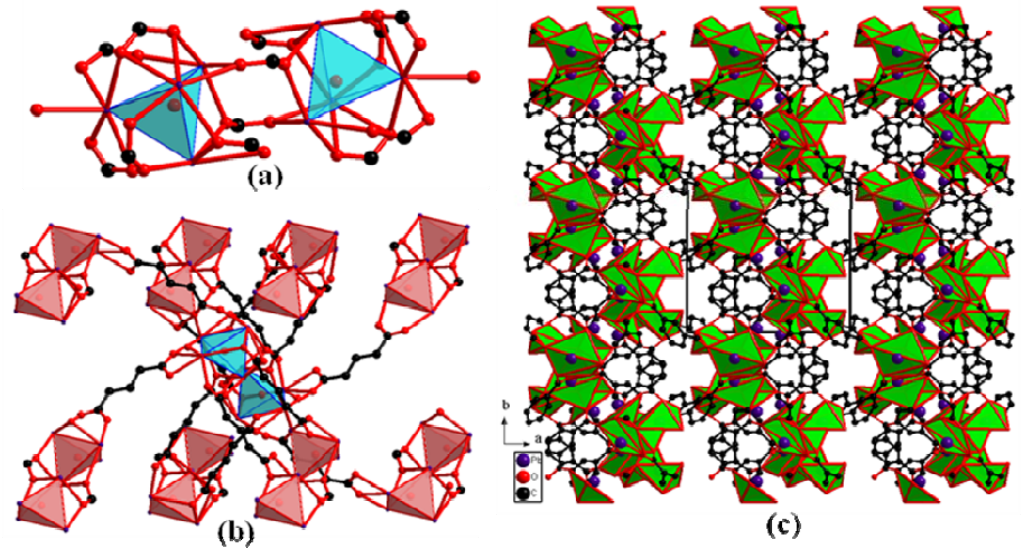

Fig. 2.4.22. (a) $Pb_8O_{28}C_2$ SBU made up of two tetrahedral Pb_4O_{14} units (b) view of the eight connected SBU and (c) view of the 3D structure of **XVIII** along the *c* axis.

These connectivities in four polyhedra lead to the formation of a tetrahedral unit, Pb_4O_{14}, with the four Pb atoms in the corner and the oxo anion in the centre. Two such tetrahedra are connected by two carboxylate groups in to a secondary building unit (SBU) of $Pb_8O_{28}C_2$ (Fig. 2.4.22a). Each 1,3-BDC anion connects two such SBUs and acts as a 2-connecting node. Each SBU is connected to eight such SBUs through twelve 1,3-BDC anions, thus acts as 8-connecting node (Fig. 2.4.22b). Among the these eight SBUs, four are connected to the central SBU through one 1,3-BDC anion each and four other SBUs through two 1,3-BDC anions. These connectivities of 8-connected SBUs and 2-connected 1,3-BDC

anions lead to an infinite three dimensional-structure ($\boldsymbol{I^0O^3}$) of (2,8) 3D-periodic net (Fig. 2.4.22c).

2.4.2. Hybrid Networks of Metal Benzenedicarboxylates with Extended Inorganic Connectivity

2.4.2.1. Metal 1,2-benzenedicarboxylates with chelating amines

$[M_3(1,2\text{-BDC})_4(1,10\text{-phen})_3(H_2O)]\cdot 0.5H_2O$, **XIX**, (where M = La and Pr) has a one-dimensional structure with one-dimensional inorganic connectivity ($\boldsymbol{I^1O^0}$). It has an asymmetric unit with 94.5 non-hydrogen atoms. There are three M^{3+} cations in three crystallographically distinct positions, four phthalate (1,2-BDC) dianions, three chelating 1,10-phenanthroline molecules, a bridging water molecule and a lattice water molecule (with 0.5 occupancy) in the asymmetric unit. The four BDC anions [acid-1, acid-2, acid-3 and acid-4] exhibit two different coordination modes with the torsional angles of 44.36(3), 70.24(2), 48.43(1) and 40.88(4)º respectively. Acids-1,-3 and -4 have (1121) connectivity and acid-2 has (1111) connectivity. Each acid (-1 to -4) binds to three M^{3+} cations [one each of M(1), M(2) and M(3)].

M(1) is ten-coordinated (MN_2O_8) with eight oxygen atoms from four different 1,2-BDC anions (one each of acid-1 to -4) and two nitrogen atoms from a chelating 1,10-phenanthroline molecule. Among the eight oxygen atoms of $M(1)N_2O_8$ (blue), five have $\boldsymbol{\mu_2}$ connectivity and the other three have $\boldsymbol{\mu_3}$ connectivity. These $\boldsymbol{\mu_3}$ oxygen atoms link M(1) to M(2) by an edge ($^3\mathbf{D_2}$ SBU) and to M(3) by a corner ($^2\mathbf{D_1}$ SBU). M(2) is nine-coordinated (MN_2O_7) with two nitrogen atoms from a chelating 1,10-phenanthroline molecule, a bridging water molecule and six oxygen atoms from four different 1,2-BDC anions (one each of

acid-1 to -4). Among these six carboxylate oxygens of $M(2)N_2O_7$ (green), four oxygen atoms having μ_2 connectivity and other two are with μ_3 connectivity. These connectivities link M(2) to M(1) by an edge, ($^3\mathbf{D_2}$ SBU) and to M(3) by a corner (bridging water, $^2\mathbf{D_1}$ SBU). M(3) is eight-coordinated (MN_2O_6) with two nitrogen atoms from a chelating 1,10-phenanthroline molecule, a bridging water molecule and five oxygen atoms from four different 1,2-BDC anions (one each of acid-1 to -4). Among these five carboxylate oxygens of $M(3)N_2O_6$ (red), four oxygen atoms having μ_2 connectivity and remaining one with μ_3 connectivity. These connectivities link M(3) to M(1) by a corner ($^2\mathbf{D_1}$ SBU) and to M(2) by another corner (bridging water , $^2\mathbf{D_1}$ SBU). The M-O bond lengths are in the 2.358(4) – 2.754(3) range for M = La and 2.305(4) – 2.724(3) Å range for M = Pr. The M-N bond lengths are 2.706(4) - 2.791(4) (5) Å range for M = La and 2.673(4) - 2.755(4) Å range for M = Pr.

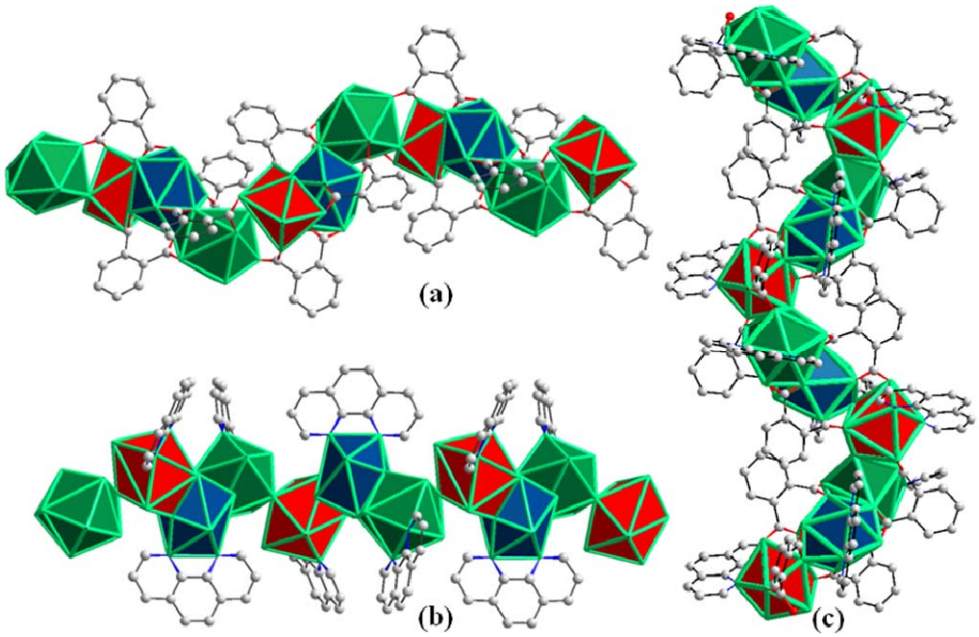

Fig. 2.4.23. View of the infinite M-O-M 1D chain structure (a) without 1,10-phen (b) without 1,2-BDC anions in **XIX** and (c) the 1D structure of **XIX** .

The connectivities in these three polyhedra lead to the formation of a trimer of M(1)-M(2)-M(3) polyhedral (blue-green-red). These trimers are further connected sequentially in (-123-123-123-) manner by the 1,2-BDC anions in to an infinite one-dimensional structure ($\boldsymbol{I^1O^0}$) (Fig. 2.4.23a). The chelating 1,10-phenanthroline molecules are decorating this chain structure (Fig. 2.4.23b). The one-dimensional chain structure (Fig. 2.4.23c) is further stabilized by π…π and C-H…π interactions among the BDC anions and 1,10-phenanthroline molecules and also between BDC anions and 1,10-phenanthroline molecules.

$[M_3(1,2\text{-BDC})_4(1,10\text{-phen})_2(NO_3)]\cdot H_2O$, **XX,** (M = La, Pr) has 85 non-hydrogen atoms in the asymmetric unit. There are three crystallographically distinct M^{3+} ions and four phthalate anions. The M^{3+} ions are connected to four phthalate anions, a nitrate anion and two 1,10-phenanthroline ligands. The four phthalate anions can be classified into three different types based on their coordination modes with the metal atoms {acid-1- (1210), acid-2 and -4 (1221), and acid-3- (1121)}. The metal atom, M(1), is surrounded by ten oxygen atoms and has a distorted bicapped square antiprism environment (MO_{10}). Among the ten, two oxygen atoms are from the nitrate group and the remaining eight oxygens are from the four phthalate anions. Five oxygen atoms, have $\boldsymbol{\mu_3}$ connections linking two metal centres and a carbon atom. M(2) is eight-coordinated by six oxygen atoms and two nitrogen atoms and has a distorted dodecahedral environment (MO_6N_2, blue). The two nitrogen atoms are from the 1,10-phenanthroline ligand and the six oxygen atoms are from the four phthalate anions. Three oxygen atoms, have $\boldsymbol{\mu_3}$ connectivity. M(3) is ten-coordinated by eight oxygen atoms and two nitrogen atoms and has a distorted bicapped square anti-prism environment (MO_8N_2, cyan). The two nitrogen atoms are from the 1,10-phenanthroline ligand

and the eight oxygen atoms are from the four phthalate anions. Four oxygen atoms, have μ_3 connectivity. The M–O bonds have distances in the range 2.456(4)–2.729(4) Å and the M–N bonds have distances in the range 2.662(5)–2.747(5) Å.

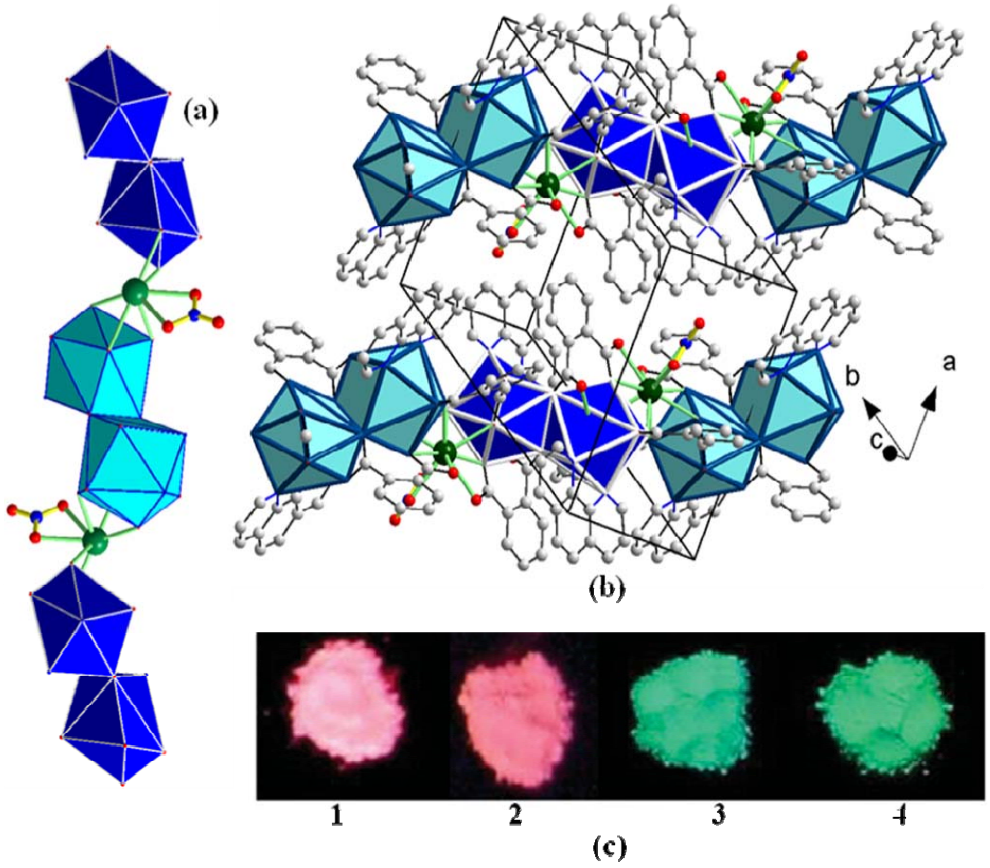

Fig. 2.4.24. (a) Infinite M-O-M 1D chain in **XX** (b) packing arrangement in **XX** and (c) emission by partially doped **XX** with Eu (2 and 4 mol% **1** and **2**) and Tb (2 and 4 mol% **3** and **4**) in place of La under UV excitation.

The structure of **XX** can be explained by considering smaller building units. Thus, two $M(2)^{3+}$ ions are connected through two μ_3 oxygen atoms, from two different phthalate anions (both are acid 1) to form an edge-shared $M_2O_{12}N_4$ dimer, $^2\mathbf{d_2}$ SBU, (blue). Similarly, two $M(3)^{3+}$ ions are connected through two μ_3 oxygen atoms, from two different phthalate anions (both are acid 4) to form an edge-shared $M_2O_{16}N_4$ dimer, $^2\mathbf{D_2}$ SBU, (cyan). The two dimers M(2) and M(3), are independently connected to each other by the acid 2 and acid 3. In addition, the M(2) and M(3) dimers are also linked to M(1) by μ_3 oxygen atoms. Thus, the M(2)

dimer is connected with M(1) by sharing the edge, $^{3}\mathbf{D_2}$ SBU, whereas M(3) dimer is connected with M(1) by sharing the face resulting in a head–tail type of arrangement with $^{3}\mathbf{D_3}$ SBU. [(M(2)-dimer as the head and M(3)-dimer as the tail or vice versa] (Fig. 2.4.24a) The arrangement of these polyhedra gives rise to an infinite one-dimensional M–O–M chain structure decorated with phthalates, nitrates and 1,10-phenanthroline ligands as shown in Fig. 2.4.24b. The structural stability in a low-dimensional structure is, in general, derived from weak non-covalent interactions. In the present case, we find $\pi\ldots\pi$ and C-H…π interactions dominate and probably lend stability to the structure. The $\pi\ldots\pi$ interactions can be classified into three different types: acid–acid, phenanthroline–acid and phenanthroline–phenanthroline. We find the centroid-to-centroid distances between all the participating aromatic rings to be in the range 3.622–3.716 Å and the dihedral angles to be in the range 0–5.7^{o}. The C-H to centroid distances are in the range 2.785–3.399 Å and the angles in the range 87.77–153.14^{o}.

The lanthanide-centered emission is sensitized by the molecules having p systems. Recently, lanthanide-centered luminescence sensitized by the diketonate type ligands was reported. Férey et al reported the luminescence behaviour of doped lanthanide carboxylates, which also contains M–O–M one-dimensional chains.[43–45] Since the present compound also has M–O–M chains, we investigated the luminescence behaviour of **XX**. In order to investigate the luminescence from the metal center, we have partially doped Eu (2 and 4 mol%) and Tb (2 and 4 mol%) in place of La.

The room temperature photoluminescence properties of all the compounds were studied using an excitation wavelength of 252 nm. The emission spectrum of the pure compounds show a broad peak centered at ~400 nm. This emission may

be attributed to the intra ligand luminescence (n←π*) or (π←π*). Generally, in metal-coordination compounds, the ligand is excited to the singlet state, from where part of the energy is transferred onto the triplet excited state through inter-system crossing (ISC). The triplet exited state then comes to the ground state through radiative emission. This emission also has a competing process called ligand-sensitized energy transfer to the metal center, if the energy levels are favorable.[46,47] This would result in a metal centered luminescence, showing characteristic spectra of the central metal ion. The success of the energy transfer to the metal ion is clearly indicated in the suppression of the intraligand emission in the luminescence spectra. A preliminary optical emission of the doped compounds, **1** (2 mol% Eu), **2** (4 mol% Eu), **3** (2 mol% Tb) and **4** (4 mol% Tb) was observed under UV irradiation. As shown in Fig. 2.4.24c, very efficient pink/red and green emissions were observed for the Eu^{3+} and Tb^{3+} doped samples, respectively.

The room temperature photoluminescence spectra of the Eu and Tb doped samples are given in Fig. 2.4.25a and b. As can be seen, the main emission band is suppressed followed by the strong red luminescence, characteristics of the $^5D_0 \rightarrow {}^7F_j$ (j = 0, 1, 2, 3, 4) emission bands of the Eu^{3+} ion.[48] The excitation spectrum of 1 and 2 has a band maximum around 250nm, confirming that the energy transfer takes place from the ligand to Eu^{3+} ion. Under these circumstances, the intersystem crossing (ISC) from the singlet to the triplet excited state of the ligands (1,2-BDC and 1,10-phenanthroline) occurs, followed by the energy transfer to the ^5D_j, j = 3, 2, 1, 0 state of Eu^{3+} ions (Fig. 2.4.25c). A schematic of the various possible energy levels in the doped compounds is given in Fig. 2.4.19c. In compounds **1** and **2**, the emission from the $^5D_0 \rightarrow {}^7F_j$ states is responsible for the red/pink luminescence. Thus, the emissions at 580, 543, 615, 650 and 700 nm corresponds to $^5D_0 \rightarrow {}^7F_0$,

$^5D_0 \rightarrow {}^7F_1$, $^5D_0 \rightarrow {}^7F_2$, $^5D_0 \rightarrow {}^7F_3$, and $^5D_0 \rightarrow {}^7F_4$ transitions, respectively. In the case of **1** (2 mol% Eu) the overall energy transfer is not complete since intra-ligand emission is not quenched fully.[49] For **2** (4 mol% Eu), on the other hand, the quenching appears to be more and hence more energy would have been transferred from the ligands. It is likely that the increased concentration of the Eu^{3+} ions in **2** would have resulted in this behaviour. This behaviour is not expected to be linear as for higher concentrations of Eu^{3+}, the metal centered luminescence may be affected by self-quenching.

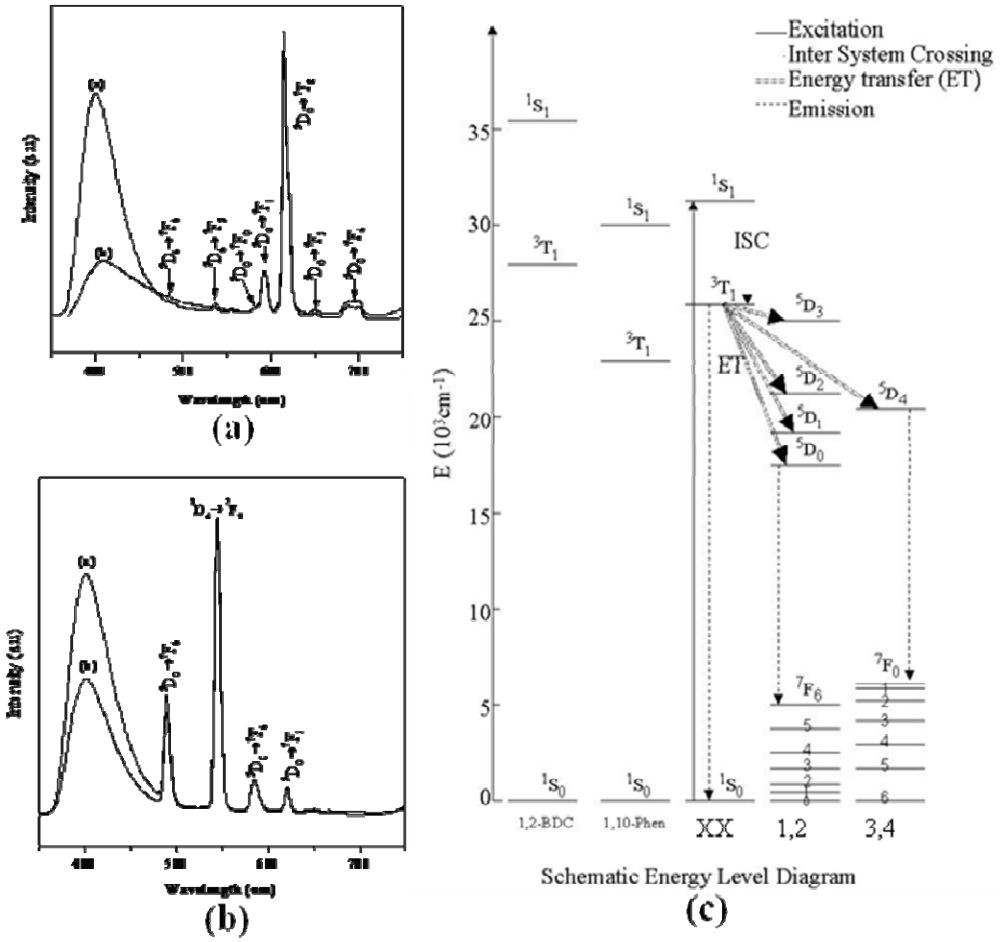

Fig. 2.4.25. Room-temperature photoluminescence spectra of the doped compounds of XX (a) **1** (2 mol% Eu) and **2** (4 mol% Eu) (b) **3** (2 mol% Tb) and **4** (4 mol% Tb). Schematic energy level diagram for the pure ligands, pure XX, and doped samples **1**–**4** showing the various possible energy transfer processes. (ISC denotes inter-system crossing).

It has been observed that the emission bands of the $^5D_0 \rightarrow {}^7F_j$ peaks also give an idea about the coordination environment. For example, a (2J + 1) splitting is observed in the emission band for a single type of environment (coordination environment and site symmetry) around the metal ion.[44] In the present case, only one emission band has been observed in the $^5D_0 \rightarrow {}^7F_0$ degenerate transition around 580 nm. This indicates that the Eu^{3+} ion occupies only one of the three crystallographic sites. Of the three available positions, two are coordinated with 1,10-phenanthroline as a secondary ligand along with the phthalate anions and the remaining site is coordinated to the nitrate and the phthalate anions. The emission at 593 nm corresponds to $^5D_0 \rightarrow {}^7F_1$ transition, which is induced by magnetic dipole moment and is fairly insensitive to the coordination environment.[44] The emission at 615nm corresponds to the $^5D_0 \rightarrow {}^7F_2$ transition, which is induced by the electric dipole moment and also sensitive to the environment. At room temperature these are not resolved very well. The intensity ratio, $I(^5D_0 \rightarrow {}^7F_2)/I(^5D_0 \rightarrow {}^7F_1)$ = ~6, indicates a lower symmetry level of the coordination environment of the Eu3+ occupied site.[50] It may be noted that in the present case, the metal ions with CN = 10 is less symmetric than with CN = 8. In **XX**, there are two sites, La(1) and La(3), which are 10 coordinated. It is likely that the Eu^{3+} ions occupy the La(3) sites, which are coordinated by oxygen and nitrogen atoms, rather than the La(1) sites, which are completely coordinated by oxygen atoms.

Similarly, in the case of Tb^{3+} doped samples (**3** and **4**), we find a band maximum ~250 nm in the excitation spectrum, indicating that the energy transfer takes place again from the ligand to the Tb^{3+} ions. The emission spectra shows the typical peaks, and the energy transfer occurs from the triplet excited state of the ligand to the $^5D_4$ state of the Tb^{3+} ions.[49] The resultant emission occurs from $^5D_4$ to

the ^7F_j (j = 3, 4, 5, 6) states giving green luminescence. The various peaks are assigned as follows: $^5D_4 \rightarrow {}^7F_6$ (~490nm), $^5D_4 \rightarrow {}^7F_5$ (~545nm), $^5D_4 \rightarrow {}^7F_4$ (~580nm) and $^5D_4 \rightarrow {}^7F_3$ (~620nm) (Fig. 2.4.25b). As can be noted, the higher concentration of Tb^{3+} in **4** shows more quenching of intra-ligand transition giving rise to more intense green emission.

Considering all the four doped compounds, it is becoming obvious that the energy transfer from the ligand to the metal is more pronounced in the Eu^{3+} doped compounds (**1** and **2**) compared to the Tb^{3+} doped ones (**3** and **4**). It is likely that the availability of more energy levels for Eu^{3+} (^5D_j, j = 3, 2, 1, 0) compared to Tb^{3+} ($^5D_4$) would have resulted in the efficient energy transfer. The $^5D_0 \rightarrow {}^7F_2$ (~615 nm) emission for **1** and **2** and the $^5D_4 \rightarrow {}^7F_5$ (~545nm) emission for **3** and **4**, respectively, correspond to the red and green region of the visible spectrum. The present results are qualitative in nature, and the emission observed in these compounds could be compared to the emissions of the commercial red phosphors (i) $Y_2O_3 : Eu^{3+}$ with 611 nm emission (ii) $(Y,Gd)(P,V)O_4 : Eu^{3+}$ with 615 nm emission and green phosphors (i) $LaPO_4 : Ce^{3+},Tb^{3+}$ with 545 nm emission (ii) $(Ce,Gd,Tb)MgB_5O_{10}$ with 542 nm emission (iii) $(Ce,Tb)MgAl_{11}O_{19}$ with 541 nm emission.[51] This opens up a new way of introducing luminescent properties into the hybrid solids with the extended inorganic network structure. In addition, the presence of aromatic linkers with delocalized π electrons (benzene carboxylate and 1,10-phenanthroline) appears to enhance the optical properties.

2.4.2.2. Metal benzenedicarboxylates without chelating amines

(a) 1,2-Benzenedicarboxylates

Two polymorphs of the same formula, $M_2(1,2\text{-BDC})_3(H_2O)$, (Y=**XXI**, and Dy= **XXII**), have been obtained with two-dimensional structure with one-

dimensional inorganic connectivity. Though the inorganic connectivity and the M…M interaction within the layer are different, the interlayer $\pi\ldots\ \pi$ interactions appear to be similar for these two structures.

The asymmetric unit of $Y_2(1,2\text{-BDC})_3(H_2O)$, **XXI**, contains 78 non-hydrogen atoms, of which four Y atoms are crystallographically independent. All the four Y atoms have different coordination environment with respect to its nearest neighbour oxygen atoms. Thus, the Y(1) binds to six oxygen atoms belonging to the carboxylate groups of six 1,2-BDC atoms, Y(2) binds eight oxygen atoms from the carboxylate groups of five 1,2-BDC anions, Y(3) bind with seven oxygen atoms, five of which are from the carboxylate groups of five 1,2-BDC and the other two are terminal ones (two coordinated water molecules) and Y(4) is coordinated to nine oxygen atoms of the carboxylate groups of six 1,2-BDC anions. It is rare that the same metal ion has four different coordination environments within the same compound. The geometry of each of the Y atoms can be described as octahedron (Y(1), CN = 6), pentagonal bipyramid (Y(3), CN = 7), dodecahedron (Y(2), CN = 8) and capped square antiprism (Y(4), CN = 9). The Y atoms have varying distances depending on the coordination arrangement with oxygen atoms. The Y–O distances are in the range 2.221(3)-2.886(3) Å. There are six carboxylate anions which have been grouped into three types based on their connectivity {acids-1 and -5 (1212) with two chelation}, {acids-2, -3 and -6 (1111) no chelation} and {acid-4 (1111) with one chelation}. The torsion angles, in general, represent the degree of distortion in the carboxylate units from the plane of the benzene ring due to the bonding with the metal atoms. In **XXI**, the torsion angles suspended between the two carboxylate groups from the benzene ring and are in the 0.32 – 7.98° range. The carboxylate groups of the acids -2, -3 and -6 are

more distorted compared to -1, -4 and -5. The six 1,2-BDC anions also show distinct differences in their connection modes with the Y atoms.

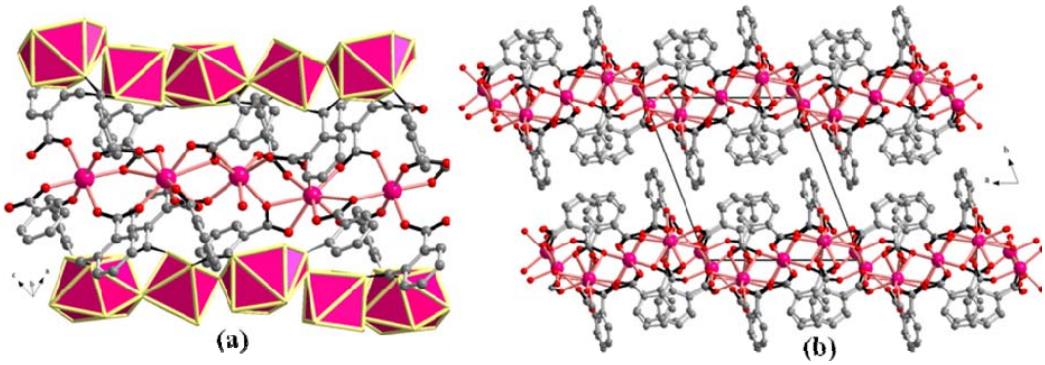

Fig. 2.4.26. (a) Showing the connectivity of 1D chains into 2D layer and (b) packing arrangement in **XXI**.

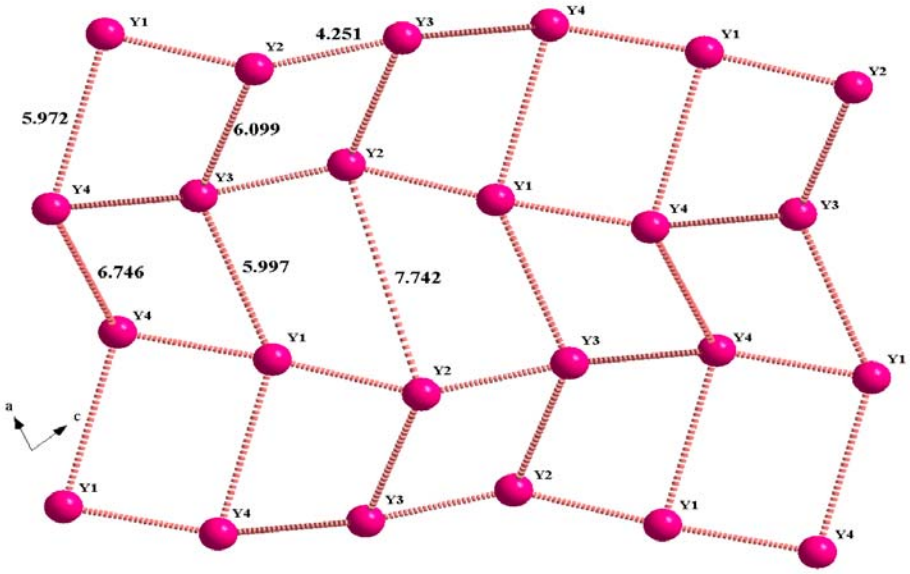

Fig. 2.4.27. Showing the Y atom connectivity within the corrugated layer of **XXI**.

The two-dimensional structure of **XXI** consists of a network of Y polyhedra connected together through their corners ($^3\mathbf{D_1}$ dimer SBUs) to give rise to an infinite one-dimensional Y–O–Y chains. The one-dimensional Y–O–Y chains are connected through the 1,2-BDC anions to form the layer structure ($\boldsymbol{I^1O^1}$) (Fig. 2.4.26a). Within the layer, the large number of $\pi\ldots\ \pi$ interactions creates a corrugated nature to the sheets (Fig. 2.4.26b). The 1,2-BDC, in general, suspends

an angle of 60° between the carboxylate groups. This would presumably give rise to interesting $\pi\ldots\pi$ interactions with in a solid.

The role of $\pi\ldots\pi$ interactions for the stability of organic compounds has been discussed recently, with particular emphasis on the centroid–centroid distances (*d*) and the angle (*q*) suspended between the benzene rings.[52] A correlation between the two (*d* and *q*) has been discussed in terms of a phase-diagram with the distances and angles having a unique relationship. From this, the following interactions appear to be important for different values of the centroid–centroid distance (*d*) and angles (*q*): (i) *d* = 0–3 Å and *q* = 50–90°, (ii) *d* = 3–7 Å and *q* = 0–50°, (iii) *d* = 4–7.5 Å, *q* = 140–180° and (iv) *d* = 6–7 Å and *q* = 0–145°. In the present structure, two distinct $\pi\ldots\pi$ interactions have been observed: one is the intra-layer and the other is the inter-layer. The interactions between the acids 1 and 2 within the layer (intra) with *d* = 4.205 Å and *q* = 8.19° and acids 3 and 6 with *d* = 5.027 Å and *q* = 118.43° are can be classified as moderate. Compared to the intra-layer, the inter-layer interactions appear to be more and in number. Thus the interactions between the acids 1 and 5 (*d* = 6.568 Å, *q* = 92.98°), 3 and 3' (*d* = 5.022 Å, *q* = 0°), 3 and 6 (*d* = 4.66 Å, *q* = 3.85°) and 5 and 2 (*d* = 5.217 Å, *q* = 8.43°) appear to be moderate. Since there are no other interactions between the layers, the $\pi\ldots\pi$ interactions appear to be the dominant interactions responsible for holding the layers apart and intact. The connectivity between the Y atoms within the layer is shown in Fig. 2.4.27. As can be seen, the Y–Y distances have different values ranging from 4.251–7.742 Å. The Y distances within the chain are the following: Y(1)-Y(2) = 4.33, Y(2)-Y(3) = 4.251, Y(3)-Y(4) = 4.642 and Y(4)-Y(1) = 4.441 Å. The distances between the chains have generally higher values.

$Dy_2(1,2\text{-BDC})_3(H_2O)$, **XXII**, has a two-dimensional structure with one-dimensional inorganic connectivity ($\boldsymbol{I^1O^1}$). It has an asymmetric unit with 39 non-hydrogen atoms. There are two Dy^{3+} cations in two crystallographically distinct positions, three phthalate (1,2-BDC) dianions and a terminal water molecule in the asymmetric unit. The three BDC anions [acid-1 to acid-3] exhibit three different coordination modes with the torsional angle of 59.67(5), 83.84(3) and 47.42(4)º respectively. Acids-1, -2 and -3 have (1211), (2011) and (1221) connectivities respectively. Acid-1 binds to three Dy^{3+} cations. Acid-2 and -3 bind to four Dy^{3+} cations. Acid-1 binds to two Dy(1) and one Dy(2). Acid-2 and -3 each binds to two Dy(1) and two Dy(2).

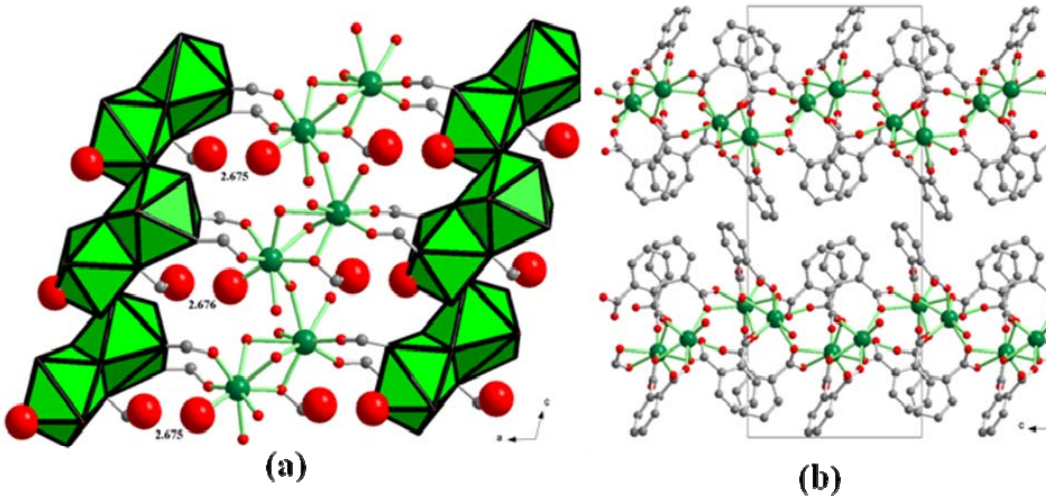

Fig. 2.4.28. (a) Showing the connectivity of 1D chains into 2D layer and (b) packing arrangement in **XXII**.

Dy(1) is eight-coordinated (DyO_8) with the oxygen atoms from six different 1,2-BDC anions. Among the eight oxygen atoms of $Dy(1)O_8$, four are having $\boldsymbol{\mu_2}$ connectivity and the remaining four are having $\boldsymbol{\mu_3}$ connectivity. These $\boldsymbol{\mu_3}$ oxygen atoms link Dy(1) to a Dy(2) through corner ($^2\mathbf{D_1}$ dimer SBUs) and to another Dy(2) through face {($^2\mathbf{d_2}$ + $^1\mathbf{D_1}$) dimer SBUs}. The Dy-O bond lengths are

in the 2.286(7) - 2.636(7) Å range. Dy(2) is also eight-coordinated (DyO_8) with seven oxygen atoms from four different 1,2-BDC anions and an oxygen atom from a terminal water molecule. Among the seven carboxylate oxygen atoms of $Dy(2)O_8$, three are having μ_2 connectivity and the remaining four are having μ_3 connectivity. These μ_3 oxygen atoms link Dy(2) to two different Dy(1) cations, one through a face and another via a corner. The Dy-O bond lengths are in the 2.305(7) - 2.854(7) Å range.

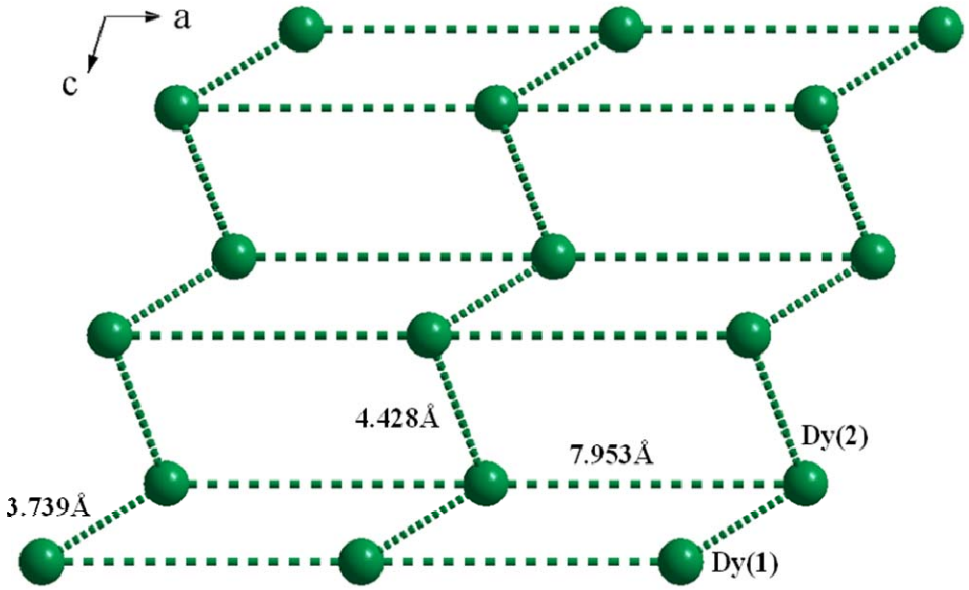

Fig. 2.4.29. Showing the Dy atom connectivity within the layer structure of **XXII**.

The connectivities in these two polyhedra lead to the formation of a face shared dimer of [Dy(1)-Dy(2)]. Each dimer is connected to two such dimers by sharing the corners. These connectivities of alternating corner and face shared polyhedra lead to the formation of an infinite one-dimensional Dy-O-Dy chain. These chains are further connected by the carboxylates of the BDC anions in to an infinite two-dimensional structure ($\boldsymbol{I^1O^1}$) (Fig. 2.4.28a). The two-dimensional layer structure is further stabilized by inter and intra-layer π…π and C-H…π interactions

among the BDC anions similar to **XXI** and intra layer hydrogen bonding interactions between the terminal water molecules and the BDC anions (Fig. 2.4.28b). The connectivity between the Dy atoms within the layer is shown in Fig. 2.4.29. The Dy-Dy distances within the chain are the following: Dy(1)-Dy(2) = 3.739 Å {($^2\mathbf{d_2}$ + $^1\mathbf{D_1}$) dimer SBUs}, and Dy(1)-Dy(2) = 4.428 Å ($^2D_1$ dimer SBUs). The distance between the chains Dy(1)-Dy(1) and Dy(2)-Dy(2) = 7.953 Å.

[M_2(1,2-BDC)$_2$(PipDPDA)], **XXIII**, (where M = La, Pr and PipDPDA = N,N'-Piperazine diphthalidodiamide dianion) has a two-dimensional structure with one-dimensional inorganic connectivity (***I*^{1}*O*^{1}**). It has an asymmetric unit with 27 non-hydrogen atoms (Fig. 2.4.30). There are one M^{3+} cation, one phthalate (1,2-BDC) dianion and one-half of the *in-situ* generated PipDPDA dianion (with two carboxylate and two amide groups, Scheme 1) in the asymmetric unit. The BDC anion exhibits (1221) connectivity with a chelating bi dentate coordination mode in each carboxylate group. The torsional angle is 28.72(3)º. It binds to three M^{3+} cations. The hexadentate diacid-diamide, PipDPA, is *in-situ* generated from two 1,2-H_2BDC and a piperazine molecules by the removal of two water molecules (Scheme 1). It binds to six M^{3+} cations through its two carboxylate and two amide groups. The torsional angle between the two carboxylate group is 46.43(5)º. The M-O bond lengths are in the 2.391(3) - 2.688(3) Å range for M = La and in the 2.395(3) - 2.695(3) Å range for M = Pr.

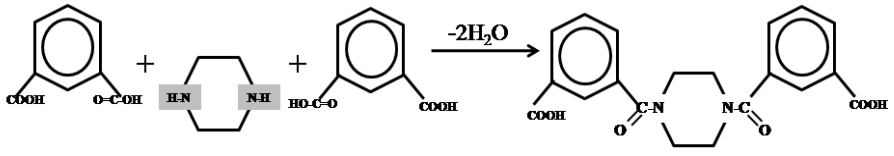

1,2-BDC Piparazine **Scheme 1** PipDPDA

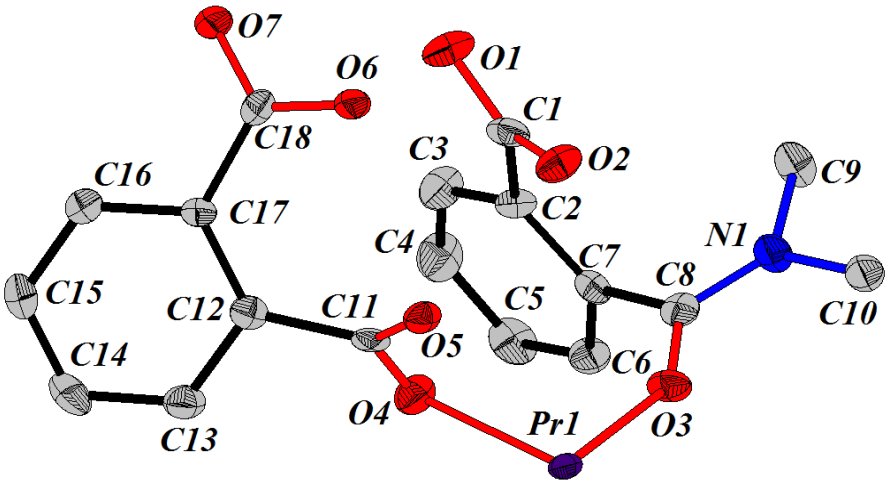

Fig. 2.4.30. ORTEP plot of **XXIII** (Thermal ellipsoids are shown at 50% probability).

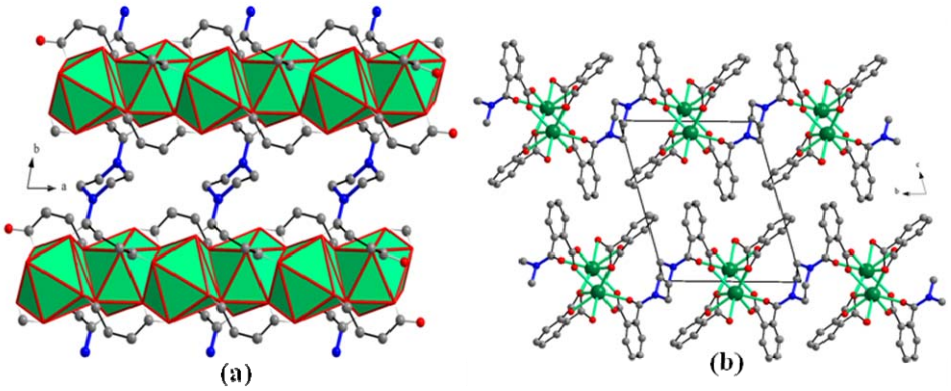

Fig. 2.4.31. (a) Showing the connectivity of 1D chains into 2D layer and (b) packing arrangement in **XXIII**.

The M^{3+} cation is nine-coordinated (MO_9) with the oxygen atoms from three different 1,2-BDC anions and three PipDPA anions. Among the nine oxygen atoms, five are having μ_2 connectivity and the remaining four are having μ_3 connectivity. These μ_3 oxygen atoms link the M^{3+} cations through edges (shared $^4\mathbf{D_2}$ dimer SBUs) into a one-dimensional chain with infinite M-O-M linkages. These chains can be also viewed as the infinite one-dimensional chains containing edge-sharing dimers ($^4\mathbf{D_2}$) of SBUs similar to paddle wheel type with two extra M-O-M bridges (an edge). These chains are further connected by the amide anions

into an infinite two-dimensional structure (***I*^{1}*O*^{1}**) (Fig. 2.4.31a, rings in BDCs are not shown). The two-dimensional layer structure is further stabilized by inter and intra-layer π…π and C-H…π interactions among the BDC anions (Fig. 2.4.31b).

(b) 1,3-Benzenedicarboxylate

We have obtained a new two-dimensional layer compound, [Cd(1,3-BDC)(H_2O)], **XXIV**, devoid of any amine, where Cd is in a distorted pentagonal bipyramidal environment (CdO_7) with Cd–O bond distances in the 2.238–2.680 Å range. Asymmetric unit of **XXIV** is shown in Fig. 2.4.32a. The CdO_7 polyhedron is formed by a coordinated water molecule and six oxygens from tridentate carboxylic acid groups of the four different molecules with (2121) connectivity. The edge sharing polyhedra are connected by the carboxylic acid molecules (**$^2D_2$** dimer SBUs) to form one-dimensional chains. The chains get interconnected by the carboxylic acids to form an extended two-dimensional layer structure (***I*^{1}*O*^{1}**) (Fig. 2.4.32b). The structure is stabilized by interlayer C-H···$\boldsymbol{\pi}$ interactions (2.823 Å, 119.0^o) between the 1,3-BDC rings.

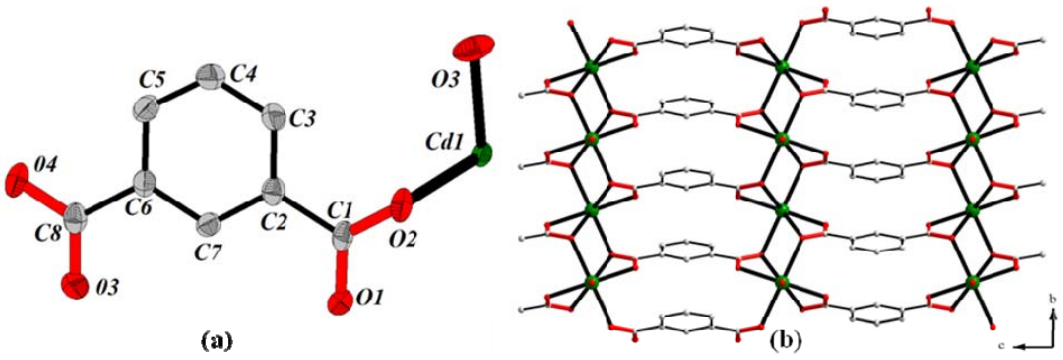

Fig. 2.4.32. (a) ORTEP plot of **XXIV** (Thermal ellipsoids are shown at 50% probability) and (b) view of the 2D layer with infinite Cd-O-Cd chains along the *a* axis in **XXIV**.

c) 1,4-Benzenedicarboxylate

The terephthalate, Pb(1,4-BDC), **XXV**, has a three-dimensional structure with two-dimensional inorganic connectivity ($\boldsymbol{I^2O^1}$). It has an asymmetric unit of 13 non-hydrogen atoms. The asymmetric unit contains a Pb^{2+} ion and a terephthalate dianion (Fig. 2.4.33a). The terephthalte anion exhibits a coordination mode with (1222) connectivity with the torsional angle of 30.71(2) º. The chelating tridentate and bis(bidentate) are the two coordination modes exhibited by the two carboxylate groups of the dicarboxylate anion.

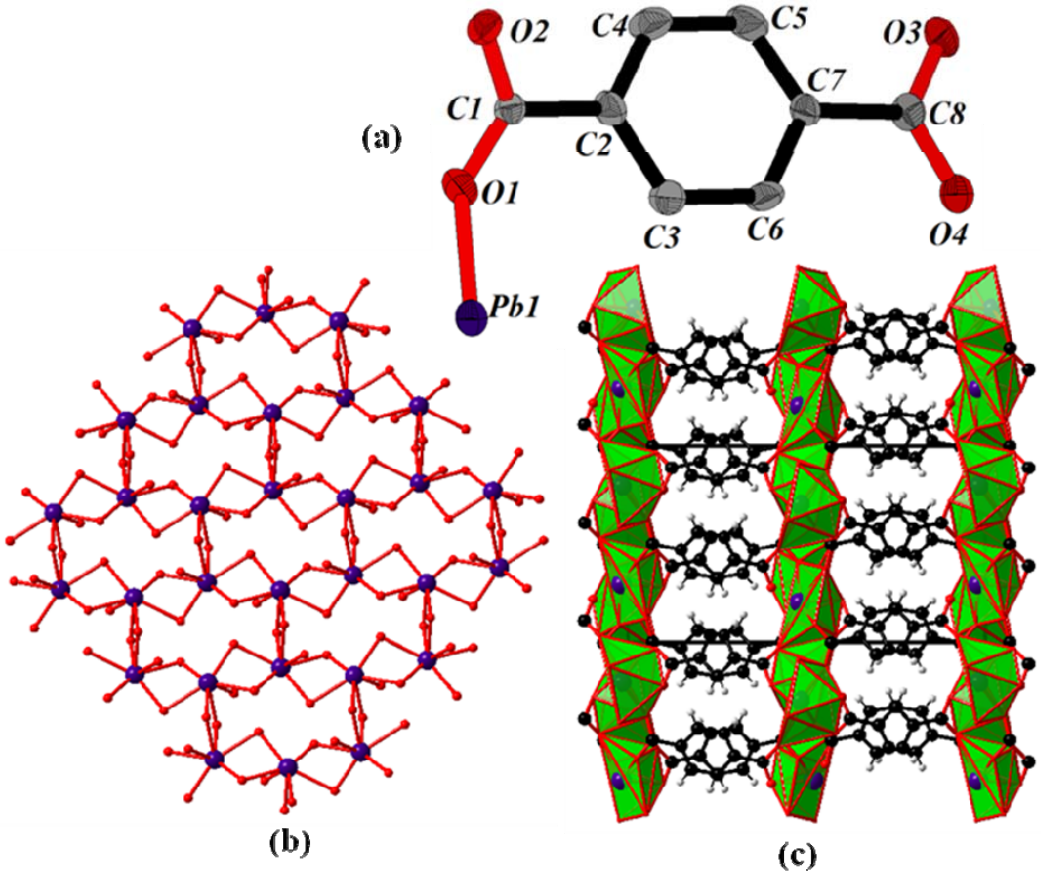

Fig. 2.3.33. (a) ORTEP plot of **XXV** (Thermal ellipsoids are shown at 50% probability) and (b) view of the 2D layer with infinite Cd-O-Cd connectivity (c) view of the 3D structure of **XXIV** showing the connectivity of the layers.

The Pb atom is hemi-directed and seven-coordinated by oxygen atoms (PbO_7) from six different terephthalate anions. Six of the oxygens have $\boldsymbol{\mu}_3$

connections linking each Pb with three other Pb atoms. The remaining one has μ_2 connection. Thus, a PbO_7 polyhedron shares its three edges with three different PbO_7 polyhedra forming an infinite two-dimensional Pb-O-Pb layer of the I^2O^0 type, with a (3,6) 2D-net topology having 'T' shaped 3-connecting nodes and six membered rings (Fig. 2.4.33b). This layer can be viewed as chains of edge ($^2\mathbf{d}_2$)shared PbO_7 polyhedra connected through the edges ($^2\mathbf{D}_2$) of PbO_7 polyhedra of the adjacent chains. The layers get further connected to each other through terephthalate anions into a three-dimensional structure of the I^2O^1 type (Fig. 2.4.33c). The Pb-O bond lengths are in the 2.531 – 2.782 Å range.

2.4.3. Process of formation of a three-dimensional zinc terephthalate

In the absence of any chelating amine, we find that Zn forms 1,4-BDCs with a one-dimensional (I^0O^1) chain structure, [Zn(1,4-BDC)$(H_2O)_2$], **A**, and a three-dimensional (I^0O^3) structure [Zn(1,4-BDC)(H_2O)], **B**, both of which have been reported earlier[53,54] (Fig. 2.4.34). In **A**, Zn is in a distorted tetrahedral environment with two coordinating water molecules and two oxygens from the monodentate carboxylate, the polyhedra being connected by the carboxylate units to form the one-dimensional chains. In **B**, Zn is in a trigonal bipyramidal environment with a coordinated water and four oxygens from the carboxylate. The zig-zag chains of ZnO_5 and 1,4-BDC units are connected to form the three-dimensional structure with a one-dimensional channel along the b-axis. Since we could readily form both one and three-dimensional zinc 1,4-BDCs in the absence of a chelating amine, we considered it of significance to examine the relation between the two 1,4-BDCs of different dimensionalities. For this purpose, we have studied the time and temperature dependence of the products obtained from a starting reaction mixture containing $ZnSO_4.4H_2O$, 1,4-BDC and NaOH in H_2O

with the molar ratio (1:1:2:278) maintained at a fixed temperature. On keeping the reaction mixture at 75°C for 72h, we obtained the one-dimensional compound [Zn(1,4-BDC)(H_2O)$_2$], **A**, in pure form. On keeping the reaction mixture at 180°C for 72h, the three-dimensional compound [Zn(1,4-BDC)(H_2O)], **B** was obtained.

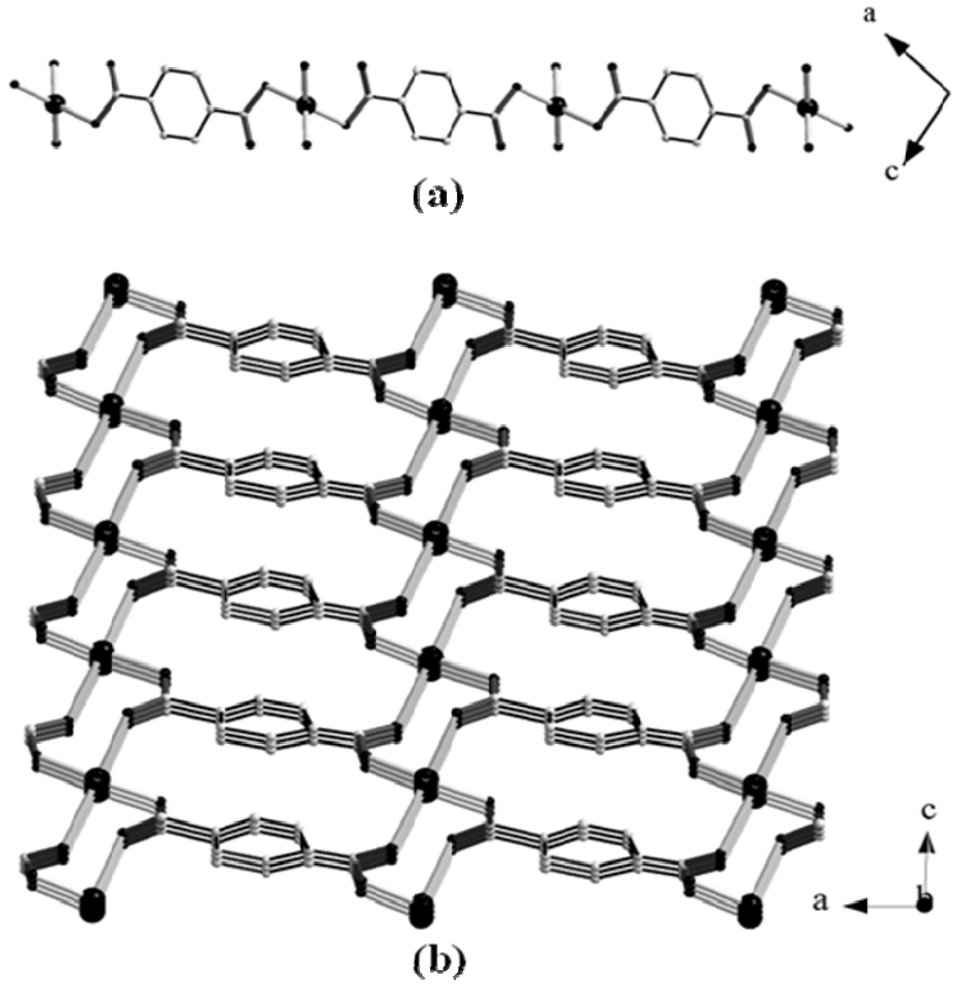

Fig. 2.4.34. (a) one-dimensional structure of [Zn(1,4-BDC)(H_2O)$_2$], **A** and (b) 3D structure of [Zn(1,4-BDC)(H_2O)], **B**.

The powder XRD patterns of **A** and **B** obtained at 75°C and 180°C are shown in Fig. 2.4.35a. On keeping the reaction mixture at 125°C for 72h, we obtained a new compound designated as **N**. we show the powder XRD pattern of **N** in Fig. 2.4.35a. It is possible that **N** has a two-dimensional layer structure, but we have not been able to establish the structure based on a single-crystal study. The

water content decreases on going from the one-dimensional **A** to three-dimensional **B** and the coordination mode of the carboxylate also changes. Thus, the carboxylate changes from a bidentate (1010) to a tetradentate (1111) ligand with the coordination number of zinc increasing from four to five. These results are similar to those reported by Foster and Cheetham, who find an increase in dimensionality and a decrease in water content in cobalt succinate with the increase in the reaction temperature.[27]

In order to establish the relation between one-dimensional **A** and three-dimensional **B**, we have studied the effect of time and temperature on **VI** under hydrothermal conditions. At 150^{o}C, **A** transforms to a mixture of **A** and the new phase **N** after 3h as shown in Fig. 2.4.35b. After 72h, we obtain a mixture of **A** and **B** as shown in 2.4.35b. However, at 180^{o}C **A** transforms into **B** in 3h. These studies show that it is likely that the three-dimensional structure is formed by the transformation of one-dimensional structure. We are not certain that the transformation proceeds through a two-dimensional structure. In this context, the observation of an intermediate phase **N** is significant. The transformation of a one-dimensional structure to a three-dimensional structure and the possible presence of a dimensional hierarchy in the BDCs find a counterpart in open-framework metal phosphates.[55-59] It has been found that there is a progressive building-up of dimensionality in the open-framework metal phosphates and that the zero- and one-dimensional structures transform to higher dimensional structures on heating for a period of time at an appropriate temperature.

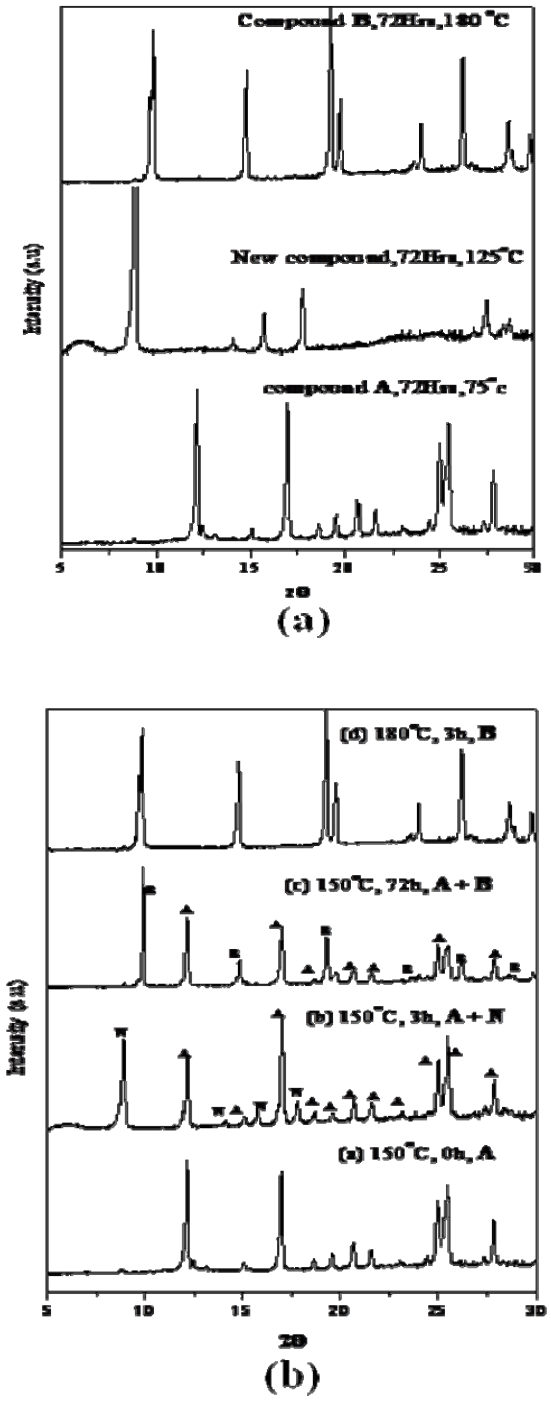

Fig. 2.4.35. (a) Powder XRD patterns of a reaction product obtained on heating a reaction mixture for 72 h at different temperature and (b) powder XRD patterns of products obtained on heating the one-dimensional compound **A**.

2.5. Conclusions

A systematic study of the metal-benzenedicarboxylates (BDCs) formed by the three isomeric dicarboxylic acids in the presence or absence of chelating amines has been carried out. Several coordination polymers and the hybrids with extended inorganic connectivity of BDCs in different dimensionality have been prepared under hydrothermal conditions and their structures established by X-ray crystallography. Summary of the structural features of the various compounds discussed in this chapter are tabulated in Tables **2.12 - 2.15**.

Six one-dimensional (I^0O^1) coordination polymers [with zero inorganic connectivity (I^0O^1)] of metal 1,2-benzenedicarboxylates with 1,10-phenanthroline or 2,2'-bipyridine as the chelating amines have been obtained. Four 1,3-benzenedicarboxylates of lanthanides with 1,10-phenanthroline or 2,2'-bipyridine as the chelating amines have been obtained. A cadmium terephthalate with a two-dimensional layer structure (I^0O^2) is obtained. Three heteroleptic mixed benzenedicarboxylates with chelating amines have been obtained with two-dimensional (I^0O^2) and three-dimensional (I^0O^3) structures, where ladders formed by the the 1,2-BDC anions are connected by the 1,3-BDC or 1,4-BDC anions into the higher dimensional structure. Two heteroleptic mixed benzenedicarboxylates without chelating amines have been obtained with three-dimensional (I^0O^3) structures, where layers formed by the the 1,2-BDC anions are connected by the 1,4-BDC anions into the three-dimensional dimensional structure.

Five hybrid frameworks of metal benzenedicarboxylates with extended inorganic connectivity were obtained with or without chelating amines. Eu and Tb doped compounds of a one-dimensional structure exhibit the lanthanide-centered red and green emission respectively at room temperature, sensitized by the ligands.

A two-dimensional compound with an *in-situ* generated ligand has been synthesized. Transformation studies in the zinc terephthalate system have been carried out. These studies show that the transformation of a one-dimensional structure to a three-dimensional structure and the possible presence of a dimensional hierarchy.

Presence of secondary ligands and chelating amines such as 1,10-phenanthroline and 2,2-bipyridine, decrease the overall dimensionality of the compounds, but stabilizes the low dimensional crystal structure. The chelating amines project into opposite sides of the layer structures, thereby preventing the formation of a three-dimensional interpenetrating network of the 1,4-BDC. Variation in the chelating amines results in the variation of supramolecular interactions in the structures and this in turn offers a method to design hybrids with tunable inorganic connectivity.

1,2-benzenedicarboxylic acid favors the formation of low dimensional compounds and extended inorganic connectivity. Higher dimensional structures are however, favored most in the case of 1,3- and 1,4-benzenedicarboxylic acids because of the right disposition of the two carboxylic groups in the benzene ring.

Increase in the size of the metal cation also favors the formation of higher dimensional compounds and extended inorganic connectivity through the increased coordination number. It is noteworthy that dimensional hierarchy and progressive building-up of dimensionality are both found in the zinc 1,4-benzenedicarboxylates.

Table 2.12. Coordination polymers with chelating amines.

Compound No.	Formula	Dimensionality	Connectivity	Dimer SBUs
I	$[Zn(H_2O)(1,2\text{-BDC})(1,10\text{-phen})].H_2O$	**1**	I^0O^1	**Helical chain**
II	$[Cd(H_2O)(1,2\text{-BDC})(2,2'\text{-bipy})]$	**1**	I^0O^1	**Helical chain**
III	$[Cd(H_2O)(1,2\text{-BDC})(1,10\text{-phen})]$	**1**	I^0O^1	$^2D_2$
IV	$[Y_2(1,2\text{-BDC})_3(1,10\text{-phen})_2]\cdot H_2O$	**1**	I^0O^1	$^2D_0$ & $^4D_2$
V	$[M_2(1,2\text{-BDC})_3(1,10\text{-phen})]$, (M = Y, Gd and Dy)	**1**	I^0O^1	$^4D_0$ & $^4D_2$
VI	$[Dy_2(1,2\text{-BDC})_3(1,10\text{-phen})]$	**1**	I^0O^1	$^2D_0$ & $^2D_2$
VII	$[M_2(1,3\text{-BDC})_3(2,2'\text{-bipy})_2]$, (M = Y, Gd and Dy)	**2**	I^0O^2	$^4D_0$
VIII	$[M_2(1,3\text{-BDC})_3(2,2'\text{-bipy})_2]\cdot H_2O$ (M = Y, Gd and Dy)	**3**	I^0O^3	$^4D_0$
IX	$[Y_2(1,3\text{-BDC})_3(1,10\text{-phen})_2]$	**3**	I^0O^3	$^2D_0$ & $^4D_0$
X	$[Nd_2(1,3\text{-BDC})_3(1,10\text{-phen})_2]$	**2**	I^0O^2	$^4D_0$ & $^4D_2$
XI	$[Cd(1,4\text{-BDC})(1,10\text{-phen})].H_2O$	**2**	I^0O^2	$^2D_2$

Table 2.13. Mixed-acid coordination polymers with chelating amines.

Compound No.	Formula	Dimensionality	Connectivity	Dimer SBUs
XII	$[Y_2(1,2\text{-BDC})_2(1,3\text{-BDC})(1,10\text{-phen})_2]$	**2**	I^0O^2	$^2D_0$
XIII	$[Y_2(1,2\text{-BDC})_2(1,4\text{-BDC})(1,10\text{-phen})_2]$	**2**	I^0O^2	$^2D_0$
XIV	$[Pr_2(1,2\text{-BDC})_2(1,4\text{-BDC})(1,10\text{-phen})_2(H_2O)_2]\cdot H_2O$	**3**	I^0O^3	$^2D_2$

Table 2.14. Coordination polymers without chelating amines.

Compound No.	Formula	Dimensionality	Connectivity	Dimer SBUs
XV	$[M_2(1,2BDC)_2(1,4BDC)(H_2O)_4]$, (M = La and Pr)	**3**	I^0O^3	$^3D_2$
XVI	$[M_2(1,2BDC)_2(1,4BDC)(H_2O)_4]$, (M = Gd, Dy, and Y)	**3**	I^0O^3	$^2D_0$
XVII	$[Gd_2(1,2\text{-}BDC)_4(H_2O)_2].(H_2Pip)$	**2**	I^0O^2	$^2D_0$
XVIII	$(OPb_4)(1,3\text{-}BDC)_3(H_2O)$	**3**	I^0O^3	**Octamer**

Table 2.15. Hybrids with extended inorganic connectivity.

Compound No.	Formula	Dimensionality	Connectivity	Dimer SBUs
XIX	$[M_3(1,2\text{-}BDC)_4(1,10\text{-}phen)_3(H_2O)]\cdot 0.5H_2O$, (M = La and Pr)	**1**	I^1O^0	$^3D_2$ & $^2D_1$
XX	$[M_3(1,2\text{-}BDC)_4(1,10\text{-}phen)_2(NO_3)]\cdot H_2O$, (M = La and Pr)	**1**	I^1O^0	$^2d_2$,$^2D_2$ & $^3D_2$
XXI	$Y_2(1,2\text{-}BDC)_3(H_2O)$	**2**	I^1O^1	$^3D_1$
XXII	$Dy_2(1,2\text{-}BDC)_3(H_2O)$	**2**	I^1O^1	($^2d_2$ + $^1D_1$) & $^2D_1$
XXIII	$[M_2(1,2\text{-}BDC)_2(PipDPA)]$, (M = La and Pr)	**2**	I^1O^1	$^4D_2$
XXIV	$[Cd(1,3\text{-}BDC)(H_2O)]$	**2**	I^1O^1	$^2D_2$
XXV	[Pb(1,4-BDC)]	**3**	I^2O^1	$^2d_2$ & $^2D_2$

2.5. References

1) M. Jansen, J. C. Schön, *Angew. Chem. Int. Ed.*, **2006**, 45, 3406.

2) M. Jansen, *Angew. Chem. Int. Ed.*, **2002**, 41, 3746.

3) C. N. R. Rao, S. Natarajan and R. Vaidhyanathan, *Angew. Chem. Int. Ed*., **2004**, 43, 1466.

4) S. Batten and R. Robson, *Angew. Chem., Int. Ed*., **1998**, 37, 1460.

5) J. Hagrman, D. Hagrman and J. Zubieta, Angew. Chem., Int. Ed., **1999**, 38, 2638.

6) M. Eddaoudi, D. Moler, H. Li, B. Chen, T. M. Reineke,M. O'Keeffee and O. M. Yaghi, *Acc. Chem. Res*., **2001**, 34, 319.

7) B. Moulton and M. J. Zawarotko, *Chem. Rev*., **2001**, 101, 1629.

8) O. M. Yaghi, H. L. Li, C. Davis, D. Richardson and T. L. Groy, *Acc. Chem. Res.*, **1998**, 31, 474.

9) C. Serre, F. Taulelle and G. Férey, *Chem. Commun*., **2003**, 2755.

10) F. Millange, C. Serre and G. Férey, *Chem. Commun.*, **2002**, 822.

11) C. Serre, F. Millange, C. Thouvenot, M. Noguès, G. Marsolier, D. Louër and G. Férey, *J. Am. Chem. Soc*, **2002**, 124, 13519.

12) K. Barthelet, J. Marrot, G. Férey and D. Riou, *Chem. Commun.*, **2004**, 520.

13) K. Barthelet, K. Adil, F. Millange, C. Serre, D. Riou and G. Férey, *J. Mater. Chem*., **2003**, 13, 2208.

14) M. Eddaoudi, J. Kim, D. Vodak, A. Sudik, J. Wachfer, M. O'Keeffe and O. M. Yaghi, *Proc. Natl. Acad. Sci, USA*, **2002**, 99, 4900.

15) D. T. Vodak M. E. Braun, J. Kim, M. Eddaoudi, and O. M. Yaghi, *Chem. Commun.*, **2001**, 2532.

16) M. Eddaoudi, J. Kim, D. Vodak, A. Sudik, J. Wachfer, M. O'Keeffe and O. M. Yaghi, *Science*, **2002**, 295, 4900.

17) H. Li, C. E. Davis, T. L. Groy, D. G. Kelley and O. M. Yaghi, *J. Am. Chem. Soc*., **1998**, 120, 2186.

18) S. A. Bourne, J. Lu, A. Mondal, B. Moulton and M. J. Zawarotko, *Angew. Chem. Int. Ed*., **2001**, 40, 2111.

19) B. Moulton, H. Abourahma, M. W. Bradner, J. Lu, G. J. McManus and M. J. Zaworotko, *Chem. Commun.*, **2003**, 1342.

20) B. Moulton, J. Lu, R. Hajndl, S. Hariharan and M. J. Zaworotko, *Angew. Chem. Int. Ed*., **2002**, 41, 2821.

21) J. S. Seo, D. Whang, H. Lee, S. I. Jun, J. Oh, Y. J. Jeon and K. Kim, *Nature*, **2000**, 404, 982.

22) P. M. Forster and A. K. Cheetham, *Angew. Chem. Int. Ed*., **2002**, 41, 457.

23) R. Kitaura, K. Fujimoto, S. Noro, M. Kondo and S. Kitagawa, *Angew. Chem. Int. Ed*., **2002**, 41, 133.

24) N. L. Rosi, J. Eukert, M. Eddaoudi, D. T. Vodak, J. Kim, M. O'Keeffe and O. M. Yaghi, *Science*, **2003**, 300, 1127.

25) J. L. C. Rowsell, A. R. Millward, K. S. Park and O. M. Yaghi, *J. Am. Chem. Soc*., **2004**, 126, 5666.

26) B. Panella and M. Hirscher, *Adv. Mater*., **2005**, 17, 538.

27) P. M. Forster, A. R. Burbank, C. Livage G. Férey and A. K. Cheetham, *Chem. Commun*., **2004**, 368.

28) L. Yi, B. Ding, B. Zhao, P. Cheng, D-Z. Liao, S-P. Yan and Z-H. Jiang, *Inorg. Chem*., **2004**, 43, 33.

29) H. K. Fun, S. S. S. Raj, R. G. Xiong, J. L. Zuo, Z. Yu, X. Z. You, *J. Chem. Soc., Dalton Trans.* **1999**, 1915.

30) O. R. Evans, R. G. Xiong, Z. Wang, G. K. Wong, W. Lin, *Angew. Chem. Int. Ed.* **1999**, *38*, 536.

31) D. Sun, R. Cao, Y. Liang, Q. Shi, W. Su, M. Hong, *J. Chem.Soc., Dalton Trans.* **2001**, 2335.

32) S. Barbara, *Infrared Spectroscopy: Fundamentals and Applications*; Wiley: New York, **2004**.

33) R. M. Silverstein, G. C. Bassler, T. C. Morrill, *Spectrometric Identification of Organic Compounds*; John Wiley & Sons: New York, **1963.**

34) K. Nakamoto, *Infrared and Raman Spectra of Inorganic and Coordination Compounds*; Wiley: New York, **1978**.

35) G. M. Sheldrick, *SADABS Siemens Area Detector Absorption Correction Program*, University of Göttingen, Gottingen, Germany, **1994.**

36) G. M. Sheldrick, SHELXTL-PLUS *Program for Crystal Structure Solution and Refinement*, University of Göttingen, Gottingen, Germany, **1997**.

37) For description of connectivity see, D. Massiot, S. Drumel, P. Janvier, M. B. Doeuff, B. Buujoli, *Chem Mater*. **1997**, 9, 6.

38) Oliver, S. R. J.; Clark, T. D.; Bowden, N.; Whitesides, G. M. *J. Am. Chem. Soc*. **2001**, *123*, 8119.

39) K. N. Power, T. L. Hennigar, M. J. Zaworotko, *Chem. Commun*., **1998**, 595.

40) M. J. Plater, M. R. J. Foreman, J. M. S. Skakle, *Cryst. Eng*. **2001**, *4*, 319.

41) M. O'Keeffe, B. G. Hyde, *Crystal Structures I. Patterns and Symmetry*; Mineralogical Society of America, Washington D. C., **1996**.

42) Bonefacic, A. *Acta Crystallogr.* **1961**, *14*, 116.

43) C. Serre, F. Pelle, N. Gardant and G. Férey, *Chem. Mater*., **2004**, 16, 1177.

44) F. Millange, C. Serre, J. Marrot, N. Gardant, F. Pelle and G. Férey, *J. Mater. Chem*., **2004**, 14, 642.

45) C. Serre, F. Millange, C. Thouvenot, N. Gardant, F. Pelle and G. Férey, J. Mater. Chem., **2004**, 14, 1530.

46) J.-C. G. Bunzli and G. R. Choppin, *Lanthanide Probes in Life*, Chemical and Earth Sciences. Theory and Practice, Elsevier, Amsterdam, **1989**.

47) P. R. Selvin, *Nat. Struct. Biol*., **2000**, 7, 730.

48) N. Sabbatini, M. Guardigli and J-M. Lahn, *Coord. Chem. Rev*., **1993**, 123, 201.

49) F. S. Richardson, *Chem. Rev*., **1982**, 82, 541.

50) S. L. Murov, I. Carmicael and G. L. Hug, Handbook of Photochemistry, Marcel Dekker, New York, **1993**.

51) G. Blasse and B. C. Grabmaier, *Luminescent Materials*, Springer, Berlin, **1994**.

52) C. A. Hunter, J. Singh and J. M. Thronton, *J. Mol. Biol.*, **1991**, 218, 837.

53) G. Guilera and J. W. Steed, *Chem. Commun*., **1999**, 1563.

54) M. Edgar, R. Mitchell, A. M. Z. Slawin, P. Lightfoot and P. A. Wright, *Chem.—Eur. J*., **2001**, 7, 5168.

55) C. N. R. Rao, S. Natarajan, A. Choudhury, S. Neeraj and A. A. Ayi, *Acc. Chem. Res*., **2001**, 34, 80.

56) A.A.Ayi, A. Choudhury, S.Natarajan, S.Neeraj and C. N. R. Rao, *J.Mater. Chem*., **2001**, 11, 1181.

57) A. Choudhury, S. Neeraj, S. Natarajan and C. N. R. Rao, *J. Mater. Chem*., **2001**, 11, 1537.

58) A. Choudhury, S. Neeraj, S. Natarajan and C. N. R. Rao, *J. Mater. Chem*., **2002**, 12, 1047.

59) R. Murugavel, M. G. Walawalkar, M. Dan, H. W. Roesky and C. N. R. Rao, *Acc. Chem. Res.*, **2004**, 37, 763.

2.7. Appendix

a) Description of dimer SBUs and terminology

The complex structures and topology of framework solids can be understood on the basis of their construction from the simple fundamental building units. The use of such building units known as secondary building units (SBUs) is very common among zeolite scientists. Structures of hybrid inorganic-organic framework solids also can be understood on the basis of SBUs. The simple SBU in hybrid solids would be a dimer of metals. The metals in the dimer can be bridged by the ligands in various coordinational modes. In carboxylate based hybrid solids the carboxylate ligands are available for binding mainly in two bridging modes namely i) "*end on*" and ii) "*end to end*" binding. Dimers can be constructed using these two bridging modes separately or a combination of them.

The dimer constructed only with the *end on* carboxylates is represented with the term $^{\mathbf{x}}\mathbf{d}_{\mathbf{y}}$, where **x** = number of bridging *end on* carboxylate groups and **y** = number of bridging oxygens ($\boldsymbol{\mu}_3$ oxygens of carboxylates and solvent molecules like water, bridging three atoms). In the case of these *end on* dimers, it is always **x** = **y**.

The dimer constructed only with the *end to end* carboxylates is represented with the term $^{\mathbf{X}}\mathbf{D}_{\mathbf{Y}}$, where **X** = number of bridging *end to end* carboxylate groups and **Y** = number of bridging oxygens ($\boldsymbol{\mu}_3$ oxygens of carboxylates and solvent molecules like water). In the case of these *end on* dimers, $\mathbf{X} \geq \mathbf{Y}$.

The dimer constructed by the combination of *end on* and *end to end* carboxylates can be represented as ($^{\mathbf{x}}\mathbf{d}_{\mathbf{y}} + {}^{\mathbf{X}}\mathbf{D}_{\mathbf{Y}}$). Higher SBUs like linear trimer, tetramer, pentamer, etc also can be understood and represented as these *end on*,

end to end or combination of these dimers. Other complex SBUs like triangular-trinuclear and tedrahedral-tetranuclear units, with bridging oxo anion are also common in the hybrid solids of carboxylate, but not represented by the dimer terminology for the reason of simplicity. Fig. A.2.1 and A. 2.2 show some of the SBUs of *end on*, *end to end* or combination of these dimers. Fig. A.2.3 shows some of the other higher SBUs.

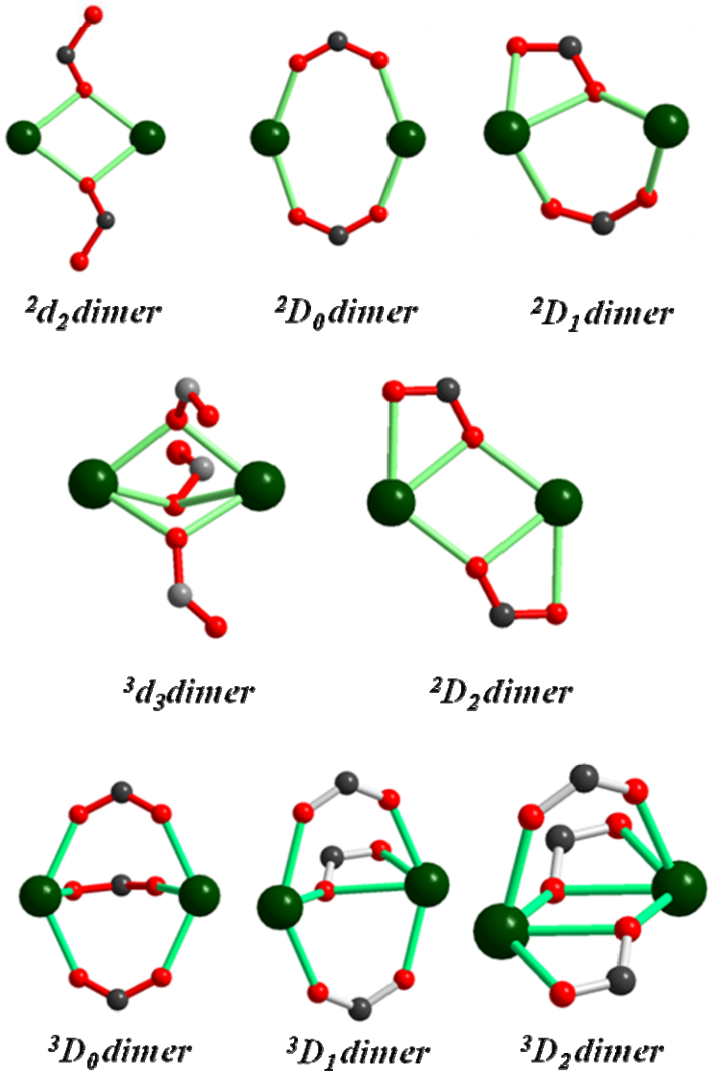

Fig. A.2.1.

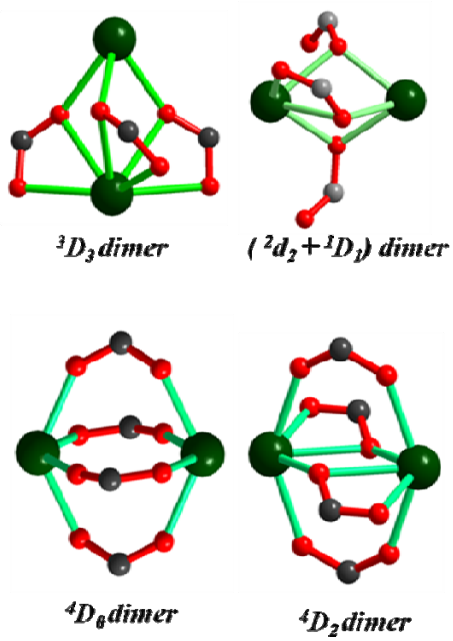

Fig. A.2.2

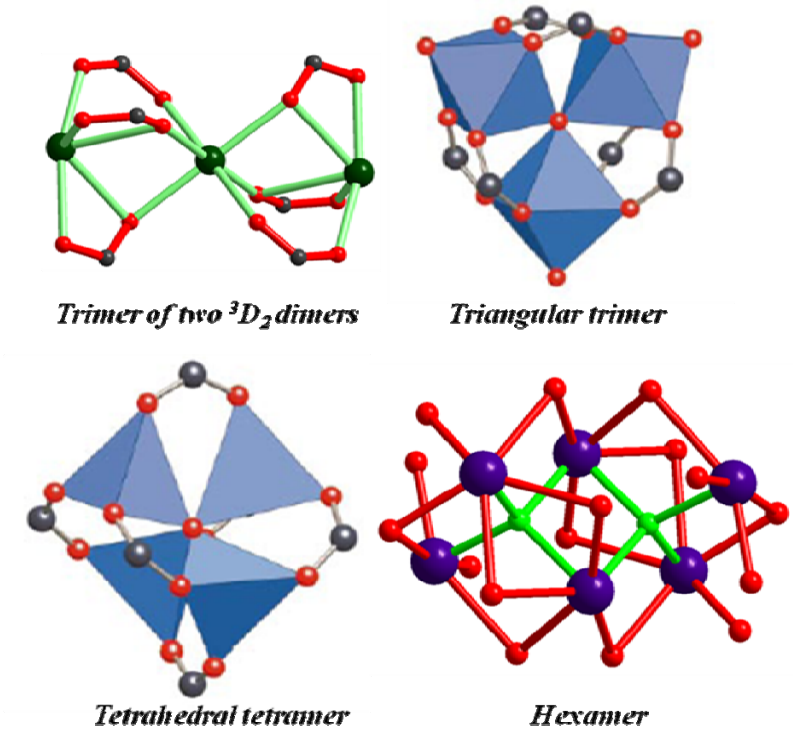

Fig. A.2.3

2.7. Appendix

(b) Tables of atomic coordinates

Table A2.1
Atomic Coordinates and Equivalent Isotropic Displacement Parameters [Å^2] for [Zn(H_2O)(1,2-BDC)(1,10-phen)].H_2O, **I**.

Atom	x	y	z	U(eq)
Zn1	0.80574	0.60871	0.16139	0.0294
O1	0.60888	0.47068	0.19608	0.0406
O2	0.65836	0.70065	0.22342	0.0362
O3	0.53650	0.25272	0.33842	0.0355
O4	0.67495	0.45051	0.34342	0.0481
O5	0.91259	0.48526	0.23117	0.0371
N1	0.86565	0.44998	0.09212	0.0303
N2	0.67984	0.67198	0.08162	0.0343
C1	0.95879	0.34217	0.09800	0.0393
C2	0.99926	0.25376	0.04774	0.0470
C3	0.94162	0.27789	-0.00983	0.0462
C4	0.84050	0.38904	-0.01779	0.0397
C5	0.77298	0.42212	-0.07662	0.0501
C6	0.67388	0.52712	-0.08102	0.0502
C7	0.63556	0.61447	-0.02769	0.0407
C8	0.53325	0.72588	-0.02890	0.0520
C9	0.50679	0.80601	0.02402	0.0526
C10	0.58394	0.77790	0.07841	0.0451
C11	0.70387	0.58970	0.02982	0.0330
C12	0.80575	0.47273	0.03496	0.0317
C21	0.58236	0.58559	0.22608	0.0300
C22	0.45453	0.58943	0.26563	0.0277
C23	0.34696	0.68663	0.25072	0.0389
C24	0.22408	0.68299	0.28428	0.0464
C25	0.21012	0.58290	0.33287	0.0435
C26	0.31719	0.48720	0.34783	0.0354

U(eq) is defined as one third of the trace of the orthogonalized Uij tensor.

Table A2.2a
Atomic Coordinates and Equivalent Isotropic Displacement Parameters [Å^2] for [Cd(H_2O)(1,2-BDC)(2,2'-bipy)], **IIA**.

Atom	x	y	z	U(eq)
Cd1	0.22575	0.19438	0.34029	0.0336
O1	0.03039	0.30896	0.33974	0.0504
O2	0.11861	0.04703	0.23995	0.0478
O3	0.13854	0.77061	0.24951	0.0491
O4	0.07756	0.57588	0.19463	0.0446
O5	0.19146	0.46791	0.35194	0.0473
N1	0.38874	0.23593	0.45198	0.0341
N2	0.19911	0.03247	0.43394	0.0352
C1	0.48787	0.32979	0.45548	0.0431
C2	0.59720	0.34298	0.51658	0.0436
C3	0.60543	0.25536	0.57723	0.0407
C4	0.50583	0.15731	0.57439	0.0380
C5	0.39648	0.14933	0.51089	0.0308
C6	0.28493	0.04527	0.50390	0.0335
C7	0.26904	-0.03681	0.56515	0.0439
C8	0.16587	-0.13336	0.55422	0.0509
C9	0.08203	-0.14887	0.48319	0.0510
C10	0.10078	-0.06382	0.42476	0.0443

C11	0.06347	0.66573	0.24041	0.0344
C12	-0.04649	0.64779	0.28754	0.0343
C13	-0.15683	0.73986	0.27874	0.0454
C14	-0.26513	0.71961	0.31566	0.0578
C15	-0.26385	0.60992	0.36281	0.0619
C16	-0.15711	0.51896	0.37182	0.0526
C17	-0.04730	0.53518	0.33363	0.0344
C18	0.06832	0.43146	0.34263	0.0364

U(eq) is defined as one third of the trace of the orthogonalized Uij tensor.

Table A2.2b

Atomic Coordinates and Equivalent Isotropic Displacement Parameters [Å^2] for [Cd(H_2O)(1,2-BDC)(2,2'-bipy)], **IIB**.

Atom	x	y	z	U(eq)
Cd1	0.36665(1)	-0.06058(1)	0.90097(5)	0.0325(1)
O1	0.2973(2)	0.03136(10)	0.7510(3)	0.0449(7)
O2	0.4360(2)	0.05580(10)	0.9401(3)	0.0440(9)
O3	0.4951(2)	0.11095(11)	0.5611(3)	0.0449(8)
O4	0.36976(19)	0.16686(12)	0.3908(5)	0.0647(9)
O5	0.4549(2)	-0.12055(11)	0.6916(3)	0.0462(8)
N1	0.2317(3)	-0.04869(13)	1.1254(3)	0.0411(9)
N2	0.1730(3)	-0.11697(12)	0.8592(3)	0.0378(9)
C1	0.2684(4)	-0.01831(19)	1.2590(4)	0.0567(12)
C2	0.1928(4)	-0.01606(18)	1.3924(7)	0.0682(13)
C3	0.0734(4)	-0.0447(2)	1.3866(9)	0.0720(16)
C4	0.0331(4)	-0.0762(2)	1.2499(5)	0.0573(12)
C5	0.1145(3)	-0.07852(16)	1.1200(4)	0.0399(10)
C6	0.0816(3)	-0.11390(14)	0.9711(4)	0.0367(9)
C7	-0.0369(3)	-0.14517(18)	0.9466(4)	0.0562(13)
C8	-0.0588(4)	-0.1807(2)	0.8068(5)	0.0687(16)
C9	0.0353(4)	-0.1837(2)	0.6955(5)	0.0670(16)
C10	0.1493(3)	-0.15076(19)	0.7238(4)	0.0553(12)
C11	0.3580(3)	0.07350(16)	0.8334(4)	0.0332(10)
C12	0.3231(3)	0.14771(15)	0.8110(3)	0.0327(9)
C13	0.2629(3)	0.18006(16)	0.9374(4)	0.0453(11)
C14	0.2082(3)	0.24432(15)	0.9175(5)	0.0534(13)
C15	0.2132(3)	0.27583(16)	0.7719(5)	0.0536(14)
C16	0.2762(3)	0.24469(15)	0.6483(4)	0.0447(11)
C17	0.3321(3)	0.18058(14)	0.6652(4)	0.0337(9)
C18	0.4047(3)	0.15058(15)	0.5263(4)	0.0365(9)

U(eq) is defined as one third of the trace of the orthogonalized Uij tensor.

Table A2.3

Atomic Coordinates and Equivalent Isotropic Displacement Parameters [Å^2] for [Cd(H_2O)(1,2-BDC)(1,10-phen)], **III**.

Atom	x	y	z	U(eq)
Cd1	0.08675(1)	0.67313(2)	-0.02422(1)	0.0311(1)
Cd2	0.02987(1)	0.67874(2)	0.19760(1)	0.0302(1)
O1	0.17758(14)	0.6305(3)	0.03960(11)	0.0708(11)
O2	0.08633(11)	0.5485(3)	0.03818(8)	0.0418(9)
O3	0.13543(13)	0.6504(2)	-0.07867(9)	0.0450(9)
O4	0.15163(12)	0.4332(2)	-0.07565(8)	0.0443(9)
O5	0.01654(12)	0.5264(3)	-0.06698(9)	0.0473(9)
O11	0.06310(12)	0.3836(3)	-0.22093(8)	0.0415(9)
O12	0.05049(10)	0.4590(2)	-0.15659(8)	0.0379(8)
O13	0.09581(12)	0.5310(3)	0.18638(8)	0.0468(10)
O14	0.09874(14)	0.6638(3)	0.13070(9)	0.0562(11)
N1	0.12548(12)	0.8874(3)	-0.00991(9)	0.0308(10)

N2	0.00757(13)	0.8282(3)	-0.05364(9)	0.0311(10)
N3	-0.02975(13)	0.8572(3)	0.16443(9)	0.0294(10)
N4	0.07733(13)	0.8729(3)	0.22814(9)	0.0312(10)
C1	0.18378(17)	0.9158(4)	0.00842(12)	0.0415(12)
C2	0.20626(18)	1.0440(4)	0.01410(13)	0.0474(14)
C3	0.16651(18)	1.1453(4)	0.00093(13)	0.0431(14)
C4	0.10414(17)	1.1191(4)	-0.01836(11)	0.0344(12)
C5	0.06078(19)	1.2219(4)	-0.03418(13)	0.0416(14)
C6	0.00299(18)	1.1936(3)	-0.05574(12)	0.0400(12)
C7	-0.01700(16)	1.0595(3)	-0.06389(11)	0.0321(11)
C8	-0.07569(16)	1.0267(4)	-0.08826(12)	0.0402(14)
C9	-0.09125(17)	0.8986(4)	-0.09530(13)	0.0454(16)
C10	-0.04878(17)	0.8021(4)	-0.07721(13)	0.0439(14)
C11	0.02362(15)	0.9571(3)	-0.04723(10)	0.0260(11)
C12	0.08583(15)	0.9879(3)	-0.02375(10)	0.0276(11)
C21	-0.08348(17)	0.8496(4)	0.13542(12)	0.0360(12)
C22	-0.11751(17)	0.9601(4)	0.11904(12)	0.0426(14)
C23	-0.09515(18)	1.0820(4)	0.13087(12)	0.0411(12)
C24	-0.03761(17)	1.0939(3)	0.16133(12)	0.0355(12)
C25	-0.0106(2)	1.2187(4)	0.17548(14)	0.0460(16)
C26	0.0425(2)	1.2268(4)	0.20599(14)	0.0499(16)
C27	0.07415(17)	1.1103(4)	0.22520(12)	0.0371(12)
C28	0.12823(18)	1.1128(4)	0.25889(13)	0.0468(16)
C29	0.15484(18)	0.9992(4)	0.27577(13)	0.0454(14)
C30	0.12820(17)	0.8808(4)	0.25983(12)	0.0399(12)
C31	0.04997(16)	0.9863(3)	0.21098(11)	0.0304(11)
C32	-0.00716(16)	0.9786(3)	0.17774(11)	0.0291(11)
C41	0.15108(15)	0.5425(4)	-0.09356(11)	0.0307(11)
C42	0.17532(15)	0.5565(3)	-0.13567(11)	0.0297(11)
C43	0.23235(17)	0.6203(4)	-0.13169(13)	0.0457(14)
C44	0.26014(18)	0.6326(4)	-0.16735(14)	0.0524(16)
C45	0.23197(17)	0.5811(4)	-0.20804(13)	0.0456(14)
C46	0.17527(16)	0.5202(4)	-0.21292(12)	0.0365(12)
C47	0.14639(15)	0.5074(3)	-0.17734(11)	0.0283(11)
C48	0.08287(16)	0.4462(3)	-0.18542(11)	0.0300(11)
C51	0.14340(17)	0.5601(3)	0.05591(11)	0.0342(12)
C52	0.17182(14)	0.4709(3)	0.09417(11)	0.0284(11)
C53	0.21580(16)	0.3839(4)	0.08464(12)	0.0369(12)
C54	0.24248(17)	0.2885(4)	0.11465(13)	0.0422(14)
C55	0.22647(16)	0.2803(4)	0.15532(13)	0.0389(12)
C56	0.18410(15)	0.3677(3)	0.16575(11)	0.0322(12)
C57	0.15656(14)	0.4640(3)	0.13581(11)	0.0264(10)
C58	0.11342(15)	0.5613(3)	0.15113(11)	0.0301(11)

U(eq) is defined as one third of the trace of the orthogonalized Uij tensor.

Table A2.4

Atomic Coordinates and Equivalent Isotropic Displacement Parameters [$Å^2$] for $[Y_2(1,2\text{-BDC})_3(1,10\text{-phen})_2]\cdot H_2O$, **IV**.

Atom	x	y	z	
Y1	0.14053(4)	0.21073(3)	0.59095(3)	0.0304(2)
Y2	0.57423(4)	0.62680(3)	0.99463(3)	0.0283(2)
O1	0.1614(6)	0.2386(5)	0.4627(4)	0.039(2)
O2	0.0781(6)	0.0453(5)	0.4599(5)	0.044(2)
O3	-0.0677(6)	-0.0931(6)	0.3502(5)	0.050(3)
O4	0.1618(6)	0.3104(5)	0.7527(5)	0.048(3)
O5	0.3131(5)	0.1145(5)	0.6297(5)	0.045(3)
O6	0.3513(5)	0.2982(5)	0.6731(5)	0.040(2)
O7	0.2278(5)	0.3277(5)	0.9087(5)	0.037(2)
O8	0.5978(5)	0.4655(5)	0.8822(4)	0.036(2)

O9	0.4942(5)	0.3212(5)	0.8825(4)	0.036(2)
O10	0.3799(5)	0.5088(5)	0.9248(4)	0.0329(19)
O11	0.3695(5)	0.6759(5)	0.9198(5)	0.042(2)
O12	0.3091(7)	0.1762(6)	0.4180(5)	0.059(3)
N1	0.1044(7)	0.4105(6)	0.6077(5)	0.038(3)
N2	-0.0766(7)	0.2378(6)	0.5287(6)	0.040(3)
N3	0.6204(6)	0.8371(6)	1.0490(5)	0.033(3)
N4	0.5806(7)	0.6947(6)	0.8629(5)	0.037(3)
C1	0.1925(9)	0.4940(8)	0.6374(7)	0.048(4)
C2	0.1732(10)	0.6074(9)	0.6631(8)	0.054(4)
C3	0.0629(10)	0.6326(9)	0.6586(8)	0.055(4)
C4	-0.0318(10)	0.5442(8)	0.6277(8)	0.047(4)
C5	-0.1518(11)	0.5643(10)	0.6204(9)	0.061(5)
C6	-0.2390(11)	0.4803(10)	0.5868(9)	0.063(5)
C7	-0.2193(9)	0.3656(9)	0.5519(8)	0.048(4)
C8	-0.3114(10)	0.2734(10)	0.5074(8)	0.057(4)
C9	-0.2871(10)	0.1686(9)	0.4714(8)	0.054(4)
C10	-0.1695(9)	0.1537(9)	0.4833(8)	0.047(4)
C11	-0.1031(8)	0.3445(8)	0.5611(7)	0.037(3)
C12	-0.0068(9)	0.4366(8)	0.6006(7)	0.038(3)
C21	0.6445(9)	0.9042(8)	1.1403(7)	0.044(3)
C22	0.6721(9)	1.0213(8)	1.1713(8)	0.047(3)
C23	0.6699(8)	1.0675(8)	1.1044(8)	0.047(4)
C24	0.6471(8)	0.9983(8)	1.0072(7)	0.040(3)
C25	0.6441(9)	1.0407(9)	0.9331(9)	0.054(4)
C26	0.6186(9)	0.9714(9)	0.8418(9)	0.056(4)
C27	0.5959(9)	0.8533(8)	0.8122(8)	0.043(4)
C28	0.5697(10)	0.7780(10)	0.7187(8)	0.055(4)
C29	0.5482(10)	0.6641(9)	0.6963(8)	0.052(4)
C30	0.5556(10)	0.6272(8)	0.7717(7)	0.048(4)
C31	0.5989(8)	0.8081(8)	0.8846(7)	0.035(3)
C32	0.6238(8)	0.8823(7)	0.9827(7)	0.034(3)
C41	0.3176(8)	0.5866(8)	0.9125(6)	0.033(3)
C42	0.1870(8)	0.5728(7)	0.8937(6)	0.033(3)
C43	0.1293(9)	0.6674(8)	0.9095(8)	0.047(4)
C44	0.0112(10)	0.6589(10)	0.8977(10)	0.071(5)
C45	-0.0552(10)	0.5538(10)	0.8653(10)	0.069(5)
C46	0.0006(9)	0.4598(9)	0.8451(9)	0.055(4)
C47	0.1202(8)	0.4677(7)	0.8603(7)	0.034(3)
C51	0.2007(9)	0.1736(8)	0.4032(7)	0.038(3)
C52	0.1126(8)	0.0937(8)	0.3058(7)	0.038(3)
C53	-0.0469(8)	-0.0615(8)	0.1933(6)	0.040(3)
C54	-0.0368(10)	-0.0450(10)	0.1148(8)	0.059(4)
C55	0.0472(12)	0.0408(11)	0.1291(8)	0.077(5)
C56	0.1213(10)	0.1075(9)	0.2240(7)	0.059(4)
C57	0.0244(7)	0.0103(7)	0.2890(7)	0.032(3)
C58	0.0113(7)	-0.0047(10)	0.3757(7)	0.047(4)
C61	0.5613(8)	0.3625(7)	0.8529(6)	0.031(3)
C62	0.6021(8)	0.2816(7)	0.7824(7)	0.031(3)
C63	0.5176(8)	0.1989(7)	0.6960(7)	0.031(3)
C64	0.5601(8)	0.1164(7)	0.6394(7)	0.039(3)
C65	0.6825(10)	0.1131(8)	0.6662(8)	0.053(4)
C66	0.7639(10)	0.1937(10)	0.7499(9)	0.061(4)
C67	0.7245(8)	0.2782(8)	0.8082(8)	0.045(3)
C71	0.3867(8)	0.2048(8)	0.6653(7)	0.037(3)
C81	0.1745(8)	0.3615(7)	0.8376(7)	0.033(3)
O100	0.4510(8)	0.3856(8)	0.5568(8)	0.072(3)

U(eq) is defined as one third of the trace of the orthogonalized Uij tensor.

Table A2.5
Atomic Coordinates and Equivalent Isotropic Displacement Parameters [$Å^2$] for $[Y_2(1,2\text{-BDC})_3(1,10\text{-phen})]$, **V**.

Atom	x	y	z	U(eq)
Y1	0.53293(4)	0.16462(4)	0.11557(3)	0.0210(2)
Y2	0.62713(4)	0.02650(4)	0.43740(3)	0.0218(2)
O1	0.5046(4)	0.2541(3)	0.2747(3)	0.0414(14)
O2	0.6412(4)	0.1859(3)	0.3684(3)	0.0448(16)
O3	0.3756(3)	0.1814(3)	0.5687(3)	0.0331(12)
O4	0.4772(3)	0.1057(3)	0.4742(3)	0.0267(11)
O5	0.2716(3)	-0.1383(3)	0.3741(3)	0.0350(11)
O6	0.4238(3)	-0.1104(3)	0.3012(3)	0.0289(11)
O7	0.3951(3)	-0.0129(3)	0.1230(3)	0.0337(11)
O8	0.6044(3)	0.1910(3)	-0.0214(3)	0.0311(11)
O9	0.3097(3)	0.0380(3)	-0.2903(2)	0.0247(10)
O10	0.1508(3)	-0.0912(3)	-0.4513(3)	0.0387(11)
O11	0.3361(3)	0.1172(3)	-0.0221(3)	0.0306(11)
O12	0.6723(3)	0.0650(3)	0.1224(3)	0.0279(11)
N1	0.7480(4)	0.3498(3)	0.2335(3)	0.0265(12)
N2	0.5249(4)	0.3788(3)	0.1227(3)	0.0237(12)
C1	0.8551(5)	0.3379(5)	0.2902(4)	0.0332(17)
C2	0.9754(5)	0.4397(5)	0.3573(4)	0.0428(19)
C3	0.9849(5)	0.5585(5)	0.3676(4)	0.0434(19)
C4	0.8738(5)	0.5760(4)	0.3100(4)	0.0315(17)
C5	0.8754(6)	0.6990(5)	0.3199(5)	0.043(2)
C6	0.7669(6)	0.7129(5)	0.2657(5)	0.042(2)
C7	0.6441(5)	0.6059(4)	0.1974(4)	0.0312(17)
C8	0.5285(6)	0.6192(5)	0.1454(4)	0.0353(19)
C9	0.4155(6)	0.5150(5)	0.0853(4)	0.0356(19)
C10	0.4177(5)	0.3961(5)	0.0758(4)	0.0316(17)
C11	0.6388(5)	0.4839(4)	0.1858(4)	0.0240(16)
C12	0.7560(5)	0.4691(4)	0.2424(4)	0.0242(17)
C21	0.5787(5)	0.2552(4)	0.3637(4)	0.0296(17)
C22	0.6001(4)	0.3541(4)	0.4690(4)	0.0256(11)
C23	0.6753(5)	0.4790(5)	0.4879(4)	0.0348(12)
C24	0.7013(5)	0.5762(5)	0.5815(4)	0.0379(13)
C25	0.6500(5)	0.5519(5)	0.6573(5)	0.0451(14)
C26	0.5713(5)	0.4295(5)	0.6374(4)	0.0374(13)
C27	0.5467(4)	0.3298(4)	0.5446(4)	0.0250(10)
C28	0.4603(5)	0.2000(4)	0.5282(4)	0.0275(17)
C31	0.3067(5)	-0.1480(4)	0.2928(4)	0.0283(17)
C32	0.1995(5)	-0.2128(5)	0.1783(4)	0.0326(17)
C33	0.0739(5)	-0.2817(6)	0.1671(5)	0.064(2)
C34	-0.0282(7)	-0.3430(9)	0.0653(6)	0.107(4)
C35	-0.0082(7)	-0.3399(8)	-0.0283(6)	0.095(3)
C36	0.1171(5)	-0.2739(6)	-0.0198(5)	0.056(2)
C37	0.2225(5)	-0.2076(4)	0.0837(4)	0.0292(17)
C38	0.3490(4)	-0.1317(4)	0.0790(4)	0.0233(16)
C41	0.1905(5)	-0.0313(4)	-0.3481(4)	0.0244(17)
C42	0.0944(4)	-0.0433(4)	-0.2937(4)	0.0220(14)
C43	-0.0374(5)	-0.0720(4)	-0.3548(4)	0.0309(17)
C44	-0.1244(5)	-0.0720(5)	-0.3036(4)	0.0376(19)
C45	-0.0805(5)	-0.0435(5)	-0.1906(4)	0.0423(14)
C46	0.0497(5)	-0.0155(5)	-0.1292(4)	0.0357(12)
C47	0.1393(4)	-0.0143(4)	-0.1786(4)	0.0220(10)
C48	0.2779(4)	0.0143(4)	-0.1053(4)	0.0237(10)

U(eq) is defined as one third of the trace of the orthogonalized Uij tensor.

Table A2.6
Atomic Coordinates and Equivalent Isotropic Displacement Parameters [$Å^2$] for $[Dy_2(1,2\text{-BDC})_3(1,10\text{-phen})]$, **VI**.

Atom	x	y	z	U(eq)
Dy1	0.38835(5)	0.13938(3)	0.02767(3)	0.0267(2)
Dy2	0.26696(5)	0.12029(3)	0.23275(3)	0.0239(2)
Dy3	0.20129(5)	0.31666(4)	0.31692(3)	0.0284(2)
Dy4	0.10974(5)	0.38259(3)	0.50807(3)	0.0254(2)
O1	0.3411(8)	0.0379(5)	-0.0072(4)	0.039(3)
O2	0.4246(8)	-0.1082(6)	0.0286(4)	0.045(3)
O3	0.3167(7)	0.0442(5)	0.1253(4)	0.029(3)
O4	0.1289(7)	0.0889(5)	0.1678(4)	0.035(3)
O5	0.1677(8)	0.2155(6)	0.0172(4)	0.047(3)
O6	0.2558(7)	0.2279(5)	0.1063(4)	0.029(2)
O7	0.0989(7)	0.2523(5)	0.2170(4)	0.037(3)
O8	0.1273(8)	0.3821(5)	0.1975(4)	0.040(3)
O9	0.5389(7)	0.1239(5)	0.1078(4)	0.033(3)
O10	0.4859(7)	0.0787(5)	0.2196(4)	0.030(3)
O11	0.3536(7)	0.2268(5)	0.2466(4)	0.039(3)
O12	0.4102(8)	0.3230(7)	0.2744(5)	0.056(4)
O13	0.3398(7)	0.0698(5)	0.3514(4)	0.031(3)
O14	0.1851(7)	0.1790(5)	0.3709(4)	0.032(3)
O15	0.3347(7)	0.2483(5)	0.4184(4)	0.035(3)
O16	0.2664(9)	0.2550(6)	0.5228(5)	0.055(3)
O17	-0.0292(7)	0.3629(5)	0.3154(4)	0.039(3)
O18	0.0447(7)	0.3422(5)	0.4194(4)	0.032(3)
O19	-0.0864(7)	0.4879(5)	0.4589(4)	0.033(3)
O20	-0.2783(7)	0.5816(5)	0.4449(4)	0.036(3)
O21	0.0478(9)	0.6829(6)	0.4325(4)	0.054(3)
O22	-0.0714(8)	0.6514(6)	0.3698(4)	0.043(3)
O23	0.1893(8)	0.4543(5)	0.3097(4)	0.045(3)
O24	0.1708(8)	0.4826(5)	0.4101(4)	0.041(3)
N1	0.3139(9)	0.2297(7)	-0.0996(5)	0.038(4)
N2	0.4355(9)	0.2883(6)	-0.0231(5)	0.036(3)
N3	0.3396(9)	-0.0496(5)	0.2845(5)	0.029(3)
N4	0.1103(9)	0.0567(6)	0.3124(4)	0.027(3)
C1	0.2489(14)	0.2040(11)	-0.1355(7)	0.062(6)
C2	0.1974(16)	0.2562(12)	-0.2040(8)	0.077(7)
C3	0.2209(17)	0.3345(12)	-0.2362(8)	0.076(7)
C4	0.2892(15)	0.3641(10)	-0.2002(7)	0.056(6)
C5	0.3214(18)	0.4435(9)	-0.2310(8)	0.075(7)
C6	0.3919(17)	0.4676(10)	-0.1954(8)	0.069(6)
C7	0.4373(13)	0.4163(8)	-0.1242(7)	0.048(5)
C8	0.5073(14)	0.4405(10)	-0.0840(9)	0.060(6)
C9	0.5382(15)	0.3917(9)	-0.0160(9)	0.062(6)
C10	0.4983(14)	0.3168(9)	0.0119(8)	0.054(5)
C11	0.4045(12)	0.3378(8)	-0.0916(6)	0.037(4)
C12	0.3354(11)	0.3082(9)	-0.1311(6)	0.038(4)
C21	0.4492(12)	-0.1007(8)	0.2720(7)	0.041(5)
C22	0.5030(14)	-0.1897(9)	0.3142(8)	0.060(6)
C23	0.4380(14)	-0.2283(8)	0.3691(8)	0.057(5)
C24	0.3175(13)	-0.1773(8)	0.3824(7)	0.042(5)
C25	0.2383(16)	-0.2123(10)	0.4374(7)	0.054(5)
C26	0.1258(16)	-0.1605(10)	0.4479(7)	0.056(6)
C27	0.0748(13)	-0.0679(8)	0.4060(6)	0.040(5)
C28	-0.0428(15)	-0.0108(10)	0.4176(7)	0.058(6)
C29	-0.0846(13)	0.0781(10)	0.3772(7)	0.049(5)
C30	-0.0012(12)	0.1083(9)	0.3257(6)	0.041(5)

C31	0.1477(11)	-0.0308(8)	0.3519(6)	0.032(4)
C32	0.2696(12)	-0.0862(7)	0.3385(6)	0.035(4)
C41	0.3367(11)	-0.0399(9)	0.0261(6)	0.030(4)
C42	0.2126(10)	-0.0507(7)	0.0588(6)	0.029(4)
C43	0.1619(13)	-0.1061(9)	0.0404(7)	0.048(5)
C44	0.0453(14)	-0.1164(10)	0.0646(8)	0.058(6)
C45	-0.0185(14)	-0.0741(10)	0.1105(9)	0.065(6)
C46	0.0328(11)	-0.0210(8)	0.1305(7)	0.043(5)
C47	0.1493(11)	-0.0088(7)	0.1048(6)	0.031(4)
C48	0.2007(10)	0.0460(7)	0.1324(6)	0.026(3)
C51	0.1621(12)	0.2533(8)	0.0619(6)	0.037(4)
C52	0.0436(10)	0.3302(7)	0.0578(6)	0.030(4)
C53	-0.0336(12)	0.3683(9)	-0.0029(7)	0.049(5)
C54	-0.1377(14)	0.4461(10)	-0.0165(8)	0.056(5)
C55	-0.1600(13)	0.4849(10)	0.0336(8)	0.054(5)
C56	-0.0851(11)	0.4488(8)	0.0954(7)	0.042(5)
C57	0.0160(10)	0.3702(7)	0.1083(6)	0.031(4)
C58	0.0878(11)	0.3328(8)	0.1784(6)	0.031(4)
C61	0.5405(10)	0.1224(7)	0.1701(6)	0.026(4)
C62	0.6143(10)	0.1761(7)	0.1844(5)	0.028(4)
C63	0.7365(11)	0.1651(9)	0.1583(6)	0.039(4)
C64	0.8146(12)	0.2116(9)	0.1648(7)	0.044(5)
C65	0.7678(12)	0.2717(9)	0.1984(7)	0.049(5)
C66	0.6476(11)	0.2851(8)	0.2239(6)	0.037(4)
C67	0.5686(11)	0.2372(7)	0.2191(6)	0.029(4)
C68	0.4358(11)	0.2631(8)	0.2479(6)	0.031(4)
C71	0.2801(11)	0.1071(7)	0.3919(6)	0.027(4)
C72	0.3213(10)	0.0655(8)	0.4682(6)	0.030(4)
C73	0.3502(10)	-0.0284(8)	0.4974(6)	0.032(4)
C74	0.3799(11)	-0.0689(8)	0.5697(6)	0.038(4)
C75	0.3803(12)	-0.0218(9)	0.6123(6)	0.042(5)
C76	0.3516(12)	0.0705(9)	0.5828(6)	0.043(5)
C77	0.3240(10)	0.1141(7)	0.5107(6)	0.025(3)
C78	0.3069(10)	0.2135(7)	0.4808(7)	0.033(4)
C81	-0.0477(10)	0.3633(7)	0.3763(6)	0.025(4)
C82	-0.1877(10)	0.3830(7)	0.3961(5)	0.025(3)
C83	-0.2541(11)	0.3354(7)	0.3783(6)	0.034(4)
C84	-0.3836(12)	0.3469(9)	0.3891(6)	0.042(5)
C85	-0.4520(12)	0.4124(9)	0.4163(7)	0.047(5)
C86	-0.3900(11)	0.4617(8)	0.4323(6)	0.035(4)
C87	-0.2574(10)	0.4476(7)	0.4248(5)	0.024(4)
C88	-0.2055(11)	0.5087(8)	0.4435(5)	0.028(4)
C91	0.0281(12)	0.6678(7)	0.3791(6)	0.033(4)
C92	0.1272(11)	0.6697(8)	0.3237(6)	0.034(4)
C93	0.1511(14)	0.7500(8)	0.2871(7)	0.048(5)
C94	0.2337(14)	0.7561(10)	0.2334(8)	0.061(6)
C95	0.2939(16)	0.6838(10)	0.2149(8)	0.073(7)
C96	0.2733(14)	0.6046(9)	0.2497(7)	0.059(5)
C97	0.1939(12)	0.5950(8)	0.3052(6)	0.036(4)
C98	0.1808(11)	0.5052(7)	0.3449(7)	0.033(4)

U(eq) is defined as one third of the trace of the orthogonalized Uij tensor.

Table A2.7
Atomic Coordinates and Equivalent Isotropic Displacement Parameters [Å^2] for [Y_2(1,3-BDC)$_3$(2,2'-bipy)$_2$], **VII**.

Atom	x	y	z	U(eq)
Y1	-0.08174(2)	0.12668(2)	0.46579(1)	0.0186(1)
Y2	0.15407(2)	0.49490(2)	0.10991(1)	0.0199(1)

O1	0.1137(3)	0.0995(3)	0.47279(17)	0.0283(10)
O2	-0.0041(3)	0.1349(3)	0.61569(17)	0.0302(10)
O3	0.2559(3)	0.0022(3)	0.49724(18)	0.0297(10)
O4	-0.1213(3)	-0.0189(3)	0.35086(17)	0.0313(10)
O5	-0.0860(3)	0.2363(3)	0.34526(17)	0.0285(10)
O6	-0.2740(3)	0.1318(3)	0.35196(17)	0.0275(9)
O7	-0.0534(3)	0.3764(3)	0.0721(2)	0.0444(12)
O8	0.1215(3)	0.4033(3)	0.97695(18)	0.0395(11)
O9	-0.2290(3)	0.3465(3)	-0.03778(19)	0.0449(11)
O10	-0.0382(3)	0.3837(3)	0.8574(2)	0.0436(11)
O11	0.1923(3)	0.3073(3)	0.14176(18)	0.0391(11)
O12	0.1722(3)	0.4108(3)	0.24560(18)	0.0371(10)
N1	0.0855(4)	0.3322(3)	0.5391(2)	0.0342(12)
N2	-0.1675(4)	0.2776(3)	0.5222(2)	0.0304(11)
N3	0.3316(4)	0.6650(3)	0.2176(2)	0.0408(14)
N4	0.3907(4)	0.5091(4)	0.1292(3)	0.0507(17)
C1	0.2125(5)	0.3559(4)	0.5508(3)	0.0489(19)
C2	0.3037(6)	0.4511(5)	0.6023(4)	0.059(2)
C3	0.2649(6)	0.5273(5)	0.6424(4)	0.068(2)
C4	0.1362(6)	0.5061(4)	0.6328(3)	0.0546(19)
C5	0.0486(5)	0.4074(4)	0.5807(3)	0.0345(14)
C6	-0.0911(5)	0.3807(4)	0.5674(3)	0.0339(16)
C7	-0.2730(6)	0.4291(5)	0.5840(3)	0.061(2)
C8	-0.3509(5)	0.3241(5)	0.5378(3)	0.0482(19)
C9	-0.2944(4)	0.2513(4)	0.5086(3)	0.0355(17)
C10	-0.1427(6)	0.4577(5)	0.5991(3)	0.0513(19)
C11	0.2988(7)	0.7418(5)	0.2586(3)	0.062(2)
C12	0.3842(9)	0.8439(6)	0.3056(4)	0.090(3)
C13	0.5104(10)	0.8672(7)	0.3112(5)	0.109(4)
C14	0.5468(7)	0.7903(7)	0.2701(5)	0.091(3)
C15	0.4547(5)	0.6880(5)	0.2225(3)	0.055(2)
C16	0.4875(5)	0.6008(6)	0.1756(4)	0.057(2)
C17	0.6147(6)	0.6104(9)	0.1799(6)	0.102(4)
C18	0.6384(8)	0.5270(10)	0.1358(7)	0.118(5)
C19	0.5415(8)	0.4332(8)	0.0897(6)	0.090(4)
C20	0.4154(6)	0.4265(6)	0.0872(5)	0.071(3)
C21	0.0675(4)	0.0894(3)	0.6680(3)	0.0251(12)
C22	0.0883(4)	0.1212(4)	0.7608(3)	0.0287(16)
C23	0.1404(6)	0.0563(5)	0.8202(3)	0.060(2)
C24	0.1601(7)	0.0843(6)	0.9058(3)	0.080(3)
C25	0.1311(6)	0.1802(5)	0.9327(3)	0.057(2)
C26	0.0783(4)	0.2461(4)	0.8738(3)	0.0305(16)
C27	0.0540(4)	0.2144(4)	0.7877(3)	0.0287(16)
C28	0.0508(4)	0.3513(4)	0.9045(3)	0.0311(16)
C31	-0.2052(4)	0.1861(4)	0.3105(3)	0.0229(14)
C32	-0.2644(4)	0.1884(4)	0.2167(3)	0.0243(12)
C33	-0.3892(4)	0.1200(4)	0.1755(3)	0.0336(16)
C34	-0.4415(5)	0.1175(5)	0.0885(3)	0.0439(17)
C35	-0.3716(4)	0.1837(4)	0.0434(3)	0.0392(16)
C36	-0.2452(4)	0.2540(4)	0.0839(3)	0.0262(12)
C37	-0.1927(4)	0.2539(4)	0.1711(3)	0.0236(12)
C38	-0.1707(5)	0.3308(4)	0.0359(3)	0.0319(16)
C41	0.2020(4)	0.3266(4)	0.2185(3)	0.0289(17)
C42	0.2598(4)	0.2526(4)	0.2803(3)	0.0267(12)
C43	0.3688(4)	0.2293(4)	0.2726(3)	0.0383(17)
C44	0.4306(5)	0.1659(5)	0.3293(3)	0.0442(19)
C45	0.3779(4)	0.1191(4)	0.3897(3)	0.0324(16)
C46	0.2669(4)	0.1380(3)	0.3971(3)	0.0240(12)
C47	0.2091(4)	0.2072(4)	0.3430(3)	0.0252(12)

C48	0.2092(4)	0.0769(3)	0.4596(2)	0.0218(12)

U(eq) is defined as one third of the trace of the orthogonalized Uij tensor.

Table A2.8
Atomic Coordinates and Equivalent Isotropic Displacement Parameters [Å^2] for [Y_2(1,3-BDC)$_3$(2,2'-bipy)$_2$]·H_2O, **VIII**.

Atom	x	y	z	U(eq)
Y1	0.51816(2)	0.36192(2)	0.06799(2)	0.0188(1)
O1	0.51198(13)	0.51402(15)	0.12731(11)	0.0292(7)
O2	0.46880(13)	0.27805(17)	0.15155(11)	0.0355(7)
O3	0.37812(12)	0.40434(17)	0.01801(12)	0.0333(7)
O4	0.51151(12)	0.65815(16)	0.06295(11)	0.0296(7)
O5	0.61779(12)	0.46059(16)	0.05191(12)	0.0328(7)
O6	0.43786(13)	0.19717(17)	0.04165(13)	0.0382(8)
N1	0.63735(15)	0.33994(19)	0.19817(14)	0.0262(8)
N2	0.63041(16)	0.2343(2)	0.07486(15)	0.0341(9)
C1	0.6343(2)	0.3825(3)	0.26186(18)	0.0347(11)
C2	0.6982(2)	0.3797(3)	0.33212(19)	0.0435(11)
C3	0.7693(2)	0.3301(3)	0.3380(2)	0.0496(14)
C4	0.7731(2)	0.2844(3)	0.2735(2)	0.0454(11)
C5	0.70606(18)	0.2893(2)	0.20383(18)	0.0292(10)
C6	0.70435(19)	0.2353(3)	0.13407(19)	0.0338(11)
C7	0.7725(2)	0.1865(3)	0.1292(2)	0.0551(16)
C8	0.7656(3)	0.1332(3)	0.0644(3)	0.0704(17)
C9	0.6909(3)	0.1288(3)	0.0053(3)	0.0702(19)
C10	0.6250(3)	0.1803(3)	0.0129(2)	0.0541(14)
C11	0.51074(17)	0.6092(2)	0.12074(16)	0.0234(10)
C12	0.50668(17)	0.6702(2)	0.18781(16)	0.0211(9)
C13	0.50805(18)	0.7759(2)	0.18898(17)	0.0290(10)
C14	1/2	0.8290(3)	1/4	0.0351(16)
C15	1/2	0.6183(3)	1/4	0.0217(12)
C21	0.34660(17)	0.4625(2)	-0.03845(17)	0.0240(10)
C22	0.26164(17)	0.4379(2)	-0.09423(16)	0.0223(9)
C23	0.23983(19)	0.4661(2)	-0.17066(18)	0.0313(11)
C24	0.16490(19)	0.4363(3)	-0.22516(18)	0.0384(11)
C25	0.11221(19)	0.3766(3)	-0.20325(18)	0.0349(11)
C26	0.13104(17)	0.3527(2)	-0.12622(17)	0.0257(10)
C27	0.20658(17)	0.3818(2)	-0.07203(17)	0.0230(9)
C28	0.42867(17)	0.2102(2)	0.10439(18)	0.0277(10)
O100	0.0442(9)	0.4705(10)	0.0714(6)	0.131(5)

U(eq) is defined as one third of the trace of the orthogonalized Uij tensor.

Table A2.9
Atomic Coordinates and Equivalent Isotropic Displacement Parameters [Å^2] for [Y_2(1,3-BDC)$_3$(1,10-phen)$_2$], **IX**.

Atom	x	y	z	U(eq)
Y1	0.21394	0.36028	0.89629	0.0299
Y2	-0.07272	0.16586	0.55945	0.0272
O1	0.01324	0.39495	0.91209	0.0433
O2	-0.15087	0.55226	0.97802	0.0450
O3	0.15245	0.52269	0.81023	0.0528
O4	0.38688	0.28309	0.76907	0.0488
O5	0.25098	0.21064	0.80839	0.0496
O6	0.30493	0.49482	0.86409	0.0463
O7	0.80216	0.07906	0.56439	0.0411
O8	0.85557	-0.08635	0.50586	0.0435
O9	0.02013	1.00122	0.63400	0.0457

O10	0.07292	0.83349	0.57890	0.0503
O11	-0.04472	0.25543	0.66026	0.0386
O12	-0.20924	0.21636	0.70701	0.0391
N1	0.19199	0.20778	1.00556	0.0509
N2	0.40413	0.23800	0.94869	0.0473
N3	-0.03855	0.33717	0.47509	0.0375
N4	-0.27428	0.35992	0.56569	0.0370
C1	0.09394	0.18512	1.03132	0.0688
C2	0.07309	0.11339	1.10142	0.0949
C3	0.16216	0.06747	1.14392	0.1008
C4	0.26944	0.08589	1.12080	0.0806
C5	0.37104	0.03791	1.16259	0.1095
C6	0.47506	0.05512	1.13334	0.1206
C7	0.49218	0.12205	1.06031	0.0754
C8	0.60080	0.13892	1.02631	0.0980
C9	0.61132	0.20222	0.95482	0.0922
C10	0.51093	0.24967	0.91857	0.0675
C11	0.39469	0.17469	1.01856	0.0540
C12	0.28270	0.15741	1.04915	0.0566
C21	0.07410	0.32719	0.42738	0.0538
C22	0.09394	0.41532	0.37715	0.0707
C23	-0.00837	0.51996	0.37766	0.0697
C24	-0.13184	0.53637	0.42714	0.0548
C25	-0.24425	0.64337	0.43181	0.0734
C26	-0.35866	0.65647	0.48048	0.0728
C27	-0.37488	0.56225	0.52812	0.0518
C28	-0.49231	0.57128	0.57863	0.0672
C29	-0.50080	0.47779	0.62084	0.0595
C30	-0.38872	0.37360	0.61241	0.0488
C31	-0.26568	0.45382	0.52392	0.0375
C32	-0.14197	0.44124	0.47445	0.0408
C41	-0.10220	0.46796	0.92934	0.0344
C42	-0.18528	0.44998	0.88911	0.0314
C43	-0.31779	0.51492	0.91702	0.0611
C44	-0.39307	0.49699	0.87973	0.0716
C45	-0.33950	0.41778	0.81441	0.0521
C46	-0.20733	0.35342	0.78652	0.0356
C47	-0.13102	0.36996	0.82395	0.0328
C51	0.22936	0.55500	0.82133	0.0395
C52	0.22515	0.66758	0.78284	0.0358
C53	0.28595	0.71659	0.80837	0.0624
C54	0.27644	0.82295	0.77788	0.0808
C55	0.20641	0.87859	0.72182	0.0591
C56	0.14813	0.83051	0.69285	0.0303
C57	0.15995	0.72227	0.72419	0.0302
C62	0.64310	0.01750	0.59200	0.0275
C63	0.60218	-0.05600	0.57233	0.0435
C64	0.47796	-0.03909	0.61266	0.0534
C65	0.39626	0.04585	0.67261	0.0424
C66	0.43610	0.11979	0.69185	0.0273
C67	0.55897	0.10442	0.65121	0.0297
C71	0.35176	0.21016	0.75976	0.0322
C81	-0.14870	0.26794	0.71444	0.0360
C91	0.07380	0.89383	0.63054	0.0329
C101	0.77674	0.00199	0.55100	0.0310

U(eq) is defined as one third of the trace of the orthogonalized Uij tensor.

Table A2.10

Atomic Coordinates and Equivalent Isotropic Displacement Parameters [$Å^2$] for [Nd_2(1,3-BDC)$_3$(1,10-phen)$_2$], **X**.

Atom	x	y	z	U(eq)
Nd1	0.14994(3)	0.58928(2)	0.47647(2)	0.0222(1)
Nd2	-0.14394(3)	0.93558(2)	0.06767(2)	0.0262(1)
O1	0.2800(3)	0.5910(2)	0.3545(3)	0.0373(12)
O2	0.0984(3)	0.6529(2)	0.3157(2)	0.0333(12)
O3	0.0737(4)	0.9057(3)	0.1081(3)	0.0497(16)
O4	0.2194(4)	0.9387(2)	0.0249(3)	0.0421(16)
O5	-0.0474(3)	0.6529(2)	0.4624(3)	0.0316(11)
O6	0.2240(3)	0.4425(2)	0.5225(3)	0.0341(11)
O7	-0.1060(3)	0.8849(2)	0.2312(3)	0.0357(12)
O8	-0.3017(3)	0.9222(2)	0.1690(3)	0.0381(12)
O9	-0.0284(3)	0.4696(2)	0.3892(2)	0.0294(11)
O10	0.1631(3)	0.6644(2)	0.6371(3)	0.0352(12)
O11	-0.0445(4)	0.0803(2)	0.1619(3)	0.0470(16)
O12	0.0927(4)	0.1231(3)	0.0747(3)	0.0544(17)
N1	0.3998(4)	0.6409(3)	0.5709(3)	0.0313(17)
N2	0.2472(4)	0.7693(3)	0.4954(3)	0.0363(16)
N3	-0.3815(4)	0.8670(3)	-0.0475(3)	0.0309(11)
N4	-0.2298(4)	0.7537(3)	0.0583(3)	0.0301(16)
C1	0.4787(5)	0.5798(4)	0.6031(4)	0.038(2)
C2	0.6068(6)	0.6046(5)	0.6583(4)	0.052(3)
C3	0.6539(6)	0.6961(5)	0.6808(5)	0.056(3)
C4	0.5764(6)	0.7654(4)	0.6488(4)	0.047(2)
C5	0.6213(7)	0.8641(5)	0.6701(5)	0.063(3)
C6	0.5432(7)	0.9261(4)	0.6366(5)	0.064(3)
C7	0.4148(6)	0.8979(4)	0.5759(5)	0.050(2)
C8	0.3316(7)	0.9599(4)	0.5348(6)	0.067(3)
C9	0.2132(7)	0.9269(4)	0.4777(6)	0.072(3)
C10	0.1739(6)	0.8321(4)	0.4594(5)	0.054(3)
C11	0.3674(5)	0.8015(3)	0.5539(4)	0.0345(19)
C12	0.4492(5)	0.7337(3)	0.5923(4)	0.0316(17)
C21	-0.4632(5)	0.9201(4)	-0.0949(4)	0.040(2)
C22	-0.5789(6)	0.8861(4)	-0.1615(4)	0.048(2)
C23	-0.6110(6)	0.7928(4)	-0.1845(4)	0.046(2)
C24	-0.5286(5)	0.7322(4)	-0.1366(4)	0.0368(19)
C25	-0.5565(6)	0.6334(4)	-0.1554(5)	0.050(2)
C26	-0.4794(6)	0.5774(4)	-0.1062(5)	0.048(2)
C27	-0.3673(5)	0.6151(3)	-0.0317(4)	0.036(2)
C28	-0.2892(6)	0.5599(4)	0.0259(5)	0.051(3)
C29	-0.1872(6)	0.6007(4)	0.0985(5)	0.050(2)
C30	-0.1604(6)	0.6980(4)	0.1130(4)	0.040(2)
C31	-0.3348(5)	0.7133(3)	-0.0122(4)	0.0299(19)
C32	-0.4154(5)	0.7732(3)	-0.0673(4)	0.0298(17)
C41	0.2069(5)	0.6396(3)	0.3025(4)	0.0284(17)
C42	0.2479(5)	0.6842(3)	0.2212(4)	0.0275(17)
C43	0.3405(6)	0.6520(4)	0.1816(4)	0.044(2)
C44	0.3787(6)	0.6953(4)	0.1106(4)	0.045(2)
C45	0.3269(5)	0.7746(4)	0.0772(4)	0.041(2)
C46	0.2342(5)	0.8082(3)	0.1160(4)	0.0291(17)
C47	0.1960(5)	0.7624(3)	0.1882(4)	0.0292(17)
C48	0.1708(5)	0.8909(3)	0.0807(4)	0.0343(19)
C51	-0.1679(5)	0.6319(3)	0.4516(3)	0.0279(19)
C52	-0.2520(5)	0.7003(3)	0.4042(3)	0.0254(17)
C53	-0.3754(5)	0.7047(3)	0.4161(4)	0.0333(17)
C54	-0.4484(5)	0.7692(3)	0.3706(4)	0.0357(19)
C55	-0.4012(5)	0.8270(3)	0.3102(4)	0.0344(19)
C56	-0.2789(5)	0.8230(3)	0.2976(3)	0.0279(17)

C57	-0.2043(5)	0.7600(3)	0.3448(3)	0.0261(17)
C58	-0.2256(6)	0.8817(3)	0.2301(4)	0.0316(19)
C61	-0.0753(5)	0.3892(4)	0.3417(4)	0.0276(17)
C62	-0.0244(5)	0.3613(3)	0.2601(3)	0.0256(17)
C63	0.0273(5)	0.4304(4)	0.2111(4)	0.036(2)
C64	0.0700(6)	0.4046(4)	0.1331(4)	0.043(2)
C65	0.0674(5)	0.3115(4)	0.1073(4)	0.042(2)
C66	0.0206(5)	0.2422(3)	0.1567(4)	0.0285(17)
C67	-0.0290(5)	0.2679(3)	0.2323(4)	0.0269(17)
C68	0.0231(6)	0.1410(4)	0.1295(4)	0.0347(19)

U(eq) is defined as one third of the trace of the orthogonalized Uij tensor.

Table A2.11

Atomic Coordinates and Equivalent Isotropic Displacement Parameters [$Å^2$] for [Cd(1,4-BDC)(1,10-phen)].H_2O, **XI.**

Atom	x	y	z	U(eq)
Cd1	0.53237	0.58773	0.12246	0.0293
O1	0.75856	0.55401	0.14859	0.0449
O2	0.64263	0.51261	-0.01414	0.0458
O3	0.44975	0.72224	0.00431	0.0524
O4	0.60464	0.76372	0.15102	0.0495
N1	0.53286	0.45570	0.24218	0.0331
N2	0.41299	0.63960	0.24538	0.0339
C1	0.59359	0.36751	0.24298	0.0449
C2	0.58209	0.28544	0.30883	0.0482
C3	0.50347	0.29671	0.37418	0.0461
C4	0.43822	0.39007	0.37690	0.0379
C5	0.35753	0.40834	0.44640	0.0469
C6	0.29981	0.49947	0.44907	0.0478
C7	0.31759	0.58082	0.38273	0.0362
C8	0.26420	0.67802	0.38601	0.0450
C9	0.28637	0.75318	0.32160	0.0474
C10	0.36019	0.73044	0.25138	0.0437
C11	0.39374	0.56566	0.31147	0.0303
C12	0.45636	0.46767	0.30924	0.0299
C21	0.75222	0.52528	0.05636	0.0331
C22	0.88120	0.51038	0.02736	0.0272
C23	1.00326	0.52230	0.10318	0.0349
C24	0.87980	0.48827	-0.07586	0.0361
C31	0.52360	0.78743	0.06408	0.0365
C32	0.51051	0.89812	0.03035	0.0310
C33	0.44691	0.92523	-0.07469	0.0348
C34	0.56303	0.97369	0.10442	0.0335
O100	0.33054	0.22624	0.61176	0.0509

U(eq) is defined as one third of the trace of the orthogonalized Uij tensor.

Table A2.12

Atomic Coordinates and Equivalent Isotropic Displacement Parameters [$Å^2$] for [Y_2(1,2-BDC)$_2$(1,3-BDC)(1,10-phen)$_2$], **XII**.

Atom	x	y	z	U(eq)
Y1	0.83028	0.15221	0.49765	0.0234
O1	0.96795	0.29449	0.48992	0.0563
O2	0.81429	0.29095	0.53800	0.0770
O3	0.52690	0.13414	0.53862	0.0286
O4	1.09890	0.11868	0.54763	0.0295
O5	0.74775	0.11488	0.62089	0.0364
O6	0.77833	0.01304	0.46246	0.0301
N1	0.66540	0.20936	0.38644	0.0313

N2	0.99451	0.14028	0.37463	0.0263
C1	0.50857	0.24849	0.39254	0.0484
C2	0.41399	0.28111	0.32830	0.0561
C3	0.47751	0.26939	0.25763	0.0542
C4	0.64471	0.22938	0.24867	0.0470
C5	0.72177	0.21667	0.17580	0.0574
C6	0.87994	0.18133	0.16920	0.0570
C7	0.98303	0.15447	0.23613	0.0438
C8	1.15266	0.11706	0.23267	0.0498
C9	1.23742	0.09257	0.29653	0.0451
C10	1.15327	0.10529	0.36665	0.0417
C11	0.73339	0.20052	0.31519	0.0343
C12	0.90827	0.16425	0.30773	0.0347
C21	0.58317	0.11431	0.60514	0.0272
C22	0.45393	0.08965	0.66556	0.0233
C23	0.51542	0.09202	0.74018	0.0371
C24	0.40572	0.07218	0.79995	0.0502
C25	0.22923	0.04936	0.78377	0.0442
C26	0.16701	0.04786	0.71040	0.0330
C27	0.27773	0.06698	0.65063	0.0216
C31	1.19672	0.05838	0.57190	0.0237
C41	0.88840	0.28580	0.51690	0.0500
C42	0.86463	0.34933	0.51804	0.0068
C43	1.01310	0.42765	0.50533	0.0300
C44	1.17139	0.38719	0.48653	0.0412
C45	1	1/2	1/2	0.0505
C46	0.71140	0.39590	0.54380	0.0500
C47	0.70426	0.44475	0.53726	0.0850
C48	1.31643	0.43870	0.46874	0.0496
C49	0.86495	0.42494	0.51528	0.0516

U(eq) is defined as one third of the trace of the orthogonalized Uij tensor.

Table A2.13

Atomic Coordinates and Equivalent Isotropic Displacement Parameters [Å^2] for [Y_2(1,2-BDC)$_2$(1,4-BDC)(1,10-phen)$_2$], **XIII**.

Atom	x	y	z	U(eq)
Y1	0.15085	0.34656	0.49416	0.0199
O1	0.22123	0.20475	0.53694	0.0399
O2	-0.04862	0.22582	0.47760	0.0396
O3	0.23949	0.37825	0.62131	0.0341
O4	0.46623	0.36589	0.53982	0.0280
O5	0.22180	0.47793	0.45753	0.0311
O6	-0.11582	0.39225	0.54302	0.0308
N1	-0.01913	0.36225	0.36715	0.0258
N2	0.32132	0.28931	0.38461	0.0268
C1	-0.18590	0.39748	0.35822	0.0334
C2	-0.27748	0.40720	0.28709	0.0401
C3	-0.19203	0.37973	0.22310	0.0413
C4	-0.01452	0.34203	0.22923	0.0344
C5	0.08389	0.31116	0.16503	0.0408
C6	0.25143	0.27476	0.17386	0.0432
C7	0.33842	0.26476	0.24797	0.0317
C8	0.51045	0.22448	0.26069	0.0409
C9	0.58379	0.21830	0.33302	0.0394
C10	0.48653	0.25181	0.39330	0.0333
C11	0.24663	0.29532	0.31246	0.0273
C12	0.06564	0.33438	0.30327	0.0282
C21	0.41133	0.38313	0.60591	0.0236
C22	0.54620	0.41034	0.66736	0.0231

C23	0.72497	0.43993	0.65203	0.0202
C24	0.84395	0.46232	0.71281	0.0306
C25	0.78560	0.45749	0.78716	0.0409
C26	0.61014	0.42869	0.80195	0.0441
C27	0.49204	0.40564	0.74265	0.0349
C28	0.20138	0.54834	0.42745	0.0206
C31	0.07086	0.17767	0.50748	0.0280
C32	0.03323	0.08551	0.50581	0.0260
C33	-0.14576	0.05552	0.49011	0.0313
C34	0.17931	0.02910	0.51588	0.0317

U(eq) is defined as one third of the trace of the orthogonalized Uij tensor.

Table A2.14
Atomic Coordinates and Equivalent Isotropic Displacement Parameters [Å^2] for [Pr_2(1,2-BDC)$_2$(1,4-BDC)(1,10-phen)$_2$ (H_2O)$_2$]·H_2O, **XIV**.

Atom	x	y	z	U(eq)
La1	0.13078(1)	0.01658(1)	0.42050(1)	0.0189(1)
O1	-0.07007(16)	0.04798(9)	0.46219(14)	0.0278(7)
O2	0.00531(17)	0.09648(10)	0.35913(15)	0.0316(8)
O3	-0.26138(17)	0.07161(10)	0.16358(14)	0.0319(8)
O4	-0.14993(18)	0.02530(9)	0.25164(15)	0.0293(8)
O5	0.15873(17)	0.09959(9)	0.51239(15)	0.0298(8)
O6	0.0796(3)	0.14874(11)	0.6123(2)	0.0708(13)
O7	-0.0016(2)	-0.04732(11)	0.34464(16)	0.0343(8)
N1	0.2549(2)	-0.07435(11)	0.37551(18)	0.0318(10)
N2	0.3052(2)	-0.00957(11)	0.51992(19)	0.0267(9)
C1	0.2298(3)	-0.10703(16)	0.3075(3)	0.0438(12)
C2	0.2911(3)	-0.15364(18)	0.2809(3)	0.0554(16)
C3	0.3818(3)	-0.16681(16)	0.3262(3)	0.0513(16)
C4	0.4126(3)	-0.13321(15)	0.3988(3)	0.0366(12)
C5	0.5058(3)	-0.14488(17)	0.4512(3)	0.0459(14)
C6	0.5304(3)	-0.11326(17)	0.5220(3)	0.0445(14)
C7	0.4634(3)	-0.06690(14)	0.5487(2)	0.0330(11)
C8	0.4843(3)	-0.03465(16)	0.6243(3)	0.0395(12)
C9	0.4164(3)	0.00807(16)	0.6467(3)	0.0397(12)
C10	0.3282(3)	0.01900(14)	0.5928(2)	0.0319(12)
C11	0.3713(2)	-0.05348(14)	0.4979(2)	0.0260(10)
C12	0.3455(3)	-0.08725(13)	0.4218(2)	0.0286(11)
C21	-0.0741(3)	0.08476(13)	0.4005(2)	0.0225(10)
C22	-0.1744(3)	0.11772(12)	0.3808(2)	0.0238(10)
C23	-0.2027(3)	0.15945(14)	0.4408(2)	0.0353(11)
C24	-0.2900(3)	0.19448(16)	0.4249(3)	0.0454(14)
C25	-0.3501(3)	0.18826(16)	0.3498(3)	0.0431(14)
C26	-0.3237(3)	0.14695(14)	0.2902(2)	0.0335(11)
C27	-0.2365(2)	0.11076(13)	0.3047(2)	0.0232(10)
C28	-0.2143(2)	0.06622(13)	0.2370(2)	0.0221(10)
C31	0.1398(3)	0.14620(14)	0.5513(2)	0.0298(11)
C32	0.1951(3)	0.20025(13)	0.5242(2)	0.0253(11)
C33	0.2025(3)	0.24834(13)	0.5789(2)	0.0307(11)
C34	0.2425(3)	0.20249(13)	0.4450(2)	0.0297(11)
O100	1/2	0.2884(2)	1/4	0.082(2)
O200	0	0.20585(18)	1/4	0.090(2)

U(eq) is defined as one third of the trace of the orthogonalized Uij tensor.

Table A2.15
Atomic Coordinates and Equivalent Isotropic Displacement Parameters [Å^2] for [La_2(1,2BDC)$_2$(1,4BDC)(H_2O)$_4$], **XV**.

Atom	x	y	z	U(eq)
La1	0.42731	0.84908	0.19980	0.0169
La2	0.67838	0.43265	0.29472	0.0182
O1	0.49434	0.56218	0.19426	0.0288
O2	0.11181	0.82362	0.26190	0.0278
O3	0.66877	1.02184	0.18239	0.0315
O4	0.42188	0.86948	0.09904	0.0359
O5	0.82963	0.68553	0.16596	0.0350
O6	0.16391	0.13132	0.20459	0.0322
O7	0.10098	0.86681	0.13813	0.0274
O8	0.47988	0.96736	0.29075	0.0308
O9	0.67916	0.71680	0.28116	0.0236
O10	0.28958	0.60011	0.30330	0.0352
O11	0.63813	0.51270	0.39016	0.0432
O12	0.91260	0.14581	0.30200	0.0475
O13	0.43782	0.27062	0.33234	0.0315
O14	-0.00111	0.38335	0.22526	0.0273
O15	0.98619	0.41023	0.35935	0.0359
O16	0.53386	0.31794	0.21748	0.0262
C1	0.63160	0.84400	0.30541	0.0180
C2	0.76122	0.85503	0.35242	0.0192
C3	0.63999	0.93079	0.39821	0.0295
C4	0.75958	0.93493	0.44291	0.0487
C5	0.99160	0.86677	0.44246	0.0420
C6	1.11441	0.79499	0.39609	0.0347
C7	0.99883	0.79222	0.35195	0.0218
C11	0.84532	0.46703	0.39752	0.0253
C12	0.92689	0.48147	0.45014	0.0272
C13	0.77037	0.55287	0.49157	0.0351
C14	1.16042	0.43159	0.45936	0.0360
C21	0.46264	0.43261	0.18658	0.0206
C22	0.34882	0.41127	0.13809	0.0190
C23	0.39329	0.47195	0.09019	0.0384
C24	0.29375	0.44117	0.04543	0.0452
C25	0.14853	0.35349	0.04860	0.0470
C26	0.09995	0.29230	0.09873	0.0329
C27	0.19817	0.32421	0.14279	0.0302
C31	0.21421	0.88613	0.09750	0.0264
C32	0.10139	0.93984	0.04652	0.0204
C33	-0.13491	0.99348	0.04547	0.0297
C34	0.23382	0.94795	0.00175	0.0261
C51	0.14107	0.73212	0.30116	0.0234
C61	0.11795	0.27533	0.19484	0.0174

U(eq) is defined as one third of the trace of the orthogonalized Uij tensor.

Table A2.16

Atomic Coordinates and Equivalent Isotropic Displacement Parameters [$Å^2$] for $[Y_2(1,2BDC)_2(1,4BDC)(H_2O)_4]$, **XVI**.

Atom	x	y	z	U(eq)
Y1	0.21642	0.21326	0.13301	0.0147
Y2	0.50442	0.76534	0.33403	0.0143
O1	0.46199	0.47616	0.13066	0.0272
O2	1.18352	0.95299	0.15321	0.0357
O3	0.08719	0.23008	0.29627	0.0171
O4	-0.18595	0.04098	0.09651	0.0180
O5	-0.01308	0.37896	0.09970	0.0269
O6	0.13893	0.16679	-0.05767	0.0308

O7	0.56581	0.26442	0.26767	0.0247
O8	0.47656	0.16467	0.01710	0.0300
O9	0.53308	0.02665	0.32673	0.0265
O10	0.26461	0.50590	0.34177	0.0200
O11	0.74687	0.60360	0.36336	0.0316
O12	0.58451	-0.19109	-0.47646	0.0207
O13	1.15608	0.71201	0.19688	0.0179
O14	0.23323	-0.18658	-0.55435	0.0261
O15	0.91799	0.93968	0.37849	0.0267
O16	0.62303	0.74318	0.17092	0.0245
C1	0.32851	0.13419	-0.06436	0.0137
C2	0.35011	0.06590	-0.16645	0.0144
C3	0.52934	0.01138	-0.17770	0.0183
C4	0.53632	-0.07910	-0.27993	0.0185
C5	0.37230	-0.08967	-0.35972	0.0278
C6	0.18893	-0.01901	-0.35702	0.0412
C7	0.17532	0.04802	-0.26820	0.0341
C11	1.10705	0.79564	0.13354	0.0156
C21	0.61635	0.17223	0.33453	0.0240
C31	0.58978	0.61919	0.11631	0.0263
C32	0.70337	0.61681	0.01036	0.0228
C33	0.93970	0.71274	0.02586	0.0182
C34	1.04204	0.72600	-0.06571	0.0228
C35	0.89849	0.65685	-0.16559	0.0308
C36	0.65104	0.56352	-0.17644	0.0302
C37	0.54412	0.53690	-0.08791	0.0249
C41	0.13207	0.36705	0.35721	0.0058
C42	0.02115	0.35010	0.44569	0.0128
C43	0.77259	0.26024	0.44323	0.0205
C44	0.67046	0.24595	0.52962	0.0348
C45	0.80559	0.32501	0.63174	0.0409
C46	1.04105	0.41510	0.64042	0.0385
C47	0.14415	0.42683	0.54806	0.0260
C51	0.41020	-0.16461	-0.46682	0.0271

U(eq) is defined as one third of the trace of the orthogonalized Uij tensor.

Table A2.17

Atomic Coordinates and Equivalent Isotropic Displacement Parameters [Å^2] for $[Gd_2(1,2\text{-BDC})_4(H_2O)_2].(H_2Pip)$, **XVII**.

Atom	x	y	z	U(eq)
Gd1	0.10332(2)	0.88625(2)	0.46410(2)	0.0171(1)
O1	0.2091(3)	0.7509(2)	0.5620(3)	0.0276(11)
O2	0.0641(3)	1.0526(3)	0.4324(4)	0.0342(12)
O3	0.2005(3)	0.9479(2)	0.6837(3)	0.0293(11)
O4	-0.0828(3)	0.8906(2)	0.2796(3)	0.0241(11)
O5	-0.0089(3)	0.7991(2)	0.5545(3)	0.0253(11)
O6	0.1532(3)	0.6058(2)	0.7796(3)	0.0284(11)
O7	0.2880(3)	0.5714(3)	0.9728(3)	0.0282(12)
O8	-0.0039(3)	0.7454(2)	0.3148(3)	0.0213(11)
O9	0.3088(3)	0.7836(3)	0.7751(3)	0.0428(14)
C1	0.2553(4)	0.5835(4)	0.8532(5)	0.0227(17)
C2	0.3336(4)	0.5661(3)	0.7905(4)	0.0216(17)
C3	0.3982(5)	0.4830(4)	0.8172(5)	0.0346(19)
C4	0.4631(5)	0.4630(4)	0.7510(6)	0.046(2)
C5	0.4604(5)	0.5245(4)	0.6546(5)	0.039(2)
C6	0.3962(5)	0.6086(4)	0.6264(5)	0.0326(19)
C7	0.3355(4)	0.6316(3)	0.6953(4)	0.0221(17)
C8	0.2788(4)	0.7305(3)	0.6771(5)	0.0241(17)

C11	-0.0853(4)	0.8006(3)	0.2508(4)	0.0191(16)
C12	-0.1895(4)	0.7620(3)	0.1412(4)	0.0204(16)
C13	-0.2927(4)	0.8044(4)	0.1152(5)	0.0308(17)
C14	-0.3888(4)	0.7710(4)	0.0165(5)	0.0368(19)
C15	-0.3860(4)	0.6943(4)	-0.0606(5)	0.0332(17)
C16	-0.2852(4)	0.6510(4)	-0.0379(5)	0.0261(17)
C17	-0.1850(4)	0.6836(3)	0.0622(4)	0.0185(16)
C18	0.0790(4)	1.1433(3)	0.4342(4)	0.0188(16)
N1	0.0851(5)	0.4282(4)	0.5274(5)	0.058(2)
C31	-0.0308(4)	0.4005(3)	0.4962(4)	0.0115(14)
C32	0.0896(5)	0.5239(4)	0.4640(5)	0.0335(19)

U(eq) is defined as one third of the trace of the orthogonalized Uij tensor.

Table A2.18

Atomic Coordinates and Equivalent Isotropic Displacement Parameters [$Å^2$] for $(OPb_4)(1,3\text{-}BDC)_3(H_2O)$, **XVIII**.

Atom	x	y	z	U(eq)
Pb1	0.59274(2)	0.22597(2)	0.26108(2)	0.0225(1)
Pb2	0.70917(2)	0.17441(2)	0.07725(2)	0.0237(1)
Pb3	0.57324(2)	-0.02196(2)	0.17158(2)	0.0265(1)
Pb4	1.17016(2)	0.59340(2)	0.14386(2)	0.0288(1)
O1	0.7991(3)	0.2885(3)	0.2131(4)	0.0426(17)
O2	0.7426(3)	0.3127(3)	0.3350(4)	0.0430(17)
O3	1.1234(3)	0.5998(4)	0.3136(4)	0.065(2)
O4	1.0533(4)	0.4992(4)	0.1901(5)	0.070(3)
O5	0.6896(3)	0.1313(3)	0.4346(3)	0.0284(16)
O6	0.5581(3)	0.0614(3)	0.3259(3)	0.0263(14)
O7	0.5878(3)	0.2845(3)	0.0811(3)	0.0268(14)
O8	0.5232(3)	0.2118(3)	-0.0707(3)	0.0347(16)
O9	0.4531(3)	0.1100(3)	0.1173(4)	0.0396(17)
O10	0.3825(3)	0.0112(3)	-0.0139(4)	0.0388(17)
O11	0.2788(4)	0.4020(4)	0.1749(5)	0.069(3)
O12	0.1483(4)	0.4462(4)	0.0468(5)	0.077(3)
O13	0.6698(3)	0.1099(3)	0.2047(3)	0.0211(12)
O14	1.0279(5)	0.6379(6)	-0.0350(7)	0.091(3)
C1	0.7946(4)	0.3350(4)	0.2875(5)	0.029(2)
C2	0.8595(4)	0.4229(4)	0.3254(4)	0.0222(19)
C3	0.8498(4)	0.4868(4)	0.3974(5)	0.030(2)
C4	0.9064(4)	0.5703(5)	0.4262(5)	0.034(2)
C5	0.9716(4)	0.5896(4)	0.3834(5)	0.030(2)
C6	0.9268(4)	0.4420(4)	0.2840(5)	0.0220(19)
C7	0.9841(4)	0.5246(4)	0.3135(5)	0.028(2)
C8	1.0574(4)	0.5427(5)	0.2694(6)	0.034(3)
C11	0.6263(4)	0.0642(4)	0.4126(5)	0.025(2)
C12	0.6311(4)	-0.0123(4)	0.4906(4)	0.0197(19)
C13	0.7052(4)	-0.0161(5)	0.5857(5)	0.031(2)
C14	0.7067(5)	-0.0893(4)	0.6560(5)	0.035(2)
C15	0.6344(4)	-0.1572(4)	0.6296(5)	0.027(2)
C16	0.5583(4)	-0.0807(4)	0.4651(5)	0.0209(19)
C17	0.5590(4)	-0.1532(4)	0.5345(4)	0.0164(17)
C18	0.5206(4)	0.2742(4)	-0.0078(5)	0.0222(19)
C21	0.3831(4)	0.0871(4)	0.0379(5)	0.027(2)
C22	0.2991(4)	0.1538(4)	0.0021(4)	0.0226(19)
C23	0.2277(4)	0.1419(4)	-0.0934(5)	0.028(2)
C24	0.1525(5)	0.2061(5)	-0.1304(5)	0.039(2)
C25	0.1487(5)	0.2843(5)	-0.0704(6)	0.038(3)
C26	0.2933(4)	0.2334(4)	0.0624(5)	0.028(2)
C27	0.2188(4)	0.2985(4)	0.0267(5)	0.030(2)

C28	0.2168(6)	0.3871(5)	0.0900(7)	0.050(3)

U(eq) is defined as one third of the trace of the orthogonalized Uij tensor.

Table A2.19

Atomic Coordinates and Equivalent Isotropic Displacement Parameters [$Å^2$] for $[La_3(1,2\text{-BDC})_4(1,10\text{-phen})_3(H_2O)]\cdot 0.5H_2O$, **XIX**.

Atom	x	y	z	U(eq)
La1	0.29651(2)	0.41340(2)	0.28543(2)	0.0249(1)
La2	0.09043(2)	0.26776(2)	0.28056(2)	0.0250(1)
La3	0.17352(2)	0.05888(2)	0.36153(2)	0.0260(1)
O1	0.2425(2)	0.4514(2)	0.38528(17)	0.0392(17)
O2	0.2133(2)	0.33308(19)	0.35507(16)	0.0285(14)
O3	0.1079(2)	0.2114(2)	0.38523(17)	0.0379(17)
O4	0.2361(3)	0.1827(2)	0.44369(17)	0.0419(17)
O5	0.2702(2)	0.40972(19)	0.16421(16)	0.0303(12)
O6	0.3714(3)	0.4218(2)	0.11162(18)	0.0403(16)
O7	0.2505(2)	0.2891(2)	0.24439(17)	0.0318(14)
O8	0.1361(2)	0.2519(2)	0.17444(17)	0.0379(16)
O9	0.1251(2)	0.41122(19)	0.24559(16)	0.0300(14)
O10	0.0398(2)	0.4029(2)	0.31085(18)	0.0389(16)
O11	0.1670(2)	0.5627(2)	0.1535(2)	0.0375(17)
O12	0.2367(2)	0.53604(19)	0.24980(18)	0.0352(14)
O13	0.4479(2)	0.3740(2)	0.26574(17)	0.0360(14)
O14	0.4069(2)	0.49115(19)	0.23891(16)	0.0289(14)
O15	0.5075(2)	0.6552(2)	0.25220(18)	0.0409(17)
O16	0.4864(2)	0.5800(2)	0.16944(18)	0.0342(16)
O100	0.1801(3)	0.1589(2)	0.2934(2)	0.0370(16)
N1	0.4254(3)	0.4899(3)	0.3689(2)	0.0341(17)
N2	0.4002(3)	0.3385(3)	0.3824(2)	0.0320(17)
N3	-0.0707(3)	0.2713(3)	0.3092(2)	0.0346(19)
N4	-0.0498(3)	0.3101(3)	0.1945(2)	0.0317(17)
N5	0.2808(3)	0.0053(3)	0.4679(2)	0.0368(19)
N6	0.1202(3)	0.0610(2)	0.4683(2)	0.0307(17)
C1	0.4392(4)	0.5639(4)	0.3624(3)	0.045(3)
C2	0.5118(4)	0.6015(4)	0.3968(3)	0.056(3)
C3	0.5714(4)	0.5627(4)	0.4385(3)	0.055(3)
C4	0.5608(4)	0.4854(4)	0.4467(3)	0.044(3)
C5	0.6210(4)	0.4407(4)	0.4899(3)	0.059(3)
C6	0.6075(4)	0.3663(4)	0.4958(3)	0.061(3)
C7	0.5341(4)	0.3287(4)	0.4604(3)	0.046(3)
C8	0.5168(4)	0.2519(4)	0.4670(3)	0.058(3)
C9	0.4446(4)	0.2196(4)	0.4319(3)	0.053(3)
C10	0.3878(4)	0.2654(3)	0.3908(3)	0.036(2)
C11	0.4727(4)	0.3704(3)	0.4177(3)	0.035(2)
C12	0.4863(4)	0.4508(3)	0.4107(3)	0.035(2)
C21	-0.0828(4)	0.2531(3)	0.3639(3)	0.046(3)
C22	-0.1630(4)	0.2407(4)	0.3756(4)	0.058(3)
C23	-0.2356(4)	0.2487(3)	0.3300(3)	0.055(3)
C24	-0.2259(4)	0.2696(3)	0.2716(3)	0.039(3)
C25	-0.2981(4)	0.2814(3)	0.2214(3)	0.050(3)
C26	-0.2883(4)	0.2991(4)	0.1659(3)	0.051(3)
C27	-0.2040(4)	0.3084(3)	0.1543(3)	0.038(3)
C28	-0.1914(4)	0.3265(3)	0.0958(3)	0.050(3)
C29	-0.1102(4)	0.3372(4)	0.0882(3)	0.052(3)
C30	-0.0415(4)	0.3289(3)	0.1389(3)	0.047(3)
C31	-0.1313(4)	0.3001(3)	0.2023(3)	0.030(2)
C32	-0.1423(4)	0.2804(3)	0.2626(3)	0.031(2)
C41	0.3582(4)	-0.0219(3)	0.4689(3)	0.049(3)
C42	0.4131(5)	-0.0523(4)	0.5207(4)	0.061(3)

C43	0.3861(5)	-0.0556(4)	0.5741(4)	0.071(3)
C44	0.3043(5)	-0.0282(4)	0.5761(3)	0.053(3)
C45	0.2714(6)	-0.0272(4)	0.6307(3)	0.075(4)
C46	0.1935(6)	0.0009(5)	0.6307(4)	0.074(4)
C47	0.1395(4)	0.0315(3)	0.5767(3)	0.044(3)
C48	0.0578(5)	0.0615(4)	0.5757(4)	0.052(3)
C49	0.0100(5)	0.0906(4)	0.5221(4)	0.051(3)
C50	0.0439(4)	0.0886(3)	0.4704(3)	0.039(3)
C51	0.1690(4)	0.0322(3)	0.5217(3)	0.034(2)
C52	0.2530(4)	0.0018(3)	0.5214(3)	0.038(3)
C61	0.2153(3)	0.3866(3)	0.3938(3)	0.030(2)
C62	0.1828(3)	0.3695(3)	0.4504(3)	0.030(2)
C63	0.1667(4)	0.4297(3)	0.4865(3)	0.044(3)
C64	0.1331(4)	0.4184(4)	0.5369(3)	0.056(3)
C65	0.1148(4)	0.3469(4)	0.5524(3)	0.059(3)
C66	0.1302(4)	0.2860(4)	0.5173(3)	0.040(2)
C67	0.1646(3)	0.2958(3)	0.4661(3)	0.028(2)
C68	0.1739(4)	0.2247(3)	0.4292(3)	0.032(2)
C71	0.3218(4)	0.3811(3)	0.1341(3)	0.032(2)
C72	0.3230(3)	0.2966(3)	0.1251(3)	0.032(2)
C73	0.3761(4)	0.2672(3)	0.0896(3)	0.055(3)
C74	0.3812(4)	0.1907(3)	0.0778(3)	0.060(3)
C75	0.3327(4)	0.1413(3)	0.1020(3)	0.042(3)
C76	0.2780(4)	0.1684(3)	0.1364(3)	0.034(2)
C77	0.2722(3)	0.2454(3)	0.1482(2)	0.025(2)
C78	0.2151(4)	0.2654(3)	0.1910(3)	0.027(2)
C81	0.0715(3)	0.4413(3)	0.2739(3)	0.031(2)
C82	0.0450(3)	0.5222(3)	0.2618(3)	0.0283(19)
C83	-0.0260(4)	0.5481(3)	0.2820(3)	0.047(3)
C84	-0.0527(4)	0.6223(3)	0.2744(3)	0.054(3)
C85	-0.0071(4)	0.6730(3)	0.2473(3)	0.049(3)
C86	0.0617(4)	0.6476(3)	0.2255(3)	0.038(3)
C87	0.0887(3)	0.5729(3)	0.2317(2)	0.027(2)
C88	0.1690(4)	0.5532(3)	0.2092(3)	0.029(2)
C91	0.4659(3)	0.4415(3)	0.2567(3)	0.028(2)
C92	0.5589(3)	0.4669(3)	0.2732(3)	0.028(2)
C93	0.6211(4)	0.4188(3)	0.3076(3)	0.040(3)
C94	0.7052(4)	0.4425(4)	0.3289(3)	0.052(3)
C95	0.7286(4)	0.5147(4)	0.3160(3)	0.046(3)
C96	0.6682(4)	0.5631(3)	0.2837(3)	0.040(3)
C97	0.5831(3)	0.5406(3)	0.2611(3)	0.028(2)
C98	0.5198(3)	0.5960(3)	0.2247(3)	0.033(2)
O200	0.0482(6)	0.5727(6)	0.5941(5)	0.055(4)

U(eq) is defined as one third of the trace of the orthogonalized Uij tensor.

Table A2.20

Atomic Coordinates and Equivalent Isotropic Displacement Parameters [$Å^2$] for $[La_3(1,2\text{-BDC})_4(1,10\text{-phen})_2(NO_3)]\cdot H_2O$, **XX**.

Atom	x	y	z	U(eq)
La1	0.33984	0.28874	0.24473	0.0266
La2	0.10834	0.33500	0.44979	0.0270
La3	0.33048	0.09451	0.07012	0.0276
O1	0.28252	0.37589	0.39195	0.0311
O2	0.36808	0.45050	0.30248	0.0477
O3	0.41701	0.23608	0.09477	0.0313
O4	0.12485	0.40779	0.29705	0.0375
O5	0.19658	0.25393	0.17313	0.0298
O6	0.41909	0.08424	0.19718	0.0305

O7	0.25733	0.17890	0.34218	0.0265
O8	0.32595	0.41622	0.13113	0.0449
O9	0.50661	0.19088	0.32217	0.0518
O10	0.56312	0.24252	0.21051	0.0600
O11	0.26774	0.14744	0.46566	0.0416
O12	0.09334	0.51953	0.50640	0.0389
O13	-0.01408	0.35525	0.34474	0.0441
O14	0.22076	0.38602	0.56153	0.0495
O15	0.64773	0.10586	-0.03803	0.0437
O16	0.18800	0.29316	0.05089	0.0380
O17	0.31692	-0.01690	0.19940	0.0407
O18	0.47800	0.10377	-0.04376	0.0318
O82	0.68516	0.17102	0.28950	0.0859
N1	0.00605	0.19035	0.45860	0.0480
N2	0.01618	0.28711	0.59213	0.0474
N4	0.23129	0.08990	-0.05282	0.0413
N5	0.10877	0.11313	0.09478	0.0364
N81	0.58751	0.20144	0.27386	0.0537
C1	0.02187	0.33170	0.65768	0.0620
C2	-0.05043	0.33767	0.72874	0.0789
C3	-0.12838	0.29453	0.73227	0.0841
C4	-0.13436	0.24054	0.66607	0.0685
C5	-0.20990	0.18791	0.66670	0.1010
C6	-0.21468	0.13764	0.60313	0.0979
C7	-0.14078	0.13479	0.52950	0.0746
C8	-0.14088	0.08200	0.46175	0.0920
C9	-0.06750	0.07941	0.39404	0.0857
C10	0.00436	0.13754	0.39545	0.0648
C11	-0.06556	0.18847	0.52626	0.0530
C12	-0.06096	0.24034	0.59573	0.0501
C21	0.04693	0.12740	0.16589	0.0488
C22	-0.07238	0.15734	0.18318	0.0585
C23	-0.13042	0.17029	0.12371	0.0592
C24	-0.06973	0.15348	0.04628	0.0478
C25	-0.12290	0.15969	-0.01901	0.0633
C26	-0.06012	0.14023	-0.09170	0.0608
C27	0.06088	0.11746	-0.10633	0.0470
C28	0.12940	0.09606	-0.18143	0.0583
C29	0.24488	0.07318	-0.19079	0.0596
C30	0.29164	0.07136	-0.12517	0.0522
C31	0.11609	0.11183	-0.04351	0.0361
C32	0.05142	0.12626	0.03458	0.0404
C41	0.32792	0.44592	0.37196	0.0334
C42	0.33458	0.51923	0.43370	0.0322
C43	0.40874	0.57402	0.41572	0.0476
C44	0.42192	0.63742	0.47162	0.0570
C45	0.35904	0.65097	0.54646	0.0570
C46	0.28420	0.59887	0.56522	0.0440
C47	0.27222	0.53188	0.50954	0.0322
C48	0.19178	0.47522	0.52973	0.0340
C51	0.30379	0.11598	0.39524	0.0265
C52	0.40026	0.00265	0.37253	0.0280
C53	0.45605	-0.05746	0.43070	0.0346
C54	0.54571	-0.16285	0.41413	0.0424
C55	0.57811	-0.20949	0.33894	0.0485
C56	0.52236	-0.15272	0.28087	0.0409
C57	0.43406	-0.04491	0.29652	0.0289
C58	0.38328	0.01182	0.22873	0.0312
C61	0.03309	0.39533	0.29153	0.0314

C62	-0.02765	0.43783	0.22423	0.0356
C63	-0.14261	0.51499	0.24125	0.0473
C64	-0.20434	0.56050	0.18329	0.0685
C65	-0.15241	0.53068	0.10627	0.0692
C66	-0.03901	0.45030	0.08847	0.0537
C67	0.02528	0.40487	0.14586	0.0334
C68	0.14447	0.31406	0.12166	0.0316
C71	0.38494	0.33895	0.07837	0.0317
C72	0.42184	0.36573	-0.00158	0.0321
C73	0.38741	0.47619	-0.02049	0.0450
C74	0.42754	0.50199	-0.09362	0.0532
C75	0.50446	0.41856	-0.14710	0.0565
C76	0.54001	0.30810	-0.12958	0.0480
C77	0.49825	0.27983	-0.05684	0.0330
C91	0.54339	0.15697	-0.04311	0.0328
O100	0.24317	0.04969	0.62749	0.1647

U(eq) is defined as one third of the trace of the orthogonalized Uij tensor.

Table A2.21

Atomic Coordinates and Equivalent Isotropic Displacement Parameters [$Å^2$] for Y_2(1,2-BDC)$_3$(H_2O), **XXI**.

Atom	x	y	z	U(eq)
Y1	0.50102(4)	-0.00398(3)	0.75885(3)	0.0199(2)
Y2	0.81822(4)	-0.12097(3)	0.53641(3)	0.0191(2)
Y3	1.01459(4)	0.04872(4)	0.74169(3)	0.0194(2)
Y4	0.19223(4)	0.11220(3)	0.99742(3)	0.0194(2)
O1	0.5327(3)	0.0875(3)	0.8377(2)	0.0300(12)
O2	0.3472(3)	0.1483(3)	0.7341(2)	0.0314(12)
O3	0.4692(3)	-0.0753(3)	0.6619(2)	0.0291(12)
O4	0.6482(3)	-0.1599(2)	0.7890(2)	0.0292(11)
O5	0.3548(3)	-0.0436(3)	0.8791(2)	0.0277(12)
O6	0.6469(3)	0.0417(3)	0.6415(2)	0.0276(12)
O7	0.2791(3)	0.0038(3)	0.5593(2)	0.0352(12)
O8	0.6552(3)	-0.1686(3)	0.5874(3)	0.0399(14)
O9	0.8231(3)	-0.1945(3)	0.6792(2)	0.0311(12)
O10	0.1199(3)	0.2573(2)	0.5483(2)	0.0274(11)
O11	0.8324(3)	0.0314(2)	0.5610(2)	0.0263(11)
O12	0.9717(3)	0.1928(3)	0.4671(2)	0.0273(12)
O13	1.0004(3)	0.1023(2)	0.5964(2)	0.0229(11)
O14	0.8122(3)	0.1205(3)	0.7886(2)	0.0325(12)
O15	0.2059(3)	-0.0663(3)	0.6988(3)	0.0398(12)
O16	0.1025(3)	0.1782(3)	0.6898(2)	0.0315(12)
O17	0.9735(3)	0.1443(3)	0.8590(2)	0.0365(12)
O18	0.9763(3)	-0.0913(3)	0.7101(2)	0.0372(14)
O19	0.3693(3)	0.1348(3)	0.9541(3)	0.0389(14)
O20	0.7279(3)	0.0296(3)	0.9120(2)	0.0292(12)
O21	0.1816(3)	0.1882(3)	0.8515(2)	0.0287(12)
O22	0.0154(3)	-0.1902(3)	0.9902(2)	0.0258(11)
O23	0.8532(3)	-0.1893(3)	0.8691(2)	0.0291(12)
O24	0.1695(3)	-0.0367(3)	0.9590(2)	0.0276(11)
O25	0.8637(3)	-0.3021(3)	0.9926(2)	0.0322(12)
O26	0.0128(3)	-0.0726(2)	0.8694(2)	0.0270(11)
C1	0.9300(4)	0.1689(4)	0.5501(3)	0.0207(17)
C2	0.7997(4)	0.2307(4)	0.5968(3)	0.0201(17)
C3	0.7045(4)	0.1924(3)	0.6246(3)	0.0203(17)
C4	0.5879(4)	0.2579(4)	0.6657(3)	0.0286(17)
C5	0.5660(5)	0.3582(4)	0.6820(3)	0.0360(17)
C6	0.6613(5)	0.3949(4)	0.6573(4)	0.040(2)

C7	0.7770(5)	0.3322(4)	0.6140(3)	0.0324(17)
C11	0.7291(4)	0.1140(4)	0.8599(3)	0.0236(17)
C12	0.6271(4)	0.2158(3)	0.8876(3)	0.0202(17)
C13	0.5056(4)	0.2261(3)	0.9139(3)	0.0205(17)
C14	0.4168(4)	0.3200(4)	0.9446(3)	0.0302(17)
C15	0.4476(5)	0.4020(4)	0.9503(4)	0.041(2)
C16	0.5667(5)	0.3917(4)	0.9245(4)	0.041(2)
C17	0.6563(5)	0.2993(4)	0.8932(3)	0.0312(17)
C21	0.5431(4)	-0.1458(4)	0.6109(3)	0.0243(17)
C22	0.4944(4)	-0.2104(4)	0.5838(3)	0.0226(17)
C23	0.5737(5)	-0.3070(4)	0.5500(4)	0.0369(19)
C24	0.5287(6)	-0.3732(4)	0.5327(4)	0.049(2)
C25	0.4069(6)	-0.3466(4)	0.5516(4)	0.046(2)
C26	0.3272(5)	-0.2513(4)	0.5843(4)	0.0348(19)
C27	0.3700(4)	-0.1815(3)	0.5987(3)	0.0215(17)
C31	0.8573(4)	-0.2812(4)	0.9135(3)	0.0242(17)
C32	0.8506(4)	-0.3624(4)	0.8707(3)	0.0227(17)
C33	0.8020(4)	-0.3336(4)	0.7980(3)	0.0232(17)
C34	0.7977(5)	-0.4125(4)	0.7622(4)	0.0333(17)
C35	0.8380(5)	-0.5181(4)	0.7979(4)	0.043(2)
C36	0.8852(5)	-0.5471(4)	0.8703(4)	0.041(2)
C37	0.8900(5)	-0.4702(4)	0.9066(4)	0.0339(19)
C41	0.0706(4)	-0.1539(4)	0.9151(3)	0.0219(17)
C42	0.2030(4)	-0.2156(3)	0.8777(3)	0.0197(17)
C43	0.2964(4)	-0.1851(3)	0.8753(3)	0.0198(17)
C44	0.4163(4)	-0.2536(4)	0.8428(3)	0.0306(17)
C45	0.4419(5)	-0.3450(4)	0.8100(4)	0.0384(19)
C46	0.3491(5)	-0.3730(4)	0.8102(4)	0.044(2)
C47	0.2304(5)	-0.3097(4)	0.8450(4)	0.0346(19)
C51	0.1221(4)	0.2511(4)	0.6278(3)	0.0215(17)
C52	0.1446(4)	0.3369(3)	0.6509(3)	0.0211(17)
C53	0.1943(4)	0.3188(3)	0.7218(3)	0.0228(17)
C54	0.2028(5)	0.4032(4)	0.7467(4)	0.0353(19)
C55	0.1669(5)	0.5048(4)	0.7006(4)	0.042(2)
C56	0.1205(5)	0.5235(4)	0.6298(4)	0.042(2)
C57	0.1115(5)	0.4400(4)	0.6052(3)	0.0322(19)
C71	0.7538(4)	-0.2194(4)	0.7539(3)	0.0230(17)
C81	0.2437(4)	0.2087(4)	0.7726(3)	0.0230(17)
C91	0.2792(4)	-0.0731(4)	0.6224(3)	0.0261(17)
C92	0.4669(4)	0.1422(4)	0.9028(3)	0.0245(17)
C101	0.2707(4)	-0.0824(4)	0.9066(3)	0.0214(17)
C111	0.7290(4)	0.0826(4)	0.6087(3)	0.0204(17)

U(eq) is defined as one third of the trace of the orthogonalized Uij tensor.

Table A2.22

Atomic Coordinates and Equivalent Isotropic Displacement Parameters [$Å^2$] for Dy_2(1,2-BDC)$_3$(H_2O), **XXII**.

Atom	x	y	z	U(eq)
Dy1	0.40204(3)	0.30487(1)	-0.01435(2)	0.0155(1)
Dy2	0.08515(3)	0.27387(1)	0.15831(2)	0.0142(1)
O1	0.0661(5)	0.32195(15)	-0.0308(3)	0.0202(12)
O2	0.2435(5)	0.38307(15)	-0.0511(4)	0.0241(12)
O3	-0.0852(5)	0.34364(15)	0.1457(3)	0.0210(12)
O4	-0.3720(5)	0.35730(16)	0.0722(4)	0.0231(14)
O5	0.3386(5)	0.32357(15)	0.1708(3)	0.0189(12)
O6	0.5801(5)	0.27836(15)	0.2355(4)	0.0267(16)
O7	0.6096(5)	0.24845(16)	-0.0169(4)	0.0274(16)
O8	0.8886(5)	0.22738(15)	0.0148(4)	0.0236(16)
O9	0.2588(5)	0.23356(14)	0.0405(3)	0.0176(12)
O10	0.1901(6)	0.20016(15)	-0.1420(3)	0.0250(16)

O11	0.2399(5)	0.29660(15)	-0.2339(3)	0.0189(12)
O12	0.4859(5)	0.33967(16)	-0.1828(4)	0.0274(14)
O100	-0.1067(5)	0.23573(18)	0.2566(4)	0.0260(16)
C1	0.0952(8)	0.3690(2)	-0.0440(5)	0.0186(19)
C2	-0.0450(7)	0.4086(2)	-0.0578(5)	0.0186(17)
C3	-0.0331(9)	0.4500(2)	-0.1293(6)	0.031(2)
C4	-0.1530(9)	0.4890(3)	-0.1508(7)	0.037(2)
C5	-0.2928(10)	0.4866(3)	-0.1018(7)	0.041(3)
C6	-0.3081(8)	0.4460(3)	-0.0314(6)	0.032(2)
C7	-0.1867(7)	0.4065(2)	-0.0074(5)	0.0181(17)
C8	-0.2151(8)	0.3656(2)	0.0751(5)	0.0200(19)
C11	0.4911(7)	0.3143(2)	0.2506(5)	0.0169(17)
C12	0.5510(7)	0.3511(2)	0.3510(5)	0.0179(17)
C13	0.4930(8)	0.4005(2)	0.3353(6)	0.030(2)
C14	0.5521(10)	0.4356(3)	0.4248(7)	0.040(3)
C15	0.6711(10)	0.4218(3)	0.5321(7)	0.043(3)
C16	0.7311(9)	0.3730(2)	0.5497(6)	0.033(2)
C17	0.6725(7)	0.3368(2)	0.4613(5)	0.0174(17)
C18	0.7277(8)	0.2170(2)	-0.0130(5)	0.0169(19)
C21	0.2145(7)	0.1955(2)	-0.0320(5)	0.017(2)
C22	0.2000(7)	0.1446(2)	0.0182(5)	0.0190(17)
C23	0.1291(9)	0.1060(2)	-0.0640(6)	0.029(2)
C24	0.1268(10)	0.0566(3)	-0.0246(7)	0.043(3)
C25	0.2007(10)	0.0449(3)	0.0946(7)	0.042(3)
C26	0.2725(9)	0.0826(2)	0.1752(6)	0.032(2)
C27	0.2691(8)	0.1328(2)	0.1404(5)	0.0211(17)
C28	0.3400(8)	0.3310(2)	-0.2574(5)	0.0197(19)

U(eq) is defined as one third of the trace of the orthogonalized Uij tensor.

Table A2.23
Atomic Coordinates and Equivalent Isotropic Displacement Parameters [$Å^2$] for $[Pr_2(1,2\text{-BDC})_2(PipDPA)]$, **XXIII**.

Atom	x	y	z	U(eq)
Pr1	0.74665(4)	0.49733(3)	0.07378(2)	0.0158(1)
O1	0.4893(5)	0.5740(4)	0.1851(3)	0.0298(12)
O2	0.2217(5)	0.6295(4)	0.0800(3)	0.0255(12)
O3	-0.2006(5)	0.7080(4)	0.1227(3)	0.0248(12)
O4	0.9827(5)	0.3980(4)	0.2482(3)	0.0260(12)
O5	0.9168(5)	0.6364(4)	-0.0830(3)	0.0201(12)
O6	0.5351(5)	0.6411(4)	-0.0801(3)	0.0231(12)
O7	0.7034(5)	0.2537(4)	0.1982(4)	0.0321(14)
N1	-0.0743(6)	0.9032(4)	0.0888(4)	0.0240(17)
C1	0.3148(8)	0.6151(5)	0.1709(5)	0.0226(17)
C2	0.2078(7)	0.6431(6)	0.2731(4)	0.0196(17)
C3	0.2949(8)	0.5954(6)	0.3817(5)	0.0299(19)
C4	0.1977(9)	0.6095(7)	0.4796(5)	0.034(2)
C5	0.0124(9)	0.6711(6)	0.4683(5)	0.0302(19)
C6	-0.0747(8)	0.7225(6)	0.3612(5)	0.0247(17)
C7	0.0203(7)	0.7110(5)	0.2623(4)	0.0189(17)
C8	-0.0880(8)	0.7724(6)	0.1505(5)	0.0201(17)
C9	0.0498(8)	0.9895(6)	0.1165(5)	0.0274(19)
C10	-0.1812(8)	0.9733(6)	-0.0197(5)	0.0270(17)
C11	1.0951(7)	0.3324(5)	0.1935(5)	0.0184(17)
C12	1.2323(7)	0.2015(5)	0.2594(4)	0.0191(17)
C13	1.1479(8)	0.1072(6)	0.3412(5)	0.0242(17)
C14	1.2489(9)	-0.0224(6)	0.4053(5)	0.0325(19)
C15	1.4354(9)	-0.0564(6)	0.3898(6)	0.039(2)
C16	1.5226(8)	0.0380(6)	0.3125(5)	0.0335(19)
C17	1.4236(7)	0.1681(5)	0.2455(5)	0.0195(17)

C18	0.4635(7)	0.7349(5)	-0.1703(5)	0.0200(17)

U(eq) is defined as one third of the trace of the orthogonalized Uij tensor.

Table A2.24
Atomic Coordinates and Equivalent Isotropic Displacement Parameters [$Å^2$] for [Cd(1,3-BDC)(H_2O)], **XXIV**.

Atom	x	y	z	U(eq)
Cd1	-0.15397(5)	1/4	0	0.0222(2)
O1	-0.1050(3)	0.3517(4)	0.11456(11)	0.0352(8)
O2	0.1718(3)	0.4385(3)	0.05375(10)	0.0293(7)
O100	-0.4991(6)	1/4	0	0.0447(16)
C1	0.0775(4)	0.4102(4)	0.11365(15)	0.0241(10)
C2	0.1865(4)	0.4439(4)	0.18432(15)	0.0215(9)
C3	0.0861(6)	0.4106(5)	1/4	0.0213(12)
C4	0.3892(4)	0.5062(4)	0.18495(16)	0.0265(10)
C5	0.4902(6)	0.5368(6)	1/4	0.0280(16)

U(eq) is defined as one third of the trace of the orthogonalized Uij tensor.

Table A2.25
Atomic Coordinates and Equivalent Isotropic Displacement Parameters [$Å^2$] for [Pb(1,4-BDC)], **XXV**.

Atom	x	y	z	U(eq)
Pb1	0.48999(5)	-0.20334(4)	0.48128(2)	0.0243(1)
O1	0.4712(9)	0.0339(8)	0.4194(4)	0.029(2)
O2	0.3400(10)	0.2201(7)	0.4015(4)	0.032(2)
O3	0.3199(9)	0.0897(7)	0.0242(4)	0.027(2)
O4	0.3051(8)	-0.1217(6)	0.0529(4)	0.0243(19)
C1	0.3928(12)	0.1101(10)	0.3781(5)	0.023(3)
C2	0.3766(13)	0.0792(9)	0.2984(5)	0.023(3)
C3	0.4418(16)	-0.0364(10)	0.2698(6)	0.033(3)
C4	0.3099(14)	0.1716(9)	0.2520(6)	0.027(3)
C5	0.3017(13)	0.1489(10)	0.1778(6)	0.026(3)
C6	0.4302(15)	-0.0610(10)	0.1951(7)	0.031(3)
C7	0.3606(13)	0.0277(10)	0.1487(5)	0.024(3)
C8	0.3299(12)	-0.0016(9)	0.0692(5)	0.020(3)

U(eq) is defined as one third of the trace of the orthogonalized Uij tensor.

Chapter 3

Hybrid Networks of Metal Cyclohexanedicarboxylates

Summary*

As part of our effort to understand the structural features of hybrid dicarboxylate frameworks in terms of dimensionality and extended inorganic connectivity, we have employed the three isomeric (1,2-, 1,3- and 1,4-) flexible (conformational) cyclohexanedicarboxylic acids and 1,2-cyclohex(4)enedicarboxylic acid to synthesize hybrid frameworks of Mn, Cd, Pb and La with or without chelating amines.

Nine hybrid inorganic-organic cyclohexanedicarboxylates with zero inorganic connectivity (I^0O^y, y = *1* to *3*) have been synthesized and characterized. These coordination polymers are the two isomeric cyclohexanedicarboxylates (1,3- and 1,4-) of Mn, Cd and Pb and with or without chelating amines. Of these, six of them (**I-VI**) contain chelating pyridyl amines such as 1,10-pheanthroline or 2,2'-bipyridine. [Cd(1,3-CHDC)(1,10-phen)], **I**, is a two dimensional compound (I^0O^2) where edge shared cadmium $^2\mathbf{D_2}$ dimers are connected by the 1,3-CHDC anions. [Description of dimer SBUs and terminology are given in the appendix {see Appendix. 2.7(a)}]. [Mn(H_2O)(1,3-CHDC)(1,10-phen)], **II**, is a molecular compound (I^0O^0) with a ring structure where the two Mn(II) cations are connected by the two 1,3- CHDC anions. [Mn_3(1,3-CHDC)$_3$(1,10-phen].4H_2O, **III**, has an infinite one-dimensional chain (I^0O^1) structure consisting of a trinuclear $Mn_3N_4O_{12}$ units (two dimers of $^3\mathbf{D_1}$) connected by 1,3-CHDC anions. Compounds,

*Papers based on these studies have been published in *Dalton. Trans*., (2006), *Chem.—Eur.J*., (2007) and *Inorg. Chem*., (2008).

$[Mn_3(1,4\text{-CHDC})_3(1,10\text{-phen})]..4H_2O$, **IV** and $[Cd_3(1,4\text{-CHDC})_3(1,10\text{-phen})_2].4H_2O$, **V**, both have a layer structure (***I*^{0}*O*^{2}**)** consisting of one-dimensional infinite chains made up of trinuclear units connected by the 1,4-CHDC anions. $[Cd(1,4\text{-CHDC})(2,2'\text{-bipy})].H_2O$, **VI**, has a two-dimensional layer structure (***I*^{0}*O*^{2}**)**, formed by the connectivity of $^2\mathbf{D_2}$ dimer and the 1,4-CHDC anions. Compounds **I-III** and **VI**, contain CHDC anions in the (*e,e*) conformation, whereas in **IV** and **V**, they are in both (*e,e*) and (*a,e*) conformations.

Compounds **VII-XI**, contain no chelating amines. $[Cd(H_2O)_2(1,3\text{-CHDC})].H_2O$, **VII**, has a two-dimensional layer structure (***I*^{0}*O*^{2}**)** formed by the connectivity between Cd_2O_{12} dimers ($^2\mathbf{D_2}$) and the carboxylate groups. $(OPb_3)(1,3\text{-CHDC})_2$, **VIII**, has a three-dimensional structure without any inorganic connectivity (***I*^{0}*O*^{3}**)**. The hexameric Pb_6O_{18} units are connected by the 1,3-CHDC anions in the (a,*e*) conformation into an infinite three dimensional-structure where Pb(II) cation is in a hemidirected coordination environment. $[Cd(H_2O)_2(1,4\text{-CHDC})]$, **IX**, is a one-dimensional chain structure (***I*^{0}*O*^{1}**)** consisting of octahedral CdO_6 units connected by the 1,4-CHDC anions. Compounds **VII** and **IX**, contain CHDC anions in the (*e,e*) conformation.

Ten hybrid inorganic-organic cyclohexane (or hexene) dicarboxylates with extended inorganic connectivity (***I*^{x}*O*^{y}**, *x* = *1* to *2* *y* = *0* to *2***) have been synthesized and characterized. These hybrid structures in two- and three-dimensions are the three isomeric cyclohexanedicarboxylates (1,2-, 1,3- and 1,4-) and 1,2-cyclohex(4)enedicarboxylates of Cd, Pb and La without chelating amines.

[Cd(1,2-CHDC)], **X**, is a layered structure consisting of a two dimensional metal-O-metal network (***I*^{2}*O*^{0}**)**, grafted by the 1,2-CHDC anions in the (*e,e*) conformation. Cd(1,2-CHeDC)(H_2O), **XI**, was obtained in two different

polymorphic forms, **A** and **B**. In both the polymorphs, **XI** has a two-dimensional layered structure (***I*^{1}*O*^{1}**) made up of infinite one-dimensional Cd-O-Cd chains connected by the CHeDC anions in the (*a,e*) conformation. The layered structures in **A** and **B** are similar, but only differ in their packing arrangements.

Pb(1,3-CHDC)(H_2O), **XII**, contains two types of two-dimensional layers (***I*^{1}*O*^{1}**) and (***I*^{2}*O*^{0}**), alternatively packed in the crystal structure. Pb(II) cation in the (***I*^{1}*O*^{1}**) layer is in a hemidirected geometry whereas in the (***I*^{2}*O*^{0}**) layer, it is in a holodirected geometry. $[(OPb_4)_2(OH)_2(C_2O_4)(1,3\text{-CHDC})_4].H_2O$, **XIII**, has a two-dimensional structure where the octameric $Pb_8(OH)_2O_{26}$ units were connected by the oxalate and 1,3-CHDC anions into the (***I*^{2}*O*^{0}**) structure. The oxalate moiety was generated *in-situ* from the 1,3-H_2CHDC under the hydrothermal synthesis. $Pb_2(1,3\text{-CHDC})_2(H_2O)$, **XIV**, has a three-dimensional structure (***I*^{2}*O*^{1}**), where a (4,4) square lattice of tetra-nuclear Pb_4O_{18} units are connected by the 1,3-CHDC anions. Compounds **XII** - **XIV**, contain 1,3-CHDC anions in the (*e,e*) conformation. $[(OPb_3)(1,4\text{-CHDC})_2]$, **XV**, has a three-dimensional structure with one-dimensional inorganic connectivity (***I*^{1}*O*^{2}**), where the one-dimensional chains of edge sharing hexameric Pb_6O_{20} units are cross-linked by the 1,4- CHDC anions in both (*e,e*) and (*a,e*) conformations.

The lanthanum 1,4-cyclohexanearboxylates, $[La_2(1,4\text{-CHDC})_3(H_2O)_4]$, **XVI**, $[La_3(1,4\text{-HCHDC})_2(1,4\text{-CHDC})_{3.5}(H_2O)_2]\cdot H_2O$, **XVII** and $[La_2(1,4\text{-CHDC})_3(H_2O)]\cdot 2.5H_2O$, **XVIII**, all contain a three-dimensional structure of the type (***I*^{1}*O*^{2}**), where infinite one-dimensional La-O-La chains are connected by the 1,4-CHDC anions, but they differ in their one-dimensional polyhedral connectivity and contain CHDC anions in different conformations. **XVI**, contains anions in the (*e,e*)

conformation only, **XVII** contains anions in both the (*e,e*) and (*a,a*) conformations and **XVIII** contains both the (*e,e*) and (*a,e*) conformations.

3.1. Introduction

Along with the progress of purely inorganic porous solids, another innovation for the synthesis of porous materials emerged at the beginning of the 1990s with the introduction of organic molecules as constituents of the structure. Such polytopic organic ligands, generally with nitrogen- and oxygen donor ligands, connect ‘‘inorganic’’ frameworks along the space in the appropriate topology to originate connected void volumes in the structure. Metal carboxylates have emerged as a large family of open framework materials[1], next only to aluminosilicates[2,3] and phosphates.[4] Interest in metal carboxylate chemistry has enhanced recently because of the increasing importance of hybrid inorganic-organic compounds with potential applications in separation, catalysis and gas storage.[5-15] A few novel metal-organic framework and open-framework compounds with varying pore volumes and sorption properties have been reported in the last few years.[5-30] Of particular interest are the inorganic-organic hybrid compounds formed by metal carboxylates.[31-35] These hybrid compounds possess inorganic and organic connectivities of different dimensionalities. An inherent feature of such hybrid materials is that they combine the rigidity of the inorganic framework with the flexibility of the organic part. Although the design of new compounds with porous structures remains important, the primary motivation has shifted towards the design of hybrid materials that possess specific physical properties potentially useful in a commercial application. In certain circumstances, this demands the design of new molecular building blocks and/or new topologies, however, current advances are generally the result of judicious choice of known

molecular components that self-assemble into novel structure with potential properties.

In view of these features, several workers are exploring various aspects of hybrid materials employing metal carboxylates.[36-41] Studies of metal benzenedicarboxylates suggest that the 1,4-dicarboxylates generally form three-dimensional structures while the 1,2-dicarboxylates favor metal-oxygen-metal (M-O-M) linkages. Cyclohexanedicarboxylic acids would similarly be expected to be useful ligands, considering that they also occur in different conformations. There have, however, been very few metal cyclohexanedicarboxylates (CHDCs) reported in the literature.[42-57] Two and three dimensional structures of metal 1,4-CHDCs have been reported. Layered 1,2-cyclohexenedicarboxylates (CHeDCs) of Mn also possess infinite M-O-M linkages.[41] To our knowledge, there are very few investigations of the 1,3-CHDC compounds.[57]

In 1,2 derivatives, the equatorial, equatorial (*e,e*) and the axial, equatorial (*a,e*) conformers are known as the cis isomers. The axial, axial (*a,a*) conformer is known as the trans isomer. In 1,3 derivatives, the (*e,e*) and the (*a,a*) conformers are known as the cis isomers. The (*a,e*) conformer is known as the trans isomer. In 1,4 derivatives, the (*e,e*) and the (*a,a*) conformers are known as the trans isomers. The (*a,e*) conformer is known as the cis isomer.[58] It is to be noted that the (*e,e*) form is most stable in the 1,2-, 1,3- and 1,4-CHDCs and the (*a,a*) form is least stable. The (*a,e*) form is reasonably stable in the 1,4-CHDCs. We have studied the compounds formed by metals (Mn, Cd, Pb and La) with 1,2-, 1,3- and 1,4-cyclohexanedicarboxylic acids in the presence and absence of organic amines, with a view to examine the structure, conformation as well as dimensionality modulation.

3.2. Scope of the present investigations

The main aim of the present study was to understand structural features of hybrid dicarboxylate frameworks in terms of dimensionality modulation and extended inorganic connectivity. For the purpose of a systematic study, we have employed the flexible (in terms of the available conformations) isomers of the three (1,2-, 1,3- and 1,4-) cyclohexanedicarboxylic acids and 1,2-cyclohex(4)enedicarboxylic acid to synthesize coordination polymers and hybrid frameworks with extended inorganic connectivity of Mn, Cd, Pb and La with or without chelating amines.

3.2.1. Coordination Polymers of Metal Cyclohexanedicarboxylates

Nine hybrid inorganic-organic cyclohexanedicarboxylates with zero inorganic connectivity ($\boldsymbol{I^0O^y}$, $\boldsymbol{y = 1}$ to $\boldsymbol{3}$) have been synthesized and characterized. These coordination polymers are the two isomeric cyclohexanedicarboxylates (1,3- and 1,4-) of Mn, Cd and Pb with or without chelating amines. Of these, six of them (**I-VI**) contain chelating pyridyl amines such as 1,10-pheanthroline or 2,2'-bipyridine. [Cd(1,3-CHDC)(1,10-phen)], **I**, is a two-dimensional compound ($\boldsymbol{I^0O^2}$) where edge shared cadmium $\mathbf{^2D_2}$ dimers are connected by the 1,3-CHDC anions [Description of dimer SBUs and terminology are given in the appendix {see Appendix. 2.7(a)}]. [Mn(H_2O)(1,3-CHDC)(1,10-phen)], **II**, is a molecular compound ($\boldsymbol{I^0O^0}$) with a ring structure where the two Mn(II) cations are connected by the two 1,3- CHDC anions. [Mn_3(1,3-CHDC)$_3$(1,10-phen].4H_2O, **III**, has an infinite one-dimensional chain ($\boldsymbol{I^0O^1}$) structure consisting of a trinuclear $Mn_3N_4O_{12}$ units (two dimers of $\mathbf{^3D_1}$) connected by 1,3- CHDC anions. Compounds, [Mn_3(1,4-CHDC)$_3$(1,10-phen].4H_2O, **IV** and [Cd_3(1,4-CHDC)$_3$(1,10-phen)$_2$].4H_2O, **V**, both

have a similar two-dimensional layer structure (***I^{0}O^2***) consisting of one-dimensional infinite chains made up of trinuclear units connected by the 1,4-CHDC anions. [Cd(1,4-CHDC)(2,2'-bipy)].H_2O, **VI**, has a two-dimensional layer structure (***I^{0}O^2***), formed by the connectivity of ^{2}**D$_2$** dimers and the 1,4-CHDC anions. Compounds **I-III** and **VI**, contain CHDC anions in the (*e,e*) conformation, whereas in **IV** and **V**, they are in both (*e,e*) and (*a,e*) conformations.

Compounds **VII-IX** contain no chelating amines. [$Cd(H_2O)_2$(1,3-CHDC)].H_2O, **VII**, has a two-dimensional layer structure (***I^{0}O^2***), formed by the connectivity between Cd_2O_{12} dimers (^{2}**D$_2$**) and the carboxylate groups. (OPb_3)(1,3-$CHDC)_2$, **VIII**, has a three-dimensional structure without any inorganic connectivity (***I^{0}O^3***). The hexameric Pb_6O_{18} units are connected by the 1,3-CHDC anions in the (*a,e*) conformation to the infinite three dimensional-structure where Pb(II) cation is in a hemidirected coordination environment. [$Cd(H_2O)_2$(1,4-CHDC)], **IX**, is a one-dimensional chain structure (***I^{0}O^1***) consisting of octahedral CdO_6 units connected by the 1,4-CHDC anions. Compounds **VII** and **IX**, contain CHDC anions in the (*e,e*) conformation.

3.2.2. Hybrid Networks of Metal Cyclohexanedicarboxylates with Extended Inorganic Connectivity

Ten hybrid inorganic-organic cyclohexane (or hexene) dicarboxylates with extended inorganic connectivity (***I^{x}O^y***, ***x = 1*** to ***2***; ***y = 0*** to ***2***) have been synthesized and characterized. These hybrid structures in two- and three-dimensions are the three isomeric cyclohenxedicarboxylates (1,2-, 1,3- and 1,4-) and 1,2-cyclohex(4)enedicarboxylates of Cd, Pb and La without chelating amines.

[Cd(1,2-CHDC)], **X**, is a two-dimensional layered structure consisting of a two dimensional metal-O-metal network (***I*^{2}*O*^{0}**), grafted by 1,2-CHDC anions in the (*e,e*) conformation. Cd(1,2-CHeDC)(H_2O), **XI**, was obtained in two different polymorpic forms, **A** and **B**. In both the polymorphs, **XI** has a two-dimensional layered structure (***I*^{1}*O*^{1}**) made up of infinite one-dimensional Cd-O-Cd chains connected by the CHeDC anions in the (*a,e*) conformation. The layered structures in **A** and **B** are similar, but only differ in their packing arrangements.

Pb(1,3-CHDC)(H_2O), **XII**, contains two types of two-dimensional layers (***I*^{1}*O*^{1}**) and (***I*^{2}*O*^{0}**), alternatively packed in the crystal structure. Pb(II) cation in the (***I*^{1}*O*^{1}**) layer is in a hemidirected geometry whereas in the (***I*^{2}*O*^{0}**) layer, it is in a holodirected geometry. [$(OPb_4)_2(OH)_2(C_2O_4)$(1,3-CHDC)$_4$].H_2O, **XIII**, has a two-dimensional structure where the octameric $Pb_8(OH)_2O_{26}$ units were connected by the oxalate and 1,3-CHDC anions into the (***I*^{2}*O*^{0}**) structure. The oxalate moiety was generated *in-situ* from the 1,3-CHDC under the hydrothermal synthesis. Pb_2(1,3-CHDC)$_2$(H_2O), **XIV**, has a three-dimensional structure (***I*^{2}*O*^{1}**), where a (4,4) square lattice of tetra-nuclear Pb_4O_{18} units are connected by the 1,3-CHDC anions. Compounds **XII** - **XIV**, contain 1,3-CHDC anions in the (*e,e*) conformation. [(OPb_3)(1,4-CHDC)$_2$], **XV**, has a three-dimensional structure with one-dimensional inorganic connectivity (***I*^{1}*O*^{2}**), where the one-dimensional chains of edge sharing hexameric Pb_6O_{20} units are cross-linked by the 1,4- CHDC anions in both (*e,e*) and (*a,e*) conformations.

The lanthanum 1,4-cyclohexanearboxylates, [La_2(1,4-CHDC)$_3$(H_2O)$_4$], **XVI**, [La_3(1,4-HCHDC)$_2$(1,4-CHDC)$_{3.5}$ (H_2O)$_2$]·H_2O, **XVII** and [La_2(1,4-CHDC)$_3$ (H_2O)]·2.5H_2O, **XVIII**, all contain a three-dimensional structure of the type (***I*^{1}*O*^{2}**), where infinite one-dimensional La-O-La chains are connected by the 1,4-

CHDC anions, but they differ in their one-dimensional polyhedral connectivity and contain CHDC anions in different conformations. **XVI**, contains anions in the (*e,e*) conformation only, **XVII** contains anions in both the (*e,e*) and (*a,a*) conformations and **XVIII** contains both the (*e,e*) and (*a,e*) conformations.

3.3. Experimental

3.3.1. Synthesis

The metal dicarboxylates were synthesized under hydrothermal conditions by heating homogenized reaction mixtures in a 23 or 7ml PTFE-lined bomb in the temperature range 150 - 200 °C for 72 h under autogeneous pressure. The pH of the starting reaction mixture was generally in the range 5-7. The pH after the reaction did not show appreciable change. The products of the hydrothermal reactions were vacuum-filtered and dried under ambient conditions. The starting compositions and the synthetic conditions for the different compounds (**I-XVIII**) synthesized by us are given in Tables 3.1 and 3.2. All the compounds were obtained as single phase, except few. Both polymorphs (**A** and **B**) of **XI** were obtained from the same reaction mixture. Crystals of **XIII** were obtained admixed with small quantities of polycrystalline **VIII** and **XII** powder. The crystals were separated under a polarizing microscope and used for all the characterization.

3.3.2. Characterization

Powder XRD patterns of the products were recorded using Cu Kα radiation (Rich-Seifert, 3000TT). The patterns agreed with those calculated for single crystal structure determination. Thermogravimetric analysis (TGA) was carried out (Metler-Toledo) in oxygen atmosphere (flow rate = 50 ml/min) in the temperature range 25 to 800 °C (heating rate = 5 °C/min).

Elemental analyses of all the compounds were satisfactory. For **VIII**, for ($C_{16}H_{20}Pb_3O_9$) calcd: C, 19.64%; H, 2.05%. Found: C, 19.71%; H, 2.01%. For **XII**, ($C_{16}H_{24}Pb_2O_{10}$) calcd: C, 24.29%; H, 3.04%. Found: C, 24.22%; H, 3.12%. For **XIII**, ($C_{34}H_{44}Pb_8O_{25}$) calcd: C, 16.26%; H, 1.75%. Found: C, 16.33%; H, 1.69%. For **XIV**, ($C_{16}H_{22}Pb_2O_9$) calcd: C, 24.86%; H, 2.85%. Found: C, 24.80%; H, 2.91%.

Thermogravimetric analysis (TGA) was carried out (Metler-Toledo) in oxygen atmosphere (flow rate = 50 ml/min) in the temperature range 25 to 800 °C (heating rate = 5 °C/min). Analyses show single or multistep weight losses in these compounds. The total weight loss matches very well with the loss of CO_2, with or without H_2O and the formation of M_xO_y in all the cases. For **XII**, the first weight loss of 4.96% (calc. 4.55%) occurred around 180^o C and the second weight loss of 43.59% (calc. 43.02%) was in the 280-470^o C range. For **XIII**, the total weight loss of 33.2% (calc. 32.69%) occurred in the 130-450^o C range. For **XIV**, the first weight loss of 2.46% (calc. 2.33%) occurred around 150^o C and the second weight loss of 31.63% (calc. 31.07%) was in the 300-450^o C range. For **VIII**, the total weight loss of 35.0% (calc. 34.78%) occurred in the 250-425^o C range. The total weight loss matches very well with the loss of CO_2, without (**VIII**) or with (**XII-XIV**) H_2O and the formation of PbO (PDF # 00-004-0561) in all the cases.

Infrared (IR) spectra of KBr pellets of the compounds were recorded in the mid IR region (Bruker IFS-66v). Compounds show characteristic bands for the functional groups.[59-61] The bands around 1550 and 1400 cm^{-1} are assigned to carboxylate $\nu_{as\ C=O}$ and $\nu_{s\ C=O}$ stretching. Absence of a band at 1700 cm^{-1} confirms the binding of carboxylate group to the lead cation. The bands at 3558 ($\nu_{as\ O-H}$),

3470 ($\nu_{s\ O-H}$), 1245 $(\delta_{O-H})_{in\text{-}plane}$ and 616 cm^{-1} $(\delta_{O-H})_{out\text{-}of\text{-}plane}$ indicate the presence of hydroxyl groups and its ligation to the lead cation.

A suitable single crystal of each compound was carefully selected under a polarizing microscope and glued to a thin glass fiber. Crystal structure determination by X-ray diffraction was performed on a Bruker-Nonius diffractometer with Kappa geometry attached with an APEX - II-CCD detector and a graphite monochromator for the X-ray source (Mo Kα radiation, λ = 0.71073Å) operating at 50 kV and 30 mA. An empirical absorption correction based on symmetry equivalent reflections was applied using the SADABS program.[62] The structure was solved and refined using SHELXTL-PLUS suite of program.[63] For the final refinement the hydrogen atoms in the cyclohexane rings were placed geometrically and held in the riding mode. The hydrogen atoms in the water molecules were located in the difference Fourier map and the O-H distance was constrained to 0.85 Å. Final refinement included atomic positions for all the atoms, anisotropic thermal parameters for all the non-hydrogen atoms and isotropic thermal parameters for the hydrogen atoms. All the hydrogen atoms were included in the final refinement except a few. The hydrogen atoms of a water molecule in these few compounds could not be located in the difference Fourier map. Some of the carbon atoms of the CHDC anion were disordered, so the C-C distances involving these atoms were constrained to 1.550 Å. Details of the structure solution and final refinements for the compounds **I** to **XVIII** are given in Tables 3.3-3.8. Atomic coordinates for the compounds **I** to **XVIII** are given in the appendix (see 3.7. Appendix, Tables A3.1-A.3.18).

Table 3.1

Compound No.	Formula	Composition					Temperature, ºC
		Metal	Acid	Additive 1	Additive 2	Water	
I	[Cd(1,3-CHDC)(1,10-phen)]	$Cd(OAc)_2.2H_2O$ (1mmol)	1,3-H_2CHDC (1mmol)	1,10-phen (1mmol)	NaOH (2mmol)	H_2O (278mmol)	180
II	[$Mn(H_2O)$(1,3-CHDC)(1,10-phen)]	$Mn(OAc)_2.4H_2O$ (0.5mmol)	1,3-H_2CHDC (0.5mmol)	1,10-phen (0.25mmol)	Piperidine (0.5mmol)	H_2O (278mmol)	150
III	[Mn_3(1,3-CHDC)$_3$(1,10-phen].4H_2O	$Mn(OAc)_2.4H_2O$ (0.5mmol)	1,3-H_2CHDC (0.5mmol)	1,10-phen (0.25mmol)	Piperidine (0.5mmol)	H_2O (278mmol)	180
IV	[Mn_3(1,4-CHDC)$_3$(1,10-phen].4H_2O	$MnCl_2.4H_2O$ (0.5mmol)	1,4-H_2CHDC (0.5mmol)	1,10-phen (0.25mmol)	Piperidine (0.5mmol)	H_2O (278mmol)	180
V	[Cd_3(1,4-CHDC)$_3$(1,10-phen)$_2$].4H_2O	$Cd(OAc)_2.2H_2O$ (0.5mmol)	1,4-H_2CHDC (0.5mmol)	1,10-phen (0.25mmol)	NaOH (0.5mmol)	H_2O (278mmol)	180
VI	[Cd(1,4-CHDC)(2,2'-bipy)].H_2O	$Cd(OAc)_2.2H_2O$ (0.5mmol)	1,4-H_2CHDC (0.5mmol)	2,2'-bipy (0.25mmol)	Piperidine (0.5mmol)	H_2O (278mmol)	180
VII	[$Cd(H_2O)_2$(1,3-CHDC)].H_2O	$Cd(OAc)_2.2H_2O$ (1mmol)	1,3-H_2CHDC (1mmol)	-	NaOH (2mmol)	H_2O (278mmol)	180
VIII	(OPb_3)(1,3-CHDC)$_2$	$Pb(NO_3)_2$ (2mmol)	1,3-H_2CHDC (1mmol)	-	NaOH (3mmol)	H_2O (278mmol)	150
IX	[$Cd(H_2O)_2$(1,4-CHDC)]	$Cd(OAc)_2.2H_2O$ (1mmol)	1,4- H_2CHDC (1mmol)	-	Piperidine (1mmol)	H_2O (278mmol)	180

Table 3.2

Compound No.	Formula	Composition					Temperature, ºC
		Metal	Acid	Additive 1	Additive 2	Water	
X	[Cd(1,2-CHDC)]	$Cd(OAc)_2.2H_2O$ (1mmol)	1,2-CHDC anhydride (1mmol)	Piperidine (1mmol)	-	H_2O (278mmol)	180
XI (**A** and **B**)	Cd(1,2-CHeDC)(H_2O)	$Cd(OAc)_2.2H_2O$ (1mmol)	1,2-CHe(4)DC anhydride (0.5mmol)	NaOH (1mmol)	-	H_2O (278mmol)	180
XII	Pb(1,3-CHDC)(H_2O)	$Pb(NO_3)_2$ (1mmol)	1,3-H_2CHDC (0.5mmol)	NaOH (1mmol)	-	H_2O (278mmol)	150
XIII	$[(OPb_4)_2(OH)_2(C_2O_4)$ $(1,3\text{-CHDC})_4].H_2O$	$Pb(NO_3)_2$ (1mmol)	1,3-H_2CHDC (0.5mmol)	NaOH (1.5mmol)	-	H_2O (278mmol)	200
XIV	$Pb_2(1,3\text{-CHDC})_2(H_2O)$	$Pb(NO_3)_2$ (1mmol)	1,3-H_2CHDC (0.5mmol)	NaOH (0.5mmol)	-	H_2O (278mmol)	200
XV	$[(OPb_3)(1,4\text{-CHDC})_2]$	$Pb(NO_3)_2$ (1mmol)	1,4-H_2CHDC (0.5mmol)			H_2O (278mmol)	180
XVI	$[La_2(1,4\text{-CHDC})_3(H_2O)_4]$	$La(NO_3)_3.4H_2O$ (0.3mmol)	1,4-H_2CHDC (0.6mmol)	NaOH (1.2mmol)	-	H_2O (556mmol)	180
XVII	$[La_3(1,4\text{-HCHDC})_2$ $(1,4\text{-CHDC})_{3.5}(H_2O)_2]\cdot H_2O$	$La(NO_3)_3.4H_2O$ (0.3mmol)	1,4-H_2CHDC (0.3mmol)	Piperazine (0.3mmol)	K_2CO_3 (0.3mmol)	H_2O (111mmol)	180
XVIII	$[La_2(1,4\text{-CHDC})_3$ $(H_2O)]\cdot 2.5H_2O$	$La(NO_3)_3.4H_2O$ (0.3mmol)	1,4-H_2CHDC (0.3mmol)	NaOH (0.6mmol)	2,3-dihydroxybenzoic acid (0.3mmol)	H_2O (111mmol)	180

Table 3.3. Crystal data and structure refinement parameters for **I** , **II** and **III**

Structure parameter	**I**	**II**	**III**
Empirical formula	$C_{40}H_{36}Cd_2N_4O_8$	$C_{40}H_{40}Mn_2N_4O_{10}$	$C_{48}H_{54}Mn_3N_4O_{16}$
Formula weight	925.53	846.64	1107.77
Crystal system	Monoclinic	Monoclinic	Monoclinic
Space group	$P2_1/n$, (no. 14)	P21/c, (no. 14)	C2/c, (no. 15)
a./Å	11.6099(2)	9.8431(5)	8.5210(4)
b /Å	17.0455(2)	17.6527(9)	21.5643(10)
c /Å	18.5687(2)	11.6066(5)	26.7853(12)
β /°	104.8900	104.0900(10)	91.0070(10)
V /Å^3	3551.29(8)	1956.06(16)	4921.0(4)
Z	4	2	4
D (calc) /gcm^{-3}	1.731	1.437	1.495
μ /mm^{-1}	1.259	0.708	0.833
Total data collected	14758	8107	10308
Unique data	5076	2804	3546
Observed data [I > 2σ (I)]	4509	2282	2749
R_{merg}	0.0416	0.0326	0.0418
R indexes [I > 2σ (I)]	$R_1 = 0.0500$[a]; $wR_2 = 0.1336$[b]	$R_1 = 0.0718$[a]; $wR_2 = 0.1430$[b]	$R_1 = 0.05777$[a]; $wR_2 = 0.1542$[b]
R indexes [all data]	$R_1 = 0.0556$[a]; $wR_2 = 0.1375$[b]	$R_1 = 0.0889$[a]; $wR_2 = 0.1504$[b]	$R_1 = 0.0779$[a]; $wR_2 = 0.1694$[b]

[a] $R_1 = \Sigma ||F_0|-|F_c|| / \Sigma |F_0|$; [b] $wR_2 = \{\Sigma[w(F_0^2 - F_c^2)^2] / \Sigma[w(F_0^2)^2]\}^{1/2}$. $w = 1/[\sigma^2(F_0)^2 + (aP)^2 + bP]$, $P = [\max.(F_0^2,0) + 2(F_c)^2]/3$, where $a = 0.0665$ and $b = 13.3409$ for **I**, $a = 0.0271$ and $b = 4.6127$ for **II**, and $a = 0.0845$and $b = 16.1649$ for **III**.

Table 3.4. Crystal data and structure refinement parameters for **IV**, **V** and **VI**

Structure parameter	**IV**	**V**	**VI**
Empirical formula	$C_{48}H_{54}Mn_3N_4O_{16}$	$C_{48}H_{54}Cd_3N_4O_{16}$	$C_{18}H_{20}CdN_2O_5$
Formula weight	1107.77	1280.15	456.76
Crystal system	Triclinic	Triclinic	Monoclinic
Space group	P-1, (no. 2)	P-1, (no. 2)	C2/c, (no. 15)
a./Å	8.8827(15)	8.9419(2)	17.3563(4)
b /Å	11.856(2)	11.9987(3)	11.8464(3)
c /Å	12.321(2)	12.4863(2)	18.3098(5)
α /°	76.791(2)	102.4650(10)	90
β /°	87.930(3)	91.7580(10)	97.1720(10)
γ /°	68.309(2)	111.7710(10)	90
V /Å^3	1172.1(3)	1205.70(5)	3735.22(16)
Z	1	1	8
D (calc) /gcm^{-3}	1.569	1.763	1.624
μ /mm^{-1}	0.874	1.387	1.200
Total data collected	13718	5149	7651
Unique data	5463	3440	2676
Observed data [I > 2σ (I)]	4366	3118	2438
R_{merg}	0.0281	0.0179	0.0304
R indexes [I > 2σ (I)]	$R_1 = 0.0384$[a]; $wR_2 = 0.0907$[b]	$R_1 = 0.0210$[a]; $wR_2 = 0.0553$[b]	$R_1 = 0.0300$[a]; $wR_2 = 0.0805$[b]
R indexes [all data]	$R_1 = 0.0519$[a]; $wR_2 = 0.0954$[b]	$R_1 = 0.0232$[a]; $wR_2 = 0.0561$[b]	$R_1 = 0.0327$[a]; $wR_2 = 0.0827$[b]

[a] $R_1 = \Sigma ||F_0|-|F_c|| / \Sigma |F_0|$; [b] $wR_2 = \{\Sigma[w(F_0^2 - F_c^2)^2] / \Sigma[w(F_0^2)^2]\}^{1/2}$. $w = 1/[\sigma^2(F_0)^2 + (aP)^2 + bP]$, $P = [\max.(F_0^2,0) + 2(F_c)^2]/3$, where $a = 0.0505$ and $b = 0.0$ for **IV**, for $a = 0.0321$ and $b = 0.0$ for **V**, and $a = 0.0394$ and $b = 10.4253$ for **VI**.

Table 3.5. Crystal data and structure refinement parameters for **VII**, **VIII** and **IX**

Structure parameter	**VII**	**VIII**	**IX**
Empirical formula	$C_8H_{16}CdO_7$	$C_{16}H_{20}Pb_3O_9$	$C_8H_{14}CdO_6$
Formula weight	336.61	977.89	318.59
Crystal system	Orthorhombic	Monoclinic	Monoclinic
Space group	Pccn, (no. 56)	C2/c, (no. 12)	C2/c, (no. 15)
a./Å	13.1510	16.3279(6)	11.5724(3)
b /Å	20.4388(4)	13.6071(5)	5.4816(2)
c /Å	8.5602(2)	18.8434(6)	16.7944(4)
α /°	90	90	90
β /°	90	112.182(2)	102.941(2)
γ /°	90	90	90
V /Å^3	2300.81(7)	3876.7(2)	1038.30(5)
Z	8	8	4
D (calc) /gcm^{-3}	1.943	3.351	2.038
μ /mm^{-1}	1.916	26.041	2.110
Total data collected	8944	31818	2104
Unique data	1654	3347	753
Observed data [I > 2σ (I)]	1479	2752	735
R_{merg}	0.0329	0.0308	0.0376
R indexes [I > 2σ (I)]	$R_1 = 0.0309$[a]; $wR_2 = 0.0670$[b]	$R_1 = 0.0341$[a]; $wR_2 = 0.0683$[b]	$R_1 = 0.0357$[a]; $wR_2 = 0.0901$[b]
R indexes [all data]	$R_1 = 0.0373$[a]; $wR_2 = 0.0705$[b]	$R_1 = 0.0496$[a]; $wR_2 = 0.0748$[b]	$R_1 = 0.03704$[a]; $wR_2 = 0.0913$[b]

[a] $R_1 = \Sigma ||F_0|-|F_c|| / \Sigma |F_0|$; [b] $wR_2 = \{\Sigma[w(F_0^2 - F_c^2)^2] / \Sigma[w(F_0^2)^2]\}^{1/2}$. $w = 1/[\sigma^2(F_0)^2 + (aP)^2 + bP]$, $P = [\max.(F_0^2,0) + 2(F_c)^2]/3$, where $a = 0.0185$ and $b = 7.0434$ for **VII**, for $a = 0.0658$, $b = 72.9605$ for **VIII**, and $a = 0.545$ and $b = 4.8788$ for **IX**.

Table 3.6. Crystal data and structure refinement parameters for **X** and **XI-A,B**

Structure parameter	**X**	**XI-A**	**XI-B**
Empirical formula	$C_8H_{10}CdO_4$	$C_8H_{10}CdO_5$	$C_8H_{10}CdO_5$
Formula weight	282.56	298.58	298.58
Crystal system	Monoclinic	Orthorhombic	Orthorhombic
Space group	C2/c, (no. 15)	Pnc2, (no. 30)	Pbcn, (no. 60)
a./Å	27.349(7)	9.7988(13)	12.2003(1)
b /Å	4.9842(12)	12.184(2)	7.3856(1)
c /Å	12.627(3)	7.3722(2)	19.6160(1)
β /°	96.163(4)	90	90
V /Å^3	1711.3(7)	880.2(2)	1767.53(3)
Z	8	4	8
D (calc) /gcm^{-3}	2.193	2.192	2.244
μ /mm^{-1}	2.528	2.470	2.460
Total data collected	4868	7367	6618
Unique data	1994	2072	1272
Observed data [I > 2σ (I)]	1575	1908	1124
R_{merg}	0.040	0.0397	0.0350
R indexes [I > 2σ (I)]	R_1 = 0.0843[a]; wR_2 = 0.2058[b]	R_1 = 0.0553[a]; wR_2 = 0.1610[b]	R_1 = 0.0246[a]; wR_2 = 0.0615[b]
R indexes [all data]	R_1 = 0.1004[a]; wR_2 = 0.2136[b]	R_1 = 0.0597[a]; wR_2 = 0.1680[b]	R_1 = 0.0277[a]; wR_2 = 0.0629[b]

[a] $R_1 = \Sigma ||F_0|-|F_c|| / \Sigma |F_0|$; [b] $wR_2 = \{\Sigma[w(F_0^2 - F_c^2)^2] / \Sigma[w(F_0^2)^2]\}^{1/2}$. $w = 1/[\sigma^2(F_0)^2 + (aP)^2 + bP]$, $P = [\max.(F_0^2,0) + 2(F_c)^2]/3$, where for $a = 0.1345$ and $b = 0.0$ for **X**, $a = 0.0867$ and $b = 6.3045$ for **XI-A** , $a = 0.0380$ and $b = 0$ for **XI-B**.

Table 3.7. Crystal data and structure refinement parameters for **XII**, **XIII** and **XIV**

Structure parameter	**XII**	**XIII**	**XIV**
Empirical formula	$C_{16}H_{24}Pb_2O_{10}$	$C_{34}H_{44}Pb_8O_{25}$	$C_{16}H_{22}Pb_2O_9$
Formula weight	790.73	2510..20	772.74
Crystal system	Orthorhombic	Monoclinic	Triclinic
Space group	Pbca, (no. 61)	C2/m, (no. 12)	P-1, (no. 2)
a./Å	14.0078(3)	8.1086(2)	9.1442(5)
b /Å	8.8268(2)	29.9463(8)	9.7893(5)
c /Å	31.6165(7)	11.5853(3)	11.0738(6)
α /°	90	90	92.922(3)
β /°	90	103.0100(10)	97.147(2)
γ /°	90	90	107.695(2)
V /Å^3	3909.19(15)	2740.96(12)	932.89(9)
Z	8	2	2
D (calc) /gcm^{-3}	2.687	3.041	2.751
μ /mm^{-1}	17.257	24.548	18.071
Total data collected	50632	19662	17716
Unique data	3339	2407	3343
Observed data [I > 2σ (I)]	3032	2201	3035
R_{merg}	0.0201	0.0214	0.0303
R indexes [I > 2σ (I)]	R_1 = 0.0282[a]; wR_2 = 0.0688[b]	R_1 = 0.0344[a]; wR_2 = 0.1042[b]	R_1 = 0.0300[a]; wR_2 = 0.0821[b]
R indexes [all data]	R_1 = 0.0321[a]; wR_2 = 0.0701[b]	R_1 = 0.0418[a]; wR_2 = 0.1232[b]	R_1 = 0.0344[a]; wR_2 = 0.0930[b]

[a] $R_1 = \Sigma ||F_0|-|F_c|| / \Sigma |F_0|$; [b] $wR_2 = \{\Sigma[w(F_0^2 - F_c^2)^2] / \Sigma[w(F_0^2)^2]\}^{1/2}$. $w = 1/[\sigma^2(F_0)^2 + (aP)^2 + bP]$, $P = [\max.(F_0^2,0) + 2(F_c)^2]/3$, where a = 0.0182 , b = 38.2775 for **XII**, a = 0.0658 , b = 72.9605 for **XIII** and a = 0.0467, b = 6.7206 for **XIV**.

Table 3.8. Crystal data and structure refinement parameters for **XV-XVIII**.

Structure parameter	**XV**	**XIV**	**XVII**	**XVIII**
Empirical formula	$C_{16}H_{20}Pb_3O_9$	$C_{24}H_{38}La_2O_{16}$	$C_{44}H_{63}La_3O_{25}$	$C_{24}H_{37}La_2O_{15.5}$
Formula weight	977.72	860.36	1407.68	851.36
Crystal system	Monoclinic	Triclinic	Monoclinic	Triclinic
Space group	C2/c, (no. 15)	P-1, (no. 2)	P21/c, (no. 14)	P-1, (no. 2)
a /Å	12.849(3)	11.5096(1)	11.6959(2)	9.8785(3)
b /Å	20.411(4)	12.0694(3)	39.6296(7)	11.1986(4)
c /Å	15.524(3)	12.4462(2)	11.5434(1)	14.7456(4)
α /°	90	94.8310(10)	90	93.919(2)
β /°	91.762(8)	116.0460(10)	105.0000(10)	97.409(2)
γ /°	90	101.3690(10)	90	104.517(2)
V /Å^3	4069.5(15)	1493.98(5)	5168.10(14)	1557.34(8)
Z	8	2	4	1
D (calc) /gcm^{-3}	3.192	1.913	1.809	1.816
μ /mm^{-1}	24.807	2.894	2.520	2.774
Total data collected	39142	6258	21457	14013
Unique data	3509	4252	7438	5346
Observed data [$I > 2\sigma(I)$]	3296	3838	6009	4556
R_{merg}	0.0248	0.0281	0.0478	0.0242
R indexes [$I > 2\sigma(I)$]	$R_1 = 0.0311$[a]; $wR_2 = 0.0861$[b]	$R_1 = 0.0296$[a] $wR_2 = 0.0756$[b]	$R_1 = 0.0300$[a] $wR_2 = 0.0596$[b]	$R_1 = 0.0367$[a] $wR_2 = 0.0965$[b]
R indexes [all data]	$R_1 = 0.0356$[a]; $wR_2 = 0.0953$[b]	$R_1 = 0.0326$[a] $wR_2 = 0.0769$[b]	$R_1 = 0.0451$[a] $wR_2 = 0.0658$[b]	$R_1 = 0.0475$[a] $wR_2 = 0.1157$[b]

[a] $R_1 = \Sigma ||F_0|-|F_c|| / \Sigma |F_0|$; [b] $wR_2 = \{\Sigma[w(F_0^2 - F_c^2)^2] / \Sigma[w(F_0^2)^2]\}^{1/2}$. $w = 1/[\sigma^2(F_0)^2 + (aP)^2 + bP]$, $P = [\max.(F_0^2,0) + 2(F_c)^2]/3$, where $a = 0.0585$, $b = 48.3324$ for **XV**, $a = 0.0420$ and $b = 0$ for **XVI**, $a = 0.0143$ and $b = 0$ for **XVII** and $a = 0.0466$ and $b = 9.7765$ for **XVIII**.

3.4. Results and discussion

3.4.1. Coordination Polymers of Metal Cyclohexanedicarboxylates

Nine hybrid inorganic-organic cyclohexanedicarboxylates with zero inorganic connectivity (***I*^{0}*O*^{y}**, ***y* = *1*** to ***3***) have been synthesized. These coordination polymers are the two isomeric cyclohexanedicarboxylates (1,3- and 1,4-) of Mn, Cd and Pb with or without chelating amines.

3.4.1.1 Metal dicarboxylates with chelating amines

(a) 1,3-Cyclohexanedicarboxylates

The cadmium 1,3-cyclohexanedicarboxylate [Cd(1,3-CHDC)(1,10-phen)], **I**, has a two-dimensional layered structure consisting of an infinite two-dimensional (***I*^{0}*O*^{2}**) networks formed by the connectivity of $Cd_2N_4O_8$ dimers and carboxylate groups (Fig. 3.4.1 and 3.4.2).

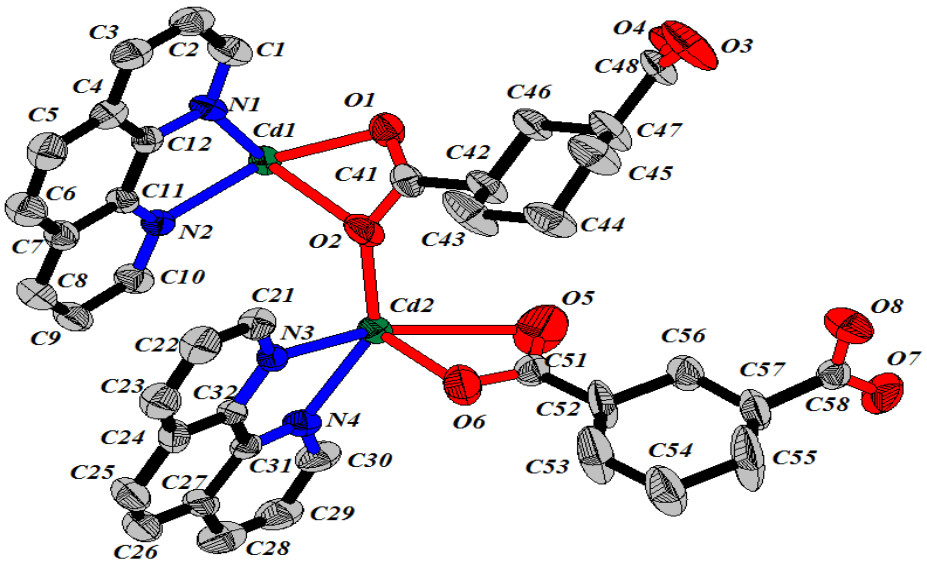

Fig. 3.4.1. ORTEP plot of **I** (Thermal ellipsoids are shown at 50% probability).

The asymmetric unit contains 54 non-hydrogen atoms (Fig. 3.4.1). The cadmium atom is in a distorted bipyramidal environment (CdN_2O_5) with Cd-O bond distances in the 2.233(5) - 2.702(5) Å range and Cd-N bond distances in the

2.362(4) - 2.405(4) Å range. The two nitrogens of the CdN_2O_5 polyhedron are from the terminal 1,10-phen molecule and the oxygens are from three different carboxyl groups with (11) or (21) connectivity.[64] Two such polyhedra form an edge-sharing dimer ($^2\mathbf{D_2}$) by sharing the $\boldsymbol{\mu}_2$ oxygen atom from a tridentate carboxylate (21). [Description of dimer SBUs and terminology are given in the appendix {see Appendix. 2.7(a)}]. The dimers get connected with four other dimers by the acid units of two types. In one type, two of the carboxylate groups are in equatorial position (*e,e*) with a torsional angle of 7.83(2)^o. The other acid molecule appears as though they have a flattened chair conformation due to the disorder. The 1,10-phen rings project on both the sides of the layer (Fig. 3.4.2b). The structure is stabilized by intralayer π-π interaction [3.546(4) Å, 7.19(1)^O] between the 1,10-phen molecules.

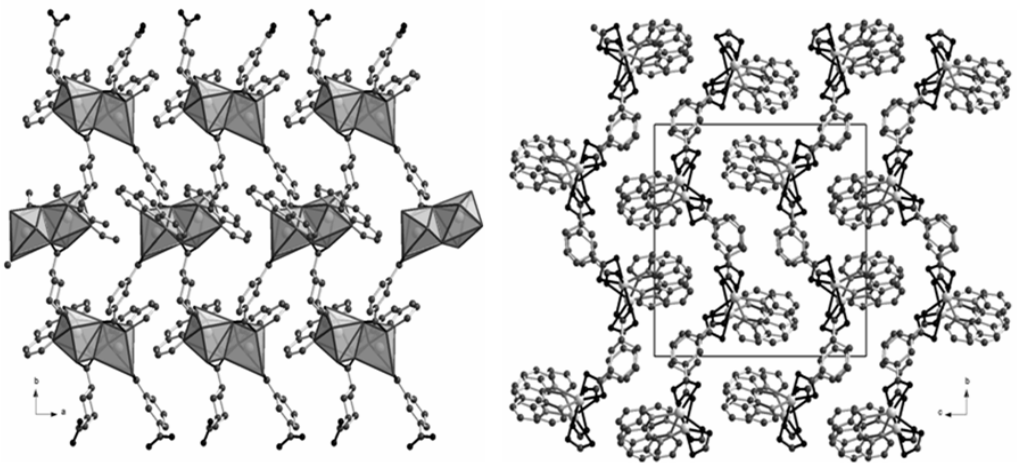

Fig. 3.4.2 (a) View of the 2D structure and (b) packing arrangement of in **I**, viewed along the *a* axis.

Zero-dimensional ($\boldsymbol{I^0O^0}$) 1,3-cyclohexanedicarboxylate, [Mn(H_2O)(1,3-CHDC)(1,10-phen)], **II**, contains 28 non-hydrogen atoms in the asymmetric unit (Fig. 3.4.3). The Mn atom here is in a distorted octahedral environment (MnN_2O_4) with Mn-O bond distances in the 2.097(4) - 2.264(5) Å range and the Mn-N bond distances are 2.244(5) and 2.265(5) Å. The two nitrogens of the MnN_2O_4

polyhedron are from the terminal 1,10-phen molecule. Among the four oxygens, one is from one terminal coordinated water and the three remaining oxygens are from two different carboxylic acid groups with (11) or (10) connectivity.[64] Two such polyhedra form a dimer (Fig. 3.4.4) with two dicarboxylates (1110 connectivity), where the two carboxylate groups are in equatorial position (*e,e*) with a torsional angle of 4.16(2)°. The structure is stabilized by intermolecular π…π interaction (3.89(1) Å, 0.56°) between the 1,10-phen molecules and intermolecular C-H…π interaction between cyclohexane and 1,10-phen rings [3.24(1) Å, 5.83°]. At 300 K, the μ_{eff} of Mn in **II** is 4.18 μ_B, larger than the expected 3.84 μ_B for a magnetically isolated Mn(II) ions in the model. Up to 300 K, the magnetic susceptibility, χ_m, could be fitted to the Curie-Weiss law, with a θ of -1.5 K. The small θ value suggests that compound is essentially paramagnetic with little or no antiferromagnetic interaction between the Mn ions.

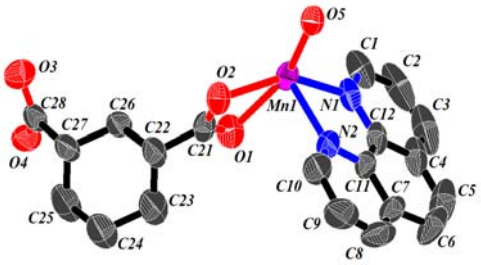

Fig.3.4.3. ORTEP plot of **II** (Thermal ellipsoids are shown at 50% probability).

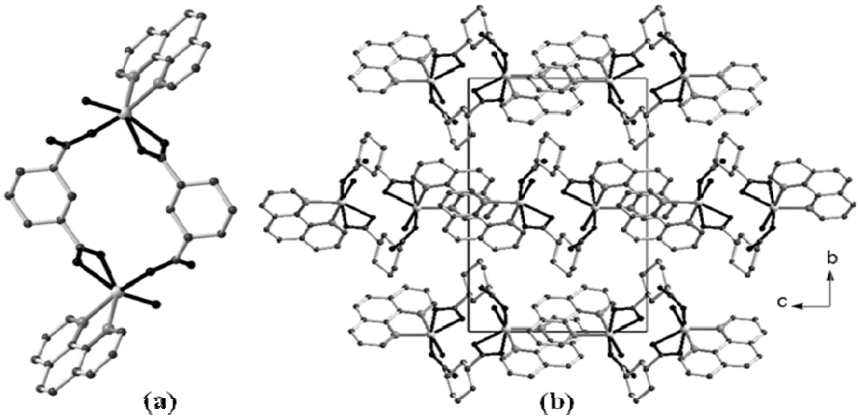

Fig. 3.4.4. (a) Structure of **II** and (b) packing arrangement in **II** viewed along the *a* axis.

The manganese 1,3-cyclohexanedicarboxylate, $[Mn_3(1,3\text{-}CHDC)_3(1,10\text{-phen}].4H_2O$, **III**, has an asymmetric unit containing 36 non-hydrogen atoms (Fig. 3.4.5) The structure consisting of the trinuclear $Mn_3N_4O_{12}$ unit connected by the carboxylate groups (two dimers of $^3\mathbf{D_1}$) (Fig. 3.4.6a) into an infinite one-dimensional chain ($\boldsymbol{I^0O^1}$).

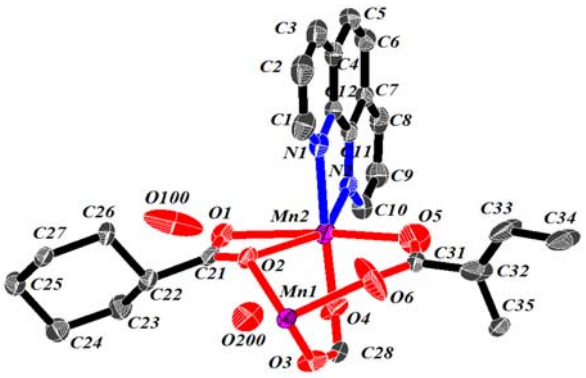

Fig. 3.4.5. ORTEP plot of **III** (Thermal ellipsoids are shown at 50% probability).

Two of the Mn atoms are in two crystallographically independent sites with Mn(1) in an octahedral environment (MnO_6) and Mn(2) in a distorted octahedral (MnN_2O_4) environment. The Mn(1) atom sits on the two-fold axis, on an inversion center, 4e. The Mn-O bond distances are in the 2.141(6) - 2.424(4) Å range and the Mn-N bond distances are 2.245(5) and 2.255(5) Å. The six oxygens of the $Mn(1)O_6$ polyhedron are from six different carboxyl with (11) or (21) connectivity.[64] The two nitrogens of the $Mn(2)N_2O_4$ polyhedron are from the terminal 1,10-phen molecule and the oxygens are from three different carboxyl groups with (11) or (21) connectivity. The $Mn(1)O_6$ polyhedron is connected to two different $Mn(2)N_2O_4$ polyhedra by the sharing of two corners, thus forming the trinuclear $Mn_3N_4O_{12}$ unit (two dimers of $^3\mathbf{D_1}$). Two $\boldsymbol{\mu_3}$ oxygen atoms from two tridentate carboxylate (21) connect the three polyhedra. The trinuclear unit gets connected to two other similar units by six different carboxylates (2111)[64] on either side resulting in the infinite one-dimensional chain structure. The connecting acid

units are in two conformations with one having the two carboxylates in equatorial position (*e,e*) (torsional angle, 1.05°) and the other acid unit appearing to have a flattened chair conformation due to the disorder. The lattice water molecules are between the chains and are hydrogen bonded to the carboxylate oxygens.

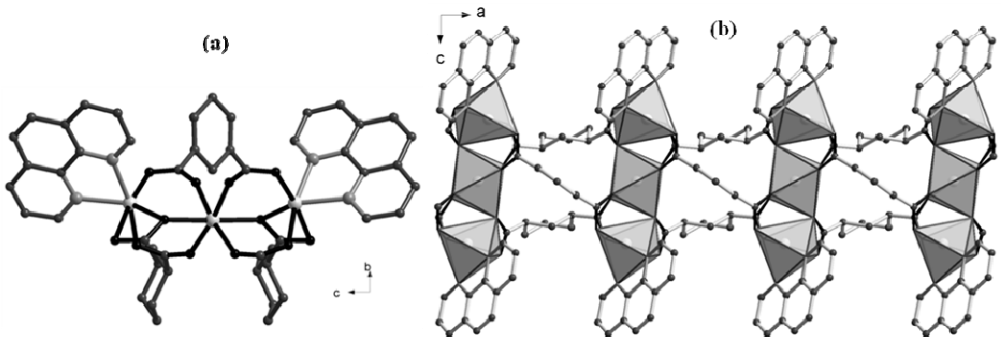

Fig. 3.4.6. (a) Structure of **III**, viewed along the *a* axis and (b) structure of **III**, viewed along the *b* axis.

The structure is stabilized by interchain π…π interaction (3.6 Å, 0°) between the 1,10-phen molecules. At 300 K, the μ_{eff} of Mn in **III** is 3.59 μ_B, larger than the expected 3.13 μ_B for a magnetically isolated Mn(II) ions in the trinuclear model. Up to 300 K, the magnetic susceptibility, χ_m, would be fitted to the Curie-Weiss law, with a θ of -18.2 K, which indicates weak antiferromagnetic interaction between the Mn(II) centres.

(b) 1,4-Cyclohexanedicarboxylates

The manganese 1,4-cyclohexanedicarboxylate, $[Mn_3(1,4\text{-CHDC})_3(1,10\text{-phen})_2].4H_2O$, **IV,** is a two-dimensional layer structure (***I^0O^2***) consisting of one-dimensional infinite chains made up of trinuclear $Mn_3N_4O_{12}$ units (two dimers of $^3\mathbf{D_1}$) connected by the carboxylate groups. The asymmetric unit contains 36 non-hydrogen atoms (Fig.3.4.7). Two Mn atoms are in crystallographically independent sites with Mn(1) in an octahedral environment (MnO_6) and Mn(2) is in a distorted octahedral environment (MnN_2O_4). The Mn(1) atom sits on the two-fold axis, on an inversion center, *1b*. The Mn-O bond distances in **IV** are in the 2.121(2) -

2.371(2) Å range and the Mn-N bond distances are 2.247(2) and 2.299(2) Å. The oxygens of the $Mn(1)O_6$ polyhedron are from six different carboxyl groups with either (11) or (21) connectivity. The two nitrogens of the $Mn(2)N_2O_4$ polyhedron are from the terminal 1,10-phen molecule and the four oxygens are from three different carboxyl groups with either (11) or (21) connectivity. The $Mn(1)O_6$ polyhedron is connected to two different $Mn(2)N_2O_4$ polyhedra by sharing the corners to form a trinuclear $Mn_3N_4O_{12}$ unit (two dimers of $^3\mathbf{D_1}$). Two of the $\boldsymbol{\mu}_3$ oxygen atoms from two tridentate carboxylates (21) connect the three polyhedra. The trinuclear unit gets connected to two other similar units by four different carboxylates (2111) on either side giving rise to an infinite one-dimensional chain structure (Fig.3.4.8a). Between the two carboxylate groups with (2111) connectivity, one is in axial position and the other is in equatorial position (*a,e*) and the torsional angle between the two carboxyl groups is 5.84(3)°. The infinite one-dimensional chains are connected with each other resulting into the infinite two-dimensional layer structure (***I*^{0}*O*^{2}**) (Fig.3.4.8b). The two carboxylate groups in the connecting acid with (1111) connectivity are in equatorial position (*e,e*) with a torsional angle of 180°. The lattice water molecules are between the layers and hydrogen bonded to the carboxylate oxygens. The structure is stabilized by interlayer π…π interaction (3.43(1) Å, 0.4°) between the 1,10-phen molecules.

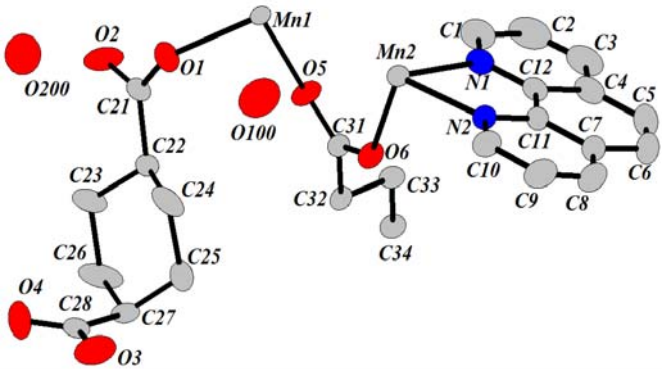

Fig. 3.4.7. Asymmetric unit of **IV** (Thermal ellipsoids are shown at 50% probability).

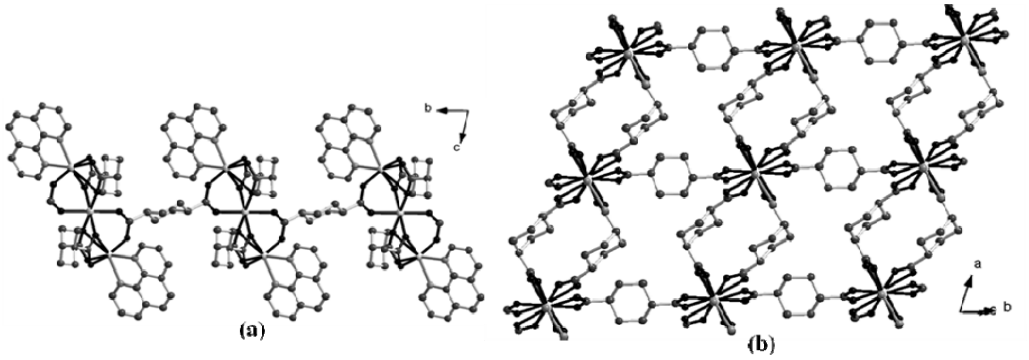

Fig. 3.4.8. (a) Structure of **IV** viewed along the *a* axis and (b) the layered structure of **IV** (the rings in 1,10-phen molecules are not shown).

We have also prepared a cadmium derivative of 1,4-cyclohexanedicarboxylic acid, $[Cd_3(1,4\text{-}CHDC)_3(1,10\text{-}phen)_2].4H_2O$, **V**, has a two-dimensional (***I*^{0}*O*^{2}**) structure (Fig.3.4.9, rings in 1,10-phen are not shown) similar to that of **IV**, except a very small difference in the trinuclear unit. Two Cd atoms are in crystallographically independent sites with Cd(1) in an octahedral environment (CdO_6) and Cd(2) is in a distorted pentagonal bipyramidal environment (CdN_2O_5). The $Cd(1)O_6$ polyhedron is connected to two different $Cd(2)N_2O_5$ polyhedra by sharing the edges to form a trinuclear $Cd_3N_4O_{12}$ unit (two dimers of $^3\mathbf{D_2}$). Four of the μ_3 oxygen atoms from four tridentate carboxylates (21) connect the three polyhedra. This increase in the coordination number results in a slightly different trinuclear unit, where Cd polyhedral share edges. Here the (*a,e*) conformer is with (2121) connectivity whereas it is (2111) in **IV**.

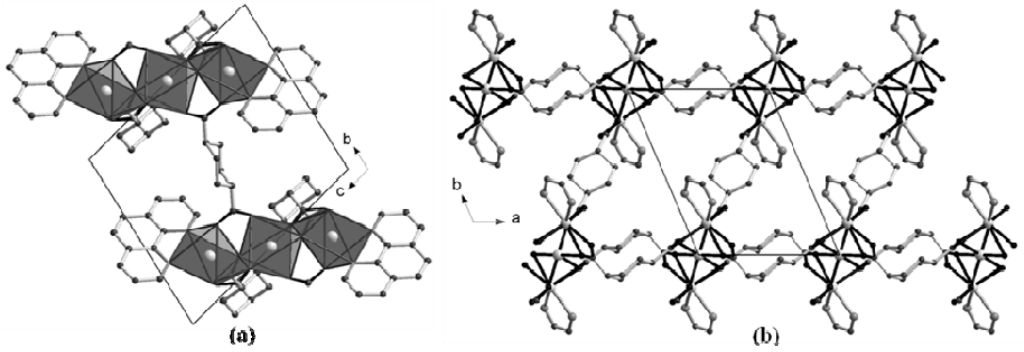

Fig. 3.4.9. (a) Structure of **V** viewed along the *a* axis and (b) structure of **V** viewed along the *c* axis (the rings in 1,10-phen molecules are not shown).

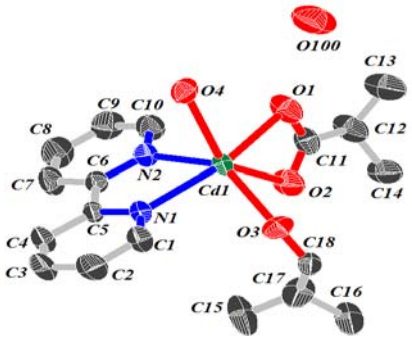

Fig. 3.4.10. ORTEP plot of **VI** (Thermal ellipsoids are shown at 50% probability).

The cadmium 1,4-cyclohexanedicarboxylate [Cd(1,4-CHDC)(2,2'-bipy)].H_2O, **VI**, is a two-dimensional layer structure (***I*^{0}*O*^{2}**), formed by the connectivity of $Cd_2N_4O_8$ dimers and the carboxylate groups (^{2}**D$_2$** dimer). The asymmetric unit of **VI** contains 27 non-hydrogen atoms (Fig. 3.4.10). The cadmium atom is in a distorted pentagonal bipyramidal environment (CdN_2O_5) with the Cd-O bond distances in the 2.269(3) - 2.624(3) Å range and Cd-N bond distances are 2.342(3) and 2.349(3) Å. The two nitrogens of the CdN_2O_5 polyhedron are from the terminal 2,2'-bipy molecule and the oxygens are from three different carboxylic acid groups with (11) or (21) connectivity. Two such polyhedra form an edge-sharing dimer (^{2}**D$_2$** dimer) by sharing the μ_3 oxygen atom from a tridentate carboxylate (21). These dimers are connected to four other dimers by four acid molecules of two types with (2111) connectivity (Fig. 3.4.11). Two of the carboxylate groups are in equatorial position (*e,e*), with a torsional angle (θ) of 7.83(4)^o between the two carboxyl groups. The other is the (*e,e*) conformation with θ = 168.61(4)^o. The 2,2'-bipy rings project on both the sides of the layer (Fig. 3.4.6b) and the structure is stabilized by interlayer π…π interaction [3.663(4) Å, 3.77(5)^O] between the adjacent bipy molecules, besides hydrogen bonding between the lattice water molecules and the carboxylate oxygens [H…O = 1.8(2) Å, O…O = 2.834(6) Å and ∠O-H…O = 164^o].

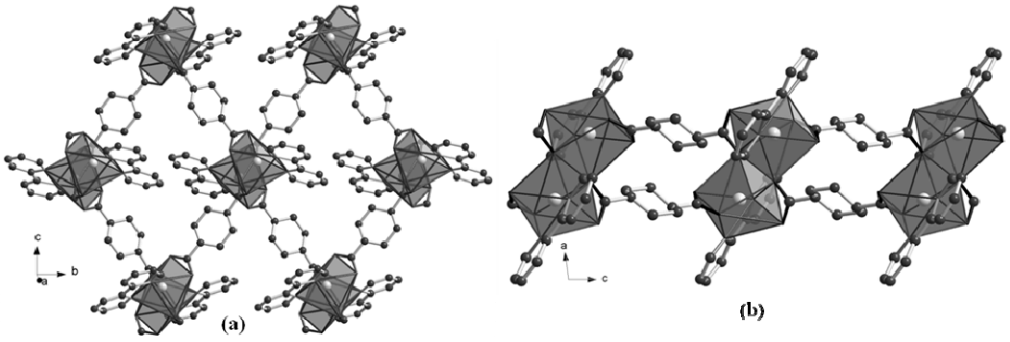

Fig. 3.4.11. (a) Structure of **VI** and (b) view of the layered structure of **VI** along the *b* axis.

3.4.1.2. Metal dicarboxylates without chelating amines

(a) 1,3-Cyclohexanedicarboxylates

The cadmium 1,3-cyclohexanedicarboxylate, $[Cd(H_2O)_2(1,3\text{-CHDC})].H_2O$, **VII**, has a two-dimensional layer structure formed by the connectivity between Cd_2O_{12} dimers ($^2\mathbf{D_2}$) and the carboxylate groups. The asymmetric unit of **VII** contains 17 non-hydrogen atoms (Fig. 3.4.12). The cadmium atom is in a distorted pentagonal bipyramidal environment (CdO_7) with Cd-O bond distances in the 2.258(4) - 2.607(4) Å range. The seven oxygens of the CdO_7 polyhedron are from two coordinated water molecules and four different carboxylic acid groups with (2111) connectivity. Each CdO_7 polyhedron shares an edge with another CdO_7 polyhedron forming the Cd_2O_{12} dimer ($^2\mathbf{D_2}$). The dimers are connected with four other dimers by a carboxylate group with (11) connectivity forming the infinite two-dimensional network. The cyclohexane rings project on both the sides of the layer. Both the carboxylate groups of the 1,3-cyclohexanedicarboxylate are in equatorial position (*e,e*) with a torsional angle of 6.11°. The two lattice water molecules are between the layers forming four-membered water clusters (Fig. 3.4.13). The O…O distances between the water molecules are in the 2.03(1) - 2.59(1) range. The short O…O distance (2.03 Å) is due to the higher thermal

parameter of the oxygen atoms (O100 and O200 with 0.5 occupancy factor). The O…O…O angles are 83.04(2) and 92.57(2)°. The adjustant clusters are twisted with respect to each other by 55.01(3)° and separated by a distance of 2.59(4) Å. The TGA curve of **VII** shows two weight losses. The first weight loss of 16.93% around 120°C and the second weight loss of 49.26% around 380°C match well with the loss of water molecules, and the cyclohexanedicarboxylate (calc. 16.04% and 50.50% respectively).

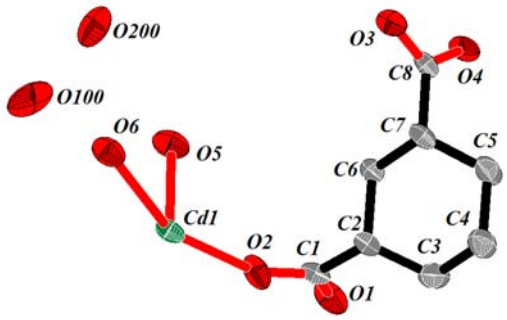

Fig. 3.4.12. ORTEP plot of **VII** (Thermal ellipsoids are shown at 50% probability).

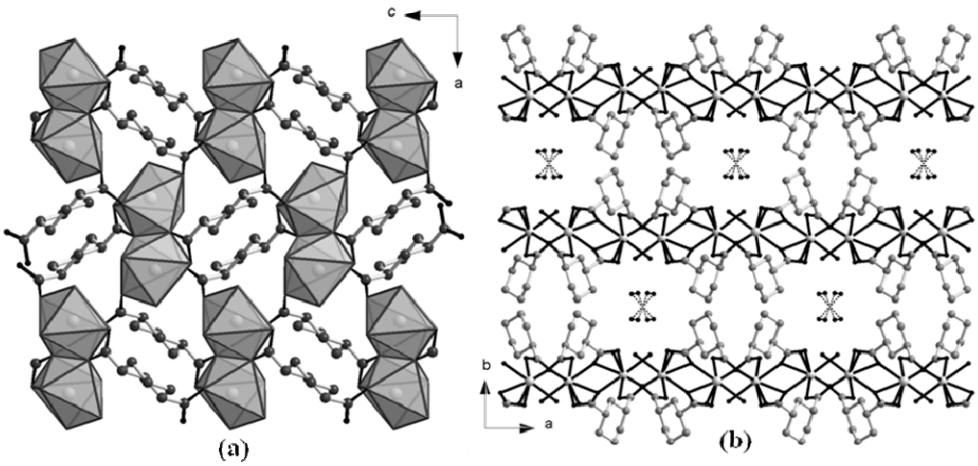

Fig. 3.4.13. 2D structure of **VII** and (b) packing arrangement of in **VII**, viewed along the *c* axis.

$(OPb_3)(1,3\text{-CHDC})_2$, **VIII**, has a three-dimensional structure without any inorganic connectivity (***I*^{0}*O*^{3}**). It has an asymmetric unit with 28 non-hydrogen atoms (Fig. 3.4.14). There are three Pb^{2+} cations in three crystallographically distinct positions, two CHDC anions and one independent oxo dianion in the

asymmetric unit. Both the CHDC anions [acid-1 and acid-2] are in the (a,*e*) conformation with the torsional angle of 120.95(1) and 99.31(1)º. They have (1222) and (1122) connectivities respectively. Acid-1 binds to seven Pb^{2+} cations [two Pb(1), three Pb(2) and two Pb(3)] and acid-2 binds to five Pb^{2+} cations [one Pb(1), two Pb(2) and two Pb(3)]. The independent oxo dianion binds to four Pb^{2+} cations [two Pb(1), one Pb(2) and one Pb(3)] to form a OPb_4 tetrahedron.

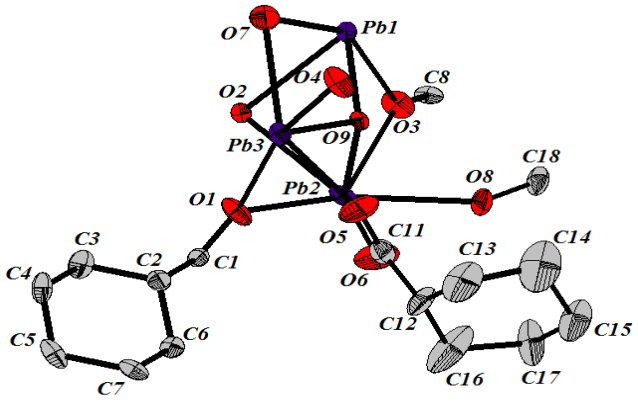

Fig. 3.4.14. ORTEP plot of **VIII** (Thermal ellipsoids are shown at 50% probability).

Pb(1) is hemidirected and coordinated by six oxygen atoms (PbO_6). Among the six oxygens of $Pb(1)O_6$, four with μ_3 connectivity are from three different CHDC anions and the remaining two with μ_4 connectivity are from two different oxo dianions. These oxygen atoms link Pb(1) with an another Pb(1) by sharing an edge, with two different Pb(2) atoms by sharing an edge with one and by sharing a face with another, and with two different Pb(3) by sharing a corner to one and by sharing an edge to another. The Pb-O bond lengths are in the 2.286 – 2.871 Å range. Pb(2) is also hemidirected and coordinated by six oxygen atoms (PbO_6). Among the six oxygens of $Pb(2)O_6$, one oxo anion has μ_4 connectivity. The remaining oxygens are from five different CHDC anions, with one oxygen having μ_2 connectivity and other four with μ_3 connectivity. These oxygens link Pb(2) with

two Pb(1) and also connect Pb(2) with one Pb(3) by edge sharing. The Pb-O bond lengths are in the 2.245 – 2.764 Å range. Pb(3) is also hemidirected but coordinated by five oxygen atoms (PbO_5). Among the five oxygens of $Pb(3)O_5$, one oxo anion is having μ_4 connectivity. The remaining four oxygens are from four different CHDC anions and two are with μ_3 connectivity and the other two are with μ_2 connectivity. These oxygens linking Pb(3) with two other Pb(1), and one Pb(2), by sharing an edge. The Pb-O bond lengths are in the 2.305 – 2.700 Å range.

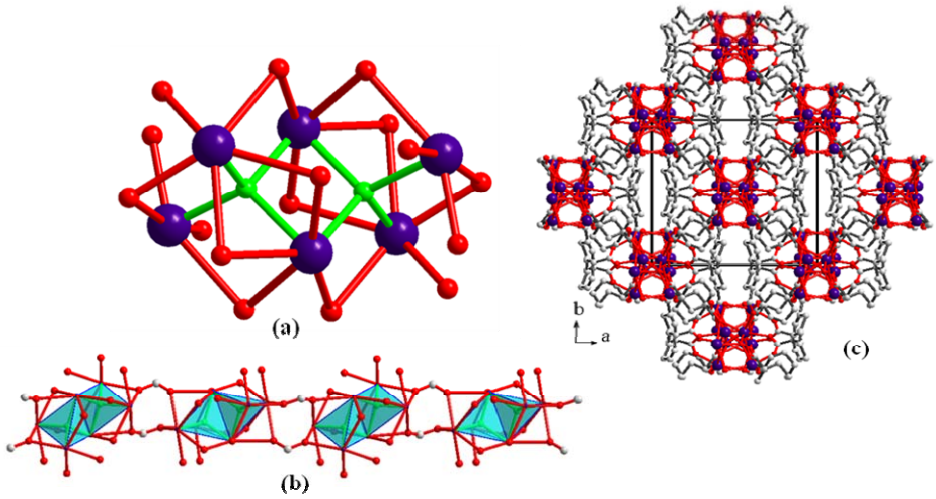

Fig. 3.4.15. (a) Pb_6O_{18} SBU (b) 1D chain and (c) view of the 3D structure in **VIII** viewed along the *c* axis.

These connectivities lead to the formation of a secondary building unit (SBU) of Pb_6O_{18}, which includes two edge-shared OPb_4 tetrahedra (Fig. 3.4.15a). The SBU is constructed by sharing $Pb(1)O_6$, $Pb(2)O_6$ and $Pb(3)O_5$ polyhedra. A carboxylate of acid-2 connects the adjacent SBUs to form an infinite 1-D chain (Fig. 3.4.15b) and the chains get connected to four other adjacent chains by CHDC anions to form the infinite three-dimensional structure ($\boldsymbol{I^0O^3}$) (Fig. 3.4.15c).

(b) 1,4-Cyclohexanedicarboxylate

The cadmium 1,4-cyclohexanedicarboxylate $[Cd(H_2O)_2(1,4\text{-}CHDC)]$, **IX**, is a one-dimensional chain structure, consisting of octahedral CdO_6 units connected by the carboxylate groups, with an asymmetric unit containing 8 non-hydrogen atoms (Fig. 3.4.16).

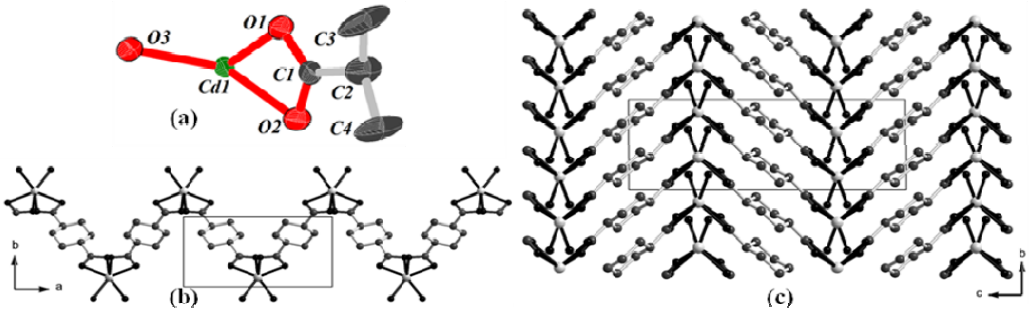

Fig.3.4.16. (a) ORTEP plot of **IX** (Thermal ellipsoids are shown at 50% probability) (b) 1D chain and (c) packing arrangement in **IX**, viewed along the *a* axis.

The cadmium atom sits on the two-fold axis, on an inversion center, 4e. This Cadmium atom is in a distorted octahedral environment (CdO_6) with the Cd-O bond distances in the 2.295(4) - 2.404(4) Å range. Two of the oxygens in the CdO_6 polyhedron are from the coordinated water molecules and the remaining four oxygens are from two different carboxyl groups with (11) connectivity. The polyhedra are connected to each other by the dicarboxylates with (1111) connectivity, resulting in a one-dimensional infinite zig-zag chain. The cyclohexane ring lies about an inversion center. The two carboxylate groups are in equatorial position (*e,e*), the torsional angle (θ) between the two being 180°. The structure is stabilized by inter chain hydrogen bonding interaction between the water molecules and the carboxylate oxygen [H…O = 1.85(3)-1.90 (3) Å, O…O = 2.708(3)-2.731(2) Å and ∠O-H…O = 168(2)-173(2)°].

3.4.2. Hybrid Networks of Metal Cyclohexanedicarboxylates with Extended Inorganic Connectivity

Hybrid inorganic-organic cyclohexane(or hexene)dicarboxylates with extended inorganic connectivity (I^xO^y, x = *1* to *2*; y = *0* to *2*) have been synthesized. These hybrid structures in two- and three-dimensions are the three isomeric cyclohenxedicarboxylates (1,2-, 1,3- and 1,4-) and 1,2-cyclohex(4)enedicarboxylates of Cd, Pb and La without chelating amines.

(a) 1,2-Cyclohexanedicarboxylate

The cadmium 1,2-cyclohexanedicarboxylate, [Cd(1,2-CHDC)], **X**, is a two dimensional layered structure consisting of a two dimensional metal-O-metal network grafted by the carboxylate groups (I^2O^0).

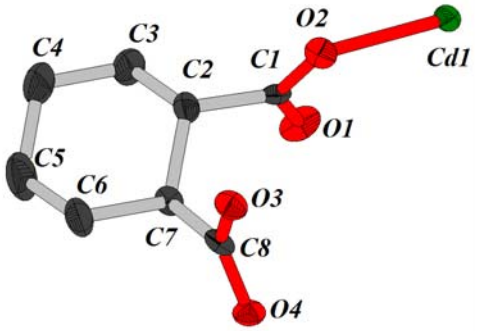

Fig. 3.4.17. ORTEP plot of **X** (Thermal ellipsoids are shown at 50% probability)

The asymmetric unit of **X** contains 13 non-hydrogen atoms (Fig. 3.4.17). The Cd atom is in a distorted octahedral environment with Cd-O bond distances in the 2.227(7) - 2.413(6) Å range. The six oxygens of CdO_6 polyhedron are from five different carboxyl groups with (2121) connectivity. Each CdO_6 polyhedron shares its edge with another CdO_6 octahedron to form an edge-shared Cd_2O_{10} dimer ($^2\mathbf{d}_2$). These dimers are connected with four other dimers by sharing the corners ($^1\mathbf{d}_1$), thus forming the infinite two-dimensional metal-O-metal network with six-

membered Cd rings, grafted with the carboxylate groups (Fig. 3.4.18a). The cyclohexane rings in **X** project on both the sides of the layer (Fig. 3.4.18b). Both of the carboxylate groups of the 1,2-cyclohexanedicarboxylate are in equatorial position (*e*,*e*) with a torsional angle of 60.59(1)^{o}.

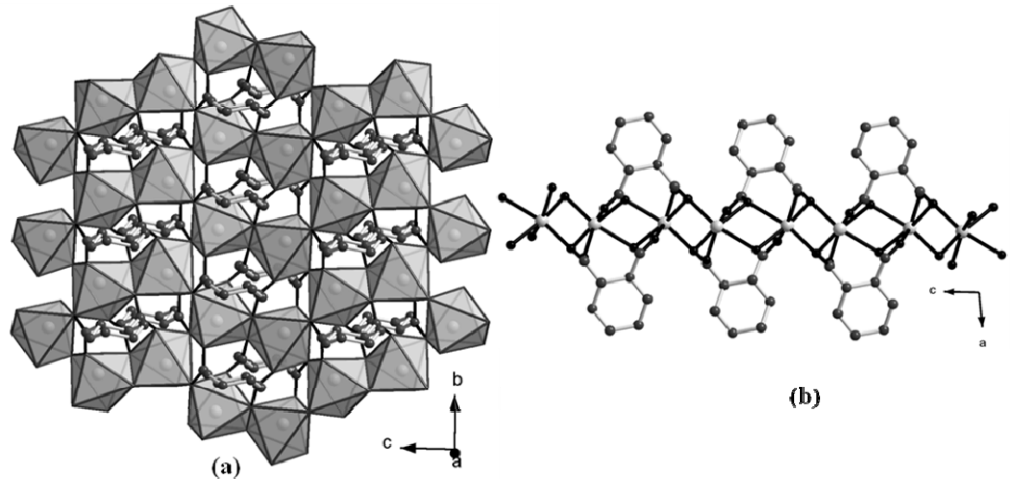

Fig. 3.4.18. View of the layered structure of **X** (a) along the *a* axis and (a) along the *b* axis.

(b) 1,2-Cyclohexenedicarboxylates

Cadmium 4-cyclohexene-1,2-dicarboxylate, Cd(1,2-CHeDC)(H_2O), **XI**, was obtained in two different polymorphic forms, **A** and **B**. In both the polymorphs, **XI** has a two-dimensional layered structure (***I*^{1}*O*^{1}**) made up of infinite one-dimensional Cd-O-Cd chains connected by the CHeDC anions. Both were crystallized in orthorhombic system, albeit in different space groups [Pnc2 (no.30) for **A** and Pbcn (no.60) for **B**]. The layered structures in **A** and **B** are similar, but only differ in their packing arrangements.

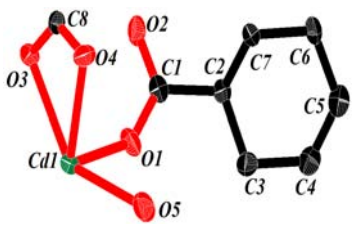

Fig. 3.4.19. ORTEP plot of **XI** (Thermal ellipsoids are shown at 50% probability).

The asymmetric unit of both **A** and **B** have 14 non-hydrogen atoms (Fig. 3.4.19). The Cd^{2+} ion is in a distorted octahedral environment, coordinated by six oxygen atoms. Five of the oxygen atoms are from three different CHeDC anions and the sixth one is from a water molecule. Among the five oxygen atoms of the carboxylate anions, two have μ_3 connections (connecting two metal centers and a carbon). Thus, each CdO_6 octahedron shares its corner ($^2\mathbf{D_1}$) with two other CdO_6 octahedra, forming an infinite Cd-O-Cd chain. The Cd-O bond distances are in the range 2.208-2.403 Å. The CHeDC anions are in the (*a,e*) conformation with a connectivity of (1211) as shown in Fig. 3.4.11a. The torsional angle are 70.41º and 67.96º respectively in the **A** and **B** polymorphs. The Cd-O-Cd chains in **XI** are further connected by the CHeDC anions through the carboxylate groups with (12) and (11) connectivity. Thus, each CHeDC anion connects two different chains, forming an infinite two-dimensional layered network as shown in Fig. 3.4.20a.

Both the sides of the layer structure in **XI** are decorated by the CHeDC rings (Fig. 3.4.20b). The rings on either side of a layer are oriented in the same direction. These layers are packed differently in the third dimension in the **A** and **B** polymorphs as shown in Fig. 3.4.19c and d. The orientation (along the *a*- axis) of the projected rings of the two adjacent layers is the same in **A** (Fig. 3.4.20c), but is in opposite directions (along the *b*-axis) in **B** (Fig. 3.4.20d). This leads to different nearest ring-ring interactions in the two polymorphs. The nearest C…C distance between the adjacent layers is 1.683 Å in **A** and 3.7 Å for **B**. Thus, the heat of formation for **A** is more endothermic than that of **B** by 26 kcal/mol, as calculated by the AM1 level Gaussian 03 suite of programs.[65] The occurrence of polymorphism, involving different arrangements of packing, indicates that the

layers are first formed through covalent connectivity, followed by packing through supramolecular interactions.

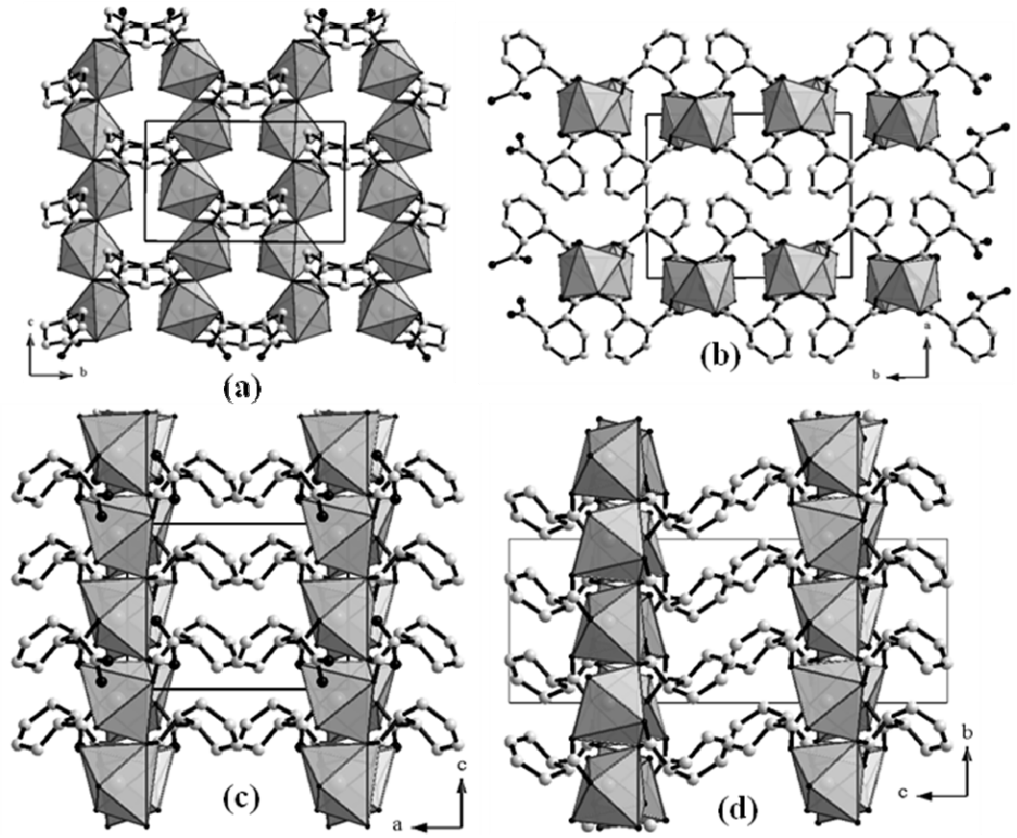

Fig. 3.4.20. (a) Layered structure of **XI** (b) the packing arrangement viewed along the c axis in compound **XI-A** (c) The packing arrangement in **XI-A** viewed along the b axis and (d) in **XI-B** viewed along the a axis.

In the recent literature, two Mn 1,2-cyclohexenedicarboxylates, $Mn(H_2O)$(1,2-CHeDC) and $[Mn_4(H_2O)$(1,2-CHeDC)].0.3$(H_2O)]$ have been reported.[41] Both these have layered structures and contain infinite M-O-M linkages. We find that the 1,2-CHeDc anions in these compounds are in the (*e,e*) conformation unlike in **XI,** which has the (*a,e*) conformation.

(c) 1,3-Cyclohexanedicarboxylates

Three hybrid inorganic-organic lead 1,3-cyclohexanedicarboxylates with extended inorganic connectivity (I^xO^y, ***x = 1*** and ***2; y = 0*** to ***2***) have been synthesized.

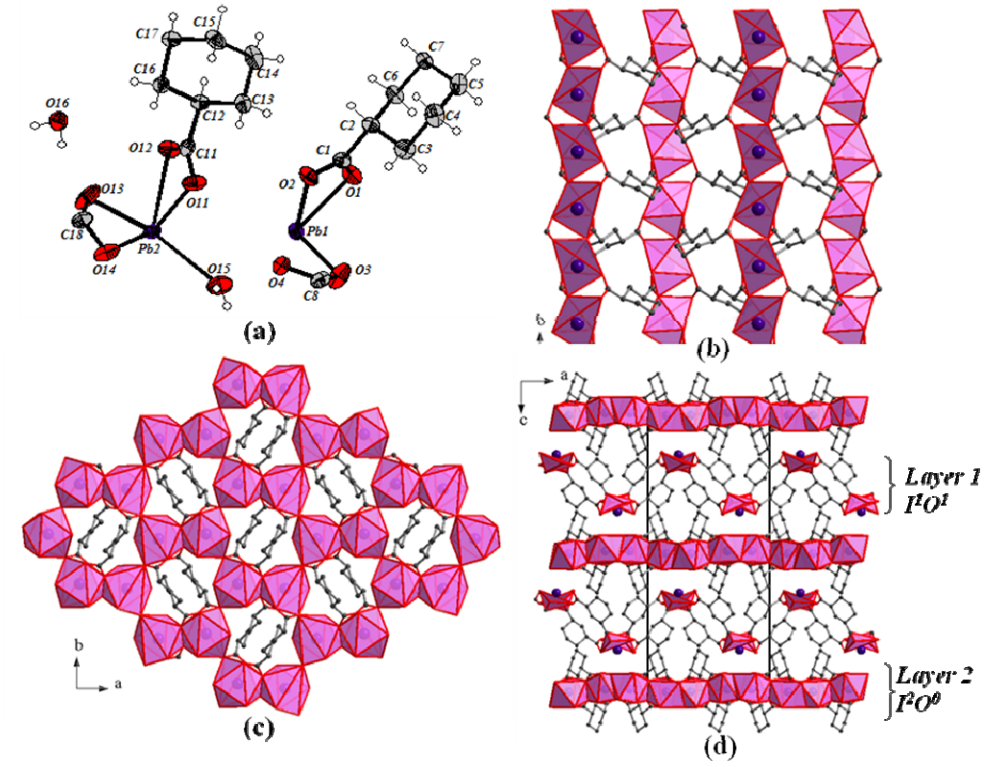

Fig. 3.4.21. (a) ORTEP plot of **XII (**Thermal ellipsoids are shown at 50% probability). Views of the layers and the infinite Pb-O-Pb linkages in (b) layer-1 and (c) layer-2 of **XII** and (d) Packing arrangement in **XII** (viewed along the *b*-axis).

The 1,3-cyclohexanedicarboxylate, Pb(1,3-CHDC)(H_2O), **XII**, has a two-dimensional structure with an asymmetric unit of 28 non-hydrogen atoms (Fig. 3.4.21a). There are two crystallographically distinct Pb^{2+} ions Pb(1) and Pb(2), two CHDC anions and two terminal water molecules in the asymmetric unit. The anions exhibit two types of coordination modes with acid-1 having (1121) connectivity and acid-2 having (1212) connectivity. Both of them are in the (*e*,*e*) conformation with torsional angles in the 172.33-172.66 ° range. Pb(1) is hemidirected and five-coordinated by oxygen atoms (PbO_5) from four different CHDC anions [acid-1]. Two of the oxygens have μ_3 connections linking Pb(1) with two other Pb(1) atoms. Thus, Pb(1)O_5 polyhedra share corners ($^2\mathbf{D_1}$) with each other forming an infinite one-dimensional Pb-O-Pb chain. The chains are

further connected by CHDC anions [acid-1], each anion binding to four different Pb^{2+} cations of adjacent Pb-O-Pb chains to form an infinite two-dimensional layer structure. This gives rise to a $\boldsymbol{I^1O^1}$ type hybrid structure (Fig. 3.4.21b). The active lone pair of the hemidirected $Pb(1)O_5$ polyhedra projects on both sides of the layer (Layer-1) as in Fig. 3.4.21d. The Pb-O bond lengths are in the 2.388 – 2.805 Å range.

Pb(2) is eight-coordinated by oxygen atoms (PbO_8) and has a holodirected geometry. Among the eight oxygens of (PbO_8), two are from two different terminal water molecules and the other six from four different CHDC anions, [acid-2]. Four among these six oxygens have $\boldsymbol{\mu_3}$ connections linking Pb(2) with three other Pb(2). Thus, each $Pb(2)O_8$ polyhedron shares an edge with another $Pb(2)O_8$, forming a dimer ($^2\mathbf{D_2}$) of Pb_2O_{14}. The dimers are further connected to each other by sharing a corner ($^1\mathbf{d_1}$) each with four dimers, forming an infinite two-dimensional Pb-O-Pb layer with a (4,4) square lattice and a hybrid connectivity of the type $\boldsymbol{I^2O^0}$ (Fig. 3.4.21c). The CHDC anions (acid-4) decorate both sides of the layer (Layer-2) as in Fig. 3.4.21c. The Pb-O bond lengths are in the 2.453 – 2.834 Å range. There is no apparent hydrogen-bonding in **XII**, and van der Waals interactions between layers appear to be the main stabilizing factor (Fig. 3.4.21d).

We have been able to obtain a lead oxalate-cyclohexanedicarboxylate, $[(OPb_4)_2(OH)_2(C_2O_4)(1,3\text{-CHDC})_4].H_2O$, **XIII**, where the oxalate moiety was generated *in-situ* from the 1,3-CHDC under the hydrothermal synthesis. Similar cases, where the ligands are formed in situ during the synthesis have been reported in the literature.[66,67] The formation of the oxalate in the synthesis of **XIII** is rather unusual. This can happen if 1,3-H_2CHDC undergoes an oxidative decarboxylation

to produce cyclohexene or cyclohexadiene. Cyclic olefins in gas phase are known to produce oxalic acid on oxidation at high temperatures.[68-70]

XIII has a two-dimensional structure with an asymmetric unit of 16.75 non-hydrogen atoms (Fig. 3.4.22a). The Pb^{2+} cations are in three crystallographically distinct positions with Pb(1) and Pb(3) land with 0.5 occupancy in 4*f* and 4*h* special positions respectively and Pb(2) with a full occupancy. One CHDC anion, one quarter of the oxalate anion (with C at 4*h*), one hydroxyl anion (with the O at 4*f*), one independent oxo dianion (at 4*f*) and one quarter of a lattice water molecule (at 2*a*) are also in the asymmetric unit. The CHDC anion in the (*e*,*e*) conformation with a torsional angle of 176.74(2) º has (2223) connectivity and binds to six Pb^{2+} cations [three Pb(2) and three Pb(3)]. The oxalate anion has (2222) connectivity and binds to six Pb^{2+} cations [two Pb(1) and four Pb(2)]. The independent oxo dianion binds to four Pb^{2+} cations [two Pb(1) and two Pb(2)] to form a OPb_4 tetrahedron. The hydroxyl anion binds to three Pb^{2+} cations [one Pb(1) and two Pb(2)].

Pb(1) is hemidirected and coordinated by five oxygen atoms (PbO_5). Among the five oxygens of $Pb(1)O_5$ two with μ_3 connectivity are from a single oxalate anion, another two with μ_4 connectivity are from two different oxo dianions and the fifth one with a μ_4 connectivity is from the hydroxyl anion . Thus, the oxygens with μ_3 and μ_4 connections link Pb(1) with two other Pb(1) atoms by sharing edges, and two different Pb(2) atoms by sharing edges. The Pb-O bond lengths are in the 2.314 – 2.635 Å range. Pb(2) is slightly hemidirected, and coordinated by seven oxygen atoms (PbO_7). Among the seven oxygens of $Pb(2)O_7$, the oxo and the hydroxyl anions are have μ_4 connectivity, the other one with μ_3

connectivity is from the oxalate anion. The remaining four (one with mono dentate, one with μ_3 and two with μ_4 connectivity) are from three different CHDC anions. These oxygens link Pb(2) with two Pb(2) and two Pb(1) atoms, by sharing edges. They also connect Pb(2) with two Pb(3) atoms, by sharing a face each. The Pb-O bond lengths are in the 2.459 – 2.919 Å range. Pb(3) is holodirected and coordinated by eight oxygen atoms (PbO_8). All the eight oxygens are from six different CHDC anions. Among the eight oxygens, two have μ_3 connectivity and the other two μ_4 connectivity. These oxygens link Pb(3) with two other Pb(3) atoms, by sharing edges and with two different Pb(2) atoms, by sharing faces. The Pb-O bond lengths are in the 2.583 – 2.905 Å range.

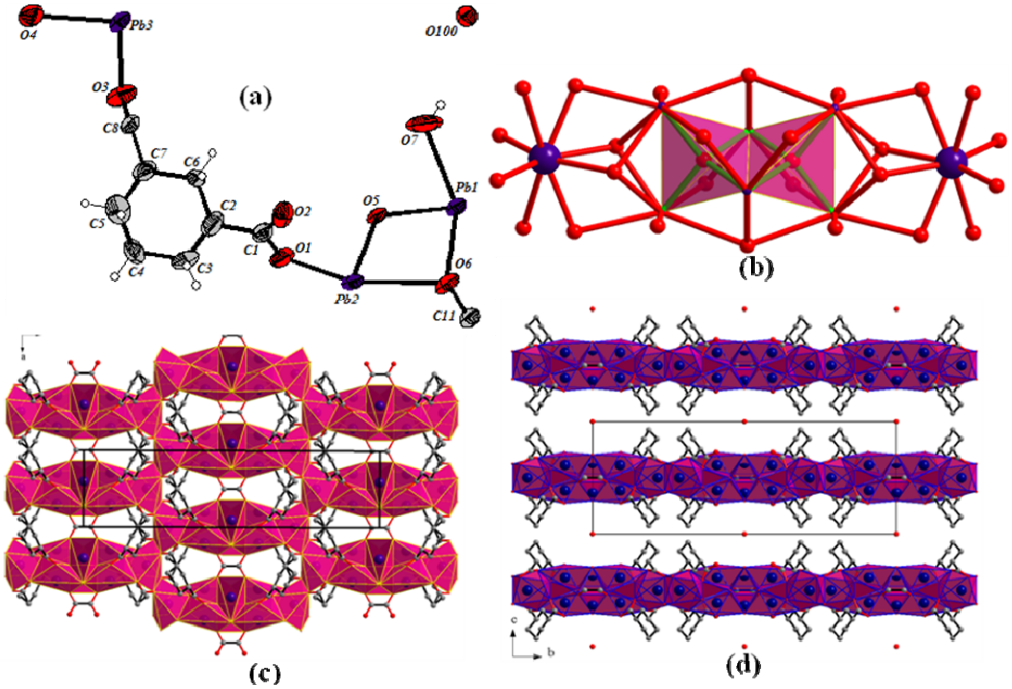

Fig. 3.4.22. (a) ORTEP plot of **XIII** (Thermal ellipsoids are shown at 50% probability). Also shown are (b) $Pb_8(OH)_2O_{26}$ secondary building unit (c) a view of the layer and the infinite Pb-O-Pb linkages in **XIII** and (d) packing arrangement in **XIII** (viewed along the *a*-axis).

These connectivities lead to the formation of a secondary building unit (SBU) of the composition $Pb_8(OH)_2O_{26}$, which includes two edge-shared OPb_4

tetrahedra and two hydroxyl groups (Fig. 3.4.22b). The SBU is made up of two $Pb(1)O_5$, four $Pb(2)O_7$ and two $Pb(3)O_8$ polyhedra. The oxalate anion connects the adjacent SBUs to form an infinite 1-D chain. Each SBU is connected to four other SBUs, leading to the formation of a (4,4) square lattice with infinite two dimensional Pb-O-Pb connectivity ($\boldsymbol{I^2O^0}$) (Fig. 3.4.22c). The CHDC anions (acid-4) decorate both sides of the layer and the lattice water molecule resides in the 1-D channel (7.1 Å × 3.0 Å) between the layers (Fig. 3.4.22d). The water molecules are H-bonded to the hydroxyl groups projecting in the channel. Platon-Solv analysis showed that 17.2% of the unit cell volume to be solvent accessible.[38,39]

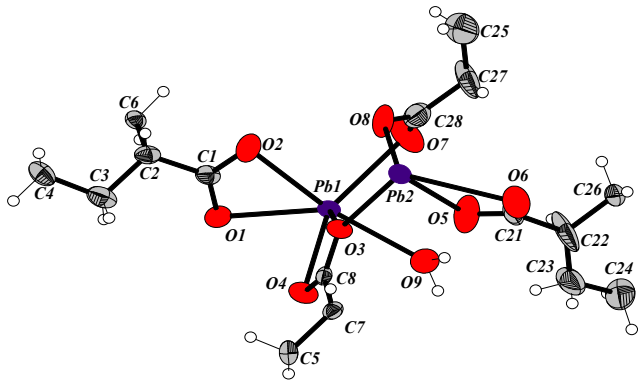

Fig. 3.4.23. ORTEP plot of **XIV** (Thermal ellipsoids are shown at 50% probability).

The 1,3-cyclohexanedicarboxylate, $Pb_2(1,3\text{-CHDC})_2(H_2O)$, **XIV**, has a three-dimensional structure with an asymmetric unit of 27 non-hydrogen atoms. There are two crystallographically distinct Pb^{2+} ions, two CHDC anions and one terminal water molecule in the asymmetric unit (Fig. 3.4.23). Based on the coordination modes, the anions can be classified in to two types: (a) acid-1 with (1222) connectivity and (b) acid- 2 with (1221) connectivity. Both of them are in the (*e*,*e*) conformation with torsional angles in the 168.9-180 ° range. Pb(1) and Pb(2) are both seven-coordinated as (PbO_7) units. Among the seven oxygens of $Pb(1)O_7$, one is from the terminal water molecule and six are from four different

CHDC anions [three acid-1 and one acid-2]. Four of these oxygens have μ_3 connections linking one Pb(1) with another Pb(1) through ($^2\mathbf{D_2}$) two oxygen atoms and with two different Pb(2) atoms through two oxygens (two $^2\mathbf{D_1}$). Thus, the $Pb(1)O_7$ polyhedra share edges with each other forming a dimeric $Pb(1)_2O_{13}$ unit ($^2\mathbf{D_2}$). The Pb-O bond lengths are in the 2.418 – 2.899 Å range.

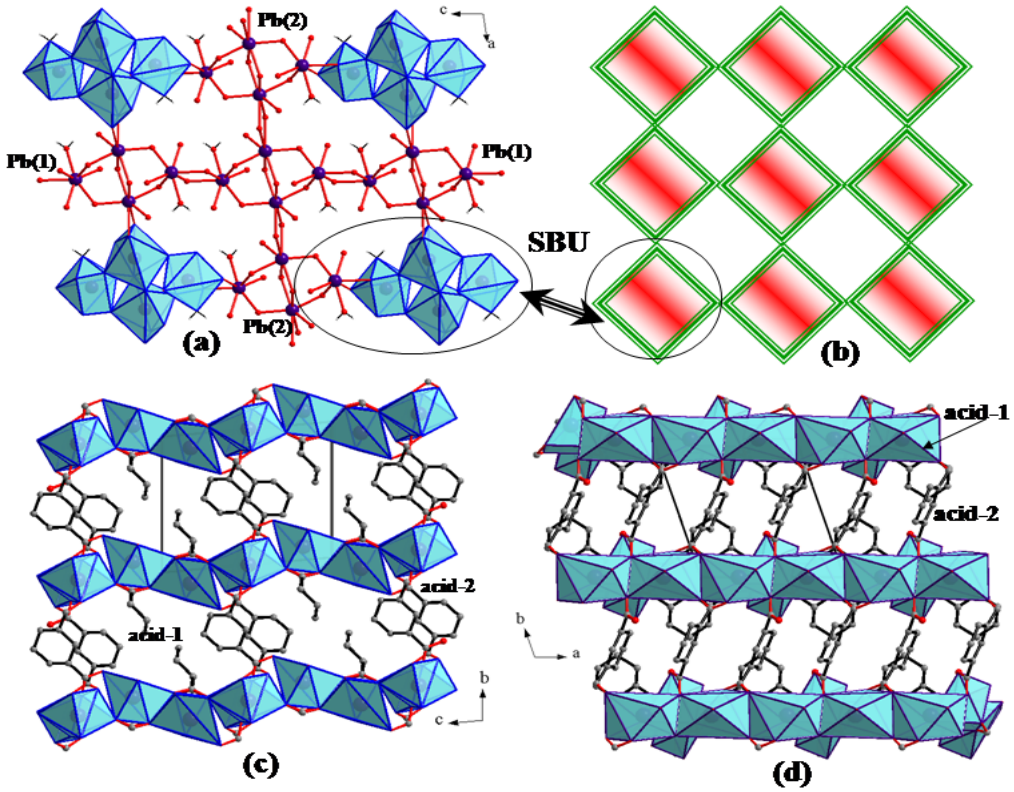

Fig. 3.4.24. (a) View of the layer with infinite Pb-O-Pb linkages in **XIV** (b) schematic of the (4,4) square lattice with the SBUs and 3D-structure of **XIV** (c) viewed along the *a*-axis and (d) viewed along the *c*-axis.

The seven oxygens of $Pb(2)O_7$ come from six different CHDC anions [two acid-1 and four acid-2]. Six of these oxygens have μ_3 connections linking Pb(2) with two different Pb(1) through two oxygen atoms and with two other Pb(2) through four oxygen atoms. Thus, each $Pb(2)O_7$ polyhedron shares an edge with another forming a dimeric $Pb(2)_2O_{13}$ unit ($^2D_2$). The dimers are connected to each other through two μ_3 oxygens, forming an infinite one-dimensional Pb-O-Pb

chain. The chains are connected by the $Pb(1)_2O_{13}$ dimer ($^2\mathbf{D_2}$) into a two-dimensional Pb-O-Pb layer (Fig. 3.4.24a). The layers can also be viewed as a (4,4) square lattice consisting of tetra-nuclear secondary building units (SBU) of Pb_4O_{18} with two Pb(1) and Pb(2) each (Fig. 3.4.24b). Acid-1 which connects the Pb cations within the layer (intralayer) decorates both sides of the layer. The layers are further connected by acid-2, forming a three-dimensional structure with the $\boldsymbol{I^2O^1}$ type (Fig. 3.4.24c and d). The Pb-O bond lengths are in the 2.450 – 2.685 Å range.

(d) 1,4-Cyclohexanedicarboxylates

Four three-dimensional hybrid inorganic-organic 1,4-cyclohexanedicarboxylates of lead and lanthanum, all with extended one-dimensional inorganic connectivity ($\boldsymbol{I^1O^2}$) have been synthesized.

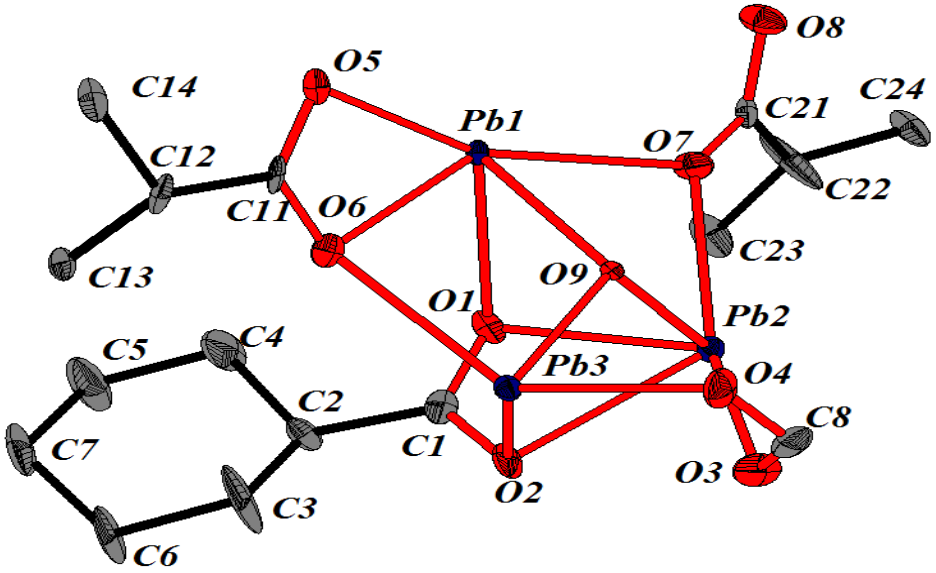

Fig. 3.4.25. ORTEP plot of **XV** (Thermal ellipsoids are shown at 50% probability).

$[(OPb_3)(1,4\text{-}CHDC)_2]$, **XV**, has a three-dimensional structure with one-dimensional inorganic connectivity ($\boldsymbol{I^1O^2}$). It has an asymmetric unit with 28 non-hydrogen atoms (Fig. 3.4.25). There are three Pb^{2+} cations in three crystallographically distinct positions, one complete 1,4-CHDC anion, half of two

different 1,4-CHDC anions and one independent oxo dianion in the asymmetric unit. There are three types of CHDC anions, acid-1, acid-2 and acid-3 with two types of conformations, (*e*,*e*) (acid-1 and -3) and (*a,a*) (acid-2). The torsional angles are 85.86(1)º for acid-1 and 0º for acid-2 and -3. They have (1122), (2222) and (2222) connectivities respectively. Acid-1 binds to five Pb^{2+} cations [one Pb(1), two each of Pb(2) and Pb(3)], acid-2 binds to six Pb^{2+} cations [two each of Pb(1), Pb(2) and Pb(3)] and acid-3 binds to eight Pb^{2+} cations [two each of Pb(1), Pb(2) and four Pb(3)]. The independent oxo dianion binds to four Pb^{2+} cations [two Pb(1), one Pb(2) and one Pb(3)] to form a OPb_4 tetrahedron.

Pb(1) is hemidirected and coordinated by six oxygen atoms (PbO_6). Among the six oxygens of $Pb(1)O_6$, four with $\boldsymbol{\mu}_3$ connectivity are from three different CHDC anions and the remaining two with $\boldsymbol{\mu}_4$ connectivity are from two different oxo dianions. These oxygen atoms link Pb(1) with an another Pb(1) by sharing an edge, with two different Pb(2) atoms by sharing an edge with one and by sharing a face with another, and with two different Pb(3) by sharing a corner to one and by sharing an edge to another. The Pb-O bond lengths are in the 2.319(6) – 2.829(7) Å range. Pb(2) is also hemidirected and coordinated by six oxygen atoms (PbO_6). Among the six oxygens of $Pb(2)O_6$, one oxo anion has $\boldsymbol{\mu}_4$ connectivity. The remaining oxygens are from four different CHDC anions with an oxygen having $\boldsymbol{\mu}_2$ connectivity and other four with $\boldsymbol{\mu}_3$ connectivity. These oxygens link Pb(2) with two Pb(1) and also connect Pb(2) with one Pb(3) by edge sharing. The Pb-O bond lengths are in the 2.201(5) – 2.736(7) Å range. Pb(3) is also hemidirected and coordinated by six oxygen atoms (PbO_6). Among the six oxygens of $Pb(3)O_5$, one oxo anion is having $\boldsymbol{\mu}_4$ connectivity. The remaining five oxygens are from five

different CHDC anions and four are with μ_3 connectivity and the remaining one is with μ_2 connectivity. These oxygens linking Pb(3) with two different Pb(1) by sharing a corner to one and by sharing an edge to another and with one Pb(2) by sharing an edge. The Pb-O bond lengths are in the 2.325(6) – 2.901(7) Å range.

These connectivities lead to the formation of a secondary building unit (SBU) of Pb_6O_{20}, which includes two edge-shared OPb_4 tetrahedra (Fig. 3.4.26a). The SBU is constructed by sharing two each of $Pb(1)O_6$, $Pb(2)O_6$ and $Pb(3)O_5$ polyhedra. Each SBU is connected to two such SBUs by sharing two edges ($^2\mathbf{d_2}$) to form a chain with an infinite 1-D inorganic connectivity ($\boldsymbol{I}^1$) and the chains get connected to the adjacent chains by CHDC anions (acid-3) to form an infinite two dimensional layer ($\boldsymbol{I}^1\boldsymbol{O}^1$) (Fig. 3.4.26b). These layers are further connected by other two CHDC anions (acid-1 and -2) into an infinite three-dimensional structure of the type ($\boldsymbol{I}^1\boldsymbol{O}^2$) (Fig. 3.4.26c).

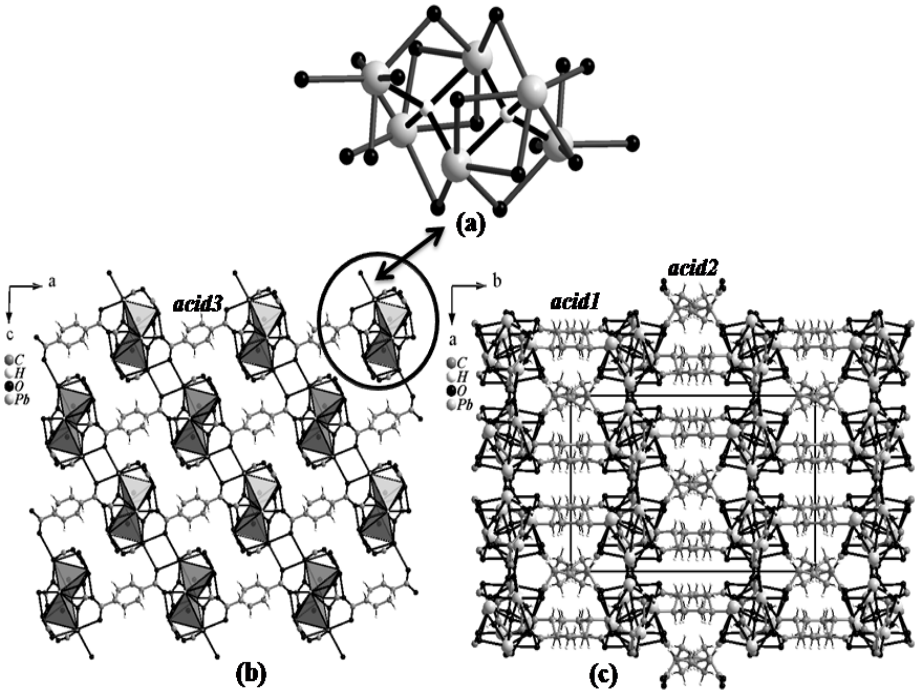

Fig. 3.4.26. (a) Pb_6O_{20} SBU (b) view of 2D layer along the *b* axis and (c) view of the 3D structure along the *c* axis in **XV**.

The lanthanum cyclohexanedicarboxylate, $[La_2(1,4\text{-CHDC})_3(H_2O)_4]$, **XVI**, has a three-dimensional structure with an asymmetric unit of 40 non-hydrogen atoms (Fig. 3.4.27). There are two crystallographically distinct La^{3+} ions, three CHDC anions and four terminal water molecules in the asymmetric unit. The anions can be categorized into four types, based on their coordination modes: (a) acid-1 (1212) (b) acid- 2 (1211) (c) acid- 3 (1111) and (d) acid 4 (1011). All of them are in (*e,e*) conformation with torsional angles in the 168.9-180 º range.

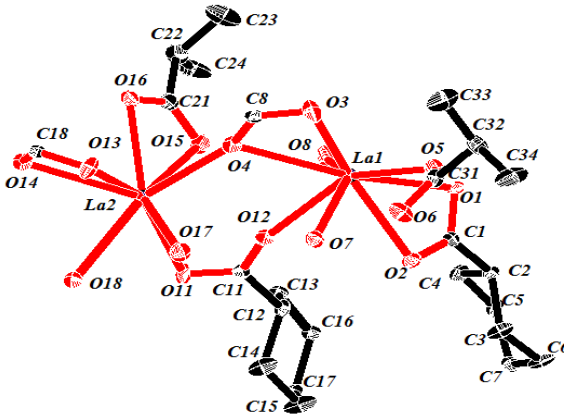

Fig. 3.4.27. ORTEP plot of **XVI** (Thermal ellipsoids are shown at 50% probability).

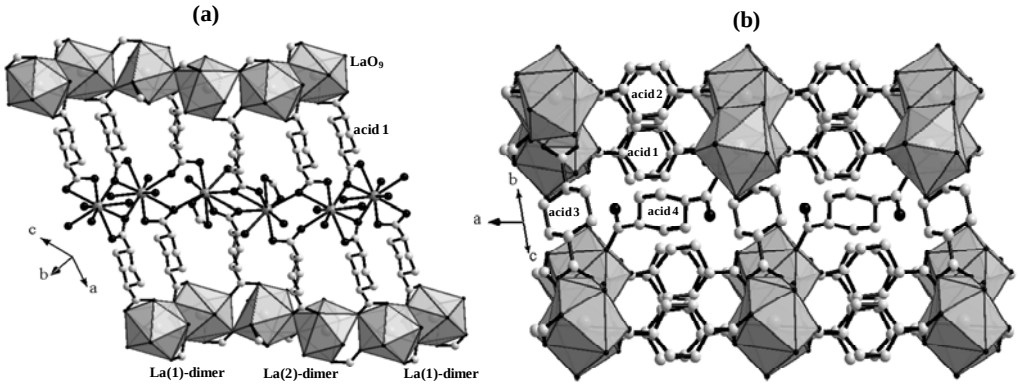

Fig. 3.4.28. (a) View of the layer and (b) the three-dimensional structure in **XVI**.

Both La(1) and La(2) are in a distorted tricapped-trigonal prism environments (LaO_9) with nine-coordinated oxygen atoms. Among the nine oxygens, two are from two terminal water molecules and seven come from five

different CHDC anions [three acid-1, one acid-2 and one acid-4 in La(1) and one acid-1, three acid-2 and one acid-3 in La(2)]. Thus, two LaO_9 polyhedra share an edge ($^2\mathbf{D_2}$) with each other forming the dimer La_2O_{16}. The dimers are connected to each other alternatively through a $\boldsymbol{\mu}_3$ oxygen atom ($^2\mathbf{D_1}$), forming an infinite one-dimensional La-O-La chain. The chains are connected by acid-1 and acid-2 into a two-dimensional layer (Fig. 3.4.28a). The layers are connected by acid-3 [which connects La(2) dimers between the layers], forming a three-dimensional structure (Fig. 3.4.28b). The La-O-La chains between the layers are cross-linked by acid-4 (which connects La(1) dimers) in the three-dimensional network (Fig. 3.4.27b). The La-O bond distances are in the range 2.501-2.755 Å. On heating at 200^o C, **XVI** loses the coordinated water molecules and transforms to another crystalline compound. The dehydrated compound reverts back to the original structure of **XVI** upon exposure to water vapor as indicated by the powder diffraction patterns.

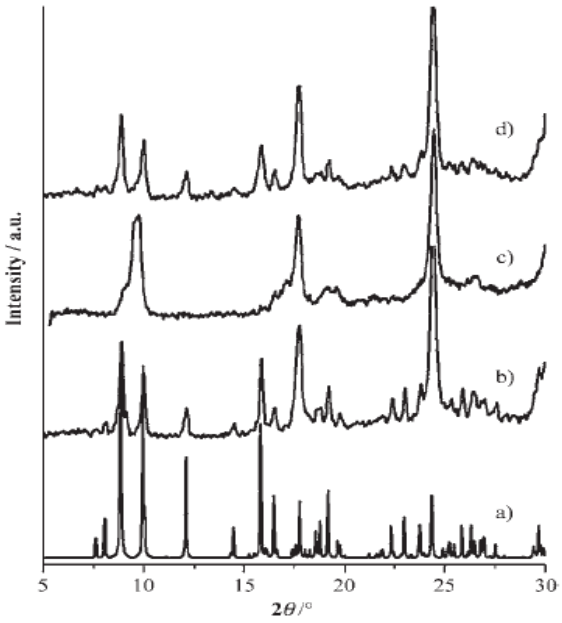

Fig. 3.4.29. Powder XRD patterns of **XVI:** (a) simulated, (b) as-synthesized, (c) after heating at 200^o C and (d) after exposing the dehydrated sample to water vapor).

$[La_3(1,4\text{-HCHDC})_2(1,4\text{-CHDC})_{3.5}(H_2O)_2]\cdot H_2O$, **XVII,** also has a three-dimensional structure with an asymmetric unit of 73 non-hydrogen atoms. There are three crystallographically independent La^{3+} ions, 5.5 cyclohexanecarboxylate anions and one lattice water molecule in the asymmetric unit (Fig. 3.4.30). The anions can be categorized into two classes based on the deprotonation level ($HCHDC^-$ and $CHDC^{2-}$), conformation and the coordination modes. La(1) is in a distorted tricapped-square antiprism environment (LaO_{11}) with eleven coordinated oxygen atoms which come from six different cyclohexanecarboxylate anions and one terminal water molecule. Among the ten oxygen atoms (of the anions), five are having $\boldsymbol{\mu}_3$ connections linking La(1) with La(2) through three oxygen atoms ($^3\mathbf{D_3}$) and La(3) through two oxygen atoms ($^2\mathbf{D_2}$).

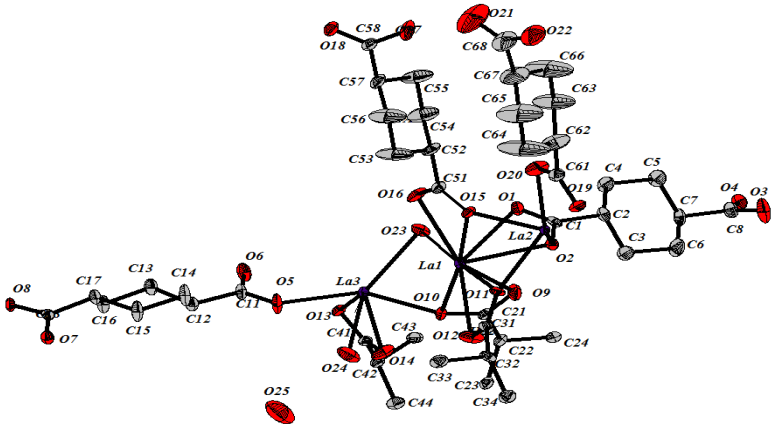

Fig. 3.4.30. ORTEP plot of **XVII** (Thermal ellipsoids are shown at 50% probability).

La(2) is in a distorted dodecahedral environment (LaO_8) and coordinated to eight oxygen atoms from eight different cyclohexanedicarboxylate anions. Among the eight oxygen atoms, four have $\boldsymbol{\mu}_3$ connections linking La(2) with La(1) through three oxygen atoms ($^3\mathbf{D_3}$) and La(3) through one oxygen ($^4\mathbf{D_1}$). La(3) also has a distorted dodecahedral environment (LaO_8) with one oxygen from a terminal water and seven from six different cyclohexanedicarboxylate anions. Among the seven

oxygen atoms, three have μ_3 connections linking La(3) with La(1) through two oxygen atoms ($^2\mathbf{D_2}$) and a(1) through one oxygen ($^4\mathbf{D_1}$). The La-O bond distances are in the range 2.406-2.744 Å. The $La(1)O_{11}$ polyhedron shares its face with $La(2)O_8$ through three μ_3 oxygen atoms forming a dinuclear unit. These units are linked to each other through $La(3)O_8$ by sharing an edge ($^2\mathbf{D_2}$) with $La(1)O_{11}$ and a corner ($^4\mathbf{D_1}$) with $La(2)O_8$, forming an infinite one-dimensional La-O-La chain along the *a*-axis (Fig. 3.4.31a). All the cyclohexanecarboxylate anions which connect these one-dimensional chains are in the trans-conformation (ten in *e,e* form and one in *a,a* form). The torsional angles are in the range 172-180º. Each La-O-La chain is connected to six similar chains to form a three-dimensional structure with two types of triangular channels along the *a*-axis (Fig. 3.4.31b). Free carboxylic acid groups (protonated) project from the walls in one type of channel [highlighted with grey (Fig. 3.4.31c)], whereas in the other type of channel, lattice water molecules are situated between the acid linkers.

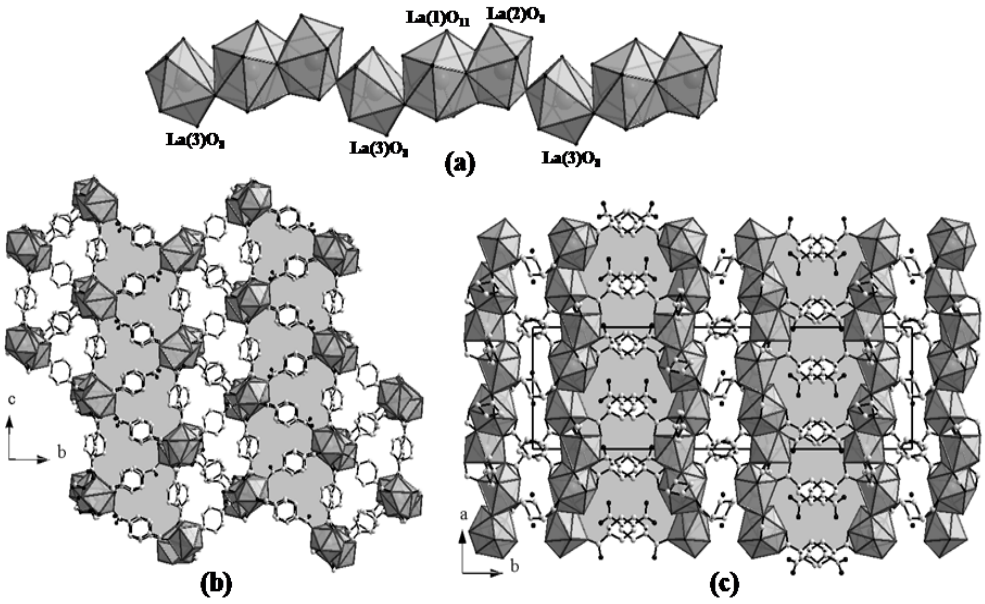

Fig. 3.4.31. (a) Infinite one-dimensional La-O-La chain (b) three-dimensional structure, showing two types of channels (viewed along a axis) and (c) the three-dimensional structure (viewed along c axis) in **XVII**.

$[La_2(1,4\text{-CHDC})_3(H_2O)].2.5H_2O$, **XVIII**, has a three-dimensional structure with an asymmetric unit of 39.5 non-hydrogen atoms. There are two crystallographically distinct La^{3+} ions, three CHDC anions, a terminal water molecule and 2.5 lattice water molecules in the asymmetric unit (Fig. 3.4.32). The three anions can be categorized into two types, based on their coordination modes: (a) acid-1 (1111) (b) acid- 2 and acid- 3 (1212). Acid-1 is in the (*e,e*) conformation where as acid-2 and acid-3 are in the (*a,e*) conformation.

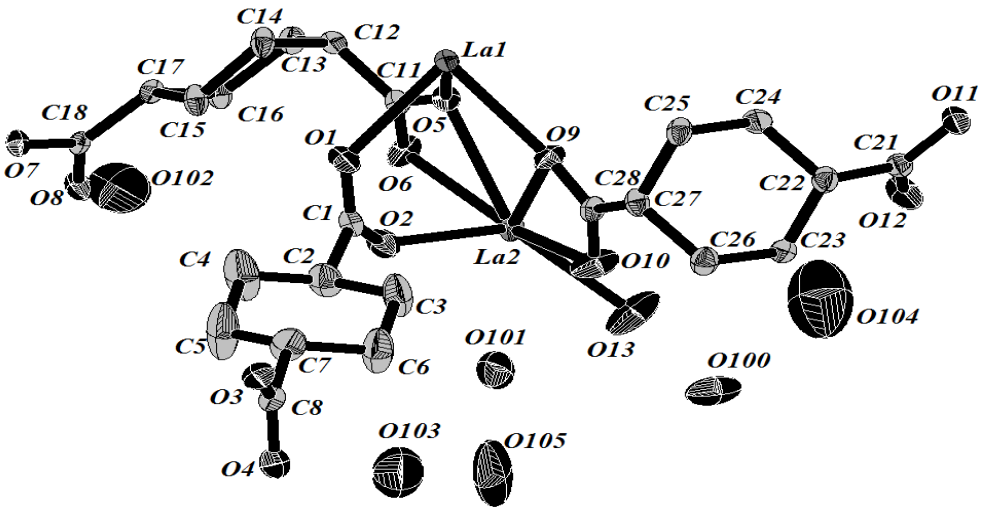

Fig. 3.4.32. ORTEP plot of **XVIII** (Thermal ellipsoids are shown at 50% probability).

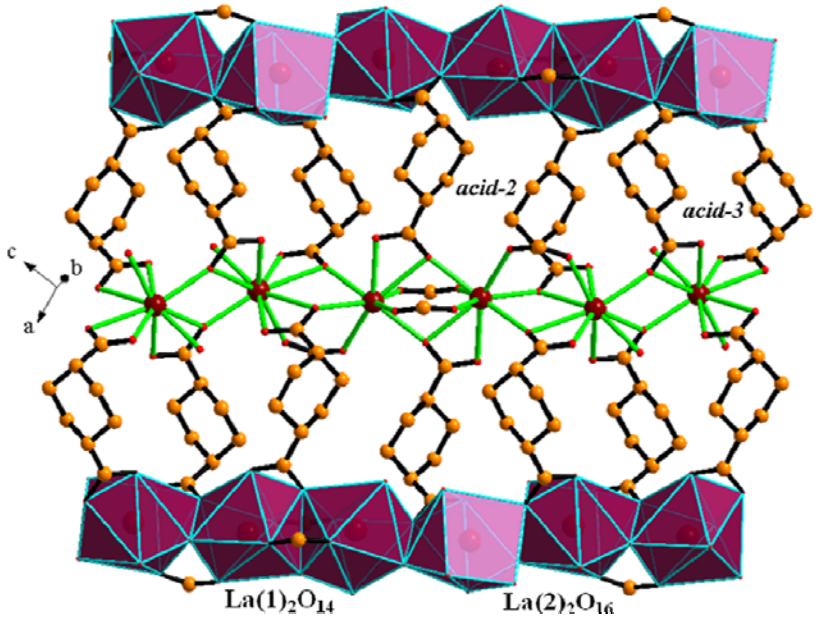

Fig. 3.4.33. View of the layer consisting of infinite La-O-La chains in **XVIII**.

La(1) is in a distorted dodecahedral environment (LaO_8), coordinated to eight oxygens from seven different cyclohexanedicarboxylate anions [three acid-1, three acid-2 and one acid-3]. Among the eight oxygens, four have μ_3 connections linking La(1) with La(1) through two oxygens ($^4\mathbf{D_2}$) and with La(2) through two oxygens ($^3\mathbf{D_2}$). La(2) is in a nine-coordinated environment (LaO_9), the nine oxygens coming from a terminal water and five different cyclohexanedicarboxylate anions [one acid-1, one acid-2 and three acid-3]. Among the nine oxygens, four have μ_3 connections linking La(2) with La(2) through two oxygens ($^2\mathbf{D_2}$) and with La(1) through two oxygens ($^3\mathbf{D_2}$). Thus, two LaO_8 polyhedra share an edge forming the La_2O_{14} dimer ($^4\mathbf{D_2}$). Similarly, two LaO_9 polyhedra share an edge forming the La_2O_{16} dimer ($^2\mathbf{D_2}$). The dimers are connected to each other alternatively through two μ_3 oxygens ($^3\mathbf{D_2}$), forming an infinite one-dimensional La-O-La chain. The chains are connected by acid-2 and acid-3 into a two-dimensional layer (Fig. 3.4.33). The layers are connected by acid-1, forming a three-dimensional structure with one-dimensional channels running along the *a*-axis (Fig. 3.4.34). The lattice water molecules are situated in these channels. The La-O bond distances are in the range 2.412-2.756 Å.

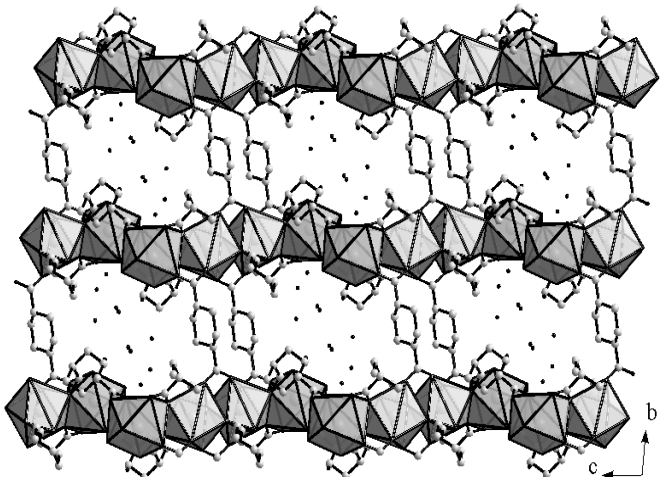

Fig. 3.4.34. View of the three-dimensional structure along the *a* axis in **XVIII**.

3.5. Conclusions

A systematic study of the metal-cyclohexanedicarboxylates (CHDCs) formed by the three isomeric dicarboxylic acids in the presence or absence of chelating amines has been carried out. Several coordination polymers and the hybrids with extended inorganic connectivity in different dimensionalities have been prepared under hydrothermal conditions and their structures established by X-ray crystallography. Summary of the structural features of the various compounds discussed in this chapter are tabulated in Tables **3.9** and **3.10**.

Nine hybrid inorganic-organic cyclohexanedicarboxylates with zero inorganic connectivity (I^0O^y, $y = 1$ to 3) have been synthesized. These coordination polymers are the two isomeric cyclohexanedicarboxylates (1,3- and 1,4-) of Mn, Cd and Pb and with or without chelating amines.

Ten hybrid inorganic-organic cyclohexane (or hexene) dicarboxylates with extended inorganic connectivity (I^xO^y, $x = 1$ to 2 $y = 0$ to 2) have been synthesized and characterized. These hybrid structures in two- and three-dimensions are the three isomeric cyclohenxedicarboxylates (1,2-, 1,3- and 1,4-) and 1,2-cyclohex(4)enedicarboxylates of Cd, Pb and La without chelating amines.

Presence of secondary ligands and chelating amines such as 1,10-phenanthroline and 2,2-bipyridine, decrease the overall dimensionality of the compounds, but helps in stabilizing the low dimensional crystal structure through supramolecular interactions. 1,2-dicarboxylic acid favors the formation of low dimensional compounds and extended inorganic connectivity. Increase in size of the metal cation also favors the formation of higher dimensional compounds and extended inorganic connectivity through increased coordination number.

In all the three isomeric cyclohexanedicarboxylates, the (*e,e*) conformation is most favored although we have often encountered other conformations (*a,a*) and (*a,e*) along with the (*e,e*) conformation {(*a,a*) and (*a,e*) in 1,4-CHDCs, (*a,e*) in 1,3-CHDCs and in (*a,e*) 1,2-CHeDCs}.

All the three isomers (1,2-, 1,3,- and 1,4-) of cyclohehanedicarboxylic acids favor the formation of hybrid compounds with extended inorganic connectivity. Both 1,2-CHDCs and 1,2-CHeDCs occur only as layered structures out of structural necessities. The three-dimensional structures are, however, formed with 1,3- and 1,4-isomers. 1,4-isomers favor higher dimensional structures irrespective of the ring conformation, but in 1,3-isomers conformation plays a crucial role in deciding the dimensionality.

Table 3.9

Comp. ID.	Formula	Conformation of the CHDC ring	Dimensionality	Connectivity	Dimer SBUs
I	[Cd(1,3-CHDC)(1,10-phen)]	**(e,e)**	**2**	I^0O^2	$^2D_2$
II	[Mn(H_2O)(1,3-CHDC)(1,10-phen)]	**(e,e)**	**0**	I^0O^0	-
III	[Mn_3(1,3-CHDC)$_3$(1,10-phen].4H_2O	**(e,e)**	**1**	I^0O^1	Trinuclear SBU from two $^3D_1$
IV	[Mn_3(1,4-CHDC)$_3$(1,10-phen].4H_2O	**(e,e) : 2(a,e)**	**2**	I^0O^2	Trinuclear SBU from two $^3D_1$
V	[Cd_3(1,4-CHDC)$_3$(1,10-phen)$_2$].4H_2O	**(e,e) : 2(a,e)**	**2**	I^0O^2	Trinuclear SBU from two $^3D_2$
VI	[Cd(1,4-CHDC)(2,2'-bipy)].H_2O	**(e,e)**	**2**	I^0O^2	$^2D_2$
VII	[Cd(H_2O)$_2$(1,3-CHDC)].H_2O	**(e,e)**	**2**	I^0O^2	$^2D_2$
VIII	(OPb_3)(1,3-CHDC)$_2$	**(a,e)**	**3**	I^0O^3	**Hexamer**
IX	[Cd(H_2O)$_2$(1,4-CHDC)]	**(e,e)**	**1**	I^0O^1	zig-zag chain

Table 3.10

Comp. ID.	Formula	Conformation of the CHDC ring	Dimensionality	Connectivity	Dimer SBUs
X	[Cd(1,2-CHDC)]	**(e,e)**	**2**	I^2O^0	$^2d_2$ & $^1d_1$
XI	Cd(1,2-CHeDC)(H_2O)	**(a,e)**	**2**	I^1O^1	$^2D_1$
XII	Pb(1,3-CHDC)(H_2O)	**(e,e)**	**2**	I^1O^1	$^2D_1$
				I^2O^0	$^2D_2$
XIII	$[(OPb_4)_2(OH)_2(C_2O_4)$ $(1,3\text{-CHDC})_4].H_2O$	**(e,e)**	**2**	I^2O^0	**Octamer**
XIV	$Pb_2(1,3\text{-CHDC})_2(H_2O)$	**(e,e)**	**3**	I^2O^1	$^2D_2$ & $^2D_1$
XV	$[(OPb_3)(1,4\text{-CHDC})_2]$	**3(e,e) : (a,e)**	**3**	I^1O^2	**Hexamer &** $^2d_2$
XVI	$[La_2(1,4\text{-CHDC})_3(H_2O)_4]$	**(e,e)**	**3**	I^1O^2	$^2D_2$ & $^2D_1$
XVII	$[La_3(1,4\text{-HCHDC})_2(1,4\text{-CHDC})_{3.5}(H_2O)_2]\cdot H_2O$	**10(e,e) : (a,a)**	**3**	I^1O^2	$^3D_3$, $^2D_2$ & $^4D_1$
XVIII	$[La_2(1,4\text{-CHDC})_3(H_2O)]\cdot 2.5H_2O$	**(e,e) : 2(a,e)**	**3**	I^1O^2	$^2D_2$, $^3D_3$ & $^4D_1$

3.6. References

1) C. N. R. Rao, S. Natarajan and R. Vaidhyanathan, *Angew. Chem. Int. Ed*., **2004**, 43, 1466.

2) D. W. Breck, *Zeolite Molecular Sieves*, Wiley, New York, **1974**

3) W. M. Meier, D. H. Oslen and C. Baerlocher, *Alas of Zeolite Structure types*, Elsevier, Londen, **1996**.

4) A K. Cheetham, G. Férey and T. Loiseau, *Angew. Chem. Int. Ed*., **1999**, 38, 3268.

5) G. Férey, C. M-Draznieks, C. Serre, F. Millange, J. Dutour, S. Surblé and I. Margiolaki, *Science*, **2005**, 309, 2040.

6) G. Férey, C. Serre, C. M-Draznieks, F. Millange, S. Surblé, J. Dutour and I. Margiolaki, *Angew. Chem. Int. Ed*., **2004**, 43, 6296.

7) B. Moulton and M. J. Zawarotko, *Chem. Rev*., **2001**, 101, 1629.

8) J. S. Seo, D. Whang, H. Lee, S. I. Jun, J. Oh, Y. J. Jeon and K. Kim, *Nature*, **2000**, 404, 982.

9) P. M. Forster and A. K. Cheetham, *Angew. Chem. Int. Ed*., **2002**, 41, 457.

10) R. Kitaura, K. Fujimoto, S. Noro, M. Kondo and S. Kitagawa, *Angew. Chem. Int. Ed*., **2002**, 41, 133.

11) N. L. Rosi, J. Eukert, M. Eddaoudi, D. T. Vodak, J. Kim, M. O'Keeffe and O. M. Yaghi, *Science*, **2003**, 300, 1127.

12) B. Paella and M. Hirscher, *Adv. Mater*., **2005**, 17, 538.

13) J. L. C. Rowsell and O. M. Yaghi, *Angew. Chem. Int. Ed*., **2005**, 44, 4670.

14) D. S. Kim, P. M. Forster, R. L. Toquin and A. K. Cheetham, *Chem. Commun*., **2004**, 2148.

15) L. Yi, B. Ding, B. Zhao, P. Cheng, D-Z. Liao, S-P. Yan and Z-H. Jiang, *Inorg. Chem*., **2004**, 43, 33.

16) O. M. Yaghi, H. L. Li, C. Davis, D. Richardson and T. L. Groy, *Acc. Chem. Res.*, **1998**, 31, 474.

17) M. Eddaoudi, J. Kim, D. Vodak, A. Sudik, J. Wachfer, M. O'Keeffe and O. M. Yaghi, *Proc. Natl. Acad. Sci, USA*, **2002**, 99, 4900.

18) M. Eddaoudi, J. Kim, D. Vodak, A. Sudik, J. Wachfer, M. O'Keeffe and O. M. Yaghi, *Science*, **2002**, 295, 4900.

19) D. T. Vodak M. E. Braun, J. Kim, M. Eddaoudi and O. M. Yaghi, *Chem. Commun.*, **2001**, 2532.

20) H. Li, C. E. Davis, T. L. Groy, D. G. Kelley and O. M. Yaghi, *J. Am. Chem. Soc*., **1998**, 120, 2186.

21) S. R. Miller, P. A. Wright, C. Serre, T. Loiseau, J. Marrot and G. Férey, *Chem. Commun.*, **2005**, 3850.

22) K. Barthelet, J. Marrot, G. Férey and D. Riou, *Chem. Commun.*, **2004**, 520.

23) C. Serre, F. Taulelle and G. Férey, *Chem. Commun*., **2003**, 2755.

24) F. Millange, C. Serre and G. Férey, *Chem. Commun.*, **2002**, 822.

25) C. Serre, F. Millange, C. Thouvenot, M. Noguès, G. Marsolier, D. Louër and G. Férey, *J. Am. Chem. Soc*, **2002**, 124, 13519.

26) S. A. Bourne, J. Lu, A. Mondal, B. Moulton and M. J. Zawarotko, *Angew. Chem. Int. Ed*., **2001**, 40, 2111.

27) B. Moulton, H. Abourahma, M. W. Bradner, J. Lu, G. J. McManus and M. J. Zaworotko, *Chem. Commun.*, **2003**, 1342.

28) Z. Lin, F. Jiang, L. Chen, D. Yaun and M. Hong, *Inorg. Chem*., **2005**, 44, 73.

29) M-B. Zhang, J. Zhang, S-T. Zheng and G-Y. Yang, *Angew. Chem. Int. Ed*., **2005**, 44, 1388.

30) Q. Fang, G. Zhu, M. Xue, J. Sun, G. Tian, G. Wu and S. Qiu, *Dalton Trans*., **2004**, 2202.

31) N. Guillou, C. Livage, W. van Beek, M. Nogues and G. Férey, *Angew. Chem. Int. Ed*., **2003**, 42, 644.

32) P. M. Forster and A. K. Cheetham, *Angew. Chem. Int. Ed*., **2003**, 42, 457.

33) R. Vaidhayanathan, S. Natarajan and C. N. R. Rao, Dalton Trans., **2003**, 1459.

34) A. Thirumurugan and S. Natarajan, *J. Mater. Chem.*, **2005**, 15, 4588.

35) A. K. Cheetham, C. N. R. Rao and R. K. Feller, *Chem. Commun*., **2006**, 4780.

36) B. Moulton, J. Lu, R. Hajndl, S. Hariharan and M. J. Zaworotko, *Angew. Chem. Int. Ed*., **2002**, 41, 2821.

37) J. L. C. Rowsell, A. R. Millward, K. S. Park and O. M. Yaghi, *J. Am. Chem. Soc*., **2004**, 126, 5666.

38) P. M. Forster, A. R. Burbank, C. Livage G. Férey and A. K. Cheetham, *Chem. Commun*., **2004**, 368.

39) S. H. Dale, M. R.J. Elsegood and S. Kainth, *Acta Cryst*., **2004**, C60, m76.

40) A. Thirumurugan and C. N. R. Rao, *J. Mater. Chem.,* **2005**, 15, 3852.

41) D. S. Kim, P. M. Forster, G. D. de Delgado, S-E. Park and A. K. Cheetham, *Dalton. Trans*., **2004**, 3365.

42) Y. J. Kim and D. Y. Jung, *Chem. Commun*., **2002**, 908.

43) M. Kurmoo, H. K. Kumagai, S. M. Hughes and C. J. Kepert, *Inorg. Chem*., **2003**, **42**, 6709.

44) Y. J. Qi, Y. H. Wang, C. W. Hu, M. H. Cao, L. Mao and E. B. Wang, *Inorg. Chem*., **2003**, 42, 73.

45) W. Bi, R. Cao, D. Sun, D. Yaun, X. Li, Y. Wang, X. Li and M. Hong, *Chem. Commun*., **2004**, 2104.

46) W. Bi, R. Cao, D. Sun, D. Yaun, X. Li and M. Hong, *Inorg. Chem. Commun*., **2003**, 6, 1426.

47) M. Du, H. Cai and X-J. Zhao, *Inorg. Chim. Acta*, **2005**, 358, 4034.

48) Y. Gong, C. W. Hu, H.Li, K. L. Huang and W. Tang, *J. Solid State Chem*., **2005**, 178, 3153.

49) M. Inoue, T. Atake, H. Kawaji and T. Tojo, *Solid State Commun*., **2005**, 134, 303.

50) Y-Z. Zheng, M-L. Tong, W-X. Zhang and X-M. Chen, *Chem. Commun*., **2006**, 165.

51) Y-Z. Zheng, M-L. Tong, W-X. Zhang and X-M. Chen, *Angew. Chem. Int. Ed*., **2006**, 45, 6310.

52) J. Chen, M. Ohba, D. Zhao, W. Kaneko and S. Kitagawa, *Cryst. Growth Des*., **2006**, 6, 664.

53) C. Lee, C. M-Draznieks, B. Slater, G. Wu, W. T. A. Harrison, C. N. R. Rao and A. K. Cheetham, *Chem. Comm*., **2006**, 2687.

54) H. Kumagai, M. A-Tanaka, K. Inoue, K. Takahashi, Hayao Kobayashi, S. Vilminot and M. Kurmoo, *Inorg. Chem*., **2007**, 46, 5949.

55) J. Yang, G-D. Li, J-J. Cao, Q. Yue, G-H. Li and J-S. Chen, *Chem.—Eur.J.,* **2007**, 13, 3248.

56) J. Lü, W-H. Bi, F-X. Xiao, S. R. Batten and R. Cao, *Chemistry - An Asian Journal*, **2008**, 3, 542.

57) S. Surblé, C. Serre, F. Millange, F. Pellé and G. Férey, *Solid State Sci.*, **2007**, 9, 131.

58) For description of conformations see, Nasipuri, D. *Stereochemistry of Organic Compounds: Principles and Applications*, Wiley: New York, **1991**.

59) S. Barbara, *Infrared Spectroscopy: Fundamentals and Applications*; Wiley: New York, **2004**.

60) R. M. Silverstein, G. C. Bassler and T. C. Morrill, *Spectrometric Identification of Organic Compounds*; John Wiley & Sons: New York, **1963.**

61) K. Nakamoto, *Infrared and Raman Spectra of Inorganic and Coordination Compounds*; Wiley: New York, **1978**.

62) G. M, Sheldrick, *SADABS Siemens Area Detector Absorption Correction Program*, University of Göttingen, Gottingen, Germany, **1994.**

63) G. M. Sheldrick, SHELXTL-PLUS *Program for Crystal Structure Solution and Refinement*, University of Göttingen, Gottingen, Germany, **1997**.

64) For description of connectivity see, D. Massiot, S. Drumel, P. Janvier, M. B Doeuff and B. Buujoli, *Chem Mater*., **1997**, 9, 6.

65) Gaussian 03, Revision C.02, M. J. Frisch, G. W. Trucks, H. B. Schlegel, G. E. Scuseria, M. A. Robb, J. R. Cheeseman, J. A. Montgomery, Jr., T. Vreven, K. N. Kudin, J. C. Burant, J. M. Millam, S. S. Iyengar, J. Tomasi, V. Barone, B. Mennucci, M. Cossi, G. Scalmani, N. Rega, G. A. Petersson, H. Nakatsuji, M. Hada, M. Ehara, K. Toyota, R. Fukuda, J. Hasegawa, M. Ishida, T. Nakajima, Y. Honda, O. Kitao, H. Nakai, M. Klene, X. Li, J. E. Knox, H. P. Hratchian, J. B. Cross, C. Adamo, J. Jaramillo, R. Gomperts, R. E. Stratmann, O. Yazyev, A. J. Austin, R. Cammi, C. Pomelli, J. W. Ochterski, P. Y. Ayala, K. Morokuma, G. A. Voth, P. Salvador, J. J. Dannenberg, V. G. Zakrzewski, S. Dapprich, A. D. Daniels, M. C. Strain, O. Farkas, D. K. Malick, A. D. Rabuck, K. Raghavachari, J. B. Foresman, J. V. Ortiz, Q. Cui, A. G. Baboul, S. Clifford, J. Cioslowski, B. B.

Stefanov, G. Liu, A. Liashenko, P. Piskorz, I. Komaromi, R. L. Martin, D. J. Fox, T. Keith, M. A. Al-Laham, C. Y. Peng, A. Nanayakkara, M. Challacombe, P. M. W. Gill, B. Johnson, W. Chen, M. W. Wong, C. Gonzalez and J. A. Pople, Gaussian Inc., Wallingford CT, **2004**.

66) D. Sun, R. Cao, Y. Liang, Q. Shi, W. Su, M. Hong, *J. Chem.Soc., Dalton Trans.* **2001**, 2335.

67) Y. Gong, H. Li, Y. G. Li, Y. H. Wang, W. Tang, C. W. Hu, *J. Coord. Chem*, **2007**, 60, 61.

68) Serguchev, Beletskaya, *Russ. Chem. Rev*., **1980**, 49, 1119.

69) Badanyan, Minasyan, vardapetyan, *Russ. Chem. Rev*., **1987**, 56, 740.

70) K. Kawamura, K. Ikushima, *Environ. Sci. Technol*., **1993**, 27, 2227.

3.7. Appendix

Table A3.1

Atomic Coordinates and Equivalent Isotropic Displacement Parameters [$Å^2$] for [Cd(1,3-CHDC)(1,10-phen)], **I**.

Atom	x	y	z	U(eq)
Cd1	0.28636	0.18776	0.64553	0.0414
Cd2	0.60403	0.25708	0.61849	0.0424
O1	0.28871	0.31935	0.67974	0.0616
O2	0.41433	0.29965	0.61291	0.0730
O3	0.25805	0.66867	0.74027	0.1030
O4	0.31153	0.57658	0.82039	0.0676
O5	0.78494	-0.12223	0.79428	0.1255
O6	0.79385	-0.14217	0.90846	0.0990
O7	0.48477	0.14163	0.67176	0.0849
O8	0.66051	0.18499	0.72620	0.0743
N1	0.10563	0.22543	0.55687	0.0430
N2	0.28137	0.13232	0.52844	0.0378
N3	0.52509	0.23692	0.48695	0.0424
N4	0.72097	0.16245	0.57308	0.0454
C1	0.01668	0.26755	0.57026	0.0601
C2	-0.08787	0.28582	0.51642	0.0608
C3	-0.10039	0.26278	0.44447	0.0570
C4	-0.00910	0.21862	0.42763	0.0460
C5	-0.01533	0.19179	0.35358	0.0637
C6	0.07291	0.15158	0.33880	0.0643
C7	0.17603	0.12794	0.39679	0.0496
C8	0.26799	0.08107	0.38416	0.0609
C9	0.36295	0.06050	0.44171	0.0611
C10	0.36534	0.08771	0.51403	0.0517
C11	0.18598	0.15195	0.47130	0.0384
C12	0.09255	0.19978	0.48617	0.0384
C21	0.42764	0.27312	0.44456	0.0538
C22	0.39052	0.26422	0.36711	0.0675
C23	0.45560	0.21850	0.33266	0.0675
C24	0.55649	0.17898	0.37456	0.0539
C25	0.62710	0.12777	0.34293	0.0718
C26	0.71981	0.08788	0.38461	0.0717
C27	0.75539	0.09837	0.46336	0.0564
C28	0.85941	0.06392	0.51054	0.0724
C29	0.89116	0.07780	0.58457	0.0730
C30	0.81946	0.12739	0.61395	0.0632
C31	0.69060	0.14974	0.49805	0.0404
C32	0.58951	0.18974	0.45348	0.0409
C41	0.36374	0.34441	0.64982	0.0490
C42	0.39992	0.42909	0.65570	0.0682
C43	0.38645	0.46540	0.58094	0.0935
C44	0.42083	0.55057	0.58624	0.0835
C45	0.35261	0.59543	0.63277	0.0860
C46	0.33517	0.47517	0.70326	0.0579
C47	0.36906	0.56086	0.70722	0.0786
C48	0.30569	0.60429	0.75792	0.0587
C51	0.75605	-0.10401	0.84969	0.0631
C52	0.67756	-0.03615	0.85251	0.1575
C53	0.63178	-0.01919	0.90713	0.1976
C54	0.54976	0.04527	0.90782	0.1260
C55	0.53556	0.09791	0.84094	0.2367

C56	0.66101	0.01936	0.78647	0.0741
C57	0.57807	0.08311	0.78532	0.1199
C58	0.57440	0.14021	0.72433	0.0501

U(eq) is defined as one third of the trace of the orthogonalized Uij tensor.

Table A3.2

Atomic Coordinates and Equivalent Isotropic Displacement Parameters [Å^2] for [Mn(H_2O)(1,3-CHDC)(1,10-phen)], **II**.

Atom	x	y	z	U(eq)
Mn1	0.70422(9)	-0.01029(5)	0.21103(7)	0.0592(3)
O1	0.8427(4)	0.0867(3)	0.1841(4)	0.0809(17)
O2	0.6759(4)	0.0502(3)	0.0347(3)	0.0704(17)
O3	1.1424(4)	0.0914(3)	-0.2038(4)	0.0855(19)
O4	1.2644(5)	0.1732(3)	-0.0745(5)	0.0899(19)
O5	0.5431(5)	-0.0935(3)	0.1446(4)	0.0647(17)
N1	0.7527(5)	-0.0122(3)	0.4103(4)	0.0696(19)
N2	0.5498(5)	0.0693(3)	0.2646(5)	0.0682(19)
C1	0.8532(7)	-0.0534(4)	0.4806(7)	0.093(3)
C2	0.8827(11)	-0.0463(7)	0.6055(8)	0.130(5)
C3	0.8085(16)	0.0019(8)	0.6550(9)	0.154(7)
C4	0.7011(12)	0.0454(6)	0.5833(7)	0.110(4)
C5	0.6163(17)	0.0988(10)	0.6290(12)	0.168(9)
C6	0.5189(15)	0.1374(9)	0.5590(14)	0.165(8)
C7	0.4908(10)	0.1327(5)	0.4312(9)	0.105(4)
C8	0.3888(11)	0.1749(5)	0.3497(14)	0.131(6)
C9	0.3696(9)	0.1626(5)	0.2327(11)	0.122(5)
C10	0.4504(8)	0.1092(4)	0.1929(8)	0.095(3)
C11	0.5695(7)	0.0807(4)	0.3833(6)	0.071(2)
C12	0.6762(8)	0.0373(4)	0.4593(6)	0.078(3)
C21	0.7787(7)	0.0923(4)	0.0779(6)	0.066(3)
C22	0.8270(7)	0.1485(4)	-0.0020(7)	0.089(3)
C23	0.8240(11)	0.2243(5)	0.0260(10)	0.150(6)
C24	0.8669(9)	0.2774(4)	-0.0642(10)	0.138(5)
C25	1.0090(10)	0.2518(5)	-0.0853(10)	0.146(5)
C26	0.9654(6)	0.1218(3)	-0.0272(6)	0.067(3)
C27	1.0147(8)	0.1756(4)	-0.1119(8)	0.096(3)
C28	1.1525(7)	0.1444(4)	-0.1314(7)	0.074(3)

U(eq) is defined as one third of the trace of the orthogonalized Uij tensor.

Table A3.3

Atomic Coordinates and Equivalent Isotropic Displacement Parameters [Å^2] for [Mn_3(1,3-CHDC)$_3$(1,10-phen].4H_2O, **III**.

Atom	x	y	z	U(eq)
Mn1	1	0.12699(5)	1/4	0.0344(4)
Mn2	1.05886(10)	0.15941(4)	0.12448(3)	0.0456(3)
O1	0.8482(4)	0.0887(2)	0.10197(14)	0.0566(14)
O2	0.8758(4)	0.12796(19)	0.17685(14)	0.0484(14)
O3	0.1610(5)	0.0634(2)	0.21587(15)	0.0608(16)
O4	0.1979(5)	0.0795(2)	0.13484(15)	0.0620(16)
O5	1.2468(8)	0.2185(3)	0.15423(19)	0.101(3)
O6	1.1507(9)	0.1997(3)	0.2251(3)	0.142(4)
N1	0.9233(5)	0.2432(2)	0.09765(18)	0.0487(17)
N2	1.1087(5)	0.1689(2)	0.04282(16)	0.0404(16)
C1	0.8331(8)	0.2784(3)	0.1246(3)	0.065(3)
C2	0.7541(9)	0.3298(4)	0.1057(4)	0.079(3)
C3	0.7724(9)	0.3451(3)	0.0567(4)	0.075(3)
C4	0.8698(7)	0.3092(3)	0.0267(3)	0.057(2)

C5	0.8957(8)	0.3218(3)	-0.0250(3)	0.067(3)
C6	0.9895(8)	0.2853(3)	-0.0517(3)	0.065(3)
C7	1.0629(7)	0.2321(3)	-0.0309(2)	0.0485(19)
C8	1.1602(8)	0.1917(3)	-0.0574(2)	0.059(2)
C9	1.2259(8)	0.1416(3)	-0.0343(2)	0.059(3)
C10	1.1979(7)	0.1318(3)	0.0159(2)	0.051(2)
C11	1.0410(6)	0.2183(3)	0.0198(2)	0.0404(17)
C12	0.9422(6)	0.2578(3)	0.0487(2)	0.0438(19)
C21	0.8122(6)	0.0886(3)	0.1471(2)	0.0437(19)
C22	0.6924(6)	0.0445(3)	0.1670(2)	0.0457(19)
C23	0.6961(7)	-0.0199(3)	0.1433(3)	0.064(3)
C24	0.5708(8)	-0.0614(3)	0.1643(3)	0.075(3)
C25	0.4066(7)	-0.0328(3)	0.1579(3)	0.060(3)
C26	0.5276(6)	0.0723(3)	0.1594(2)	0.0436(17)
C27	0.4016(6)	0.0310(3)	0.1816(2)	0.0407(19)
C28	0.2416(6)	0.0604(3)	0.1777(2)	0.0410(17)
C31	1.2480(7)	0.2231(3)	0.1991(2)	0.046(2)
C32	1.3743(10)	0.2597(4)	0.2236(3)	0.091(2)
C33	1.3771(11)	0.3220(3)	0.2235(5)	0.142(5)
C34	3/2	0.3590(5)	1/4	0.119(7)
C35	3/2	0.2239(4)	1/4	0.045(3)
O100	0.762(3)	0.0165(4)	0.0165(4)	0.432(14)
O200	0.5711(13)	0.4791(4)	0.0673(4)	0.196(6)

U(eq) is defined as one third of the trace of the orthogonalized Uij tensor.

Table A3.4

Atomic Coordinates and Equivalent Isotropic Displacement Parameters [$Å^2$] for $[Mn_3(1,4\text{-CHDC})_3(1,10\text{-phen}].4H_2O$, **IV**.

Atom	x	y	z	U(eq)
Mn1	1	0	1	0.0221(1)
Mn2	0.95998(4)	0.19229(3)	0.73577(2)	0.0270(1)
O1	0.8250(2)	0.07532(15)	0.85248(13)	0.0435(5)
O2	0.8245(2)	0.09104(19)	0.67423(15)	0.0574(7)
O3	0.1835(2)	-0.01512(18)	0.88014(16)	0.0602(7)
O4	0.1912(2)	0.06219(16)	0.70285(15)	0.0536(6)
O5	1.0239(2)	-0.18727(13)	1.00031(13)	0.0397(5)
O6	0.9570(2)	-0.28127(13)	1.16183(12)	0.0377(5)
N1	0.7227(2)	0.36398(18)	0.71685(16)	0.0379(6)
N2	0.9473(2)	0.31062(16)	0.56296(14)	0.0321(6)
C1	0.6133(3)	0.3899(3)	0.7927(2)	0.0529(10)
C2	0.4789(3)	0.5027(3)	0.7757(3)	0.0658(13)
C3	0.4586(3)	0.5890(3)	0.6791(3)	0.0637(13)
C4	0.5711(3)	0.5665(2)	0.5965(3)	0.0501(9)
C5	0.5598(4)	0.6524(2)	0.4916(3)	0.0627(10)
C6	0.6713(4)	0.6263(3)	0.4164(3)	0.0593(10)
C7	0.8063(3)	0.5101(2)	0.4363(2)	0.0450(8)
C8	0.9280(4)	0.4781(3)	0.3610(2)	0.0523(10)
C9	1.0485(4)	0.3655(3)	0.3842(2)	0.0510(10)
C10	1.0564(3)	0.2834(2)	0.48635(19)	0.0403(8)
C11	0.8215(3)	0.42203(19)	0.53787(18)	0.0338(7)
C12	0.7027(3)	0.4505(2)	0.6203(2)	0.0370(7)
C21	0.7858(3)	0.0474(2)	0.76799(18)	0.0315(6)
C22	0.6944(3)	-0.0394(2)	0.77873(18)	0.0330(7)
C23	0.5854(3)	-0.0115(3)	0.67670(19)	0.0456(9)
C24	0.5980(3)	-0.0463(3)	0.8817(2)	0.0645(12)
C25	0.5244(3)	-0.1450(3)	0.8913(3)	0.0808(11)
C26	0.5048(3)	-0.1057(3)	0.6848(3)	0.0612(11)
C27	0.4145(3)	-0.1207(2)	0.7910(2)	0.0411(8)
C28	0.2527(2)	-0.01612(19)	0.79077(18)	0.0301(6)

C31	0.9836(3)	-0.27156(18)	1.05990(18)	0.0294(6)
C32	0.9750(3)	-0.37130(18)	1.00434(17)	0.0291(6)
C33	1.1451(3)	-0.47088(19)	1.00996(19)	0.0334(7)
C34	0.8554(3)	-0.43138(19)	1.05272(18)	0.0333(7)
O100	0.8872(3)	0.2479(2)	0.2219(2)	0.0785(10)
O200	0.8435(3)	0.1105(2)	0.43731(18)	0.0760(9)

U(eq) is defined as one third of the trace of the orthogonalized Uij tensor.

Table A3.5

Atomic Coordinates and Equivalent Isotropic Displacement Parameters [$Å^2$] for $[Cd_3(1,4\text{-CHDC})_3(1,10\text{-phen})_2].4H_2O$, **V**.

Atom	x	y	z	U(eq)
Cd1	0	1	1/2	0.0213(1)
Cd2	-0.15146(2)	0.80803(2)	0.23347(2)	0.0251(1)
O1	0.0955(3)	0.9200(3)	0.1775(2)	0.0525(9)
O2	0.1136(3)	0.9213(2)	0.3521 (2)	0.0398(8)
O3	0.8313(3)	1.0040(3)	0.3615(2)	0.0582(10)
O4	0.7340(3)	0.9404(2)	0.1897(2)	0.0529(10)
O5	-0.3299(3)	0.7160(1)	0.3419(1)	0.0387(8)
O6	-0.1650(3)	0.8069(2)	0.5006(2)	0.0418(8)
N1	-0.0877(3)	0.6294(3)	0.2120(2)	0.0356(9)
N2	-0.2573(3)	0.6816(2)	0.0566(2)	0.0308(8)
C1	-0.0049(5)	0.6045(4)	0.2868(3)	0.0485(12)
C2	0.0179(5)	0.4934(4)	0.2697(4)	0.0592(16)
C3	-0.0481(5)	0.4061(4)	0.1748(4)	0.0561(14)
C4	-0.1376(4)	0.4276(3)	0.0932(3)	0.0456(14)
C5	-0.2122(5)	0.3398(3)	-0.0104(4)	0.0565(16)
C6	-0.2983(5)	0.3638(3)	-0.0848(3)	0.0550(14)
C7	-0.3172(4)	0.4806(3)	-0.0667(3)	0.0428(11)
C8	-0.4052(5)	0.5099(4)	-0.1418(3)	0.0500(11)
C9	-0.4129(4)	0.6233(4)	-0.1200(3)	0.0490(14)
C10	-0.3379(4)	0.7068(3)	-0.0191(3)	0.0397(11)
C11	-0.2437(4)	0.5703(3)	0.0342(3)	0.0317(10)
C12	-0.1539(4)	0.5431(3)	0.1162(3)	0.0328(10)
C21	0.1771(4)	0.9573(3)	0.2698(3)	0.0309(10)
C22	0.3525(4)	1.0450(3)	0.2832(3)	0.0345(10)
C23	0.4561(4)	1.0455(5)	0.3815(3)	0.0595(16)
C24	0.4322(4)	1.0253(4)	0.1788(3)	0.0424(11)
C25	0.6057(4)	1.1196(4)	0.1908(4)	0.0600(18)
C26	0.6276(5)	1.1436(5)	0.3936(4)	0.0769(18)
C27	0.7098(4)	1.1241(3)	0.2914(3)	0.0420(13)
C28	0.7608(3)	1.0159(3)	0.2808(3)	0.0291(10)
C41	-0.2904(4)	0.7257(3)	0.4411(3)	0.0297(10)
C42	-0.3973(4)	0.6277(3)	0.4966(3)	0.0281(9)
C43	-0.5749(4)	0.5675(3)	0.4466(3)	0.0317(10)
C44	-0.3262(4)	0.5293(3)	0.4923(3)	0.0319(10)
O100	0.1348(5)	0.2464(3)	0.2762(3)	0.0813(14)
O200	0.9494(5)	0.1100(3)	0.0591(3)	0.0775(14)

U(eq) is defined as one third of the trace of the orthogonalized Uij tensor.

Table A3.6

Atomic Coordinates and Equivalent Isotropic Displacement Parameters [$Å^2$] for $[Cd(1,4\text{-CHDC})(2,2'\text{-bipy})].H_2O$, **VI**.

Atom	x	y	z	U(eq)
Cd1	0.34662(1)	0.2163(2)	0.05786(1)	0.0325(1)
O1	0.3886(2)	0.3913(3)	0.11854(17)	0.0659(13)
O2	0.3249(2)	0.2710(3)	0.17667(19)	0.0616(12)
O3	0.2930 (2)	0.6915(3)	0.45525(15)	0.0461(9)

O4	0.4163(2)	0.7100(2)	0.44791(18)	0.0531(11)
N1	0.3433(2)	0.0283(3)	0.01815(17)	0.0374(10)
N2	0.4600(2)	0.1217(3)	0.10955(17)	0.0405(11)
C1	0.2846(3)	-0.0139(4)	-0.0283(2)	0.0475(12)
C2	0.2825(3)	-0.1246(4)	-0.0516(3)	0.0573(17)
C3	0.3434(3)	-0.1936(4)	-0.0263(3)	0.0586(16)
C4	0.4039(3)	-0.1519(3)	0.0208(3)	0.0516(16)
C5	0.4026(2)	-0.0392(3)	0.0431(2)	0.0359(12)
C6	0.4655(2)	0.0107(3)	0.0950(2)	0.0379(12)
C7	0.5279(3)	-0.0519(4)	0.1273(3)	0.0596(17)
C8	0.5844(3)	-0.0006(5)	0.1765(3)	0.070(2)
C9	0.5787(3)	0.1123(4)	0.1905(3)	0.0633(19)
C10	0.5159(3)	0.1704(4)	0.1558(3)	0.0535(17)
C11	0.3584(3)	0.3639(4)	0.1738(2)	0.0479(16)
C12	0.3687(4)	0.4411(4)	0.2412(3)	0.072(2)
C13	0.3819(4)	0.5580(5)	0.2295(3)	0.091(3)
C14	0.3108(3)	0.4156(4)	0.2944(3)	0.0712(19)
C15	0.3197(5)	0.4927(5)	0.3610(3)	0.107(3)
C16	0.3908(4)	0.6319(4)	0.2973(3)	0.074(2)
C17	0.3383(3)	0.6078(5)	0.3507(3)	0.072(2)
C18	0.3514(2)	0.6740(3)	0.4219(2)	0.0409(14)

U(eq) is defined as one third of the trace of the orthogonalized Uij tensor.

Table A3.7

Atomic Coordinates and Equivalent Isotropic Displacement Parameters [$Å^2$] for [$Cd(H_2O)_2$(1,3-CHDC)].H_2O, **VII**.

Atom	x	y	z	U(eq)
Cd1	0.3536(3)	-0.0115(2)	0.4869(4)	0.0301(1)
O1	0.3744(3)	0.0706(2)	0.3133(4)	0.0340(14)
O2	0.2439(3)	0.0279(2)	0.1869(4)	0.0350(14)
O3	0.4905(3)	0.0513(2)	-0.3908(5)	0.0407(14)
O4	0.6163(3)	0.0956(2)	-0.2627(5)	0.0427(14)
O5	0.2110(3)	-0.0820(2)	0.4762(5)	0.0433(14)
O6	0.4065(3)	-0.0893(2)	0.6854(5)	0.0427(17)
C1	0.5222(4)	0.0893(3)	-0.2869(6)	0.0273(19)
C2	0.4461(4)	0.1253(3)	-0.1851(6)	0.0277(17)
C3	0.4824(5)	0.1916(3)	-0.1264(7)	0.037(2)
C4	0.4010(5)	0.2244(3)	-0.0288(7)	0.041(2)
C5	0.3713(5)	0.1809(3)	0.1102(7)	0.038(2)
C6	0.4179(4)	0.0809(3)	-0.0476(6)	0.0257(17)
C7	0.3375(4)	0.1133(3)	0.0583(6)	0.0263(17)
C8	0.3158(4)	0.0676(3)	0.1941(6)	0.0250(17)
O100	0.6836(11)	0.2066(6)	0.4975(2)	0.236(9)
O200	0.7239(14)	0.2032(7)	0.2616(2)	0.265(10)

U(eq) is defined as one third of the trace of the orthogonalized Uij tensor.

Table A3.8

Atomic Coordinates and Equivalent Isotropic Displacement Parameters [$Å^2$] for (OPb_3)(1,3-CHDC)$_2$, **VIII**.

Atom	x	y	z	U(eq)
Pb1	0.39424(3)	0.4530(3)	0.4343(3)	0.0302(2)
Pb2	0.44610(4)	0.5360(4)	0.1461(3)	0.0416(2)
Pb3	0.39821(3)	0.3013(3)	0.04432(3)	0.0323(1)
O1	0.4104(7)	0.3754(7)	0.1795(5)	0.052(4)
O2	0.4046(6)	0.4230(6)	0.2893(5)	0.040(3)
O3	0.0858(7)	0.1150(7)	0.1248(5)	0.051(3)
O4	0.1432(7)	0.2414(8)	0.0878(5)	0.057(4)
O5	0.2394(7)	-0.1188(8)	0.5108(7)	0.072(4)
O6	0.2143(7)	0.0054(9)	0.4311(7)	0.077(5)
O7	0.4423(7)	0.2685(7)	0.4623(6)	0.051(4)

O8	0.3850(8)	0.3307(7)	0.5404(7)	0.069(5)
O9	0.5399(5)	0.4547(5)	0.4510(4)	0.024(2)
C1	0.3836(8)	0.3655(9)	0.2335(7)	0.032(4)
C2	0.3197(9)	0.2799(9)	0.2232(7)	0.036(4)
C3	0.3641(10)	0.1953(10)	0.2745(9)	0.054(5)
C4	0.2992(10)	0.1101(9)	0.2644(9)	0.052(5)
C5	0.2176(10)	0.1421(10)	0.2747(8)	0.050(5)
C6	0.2357(8)	0.3129(9)	0.2324(7)	0.034(4)
C7	0.1714(9)	0.2275(9)	0.2211(6)	0.036(4)
C8	0.1310(8)	0.1902(9)	0.1398(7)	0.032(4)
C11	0.2629(11)	-0.0453(12)	0.4843(8)	0.052(5)
C12	0.3589(11)	-0.0167(11)	0.5201(9)	0.060(6)
C13	0.4025(15)	-0.0352(13)	0.6029(10)	0.100(9)
C14	0.3938(19)	0.0564(12)	0.6484(12)	0.168(19)
C15	0.4303(18)	0.1494(14)	0.6230(10)	0.119(12)
C16	0.3833(17)	0.0718(11)	0.4889(10)	0.141(13)
C17	0.391(2)	0.1642(11)	0.5391(11)	0.136(14)
C18	0.4119(13)	0.2583(11)	0.5125(9)	0.061(6)

U(eq) is defined as one third of the trace of the orthogonalized Uij tensor.

Table A3.9

Atomic Coordinates and Equivalent Isotropic Displacement Parameters [Å^2] for [Cd(H_2O)$_2$(1,4-CHDC)], **IX**.

Atom	x	y	z	U(eq)
Cd1	1/2	0.1398(8)	1/4	0.0271(2)
O1	0.4856(3)	0.4247(7)	0.1481(2)	0.0344(12)
O2	0.3169(4)	0.3018(8)	0.1711(3)	0.0405(14)
O3	0.6052(4)	-0.1670(8)	0.2138(3)	0.0412(17)
C1	0.3742(5)	0.4389(11)	0.1340(3)	0.0333(17)
C2	0.3115(7)	0.6313(14)	0.0743(6)	0.062(3)
C3	0.3751(7)	0.721(2)	0.0179(7)	0.105(5)
C4	0.1844(7)	0.5905(19)	0.0422(6)	0.080(3)

U(eq) is defined as one third of the trace of the orthogonalized Uij tensor.

Table A3.10

Atomic Coordinates and Equivalent Isotropic Displacement Parameters [Å^2] for [Cd(1,2-CHDC)], **X**.

Atom	x	y	z	U(eq)
Cd1	0.2522(2)	0.3080(2)	0.1433(5)	0.0202(3)
O1	0.2001(3)	0.1388(14)	0.2524(5)	0.023(2)
O2	0.1832(3)	0.5513(13)	0.3025(6)	0.028(2)
O3	0.2044(3)	-0.1011(15)	0.5095(5)	0.0229(19)
O4	0.2216(3)	0.2739(14)	0.5974(6)	0.023(2)
C1	0.1354(4)	0.199(2)	0.3638(8)	0.026(3)
C2	0.1468(4)	0.2602(19)	0.4819(8)	0.018(2)
C3	0.1052(4)	0.169(3)	0.5455(9)	0.037(4)
C4	0.0560(5)	0.277(3)	0.4999(12)	0.048(5)
C5	0.0446(5)	0.228(3)	0.3829(12)	0.049(5)
C6	0.0857(4)	0.310(3)	0.3190(10)	0.041(4)
C7	0.1762(3)	0.3042(19)	0.3021(7)	0.017(2)
C8	0.1936(4)	0.143(2)	0.5319(7)	0.020(3)

U(eq) is defined as one third of the trace of the orthogonalized Uij tensor.

Table A3.11A

Atomic Coordinates and Equivalent Isotropic Displacement Parameters [Å^2] for Cd(1,2-CHeDC)(H_2O), **XI-A**.

Atom	x	y	z	U(eq)
Cd1	0.05137(5)	0.21041(4)	0.42721(12)	0.0182(2)
O1	0.1309(8)	0.3797(5)	0.4121(15)	0.027(2)
O2	0.2145(9)	0.3330(8)	0.1491(15)	0.044(3)

O3	0.1166(9)	0.5852(7)	0.0440(13)	0.035(3)
O4	0.0882(7)	0.7591(10)	0.1707(16)	0.024(2)
O5	0.1401(13)	0.0724(8)	0.2670(13)	0.049(3)
C1	0.2076(13)	0.3938(9)	0.2809(15)	0.032(3)
C2	0.3086(11)	0.4987(9)	0.2898(16)	0.028(3)
C3	0.4066(12)	0.5074(10)	0.1339(15)	0.031(3)
C4	0.4965(14)	0.6055(10)	0.1630(18)	0.036(4)
C5	0.4626(12)	0.6856(11)	0.2833(19)	0.032(4)
C6	0.3366(11)	0.6897(8)	0.409(4)	0.046(5)
C7	0.2345(13)	0.6044(9)	0.3344(16)	0.029(3)
C8	0.1417(10)	0.6458(7)	0.1767(13)	0.017(2)

U(eq) is defined as one third of the trace of the orthogonalized Uij tensor.

Table A3.11B

Atomic Coordinates and Equivalent Isotropic Displacement Parameters [Å^2] for Cd(1,2-CHeDC)(H_2O), **XI-B**.

Atom	x	y	z	U(eq)
Cd1	-0.21042(2)	0.00576(2)	0.27568(1)	0.0198(1)
O1	-0.16619(16)	0.2195(3)	0.35686(10)	0.0317(7)
O2	-0.11941(19)	0.4885(2)	0.31566(13)	0.0312(8)
O3	0.24120(14)	0.2658(2)	0.29458(12)	0.0217(7)
O4	0.08683(15)	0.1179(3)	0.30774(10)	0.0268(7)
O5	-0.0732(2)	-0.1575(4)	0.31917(16)	0.0469(10)
C1	-0.1032(2)	0.3518(4)	0.35455(14)	0.0221(9)
C2	-0.0049(2)	0.3673(4)	0.40172(13)	0.0206(9)
C3	0.0064(2)	0.2121(4)	0.45319(15)	0.0273(10)
C4	0.1045(2)	0.2405(4)	0.49745(16)	0.0298(10)
C5	0.1840(3)	0.3560(4)	0.48271(16)	0.0294(11)
C6	0.1891(3)	0.4658(4)	0.41895(17)	0.0277(10)
C7	0.1040(2)	0.4065(3)	0.36554(13)	0.0193(8)
C8	0.1451(2)	0.2515(3)	0.32106(14)	0.0194(8)

U(eq) is defined as one third of the trace of the orthogonalized Uij tensor.

Table A3.12

Atomic Coordinates and Equivalent Isotropic Displacement Parameters [Å^2] for Pb(1,3-CHDC)(H_2O), **XII**.

Atom	x	y	z	U(eq)
Pb1	-0.14977(2)	0.52421(3)	0.00456(1)	0.0221(1)
O1	-0.1115(4)	0.7323(7)	0.0608(2)	0.035(2)
O2	0.0076(4)	0.5985(7)	0.0362 (2)	0.0303(19)
O3	0.0895(4)	1.2763(8)	0.0425(3)	0.052(3)
O4	0.2380(4)	1.2124(8)	0.0305(2)	0.041(2)
O5	-0.3003(5)	0.5178(8)	0.0600(2)	0.041(3)
O6	-0.0988(4)	0.2959(8)	0.0598(2)	0.033(2)
C1	-0.0236(6)	0.7054(10)	0.0580(3)	0.025(3)
C2	0.0467(5)	0.8048(9)	0.0815(3)	0.021(2)
C3	0.0109(6)	0.8586(11)	0.1241(3)	0.031(3)
C4	0.0833(7)	0.9602(10)	0.1457(3)	0.037(3)
C5	0.1088(7)	1.0955(11)	0.1180(3)	0.036(3)
C6	0.0722(5)	0.9400(9)	0.0530(3)	0.024(3)
C7	0.1427(6)	1.0485(10)	0.0743(3)	0.027(3)
C8	0.1595(6)	1.1863(10)	0.0475(3)	0.028(3)
Pb2	0.25042(2)	0.15786(4)	0.35360(1)	0.0235(1)
O11	0.1638(4)	0.2064(7)	0.29025(2)	0.034(2)
O12	0.1975(4)	0.4200(7)	0.32192(2)	0.0303(17)
O13	-0.1107(4)	0.2325(7)	0.1838(2)	0.040(2)
O14	-0.1149(4)	0.4266(8)	0.13875(2)	0.0343(19)
C11	0.1613(5)	0.3471(10)	0.2914(3)	0.023(3)
C12	0.1176(5)	0.4336(9)	0.2548(3)	0.023(2)
C13	0.1981(6)	0.4797(11)	0.2245(3)	0.034(3)
C14	0.1590(7)	0.5681(11)	0.1874(3)	0.037(3)

C15	0.0810(6)	0.4813(10)	0.1640(3)	0.028(3)
C16	0.0400(6)	0.3458(10)	0.2317(3)	0.026(3)
C17	0.0005(5)	0.4371(10)	0.1946(2)	0.023(3)
C18	-0.0809(6)	0.3578(11)	0.1707(3)	0.031(3)

U(eq) is defined as one third of the trace of the orthogonalized Uij tensor.

Table A3.13
Atomic Coordinates and Equivalent Isotropic Displacement Parameters [Å^2] for $[(OPb_4)_2(OH)_2(C_2O_4)(1,3\text{-CHDC})_4].H_2O$, **XIII**.

Atom	x	y	z	U(eq)
Pb1	0.59283(8)	0	0.36909(6)	0.0324(2)
Pb2	0.29626(6)	0.09086(2)	0.38741(5)	0.0348(2)
Pb3	1/2	0.21425(2)	1/2	0.0355(2)
O1	0.5155(13)	0.0935(4)	0.2715(11)	0.055(4)
O2	0.6141(13)	0.1398(3)	0.4195(10)	0.048(4)
O3	1.2845(13)	0.1816(4)	0.3211(11)	0.057(4)
O4	1.1572(14)	0.2371(4)	0.3771(12)	0.064(4)
O5	1/2	0.0470(4)	1/2	0.029(3)
O6	0.8596(11)	0.0454(3)	0.4635(11)	0.049(3)
O7	0.261(2)	0	0.2937(19)	0.104(11)
C1	0.6106(17)	0.1244(5)	0.3172(14)	0.041(5)
C2	0.723(2)	0.1443(7)	0.2453(15)	0.062(6)
C3	0.640(3)	0.1693(11)	0.154(2)	0.118(12)
C4	0.757(3)	0.1852(14)	0.074(2)	0.164(16)
C5	0.902(3)	0.2123(9)	0.153(2)	0.090(10)
C6	0.8852(16)	0.1644(5)	0.3194(12)	0.035(4)
C7	0.9952(19)	0.1845(7)	0.2437(13)	0.053(6)
C8	1.1573(16)	0.2028(5)	0.3203(12)	0.036(4)
C11	1	0.0260(6)	1/2	0.035(6)
O100	0	0	0	0.21(3)

U(eq) is defined as one third of the trace of the orthogonalized Uij tensor.

Table A3.14
Atomic Coordinates and Equivalent Isotropic Displacement Parameters [Å^2] for $Pb_2(1,3\text{-CHDC})_2(H_2O)$, **XIV**.

Atom	x	y	z	U(eq)
Pb1	0.46506(4)	0.09979(3)	0.16941(3)	0.0274(1)
Pb2	0.26306(4)	-0.00070(3)	0.50908(3)	0.0280(1)
O1	0.2065(9)	-0.0971(10)	0.0806(7)	0.059(3)
O2	0.2364(9)	-0.0441(12)	0.2756(7)	0.073(3)
O3	-0.4010(7)	-0.0553(7)	0.2697(5)	0.033(2)
O4	-0.4548(8)	-0.1057(8)	0.0736(6)	0.038(2)
O5	1.1165(10)	0.8152(9)	0.6238(8)	0.064(3)
O6	0.9475(10)	0.8332(9)	0.4746(7)	0.059(3)
O7	0.5628(12)	0.3115(11)	0.3465(9)	0.081(4)
O8	0.5655(10)	0.1481(9)	0.4679(11)	0.076(4)
O9	0.7523(9)	0.2192(9)	0.1399(7)	0.043(2)
C1	0.1561(10)	-0.1141(11)	0.1798(8)	0.033(3)
C2	-0.0055(10)	-0.2117(10)	0.1850(8)	0.029(3)
C3	-0.0608(12)	-0.3411(11)	0.0879(9)	0.041(3)
C4	-0.2246(12)	-0.4335(10)	0.0991(9)	0.041(3)
C5	-0.3351(10)	-0.3437(10)	0.0874(9)	0.034(3)
C6	-0.1168(9)	-0.1226(9)	0.1749(7)	0.025(3)
C7	-0.2830(9)	-0.2162(9)	0.1819(7)	0.024(2)
C8	-0.3868(9)	-0.1225(9)	0.1736(7)	0.022(2)
C21	0.9865(12)	0.7695(10)	0.5626(8)	0.040(3)
C22	0.869(2)	0.6443(16)	0.6034(11)	0.117(7)
C23	0.817(2)	0.6525(15)	0.7116(13)	0.094(6)
C24	0.7169(17)	0.5182(16)	0.7520(11)	0.072(5)

C25	0.631(2)	0.4029(16)	0.6571(16)	0.115(8)
C26	0.7926(11)	0.5242(9)	0.5062(8)	0.032(3)
C27	0.6869(19)	0.3935(13)	0.5477(11)	0.077(5)
C28	0.6061(14)	0.2739(12)	0.4494(14)	0.059(5)

U(eq) is defined as one third of the trace of the orthogonalized Uij tensor.

Table A3.15

Atomic Coordinates and Equivalent Isotropic Displacement Parameters [Å^2] for [(OPb_3)(1,4-CHDC)$_2$], **XV**.

Atom	x	y	z	U(eq)
Pb1	0.29820(2)	0.16597(2)	0.51758(2)	0.0168(1)
Pb2	0.42330(3)	0.26042(2)	0.35324(2)	0.0193(1)
Pb3	0.15157(2)	0.21614(2)	0.30218(2)	0.0187(1)
O1	0.4278(5)	0.1393(3)	0.3778(5)	0.029(2)
O2	0.3476(6)	0.1681(3)	0.2560(5)	0.033(3)
O3	0.2007(7)	-0.1853(4)	0.2615(5)	0.041(3)
O4	0.3539(6)	-0.1675(4)	0.2034(5)	0.038(3)
O5	0.1097(6)	0.1241(3)	0.5623(5)	0.034(2)
O6	0.1493(5)	0.1196(3)	0.4249(4)	0.031(2)
O7	0.4634(5)	0.2426(4)	0.5148(4)	0.027(2)
O8	0.5290(5)	0.2655(4)	0.6440(5)	0.033(3)
O9	0.2712(4)	0.2445(3)	0.4113(4)	0.0137(17)
C1	0.3796(7)	0.1249(5)	0.3063(7)	0.026(3)
C2	0.3650(8)	0.0532(5)	0.2849(7)	0.027(3)
C3	0.2777(14)	0.0403(6)	0.2235(13)	0.088(7)
C4	0.368(2)	0.0096(7)	0.3589(10)	0.111(11)
C5	0.3641(19)	-0.0625(7)	0.3327(11)	0.109(8)
C6	0.2775(13)	-0.0317(5)	0.1958(10)	0.071(6)
C7	0.2725(10)	-0.0778(6)	0.2705(10)	0.055(5)
C8	0.2741(9)	-0.1484(6)	0.2445(7)	0.036(4)
C11	0.0901(8)	0.1065(4)	0.4862(7)	0.027(3)
C12	-0.0075(7)	0.0676(5)	0.4642(7)	0.029(3)
C13	0.0149(9)	0.0082(6)	0.4083(7)	0.038(4)
C14	-0.0684(8)	0.0462(5)	0.5412(8)	0.039(4)
C21	0.5384(7)	0.2537(4)	0.5655(7)	0.021(3)
C22	0.6461(10)	0.2515(9)	0.5316(12)	0.081(7)
C23	0.6717(8)	0.2015(6)	0.4718(8)	0.039(4)
C24	0.7208(8)	0.2980(6)	0.5632(8)	0.034(4)

U(eq) is defined as one third of the trace of the orthogonalized Uij tensor.

Table A3.16

Atomic Coordinates and Equivalent Isotropic Displacement Parameters [Å^2] for [La_2(1,4-CHDC)$_3$(H_2O)$_4$], **XVI**.

Atom	x	y	z	U(eq)
La1	0.46251(2)	0.16831(2)	0.0270 (2)	0.0157(1)
La2	1.48860(2)	0.43076(2)	0.3191 (2)	0.0158(1)
O1	0.6060(3)	0.0472(3)	-0.0240(3)	0.0243(10)
O2	0.6424(3)	0.2295(3)	-0.0387(3)	0.0281(10)
O3	1.2187(3)	0.1355(3)	-0.0295(3)	0.0397(11)
O4	1.3390(3)	0.2633(3)	0.1402(3)	0.0285(10)
O5	0.3297(3)	0.0917(3)	-0.2001(3)	0.0289(10)
O6	0.2465(4)	0.2318(3)	-0.2866(3)	0.0383(11)
O7	0.4034(3)	0.3448(3)	-0.0684(3)	0.0284(11)
O8	0.6271(4)	0.1250(3)	0.2246(3)	0.0440(14)
O11	0.7197(3)	0.4878(3)	0.3400(3)	0.0421(11)
O12	0.6033(3)	0.3531(3)	0.1771(3)	0.0267(10)
O13	1.2646(3)	0.4797(3)	0.2502(3)	0.0321(10)
O14	1.3743(3)	0.5176(3)	0.4497(3)	0.0241(10)
O15	1.5666(4)	0.2476(3)	0.3806(3)	0.0371(11)
O16	1.3950(3)	0.2718(3)	0.4054(3)	0.0303(10)

O17	1.4029(4)	0.5159(3)	0.1084(3)	0.0352(11)
O18	1.5772(4)	0.6502(3)	0.3702(3)	0.0346(11)
C1	0.6769(4)	0.1374(4)	-0.0346(4)	0.0198(14)
C2	0.8072(4)	0.1321(4)	-0.0328(4)	0.0203(12)
C3	0.8583(5)	0.2249(5)	-0.0898(5)	0.0343(17)
C4	0.9111(4)	0.1446(4)	0.1008(4)	0.0270(14)
C5	1.0503(4)	0.1437(4)	0.1160(4)	0.0254(14)
C6	0.9895(5)	0.2113(5)	-0.0835(5)	0.0344(17)
C7	1.0971(4)	0.2277(4)	0.0477(4)	0.0263(14)
C8	1.2254(4)	0.2073(4)	0.0538(4)	0.0236(14)
C11	0.7144(4)	0.4206(4)	0.2551(4)	0.0208(12)
C12	0.8424(4)	0.4221(4)	0.2478(4)	0.0255(14)
C13	0.9364(4)	0.3763(4)	0.3563(4)	0.0281(16)
C14	0.9112(5)	0.5430(5)	0.2476(5)	0.0392(17)
C15	1.0432(5)	0.5469(5)	0.2470(6)	0.046(2)
C16	1.0750(4)	0.3874(4)	0.3656(4)	0.0254(14)
C17	1.1397(4)	0.5078(4)	0.3564(4)	0.0221(12)
C18	1.2662(4)	0.5039(4)	0.3517(4)	0.0193(12)
C21	1.4820(5)	0.2167(4)	0.4179(4)	0.0291(14)
C22	1.4826(6)	0.1133(4)	0.4791(5)	0.0410(19)
C23	1.3872(7)	0.0083(5)	0.3889(6)	0.060(2)
C24	1.6194(7)	0.0964(5)	0.5495(6)	0.064(2)
C31	0.2453(5)	0.1279(4)	-0.2859(4)	0.0254(14)
C32	0.1333(5)	0.0402(4)	-0.3934(4)	0.0344(17)
C33	0.0076(7)	0.0172(7)	-0.3810(5)	0.071(2)
C34	0.1070(6)	0.0729(6)	-0.5133(5)	0.066(2)

U(eq) is defined as one third of the trace of the orthogonalized Uij tensor.

Table A3.17

Atomic Coordinates and Equivalent Isotropic Displacement Parameters [$Å^2$] for $[La_3(1,4\text{-HCHDC})_2(1,4\text{-CHDC})_{3.5}(H_2O)_2]\cdot H_2O$, **XVII**.

Atom	x	y	z	U(eq)
La1	0.68082(2)	0.10383(1)	0.24751(3)	0.0150(1)
La2	1.00604(2)	0.12478(1)	0.22118(3)	0.0147(1)
La3	0.34848(2)	0.08864(1)	-0.70422(3)	0.0163(1)
O1	0.6516(3)	0.14007(9)	0.0464(3)	0.0285(12)
O2	0.8098(3)	0.10802(9)	0.0836(3)	0.0212(12)
O3	0.7393(4)	0.10081(12)	-0.5236(3)	0.0555(18)
O4	0.5496(3)	0.10805(10)	-0.5906(3)	0.0305(14)
O5	1.2770(3)	0.09150(11)	0.4773(3)	0.0439(16)
O6	1.1072(3)	0.11943(10)	0.4309(3)	0.0351(14)
O7	1.2603(3)	0.09945(9)	0.0741(3)	0.0246(12)
O8	1.0940(3)	0.12919(9)	0.0396(3)	0.0253(12)
O9	0.5833(3)	0.06933(10)	0.0617(3)	0.0381(16)
O10	0.4971(3)	0.06153(9)	0.2063(3)	0.0221(12)
O11	0.8938(3)	0.07893(9)	0.3075(3)	0.0230(12)
O12	0.7566(3)	0.04249(10)	0.3128(4)	0.0446(16)
O13	1.1141(3)	0.07283(9)	0.2175(3)	0.0231(12)
O14	1.2446(3)	0.03368(9)	0.2166(4)	0.0409(14)
O15	0.8488(3)	0.14850(8)	0.3023(3)	0.0233(12)
O16	0.6762(3)	0.16775(9)	0.3123(4)	0.0422(14)
O17	1.0149(4)	0.31278(11)	0.4542(4)	0.077(2)
O18	0.9065(3)	0.32407(9)	0.5783(3)	0.0339(12)
O19	1.2580(3)	0.14438(10)	0.2872(3)	0.0369(16)
O20	1.1113(3)	0.17947(10)	0.2717(4)	0.0470(16)
O21	1.3983(6)	0.31978(17)	0.5290(7)	0.133(4)
O22	1.5556(5)	0.29940(13)	0.4882(5)	0.089(3)
O23	0.4711(3)	0.13369(11)	0.1897(4)	0.0333(16)
O24	0.4477(4)	0.04124(12)	-0.5618(4)	0.0554(17)

C1	0.7279(5)	0.12456(14)	0.0099(4)	0.0214(17)
C2	0.7281(4)	0.12285(13)	-0.1208(4)	0.0240(19)
C3	0.7083(6)	0.08677(15)	-0.1648(5)	0.045(2)
C4	0.6401(6)	0.14573(16)	-0.2021(5)	0.046(2)
C5	0.6470(7)	0.14270(16)	-0.3328(5)	0.052(3)
C6	0.7149(6)	0.08334(16)	-0.2947(5)	0.051(3)
C7	0.6298(5)	0.10659(15)	-0.3768(4)	0.0292(19)
C8	0.6412(5)	0.10459(15)	-0.5047(5)	0.032(2)
C11	1.1892(5)	0.10520(15)	0.5042(5)	0.029(2)
C12	1.1844(4)	0.10276(14)	0.6342(4)	0.0265(19)
C13	1.0803(5)	0.12137(15)	0.6602(4)	0.0314(19)
C14	1.2987(5)	0.11358(17)	0.7217(4)	0.041(2)
C15	1.2942(5)	0.10765(17)	0.8504(4)	0.037(2)
C16	1.0734(4)	0.11458(16)	0.7882(4)	0.0314(19)
C17	1.1884(4)	0.12423(14)	0.8799(4)	0.0257(19)
C18	1.1816(4)	0.11675(13)	0.0071(4)	0.0198(17)
C21	0.5082(5)	0.05437(13)	0.1002(5)	0.0247(19)
C22	0.4266(4)	0.02833(13)	0.0257(4)	0.0237(17)
C23	0.4357(5)	-0.00509(13)	0.0934(5)	0.0286(17)
C24	0.4474(5)	0.02309(13)	-0.0985(5)	0.0281(17)
C31	0.8648(5)	0.05068(14)	0.3393(5)	0.0247(19)
C32	0.9576(4)	0.02766(13)	0.4138(4)	0.0245(17)
C33	0.9641(5)	0.03150(14)	0.5467(5)	0.033(2)
C34	0.9383(5)	-0.00966(14)	0.3776(5)	0.035(2)
C41	1.1400(4)	0.04371(13)	0.1853(5)	0.0212(17)
C42	1.0453(4)	0.02252(12)	0.1053(5)	0.0242(17)
C43	1.0178(5)	0.03607(14)	-0.0239(5)	0.031(2)
C44	1.0786(5)	-0.01463(13)	0.1073(5)	0.031(2)
C51	0.7833(5)	0.17259(14)	0.3206(5)	0.0249(17)
C52	0.8398(5)	0.20647(14)	0.3523(5)	0.0336(19)
C53	0.8900(7)	0.20937(17)	0.4823(7)	0.089(3)
C54	0.7624(7)	0.23522(16)	0.3017(7)	0.073(3)
C55	0.8261(7)	0.26907(16)	0.3355(7)	0.076(3)
C56	0.9512(8)	0.24344(17)	0.5180(7)	0.090(3)
C57	0.8704(6)	0.27223(15)	0.4683(6)	0.052(3)
C58	0.9317(5)	0.30556(15)	0.5069(5)	0.037(2)
C61	1.2198(5)	0.17307(15)	0.2962(5)	0.034(2)
C62	1.3035(6)	0.20200(17)	0.3337(7)	0.060(3)
C63	1.2543(8)	0.23505(19)	0.2799(8)	0.106(4)
C64	1.3586(11)	0.2030(2)	0.4536(9)	0.169(6)
C65	1.4400(9)	0.2343(2)	0.4959(9)	0.131(5)
C66	1.3347(10)	0.2646(2)	0.3249(9)	0.151(6)
C67	1.3807(9)	0.2653(2)	0.4463(8)	0.095(4)
C68	1.4465(9)	0.2969(2)	0.4937(8)	0.076(4)
O25	0.6255(7)	-0.0021(2)	0.3979(8)	0.107(3)

U(eq) is defined as one third of the trace of the orthogonalized Uij tensor.

Table A3.18
Atomic Coordinates and Equivalent Isotropic Displacement Parameters [Å^2] for $[La_2(1,4\text{-CHDC})_3(H_2O)]\cdot 2.5H_2O$, **XVIII**.

Atom	x	y	z	U(eq)
La01	0.61803(3)	0.47520(3)	0.11755(2)	0.0226(1)
La02	0.82418(4)	0.42153(4)	0.38526(2)	0.0286(1)
O1	0.7753(5)	0.3357(5)	0.1136(3)	0.0394(17)
O2	0.8730(5)	0.3107(5)	0.2524(3)	0.0414(17)
O3	0.5630(5)	-0.2844(5)	-0.0546(3)	0.0379(17)
O4	0.6915(5)	-0.3126(5)	0.0733(3)	0.0369(16)
O5	0.8132(4)	0.5695(4)	0.2486(3)	0.0287(14)
O6	1.0154(5)	0.6022(5)	0.3349(3)	0.0382(14)

O7	0.3856(4)	0.5441(4)	0.0525(3)	0.0283(14)
O8	0.4694(5)	0.5973(5)	0.1982(3)	0.0361(16)
O9	0.5789(5)	0.3766(5)	0.2611(3)	0.0364(16)
O10	0.5892(6)	0.2485(6)	0.3623(4)	0.058(2)
O11	0.0589(5)	0.4123(5)	0.4649(3)	0.0359(17)
O12	0.2571(6)	0.3993(6)	0.5431(3)	0.0515(19)
O13	0.7566(7)	0.3398(8)	0.5328(4)	0.085(3)
O101	0.8352(15)	0.1744(7)	0.4194(8)	0.080(6)
C1	0.8187(7)	0.2706(7)	0.1711(5)	0.031(2)
C2	0.8009(10)	0.1341(8)	0.1445(7)	0.054(3)
C3	0.6572(10)	0.0628(8)	0.1569(8)	0.068(4)
C4	0.8487(14)	0.1015(9)	0.0616(10)	0.100(6)
C5	0.8179(15)	-0.0381(10)	0.0372(11)	0.113(6)
C6	0.6264(12)	-0.0756(9)	0.1310(9)	0.079(4)
C7	0.6842(10)	-0.1059(8)	0.0463(6)	0.052(3)
C8	0.6445(7)	-0.2450(6)	0.0193(4)	0.0292(19)
C11	0.9449(6)	0.6228(6)	0.2664(4)	0.0234(17)
C12	1.0079(7)	0.7127(6)	0.2012(5)	0.029(2)
C13	1.1558(7)	0.7965(6)	0.2364(5)	0.033(2)
C14	1.0052(7)	0.6431(8)	0.1068(4)	0.036(2)
C15	1.1197(7)	0.5744(7)	0.1086(5)	0.0331(19)
C16	1.2744(7)	0.7313(6)	0.2319(4)	0.0293(19)
C17	1.2660(6)	0.6651(6)	0.1372(4)	0.0264(19)
C18	0.3810(6)	0.5998(6)	0.1302(4)	0.0237(17)
C21	0.1659(7)	0.3673(7)	0.4716(4)	0.032(2)
C22	0.1853(7)	0.2876(7)	0.3907(4)	0.0330(19)
C23	0.2763(8)	0.2003(7)	0.4157(5)	0.034(2)
C24	0.2501(8)	0.3744(7)	0.3214(5)	0.035(2)
C25	0.2733(7)	0.3012(7)	0.2373(4)	0.033(2)
C26	0.3010(8)	0.1276(7)	0.3311(5)	0.035(2)
C27	0.3664(7)	0.2145(7)	0.2631(4)	0.0294(19)
C28	0.5195(7)	0.2835(6)	0.2989(4)	0.0266(19)
O102	0.6249(13)	0.7608(8)	0.3514(7)	0.052(4)
O104	-0.5122(16)	0.3204(8)	0.6120(9)	0.047(6)
O100	0.5603(12)	0.1277(3)	0.5458(7)	0.079(6)
O103	0.117(3)	0.053(2)	0.6474(9)	0.084(10)
O105	0.972(5)	0.104(2)	0.535(4)	0.24(3)

U(eq) is defined as one third of the trace of the orthogonalized Uij tensor.

Chapter 4

Hybrid Networks of Lead Aliphaticdicarboxylates with Extended Inorganic Connectivity

Summary*

As part of our effort to synthesize novel hybrid frameworks with extended inorganic connectivity, investigations were carried out by employing single and mixture of aliphatic dicarboxylicacids with the potentially lone pair active, flexible coordinating Pb(II) cation with a large ionic radii. We have synthesized and characterized five three-dimensional (**I**-**V**) and one two-dimensional (**VI**) hybrid lead dicarboxylates, all possessing two-dimensional inorganic connectivity. Of these, three of them (**I**-**III**) are homoleptic (same ligand) and the other three (**III**-**VI**) are heteroleptic (mixed ligands). The Pb glutarate, **I**, and adipate, **II**, possess one type of two-dimensional inorganic layers [contains only one ($^{X}\mathbf{D}_{\mathbf{Y}}$) type of dimer SBUs of only hemidirected Pb(II) cations] connected in to a three-dimensional structure by the dicarboxylate anions with near 90 ^{o} torsional angle. [Description of dimer SBUs and terminology are given in the appendix {see Appendix. 2.7(a)}]. On the other hand, the Pb adipate, **III**, as well as the oxalate-succinate, **IV**, and oxalate-adipate, **V**, possess another type of two-dimensional inorganic connectivity [contain two different ($^{x}\mathbf{d}_{\mathbf{y}}$ & $^{X}\mathbf{D}_{\mathbf{Y}}$) types of dimer SBUs and only holodirected Pb(II) cations] connected by the dicarboxylate anions with the zero torsional angle. The bilayer nitrate-oxalate, **VI**, is unusual in that it possesses a (6,3) net topology of the two-dimensional inorganic metal nitrate layer, with infinite M-O-M linkages. The Pb(II) cations in **VI** are in hemidirected

*An article based on this study has been published in *Journal of Solid State Chemistry* (2008).

coordination geometry.

4.1. Introduction

Metal carboxylates with different framework structures are being investigated in-depth in the last few years.[1-3] Some of the carboxylates possess interesting properties as exemplified by the metal-organic frameworks synthesized by Yaghi and coworkers[4] which show excellent hydrogen sorption properties. Then, there are trinuclear chromium cluster-based benzene di- and tri- carboxylates synthesized by Férey and coworkers[5-7] which possess very large surface areas and unit cell volumes going up to 7,00,000 $Å^3$. Of particular interest to us are the inorganic organic hybrid frameworks with infinite metal-oxygen-metal bonds. Hybrid metal carboxylates with interesting properties have been reported in the literature. Aliphatic dicarboxylic acids have been used as good linkers in the construction of hybrid compounds with interesting structures.[8-16]

Recently,[17] hybrid frameworks have been classified on the basis of the dimensionality (***n,m***) of the inorganic (***I***) and organic (***O***) connectivities, to define a characteristic $\boldsymbol{I^nO^m}$. There are not many hybrid carboxylates with $\boldsymbol{I^2O^1}$ type connectivity.[8,9,18-24] There are also very few mixed aliphatic dicarboxylates known today, the only examples, to our knowledge being the neodymium oxalate-glutarate,[25] $Nd_4(H_2O)_2(C_5H_6O_4)_4(C_2O_4)_2$, lanthanum oxalate-succinate,[26] $[La_2(C_2O_4)(C_4H_4O_4)_2(H_2O)_4]\cdot 4H_2O$, lanthanum oxalate-adipate,[26] $La_2(C_2O_4)_2(C_6H_8O_4)(H_2O)_2$, lanthanide oxalate-fumarate,[27] $[La_2(C_2O_4)(C_4H_2O_4)_2(H_2O)_4]\cdot 4H_2O$, (Ln = Eu,Tb). The compounds synthesized and characterized by us include a glutarate, $Pb(C_5H_6O_4)$, **I,** and two adipates of the same formula, $Pb(C_6H_8O_4)$, **II,** and **III,** in addition to two mixed carboxylates, an oxalate-succinate, $Pb_2(C_2O_4)(C_4H_4O_4)$, **IV,** and an oxalate-adipate, $Pb_2(C_2O_4)(C_6H_8O_4)$, **V**.

We also report a nitrate-oxalate, $(OPb_2)_2(C_2O_4)(NO_3)_2$, **VI**, where the nitrate and oxalate anions coordinate with the metal ion.

4.2. Scope of the present investigation

Synthesis of novel hybrid frameworks with extended inorganic connectivity is an important area of research. We have investigated the formation of such hybrid frameworks by employing single or mixture of two aliphatic dicarboxylicacids and a potentially lone pair active Pb(II) cation with a large ionic radii and flexible coordination geometry compared to the transition metal cations.

We have successfully synthesized and characterized five three-dimensional (**I**-**V**) and one two-dimensional (**VI**) hybrid lead dicarboxylates, all possessing two-dimensional inorganic connectivity. Of these, three of them (**I**-**III**), are homoleptic (same ligand) and the other three (**III**-**VI**), are heteroleptic (mixed ligands). The homoleptic Pb glutarate, **I**, and adipate, **II**, possess one type of two-dimensional inorganic layers (contains only one ($^{X}\mathbf{D}_{\mathbf{Y}}$) type of dimer SBUs of only hemidirected Pb(II) cations) connected in to a three-dimensional structure by the dicarboxylate anions with near 90 ^{o} torsional angle. [Description of dimer SBUs and terminology are given in the appendix {see Appendix. 2.7(a)}]. On the other hand, the homoleptic Pb adipate, **III**, as well as the heteroleptic oxalate-succinate, **IV**, and oxalate-adipate, **V**, possess another type of two-dimensional inorganic connectivity (contain two different ($^{x}\mathbf{d}_{\mathbf{y}}$ & $^{X}\mathbf{D}_{\mathbf{Y}}$) types of dimer SBUs and only holodirected Pb(II) cations) connected by the dicarboxylate anions with the zero torsional angle. The bilayer nitrate-oxalate, **VI**, is unusual in that it possesses a (6,3) net topology of the two-dimensional inorganic metal nitrate layer, with infinite M-O-M linkages. The Pb(II) cations in **VI** are in hemdirected geometry. Coordination geometry of the cation and ligands plays a crucial role in determining

the type of inorganic connectivity. The lower dicarboxylic acid in the heteroleptic hybrids participate in the formation of structures with bilayer connectivities.

4.3. Experimental

Synthesis and characterization

Materials and methods: $Pb(NO_3)_2$ (Qualigens, India, 99%), oxalic acid dihydrate ($C_2H_2O_4.2H_2O$) (S.D. Fine, India, 99.5%), succinic acid ($C_4H_6O_4$) (Qualigens, India, 99%), glutaric acid ($C_5H_8O_4$) (Spectrochem, India, 99%), adipic acid ($C_6H_{10}O_4$) (Merck, India, 99%), NaOH (Merck, India, 99%) of high purity and double distilled water were used for the synthesis.

The Pb aliphatic dicarboxylates **I** - **VI** were synthesized under hydrothermal conditions by heating the homogenized reaction mixtures in a 23 ml PTFE-lined bomb at the 180 °C temperature for 72 h under autogeneous pressure. The pH of the starting reaction mixture was generally in the range 5-6. The pH after the reaction did not show appreciable change. The products of the hydrothermal reactions were vacuum-filtered and dried under ambient conditions. The starting compositions for the different compounds synthesized by us are given in Table 4.1. All the compounds were obtained as single phase materials, except **III**, whose crystals were admixed with small quantities of lead succinate, $Pb(C_4H_4O_4)$[28]. Attempts were made unsuccessfully to prepare **III** in pure form without the addition of succinic acid. The crystals of **I**, **II**, **IV**, **V** and **VI** were separated under a polarizing microscope and used for all the characterization. Other than the single crystal X-ray diffraction, **III** could not be subjected to other methods of characterization due to the difficulty in separating the lead succinate impurity.

Elemental analyses were satisfactory. For **I**, ($C_5H_6PbO_4$) calcd: C, 17.79%; H, 1.78%. Found: C, 18.09%; H, 1.63%; For **II**, ($C_6H_8PbO_4$) calcd: C, 20.50%; H, 2.28%. Found: C, 21.06%; H, 2.15%. For **IV**, ($C_3H_2PbO_4$) calcd: C, 11.64%; H, 0.65%. Found: C, 11.92%; H, 0.87%. For **V**, ($C_4H_4PbO_4$) calcd: C, 14.85%; H, 1.24%. Found: C, 15.12%; H, 1.36%. For **VI**, ($CNPb_2O_6$) calcd: C, 2.24%; N, 2.61%. Found: C, 2.36%; N, 2.84%.

Powder XRD patterns of the products were recorded using Cu Kα radiation (Rich-Seifert, 3000TT). The patterns agreed with those calculated for single crystal structure determination. Thermogravimetric analysis (TGA) was carried out (Metler-Toledo) in oxygen atmosphere (flow rate = 50 ml/min) in the temperature range 25 to 800 °C (heating rate = 5 °C/min).

Infrared (IR) spectra of KBr pellets of the compounds were recorded in the mid IR region (Bruker IFS-66v). All the compounds show characteristic bands of the functional groups.[29-31] The bands around 1600 and 1400 cm^{-1} are assigned to the asymmetric ($\nu_{as\ C\text{-}O}$) and symmetric ($\nu_{s\ C=O}$) stretching of the carboxylate anion. The bands at 1285 ($\nu_{as\ N\text{-}O}$), 1017 ($\nu_{s\ N\text{-}O}$), 752 $(\delta_{NO3})_{in\text{-}plane}$ and 817 cm^{-1} $(\delta_{NO3})_{out\text{-}of\text{-}plane}$ indicate the presence of the nitrate groups in **VI**.

Thermogravimetric analyses of the Pb dicarboxylates are as follows. All the compounds show single step weight loss. For **I**, the weight loss of 34.36% (calc. 33.80%) occurred in the 310-450^o C range. For **II**, the weight loss of 36.82% (calc. 36.44%) occurred in the 295-440^o C range. For **IV**, the weight loss of 28.17% (calc. 27.79%) occurred in the 300-450^o C range. For **V**, the weight loss of 31.33% (calc. 30.92%) occurred in the 295-450^o C range. The total weight loss matches very well with the loss of CO_2, and H_2O as well as the formation of PbO

(PDF # 00-004-0561) in all the cases. TGA could not be performed in **VI** due to the highly exothermic nature of the decomposition.

A suitable single crystal of each compound was carefully selected under a polarizing microscope and glued to a thin glass fiber. Crystal structure determination by X-ray diffraction was performed on a Bruker-Nonius diffractometer with Kappa geometry attached with an APEX -II-CCD detector and a graphite monochromator for the X-ray source (Mo Kα radiation, λ = 0.71073Å) operating at 50 kV and 30 mA. An empirical absorption correction based on symmetry equivalent reflections was applied using the SADABS program[32]. The structure was solved and refined using SHELXTL-PLUS suite of programs[33]. For the final refinement the hydrogen atoms were placed geometrically and held in the riding mode. Final refinement included atomic positions for all the atoms, anisotropic thermal parameters for all the non-hydrogen atoms and isotropic thermal parameters for the hydrogen atoms. All the hydrogen atoms were included in the final refinement. Details of the structure solution and final refinements for the compounds **I** to **VI** are given in Tables 4.2 and 4.3. Atomic coordinates for the compounds **I** to **VI** are given in the appendix (see 4.7. Appendix, Tables A4.1-A.4.6).

Table 4.1 Synthetic conditions for the compounds I-VI.

Compound No.	Formula	Composition (Mole ratio)					Yield based on lead (%)
		$Pb(NO_3)_2$	Dicarboxylic acid		NaOH (5M soln.)	Water	
I	$Pb(C_5H_6O_4)$	(0.333g) 1	Glutaric acid (0.267g) 2		(0.5ml) 2.5	(5ml) 278	54
II	$Pb(C_6H_8O_4)$	(0.333g) 1	Adipic acid (0.295g) 2		(0.6ml) 3	(5ml) 278	61
III	$Pb(C_6H_8O_4)$	(0.333g) 1	Succinic acid (0.0596g) 0.5	Adipic acid (0.295g) 2	(0.5ml) 2.5	(5ml) 278	-
IV	$Pb_2(C_2O_4)(C_4H_4O_4)$	(0.333g) 1	Oxalic acid.$2H_2O$ (0.127g) 1	Succinic acid (0.238g) 2	(1.0ml) 5	(5ml) 278	67
V	$Pb_2(C_2O_4)(C_6H_8O_4)$	(0.333g) 1	Oxalic acid.$2H_2O$ (0.127g) 1	Adipic acid (0.295g) 2	(0.8ml) 4	(5ml) 278	64
VI	$(OPb_2)_2(C_2O_4)(NO_3)_2$	(0.333g) 1	Oxalic acid.$2H_2O$ (0.19g)1.5		(0.6ml) 3	(5ml) 278	56

Table 4.2. Crystal data and structure refinement parameters for **I** to **III**.

Structure parameter	**I**	**II**	**III**
Empirical formula	$C_5H_6PbO_4$	$C_6H_8PbO_4$	$C_6H_8PbO_4$
Formula weight	337.29	351.31	351.31
Crystal system	Monoclinic	Monoclinic	Monoclinic
Space group	$P2_1/m$, (no. 11)	$P2_1/c$, (no. 14)	$P2_1/c$, (no. 14)
a /Å	4.7454(1)	7.2156(1)	20.5361(7)
b /Å	7.2032(1)	4.7367(1)	5.0737(2)
c /Å	9.6750(1)	21.9305(4)	7.0706(2)
β /°	93.164(1)	90.417(1)	92.147(1)
V /Å^3	330.21(1)	749.52(2)	736.20(4)
Z	2	4	4
D (calc) /gcm^{-3}	3.392	3.113	3.170
μ /mm^{-1}	25.494	22.470	22.876
Total data collected	2170	4825	7160
Unique data	607	1387	1269
Observed data	591	1307	1221
[I > 2σ (I)]			
R_{merg}	0.0277	0.0349	0.0276
Goodness of fit	1.082	1.037	1.133
R indexes	$R_1 = 0.0396$[a];	$R_1 = 0.0182$[a];	$R_1 = 0.0450$[a];
[I > 2σ (I)]	$wR_2 = 0.0897$[b]	$wR_2 = 0.0416$[b]	$wR_2 = 0.1080$[b]
R indexes	$R_1 = 0.0401$[a];	$R_1 = 0.0200$[a];	$R_1 = 0.00459$[a];
[all data]	$wR_2 = 0.0906$[b]	$wR_2 = 0.0424$[b]	$wR_2 = 0.1106$[b]

[a] $R_1 = \Sigma ||F_0|-|F_c|| / \Sigma |F_0|$; [b] $wR_2 = \{\Sigma[w(F_0^2 - F_c^2)^2] / \Sigma[w(F_0^2)^2]\}^{1/2}$. $w = 1/[\sigma^2(F_0)^2 + (aP)^2 + bP]$, $P = [\max.(F_0^2,0) + 2(F_c)^2]/3$, where $a = 0.0773$, $b = 0$ for **I**, $a = 0.0183$, $b = 0.3362$ for **II** and $a = 0.0828$, $b = 0.7243$ for **III**.

Table 4.3. Crystal data and structure refinement parameters for **IV** to **VI**.

Structure parameter	**IV**	**V**	**VI**
Empirical formula	$C_3H_2PbO_4$	$C_4H_4PbO_4$	$CNPb_2O_6$
Formula weight	309.24	323.27	536.40
Crystal system	Monoclinic	Monoclinic	Monoclinic
Space group	$P2_1/c$, (no. 14)	$P2_1/m$, (no. 11)	$P2_1/c$, (no. 14)
a /Å	12.6902(5)	15.1995(8)	11.8682(3)
b /Å	5.2086(2)	5.1505(3)	5.2501(1)
c /Å	6.9389(2)	7.0289(4)	9.0989(2)
β /°	100.507(2)	98.072(3)	96.741(2)
V /Å^3	450.96(3)	544.81(5)	563.03(2)
Z	4	4	4
D (calc) /gcm^{-3}	4.555	3.941	6.328
μ /mm^{-1}	37.312	30.894	59.696
Total data collected	7700	11864	3355
Unique data	720	965	1007
Observed data	710	939	952
[I > 2σ (I)]			
R_{merg}	0.0236	0.0183	0.0915
Goodness of fit	1.136	1.214	1.058
R indexes	$R_1 = 0.0428$[a];	$R_1 = 0.0305$[a];	$R_1 = 0.0528$[a];
[I > 2σ (I)]	$wR_2 = 0.1012$[b]	$wR_2 = 0.0764$[b]	$wR_2 = 0.1187$[b]
R indexes	$R_1 = 0.0430$[a];	$R_1 = 0.0310$[a];	$R_1 = 0.0548$[a];
[all data]	$wR_2 = 0.1014$[b]	$wR_2 = 0.0768$[b]	$wR_2 = 0.1211$[b]

[a] $R_1 = \Sigma ||F_0|-|F_c|| / \Sigma |F_0|$; [b] $wR_2 = \{\Sigma[w(F_0^2 - F_c^2)^2] / \Sigma[w(F_0^2)^2]\}^{1/2}$. $w = 1/[\sigma^2(F_0)^2 + (aP)^2 + bP]$, $P = [\max.(F_0^2,0) + 2(F_c)^2]/3$, where $a = 0.0838$, $b = 0.3233$ for **IV**, $a = 0.00467$, $b = 1.7204$ for **V** and $a = 0.0764$, $b = 10.0162$ for **VI** .

4.4. Results and discussion

We have synthesized three homoleptic hybrid metal dicarboxylates of the composition, $Pb(C_5H_6O_4)$, **I,** and two polymorphs of $Pb(C_6H_8O_4)$, **II** and **III,** in addition to two heteroleptic (mixed ligands) carboxylates of lead, $Pb_2(C_2O_4)(C_4H_4O_4)$, **IV**, and $Pb_2(C_2O_4)(C_6H_8O_4)$, **V**, formed by oxalate and succinate or adipate. We have also prepared an unusual dicarboxylate, $(OPb_2)_2(C_2O_4)(NO_3)_2$, **VI**, where the nitrate ion coordinates with the metal ion along with the oxalate anion. In what follows, we discuss the structures of **I-VI**.

4.4.1. Homoleptic dicarboxylates

(a) Lead glutarate

The glutarate, $Pb(C_5H_6O_4)$, **I**, has a three-dimensional structure with an asymmetric unit of 5 non-hydrogen atoms. The asymmetric unit contains a crystallographically distinct Pb^{2+} ion and half of the glutarate anion where all the atoms have a 0.5 occupancy except O(3) which sits at the 4*f* position (Fig. 4.4.1a). The glutarate anion with a molecular mirror plane exhibits a coordination mode with (1222) connectivity[34] with the torsional angle of 95.01(2) º (Fig. 4.4.1b). The Pb atom is hemidirected and seven-coordinated by oxygen atoms (PbO_7) from five different glutarate anions. Six of the oxygens have μ_3 connections linking each Pb with four other Pb atoms. Thus, a PbO_7 polyhedron shares its two corners ($^1\mathbf{D_1}$) with two different PbO_7 polyhedra and two edges ($^2\mathbf{D_2}$) with two other PbO_7 forming an infinite two-dimensional Pb-O-Pb layer of the $\boldsymbol{I^2O^0}$ type, with a (4,4) net topology (Fig. 4.4.1c). This layer can be viewed as chains of edge shared PbO_7 polyhedra connected through the corners of PbO_7 polyhedra of the adjacent chains. The layers get further connected to each other through glutarate anions into a

three-dimensional structure of the I^2O^1 type (Fig. 4.4.1d). The Pb-O bond lengths are in the 2.399 – 2.853 Å range.

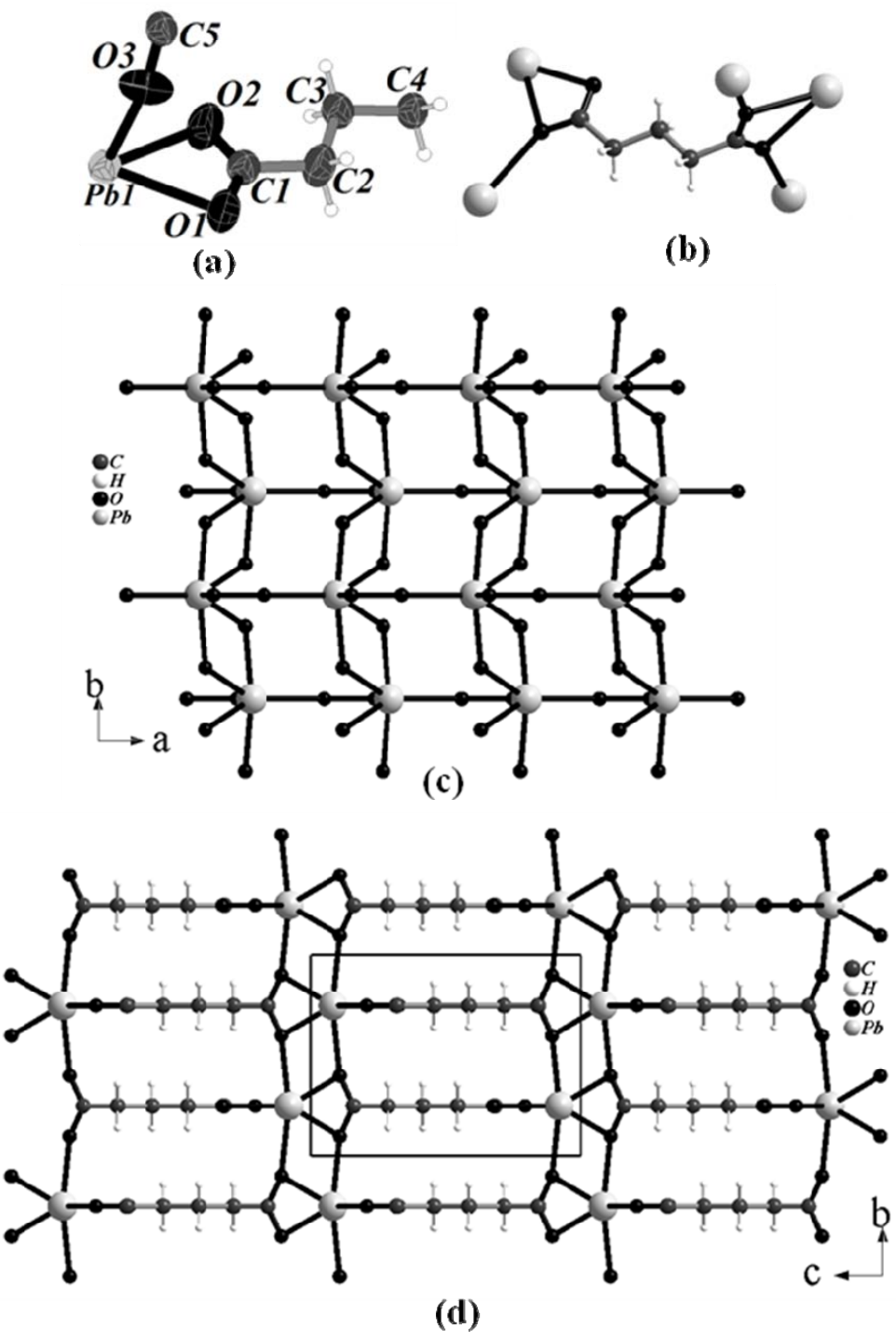

Fig. 4.4.1 (a) ORTEP plot of $Pb(C_5H_6O_4)$, **I** (Thermal ellipsoids are shown at 50% probability) (b) coordination mode of the glutarate moiety in **I** (c) view of the inorganic layer with the infinite Pb-O-Pb linkages of the I^2O^0 type in **I** and (d) the 3D-structure of **I** viewed along the *a*- axis.

(b) Lead adipates

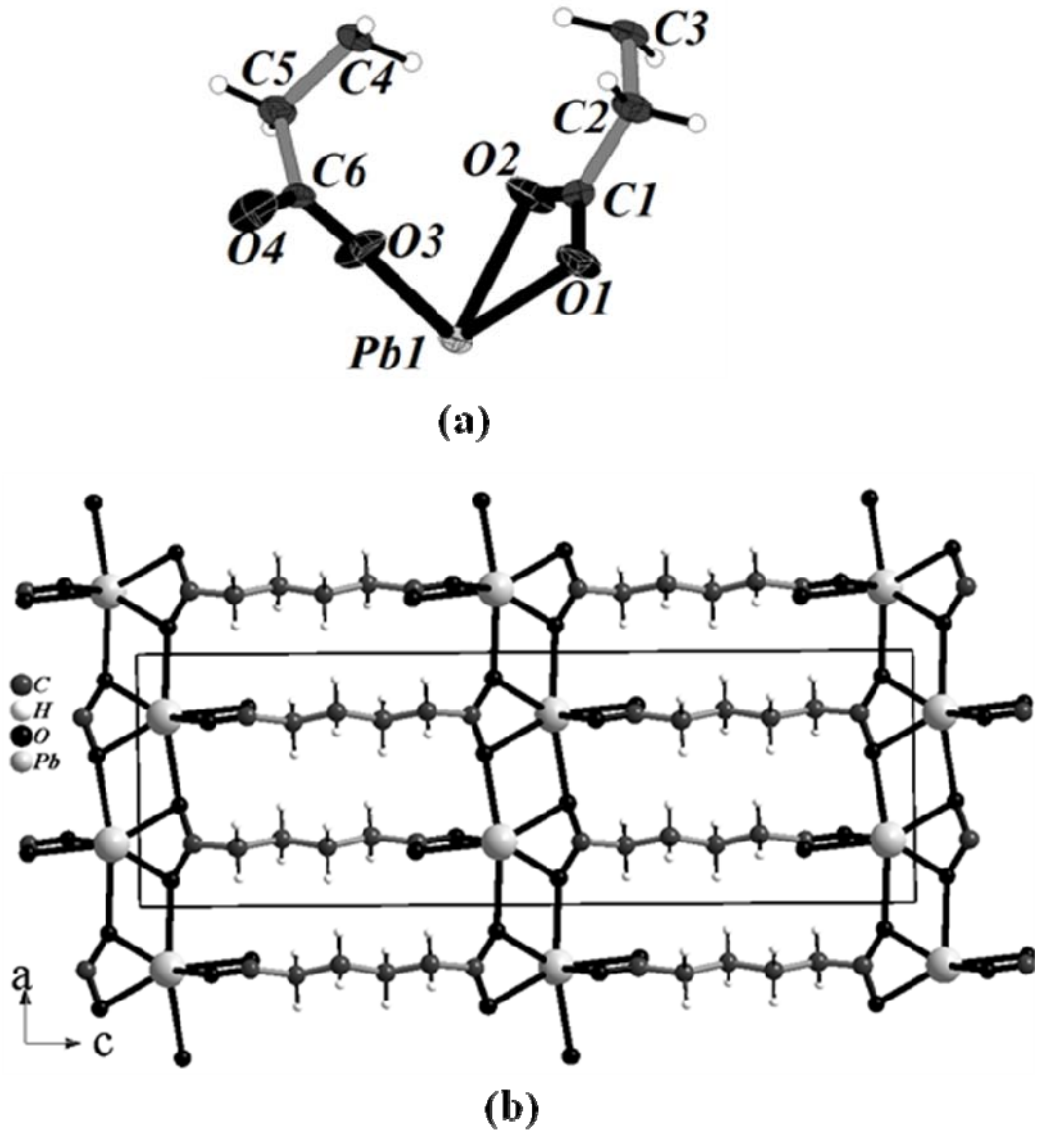

Fig. 4.4.2 (a) ORTEP plot of $Pb(C_6H_8O_4)$, **II** (Thermal ellipsoids are shown at 50% probability) (b) the 3D-structure of **II** viewed along the *b*- axis.

The adipate, $Pb(C_6H_8O_4)$, **II**, has a three-dimensional structure similar to **I**, with an asymmetric unit of 11 non-hydrogen atoms. The asymmetric unit contains a crystallographically distinct Pb^{2+} ion and one adipate anion (Fig. 4.4.2a). The adipate anion exhibits a coordination mode with (1222) connectivity and a torsional angle of 108.19(3) º. The Pb atom is hemidirected and seven-coordinated by oxygen atoms from five different adipate anions. Six of the oxygens have $\boldsymbol{\mu}_3$

connections linking each Pb with four other Pb atoms giving rise to an infinite two-dimensional Pb-O-Pb layer of the $\boldsymbol{I^2O^0}$ type, with a (4,4) net topology just as in **I** (Fig. 4.4.1c) and a three-dimensional structure of the $\boldsymbol{I^2O^1}$ type through adipate connectivity (Fig. 4.4.2b). The Pb-O bond lengths in **II** are in the 2.398 – 2.864 Å range.

Another adipate, $Pb(C_6H_8O_4)$, **III**, also has a three-dimensional structure with an asymmetric unit of 11 non-hydrogen atoms. The asymmetric unit contains a crystallographically distinct Pb^{2+} ion and an adipate anion (Fig. 4.4.3a). The adipate anion exhibits a coordination mode with (1212) connectivity and a torsional angle of 0 º (Fig. 4.4.3b). The Pb atom is holodirected and seven-coordinated by oxygen atoms from six different adipate anions. Six of the oxygens have $\boldsymbol{\mu_3}$ connections linking each Pb atom with four other Pb atoms. Thus, a PbO_7 polyhedron shares its two corners ($^2\mathbf{D_1}$) with two PbO_7 polyhedra and two of its edges **($^1\mathbf{d_1}$ + $^1\mathbf{D_1}$)** with other two PbO_7 forming an infinite two-dimensional Pb-O-Pb layer of the $\boldsymbol{I^2O^0}$ type, with a (4,4) net topology different from compounds **I** and **II** (Fig. 4.4.3c). This layer can be viewed as chains of alternative edge and corner shared PbO_7 polyhedra, connected through the corners and edges of PbO_7 polyhedra alternatively in between the adjacent chains. The layers are further connected to each other through the adipate anions into a three-dimensional structure of the $\boldsymbol{I^2O^1}$ type (Fig. 4.4.3d). The Pb-O bond lengths are in the 2.386 – 2.925 Å range.

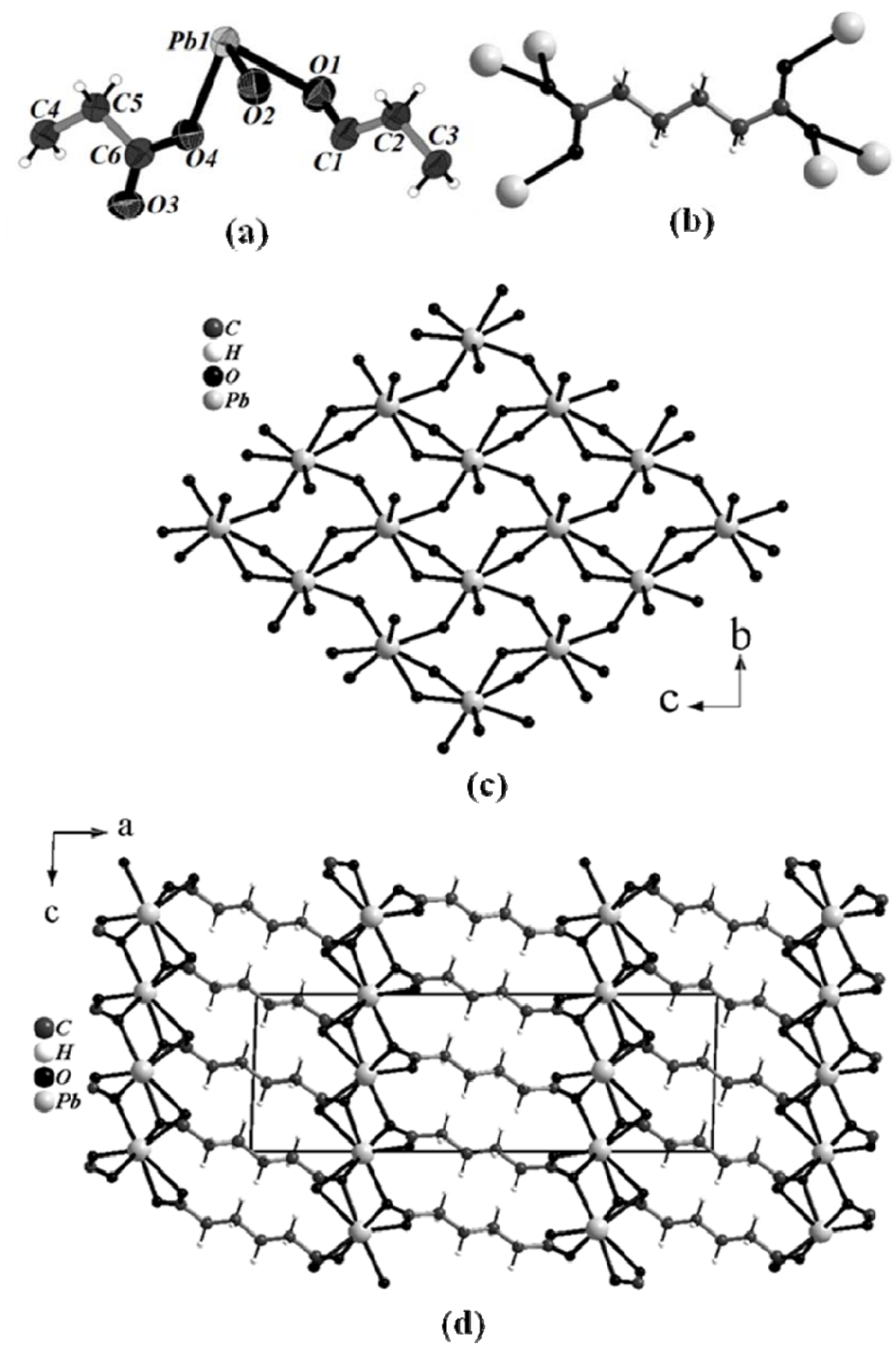

Fig. 4.4.3 (a) ORTEP plot of $Pb(C_6H_8O_4)$, **III** (Thermal ellipsoids are shown at 50% probability) (b) coordination mode of the adipate moiety in **III** (c) view of the inorganic layer with the infinite Pb-O-Pb linkages of the $\boldsymbol{I^2O^0}$ type in **III** and (d) the 3D-structure of **III** viewed along the *b*- axis.

4.4.2. Heteroleptic dicarboxylates

(a) Lead oxalate-succinate

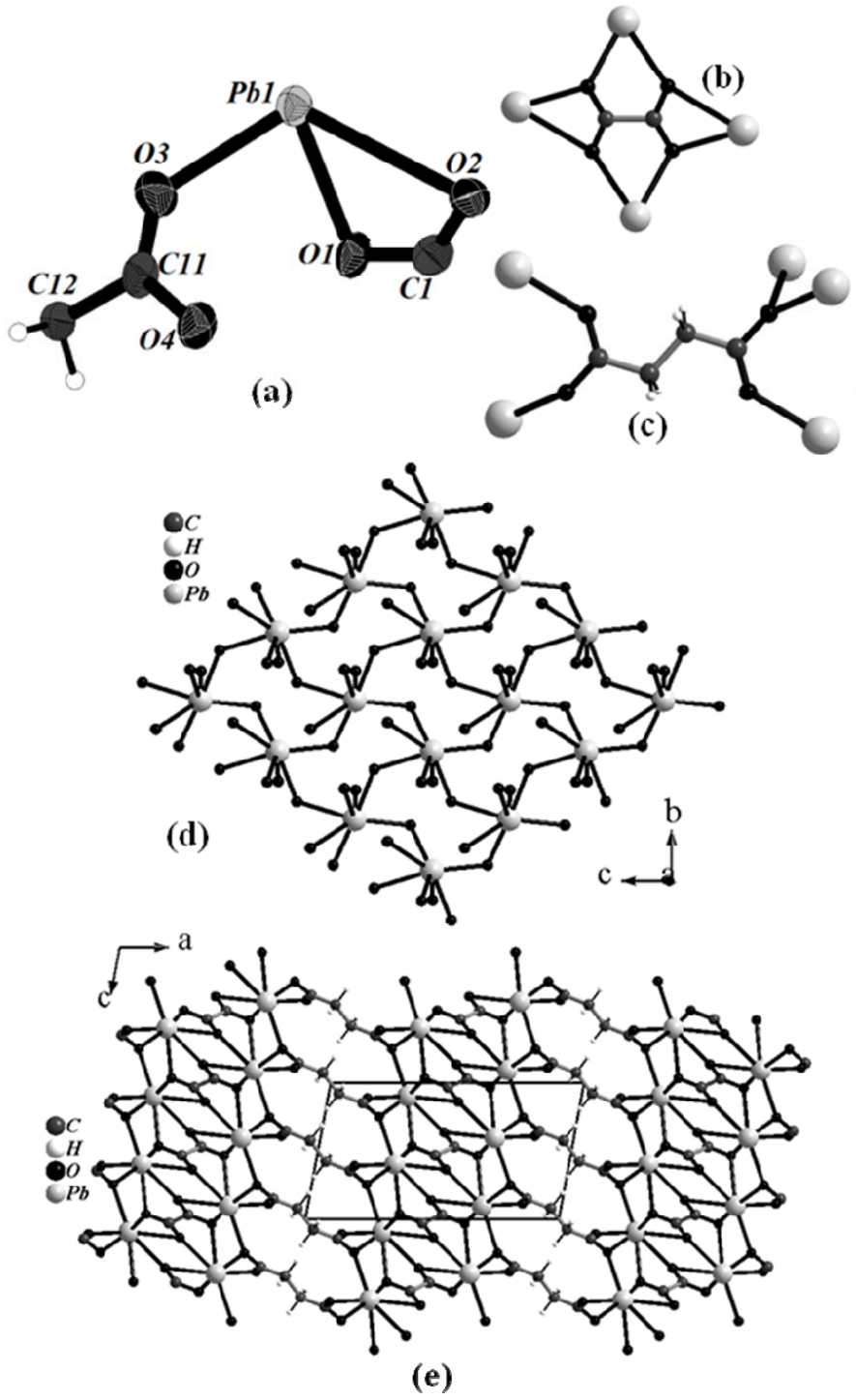

Fig. 4.4.4 (a) ORTEP plot of $Pb_2(C_2O_4)(C_4H_4O_4)$, **IV** (Thermal ellipsoids are shown at 50% probability) (b) coordination mode of the oxalate moiety in **IV** (c) coordination mode of the succinate moiety in **IV** (d) view of the inorganic layer with the infinite Pb-O-Pb linkages of the $\boldsymbol{I^2O^0}$ type in **IV** and (e) the 3D-structure of **IV** viewed along the *b*- axis.

The oxalate-succinate, $Pb_2(C_2O_4)(C_4H_4O_4)$, **IV**, has a three-dimensional structure with an asymmetric unit of 8 non-hydrogen atoms. The asymmetric unit contains a crystallographically distinct Pb^{2+} ion, one half of the oxalate and one half of the succinate anions (Fig. 4.4.4a). The oxalate and succinate anions exhibit coordination modes with (2222) and (1121) connectivities respectively, both with 0 º torsional angle (Fig. 4.4.4b and c). The Pb atom is holodirected and seven-coordinated by oxygen atoms from two oxalate and three succinate anions. Six of the oxygens have $\boldsymbol{\mu}_3$ connections linking two different Pb atoms. This leads to a connectivity wherein each Pb atom is connected with four other Pb atoms. Thus, each PbO_7 polyhedron shares four of its corners {two ($^1\mathbf{d_1}$) and two ($^2\mathbf{D_1}$)} with four other PbO_7 polyhedra forming an infinite two-dimensional Pb-O-Pb layer of the $\boldsymbol{I^2O^0}$ type, with a (4,4) net topology very similar to that in **III** (Fig. 4.3.4d). This layer can be viewed as chains of only corner shared PbO_7 polyhedra and connected through the corners of PbO_7 polyhedra in the adjacent chains. Two of these layers are connected to each other through the oxalate anions into a bilayer structure. These bilayers are further connected to each other through succinate anions into a three-dimensional structure of the $\boldsymbol{I^2O^1}$ type (Fig. 4.3.4e). The Pb-O bond lengths are in the 2.394 – 2.890 Å range.

(b) Lead oxalate-adipate

The oxalate-adipate, $Pb_2(C_2O_4)(C_6H_8O_4)$, **V**, has a three-dimensional structure similar to **IV**, with an asymmetric unit of 9 non-hydrogen atoms. The asymmetric unit contains a crystallographically distinct Pb^{2+} ion, one half of the oxalate and one half of the adipate anions (Fig. 4.4.5a). The oxalate (Fig. 4.4.4b) and adipate anions (Fig. 4.4.5b) exhibit coordination modes with (2222) and (1212) connectivities respectively, both with 0 º torsional angle. The Pb atom is

holodirected and seven-coordinated by oxygen atoms from two different oxalate and three different succinate anions. Six of the oxygens have μ_3 connections linking two different Pb atoms, leading to a connectivity just as in **IV**, giving rise to an infinite two-dimensional Pb-O-Pb layer of the I^2O^0 type, with a (4,4) net topology. The layers are connected to each other through the oxalate anions to form bilayers (Fig. 4.4.5c). The bilayers further get connected through adipate anions into a three-dimensional structure of the I^2O^1 type (Fig. 4.4.5c). The Pb-O bond lengths are in the 2.402 – 2.867 Å range.

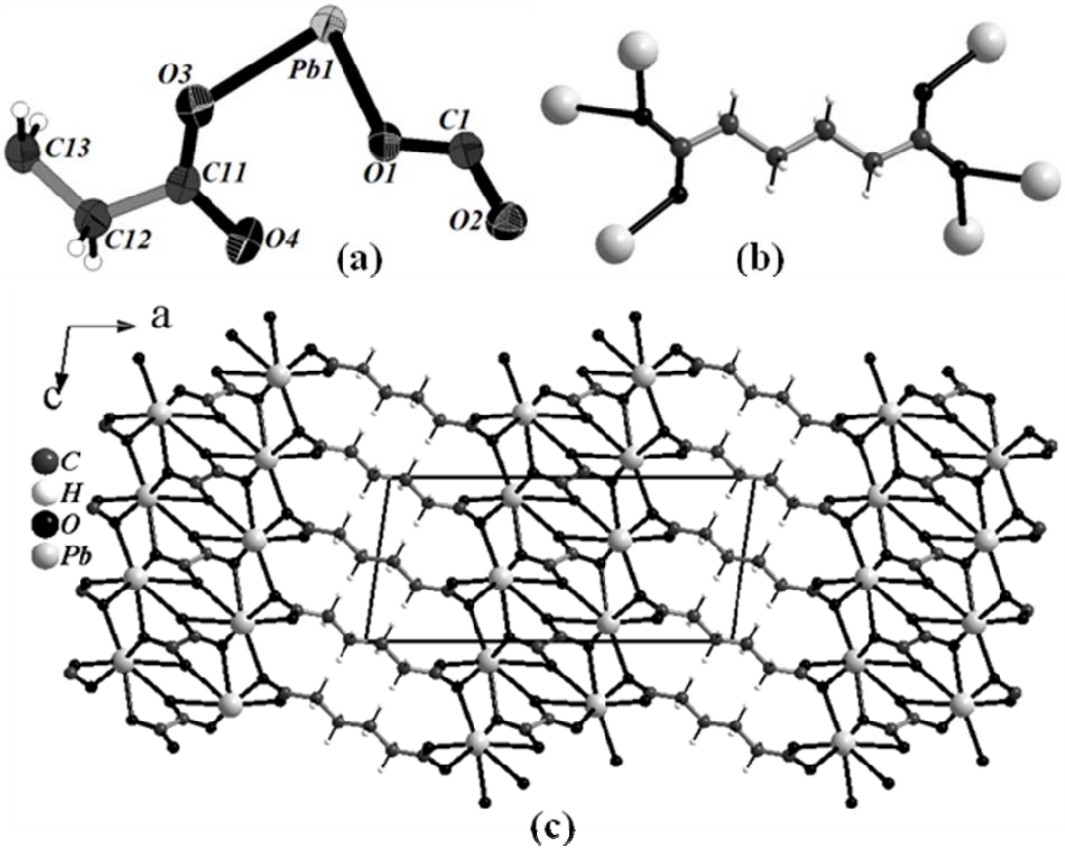

Fig. 4.4.5 (a) ORTEP plot of $Pb_2(C_2O_4)(C_6H_8O_4)$, **V** (Thermal ellipsoids are shown at 50% probability) (b) coordination mode of the succinate moiety in **V** and (c) the 3D-structure of **V** viewed along the *b*- axis.

The three-dimensional lead aliphatic dicarboxylates, **I** to **III** (homoleptic) and **IV** and **V** (heteroleptic) all possess infinite two-dimensional layers of the I^2O^0 type which are connected by the dicarboxylate moiety. The inorganic layers can be

further categorized in to two types: Type **A**: compounds **I** to **II** (Fig. 4.4.1c) and Type **B**: **III** - **V** (Fig. 4.4.3c and 4.4.4d). The difference between **A** and **B** arises from the different polyhedral connectivities in the inorganic layers. The origin of the difference can be attributed to the torsional angles of the dicarboxylate moieties. In type **A**, the torsional angles are close to 100°, whereas it is zero in type **B**. This observation gains support from the structures of other lead aliphatic dicarboxylates. Thus, lead azelate,[35] $Pb(C_9H_{14}O_4)$, with a torsional angle of 93.11°, possesses **A** type inorganic layers connected by the azelate moieties. Lead succinate, $Pb(C_4H_4O_4)$,[28] with a torsional angle of 90.41°, possesses M-O-M inorganic chains, closely related to the connectivity in **A** type layers. In lead succinates,[28,36] the conformation of the acid plays a role in determining the structure. In the lower dicarboxylates, such as malonates,[37,38] and oxalates,[39-41] the main factor is the coordination mode of the acid, coordination number (CN) and the geometry of lead cation, since the torsional angle being always close to zero.

The heteroleptic three-dimensional compounds, **IV** (oxalate-succinate) and **V** (oxalate-adipate), possess a unique bilayer oxalate with the inorganic layer of the $\boldsymbol{I^2O^1}$ type (Figure 4d) connected by the succinate or adipate anions into three-dimensional structures. The other known hybrid heteroleptic aliphatic dicarboxylates are neodymium oxalate-glutarate,[25] $Nd_4(H_2O)_2(C_5H_{63}O_4)_4(C_2O_4)_2$, lanthanum oxalate-succinate,[26] $[La_2(C_2O_4)(C_4H_4O_4)_2(H_2O)_4]\cdot 4H_2O$, lanthanum oxalate-adipate,[26] $La_2(C_2O_4)_2(C_6H_8O_4)\ (H_2O)_2$, and lanthanide oxalate-fumarate,[27] $[La_2(C_2O_4)(C_4H_2O_4)_2\ (H_2O)_4]\cdot 4H_2O$, (Ln = Eu,Tb). The first three are the three-dimensional compounds possessing one-dimensional $\boldsymbol{I^1O^0}$ type M-O-M infinite chains. The oxalate-fumarate is a coordination polymer of the $\boldsymbol{I^0O^3}$ type where four member Ln clusters are connected by carboxylate moieties.

(c) Lead oxalate-nitrate

The oxalate-nitrate, $(OPb_2)_2(C_2O_4)(NO_3)_2$, **VI**, has a two-dimensional structure with an asymmetric unit of 10 atoms. There are two crystallographically distinct Pb^{2+} ions Pb(1) and Pb(2) in the asymmetric unit (Fig. 4.4.6a). One nitrate anion, one half of the oxalate anion and one independent oxo dianion are also in the asymmetric unit. The oxalate anion exhibits a coordination mode with (1221) connectivity with zero torsional angle and the planar nitrate anion is having (233) connectivity (Fig. 4.4.6b).

Pb(1) is hemidirected and seven-coordinated by oxygen atoms (PbO_7) from three different nitrate anions and an apical oxo dianion. Six of the oxygens have $\boldsymbol{\mu}_4$ connections linking Pb(1) with two other Pb(1) atoms and one Pb(2) atom. Thus, a $Pb(1)O_7$ polyhedron shares its six corners with other $Pb(1)O_7$ polyhedra forming an infinite two-dimensional Pb-O-Pb layer of the $\boldsymbol{I^2O^0}$ type, with a (6,3) 2-D net topology (Fig. 4.4.6c). The oxo dianion has $\boldsymbol{\mu}_2$ connectivity and links each Pb(1) with a Pb(2) atom. Pb(2) is hemidirected and six-coordinated by oxygen atoms (PbO_6) from an oxo dianion, two different nitrate anions and two different oxalate anions. These oxgens have $\boldsymbol{\mu}_2$, $\boldsymbol{\mu}_4$ and $\boldsymbol{\mu}_3$ connections respectively. Thus, each $Pb(2)O_6$ polyhedron is linked by the oxalate anion to two of the polyhedron by corner-sharing to give rise an infinite one-dimensional chain. The chains of $Pb(2)O_6$ polyhedra are further connected to the layers formed by $Pb(1)O_7$ units through oxo and nitrate anions, forming an infinite two-dimensional layer with Pb-O-Pb linkages (Fig. 4.4.7a).

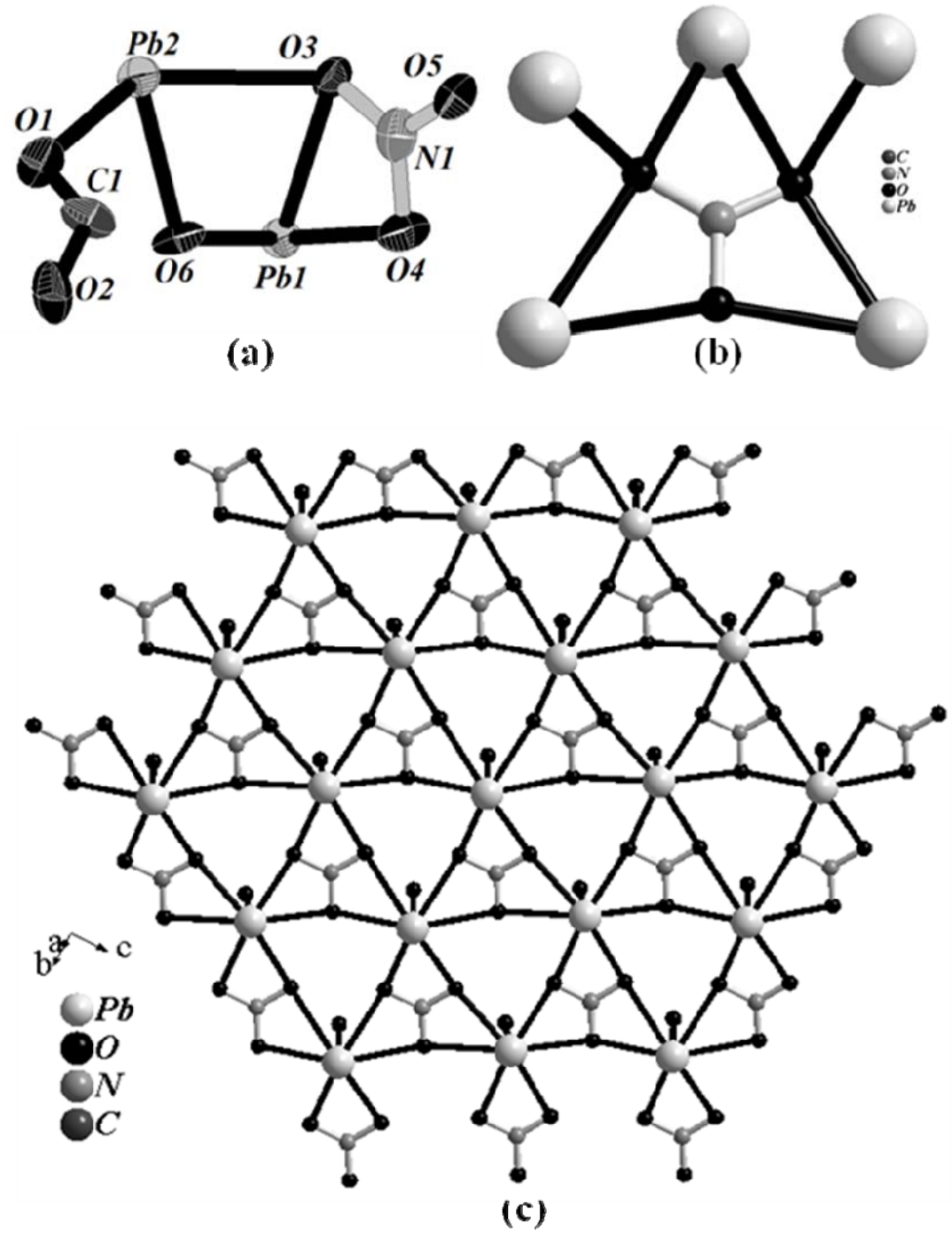

Fig. 4.4.6 (a) ORTEP plot of $(OPb_2)_2(C_2O_4)(NO_3)_2$, **VI** (Thermal ellipsoids are shown at 50% probability) (b) coordination mode of the nitrate moiety in **VI** and (c) view of the inorganic layer with the infinite Pb-O-Pb linkages of the $\boldsymbol{I^2O^0}$ type in **VI**.

While the active lone pair electron of the Pb(1) projects out on one side of the layer, the other side is decorated with chains of hemidirected $Pb(2)O_6$ polyhedra. The oxalate anions connecting these layers through the Pb(2) atom, form a double layer structure with the lone pair of electrons projecting out from

both the sides of the double layer (Fig. 4.4.7b). These layers are packed in a …AAA… manner without any H-bonding interactions. The Pb-O bond lengths are in the 2.268 – 2.830 Å range.

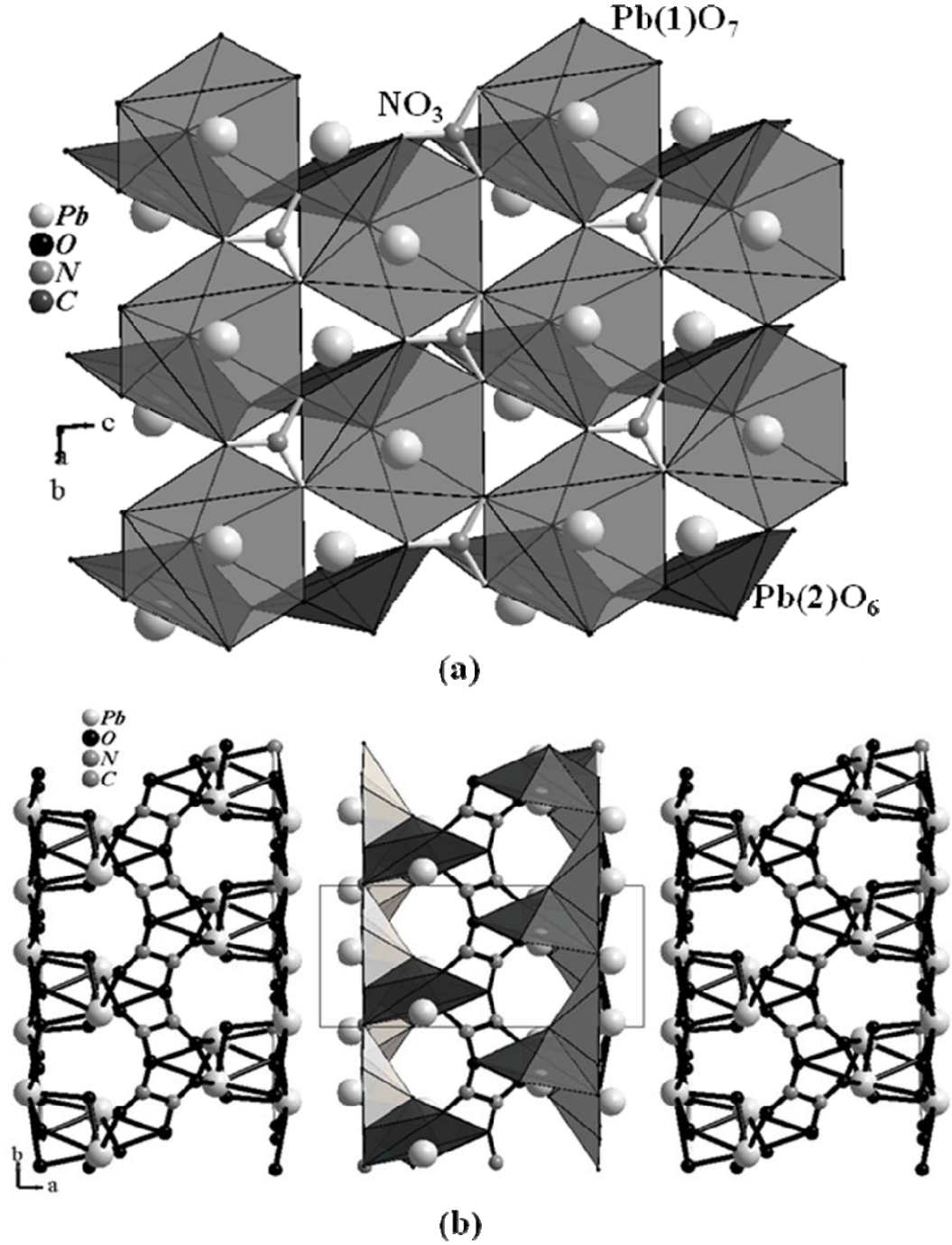

Fig. 4.4.7 (a) View of the inorganic layer with the infinite Pb-O-Pb linkages of the $\boldsymbol{I^2O^0}$ type in $(OPb_2)_2(C_2O_4)(NO_3)_2$, **VI** showing the polyhedral connectivity between $Pb(1)O_7$, $Pb(2)O_7$ and NO_3 moieties and (b) the packing arrangement in **VI**.

The oxalate-nitrate, **VI** is a unique hybrid framework wherein infinite two dimensional layers of lead nitrate of the $\boldsymbol{I^2O^0}$ type are connected by the oxalate moiety into a bilayer structure. Unlike the nitrate anion, oxy-anions such as phosphate, sulfate, sulfite and selenate are known to form organically templated inorganic framework compounds.[42,43] There are, however few organic inorganic hybrid compounds, wherein the nitrate anion is involved in the network formation.[44-54] Most of these compounds are with low-dimensional inorganic connectivity, $\boldsymbol{I^m}$ (m<2). The value of m depends on the nature of chelation, ligation number, coordination mode and connectivity of the nitrate ions. The commonly observed connectivities in the low dimensional hybrids are (110), (111), (112) and (122) with zero to two chelation per single nitrate moiety. The hybrid compound **VI** is appears to be only the second example after $Ag(C_5H_5NO)NO_3$,[54] possessing a two-dimensional inorganic metal nitrate layer with infinite M-O-M linkages. The connectivities of the nitrate in **VI** are unique with (233) connectivity with three chelations (Fig. 4.4.6b). In $Ag(C_5H_5NO)NO_3$, the connectivity is (222) with three chelations.

4.4.3. Coordination geometry of lead

The coordination geometry of the PbO_n polyhedra in Pb(II) compounds is hemidirected for low coordination numbers (2-5) and holodirected for high coordination numbers (9,10). For intermediate coordination numbers (6-8) either type of stereochemistry is found.[55,56] Ab initio molecular orbital studies of gas-phase Pb(II) complexes show that a hemidirected geometry occurs if the ligand coordination number is low, the ligands are hard, and there are attractive interactions between the ligands.[57,58] In such cases, the lone pair orbital has a p character and fewer electrons are transferred from the ligands to the bonding

orbitals of Pb(II), giving rise to more ionic bonds. Holodirected geometry occurs when the coordination number is high and the ligands are soft and bulky or show strong interligand repulsion. The lone pair orbital has negligible p character when the geometry is holodirected, and the bonds are more covalent than in the hemidirected structures.

The Pb(II) cations in **I** to **V** exhibit either hemi- and holo-directed geometry with a CN of 7. **I** and **II**, with type **A** inorganic layers possess Pb(II) cations which in hemidirected geometry with a CN of 7, whereas **III** - **V**, with type **B** inorganic layers possess Pb(II) cations in holo-directed geometry with a CN of 7. The two-dimensional compound, **VI**, with a inorganic bilayer structure has two Pb(II) cations both in hemidirected geometry with CN of 6 and 7. A situation has been reported in another Pb carboxylate where the Pb(II) cations are present with both hemi- and holo-directed geometries[24].

4.5. Conclusions

In conclusion, we have synthesized and characterized five three-dimensional (**I-V**) and one two-dimensional (**VI**) hybrid lead dicarboxylates, all possessing two-dimensional inorganic connectivity. Of these, two of them, the Pb glutarate, **I**, and adipate, **II**, possess one type of two-dimensional inorganic connectivity with near 90 ^{o} torsional angle of the dicarboxylate anions, contains only one ($^{X}\mathbf{D}_{\mathbf{Y}}$) type of dimer SBU and hemidirected Pb(II) cations. The Pb adipate, **III**, as well as the oxalate-succinate, **IV**, and oxalate-adipate, **V**, possess another type of two-dimensional inorganic connectivity with the dicarboxylate anions in the zero torsional angle, contain two different ($^{x}\mathbf{d}_{\mathbf{y}}$ & $^{X}\mathbf{D}_{\mathbf{Y}}$) types of dimer SBUs and holodirected Pb(II) cations. The bilayer nitrate-oxalate, **VI**, is unusual in that it possesses a (6,3) net topology of the two-dimensional inorganic metal nitrate layer,

with infinite M-O-M linkages. The Pb(II) cations in **VI** are in hemidirected geometry with CN 6 and 7. Summary of the structural features of the various compounds discussed in this chapter are tabulated in Table **4.4**.

Table 4.4

Comp. ID.	Formula	Dimensionality	Connectivity	Dimer SBUs
I	Pb(glutarate)	**3**	I^2O^1	$^2D_2$ & $^1D_1$
II	Pb(adipate)	**3**	I^2O^1	$^2D_2$ & $^1D_1$
III	Pb(adipate)	**3**	I^2O^1	($^1d_1$ + $^1D_1$) & $^2D_1$
IV	Pb(oxalate)(succinate)	**3**	I^2O^1	$^1d_1$ & $^2D_1$
V	Pb(oxalate)(adipate)	**3**	I^2O^1	$^1d_1$ & $^2D_1$
VI	Pb(nitrate)(oxalate)	**2**	I^2O^0	**Trimers**

4.6. References

1) C. N. R. Rao, S. Natarajan and R. Vaidhyanathan, *Angew. Chem. Int. Ed*., **2004**, 43, 1466.

2) D. Maspoch, D. Ruiz-Molina and J. Veciana, *Chem. Soc. Rev*., **2007**, *3*6, 770.

3) N.Guillou, C. Livage and G. Férey, *Eur. J. Inorg. Chem*., **2007**, 4963.

4) N. L. Rosi, J. Eukert, M. Eddaoudi, D. T. Vodak, J. Kim, M.O'Keeffe and O. M. Yaghi, *Science*, **2003**, 300, 1127.

5) G. Férey, C.Mellot-Draznieks, C. Serre, F. Millange, J. Dutour, S. Surblé and I. Margiolaki, *Science*, **2005**, 309, 2040.

6) C. Serre, F. Millange, S.Surblé and G. Férey, *Angew. Chem., Int. Ed.*, **2004**, 43, 6285.

7) C. Serre, F. Millange, S.Surblé and G. Férey, *Chem. Mater.*, **2004**, 16, 2706.

8) L-S. Long, X.-M. Chen, M.-L. Tong, Z.-G. Sun, Y.-P Ren, R.-B. Huang and L-S. Zheng, *J. Chem. Soc., Dalton Trans.*, **2001**, 2888.

9) C. Livage, C. Egger, M. Noguès and G. Férey, *J. Mater. Chem.*, **1998**, 8, 2743.

10) C. Livage, C. Egger and G. Férey, *Chem. Mater.*, **1999**, 11, 1546.

11) N. Guillou, C .Livage, M. Drillon and G. Férey, *Angew. Chem. Int. Ed*., **2003**, 42, 5314.

12) P. M. Forster and A. K. Cheetham, *Angew. Chem. Int. Ed.*, **2002**, 41, 457.

13) R. Vaidhyanathan, S. Natarajan and C. N. R. Rao, *Dalton Trans.*, **2003**, 1459.

14) R. Vaidhyanathan, S. Natarajan and C. N. R. Rao, *Cryst. Growth Des*., **2003**, 3, 47.

15) S. C. Manna, E. Zangrando, A.Bencini, C. Benelli and N. R. Chaudhuri, *Inorg. Chem*., **2006**, 45, 9114.

16) S. Konar, P.S. Mukherjee, E. Zangrando, F. Lloret and N. R. Chaudhuri, *Angew. Chem. Int. Ed* ., **2002**, 41, 1561.

17) A. K. Cheetham, C.N.R. Rao and R.K. Feller, *Chem. Commun*., **2006**, 4780.

18) M. Kurmoo, H. Kumagai, S.M. Hughes and C. J. Kepert, *Inorg. Chem.*, **2003**, 42, 6709.

19) Z.-L. Huang, M. Drillon, N. Masciocchi, A. Sironi, J.-T. Zhao, P. Rabu and P. Panissod, *Chem. Mater.*, **2000**, 12, 2805.

20) K. Barthelet, K. Adil, F. Millange, C. Serre, D. Riou, G. Férey, *J. Mater. Chem*., **2003**, 13, 2208.

21) C. A. Merrill and A. K. Cheetham, *Inorg. Chem.*, **2007**, 46, 278.

22) A. Thirumurugan, , M. B. Avinash and C. N. R. Rao, *Dalton. Trans*., **2006**, 221.

23) K. P. Rao, A. Thirumurugan and C. N. R. Rao, *Chem. Eur.J.*, **2007**, **13**, 3193.

24) A. Thirumurugan, R. Sanguramath and C. N. R. Rao, *Inorg. Chem.*, **2008**, 47, 823.

25) R. Vaidhyanathan, S. Natarajan and C. N. R. Rao, *J. Solid State Chem*., **2004**, 177, 1444.

26) M. Dan, G. Cottereau and C. N. R. Rao, *Solid State Sciences,* **2005**, 7, 437.

27) W-H. Zhu, Z-M. Wang and S.Gao, *Inorg. Chem.*, **2007**, 46, 1337.

28) M.R.St J. Foreman, M.J. Plater and J.M.S. Skakle, *J.Chem.Soc., Dalton Trans.*, **2001**, 1897.

29) S. Barbara, Infrared Spectroscopy: Fundamentals and Applications, Wiley, New York, **2004**.

30) R. M. Silverstein, G. C. Bassler and T. C. Morrill, Spectrometric Identification of Organic Compounds, John Wiley & Sons, New York, **1963**.

31) K. Nakamoto, Infrared and Raman Spectra of Inorganic and Coordination Compounds, Wiley, New York, **1978**.

32) G. M. Sheldrick, SADABS Siemens Area Detector Absorption Correction Program, University of Göttingen: Göttingen, Germany, **1994**.

33) G. M. Sheldrick, SHELXTL-PLUS Program for Crystal Structure Solution and Refinement, University of Göttingen: Göttingen, Germany, **1997**.

34) For description of connectivity see, D. Massiot, S. Drumel, P. Janvier, M. B-Doeuff and B. Buujoli, *Chem Mater*., **1997**, 9, 6.

35) M.J. Plater, B. De Silva, Gelbrich, T. M.B. Hursthouse, C.L. Higgitt and D.R. Saunders, *Polyhedron,* **2003**, 22, 3171.

36) K. Nagase and H. Yokobayashi, *Chem.Lett.*, **1974**, 861.

37) J.R. Gunter, *Cryst.Res.and Technol.,* **1982**, 17, K123.

38) W. Bensch and J.R. Gunter, *Z. Kristallogr.*, **1987**, 178, 257.

39) A.V. Virovets, D.Yu. Naumov, E.V. Boldyreva and N.V. Podberezskaya, *Acta Crystallogr., Sect.C: Cryst.Struct.Commun.*, **1993**, 49,1882.

40) H. S-Hua, W. Ru-Ji and T.C.W. Mak, *J.Crystallogr.Spectrosc.Res.*, **1990**, 20, 99.

41) A. N. Christensen, D. Cox and M. S. E. Lehmann, *Acta Chem. Scand*., **1989**, 43, 19.

42) A. K.Cheetham, G. Férey and T. Loiseau, *Angew. Chem. Int. Ed*., **1999**, 38, 3268.

43) C.N. R. Rao, J. N. Behera and M. Dan, *Chem. Soc. Rev*., **2006**, 35, 375.

44) B.G. Cooksey, L.T. Gibson, A.R. Kennedy, D. Littlejohn, L. Stewart and N.H. Tennent, *Acta Crystallogr., Sect.C: Cryst.Struct.Commun.*, **1999**, 55, 324.

45) L. Zhao and T.C.W. Mak, *J. Am. Chem. Soc.*, **2004**, 126, 6852.

46) J-P. Costes, F. Dahan, A. Dupuis and J-P. Laurent *Inorg.Chem.*, **2000**, 39, 169.

47) Y-Q. Zheng, J-L. Lin and W-J. Chen, *Z.Kristallogr.-New Cryst.Struct.*, **2001**, **216**, 269.

48) C.L. Lengauer and G. Giester, *Acta Crystallogr., Sect.C: Cryst.Struct.Commun.*, **1997**, 53, 870.

49) M. Fangming, L. Xiaolan, Z. Shufen, J. Zonghui and W. Genglin, *Wuli Huaxue Xuebao(Chin.)(Acta Phys.-Chim.Sin).*, **1988**, 4, 20.

50) K. Lashgari, M. Kritikos, K. Lashgari and G. Westin, *Acta Crystallogr. ,Sect.C: Cryst.Struct.Commun.*, **1998**, 54, 1794.

51) G.A. Bowmaker, B. Assadollahzadeh, A.M. Brodie, E.W. Ainscough, G.H. Freeman and G.B. Jameson, *Dalton Trans.*, **2005**, 1602.

52) M. Hashimoto, M. Takata and A. Yagasaki, *Inorg.Chem.*, **2000**, 39, 3712.

53) G.A. Bowmaker, Effendy, S. Marfuah, B.W. Skelton and A.H White, *Inorg.Chim.Acta*, **2005**, 358, 4371.

54) G.A. Bowmaker, Effendy, M. Nitiatmodjo, B.W. Skelton and A.H. White, *Inorg.Chim.Acta*, **2005**, 358, 4327.

55) S. Ayyappan, G. Diaz de Delgado, A. K. Cheetham, G. Férey and C. N. R. Rao, *J. Chem. Soc. Dalton Trans.,* **1999**, 2905.

56) T. Glowiak, H. Kozlowski, L. S. Erre, G. Micera and B. Gulinati, *Inorg. Chim. Acta.,* **1992**, *202*, 43.

57) L. S-Livny, J. P. Glusker and C. W. Bock, *Inorg. Chem*. **1998**, 37, 1853.

58) C. W. Watson and S. C. Parker, *J. Phys. Chem. B*. **1999**, 103, 1258.

4.7. Appendix

Table A4.1
Atomic Coordinates and Equivalent Isotropic Displacement Parameters [Å^2] for Pb(glutarate), **I**.

Atom	x	y	z	U(eq)
Pb1	0.18848(6)	1/4	0.08109(3)	0.0455(2)
O1	0.2818(18)	1/4	0.2069(9)	0.070(4)
O2	0.085(2)	1/4	0.3266(10)	0.088(5)
O3	0.1443(19)	0.1000(13)	0.8921(9)	0.076(2)
C1	0.167(2)	1/4	0.3198(12)	0.048(3)
C2	0.354(3)	1/4	0.4547(14)	0.070(5)
C3	0.193(3)	1/4	0.5854(11)	0.050(4)
C4	0.385(2)	1/4	0.7143(11)	0.048(3)
C5	0.219(2)	1/4	0.8414(9)	0.046(3)

U(eq) is defined as one third of the trace of the orthogonalized Uij tensor.

Table A4.2
Atomic Coordinates and Equivalent Isotropic Displacement Parameters [Å^2] for Pb(adipate), **II**.

Atom	x	y	z	U(eq)
Pb1	0.24811(2)	-0.30072(3)	0.46464(1)	0.0217(1)
O1	0.2699(6)	0.2448(7)	0.40885(17)	0.0390(13)
O2	0.2133(5)	0.6278(7)	0.35690(14)	0.0421(11)
O3	0.4004(5)	0.1481(8)	0.05273(18)	0.0433(11)
O4	0.1042(5)	0.1703(8)	0.04037(18)	0.0435(13)
C1	0.2488(6)	0.3689(10)	0.3586(2)	0.0240(14)
C2	0.2728(8)	0.2144(9)	0.2995(3)	0.0297(14)
C3	0.2335(6)	0.3895(10)	0.24273(18)	0.0263(12)
C4	0.2655(7)	0.2284(9)	0.1842(2)	0.0273(16)
C5	0.2324(6)	0.4078(10)	0.12670(18)	0.0273(12)
C6	0.2484(6)	0.2357(9)	0.0698(2)	0.0210(12)

U(eq) is defined as one third of the trace of the orthogonalized Uij tensor.

Table A4.3
Atomic Coordinates and Equivalent Isotropic Displacement Parameters [Å^2] for Pb(adipate), **III**.

Atom	x	y	z	U(eq)
Pb1	0.24278(2)	0.47873(7)	0.00949(5)	0.0485(2)
O1	0.2982(4)	0.4317(15)	0.3349(12)	0.067(2)
O2	0.3429(3)	0.7936(12)	0.4679(8)	0.0691(17)
O3	0.1459(3)	0.2238(12)	0.2325(9)	0.0716(19)
O4	0.1986(3)	0.8567(12)	0.1794(8)	0.0640(17)
C1	0.3471(5)	0.563(2)	0.4021(14)	0.053(3)
C2	0.4127(5)	0.4393(17)	0.3934(13)	0.053(3)
C3	0.4679(4)	0.5675(18)	0.5121(13)	0.051(3)
C4	0.0280(5)	0.0558(17)	0.0622(15)	0.053(3)
C5	0.0908(3)	-0.1049(15)	0.0443(10)	0.049(2)
C6	0.1480(7)	0.0005(14)	0.1612(16)	0.049(3)

U(eq) is defined as one third of the trace of the orthogonalized Uij tensor.

Table A4.4
Atomic Coordinates and Equivalent Isotropic Displacement Parameters [Å^2] for Pb(oxalate)(succinate), **IV**.

Atom	x	y	z	U(eq)
Pb1	0.31274(3)	0.46539(10)	0.09694(5)	0.0335(3)
O1	0.3673(5)	0.8853(16)	-0.0356(10)	0.040(2)
O2	0.5175(5)	0.7219(13)	0.1374(9)	0.0379(17)
O3	0.1552(6)	0.7125(17)	0.1108(11)	0.047(2)
O4	0.2159(6)	0.0838(15)	0.2476(11)	0.043(2)
C1	0.4652(9)	0.885(3)	0.0314(15)	0.037(3)
C11	0.1412(10)	0.943(2)	0.1469(18)	0.036(4)
C12	0.0391(8)	1.0720(18)	0.0772(17)	0.035(3)

U(eq) is defined as one third of the trace of the orthogonalized Uij tensor.

Table A4.5
Atomic Coordinates and Equivalent Isotropic Displacement Parameters [Å^2] for Pb(oxalate)(adipate), **V**.

Atom	x	y	z	U(eq)
Pb1	0.34459(2)	0.46341(6)	0.11597(4)	0.0341(2)
O1	0.3907(4)	0.6147(13)	0.4753(8)	0.0396(19)
O2	0.5136(4)	0.7822(11)	0.6406(8)	0.0407(19)
O3	0.2115(4)	0.7046(14)	0.1414(9)	0.048(2)
O4	0.2669(5)	0.0721(13)	0.2764(9)	0.044(2)
C1	0.4718(6)	0.6133(17)	0.5329(10)	0.032(2)
C11	0.2027(7)	0.9329(17)	0.1892(12)	0.036(3)
C12	0.1143(7)	1.0597(17)	0.1571(13)	0.041(3)
C13	0.0445(6)	0.9291(17)	0.0139(12)	0.038(3)

U(eq) is defined as one third of the trace of the orthogonalized Uij tensor.

Table A4.6
Atomic Coordinates and Equivalent Isotropic Displacement Parameters [Å^2] for Pb(nitrate)(oxalate), **VI**.

Atom	x	y	z	U(eq)
Pb1	0.40167(4)	0.46644(11)	0.31890(6)	0.0293(2)
Pb2	0.18042(4)	0.90156(11)	0.15279(6)	0.0321(2)
O1	-0.0217(9)	0.742(2)	0.1264(13)	0.041(3)
O2	-0.1208(10)	0.387(3)	0.0762(14)	0.049(4)
O3	0.3612(9)	0.728(2)	0.0458(11)	0.034(3)
O4	0.3689(10)	0.293(2)	0.0470(11)	0.040(3)
O5	0.3621(10)	0.986(2)	0.3379(12)	0.035(3)
O6	0.2119(10)	0.5069(18)	0.2505(12)	0.035(3)
N1	0.3630(12)	0.513(3)	-0.0248(15)	0.037(4)
C1	-0.0415(13)	0.544(3)	0.0576(16)	0.036(5)

U(eq) is defined as one third of the trace of the orthogonalized Uij tensor.

Chapter 5

Hybrid Network of Lead Dihydroxybenzoate

Summary*

As part of our effort to synthesize novel hybrid frameworks with multifunctional ligands, investigations were carried out by employing 2,6-dihydroxybenzoicacid with the potentially lone pair active, flexible coordinating Pb(II) cation. A three-dimensional lead 2,6-dihydroxybenzoate coordination polymer of the formula $Pb(C_{14}H_{10}O_8)$, **I,** has been synthesized and characterized by X-ray crystallography and spectroscopic techniques. This is the first three-dimensional metal dihydroxybenzoate structure, comprising 3,6-connected periodic net and possessing channels with the dimensions 3.8 × 3.8 $Å^2$ and 10.8 × 3.8 $Å^2$ measured from carbon-to-carbon and cenrtoid-to-centroid of the aromatic ring without considering the radii of the atoms. The coordination geometry of the PbO_8 polyhedron is holodirected and the electron lone pair of the lead is, therefore, not manifested in **I**. It exhibits photoluminescence in the violet, green and red when excited at 240, 390 and 525 nm respectively.

*An article based on this study has been published in *Z. Anorg. Allg. Chem.* (2007).

5.1. Introduction

Although metal silicates and phosphates abound in the literature on open framework materials[1-3], recent studies on metal carboxylates have added a new dimension to this area as well as to inorganic-organic hybrid materials.[4] These studies show how a variety of hybrid materials of different dimensions can be designed using carboxylic acids.[5-10] Dihydroxybenzoic acids are interesting organic linkers because of the availability of both the carboxyl and hydroxyl functional groups for the connectivity.[11-22] A recent study of strontium and lanthanum derivatives of various isomeric dihydroxybenzoic acids has revealed the formation of diverse structures with one and two dimensionalities.[23] However, no three-dimensional metal dihydroxybenzoate has been found to date. We have, therefore, explored the possibility of synthesizing a three-dimensional dihydroxybenzoate.

5.2. Scope of the present investigation

Synthesis of novel hybrid coordination polymers with novel architecture is an important area of research. We have investigated the formation of such networks by employing multifunctional 2,6-dihydroxybenzoicacid and a potentially lone pair active Pb(II) cation with a large ionic radii and flexible coordination geometry. We have successfully synthesized a three-dimensional lead 2,6-dihydroxybenzoate coordination polymer of the formula $Pb(C_{14}H_{10}O_8)$, **I,** and characterized it by X-ray crystallography and spectroscopic techniques. This is the first three-dimensional metal dihydroxybenzoate structure, comprising 3,6-connected periodic net and possessing channels with the dimensions 3.8×3.8 Å^2 and 10.8×3.8 Å^2 measured from carbon-to-carbon and cenrtoid-to-centroid

without considering the radii of the atoms. The coordination geometry of the PbO_8 polyhedron is holodirected and the electron lone pair of the lead is, therefore, not manifested in **I**. It exhibits photoluminescence in the violet, green and red when excited at 240, 390 and 525 nm respectively.

5.3. Experimental

Synthesis and characterization

Materials and methods: $Pb(NO_3)_2$ (Qualigens, India, 99%), 2,6-dihydroxybenzoicacid (Aldrich, 99%) of high purity and double distilled water were used for the synthesis.

Lead 2,6-dihydroxybenzoate, $Pb(2,6\text{-}DHB)_2$ was synthesized by mixing 0.1 g, 0.3 mmol of $Pb(NO_3)_2$ and 0.047 g, 0.3 mmol of 2,6-dihydroxybenzoaic acid in 5ml H_2O. The mixture was stirred with heating at 80^oC for 45 minutes. The homogenized reaction mixture was left at room temperature for crystallization. Rod-shaped crystals suitable for single crystal structure determination were obtained after two days. The pH of the starting reaction mixture was 2. The pH after the reaction did not show any appreciable change. The product was washed with H_2O, vacuum-filtered and dried under ambient condition.

The powder XRD pattern of the product was recorded using Cu Kα radiation (Rich-Seifert, 3000TT). The pattern agreed with that calculated from single crystal structure determination. Thermogravimetric analysis (TGA) was carried out (Metler-Toledo) in an oxygen atmosphere (flow rate = 50 ml/min) in the temperature range 25 to 900 °C (heating rate = 5 °C/min). Infra-red (IR) spectroscopic studies were carried out in the mid-IR region as a KBr pellet (Bruker

IFS-66v). Room temperature photoluminescence spectra were recorded on a powdered sample. A Perkin-Elmer spectrometer (LS-55) with a single beam set-up was employed using a xenon lamp (50 watt) as the source and a photo-multiplier tube as the detector.

Thermogravimetric analysis of **I** shows two weight losses. The first weight loss of 35.74% occurred around 215^{o} C and the second weight loss of 23.52% was in the 215-900^{o} C range. The total weight loss of 59.26% matches very well with the loss of CO_2 and H_2O (calc. 59.65%) along with the formation of PbO.

The infra-red (IR) spectrum of **I** shows characteristic bands of the carboxylate and hydroxyl units. The bands around 1591 and 1390 cm^{-1} are assigned to carboxylate $\nu_{as\ C=O}$ and $\nu_{s\ C=O}$ stretching. Absence of a band at 1700 cm^{-1} confirms the binding of carboxylate group to the lead anion. The bands at 3566 ($\nu_{as\ O-H}$), 3476 ($\nu_{s\ O-H}$), 1242 $(\delta_{O-H})_{in\text{-}plane}$ and 611 cm^{-1} $(\delta_{O-H})_{out\text{-}of\text{-}plane}$ indicates the presence of hydroxyl groups and its ligation to the lead cation.

Single crystal structure determination

A suitable single crystal of the compound was carefully selected under a polarizing microscope and glued to a thin glass fiber. Crystal structure determination by X-ray diffraction was performed on a Bruker Smart-CCD diffractometer equipped with a normal focus, 2.4 kW sealed tube X-ray source (Mo Kα radiation, λ = 0.71073Å) operating at 50 kV and 30 mA. An empirical absorption correction based on symmetry equivalent reflections was applied using the SADABS program.[24] The structure was solved and refined using SHELXTL-PLUS suite of program.[25] For the final refinement, the hydrogen atoms on the ring were placed geometrically and held in the riding mode. The hydrogen atoms of the

hydroxyl group were located in the difference Fourier map and the O-H distance was constrained to 0.85 Å. Final refinement included atomic positions for all the atoms, anisotropic thermal parameters for all the non-hydrogen atoms and isotropic thermal parameters for the hydrogen atoms. Details of the structure solution and final refinements and selective bond lengths for the compound are given in Tables 5.1 and 5.2 respectively. Atomic coordinates are given in the appendix (see 5.7. Appendix, Table A5.1).

Table 5.1. Crystal data and structure refinement parameters for **I**.

Structure parameter	$Pb(2,6\text{-}DHB)_2$
Empirical formula	$C_{14}H_{10}PbO_8$
Formula weight	513.2
Crystal system	Monoclinic
Space group	C2/c, (no. 15)
a /Å	11.2155(2)
b /Å	9.2942(2)
c /Å	13.5112(3)
α /°	90
β /°	96.510(1)
γ /°	90
V /Å^3	1399.31(5)
Z	4
D (calc) /gcm^{-3}	2.437
μ /mm^{-1}	12.099
Total data collected	15569
Unique data	8721
Observed data [I > 2σ (I)]	6391
R_{merg}	0.0334
Goodness of fit	1.020
R indexes [I > 2σ (I)]	$R_1 = 0.0314$[a]; $wR_2 = 0.0663$[b]
R indexes [all data]	$R_1 = 0.0533$[a]; $wR_2 = 0.0731$[b]

[a] $R_1 = \Sigma ||F_0|-|F_c|| / \Sigma |F_0|$; [b] $wR_2 = \{\Sigma[w(F_0^2 - F_c^2)^2] / \Sigma[w(F_0^2)^2]\}^{1/2}$. $w = 1/[\sigma^2(F_0)^2 + (aP)^2 + bP]$, $P = [\max.(F_0^2,0) + 2(F_c)^2]/3$, where $a = 0.0344$ and $b = 0$.

Table 2. Selected bond distances and angles for $Pb(2,6\text{-}DHB)_2$, **I**.

Bond	Distance (Å)
Pb(1) - O(1)	2.473(2)
Pb(1) - O(1)#1	2.473(2)
Pb(1) - O(2)	2.548(2)
Pb(1) - O(2)#1	2.548(2)
Pb(1) - O(3)#2	2.803(1)
Pb(1) - O(3)#3	2.803(1)
Pb(1) - O(4)#4	2.907(1)
Pb(1) - O(4)#5	2.907(1)
C(1) - O(1)	1.269(3)
C(1) - O(2)	1.269(3)
C(3) - O(3)	1.363(3)
C(7) - O(4)	1.361(3)

Symmetry transformations used to generate equivalent atoms: #1 -x,y,1/2-z, #2 1/2-x,1/2+y,1/2-z,, #3 -1/2+x,1/2+y,z, #4 x,1-y,1/2+z, #5 -x,1-y,-z.

5.4. Results and discussion

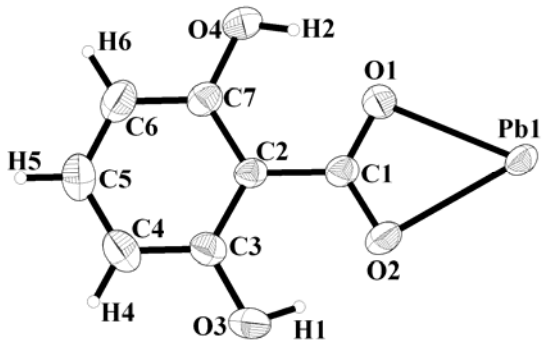

Fig. 5.4.1 ORTEP plot of Pb(2,6-DHB)$_2$, **I**. Thermal ellipsoids are shown at 50 % probablility.

Lead 2,6-dihydroxybenzoate, Pb($C_{14}H_{10}O_8$), **I**, has a three-dimensional structure with an asymmetric unit of 11.5 non-hydrogen atoms (Fig. 5.4.1). Lead is in the 2+ oxidation state and is coordinated to eight oxygen atoms with a distorted dodecahedral environment (PbO_8). The lead cation sits at 4*e* position and have 0.5 occupancy factor.

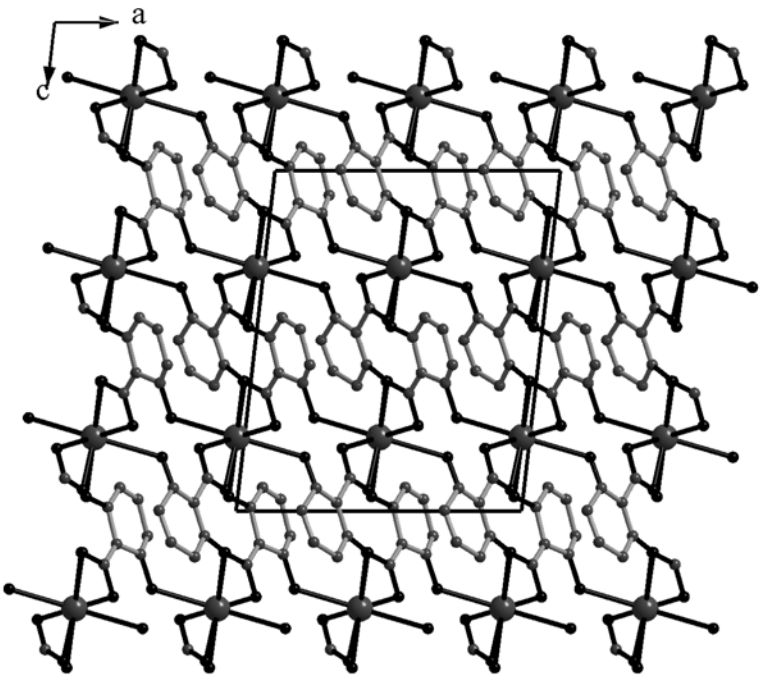

Fig. 5.4.2. 3D-structure viewed along the *b*- axis in Pb(2,6-DHB)$_2$, **I**.

The eight oxygen atoms are from six different dihydroxybenzoates (DHBs). Each carboxylate group of the DHB anion binds with a single Pb cation in a chelating coordination mode. The hydroxyl groups of the DHB anions are also participating in the ligation to the Pb cations with a mono-dentate coordination mode. Among the eight oxygen atoms of the PbO_8, four are from two chelating carboxylate groups of the two different DHB anions. The remaining four are from hydroxyl groups of four different DHB anions (Fig. 5.4.2). Thus, each PbO_8 polyhedron is connected to six DHB anions and each DHB anion coordinates to three Pb(II) atoms forming a 3,6-connected three-dimensional net (Fig. 5.4.3).

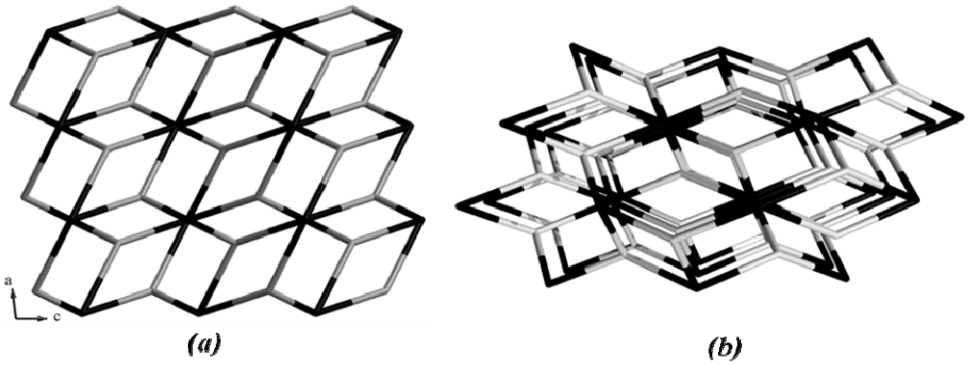

Fig. 5.4.3. Views of 3,6-Connected three-dimensional net derived from the structure of **I**. Grey 3-connected nodes represent DHB ligands, while black 6-connected nodes represent PbO_8 polyhedron.

The structure involves no Pb-O-Pb linkages and can therefore be considered to be a 3-D coordination polymer of the $\boldsymbol{I^0O^3}$ type according to the recent classification.[4] The three-dimensional structure consists of infinite one-dimensional channels along two directions, one perpendicular to the *c*-axis with channel dimensions of 10.8 × 3.8 $Å^2$ measured from carbon-to-carbon and cenrtoid-to-centroid without considering the radii of the atoms (Fig. 5.4.4) and the other along the *c*-axis with channel dimensions of 3.8 × 3.8 $Å^2$ (Fig. 5.4.5). The three-dimensional net structure has intramolecular hydrogen bondings involving

carboxylate and hydroxyl groups (D···A distances in the range 2.542-2.545 Å and the D-H···A angles in the range 145-154^o) as well as $\pi...\pi$ interactions (3.75-3.86 Å and 2.77^o) involving the aromatic rings (Fig. 5.4.5). The Pb-O bond distances are in the range 2.473 - 2.907 Å.

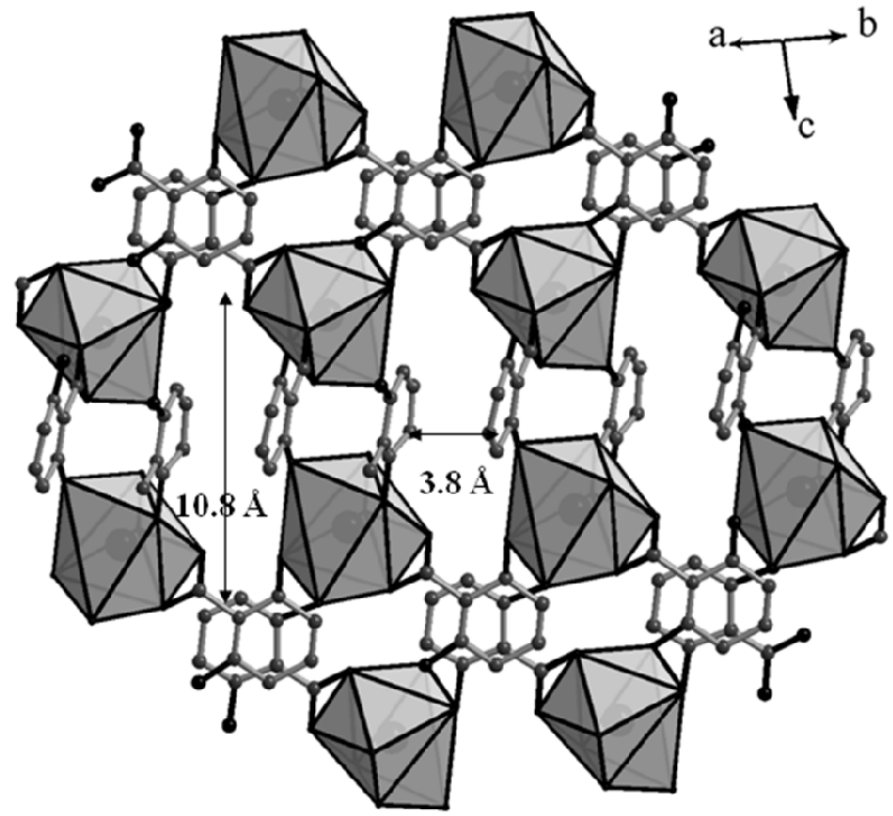

Fig. 5.4.4. 3D-structure viewed perpendicular to the *c*- axis with channel dimensions of 10.8 × 3.8 Å^2 in Pb(2,6-DHB)$_2$, **I**.

The coordination geometry of the PbO_n polyhedron in Pb(II) compounds is hemidirected for low coordination numbers (2-5) and holodirected for high coordination numbers (9,10). For intermediate coordination numbers (6-8) either type of stereochemistry is found.[26] Ab initio molecular orbital studies of gas-phase Pb(II) complexes show that a hemidirected geometry is favored if the ligand coordination number is low, the ligands are hard, and there are attractive interactions between the ligands. In such complexes, the lone pair orbital has p

character and fewer electrons are transferred from the ligands to the bonding orbitals of Pb(II), resulting in bonds that are more ionic. Holodirected geometry is favored when the coordination number is high and the ligands are soft and bulky or show strong interligand repulsion. The lone pair orbital has little or no p character when the geometry is holodirected, and the bonds are more covalent than in the hemidirected structures.[27] The PbO_8 polyhedron in **I** is holodirected, wherein the lone pair electron of the lead is not manifested. This is not always the case in Pb(II) hybrids. For example, the Pb(II) carboxyethylphosphonate exhibits hemidirected bonding.[28]

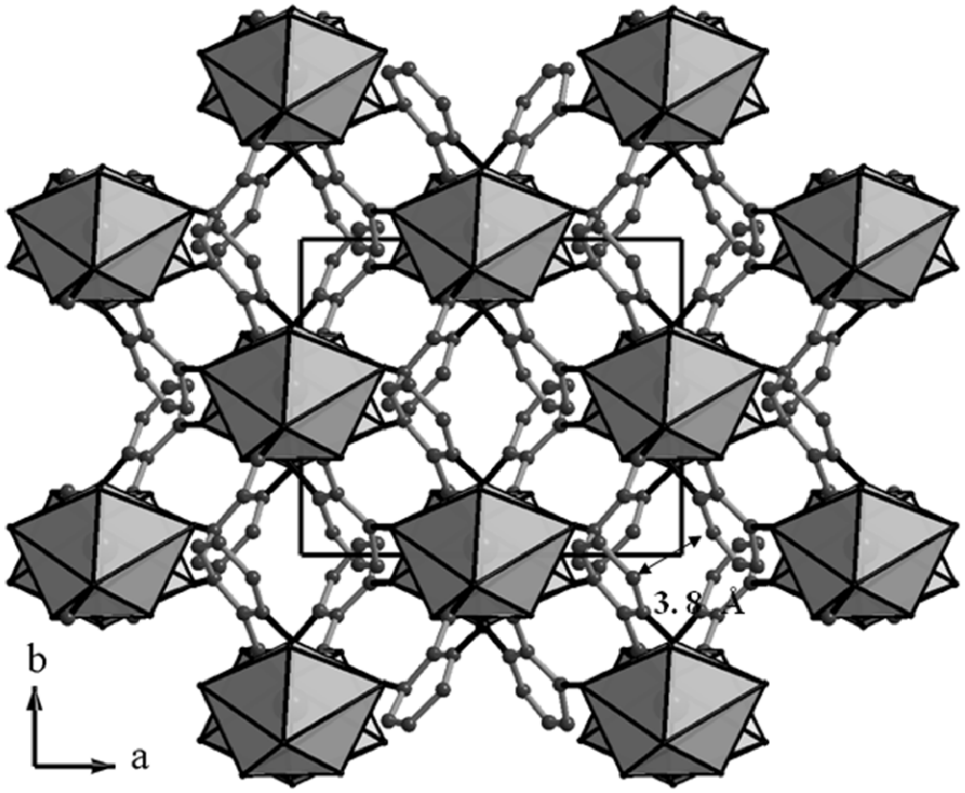

Fig. 5.4.5. 3D-structure viewed along the *c*- axis with channel dimensions of 3.8 × 3.8 Å showing $\pi...\pi$ interactions involving the aromatic rings in $Pb(2,6\text{-}DHB)_2$, **I**.

The 2,6-dihydroxybenzoic acid shows luminescence bands in the 350 – 450nm region when excited at 240nm. When excited at the same wavelength, **I** exhibits characteristic photoluminescence (PL) spectra with bathochromic-shifted

peaks in the 350 – 450nm range (Fig. 5.4.6a). These peaks can be assigned to the intraligand emission.[11-22] Emissions at 553 and 671 nm were observed when **I** was excited at 390 and 525 nm respectively, unlike the ligand, 2,6-dihydroxybenzoic acid. These peaks can be assigned to the emissions related to either metal to ligand or ligand to metal charge transfer (Fig. 5.4.6b and c).

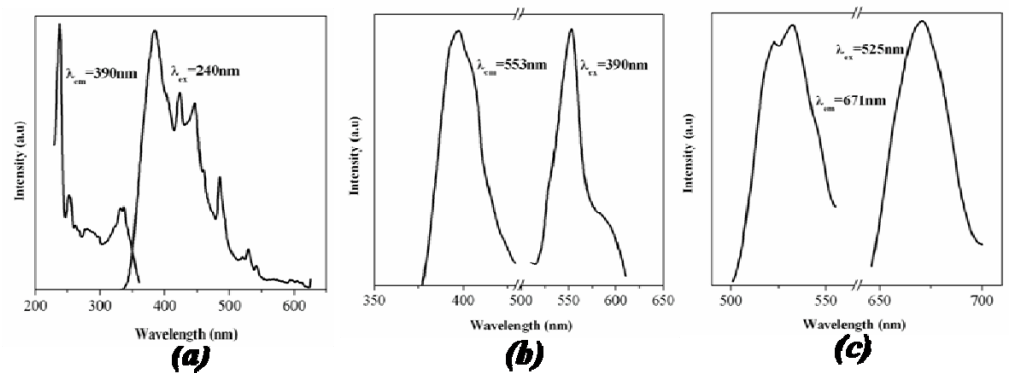

Fig. 5.4.6. Photo luminescence spectra of $Pb(2,6\text{-}DHB)_2$, **I**, when excited at a) 240 nm b) 390 nm and c)525 nm at room temperature.

5.5. Conclusions

While the recent literature reports one- and two- dimensional metal dihydroxybenzoates, it has been possible to synthesize a three-dimensional lead 2,6-dihydroxybenzoate for the first time. The 3,6-connected three-periodic net in this compound possesses channels with dimensions of 3.8×3.8 Å^2 and 10.86×3.8 Å^2. The electron in the PbO_8 polyhedron with the holodirected coordination geometry gives rise to negligible p-character in the lone pair of Pb(II).

5.6. References

(1) D. W. Breck, *Zeolite Molecular Sieves*, Wiley, New York, **1974**.

(2) W. M. Meier, D. H.Oslen, C. Baerlocher, *Atlas of Zeolite Structure Types*, Elsevier: London, **1996**.

(3) A K. Cheetham, G. Férey, T. Loiseau, *Angew. Chem. Int. Ed*., **1999**, 38, 3268.

(4) C. N. R. Rao, S. Natarajan, R. Vaidhyanathan, *Angew. Chem. Int. Ed*., **2004**, 43, 1466.

(5) B. Moulton, M. J. Zawarotko, *Chem. Rev*., **2001**, 101, 1629.

(6) (b) P. M. Forster, A. K. Cheetham, *Angew. Chem.*, **2002**, 114, 475.

(7) R. Kitaura, K. Fujimoto, S. Noro, M. Kondo, S. Kitagawa, *Angew. Chem.*, **2002**, 114, 141.

(8) G. Férey, C. M-Draznieks, C. Serre, F. Millange, J. Dutour, S. Surblé, I. Margiolaki, *Science*, **2005**, 309, 2040.

(9) J. L. C. Rowsell, O. M. Yaghi, *Angew. Chem.*, **2005**, 117, 4748; *Angew. Chem. Int. Ed*., **2005**, 44, 4670.

(10) A. K. Cheetham, C. N. R. Rao, R. K. Feller, *Chem. Commun*., **2006**, 4780.

(11) M. P.Suh, K. S.Min, J. W.Ko, H. J. Choi, *Eur. J. Inorg. Chem.,* **2003**, 1373.

(12) H-Y. Wang, S. Gao, S. W. Ng, *Acta Cryst.,* **2005**, *E61*, m2639.

(13) T. Glowiak, H. Kozlowski, L. S. Erre, G. Micera, B. Gulinati, *Inorg. Chim. Acta.,* **1992**, *202*, 43.

(14) C. Litos, A. Terzis, C. Raptopoulou, A. Rontoyianni, A. Karaliota, *Polyhedron,* **2006**, *25*, 1337.

(15) W. P. Griffith, H. I. S. Nogueira, B. C. Parkin, R. N.Sheppard, A. J. P. White, D. J.Williams, *J. Chem. Soc. Dalton Trans.,* **1995**, 1775.

(16) G.Micera, L. S. Erre, F. Cariati, G. Ciani, A. Sironi, *Inorg. Chim. Acta.*, **1985**, *108*, L1.

(17) G. S.Papaefstathiou, B. G. Darrow, , L. R. MacGillivray*J. Chem. Cryst.,* **2002**, *32*,191.

(18) F. Cariati, L. Erre, G. Micera, A. Panzanelli, G. Ciani, A. Sironi, I*norg. Chim.Acta,* **1983**, *80*, 57.

(19) E. Garriba, G. Micera, M. Zema, *Inorg. Chim. Acta,* **2004**, *357*, 2038.

(20) P. C. R. Soares-Santos, H. I. S. Nogneira, F. A. A. Paz, R. A. SaFerreira, L. D. Carlos, J. Klinowski, T. Trindade, *Eur. J. Inorg. Chem.,* **2003**, 3609.

(21) S. F. M. Ali, V. R. Rao, *J. Inorg. Nucl. Chem.*, **1975**, *37*, 1041.

(22) P. C. R. Soares-Santos, H. I. S. Nogueira, F. A. A. Paz, R. A. Sa Ferreira, L. D. Carlos, J. Klinowski, T. Trindade, *J. Alloys Comounds*, **2004**, *374*, 344.

(23) M. Dan, C. N. R. Rao, *Inorg. Chem*., **2006**, 45, 8227.

(24) G. M. Sheldrick, *SADABS Siemens Area Detector Absorption Correction Program*, University of Göttingen, Gottingen, Germany (**1994**).

(25) G. M. Sheldrick, SHELXTL-PLUS *Program for Crystal Structure Solution and Refinement*, University of Göttingen, Gottingen, Germany (**1997**).

(26) L. S-Livny, J. P. Glusker, C. W. Bock, *Inorg. Chem*., **1998**, 37, 1853.

(27) C. W. Watson, S. C. Parker, *J. Phys. Chem. B*., **1999**, 103, 1258.

(28) S. Ayyappan, G. Diaz de Delgado, A K. Cheetham, G. Férey, C. N. R. Rao, *J. Chem. Soc. Dalton Trans.,* **1999**, 2905.

5.7. Appendix

Table A5.1
Atomic Coordinates and Equivalent Isotropic Displacement Parameters [$Å^2$] for Pb(glutarate), **I**.

Atom	x	y	z	U(eq)
Pb1	0	0.52393(1)	1/4	0.0303(1)
O1	0.0094(2)	0.3955(3)	0.09080(15)	0.0414(6)
O2	0.12844(16)	0.3069(3)	0.21661(14)	0.0386(5)
O3	0.25826(19)	0.0898(3)	0.19199(18)	0.0469(7)
O4	-0.0047(2)	0.2822(3)	-0.08163(16)	0.0447(6)
C1	0.08598(19)	0.3026(3)	0.12541(17)	0.0295(5)
C2	0.12253(18)	0.1889(3)	0.05957(16)	0.0271(5)
C3	0.20517(19)	0.0827(3)	0.0964(2)	0.0328(6)
C4	0.2342(3)	-0.0302(3)	0.0360(3)	0.0452(9)
C5	0.1845(4)	-0.0344(4)	-0.0614(3)	0.0491(11)
C6	0.1056(3)	0.0706(4)	-0.1014(2)	0.0436(8)
C7	0.0742(2)	0.1812(3)	-0.04094(18)	0.0321(6)

U(eq) is defined as one third of the trace of the orthogonalized Uij tensor.

Chapter 6

Use of Ionic Liquids as Solvents for Materials Synthesis

Summary*

Ionic liquids (ILs) are salts with low melting points (<100^{o}C), consisting of a bulky organic cation and an organic or inorganic anion. ILs provide a unique medium to carry out the synthesis of a variety of materials. We have employed ILs for the synthesis of certain nanomaterials as well as other compounds.

By heating imidazolium bromide-based ionic liquids with lead (II) salts under ionothermal conditions, we have been able to obtain two imidazolium bromoplumbates, (EMIm)$PbBr_3$, **I** and $(BMIm)_2PbBr_4$, **II**, where EMIm and BMIm stand for 1-ethyl-3-methyl and 1-butyl-3-methyl imidazolium cations respectively. Interestingly, both these compounds exhibit supramolecular organization wherein dialkylimidazolium cations arrange themselves in a cylindrical fashion giving rise to channel structures. The bromoplumbate anions reside in the channels. These fascinating structures are the result of weak C-H$\cdots$Br^{-} hydrogen bonding and alkyl-alkyl interactions. The lead (II) cation exhibits either hemi- or holodirected coordination geometry.

Nanocrystals of elemental chalcogens have been synthesized solvothermally by using elemental chalcogen powder (Se and Te) and $NaBH_4$ in imidazolium [BMIM]-based ionic liquids as solvents at 180 – 200 °C. Nanorods and nanowires of Se and Te have been obtained when polyethyleneglycol was used as a co-solvent. Se nanowires have been prepared by using an ionic liquid with a

*Papers based on these studies have been published in *Bulletin of Material Science* (2007) and *Crystal Growth & Design* (2008).

small amount of water at room temperature. Sulfur microspheres have been prepared by heating sulfur powder in a mixture of [BMIM][BF_4] and polyethyleneglycol over the temperature range of 150-250 ºC. The nanostructures obtained are single crystalline in all the cases.

Nanoparticles of TiO_2 in the anatase form have been synthesized ionothermally by heating titanium isopropoxide and methyl alcohol or titania hydro-gel in [BMIM][BF_4] ionic liquid in the 100 – 200 °C range. Amorphous nanotapes of V_2O_5 have been prepared by heating vanadia gel in [BMIM][BF_4] ionic liquid at 200 °C. Nanowires of amorphous boehmite have been synthesized by heating aluminium isopropoxide and methyl alcohol in [BMIM][Br] or [EMIM][Br] ionic liquid at 180 °C. Crystalline nanowires of $Al_2O_3.3H_2O$ have been synthesized by heating alumina hydro-gel in [BMIM][Br] / [EMIM][Br] ionic liquid at 180 °C. Amorphous silica microspheres have been prepared by heating tetraethylorthosilicate in a mixture of [BMIM][BF_4] and methanol at 180 ºC.

6.1. Introduction

Ionic liquids (ILs) are salts with low melting points (<100^oC), consisting of a bulky organic cation and an organic or inorganic anion.[1] ILs have attracted much attention as potential solvents and reaction media for organic synthesis, catalysis, electrochemistry and solvent extraction, due to their unique chemical and physical properties such as tunable acidity, low vapor pressure, nonflammability, a wide liquid-state temperature range and extended electrochemical windows.[2-6] In recent years ILs have also been used as solvents for the synthesis of nanomaterials,[7-10] and inorganic as well as hybrid framework solids.[11-17] ILs are considered to be

green solvents and their unique properties have been understood on the basis of the interactions between the cations and anions which determine the nature and dominance of the supramolecular self-assembling forces.[18,19] The role of electrostatic, hydrogen bonding, hydrophobic and other interactions have been examined, along with aspects related to factors such as the length of the alkyl chain, nature of the anion, polymorphism and structural disorder.[20-22] Such studies have, by and large, been devoted to spectroscopic, crystallographic investigations, computer simulations and other theoretical calculations.[23-30] In spite of several investigations, properties of ILs are not entirely understood. Low melting points in halogenometalate-based ILs have evoked some interest and have been used as models to understand their properties.[31-35]

Nanocrystals and nanorods of inorganic materials have been prepared by variety of methods, especially those involving solvothermal and hydrothermal methods.[36-39] In the last two to three years, there have been attempts to use ionic liquids as media for the synthesis of inorganic nanomaterials.[8,40] The low interface tension and the associated high nucleation rate as well as high thermal stability make ionic liquids attractive for carrying out the synthesis of nanostructures. However, there have been very few reports in the literature on the synthesis of inorganic nanomaterials such as elemental chalcogens and metal and non metal oxides. Nanoparticles of Rh and Ir have been prepared by the reduction of the appropriate compound in 1-n-butyl-3- methylimidazolium hexafluorophosphate, ([BMIM][PF_6]), in the presence of hydrogen.[41] Synthesis and functionalization of gold nanoparticles in ionic liquids is also reported, wherein the colour of gold nanoparticles can be tuned by changing the anion of ionic liquid.[10] Single crystalline Te nanorods and nanowires have been obtained by a microwave-

assisted synthesis in liquid n-butylpyridinium tetrafluoroborate and polyvinylpyrrolidone.[42] Nanoparticles, nanorods and nanowires of metal chalcogenides have been synthesized in various ([BMIM] based ionic liquids in the presence of some surfactants and amines.[43]

Nanostructures of elemental chalcogens have been reported in the literature by a few workers. A simple solution-based method have been used by involving the reaction of selenium powder with $NaBH_4$ to prepare nanorods and nanowires of t-Se.[44] Single crystalline t-Se nanowires were obtained by the reduction of selenious acid with excess hydrazine under refluxing conditions,[45] while ascorbic acid along with β-cyclodextrin have been also used for the reduction in an another method.[46] Single crystalline selenium nanorods have been obtained by the reduction of selenious acid solution with hydrazine hydrate in the presence of poly(vinylpyrrolidone) (PVP) at the liquid-liquid interface between water and *n*-butyl alcohol.[47] t-Te nanorods, nanowires and nanobelts have been prepared by a solution-based method involving $NaBH_4$ and sodium dodecylbenzenesulfonate starting with Te powder.[48] Single crystalline Te nanotubes have been synthesized by the polyol process.[49] Te nanorods, nanowires, and tubes have also been prepared by the reduction of TeO_2 using polyvinylpyrrolidone or polyethylene glycol.[50] To date, there is no report of synthesis of the nanostructures of sulfur.

Titanium dioxide (TiO_2) has been widely used material for many applications, which can be roughly divided into "energy" and "environmental" categories, many of which depend not only on the properties of the TiO_2 material itself but also on the modifications of the size, shape, material host (e.g., with inorganic and organic dyes) and on the interactions with the environment. As continued breakthroughs have been made in the applications of TiO_2 nanomaterials

in recent years, syntheses of TiO_2 nanomaterials in various forms such as nanoparticles, nanorods, nanowires, and nanotubes are primarily gained importance.[51] TiO_2 nanomaterials have been synthesized with the sol-gel method from hydrolysis of a titanium precursor. Highly crystalline anatase TiO_2 nanoparticles with different sizes and shapes could be obtained with the polycondensation of titanium alkoxide in the presence of tetramethylammonium hydroxide.[52] By a combination of the sol-gel method and an anodic alumina membrane (AAM) template, TiO_2 nanorods have been successfully synthesized by dipping porous AAMs into a boiled TiO_2 sol followed by drying and heating processes.[53] TiO_2 nanotubes can also be obtained using the sol-gel method by templating with an AAM and other organic compounds.[54,55] Micelles and inverse micelles are commonly employed to synthesize TiO_2 nanomaterials. The values of H_2O/surfactant, H_2O/titanium precursor, ammonia concentration, feed rate, and reaction temperature were significant parameters in controlling TiO_2 nanoparticle size and size distribution.[56] With the aid of surfactants, different sized and shaped TiO_2 nanorods can be synthesized.[57] TiO_2 nanoparticles were prepared by hydrothermal reaction of titanium alkoxide in an acidic ethanol-water solution.[58] TiO_2 nanowires have been prepared with the hydrothermal method by treating TiO_2 white powders in NaOH aqueous solution.[59] Nanocrystalline TiO_2 particles have been obtained via an alkoxide sol-gel method employing a water-immiscible IL (1-butyl-3-methylimidazolium hexafluorophosphate, [bmim][PF6]) as a new solvent medium and further modified with nonionic surfactant (polyoxyethylenesorbitan monooleate) as a pore templating material.[60]

Vanadium oxides are promising materials for applications such as lithium batteries, catalysts, electrochromic devices (ECDs), and supercapacitors due to the

ease with which it can be reduced and its ions intercalated into layered structures.[61] In recent years, there has been increasing interest in low-dimensional vanadium oxide nanostructures because of their size-dependent properties and potential applications in lithium batteries, electric field-effect transistors, chemical sensors or actuators, and nanodevices.[62] Urchin-like nanostructures consisting of high-density spherical nanotube radial arrays of vanadium oxide nanocomposite were successfully synthesized by a simple chemical route using an ethanolic solution of vanadium tri-isopropoxide and alkylamine hexadecylamine.[63] Single-crystalline vanadium oxide nanobelts were obtained through a sodium dodecylsulfate (SDS) surfactant-directed growth process under hydrothermal conditions using V_2O_5 as a precursor.[64] Some low-valent vanadium oxides are very unique. For example, VO_2 can undergo a first-order transition from a high-temperature metallic phase to a low temperature insulating phase at around 340 K and exhibits excellent optical, electrical, and electrochemical properties.[65,66] Low-valent vanadium oxide nanostructures have been synthesized by a variety of methods, such as thermal evaporation, surfactant-assisted solution, and hydrothermal/solvothermal synthesis.[67,68] An ethylene glycol reduction process have been used to prepare monoclinic VO_2 nanowire arrays under hydrothermal conditions.[69] VO_2 nanobelts have been obtained by the reduction of V_2O_5 powder using oxalic acid as the reductant.[70] $H_2V_3O_8$ nanobelts have been also prepared by the reduction of V_2O_5 powder with ethanol.[70]

Alumina is most cost effective and widely used material in the family of engineering ceramics. Owing to its special properties, such as high elastic modulus, thermal and chemical stability, high strength and toughness, and excellent dielectric properties, alumina has been regarded as a material of

outstanding performance especially under tension or bending conditions.[71] Recent efforts have been devoted to the synthesis of various alumina nanostructures. One-dimensional structured boehmite have been used as the precursor for Al_2O_3 nanofibers and nanorods, which possess nanoscale thickness and have potential for applications in advanced catalysts, adsorbents, composite materials, and ceramics.[72] A simple solid-phase method was developed for synthesis of high-quality boehmite nanorods by steam-assisted wet-gel conversion process. Al_2O_3 nanorods with clear-cut edge have been successfully obtained by thermal treatment of boehmite nanorods at 600 °C for 5 h.[73] Boehmite nanofibers were reported to be assembled with the assistance of poly(ethylene oxide) (PEO) surfactant, and tubular Al_2O_3 was fabricated via soft solution route using *N*-cetyl-*N*,*N*,*N*-trimethylammonium bromide surfactant. [74,75] $Al(OH)_3$ nanorods were obtained by a very simple reaction of Al metal powder or foil with water in the 25–75 °C range.[76] The colloidal particles have diameters between 10 and 50 nm and a shell with a thickness of 3.5 nm, made of noncrystalline ordered Al-O polycations. By introducing poly(ethylene oxide) surfactant to aluminum hydrate colloids, fibrous nanocrystallites of boehmite and alumina have been obtained.[77]

Recently, mesoporous materials have attracted much attention because of their emerging applications in catalysis, adsorption, sensors, and separations.[78] Mesoporous silica is synthesized by polymerizing a silica source in the presence of a surfactant template. Two different mesostructured IL /silica materials prepared from precursors solutions with varying the ratio of IL to silica precursor.[8] Hexagonal mesostructures were obtained with an excess of water. Lamellar mesostructure were obtained with only stoichiometric amounts of water and keeping the natural H-bonding network intact. Monodispersed conducting solid

microsilica spheres by hydrolyzing tetramethylorthosilicate (TMOS) and tetraethylorthosilicate (TEOS) in an ionic liquid, 1-butyl-3-methylimidazolium hexafluorophosphate, at room temperature.[79]

Molecular dynamics simulations show that RTILs and their binary mixtures are nanostructurally organized with ionic networks and nonpolar regions.[80] Quantum chemical calculations have been used to investigate the interaction between water molecules and ionic liquids based on the imidazolium cation with the anions [Cl^-], [Br^-], [BF_4^-], and [PF_6^-].[81] The predicted geometries and interaction energies implied that the water molecules interact with the Cl^-, Br^-, and BF_4^- anions to form $X^-\cdots W$ (X = Cl or Br, W = H_2O), $2X^-\cdots 2W$, $BF_4^-\cdots W$, and $W\cdots BF_4^-\cdots W$ complexes. The hydrophobic PF_6^- anion could not form a stable complex with the water molecules at the density functional theory (DFT) level. Further studies indicate that the cation could also form a strong interaction with the water molecules. So it is considered as rewarding to explore the use of ionic liquids for the synthesis of nano and hybrid network structures.

6.2. Scope of the present investigation

Research on ILs has focused on the synthesis of organic compounds and green chemistry. Recently, however, ILs have also received attention from the inorganic materials community. Ionic liquids can act as solvents for reactants and morphology templates for the products at the same time, which enables the synthesis of inorganic materials with novel or improved properties. In our effort to utilize ILs as solvents to synthesize novel hybrid frameworks and nano materials, investigations were carried out. We have obtained two supramolecular

dialkylimidazolium bromoplumbates with channel architecture, nanostructures of three elemental chalcogens and nanostructures of four oxide materials. We have examined the effects of changing the anion of the ionic liquid, as well as the presence of water and surfactants on the crystallinity, size and shape of the nanostructures of these materials.

(a) Dialkylimidazolium bromoplumbates

By heating imidazolium bromide-based ionic liquids with lead (II) salts under ionothermal conditions, we have been able to obtain two imidazolium bromoplumbates, $(EMIm)PbBr_3$, **I** and $(BMIm)_2PbBr_4$, **II**, where EMIm and BMIm stand for 1-ethyl-3-methyl and 1-butyl-3-methyl imidazolium cations respectively. Interestingly, both these compounds exhibit unusual supramolecular organization wherein dialkylimidazolium cations arrange themselves in a cylindrical fashion giving rise to channel structures. The bromoplumbate anions reside in the channels. These fascinating structures are the result of weak C-H···Br^- hydrogen bonding and alkyl-alkyl interactions. The lead (II) cation exhibits either hemi- or holodirected coordination geometry.

(b) Nanocrystals of elemental chalcogens

Nanocrystals of elemental chalcogens have been synthesized solvothermally by using elemental chalcogen powder (Se and Te) and $NaBH_4$ in imidazolium[BMIM]-based ionic liquids as solvents at 180 – 200 °C. Nanorods and nanowires of Se and Te have been obtained when polyethyleneglycol was used as a co-solvent. Se nanowires have been prepared by using an ionic liquid with a small amount of water at room-temperature. Sulfur microspheres have been

prepared by heating sulfur powder in a mixture of [BMIM][BF_4] and polyethyleneglycol over the temperature range of 150-250 ºC. The nanostructures obtained are single crystalline in all the cases.

(c) Nanocrystals of oxides

Nanoparticles of TiO_2 in the anatase form have been synthesized ionothermally by heating titanium isopropoxide and methyl alcohol or titania hydro-gel in [BMIM][BF_4] ionic liquid in the 100 – 200 °C range. Amorphous nanotapes of V_2O_5 have been prepared by heating vanadia gel in [BMIM][BF_4] ionic liquid at 200 °C. Nanowires of amorphous boehmite have been synthesized by heating aluminiumisopropoxide and methyl alcohol in [BMIM][Br] or [EMIM][Br] ionic liquid at 180 °C. Crystalline nanowires of $Al_2O_3.3H_2O$ have been synthesized by heating alumina hydro-gel in [BMIM][Br] / [EMIM][Br] ionic liquid at 180 °C. Amorphous silica microspheres have been prepared by heating tetraethylorthosilicate in a mixture of [BMIM][BF_4] and methanol at 180 ºC.

6.3. Experimental

Synthesis and characterization

The imidazolium bromoplumbates **I** and **II** were synthesized under ionothermal conditions by heating homogenized reaction mixtures in a 7ml PTFE-lined bomb at the 180 °C temperature for 72 h under autogeneous pressure. For the synthesis of **I**, the reaction mixture of the following composition was used. $Pb(NO_3)_2$ (0.3mmol), 1,3-cyclohexanedicarboxylic acid (0.3mmol), NaOH (0.3mmol), methanol (2ml) and 0.5g of EMImBr. For the synthesis of **II**, the reaction mixture

of the following composition was used. $Pb(NO_3)_2$ (0.3mmol), 1,3-benzenedicarboxylic acid (0.15mmol) , NaOH (0.3mmol) , methanol (2ml) and 0.5g of BMImBr. The change of the starting compositions or omission of either carboxylic acid or NaOH did not yield any crystals but resulted in powders or gel-like products. The pH of the starting reaction mixture was 6-6.5. The pH after the reaction did not show appreciable change. The products of the ionothermal reaction were washed with methanol and ethanol without any residual carboxylic acid, vacuum-filtered and dried under ambient conditions. Both the compounds were obtained as single phase materials. The crystals were separated under a polarizing microscope and used for all the characterization.

Elemental analyses of **I** and **II** were satisfactory. For **I**, ($C_6H_{11}N_2PbBr_3$) calcd: C, 12.90%; H, 1.97%; N, 5.02%. Found: C, 12.86%; H, 2.13%; N, 5.23%. For **II**, ($C_{16}H_{30}N_4PbBr_4$) calcd: C, 23.84%; H, 3.73%; N, 6.95%. Found: C, 24.16%; H, 4.02%; N, 6.72%. Powder X-ray diffraction (XRD) patterns of the products were recorded using Cu Kα radiation (Rich-Seifert, 3000TT). The patterns agreed with those calculated for single crystal structure determination. Thermogravimetric analysis (TGA) was carried out (Metler-Toledo) in air (flow rate = 50 ml/min) in the temperature range 25 to 800 °C (heating rate = 5 °C/min). Infrared (IR) spectra of KBr pellets of the compounds were recorded in the mid IR region (Bruker IFS-66v). The compounds show characteristic bands of the imidazole ring and the alkyl chains.[82-84]

Thermogravimetric analyses gave the following results. Both the compounds show weight loss at two temperature ranges. For **I**, the first weight loss of 26.42% occurred in the 280-380^o C range and the second weight loss of 65.12% occurred in the 380-700^o C range. For **II**, the first weight loss of 44.58% occurred

in the 260-370^{o} C range and the second weight loss of 48.50% occurred in the 370-700^{o} C range. The first step in the weight loss is attributed to the loss of organic cations and the second to the decomposition of the bromoplumbate. Differential thermal analysis (DTA) of **I** shows an endothermic peak around 209^{o} C (melting point) and a small exothermic peak around 400^{o} C. **II** shows an endothermic peak around 138^{o} C (melting point) and an exothermic peak around 375^{o} C.

A suitable single crystal of each compound was carefully selected under a polarizing microscope and glued to a thin glass fiber. Crystal structure determination by X-ray diffraction was performed on a Bruker-Nonius diffractometer with Kappa geometry attached with an APEX -II-CCD detector and a graphite monochromator for the X-ray source (Mo Kα radiation, λ = 0.71073Å) operating at 50 kV and 30 mA. An empirical absorption correction based on symmetry equivalent reflections was applied using the SADABS program.[85] The structure was solved and refined using SHELXTL-PLUS suite of program.[86] For the final refinement the hydrogen atoms were placed geometrically and held in the riding mode. Final refinement included atomic positions for all the atoms, anisotropic thermal parameters for all the non-hydrogen atoms and isotropic thermal parameters for the hydrogen atoms. All the hydrogen atoms were included in the final refinement, selected bond distances along with the details of the structure solution and final refinements of **I** and **II** are given in Tables 6.1, 6.2 and 6.3. Atomic coordinates for the compounds **I** to **VI** are given in the appendix (see 6.7. Appendix, Tables A6.1 and A.6.2).

Table 6.1. Selected bond distances in (EMIm)$PbBr_3$, **I**.

Bond	Distance (Å)
Pb(1) - Br(1)	2.789(1)
Pb(1) - Br(2)	2.886(1)
Pb(1) - Br(2)#1	3.219(1)
Pb(1) - Br(3)	2.9748(9)
Pb(1) - Br(3)#2	3.1177(9)

Symmetry transformations used to generate equivalent atoms: #1 -0.5+x,0.5-y,1-z, #2 0.5+x,0.5-y,1-z

Table 6.2. H-bonding interactions in **I** and **II**.

Compound	D–H···A	Distance (Å) D–H	Distance (Å) H···A	Distance (Å) D···A	Angle (°) D–H···A
I	C(4)-H(4b)···Br(2)	0.9600	2.896(2)	3.781(4)	153.7
	C(4)-H(6a)···Br(1)	0.9600	2.975(6)	3.773(4)	141.9
	C(4)-H(4c)···Br(2)	0.9600	2.942(5)	3.813(5)	151.4
II	C(2)-H(2)···Br(4)	0.9600	2.842(3)	3.738(8)	161.6

Table 6.3. Crystal data and structure refinement parameters for $(EMIm)PbBr_3$, **I** and $(BMIm)_2PbBr_4$, **II**.

Structure parameter	**I**	**II**
Empirical formula	$C_6H_{11}N_2PbBr_3$	$C_{16}H_{30}N_4PbBr_4$
Formula weight	558.07	805.24
Crystal system	Orthorhombic	Trigonal
Space group	$P2_12_12_1$, (no. 19)	R-3, (no. 148)
a /Å	8.2131(7)	16.6041(2)
b /Å	9.7717(8)	16.6041(2)
c /Å	15.4345(13)	24.1297(5)
V /Å^3	1238.71(18)	5761.20(15)
Z	4	3
D (calc) /gcm^{-3}	2.993	2.089
μ /mm^{-1}	23.255	12.838
Total data collected	28200	15008
Unique data	2297	2391
Observed data	1995	1984
[$I > 2\sigma(I)$]		
R_{merg}	0.0335	0.0233
Goodness of fit	1.016	1.021
R indexes	$R_1 = 0.0282$[a];	$R_1 = 0.0249$[a];
[$I > 2\sigma(I)$]	$wR_2 = 0.0563$[b]	$wR_2 = 0.0605$[b]
R indexes	$R_1 = 0.0399$[a];	$R_1 = 0.0348$[a];
[all data]	$wR_2 = 0.0600$[b]	$wR_2 = 0.0642$[b]

[a] $R_1 = \Sigma ||F_0|-|F_c|| / \Sigma |F_0|$; [b] $wR_2 = \{\Sigma[w(F_0^2 - F_c^2)^2] / \Sigma[w(F_0^2)^2]\}^{1/2}$. $w = 1/[\sigma^2(F_0)^2 + (aP)^2 + bP]$, $P = [\max.(F_0^2,0) + 2(F_c)^2]/3$, where $a = 0.0247$, $b = 4.1206$ for **I** and $a = 0.0344$, $b = 12.3057$ for **II**.

In order to prepare sulfur nanostructures, 0.025 g sulfur powder was dispersed in 1.5 mL of polyethyleneglycol (PEG-600) and 1 mL of the ionic liquid 1-butyl-3-methylimidazolium tetrafluroborate, ([BMIM][BF_4]). The mixture was heated in a 7 mL Teflon-lined stainless steel autoclave at 180 ºC for 12 hrs. After cooling to room temperature the product was washed with water and ethyl alcohol several times.

In order to prepare Se nanostructures several procedures were employed: (a) In one procedure, 0.01 g Se powder and 0.05 g $NaBH_4$ were dispersed in 1 mL of the ionic liquid 1-butyl-3-methylimidazolium hexafluorophosphate, ([BMIM][PF_6]). The mixture was heated in a 7 mL Teflon-lined stainless steel autoclave at 200 ºC for 10 hrs. After cooling to room temperature, the product was washed with water and acetonitrile several times. (b) In another preparation 0.025 g Se powder and 0.03 g $NaBH_4$ were dispersed in a mixture of 1 mL of PEG-600, 2 mL of [BMIM][BF_4] and 2 mL H_2O. The mixture was stirred and kept at room temperature for 48 hrs. The product was washed several times with water and ethyl alcohol. (c) Nanostructures were also prepared from a mixture of 0.025 g Se powder and 0.03 g $NaBH_4$ dispersed in 1 mL of PEG-600, 2 ml of [BMIM][BF_4] and 2 mL H_2O. The mixture was stirred and heated at 75 ºC for 24 hrs. After cooling to room temperature, the product was washed with water and ethyl alcohol. (d) A mixture of 0.01 g Se powder and 0.05 g $NaBH_4$ dispersed in 1 mL of PEG-600 and 1 mL of [BMIM][PF_6]. The mixture was stirred and heated at 200 ºC for 10 hrs. After cooling to room temperature, the product was washed several times with water and acetonitrile.

In order to prepare Te nanostructures the following procedures were used: (a) Te nanoparticles were prepared from a mixture of 0.015 g Te powder and 0.05

g $NaBH_4$ dispersed in 1 mL of [BMIM][PF_6]. The mixture was heated in a 7 mL Teflon lined stainless still autoclave at 200 ºC for 10 hrs. After cooling to room temperature, the product was washed several times with water and acetonitrile. (b) In a second set of reactions a mixture of 0.015 g Te powder and 0.05 g $NaBH_4$ dispersed in 2 mL of PEG-600 and 2 mL of [BMIM][PF_6]. The mixture was heated in a 7 mL Teflon lined stainless steel autoclave at 200 ºC for 10 hrs. After cooling to room temperature, the product was washed several times with water and acetonitrile. (c) In another set of reactions, a mixture of 0.015 g Te powder, 0.02 g cetyltrimethylammoniumbromide (CTAB) and 0.05 g $NaBH_4$ dispersed in 2 mL of [BMIM][PF_6]. The mixture was heated in a 7 mL Teflon-lined stainless steel autoclave at 200 ºC for 10 hrs. After cooling to room temperature, the product was washed several times with water and acetonitrile.

TiO_2 nanostructures have been prepared by two methods. In the first method, 0.5 mL of titanium isopropoxide was mixed with a mixture of 1 mL of the ionic liquid 1-butyl-3-methylimidazolium tetrafluroborate, ([BMIM][BF_4]) and 1 mL of methyl alcohol and stirred for 30 minutes. The mixture was heated in a 7 mL Teflon-lined stainless steel autoclave at 180 ºC for 20 hrs. After cooling to room temperature the product was washed with water and ethyl alcohol several times. In the second method, 0.1 g of titania gel was dispersed in 1 mL of [BMIM][BF_4]. The mixture was stirred for 30 minutes and then heated in a 7 mL Teflon-lined stainless steel autoclave at 180 ºC for 20 hrs. TiO_2 nanostructures were also obtained by adding surfactants to the above two reactions mixtures followed by heating them in the 100-200 ºC for 20-48 hrs. Titania gel was obtained by stirring titanium isopropoxide in ethyl alcohol followed by the addition of aceticacid till pH 3, which lead to the precipitation of the gel after 2hrs.

V_2O_5 nanostructures have been prepared as follows; 0.4 g of vanadia gel was mixed in 1 mL of the ionic liquid ([BMIM][BF_4]) and stirred for 60 minutes. The mixture was heated in a 7 mL Teflon-lined stainless steel autoclave at 200 ºC for 48 hrs. After cooling to room temperature the product was washed with water and ethyl alcohol several times. Vandia gel was obtained by stirring ammonium vanadate in water followed by the addition of nitric acid till the pH of the solution is 2. Then the mixture is heated and dried at 100 ºC for 3hrs.

Boehmite nanostructures have been prepared by the following method. 0.1 g of aluminiumisopropylate was mixed with 1 g of the ionic liquid 1-butyl-3-methylimidazolium bromide, [BMIM][Br] or 1-ethyl-3-methylimidazolium bromide, [EMIM][Br] and 1mL of methyl alcohol and stirred for 60 minutes. The mixture was heated in a 7 mL Teflon-lined stainless steel autoclave at 180 ºC for 24 hrs. After cooling to room temperature the product was washed with water and ethyl alcohol several times. $Al_2O_3.3H_2O$ nanostructures have been prepared by the following method. 0.1 g of the alumina gel was mixed with 1 g of the ionic liquid 1-butyl-3-methylimidazolium bromide, [BMIM][Br] or 1-ethyl-3-methylimidazolium bromide, [EMIM][Br] and stirred for 60 minutes. The mixture was heated in a 7 mL Teflon-lined stainless steel autoclave at 180 ºC for 24 hrs. After cooling to room temperature the product was washed with water and ethyl alcohol several times. Nanostructures were also obtained by adding methyl alcohol or surfactants to the above two reactions mixtures followed by heating them at 180 ºC for 24 hrs. Alumina gel was obtained by stirring sodium aluminate in acetic acid till the pH is 4. Precipitation of the gel occurred after 2hrs which is washed with water several times.

In order to prepare silica nanostructures, 0.1 mL of tetraethylorthosilicate was mixed in 1.0 mL of methyl alcohol and 1 mL of the ionic liquid [EMIM][Br]. The mixture was stirred for 5hrs and then heated in a 7 mL Teflon-lined stainless steel autoclave at 180 ºC for 48 hrs. After cooling to room temperature the product was washed with water and ethyl alcohol several times.

TEM images of the nanostructures were obtained by taking a drop of ethanol solution of the compound on the holey carbon-coated Cu grids. The grids were allowed to dry in the air and examined by using a JEOL (JEM3010) microscope operating with an accelerating voltage of 300 kV. The nanostructures also characterized by powder X-ray diffraction (XRD) using a Phillips X'Pert diffractometer employing the Bragg-Brentano configuration and energy dispersive X-ray analysis (EDX) (using a scanning electron microscope Leica S4401 fitted with a Link ISIS software). Field emission SEM images of nanostructures were recorded by taking a drop of the ethanol solution on the aluminum sample holder.

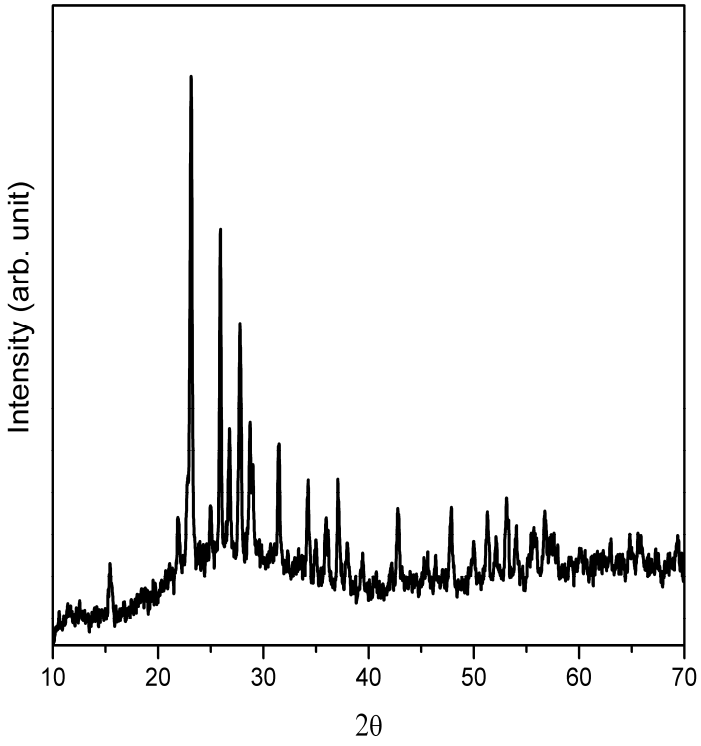

Fig. 6.3.1. Powder XRD pattern of S micropheres.

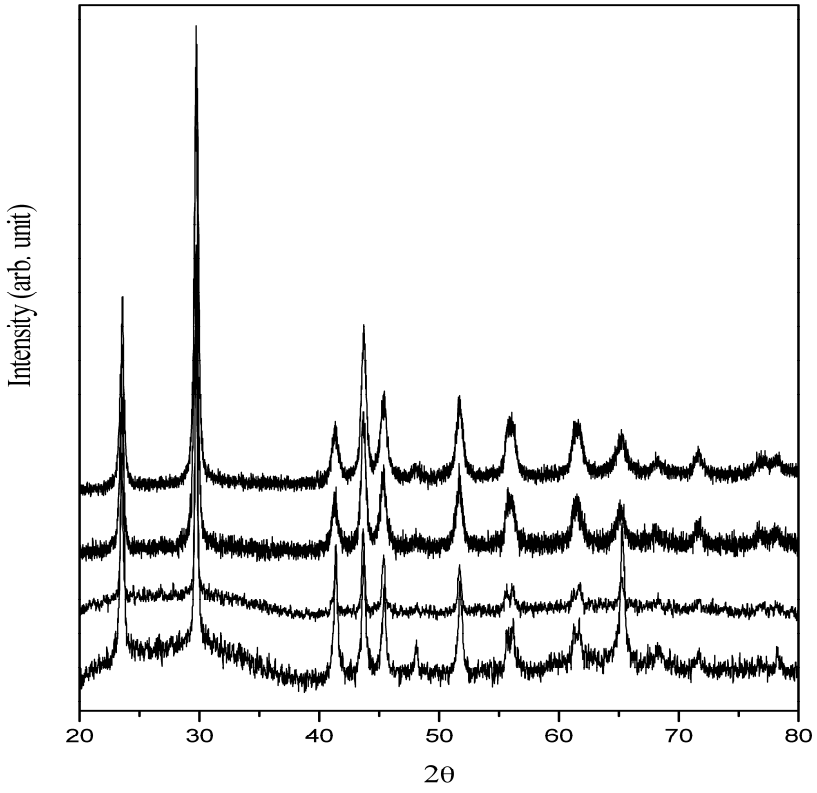

Fig. 6.3.2. Powder XRD pattern of hexagonal Se structures.

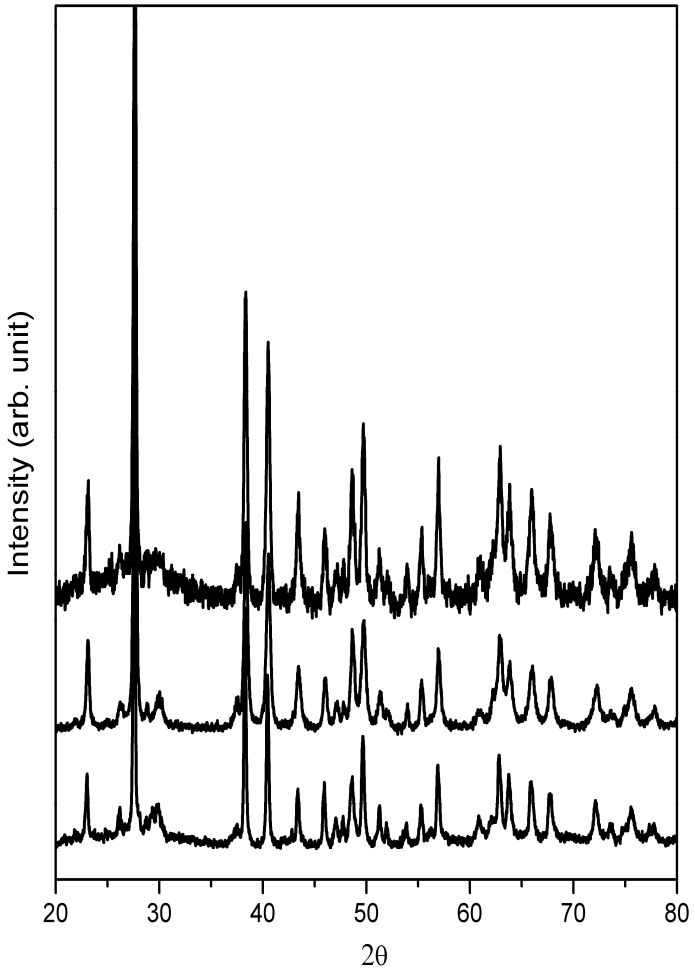

Fig. 6.3.3. Powder XRD pattern of hexagonal Te structures.

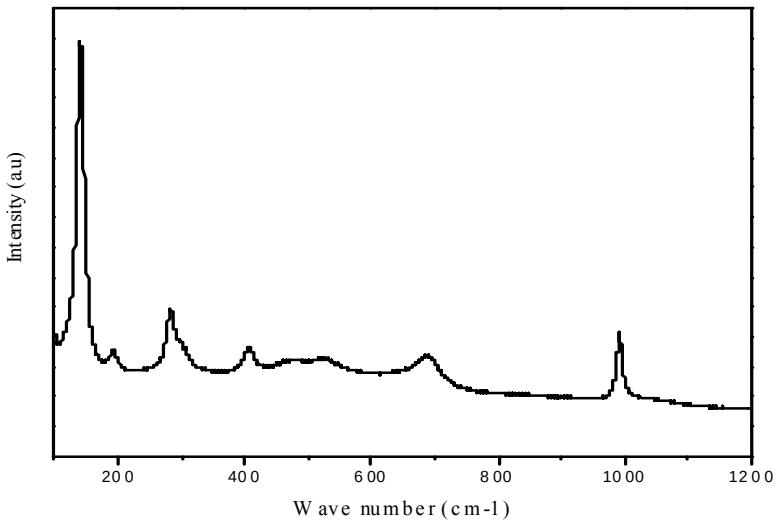

Fig. 6.3.4. Raman Spectra of V_2O_5 nanobelts.

6.4. Results and discussion

(a) Dialkylimidazolium bromoplumbates

We have synthesized two compounds of imidazolium bromoplumbates, 1-ethyl-3-methyl imidazolium tribromoplumbate, (EMIm)$PbBr_3$, **I**, and bis(1-butyl-3-methyl imidazolium) tetrabromoplumbate, $(BMIm)_2PbBr_4$, **II**. Both **I** and **II** possess structures with one-dimensional channels made up of imidazolium cations and filled with the lead bromide anions.

1-Ethyl-3-methyl imidazolium tribromoplumbate, (EMIm)$PbBr_3$, **I**, has an asymmetric unit of 12 non-hydrogen atoms. The asymmetric unit contains a crystallographically distinct Pb^{2+} cation, one $EMIm^+$ cation and three distinct Br^- anions. The Pb atom is hemidirected and five-coordinated by bromine atoms ($PbBr_5$) from three different types of Br^- anions. The Pb-Br bond lengths are in the 2.789 – 3.219 Å range (Table 6.1) and all the bond distances are within the van der Waals contact limits. Four of the bromine anions have μ_2 connections linking each Pb with two other Pb atoms. Thus, a $PbBr_5$ polyhedron shares two of its edges with two different $PbBr_5$ polyhedra forming an infinite one-dimensional Pb-Br-Pb chain (Fig. 6.4.1a). $EMIm^+$ cations exhibit weak C-H···Br interactions through the alkyl groups in the imidazolium ring with three different Br^- anions (Figure 6.4.1b), (Table 6.2). These weak interactions lead to the formation of channels with the dimension ~6.8 × 7.8 $Å^2$, where the assembly of $EMIm^+$ anions serves as walls. The channels are occupied with the infinite $PbBr_3$ chains and surrounded by the $EMIm^+$ cations (Fig. 6.4.2). The structure is further stabilized by the alkyl-alkyl interactions between two neighboring $EMIm^+$ cations.

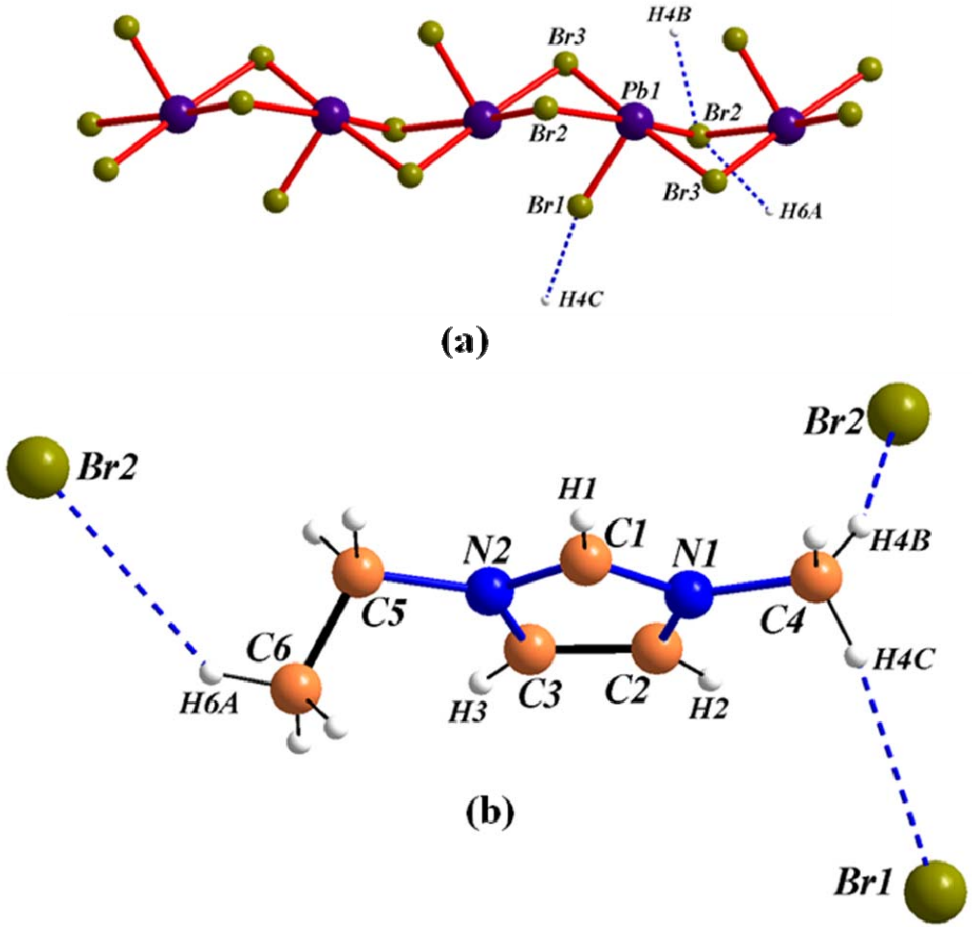

Fig. 6.4.1(a) Infinite 1-D of Pb-Br-Pb chain in (EMIm)$PbBr_3$, **I**. The dotted lines show H-bonding interactions between the cations and anions (b) view of the C-H···Br interactions between the $EMIm^+$ cations and Br^- anions in **I**.

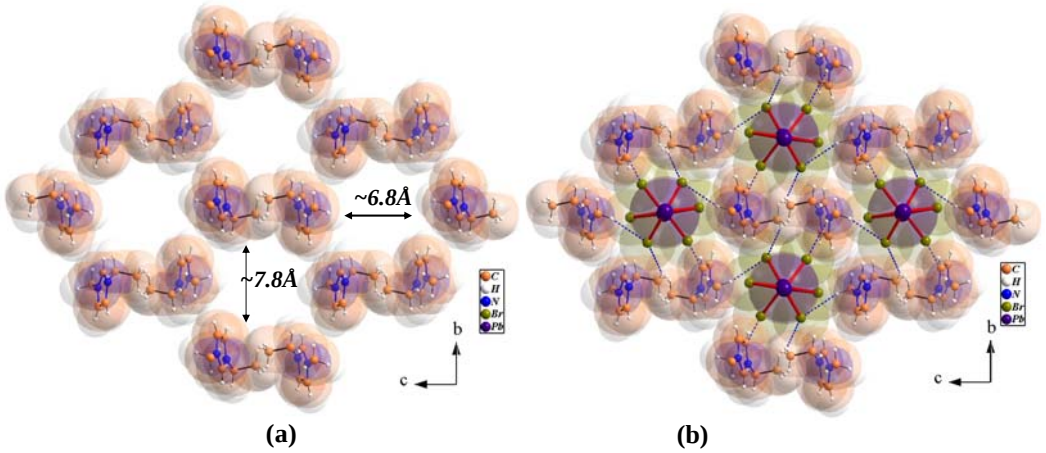

Fig. 6.4.2 (a) View of the infinite 1-D empty channels and ethyl-ethyl (cation-cation) interactions along the *a*-axis and (b) Crystal structure packing and H-bonding interactions in (EMIm)$PbBr_3$,**I**, viewed along the *a*-axis. Superimposed models of ball-stick and van der Waals spheres.

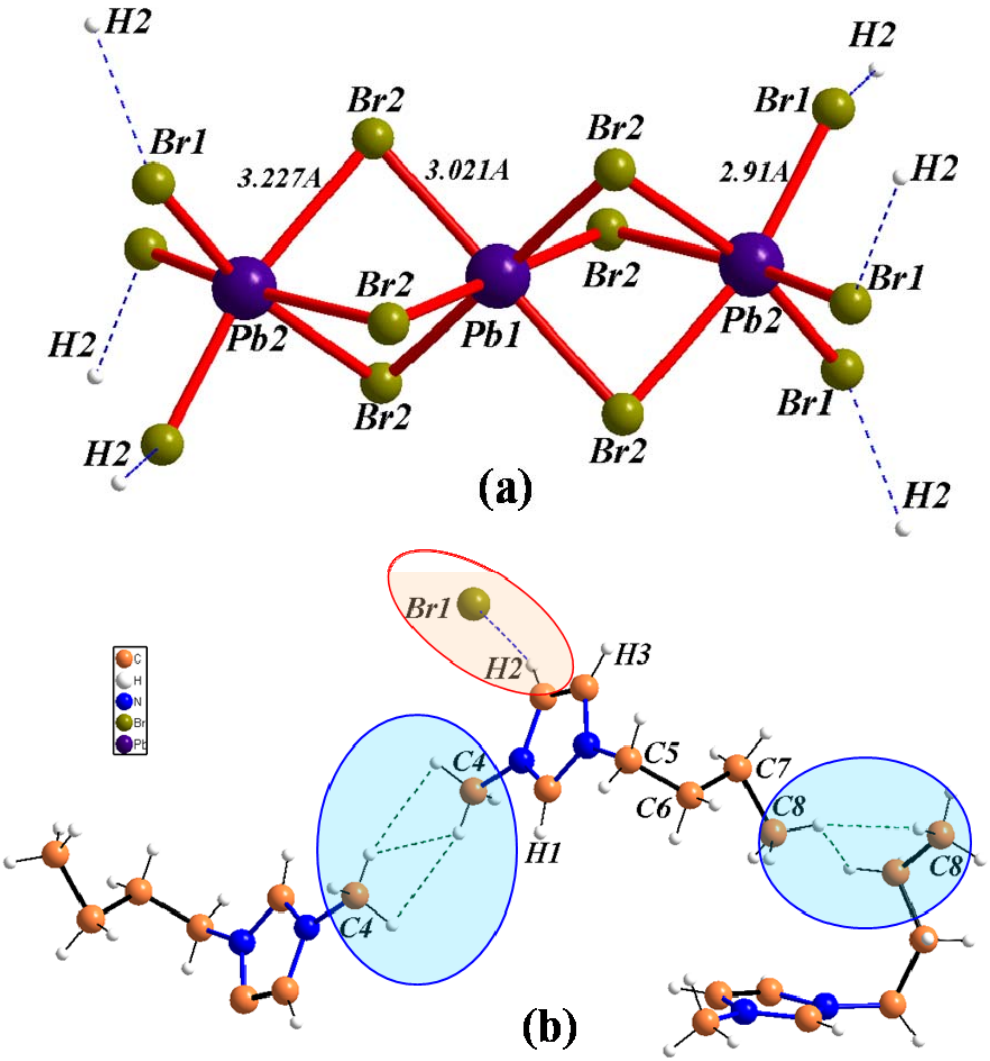

Fig. 6.4.3 (a) The Pb_3Br_{12} unit and its H-bonding interactions with the cations in $(BMIm)_2PbBr_4$, **II** and (b) View of the H-bonding interactions (highlighted in red, cation-anion interaction) between $BMIm^+$ cation and Br^- anion and alkyl-alkyl interactions (highlighted in blue, cation-cation interaction) between the $BMIm^+$ cations.

Bis(1-butyl-3-methyl imidazolium) tetrabromoplumbate, $(BMIm)_2PbBr_4$, **II**, has an asymmetric unit of 12.5 non-hydrogen atoms. The asymmetric unit contains two crystallographically distinct Pb^{2+} cations, one $BMIm^+$ cation and two distinct Br^- anions. Pb(1) has a 1/6 occupancy and sits at the 3*b* position. Pb(2) has a 1/3 occupancy and sits at the 6*c* position. Pb(1) is holodirected and coordinated

by six bromine atoms of the same type, Br(1), into a perfect octahedron $PbBr_6$. The Pb-Br bond length is 3.021 Å. Pb(2) is also holodirected and coordinated to six bromine atoms of two types, three Br(1) and three Br(2), in to a slightly distorted octahedron $PbBr_6$. The Pb(2)-Br(1) bond length is 2.91 and the Pb(2)-Br(2) bond length is 3.227 Å, all within the van der Waals contact limit. All the six Br(2) anions have $\boldsymbol{\mu}_2$ connections linking each Pb(1) with two Pb(2) atoms. Thus, a $Pb(1)Br_6$ polyhedron shares its two faces with two different $Pb(2)Br_6$ polyhedra forming a linear Pb_3Br_{12} unit (Fig. 5.4.3a). Each of the $BMIm^+$ cation is hydrogen-bonded to Br(1) anions through H(2) in the imidazole ring (Fig. 6.4.3b), (Table 6.2). The $BMIm^+$ anions interact with each other through methyl-methyl and butyl-butyl interactions (Fig. 6.4.3b).

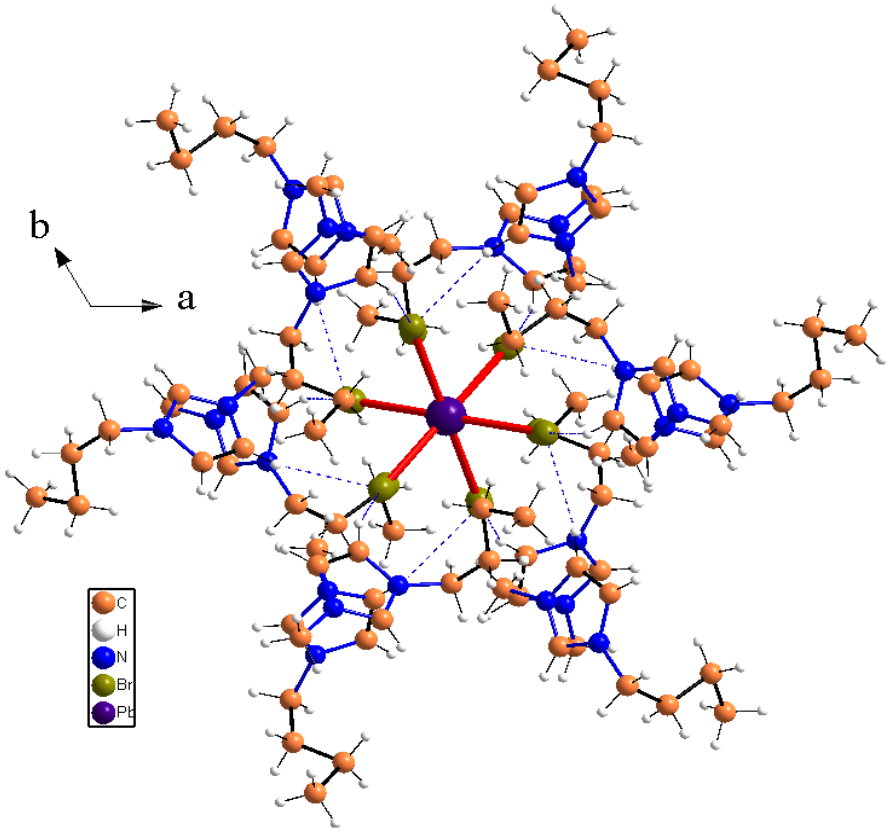

Fig. 6.4.4. View of a single capsule with the Pb_3Br_{12} unit and its H-bonding interactions with the $BMIm^+$ cations in $(BMIm)_2PbBr_4$, **II.**

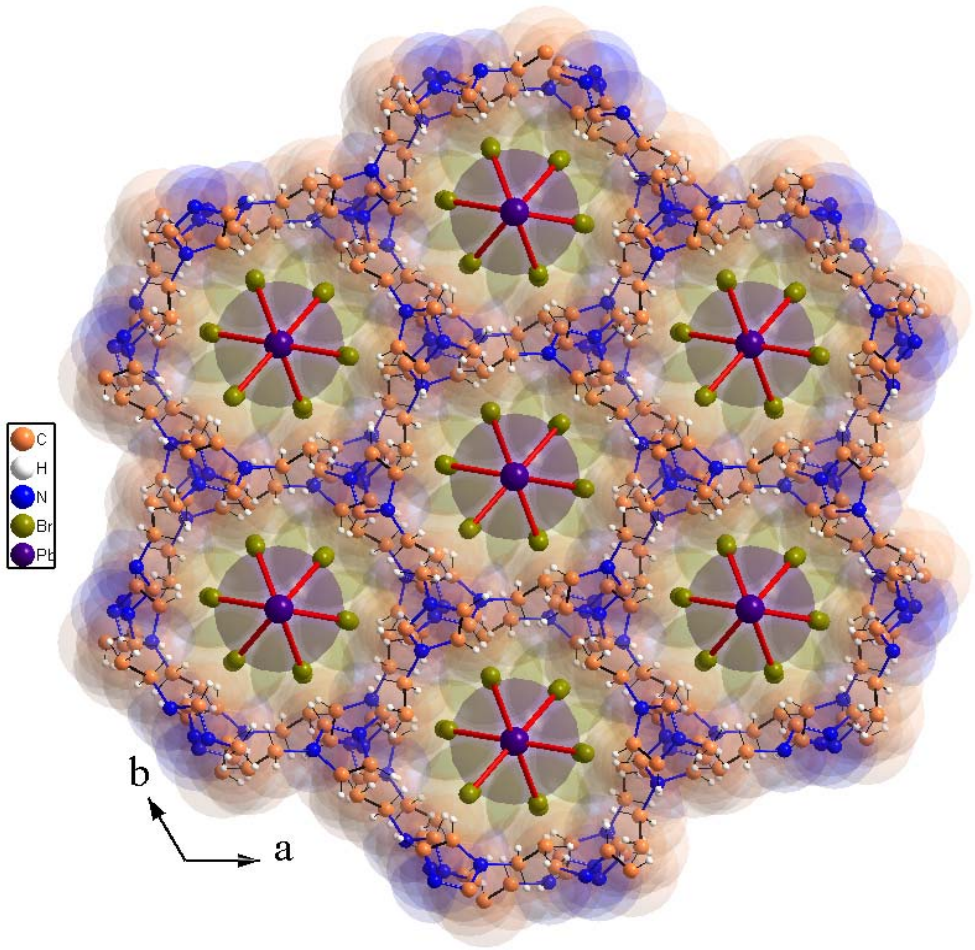

Fig. 6.4.5. View of the crystal structure packing in $(BMIm)_2PbBr_4$, **II**, along the *c* axis. Superimposed models of ball-stick and van der Waals spheres.

These interactions lead to the formation of a one-dimensional channel, where the $BMIm^+$ assembly serves as a wall. The channel is made up of capsules or cavities of the dimensions ~8.5 × 8.0 $Å^2$ and the Pb_3Br_{12} units reside in the cavities, getting hydrogen-bonded to the $BMIm^+$ cations (Fig. 6.4.4 and 6.4.5). The capsules are connected to form the infinite one dimensional channel by a small window of the dimension ~3.6 Å. This small window results due to the dangling butyl groups of the $BMIm^+$ anions into the 1D channel (Fig.6.4.6). The structure is further stabilized by the alkyl-alkyl interactions between two neighboring $BMIm^+$

cations. The difference between the channels in **I** and **II** arises due to the longer alkyl group in the latter. **I** possesses a whole simple rhombic 1-D channel, while **II** has a capsulized 1-D channel with small and large windows due to the dangling butyl groups.

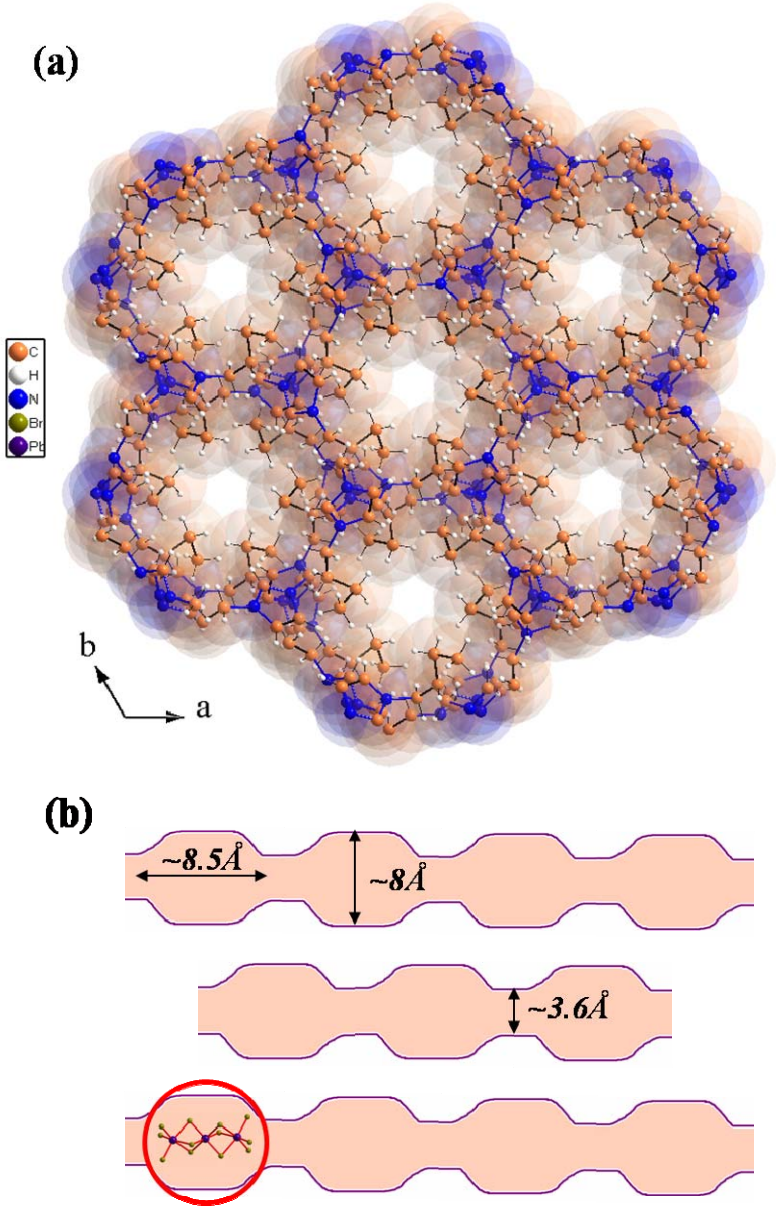

Fig. 6.4.6 (a) View of the infinite 1-D empty channels and dangling butyl groups at the small window along the *c*-axis. Superimposed models of ball-stick and van der Waals spheres and (b) view of the schematic of the packing of the 1-D channels with capsules (Pb_3Br_{12} unit in the capsule is highlighted in red), along the *a*-axis in $(BMIm)_2PbBr_4$, **II**.

An important conformational feature of the $BMIm^+$ cation is the torsional angle around C(5)-C(6) bond of the butyl chain. This angle is close to 60° for *gauche* and near 120° for the *anti* conformation. $BMIm^+$ cations with butyl chains in both the *gauche* and the *anti* conformation are reported. In the *gauche* conformation,[27,87-89] the butyl chain is twisted towards the imidazolium ring, whereas in the *anti* conformation,[90,91] it is projected away from the ring. These conformations are crucially affecting the hydrogen bonding and alkyl-alkyl interactions. In **II**, this angle is 57.88° with a *gauche* conformation of the twisted butyl chain. Another important feature is the angle between the imidazolium ring and the butyl chain. Butyl chains in most of the $BMIm^+$ cations are directed perpendicular to the ring. Coplanar butyl chains are formed rarely[92]. The butyl chain in **II** makes an interplanar angle of 88.67° with the ring.

The melting points of **I** and **II** are 209° and 138° C respectively, as confirmed from DTA. Both the compounds crystallize (polycrystalline powder) back to the original structures on cooling the melts. **I** has three H-bonding interactions per cation with three anions through alkyl groups. **II** has only one H-bonding interaction per cation with a Br^- anion through a hydrogen atom from the imidazolium ring. Both **I** and **II** are stabilized by alkyl-alkyl interactions. The role of cooperative H-bonding interactions in directing and influencing the electronic properties of hybrid perovskites has been demonstrated in the recent literature.[93]

The stereochemical activity of lone-pair electrons in Pb^{2+} cation plays a role in the coordination geometry and thereby crystal engineering.[94] The coordination geometry of the PbO_n polyhedra in Pb(II) compounds is hemidirected for low coordination numbers (2-5) and holodirected for high coordination numbers (9,10). For intermediate coordination numbers (6-8) either type of

stereochemistry is found.[95,96] Ab initio molecular orbital studies of gas-phase Pb(II) complexes show that stereochemically active hemidirected geometry occurs if the ligand coordination number is low, the ligands are hard, and there are attractive interactions between the ligands.[97,98] In such cases, the lone pair orbital has a p character and fewer electrons are transferred from the ligands to the bonding orbitals of Pb(II), giving rise to more ionic bonds. Holodirected geometry occurs when the coordination number is high and the ligands are soft and bulky or show strong interligand repulsion. The lone pair orbital has negligible p character when the geometry is holodirected, and the bonds are more covalent than in the hemidirected structures. In the case of holodirected geometry, with weak donors and high Pb-L distances, the lone pair is still considered to be active with discern holes in the coordination spheres.[94] The Pb^{2+} cations in **I** exhibit hemidirected geometry with coordination number 5. The Pb^{2+} cations in **II** exhibit holodirected geometry with coordination number 6. One of the Pb^{2+} in **II** (Pb2) with slightly long Pb-Br distances may be considered to be holodirected, with active lone- pairs in the discernable holes of the coordination spheres.

(b) Nanocrystals of elemental chalcogens

Disolving sulfur powder in [BMIM][BF_4] or polyethyleneglycol alone and heating the solution to 200 °C did not yield in any nanostructures. Addition of $NaBH_4$ to the solution had no effect. However, heating sulfur powder in a mixture of [BMIM][BF_4] and polyethyleneglycol over the temperature range of 150-250 ºC resulted sulfur microspheres rather than any nanostructures. In Figure 6.4.7 (a), we show a SEM image of the sulfur microspheres prepared in a mixture of [BMIM][BF_4] and polyethyleneglycol at 180 °C for 12 hrs. The microspheres are

reasonably monodisperse with an average diameter of 18 μm. The microspheres are crystalline and the powder XRD pattern could be indexed based on the orthorhombic (*Fddd*) space group.

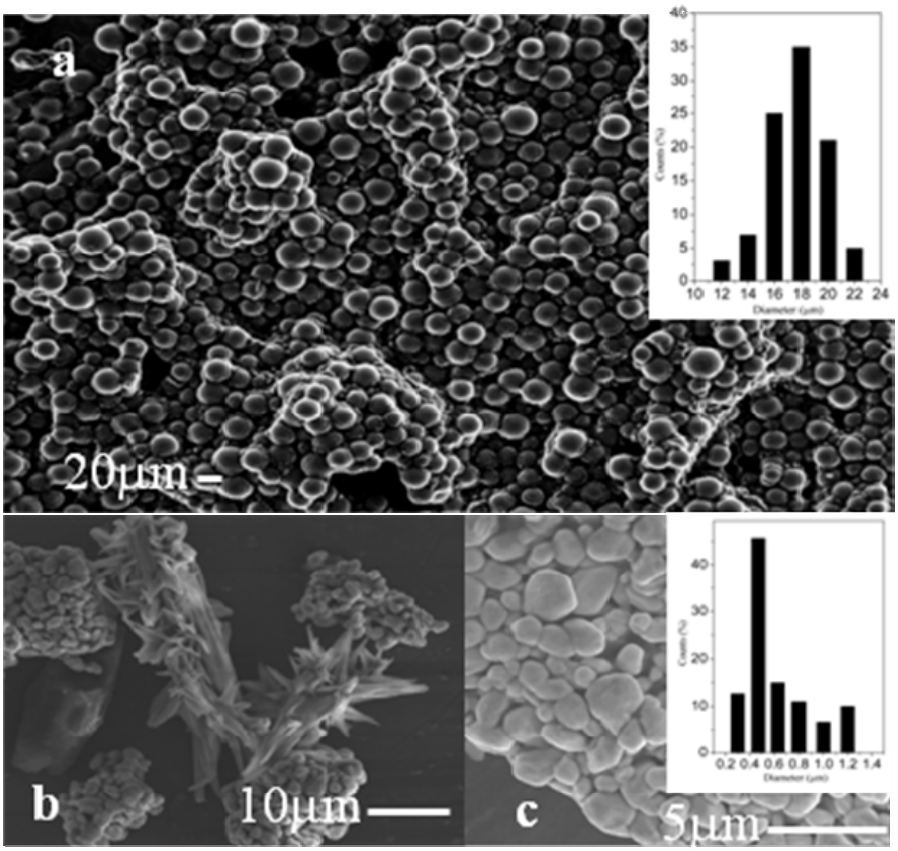

Fig. 6.4.7 (a) SEM image of S microspheres prepared in a mixture of [BMIM][BF_4] and polyethylene glycol at 180 °C for 12 hrs. Inset shows the size distribution histogram. (b) SEM image of Se particles and flower like structures prepared in a mixture of [BMIM][PF_6] and $NaBH_4$ at 200 °C for 10 hrs and (c) SEM image of Te micro crystals prepared in a mixture of [BMIM][PF_6] and $NaBH_4$ at 200 °C for 10 hrs. Inset shows the size distribution histogram**.**

Heating Se powder in a mixture of $NaBH_4$ and [BMIM][PF_6] at 200 °C for 10 hrs gives rise to Se particles and flower-like structures as shown in the SEM image in Figure 6.4.7 (b). These Se structures are crystalline and the powder XRD pattern could be indexed based on the hexagonal ($P3_12_1$) space group. Under similar conditions, heating Te powder in [BMIM][PF_6] in the presence of $NaBH_4$

gives rise to Te particles with an average diameter of 450 nm. The particles are crystalline and the powder XRD pattern could be indexed based on the hexagonal ($P3_12_1$) space group. Figure 6.4.7 (c) shows a SEM image of the Te microcrystals obtained in this manner.

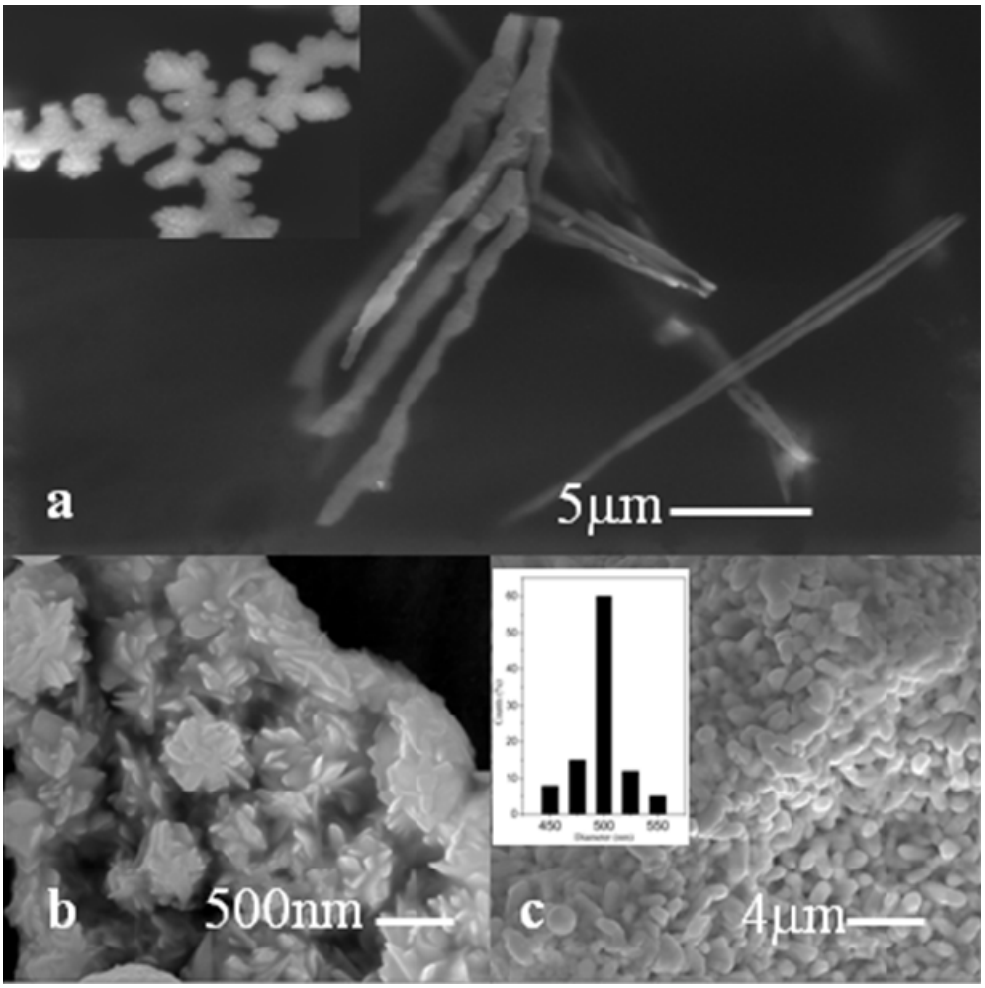

Fig. 6.4.8 (a) SEM image of Se nanowires and the inset shows dendritic structure of Se particles prepared in a mixture o[BMIM][BF_4], polyethyleneglycol, $NaBH_4$ and H_2O at room temperatures for 48 hrs, (b) SEM images of Se plate-like structures prepared in [BMIM][BF_4], polyethyleneglycol, $NaBH_4$ and H_2O at 75 °C for 24 hrs and (c) SEM image of Se rod-like structures prepared in a mixture of [BMIM][PF_6], polyethyleneglycol and $NaBH_4$ at 200 °C for 10 hrs. Inset shows the size distribution histogram.

A mixture of Se nanowires and dendritic structures of particles was obtained by keeping Se powder in a mixture of [BMIM][BF_4], polyethyleneglycol,

$NaBH_4$ and H_2O at 30 ºC for 48 hrs. The wires have a diameter of around 150 nm and of 10 μm length. The particles in the dendrite structures are crystalline and have an average diameter of 100 nm. Figure 6.4.8 (a) shows a SEM image of the Se nanowires, with the inset showing the dendritic structures. The above reaction mixture when heated at 75 °C for 24 hrs, gave aggregates of crystalline plate-like structures. Figure 6.4.8 (b) shows a SEM image of the plate-like structures prepared. Rod-like structures of Se were obtained, when Se powder was heated in a mixture of [BMIM][PF_6], polyethyleneglycol and $NaBH_4$ at 200 °C for 10 hrs. The rods are crystalline and reasonably monodisperse with an average diameter of 500 nm and a length of 2-3 μm. Figure 6.4.8 (c) shows a SEM image of the rod-like structures. The powder XRD pattern of these Se nanostructures could be indexed based on the hexagonal ($P3_12_1$) space group.

Te nanowires with an average thickness of 75 nm and several microns in length were obtained when Te powder was heated at 200 °C for 10 hrs in a mixture of [BMIM][PF_6], polyethyleneglycol and $NaBH_4$. Figure 6.4.9 (a) shows a SEM image of the Te nanowires and Figure 6.4.9 (b) shows a TEM image. A high-resolution electron microscope (HREM) image of a single nanowire is shown in Figure 6.4.9 (c). The inset in Figure 6.4.9 (c) shows the selected area electron diffraction (SAED) pattern with a lattice spacing of 5.9 Å corresponding to the (001) planes of the hexagonal Te structure. When the polyethyleneglycol was replaced by CTAB in the reaction mixture Te nanorods with an average diameter of 100 nm and a length of 300-400 nm were obtained under the similar reaction conditions. Few Y-junctions were also found in the product. In Figure 6.4.9 (d), we show a SEM image of the Te nanorods obtained from a mixture of [BMIM][PF_6],

CTAB and $NaBH_4$ at 200 °C after 10 hrs. The insets show the Y junctions and the size distribution histogram. All the Te nanostructures are crystalline and the powder XRD patterns could be indexed based on the hexagonal ($P3_12_1$) space group.

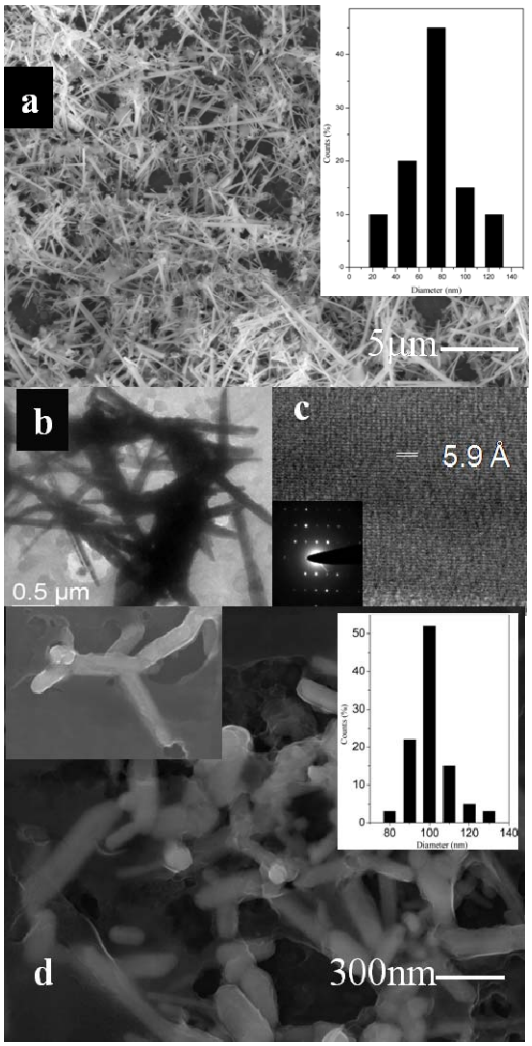

Fig. 6.4.9. (a) SEM image of Te nanowires prepared in a mixture of [BMIM][PF_6], polyethylene glycol and $NaBH_4$ at 200 °C for 10 hrs. Inset shows the size distribution histogram. (b) TEM images of Te nanowires, (c) HREM image of a single nanowire and the inset shows electron diffraction patterns and (d) SEM image of Te nanorods prepared in a mixture of [BMIM][PF_6], CTAB and $NaBH_4$ at 200 °C for 10 hrs. Insets show the Y junction and the size distribution histogram.

(c) Nanocrystals of oxides

Heating titanium isopropoxide in [BMIM][BF_4] and methyl alcohol at 180 ºC for 20 hrs gives rise to TiO_2 nanoparticles with an average diameter of 10 nm. Similar size nanoparticles were also obtained by treating the titania hydrogel in [BMIM][BF_4] at 180 ºC for 20 hrs. Addition of surfactant or variation of time and temperature of the reaction did not yield any change in the size or shape of the particles. Figure 6.4.10 shows a SEM image of the TiO_2 nanoparticles and Figure 6.4.11 (a) shows a TEM image. The inset in Figure 6.4.11 (a) shows the electron diffraction (SAED) pattern. The powder XRD pattern of these TiO_2 nanoparticles could be indexed based on anatase phase of the TiO_2.

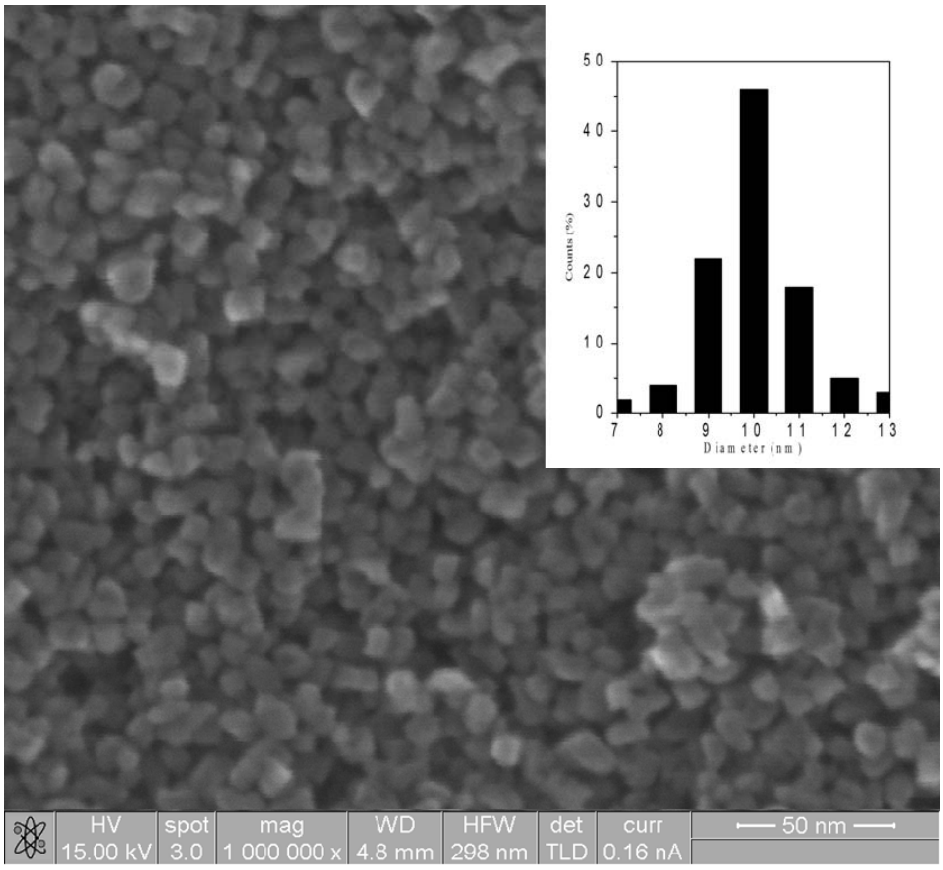

Fig. 6.4.10. SEM image of TiO_2 nanoparticles prepared in a mixture of [BMIM][BF4] and methyl alcohol at 180 °C for 20 hrs. Inset shows the size distribution histogram.

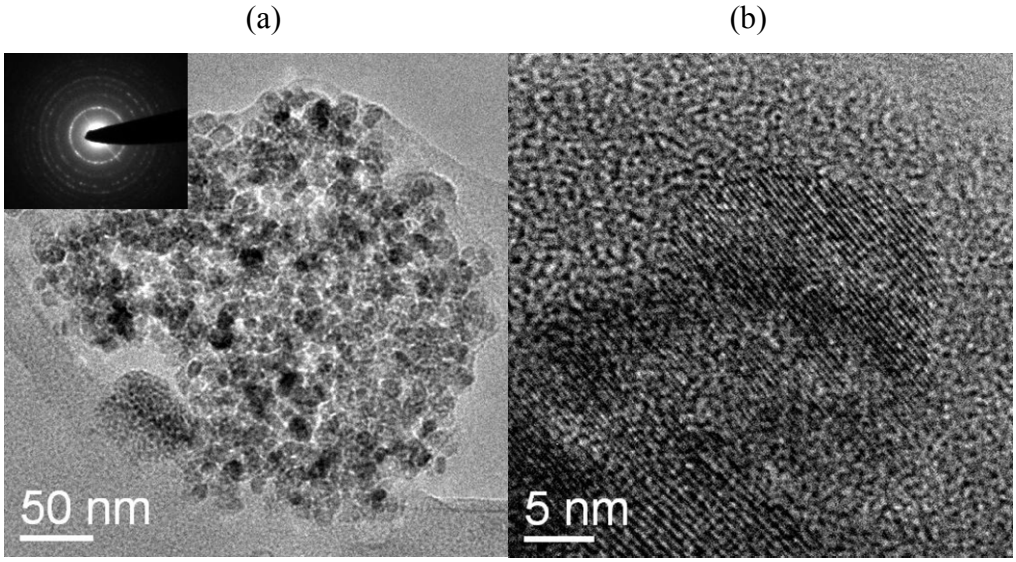

Fig. 6.4.11. (a) TEM images of TiO_2 nanoparticles (b) HREM image of a single nanoparticle.

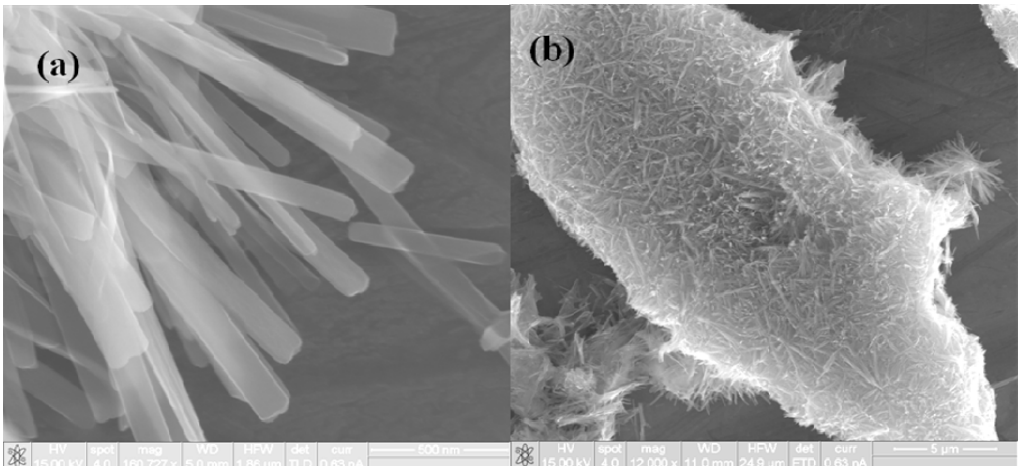

Fig. 6.4.12. SEM images of (a) of the V_2O_5 nanotapes and (b) a bunch of V_2O_5 nanotapes.

V_2O_5 nanotapes with an average thickness of 15 nm, an average width of 100nm and up to 3 microns in length were obtained by heating the vanadia gel in the ionic liquid [BMIM][BF_4] at 200 ºC for 48 hrs. Addition of any surfactant or variation of time and temperature of the reaction did not yield any change in the size or shape of the nanotapes. Figure 6.4.12 (a) shows a SEM image of the dispersed V_2O_5 nanotapes and Figure 6.4.12 (b) shows a SEM image of a bunch of

V_2O_5 nanotapes. The nanotapes are not crystalline and the powder XRD pattern did not show any peaks.

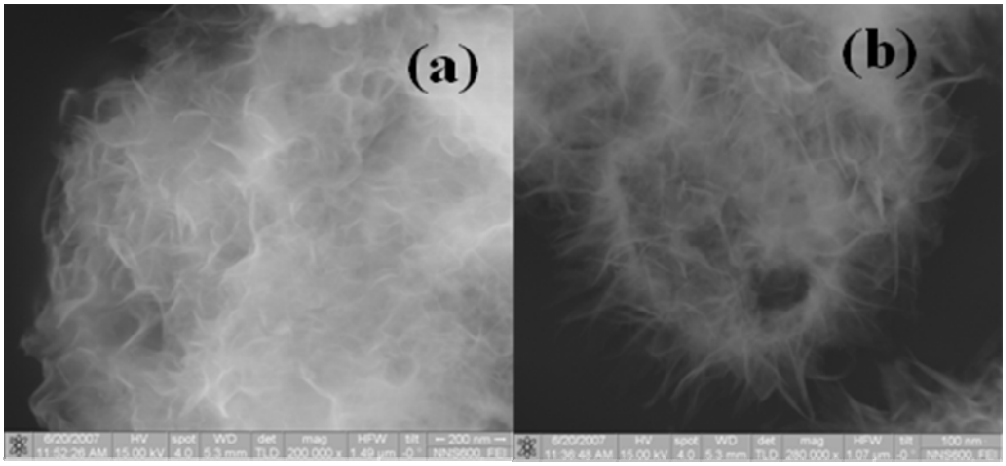

Fig. 6.4.13. SEM images of (a) Boehmite nanowires prepared in a mixture of aluminium isopopylate with [BMIM][Br] and methyl alcohol heated at 180^{o}c for 24h (b) $Al_2O_3.3H_2O$ nanowires prepared in a mixture of alumina hydrogel with [BMIM][Br] heated at 180^{o}c for 24h.

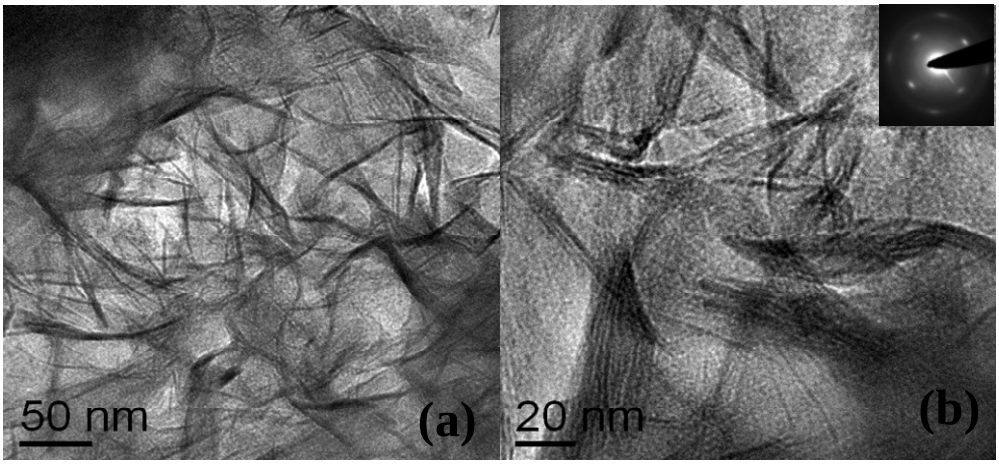

Fig. 6.4.14. TEM images of (a) Boehmite nanowires prepared in a mixture of aluminium isopopylate with [BMIM][Br] and methyl alcohol heated at 180^{o}c for 24h (b) $Al_2O_3.3H_2O$ nanowires prepared in a mixture of alumina hydrogel with [BMIM][Br] heated at 180^{o}c for 24h.

Heating aluminium isopropylate in [BMIM][Br] or [EMIM][Br] and methyl alcohol at 180 ºC for 24 hrs gives rise to bunches of boehmite nanowires with an average diameter of 3 nm and up to few hundreds of nm in length. Similar size nanowires of $Al_2O_3.3H_2O$ were also obtained in bunches by treating the

alumina gel in [BMIM][Br] or [EMIM][Br] at 180 ºC for 24 hrs. Addition of surfactant or variation of time and temperature of the reaction did not yield any change in the size or shape of the nanostructure. Figure 6.4.13 (a) shows a SEM image of the bunch of boehmite nanowires Figure 6.4.13 (b) shows a SEM image of the bunch of $Al_2O_3.3H_2O$ nanowires. Figure 6.4.14 (a) shows a TEM image of the bunch of boehmite nanowires. Figure 6.4.14 (b) shows a TEM image of the bunch of $Al_2O_3.3H_2O$ nanowires. The inset in Figure 6.4.14 (b) shows the selected area electron diffraction (SAED) pattern indicating the single crystallinity.

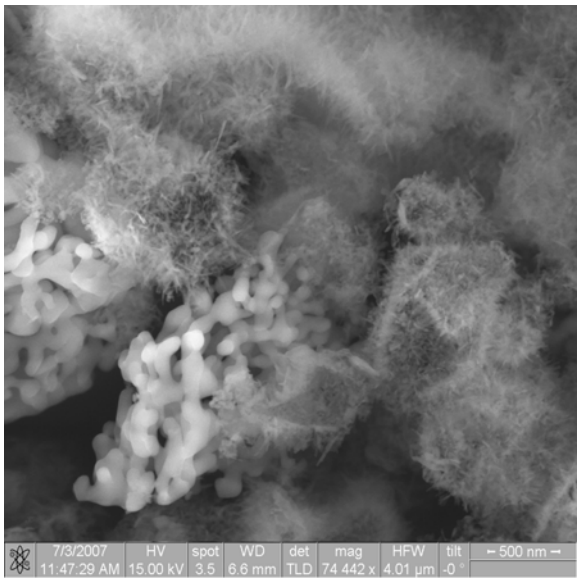

Fig. 6.4.15. SEM images of partially converted porous alumina (Al_2O_3) structures by heating the boehmite nanowires prepared in a mixture of aluminium isopopylate with [BMIM][Br] and methyl alcohol heated at 180^{o}c for 24h.

Boehmite nanowires are not crystalline and the powder XRD pattern did not show any peaks. These amorphous boehmite nanowires on heating at 1100^{o}c, were converted into crystalline porous alumina (Al_2O_3) structures. Figure 6.4.15 shows a SEM image of the partially converted porous alumina (Al_2O_3) structures. The powder XRD pattern of the $Al_2O_3.3H_2O$ nanowires could be indexed based on the monoclinic β- $Al_2O_3.3H_2O$ (PDF- 000010307). This result indicates role of a

small amount of water in the precursor on the product formation and its crystallinity.

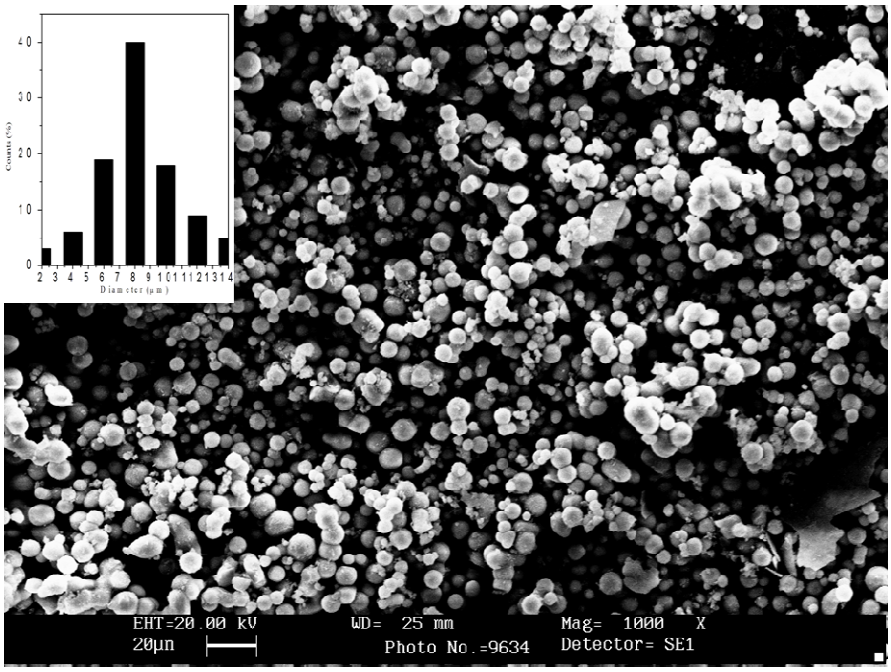

Fig. 6.4.16. SEM images of silica microspheres prepared from a mixture of TEOS in [EMIM][Br] and methyl alcohol.

Treating tetraethylorthosilicate (TEOS) in methyl alcohol or in the ionic liquid [EMIM][Br] alone and heating the solution up to 200 °C did not yield in any nanostructures. However, heating the mixture of tetraethylorthosilicate in methyl alcohol and ionic liquid [EMIM][Br] at 180 °C for 48hrs resulted silica microspheres rather than any nanostructures. Addition of surfactant to the solution did not yield any defined micro structures. Figure 6.4.16 shows a SEM image of the silica microspheres prepared in the mixture of [EMIM][Br] and methyl alcohol at 180 °C for 12 hrs. The diameters of the microspheres are in the 4-12 μm range. The microspheres are not crystalline and the powder XRD pattern did not show any peaks.

6.5. Conclusions

Ionothermal synthesis has enabled us to obtain two dialkylimidazolium bromoplumbates, (EMIm)$PbBr_3$, **I** and $(BMIm)_2PbBr_4$, **II**, derived from the corresponding ionic liquids. These compounds exhibit novel supramolecular architectures wherein the dialkylimidazolium cations organize themselves into channel structures with the bromoplumbate moieties residing in the channels. The difference between the channels of the two structures arises from the presence of the twisted, longer butyl chain with *gauche* conformation and the participation of ring hydrogen of **II** in hydrogen bonding interaction. The lead (II) cation in these compounds exhibits either hemi- or holodirected coordination geometry.

Preparation of nanowires and nanorods of Se and Te, based on the aqueous solution method at room temperature by using elemental chalcogen powder and $NaBH_4$ have been reported earlier. We could not obtain nanowires of Se and Te at room temperature using an ionic liquid alone. However we could obtain Se nanowires by using ionic liquid with a small amount of water at room temperature. We could synthesize other nanostructures of elemental chalcogens at 180 – 200 °C. Sulfur microspheres could be prepared by heating sulfur powder in a mixture of [BMIM][BF_4] and polyethyleneglycol.

We could synthesize TiO_2 nanoparticles with anatase structure by heating titaniumisopropoxide and methyl alcohol or a hydrogel of titania in the ionic liquid [BMIM][BF_4]. We could synthesize amorphous boehmite nanowires by heating aluminium isopropoxide in ionic liquids like [BMIM][Br] or [EMIM][Br] and methyl alcohol. These amorphous boehmite nanowires on heating at 1100^{o}c, were converted into crystalline porous alumina (Al_2O_3) structures. By using a different

precursor (alumina hydrogel) which contains a small amount of water in ionic liquids, crystalline nano wires of $Al_2O_3.3H_2O$ were obtained. We have also found that surfactant have no role in the formation of nanostructures in ionic liquids for this particular case. We could synthesize amorphous silica spheres by heating tetraethylorthosilicate in ionic liquids, [BMIM][Br] or [EMIM][Br], as solvents at 180 °C for 24Hrs.

6.6. References

1) T. Welton, *Chem. Rev.*, **1999**, 1, 223.

2) R. Sheldon, *Chem. Commun*., **2001**, 2399.

3) A. E. Visser, R. P. Swatloski, W. M. Reichert, J. H. Davis Jr., R. D. Rogers, R. Mayton, S. Sheff and A. Wierzbicki, *Chem. Commun*., **2001**, 135.

4) Y. S. Vygodskii, E. I. Lozinskaya and A. S. Shaplov, *Macromol. Rapid Commun.*, **2002**, 23, 676.

5) J. S. Wilkes, J. A. Levisky, R. A. Wilson and C. L. Hussey, *Inorg. Chem.,* **1982**, 21, 1263.

6) R. Ludwig and U. Kragl, *Angew. Chem. Int. Ed.*, **2007**, 46, 6582.

7) A. Taubert, *Acta Chim. Slov.*, **2005**, *52*, 183.

8) M. Antonietti, D. Kuang, B. Smarsly and Y. Zhou, *Angew. Chem. Int. Ed.*, **2004**, 43, 4988.

9) K. Biswas and C. N. R. Rao, *Chem. Eur.J.*, **2007**, 13, 6123.

10) H. Itoh, K. Naka and Y. Chujo, *J. Am. Chem. Soc*., **2004**, 126, 3026.

11) G. Buhler and C .Feldmann, *Angew. Chem. Int. Ed.* **2004**, 45, 4864.

12) E. R. Parnham and R. E. Morris, *Acc. Chem. Res*. **2007**, 40, 1005.

13) E. R. Parnham and R. E. Morris, *J. Mater. Chem*., **2006**, 16, 2208.

14) E. R. Parnham and R. E. Morris, *Chem. Mater.*, **2006**, 18, 4882.

15) Z. Lin, D. S. Wragg, J. E. Warren and R. E. Morris, *J. Am. Chem. Soc*., **2007**, 129, 10335.

16) E. R. Cooper, C. D. Andrews, P. S. Wheatley, P. B. Webb, P. Wormald and R. E. Morris, *Nature*, **2004**, 430, 1012.

17) J-H. Liao, P-C. Wu and W-C. Huang, *Cryst. Growth Des.*, **2006**, 6, 3682.

18) K. R. Seddon, *Chem. Technol. Biotechnol.*, **1997**, 68, 351.

19) J. G. Huddleston, A. E. Visser, W. M. Reichert, H. D. Willauer, G. A. Broker and R. D. Rogers, *Green Chem*., **2001**, 3, 156.

20) Y-F. Hu and C-M. Xu, *Chem. Rev.*, **2006**, ASAP Article,

DOI: 10.1021/cr0502044

21) W. M. Reichert, J. D. Holbrey, K. B. Vigour, T. D. Morgan, G. A. Broker and R. D. Rogers, *Chem. Commun*., **2006**, 4767.

22) B.Kirchner and A. P. Seitsonen, *Inorg. Chem.*, **2007**, 46, 2751.

23) L. P. N. Rebelo J. N. C. Lopes, J. M. S. S. Esperanca and E. Filipe, *J. Phys. Chem. B*, **2005**, 109, 6040.

24) S. Hayashi, R. Ozawa and H-O. Hamaguchi, *Chem. Lett.*, **2003**, 32, 498.

25) J. D. Holbery, W. M. Reichert, M. Nieuwenhuyzen, S. Johnston, K. R. Seddon and R. D. Rogers, *Chem. Commun*., **2003**, 1636.

26) D. G. Golovanov, K. A. Lyssenko, Ya. S. Vygodskii, E. I. Lozinskaya, A. S. Shaplov and M. Yu. Antipin, *Russ.Chem.Bull., Int.Ed.*, **2006**, 55, 1989.

27) A. R. Choudhury, N. Winterton, A. Steiner, A. I. Cooper and K. A. Johnson, *J. Am. Chem. Soc*. **2005**, 127, 16792.

28) N. Sieffert and G.Wipff, *J. Phys. Chem. A*., **2006**, 110, 1106.

29) B.L. Bhargava and S. Balasubramanian, *J. Am. Chem. Soc*., **2006**, 128, 10073.

30) R. M. L-Bell, M. G. Del Pópolo, T. G. Youngs, J. Kohanoff, C.G. Hanke, J. B. Harper and C.C. Pinilla, *Acc. Chem. Res*., **2007**, 40, 1138.

31) P. B. Hitchcock, K. R. Seddon and T. Welton, *J. Chem. Soc., Dalton Trans.*, **1993**, 2639.

32) A. Elaiwi, P. B.Hitchcock, K. R. Seddon, N. Srinivasan, Y.M. Tan, T. Welton and J. A. Zora, *J. Chem. Soc., Dalton Trans.*, **1995**, 3467.

33) K. Matsumoto, T. Tsuda, R. Hagiwara, Y. Ito and O.Tamada, *Solid State Sci.* **2002**, 4, 23.

34) M. Hasan, I.V. Kozhevnikov, M.R.H. Siddiqui, C. Femoni, A. Steiner and N. Winterton, *Inorg. Chem.*, **2001**, 40, 795.

35) M.F. Ortwerth, M.J. Wyzlic and R.G. Baughman, *Acta Cryst. C*, **1998**, 54, 1594.

36) C. N. R. Rao, A. Mueller and A. K. Cheetham, (Eds.), *The Chemistry of Nanomaterials*, Weinheim: Wiley-VCH, **2004**.

37) G. Schmid, (Ed), *Nanoparticles: Theory to Application*, , Weinheim: Wiley-VCH, **2004**.

38) C. Burda, X. Chen, R. Narayanan and M. A. El-Sayed, *Chem. Rev.*, **2005**, 105, 1025.

39) C. N. R. Rao and A. Govindaraj, *Nanotubes and nanowires*, *RSC series on nanoscience and nanotechnology*, Cambridge: RSC, **2006**.

40) Y. Zhou, *Current Nanoscience*, 2005, 1, 35.

41) G. S. Fonseca, A. P. Umpierre, P. F. P. Fichtner, S. R. Teixeira and J. Dupont, *Chem. Eur. J.*, **2003**, 9, 3263.

42) Y-J. Zhu, W-W. Wang, R-J. Qi and X-L. Hu, *Angew. Chem. Int. Ed.*, **2004**, 43, 1410.

43) K. Biswas and C.N.R. Rao, *Chem. Eur. J.*, **2007**, 13, 6123.

44) U. K. Gautam, M. Nath and C. N. R. Rao, *J. Mater. Chem.*, **2003**, 135, 2845.

45) B. Gates, B. Mayers, B. Cattle and Y. Xia, *Adv. Funct. Mater .,* **2002**, 12, 219.

46) Q. Li and V. W-W. Yam, *Chem. Commun.*, 2006,1006.

47) J-M. Song, J-H. Zhu and S-H. Yu, *J. Phys. Chem. B.*, **2006**, 110, 23790.

48) U. K. Gautam and C. N. R. Rao, *J. Mater. Chem.*, **2004**, 14, 2530.

49) B. Mayers and Y. Xia, *Adv. Mater.*, **2002**, 14, 279.

50) Y-J, Zhu, X-L. Hu and W-W. Wang, *Nanotechnology*, **2006**, 17, 645.

51) X. Chen and S. S. Mao, *Chem. Rev.*, **2007**, 107, 2891.

52) A. Chemseddine and T. Moritz, *Eur. J. Inorg. Chem.*, **1999**, 235.

53) L. Miao, S. Tanemura, S. Toh, K. Kaneko and M. Tanemura, *J. Cryst.Growth*, **2004**, *264*, 246.

54) M. S. Sander, M. J. Cote, W. Gu, B. M. Kile and C. P. Tripp, *Adv.Mater.*, **2004**, *16*, 2052.

55) J. H. Jung, T. Shimizu and S. Shinkai, *J. Mater. Chem.*, **2005**, *15*, 3979.

56) K. D. Kim, S. H. Kim and H. T. Kim, *Colloids Surf., A*, **2005**, *254*, 99.

57) P. D. Cozzoli, M. L. Curri and A. Agostiano, *Chem. Commun.*, **2005**, 3186.

58) S. Y. Chae, M. K. Park, S. K. Lee, T. Y. Kim, S. K. Kim and W. I. Lee, *Chem. Mater.*, **2003**, *15*, 3326.

59) A. R. Armstrong, G. Armstrong, J. Canales, R. Garcia and P.G. Bruce, *Adv. Mater.*, **2005**, *7*, 862.

60) H. Choi, Y. J. Kim, R. S. Varma, and D. D. Dionysiou, *Chem. Mater.*, **2006**, 18, 5377.

61) C. Xiong, A. E. Aliev, B. Gnade and K. J. Balkus Jr., *ACS Nano*, **2008**, 2, 293.

62) Y. Wang and G. Cao, *Chem. Mater.*, **2006,** *18,* 2787.

63) C. O'Dwyer, D. Navas, V. Lavayen, E. Benavente, M. A. Santa Ana, G. González, S. B. Newcomb and C. M. S. Torres, *Chem. Mater.*, **2006,** *18,* 3016.

64) S. Shi, M. Cao, X. He and H. Xie, *Cryst. Growth Des.*, **2007,** 7, 1893.

65) S. Biermann, A. Poteryaev, A. I. Lichtenstein and A. Georges, *Phys.Rev. Lett.*, **2005**, *94*, 26404.

66) T. D. Manning, I. P. Parkin, M. E. Pemble, D. Sheel, D. Vernardou, *Chem. Mater.*, **2004**, *16*, 744.

67) B. S. Guiton, Q. Gu, A. L. Prieto, M. S. Gudiksen and H. Park, *J. Am.Chem. Soc.*, **2005**, *127*, 498.

68) J. Wu, Q. Gu, B. S. Guiton, N. P. Leon, L. Ouyang and H. Park, *Nano Lett.*, **2006**, *6*, 2313.

69) X. Chen, X. Wang, Z. Wang, J. Wan, J. Liu and Y. Qian, *Nanotechnology*, **2004**, *15*, 1685.

70) G. Li, K. Chao, H. Peng, K. Chen and Z. Zhang, *Inorg. Chem.*, **2007,** 46, 5787.

71) G. Das, *Ceram. Eng. Sci. Proc*., **1995**, 16, 977.

72) A. P. Philipse, A-M. Nechifor and C. Pathmamanoharan, *Langmuir*, **1994**, *10*, 4451.

73) S. C. Shen, Q. Chen, P. S. Chow, G. H. Tan, X. T. Zeng, Z. Wang and R. B. H. Tan, *J. Phys. Chem. C*, **2007**, *111,* 700.

74) H. Y. Zhu, X. P. Gao, D. Y. Song, Y. Q. Bai, S. P. Ringer, Z. Gao, Y. X. Xi, W. Martens, J. D. Riches and R. L. Frost, *J. Phys. Chem.B*, **2004**, *108*, 4245.

75) D. B. Kuang, Y. P. Fang, H. Q. Liu, C. Frommen, D. Fenske, *J.Mater. Chem.*, **2003**, *13*, 660.

76) A.S. Panchakarla, M.A. Shah, A. Govindaraj and C.N.R. Rao, *J. Solid State Chem.*, **2007,** 180, 3106.

77) H. Y. Zhu, J. D. Riches, and J. C. Barry, *Chem. Mater.*, **2002,** *14,* 2086.

78) M. E. Davis, *Nature*, **2002**, 417, 813.

79) D. S. Jacob, A. Joseph, S. P. Mallenahalli, S. Shanmugam, S. Makhluf, J. C-Moreno, Y. Koltypin, and A. Gedanken, *Angew. Chem. Int. Ed*., **2005**, 44, 6560.

80) D. Xiao, J. R. Rajian, S. Li, R. A. Bartsch, and E. L. Quitevis, *J. Phys. Chem. B*, **2006**, *110,* 16174.

81) Y. Wang, H. Li and S. Han, *J. Phys. Chem. B*, **2006**, *110,* 24646.

82) S. Barbara, Infrared Spectroscopy: Fundamentals and Applications, Wiley, New York, **2004**.

83) R. M. Silverstein, G. C. Bassler and T. C. Morrill, Spectrometric Identification of Organic Compounds, John Wiley & Sons, New York, **1963**.

84) K. Nakamoto, Infrared and Raman Spectra of Inorganic and Coordination Compounds, Wiley, New York, **1978**.

85) G. M. Sheldrick, SADABS Siemens Area Detector Absorption Correction Program, University of Göttingen: Göttingen, Germany, **1994**.

86) G. M. Sheldrick, SHELXTL-PLUS Program for Crystal Structure Solution and Refinement, University of Göttingen: Göttingen, Germany, **1997**.

87) J. E. L. Dullius, P. A. Z. Suarez, S. Einloft, R. F. De Souza, J. Dupont, J. Fischer and A. De Cian, *Organometallics*, **1998**, 17, 815.

88) J. Dupont, P. A. Z. Suarez, R. F. De Souza, R. A. Burrow and J.-P. Kintzinger, *Chem. Eur. J.*, **2000**, 6, 2377

89) O. Stentzel, H. G. Raubenheimer and C. Esterhuyzen, *J. Chem. Soc., Dalton Trans.*, **2002**, 1132.

90) A. E. Bradley, J. E. Hatter, M. Nieuwenhuyzen, W. R. Pitner, K. R. Seddon and R. C. Theid, *Inorg. Chem.*, **2002**, 41, 1692.

91) J. van den Broeke, M.Stam, M. Lutz, H. Kooijman, A.L. Spek, B-J. Deelman and G.van Koten, *Eur.J.Inorg.Chem.*, **2003**, 2798.

92) D. G. Golovanov, K. A. Lyssenko, M. Y. Antipin, Y. S. Vygodskii, E. I. Lozinskaya and A. S. Shaplov, *Cryst. Growth Des*., **2005**, 5, 337.

93) N. Mercier, S. Poiroux, A. Riou and P. Batail, *Inorg. Chem*., **2004**, 43, 8361.

94) A. K. Hall, J. M. Harrowfield, A. Morsali, A. A. Soudi and A.Yanovsky, *CrystEngComm*., **2000**, 82.

95) S. Ayyappan, G. D. de Delgado, A. K. Cheetham, G. Férey and C. N. R. Rao, *J. Chem. Soc. Dalton Trans.,* **1999**, 2905.

96) T. Glowiak, H. Kozlowski, L. S. Erre, G. Micera and B. Gulinati, *Inorg. Chim. Acta.,* **1992**, *202*, 43.

97) L. S-Livny, J. P. Glusker and C. W. Bock, *Inorg. Chem*., **1998**, 37, 1853.

98) C. W. Watson, S. C. Parker, *J. Phys. Chem. B*., **1999**, 103, 1258.

6.7. Appendix

Table A6.1

Atomic Coordinates and Equivalent Isotropic Displacement Parameters [Å^2] for (EMIm)$PbBr_3$, **I**.

Atom	x	y	z	U(eq)
Pb1	0.35723(3)	0.25740(3)	0.50210(2)	0.0305(1)
Br1	0.18336(13)	0.06194(9)	0.59583(6)	0.0490(3)
Br2	0.56667(13)	0.05088(8)	0.42824(6)	0.0397(3)
Br3	0.12579(11)	0.21708(9)	0.35606(5)	0.0413(3)
N1	0.6657(9)	0.2184(7)	0.1924(4)	0.029(2)
N2	0.9139(9)	0.2550(7)	0.1506(4)	0.034(2)
C1	0.7744(13)	0.3146(9)	0.1696(5)	0.036(3)
C2	0.7396(13)	0.0949(9)	0.1886(5)	0.040(4)
C3	0.8967(13)	0.1167(9)	0.1601(5)	0.042(4)
C4	0.4957(11)	0.2415(11)	0.2185(5)	0.043(3)
C5	1.0630(13)	0.3262(11)	0.1195(6)	0.049(4)
C6	1.0978(12)	0.2964(11)	0.0281(6)	0.053(4)

U(eq) is defined as one third of the trace of the orthogonalized Uij tensor.

Table A6.2

Atomic Coordinates and Equivalent Isotropic Displacement Parameters [Å^2] for $(BMIm)_2PbBr_4$, **II.**

Atom	x	y	z	U(eq)
Pb1	1/3	2/3	1/6	0.0467(1)
Pb2	1/3	2/3	-0.00223(1)	0.0477(1)
Br1	0.30220(8)	0.50183(4)	-0.06260(3)	0.0855(2)
Br2	0.45985(7)	0.63889(4)	0.08878(2)	0.0636(2)
N1	0.3461(3)	0.3520(6)	0.07259(18)	0.0620(14)
N2	0.2280(3)	0.3111(7)	0.12490(18)	0.0682(17)
C1	0.2836(4)	0.3737(8)	0.0882(2)	0.0681(17)
C2	0.3307(4)	0.2745(8)	0.1001(3)	0.076(2)
C3	0.2568(4)	0.2489(9)	0.1323(3)	0.082(2)
C4	0.4225(4)	0.4055(9)	0.0331(3)	0.088(3)
C5	0.1457(5)	0.3074(10)	0.1492(3)	0.104(3)
C6	0.0673(7)	0.2648(17)	0.1083(6)	0.373(15)
C7	0.0303(8)	0.1698(17)	0.0837(8)	0.206(8)
C8	-0.0256(13)	0.185(2)	0.0403(7)	0.310(11)

U(eq) is defined as one third of the trace of the orthogonalized Uij tensor.